Analysis Report for AP-203

Analysis Report Documenting the Data, Generation, and Calibration of T-fields for CRA-2024

AP-203: Analysis Plan for Evaluation and Recalibration of Culebra Transmissivity Fields

Task Number 4.4.2.3.1

Authors:

Dale O. Bowman, II, 8882 — 5/24/23
Repository Performance Department — Date

Signature on File — 05/17/2023
Ross Kushnereit, 8882 — Date
INTERA Inc.

Signature on File — 05/17/2023
Michelle Pedrazas, 8882 — Date
INTERA Inc.

Signature on File — 05/17/2023
Patricia Johnson, 8882 — Date
INTERA Inc.

Signature on File — 05/17/2023
Neil Deeds, 8882 — Date
INTERA Inc.

Signature on File — 05/17/2023
James Pinkard, 8882 — Date
INTERA Inc.

Technical Review:

Signature on File — 05/17/2023
Kristopher Kuhlman, 8842 — Date
Nuclear Waste Disposal Research & Analysis Dept.

4.4.2.3.1:TD:QA-L:RECERT:579482
WIPP:~~1.4.2.3.TD:QA-L:DPRP1:PKG# 539221~~ DH 6/7/23

Information Only

	Signature on File James Bethune, 8881 Piru & Associates	05/17/2023 Date
QA Review:	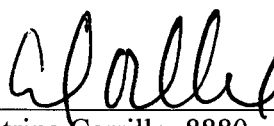 Catrina Carrillo, 8880 Edgewater, Inc	5/17/23 Date
Management Review:	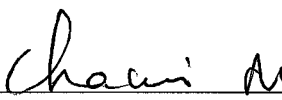 Chammi Miller, 8882 Repository Performance Department	05/24/23 Date

Information Only

Contents

1. Introduction 16

2. Task 4 – Investigation of the Impact of Boundary Conditions on the Model Domain 23

3. Task 5 – Update Flow and Optimization Programs 25

3.1 MODFLOW6 Numerical Flow Model 25

3.2 PEST++ IES Parameter Estimator 25

4. Task 6 – Evaluation of Mills Ranch Pumping Data as Optimization Targets 27

4.1 Estimation of the Mills Ranch Pumping Rate 28

5. Task 7 – Calibration of Revised T-fields 31

5.1 Observations 33

5.2 Parameters 44

5.3 Ensemble-based Inversion Process & Results 54

5.4 Calibrated Results 63

5.5 Run Control, Software, and Hardware 82

6. References 83

7. Appendix A 87

7.1 Normalized Objective Function for Observation Groups at Iteration 5 87

7.2 Distribution of Steady-State Freshwater Heads 121

7.3 Distribution of Observed vs Simulated Drawdown at Monitoring Locations for the Multi-Well Pumping Tests 145

7.4 Observed vs Simulated Drawdown at Monitoring Locations during Mills Ranch Pumping 178

7.5 Distribution of Estimated Transmissivity Values with Single-Well Performance Test Data 187

7.6 Directory Tree Structure 219

8. Appendix B – Routine Calculations 229

Tables

Table 1. Estimated Parameter Values Used to Generate Initial Head Surface and Assign Boundary Conditions 24

Table 2. MODFLOW6 Model Runs 31

Table 3. Fresh Water Heads (FWH) and Calculations for Selected Wells 35

Table 4. Wells with Drawdown Observations Impacted by Mills Ranch Pumping 39

Table 5. Single Well Performance Transmissivity Measurements 41

Table 6. General Observation Groups, Desired Objective Function Percentages, and Weight Multipliers 43

Information Only

Table 7. Variogram Parameters for Grid-Scale 45
Table 8. Variogram Parameters for Pilot Point Multipliers 46
Table 9. Summary Table of Hydraulic Conductivity Parameters 48
Table 10. Summary Table of Specific Storage Parameters 50
Table 11. Summary Table of Anisotropy Parameters 52
Table 12. Summary Table of Recharge Parameters 53
Table 13. 100 Selected T-Field Realizations 63
Table 14. Particle Travel Times to the LWB for 100 Selected Realizations at Iteration 5 75
Table 15. Particle Travel Times to the LWB for All the Realizations for CRP1 76
Table 16. Particle Travel Times to the LWB for All the Realizations for CRP2 76
Table 17. Particle Travel Times to the LWB for All the Realizations for CRP3 76
Table 18. Particle Travel Times to the LWB for All the Realizations for CRP4 77

Figures

Figure 1. Wells used in CRA-2009 PABC T-Fields Analysis 20
Figure 2. Wells used in CRA-2024 T-Fields Analysis 21
Figure 3. Change in Freshwater Heads (m) between CRA-2009 PABC and CRA-2024 22
Figure 4. Map of Estimated Initial Heads Surface Used to Prescribe Fixed Head Boundary Conditions 24
Figure 5. Location of Mills Ranch Culebra Well and Neighboring Culebra Wells 27
Figure 6. Recovery Data for Ten Wells from the Culebra Monitoring Network Located Near Mills Ranch Well 28
Figure 7. Drawdown Observations in Well SNL17 and Pumping Periods Selected for the Mills Ranch Pumping Well (vertical bars), Pink Fraction of Bar Represents Estimate Relative Pumping Rate 29
Figure 8. Flowchart of Calibration Workflow 33
Figure 9. Map of Single Well Performance Transmissivity Measurements 42
Figure 10. Pilot Point Multipliers in the Model Domain 46
Figure 11. Transmissivity Zones 47
Figure 12. Storativity Zones 50
Figure 13. Recharge Zonation 53
Figure 14. Evolution of Total Objective Function with IES Iteration 56
Figure 15. Evolution of Objective Function with IES Iteration for Steady-state Freshwater Heads Observation Group 57
Figure 16. Evolution of Total Objective Function with IES Iteration for Multi-Well Pumping Tests 57
Figure 17. Evolution of Total Objective Function with IES Iteration for Mills Ranch Pumping Event 58
Figure 18. Travel time statistics by iteration for CRP 1 58
Figure 19. Travel time statistics by iteration for CRP 2 59

Information Only

Figure 20. Travel time statistics by iteration for CRP 3 59
Figure 21. Travel time statistics by iteration for CRP 4 60
Figure 22. Normalized Objective Function for Observation Groups at Iteration 5 61
Figure 23. Histograms and Scatter Plots of Normalized Objective Function for Primary Observation Groups 62
Figure 24. Contour of median steady-state freshwater head in meters above sea level in black. . Mean, median, or mode of observed steady-state freshwater heads for each well are in red. 64
Figure 25. Distributions of Estimated Mills Ranch Pumping Rates for the 100 Selected Realizations 65
Figure 26. Standard Deviation of Transmissivity Across 100 Selected Realizations at Iteration 5 66
Figure 27. Mean Transmissivity Across 100 Selected Realizations at Iteration 5 67
Figure 28. Count of "High-T" Zone Membership at Iteration 0 67
Figure 29. Count of "High-T" Zone Membership at Iteration 5 68
Figure 30. Change from High-T to Low-T Membership Between Iterations 0 and 5 68
Figure 31. Change from Low-T to High-T Membership Between Iterations 0 and 5 69
Figure 32. Standard Deviation of Storativity Across 100 Selected Realizations at Iteration 5 70
Figure 33. Mean Storativity Across 100 Selected Realizations at Iteration 5 70
Figure 34. Standard Deviation of Anisotropy Across 100 Selected Realizations at Iteration 5 71
Figure 35. Mean Anisotropy Across 100 Selected Realizations at Iteration 5 72
Figure 36. Maximum Recharge Across Final 100 Selected Realizations at Iteration 5 73
Figure 37. Standard Deviation of Recharge Across Final 100 Selected Realizations at Iteration 5 73
Figure 38. Mean Recharge Across Final 100 Selected Realizations at Iteration 5 74
Figure 39. Four CRP Starting Point Locations on WIPP Layout (Figure from Bethune, 2022c) 75
Figure 40. Cumulative Distribution of Travel Times to the LWB for 100 Selected Realizations at Iteration 5 77
Figure 41. Cumulative Distribution of Travel Times to the LWB for All Realizations at Iteration 5 78
Figure 42. Cumulative Distribution of Travel Times to the LWB for All Realizations for CRP 1 78
Figure 43. Cumulative Distribution of Travel Times to the LWB for All Realizations for CRP 2 79
Figure 44. Cumulative Distribution of Travel Times to the LWB for All Realizations for CRP 3 79
Figure 45. Cumulative Distribution of Travel Times to the LWB for All Realizations for CRP 4 80
Figure 46. Cumulative Distribution of Travel Times to the LWB for CRP1 for Previous and Current Work 81
Figure 47. Distribution of Steady-State Freshwater Heads in AEC-7R for 100 Realizations at Iteration 5 121
Figure 48. Distribution of Steady-State Freshwater Heads in C-2737 for 100 Realizations at Iteration 5 122
Figure 49. Distribution of Steady-State Freshwater Heads in ERDA-9 for 100 Realizations at Iteration 5 122
Figure 50. Distribution of Steady-State Freshwater Heads in H-2b2 for 100 Realizations at Iteration 5 123

Information Only

Figure 51. Distribution of Steady-State Freshwater Heads in H-3b2 for 100 Realizations at Iteration 5 123
Figure 52. Distribution of Steady-State Freshwater Heads in H-4bR for 100 Realizations at Iteration 5 124
Figure 53. Distribution of Steady-State Freshwater Heads in H-5b for 100 Realizations at Iteration 5 124
Figure 54. Distribution of Steady-State Freshwater Heads in H-6bR for 100 Realizations from Iteration 5 125
Figure 55. Distribution of Steady-State Freshwater Heads in H-7b1 for 100 Realizations at Iteration 5 125
Figure 56. Distribution of Steady-State Freshwater Heads in H-9c for 100 Realizations at Iteration 5 126
Figure 57. Distribution of Steady-State Freshwater Heads in H-10cR for 100 Realizations from Iteration 5 126
Figure 58. Distribution of Steady-State Freshwater Heads in H-11b4R for 100 Realizations at Iteration 5 127
Figure 59. Distribution of Steady-State Freshwater Heads in H-12R for 100 Realizations at Iteration 5 127
Figure 60. Distribution of Steady-State Freshwater Heads in H-15R for 100 Realizations at Iteration 5 128
Figure 61. Distribution of Steady-State Freshwater Heads in H-17 for 100 Realizations at Iteration 5 128
Figure 62. Distribution of Steady-State Freshwater Heads in H-19b0 for 100 Realizations at Iteration 5 129
Figure 63. Distribution of Steady-State Freshwater Heads in IMC-461 for 100 Realizations at Iteration 5 129
Figure 64. Distribution of Steady-State Freshwater Heads in P-15 for 100 Realizations at Iteration 5 130
Figure 65. Distribution of Steady-State Freshwater Heads in P-17 for 100 Realizations at Iteration 5 130
Figure 66. Distribution of Steady-State Freshwater Heads in SNL-1 for 100 Realizations at Iteration 5 131
Figure 67. Distribution of Steady-State Freshwater Heads in SNL-2 for 100 Realizations at Iteration 5 131
Figure 68. Distribution of Steady-State Freshwater Heads in SNL-3 for 100 Realizations at Iteration 5 132
Figure 69. Distribution of Steady-State Freshwater Heads in SNL-5 for 100 Realizations at Iteration 5 132
Figure 70. Distribution of Steady-State Freshwater Heads in SNL-8 for 100 Realizations at Iteration 5 133
Figure 71. Distribution of Steady-State Freshwater Heads in SNL-9 for 100 Realizations at Iteration 5 133
Figure 72. Distribution of Steady-State Freshwater Heads in SNL-10 for 100 Realizations at Iteration 5 134

Information Only

Figure 73. Distribution of Steady-State Freshwater Heads in SNL-12 for 100 Realizations at Iteration 5 134
Figure 74. Distribution of Steady-State Freshwater Heads in SNL-13 for 100 Realizations at Iteration 5 135
Figure 75. Distribution of Steady-State Freshwater Heads in SNL-14 for 100 Realizations at Iteration 5 135
Figure 76. Distribution of Steady-State Freshwater Heads in SNL-16 for 100 Realizations at Iteration 5 136
Figure 77. Distribution of Steady-State Freshwater Heads in SNL-17 for 100 Realizations at Iteration 5 136
Figure 78. Distribution of Steady-State Freshwater Heads in SNL-18 for 100 Realizations at Iteration 5 137
Figure 79. Distribution of Steady-State Freshwater Heads in SNL-19 for 100 Realizations at Iteration 5 137
Figure 80. Distribution of Steady-State Freshwater Heads in USGS-4 for 100 Realizations at Iteration 5 138
Figure 81. Distribution of Steady-State Freshwater Heads in WIPP-11 for 100 Realizations at Iteration 5 138
Figure 82. Distribution of Steady-State Freshwater Heads in WIPP-12 for 100 Realizations at Iteration 5 139
Figure 83. Distribution of Steady-State Freshwater Heads in WIPP-13 for 100 Realizations at Iteration 5 139
Figure 84. Distribution of Steady-State Freshwater Heads in WIPP-19 for 100 Realizations at Iteration 5 140
Figure 85. Distribution of Steady-State Freshwater Heads in WIPP-25 for 100 Realizations at Iteration 5 140
Figure 86. Distribution of Steady-State Freshwater Heads in WIPP-26 for 100 Realizations at Iteration 5 141
Figure 87. Distribution of Steady-State Freshwater Heads in WIPP-30 for 100 Realizations at Iteration 5 141
Figure 88. Distribution of Steady-State Freshwater Heads in WQSP-1 for 100 Realizations at Iteration 5 142
Figure 89. Distribution of Steady-State Freshwater Heads in WQSP-2 for 100 Realizations at Iteration 5 142
Figure 90. Distribution of Steady-State Freshwater Heads in WQSP-3 for 100 Realizations at Iteration 5 143
Figure 91. Distribution of Steady-State Freshwater Heads in WQSP-4 for 100 Realizations at Iteration 5 143
Figure 92. Distribution of Steady-State Freshwater Heads in WQSP-5 for 100 Realizations at Iteration 5 144
Figure 93. Distribution of Steady-State Freshwater Heads in WQSP-6 for 100 Realizations at Iteration 5 144
Figure 94. Observed vs Simulated Drawdown at DOE-1 And H11-b2 Monitoring Locations for the H-3 Multi-Well Pumping Test 145

Information Only

Figure 95. Observed vs Simulated Drawdown at H-1 and H-2b2 Monitoring Locations for the H-3 Multi-Well Pumping Test 146
Figure 96. Observed vs Simulated Drawdown at ENGLE and H-4bR Monitoring Locations for the H-9bR Multi-Well Pumping Test 147
Figure 97. Observed vs Simulated Drawdown at SNL-12 and SNL-14 Monitoring Locations for the H-9bR Multi-Well Pumping Test 148
Figure 98. Observed vs Simulated Drawdown at SNL-17 Monitoring Location for the H-9bR Multi-Well Pumping Test 149
Figure 99. Observed vs Simulated Drawdown at CB-1 and DOE-1 Monitoring Locations for the H-11 Multi-Well Pumping Test 149
Figure 100. Observed vs Simulated Drawdown at H-3b2 and H-4b Monitoring Locations for the H-11 Multi-Well Pumping Test 150
Figure 101. Observed vs Simulated Drawdown at H-12 and H-14 Monitoring Locations for the H-11 Multi-Well Pumping Test 151
Figure 102. Observed vs Simulated Drawdown at H-15 and H-17 Monitoring Locations for the H-11 Multi-Well Pumping Test 152
Figure 103. Observed vs Simulated Drawdown at P-15 and P-17 Monitoring Locations for the H-11 Multi-Well Pumping Test 153
Figure 104. Observed vs Simulated Drawdown at DOE-1 and ERDA-9 Monitoring Locations for the H-19 Multi-Well Pumping Test 154
Figure 105. Observed vs Simulated Drawdown at H-3b2 and WIPP-21 Monitoring Locations for the H-19 Multi-Well Pumping Test 155
Figure 106. Observed vs Simulated Drawdown at H-15 and H-1 Monitoring Locations for the H-19 Multi-Well Pumping Test 156
Figure 107. Observed vs Simulated Drawdown at WQSP-5 Monitoring Location for the H-19 Multi-Well Pumping Test 156
Figure 108. Observed vs Simulated Drawdown at D-268 and H-18 Monitoring Locations for the P-14 Multi-Well Pumping Test 157
Figure 109. Observed vs Simulated Drawdown at H-6b and WIPP-25 Monitoring Locations for the P-14 Multi-Well Pumping Test 158
Figure 110. Observed vs Simulated Drawdown at WIPP-26 Monitoring Locations for the P-14 Multi-Well Pumping Test 158
Figure 111. Observed vs Simulated Drawdown at C-2737 and ERDA-9 Monitoring Locations for the SNL-14 Multi-Well Pumping Test 159
Figure 112. Observed vs Simulated Drawdown at H-3b2 and H-4b Monitoring Locations for the SNL-14 Multi-Well Pumping Test 160
Figure 113. Observed vs Simulated Drawdown at H-7 and H-9c Monitoring Locations for the SNL-14 Multi-Well Pumping Test 161
Figure 114. Observed vs Simulated Drawdown at H-11b4 and H-15 Monitoring Locations for the SNL-14 Multi-Well Pumping Test 162
Figure 115. Observed vs Simulated Drawdown at H-17 and H-19b0 Monitoring Locations for the SNL-14 Multi-Well Pumping Test 163
Figure 116. Observed vs Simulated Drawdown at SNL-12 and SNL-13 Monitoring Locations for the SNL-14 Multi-Well Pumping Test 164

Information Only

Figure 117. Observed vs Simulated Drawdown at H-6b and SNL-1 Monitoring Locations for the WIPP-11 Multi-Well Pumping Test 165
Figure 118. Observed vs Simulated Drawdown at SNL-2 and SNL-3 Monitoring Locations for the WIPP-11 Multi-Well Pumping Test 166
Figure 119. Observed vs Simulated Drawdown at SNL-5 and SNL-9 Monitoring Locations for the WIPP-11 Multi-Well Pumping Test 167
Figure 120. Observed vs Simulated Drawdown at WIPP-12 and WIPP-13 Monitoring Locations for the WIPP-11 Multi-Well Pumping Test 168
Figure 121. Observed vs Simulated Drawdown at WIPP-30 and WQSP-1 Monitoring Locations for the WIPP-11 Multi-Well Pumping Test 169
Figure 122. Observed vs Simulated Drawdown at WQSP-2 and WQSP-3 Monitoring Locations for the WIPP-11 Multi-Well Pumping Test 170
Figure 123. Observed vs Simulated Drawdown at DOE-2 and H-2b2 Monitoring Locations for the WIPP-13 Multi-Well Pumping Test 171
Figure 124. Observed vs Simulated Drawdown at H-6b and P-14 Monitoring Locations for the WIPP-13 Multi-Well Pumping Test 172
Figure 125. Observed vs Simulated Drawdown at WIPP-12 and WIPP-18 Monitoring Locations for the WIPP-13 Multi-Well Pumping Test 173
Figure 126. Observed vs Simulated Drawdown at WIPP-19 and WIPP-25 Monitoring Locations for the WIPP-13 Multi-Well Pumping Test 174
Figure 127. Observed vs Simulated Drawdown at WIPP-30 Monitoring Location for the WIPP-13 Multi-Well Pumping Test 174
Figure 128. Observed vs Simulated Drawdown at H-18 and WIPP-13 Monitoring Locations for the WQSP-1 Multi-Well Pumping Test 175
Figure 129. Observed vs Simulated Drawdown at DOE-2 and H-18 Monitoring Locations for the WQSP-2 Multi-Well Pumping Test 176
Figure 130. Observed vs Simulated Drawdown at WIPP-13 and WQSP-1 Monitoring Locations for the WQSP-2 Multi-Well Pumping Test 177
Figure 131. Observed vs Simulated Drawdown at Monitoring Location C-2737 during Mills Ranch Pumping for 100 Selected Realizations from Iteration 5 178
Figure 132. Observed vs Simulated Drawdown at Monitoring Location ERDA-9 during Mills Ranch Pumping for 100 Selected Realizations from Iteration 5 179
Figure 133. Observed vs Simulated Drawdown at Monitoring Location H-2b2 during the Mills Ranch Pumping Event for 100 Selected Realizations from Iteration 5 179
Figure 134. Observed vs Simulated Drawdown at Monitoring Location H-4bR during the Mills Ranch Pumping Event for 100 Selected Realizations from Iteration 5 180
Figure 135. Observed vs Simulated Drawdown at Monitoring Location H-9bR during Mills Ranch Pumping for 100 Selected Realizations from Iteration 5 181
Figure 136. Observed vs Simulated Drawdown at Monitoring Location H-15R during Mills Ranch Event for 100 Selected Realizations from Iteration 5 181
Figure 137. Observed vs Simulated Drawdown at Monitoring Location H-16 during Mills Ranch Pumping for 100 Selected Realizations from Iteration 5 182
Figure 138. Observed vs Simulated Drawdown at Monitoring Location H-17 during Mills Ranch Pumping for 100 Selected Realizations from Iteration 5 183

Information Only

Figure 139. Observed vs Simulated Drawdown at Monitoring Location H-19b0 during Mills Ranch Pumping for 100 Selected Realizations from Iteration 5 183
Figure 140. Observed vs Simulated Drawdown at Monitoring Location SNL-10 during Mills Ranch Pumping for 100 Selected Realizations from Iteration 5 184
Figure 141. Observed vs Simulated Drawdown at Monitoring Location SNL-12 during Mills Ranch Pumping for 100 Selected Realizations from Iteration 5 184
Figure 142. Observed vs Simulated Drawdown at Monitoring Location SNL-13 during Mills Ranch Pumping for 100 Selected Realizations from Iteration 5 185
Figure 143. Observed vs Simulated Drawdown at Monitoring Location SNL-14 during Mills Ranch Pumping for 100 Selected Realizations from Iteration 5 185
Figure 144. Observed vs Simulated Drawdown at Monitoring Location SNL-17 during Mills Ranch Pumping for 100 Selected Realizations from Iteration 5 186
Figure 145. Observed vs Simulated Drawdown at Monitoring Location WIPP-19 during Mills Ranch Pumping for 100 Selected Realizations from Iteration 5 186
Figure 146. Distribution of Transmissivity Values in Model Element Containing AEC-7R for 100 Selected Realizations from Iteration 5 187
Figure 147. Distribution of Transmissivity Values in Model Element Containing C-2737 for 100 Selected Realizations from Iteration 5 188
Figure 148. Distribution of Transmissivity Values in Model Element Containing CB-1 for 100 Selected Realizations from Iteration 5 188
Figure 149. Distribution of Transmissivity Values in Model Element Containing D-268 for 100 Selected Realizations from Iteration 5 189
Figure 150. Distribution of Transmissivity Values in Model Element Containing DOE-1 for 100 Selected Realizations from Iteration 5 189
Figure 151. Distribution of Transmissivity Values in Model Element Containing DOE-2 for 100 Selected Realizations from Iteration 5 190
Figure 152. Distribution of Transmissivity Values in Model Element Containing ENGLE Well for 100 Selected Realizations from Iteration 5 190
Figure 153. Distribution of Transmissivity Values in Model Element Containing ERDA-9 for 100 Selected Realizations from Iteration 5 191
Figure 154. Distribution of Transmissivity Values in Model Element Containing H-1 for 100 Selected Realizations from Iteration 5 191
Figure 155. Distribution of Transmissivity Values in Model Element Containing H-2c for 100 Selected Realizations from Iteration 5 192
Figure 156. Distribution of Transmissivity Values in Model Element Containing H-3b1 for 100 Selected Realizations from Iteration 5 192
Figure 157. Distribution of Transmissivity Values in Model Element Containing H-4c for 100 Selected Realizations from Iteration 5 193
Figure 158. Distribution of Transmissivity Values in Model Element Containing H-5c for 100 Selected Realizations from Iteration 5 193
Figure 159. Distribution of Transmissivity Values in Model Element Containing H-6c for 100 Selected Realizations from Iteration 5 194
Figure 160. Distribution of Transmissivity Values in Model Element Containing H-7c for 100 Selected Realizations from Iteration 5 194

Information Only

Figure 161. Distribution of Transmissivity Values in Model Element Containing H-9bR for 100 Selected Realizations from Iteration 5 195
Figure 162. Distribution of Transmissivity Values in Model Element Containing H-10cR for 100 Selected Realizations from Iteration 5 195
Figure 163. Distribution of Transmissivity Values in Model Element Containing H-11b4R for 100 Selected Realizations from Iteration 5 196
Figure 164. Distribution of Transmissivity Values in Model Element Containing H-12R for 100 Selected Realizations from Iteration 5 196
Figure 165. Distribution of Transmissivity Values in Model Element Containing H-14 for 100 Selected Realizations from Iteration 5 197
Figure 166. Distribution of Transmissivity Values in Model Element Containing H-15R for 100 Selected Realizations from Iteration 5 197
Figure 167. Distribution of Transmissivity Values in Model Element Containing H-16 for 100 Selected Realizations from Iteration 5 198
Figure 168. Distribution of Transmissivity Values in Model Element Containing H-17 for 100 Selected Realizations from Iteration 5 198
Figure 169. Distribution of Transmissivity Values in Model Element Containing H-18 for 100 Selected Realizations from Iteration 5 199
Figure 170. Distribution of Transmissivity Values in Model Element Containing H-19b0 for 100 Selected Realizations from Iteration 5 199
Figure 171. Distribution of Transmissivity Values in Model Element Containing IMC-461 for 100 Selected Realizations from Iteration 5 200
Figure 172. Distribution of Transmissivity Values in Model Element Containing P-14 for 100 Selected Realizations from Iteration 5 200
Figure 173. Distribution of Transmissivity Values in Model Element Containing P-15 for 100 Selected Realizations from Iteration 5 201
Figure 174. Distribution of Transmissivity Values in Model Element Containing P-17 for 100 Selected Realizations from Iteration 5 201
Figure 175. Distribution of Transmissivity Values in Model Element Containing SNL-1 for 100 Selected Realizations from Iteration 5 202
Figure 176. Distribution of Transmissivity Values in Model Element Containing SNL-2 for 100 Selected Realizations from Iteration 5 202
Figure 177. Distribution of Transmissivity Values in Model Element Containing SNL-3 for 100 Selected Realizations from Iteration 5 203
Figure 178. Distribution of Transmissivity Values in Model Element Containing SNL-5 for 100 Selected Realizations from Iteration 5 203
Figure 179. Distribution of Transmissivity Values in Model Element Containing SNL-6 for 100 Selected Realizations from Iteration 5 204
Figure 180. Distribution of Transmissivity Values in Model Element Containing SNL-8 for 100 Selected Realizations from Iteration 5 204
Figure 181. Distribution of Transmissivity Values in Model Element Containing SNL-9 for 100 Selected Realizations from Iteration 5 205
Figure 182. Distribution of Transmissivity Values in Model Element Containing SNL-10 for 100 Selected Realizations from Iteration 5 205

Information Only

Figure 183. Distribution of Transmissivity Values in Model Element Containing SNL-12 for 100 Selected Realizations from Iteration 5 206
Figure 184. Distribution of Transmissivity Values in Model Element Containing SNL-13 for 100 Selected Realizations from Iteration 5 206
Figure 185. Distribution of Transmissivity Values in Model Element Containing SNL-14 for 100 Selected Realizations from Iteration 5 207
Figure 186. Distribution of Transmissivity Values in Model Element Containing SNL-15 for 100 Selected Realizations from Iteration 5 207
Figure 187. Distribution of Transmissivity Values in Model Element Containing SNL-16 for 100 Selected Realizations from Iteration 5 208
Figure 188. Distribution of Transmissivity Values in Model Element Containing SNL-17 for 100 Selected Realizations from Iteration 5 208
Figure 189. Distribution of Transmissivity Values in Model Element Containing SNL-18 for 100 Selected Realizations from Iteration 5 209
Figure 190. Distribution of Transmissivity Values in Model Element Containing SNL-19 for 100 Selected Realizations from Iteration 5 209
Figure 191. Distribution of Transmissivity Values in Model Element Containing USGS-1 for 100 Selected Realizations from Iteration 5 210
Figure 192. Distribution of Transmissivity Values in Model Element Containing WIPP-11 for 100 Selected Realizations from Iteration 5 210
Figure 193. Distribution of Transmissivity Values in Model Element Containing WIPP-12 for 100 Selected Realizations from Iteration 5 211
Figure 194. Distribution of Transmissivity Values in Model Element Containing WIPP-13 for 100 Selected Realizations from Iteration 5 211
Figure 195. Distribution of Transmissivity Values in Model Element Containing WIPP-18 for 100 Selected Realizations from Iteration 5 212
Figure 196. Distribution of Transmissivity Values in Model Element Containing WIPP-19 for 100 Selected Realizations from Iteration 5 212
Figure 197. Distribution of Transmissivity Values in Model Element Containing WIPP-21 for 100 Selected Realizations from Iteration 5 213
Figure 198. Distribution of Transmissivity Values in Model Element Containing WIPP-22 for 100 Selected Realizations from Iteration 5 213
Figure 199. Distribution of Transmissivity Values in Model Element Containing WIPP-25 for 100 Selected Realizations from Iteration 5 214
Figure 200. Distribution of Transmissivity Values in Model Element Containing WIPP-26 for 100 Selected Realizations from Iteration 5 214
Figure 201. Distribution of Transmissivity Values in Model Element Containing WIPP-28 for 100 Selected Realizations from Iteration 5 215
Figure 202. Distribution of Transmissivity Values in Model Element Containing WIPP-30 for 100 Selected Realizations from Iteration 5 215
Figure 203. Distribution of Transmissivity Values in Model Element Containing WQSP-1 for 100 Selected Realizations from Iteration 5 216
Figure 204. Distribution of Transmissivity Values in Model Element Containing WQSP-2 for 100 Selected Realizations from Iteration 5 216

Information Only

Figure 205. Distribution of Transmissivity Values in Model Element Containing WQSP-3 for 100 Selected Realizations from Iteration 5 217
Figure 206. Distribution of Transmissivity Values in Model Element Containing WQSP-4 for 100 Selected Realizations from Iteration 5 217
Figure 207. Distribution of Transmissivity Values in Model Element Containing WQSP-5 for 100 Selected Realizations from Iteration 5 218
Figure 208. Distribution of Transmissivity Values in Model Element Containing WQSP-6 for 100 Selected Realizations from Iteration 5 218

Information Only

Acronyms and Terms

A	horizontal anisotropy
amsl	above mean sea level
AMG	MODFLOW2000 Link Algebraic Multi-Grid package
AP	Analysis Plan
AR	Analysis Report
BAS6	MODFLOW2000 Basic File package
CDF	cumulative distribution function
CFD	continuous frequency distribution
CHD	MODFLOW Constant Heads package
CRP	Culebra Release Point
CRA	Compliance Recertification Application
DIS	MODFLOW Discretization File package
DOE	U.S. Department of Energy
DTW	depth-to-water
ft	feet
FWM	Fleetwood Mac Linux cluster
gpm	gallons per minute
hk	hydraulic conductivity
IC	MODFLOW6 Initial Conditions package
IMS	MODFLOW6 Iterative Model Solution package
LPF	MODFLOW2000 Layer Property Flow package
LWB	Land-Withdrawal Boundary
m	meters
MF2K	MODFLOW 2000
MOC	WIPP Management and Operations Contractor
NPF	MODFLOW6 Node Property File package
OC	MODFLOW Output Control package
OSE	Office of the State Engineer
PCG	MODFLOW2000 Preconditioned Conjugate-Gradient package
PEST	Parameter Estimation Optimization Software
QA	quality assurance
R	recharge
RC	run control
RCH	MODFLOW Recharge Package
RES	Regulatory Environmental Services, group within MOC
S	storativity
SNL	Sandia National Laboratories
ss	specific storage
STO	MODFLOW6 storage package
T	transmissivity
TDIS	MODFLOW6 Time Discretization File package
T-fields	transmissivity fields

Information Only

WEL	MODFLOW Well Package
WIPP	Waste Isolation Pilot Plant

Information Only

1. Introduction

The Waste Isolation Pilot Plant (WIPP), located in southeastern New Mexico, was developed by the US Department of Energy (DOE) for the deep geologic disposal of transuranic waste. The WIPP repository is located approximately 26 miles southeast of Carlsbad, New Mexico. The disposal horizon of the WIPP is approximately 2,150 feet below the ground surface in the Salado Formation of the Delaware Basin. The Salado is regionally extensive, consisting predominantly of halite, a low permeability evaporite (Powers et al., 1978). The Rustler Formation is located stratigraphically above the Salado Formation and is of particular importance in estimating the potential for radionuclide releases from the WIPP, because it contains the most hydraulically transmissive units above the repository, and consequently it is the most likely pathway for subsurface transport of radionuclides from the disposal panels to the accessible environmental outside the land withdrawal boundary (LWB). The Culebra Dolomite Member (herein referred to as Culebra) has been identified as the most transmissive unit in the Rustler Formation and consequently it is the most likely pathway for subsurface transport of radionuclides from the WIPP panels to the accessible environment outside the LWB (Kuhlman, 2010).

As summarized in Kuhlman (2010), the key steps in estimating radionuclide transport through the Culebra include the tasks listed below:

1. Construction of base geostatistical realizations of Culebra hydraulic transmissivity (T), anisotropy (A), storativity (S), and recharge (R) fields (collectively referred to as "T-fields")
2. Calibration of the T-fields to observed heads,
3. Modifying the T-fields to account for potential subsidence due to potash mining beneath the Culebra,
4. Calculating steady-state groundwater flow-fields for each mining-modified T-field, and
5. Calculating radionuclide transport through the Culebra for each flow-field. Culebra transport simulations calculate the cumulative discharge at the WIPP LWB over the 10,000-year regulatory period due to a source located at the center of the waste panel area. The source releases 1 kg for each of several radionuclides over the first 50 years of the simulation.

This Analysis Report (AR) summarizes the updated evaluation and recalibration of T-fields for the Culebra near the WIPP, which includes step 2 and additional related activities. To provide historical context regarding the past generations and calibrations of T-fields relative to the Compliance Certification Application (CCA) and Compliance Recertification Application (CRA) efforts, brief summaries of these efforts are described below:

- CCA-1996 (DOE, 1996; DOE/CAO 1996-2184) – The original generation of base T-fields, and subsequent calibration, were completed in 1996 for CCA using GRASP-INV. GRASP-INV was composed of four main routines: CONSIM II, SWIFT II, GRASP II, and PAREST. The initial T fields (consisting only of T values for the CCA) were generated through the geostatistical simulation routine called CONSIM II. The flow model grid was superimposed upon the geostatistical simulation grid and average transmissivity values were calculated for each flow model grid block. The grid-block transmissivity values were then sent to the flow model, SWIFT II, which calculated groundwater pressures and velocities across the flow model domain and sent this information to GRASP II, a sensitivity analysis routine. GRASP II first determined the objective function, which in the case of the Culebra flow model is the weighted least squares error between computed and measured steady-state and/or transient pressures. GRASP II then calculated adjoint sensitivities of the objective function to the addition of a pilot point. Having determined the most sensitive location for the addition of a pilot point into the model transmissivity field, the transmissivity value assigned to the pilot point was optimized by the PAREST routine to reduce the objective function. Constraints

Information Only

were assigned to the optimization process to ensure realistic transmissivity values at the pilot point transmissivity field was modified by determining the influence of the pilot point upon the surrounding grid block transmissivity values. The modified transmissivity field was then sent back to SWIFT II and the process repeats until the objective function is reduced to a specified minimum or until a selected maximum number of pilot points had been added.

- CRA-2004 (DOE, 2004; DOE/WIPP 2004-3231) – A two-part geologically based approach was used to generate new Culebra base T-fields (consisting only of T values for CRA-2004). In the first part, a conceptual model for geologic controls on Culebra T was formalized, and the hypothesized geologic controls were regressed against Culebra T data to determine linear regression coefficients. The regression includes one continuously varying function, Culebra overburden thickness, and three indicator functions that assume values of 0 or 1 depending on the occurrence of open, interconnected fractures, Salado dissolution, and the presence or absence of halite in units bounding the Culebra. In the second part, a method was developed for applying the linear regression model to predict Culebra T across the WIPP area. The regression model was combined with the maps of geologic factors to create 500 stochastically varying Culebra base T fields. Details about the development of the regression model and the creation of the base T fields are given in Holt and Yarbrough (2002, 2003a, 2003b).
- CRA-2009 (DOE, 2009; DOE/WIPP 09-3424, Appendix TFIELD-2009) – Only editorial and minor text changes were made to the CRA-2004 PABC, And T-fields incorporating the new data had not been completed.
- CRA-2009 Performance Assessment Baseline Calculations (PABC) (Kuhlman, 2009; Hart et al., 2008) – For PABC purposes, Hart et al. generated revised base T-fields (consisting of T, A, R, and S values for CRA-2009 PABC and after) using the same linear regression approach utilized for CRA-2004. The base T-fields were calibrated to freshwater heads and drawdown data, and 1,000 base T-fields were produced for preliminary screening and selection of the fields to calibrate or discard to generate the final 100 T-fields. The construction of the T-fields was completed using a Perl script called GEO2FIELD.
- CRA-2014 (DOE, 2014) – T-fields were used unchanged from CRA-2009 PABC in CRA-2014.
- CRA-2024 – Incorporation of new data and recalibration of the T-fields was completed in 2022 and 2023, and is documented herein. Since the T-fields resulting from these evaluations are intended as inputs to the 2024 Compliance Recertification Application, these analyses are categorized collectively as a Compliance Decision.

The CRA-2024 T-fields evaluation and recalibration efforts were completed in response to Analysis Plan 203 (AP-203) (Bowman, 2022), which includes the tasks listed below:

- Task 1 - Evaluation of Steady-State Head Optimization Targets
- Task 2 - Development of a New Steady-State Head Approach for T-field Optimization
- Task 3 - Update of T Values and Multi-Pad Pumping Test Optimization Targets
- Task 4 - Investigation of the Impact of Boundary Conditions on the Model Domain
- Task 5 - Update of Flow and Optimization Codes
- Task 6 - Evaluation of Mills Ranch Pumping Data as an Optimization Target
- Task 7 - Calibration of Revised T-fields

Tasks 1, 2, and 3, and the software qualification portion of Task 5 were completed and documented in prior reports, which are briefly referred to below.

- Task 1 – Completion of this task and the associated results are documented in Bowman (2019)
- Task 2 – Completion of this task and the associated results are documented in Farinacci and Bowman (2022)

Information Only

- Task 3 – Analyses of well tests completed since CRA-2009 were completed under AP-070 (Analysis Plan for Non-Salado Hydraulic-Test Interpretations; Bowman, 2020a) and have been documented in numerous Analysis Reports, referenced below:
  - Analysis of Culebra and Magenta Hydraulic Tests Performed Between January 2005 and August 2008 (Bowman, 2009)
  - Analysis of the IMC-461 Sinusoidal Test Conducted from 6/6/16 to 6/9/16 (Bowman, 2016)
  - Analysis of the AEC-7R Pumping Test Conducted from 3/9/15 to 3/13/15 (Bowman, 2015a)
  - Analysis of the H-9bR Pumping Test Conducted from 8/6/12 to 8/22/12 (Bowman, 2014)
  - Analysis of the H-10cR Pumping Test Conducted from 7/24/17 to 7/27/17 (Bowman, 2017)
  - Analysis of the H-11b4R Pumping Test Conducted From 6/11/12 to 6/14/12 (Bowman, 2013)
  - Analysis of the H-12R Pumping Test Conducted from 4/20/15 to 4/22/15 (Bowman, 2015b)
  - Analysis of the H-15R Pumping Test Conducted From 1/19/09 to 1/22/09 (Bowman, 2020a)
- Task 5 – To benefit from the advancements made in both the MODFLOW flow simulator and the PEST parameter estimator and to remain current with industry software, the newer program versions were qualified and include MODFLOW6 (version 6.2.2) and PEST++ (version 5.1.6). The software qualification process was completed for PEST++, an acquired code, and included compatibility assessments with MODFLOW6, also an acquired code, in August and September of 2022, and is detailed in the user's manuals and qualification documents specified below:
  - User's Manuals
    - Addendum to the User's Manual for MODFLOW6 Version 6.2.2. Sandia National Laboratories. Carlsbad, NM. ERMS 576747. (Brunell, 2022a)
    - Documentation for the MODFLOW6 Groundwater Flow Model. U.S. Geological Survey. Reston, VA. https://doi.org/10.3133/tm6A55. (Langevin et al., 2017)
    - Addendum to the Design Document and User's Manual for PEST ++ Version 5.1.6. Sandia National Laboratories. Carlsbad, NM. ERMS 576753. (Bethune, 2022a)
    - Documentation for PEST++ Version 5.1.6. https://github.com/usgs/pestpp/blob/5.1.6/documentation/pestpp_users_guide_v5.1.6.docx (PEST++ Development Team, 2021)
  - Required Document/Verifications and Validation Plan/Validation Document (RD/VVP/VD)
    - Requirements Document, Verification and Validation Plan, and Validation Document for MODFLOW 6 Version 6.2.2. Sandia National Laboratories. Carlsbad, NM. ERMS 576745. (Brunell, 2022b)
    - Requirements Document, Verification and Validation Plan, and Validation Document for PEST++ Version 5.1.6. Sandia National Laboratories. Carlsbad, NM. ERMS 576751. (Bethune, 2022b)

The work completed in response to AR-203 Tasks 4, 5 (non-qualification related), 6, and 7 are documented in detail in the remaining sections of this report, and brief summaries of the reasons these tasks were important to complete are briefly described below.

Task 4 of AP-203 involved the investigation of the impact of boundary conditions on the model domain. To support the alleviation of uncertainty associated with the peripheral constant head boundary conditions in the existing model, each geostatistical realization of the Culebra forward model was allowed to have a unique set of constant head boundaries in the north, south, and southwestern borders of the model domain. This task was completed to assess the effects of applying unique sets of head boundary conditions to each

Information Only

T field and optimizing those head boundary values. The work associated with Task 4 is discussed in Section 2.

Task 5 of AP-203 included updating the flow and optimization codes from MODFLOW 2000 (flow code) and PEST v. 9.11 (optimizer), and the qualification of the codes is documented as referenced above. The updates were completed primarily to increase the speed of the optimization and calibration processes, to allow for the incorporation of new data from pumping tests and neighboring large-scale pumping events, and to provide the analysis time required to assess the boundary condition modifications discussed in Task 4. The benefits of updating the flow and optimization codes and the associated computational methodology are further discussed in Section 3.

Task 6 of AP-203 included the evaluation of observation data impacted by Mills Ranch pumping and using this data as an optimization target. The Mills Ranch pumping event was a large-scale pumping event that occurred in an unpermitted Culebra well at a neighboring property to WIPP. The effects of this pumping were observed in the WIPP Culebra well network during pumping, which lasted approximately five years, beginning in 2013 and continuing intermittently until summer of 2018. Due to its significance and impacts on the water levels in nearby WIPP network wells, it was important to incorporate the associated Culebra water level effects into the sensitivity analyses and recalibration efforts. The work associated with this task is described in Section 4.

Task 7 of AP-203 consisted of the actual calibration of revised T-fields for CRA-2024. As stated previously, new data were incorporated into this calibration effort, and as part of these analyses, the sensitivity of the base T-fields that were calculated in 2003 (McKenna, 2003) and recalculated in 2009 (Hart et al., 2009) were evaluated to different boundary conditions and hydrogeologic parameterizations. This task is conceptually similar to the first revision of Task 7 (Hart at al., 2009) and is described in detail in Section 5. For context, the number of wells and associated freshwater head measurements included in the T-fields calibration for CRA 2009 PABC was 40 (measurements from May 2007), and for CRA 2024 is 47. These data are presented later in **Table 3**, and the wells included in each of the calibrations are shown on **Figure 1** and **Figure 2**, below, and the observed change in freshwater heads from CRA-2009PABC to the median or mode of the distributions used in CRA-2024 is shown for select wells in **Figure 3**.

Information Only

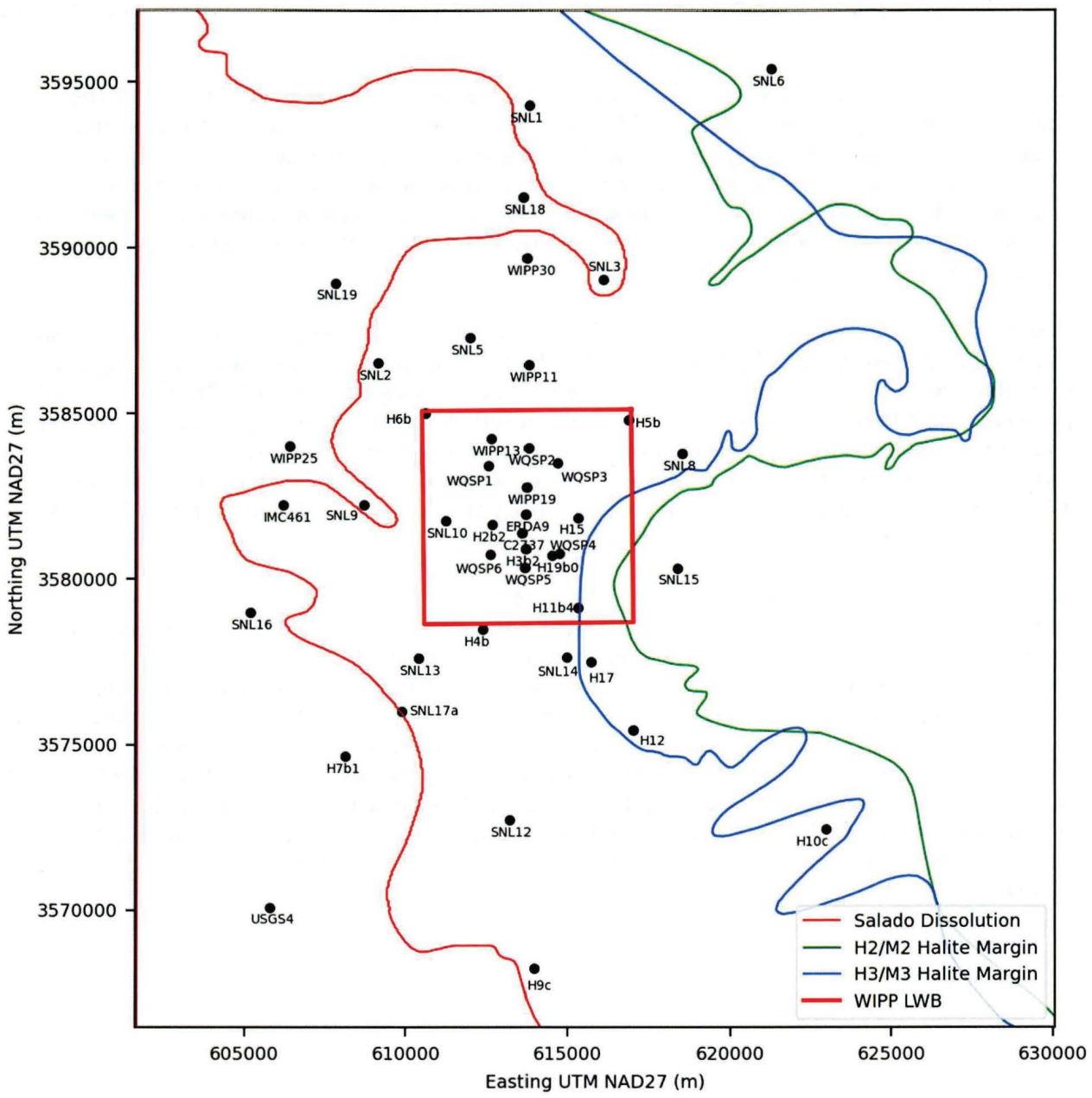

Figure 1. Wells used in CRA-2009 PABC T-Fields Analysis
(includes 40 steady state head wells and 4 observation wells)

Information Only

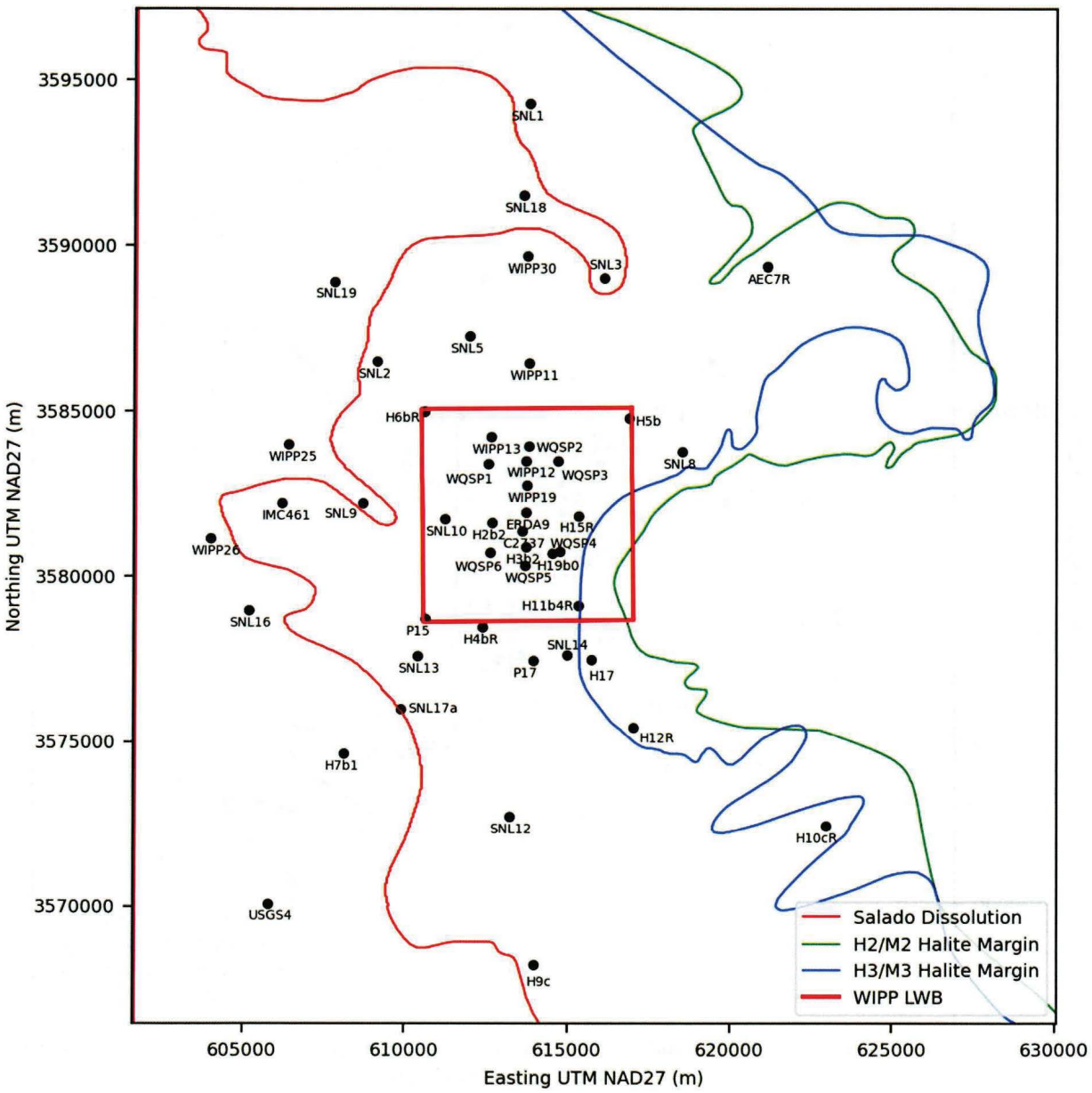

Figure 2. Wells used in CRA-2024 T-Fields Analysis
(includes 47 steady-state wells from 2022 analysis)

Information Only

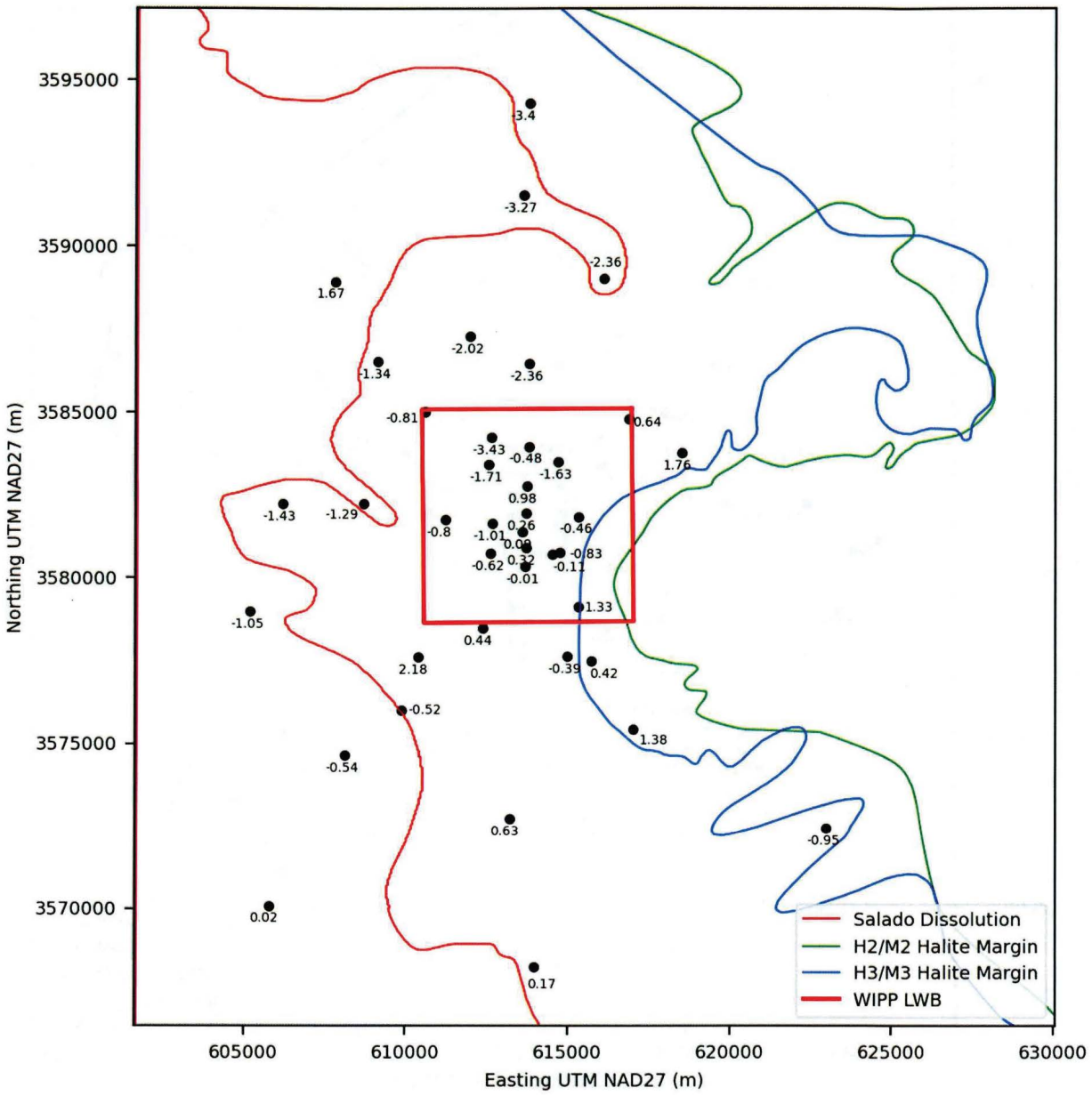

Figure 3. Change in Freshwater Heads (m) between CRA-2009 PABC and CRA-2024

Information Only

2. Task 4 – Investigation of the Impact of Boundary Conditions on the Model Domain

Boundary conditions in the form of constant head cells along the boundaries of the model domain control the north-south hydrologic gradient predicted by the Culebra flow model. **Figure 4** depicts the constant head boundaries as solid green lines. The values assigned to the constant head cells come from an extrapolated surface roughly fit to the observed potentiometric head values using the following equation:

$$\textit{Equation 1. } h_{x,y} = a + b(y + d * sin(y) * |y|^{exp}) + c(e * x^3 + f * x^2 - x)$$

Where $h_{x,y}$ is the head at the cell, x and y are the coordinates of the center of the cell (with both x and y normalized to range from -1 to $+1$), and a, b, c, d, e, f, and exp are free variables that allow the shape of the water table to adjust.

Rather than allowing the boundary condition values to be modified simultaneously with T-field values to match steady-state heads, it was decided to first estimate a single set of boundary condition heads across the entire ensemble of T-fields.

In Task 7 of AP-114, the initial head surface for setting the constant head cells in the north, south, and southwestern boundaries was created using the multivariate equation above (**Equation 1**). The equation was formulated to keep the head at the northern boundary above the measured head at SNL-1 and the head at the southern boundary below the measured head at well H-9c. These constraints helped define the constants in the equation. As a result, only cells in the northern-most row of the model domain between the northeast-to-southwest no-flow boundary to the west and the irregular constant head halite margin to the east were derived from this equation, as well as cells along the westernmost column south of the no-flow boundary, and all the cells along the southern-most row of the model. The constant head cells east of the halite margin were not subjected to this equation but were instead set to land surface elevation, as was done in Task 7 of AP-114.

Figure 4 presents a map of the initial heads surface derived from the multivariate equation, where regions in solid brick red are no-flow, and regions in solid dark blue are constant heads set to land surface elevation. The observed steady-state freshwater heads for each of the 47 wells are in red.

A similar approach to that performed in Task 7 of AP-114 was adopted, except the parameters were estimated using PEST++, rather than chosen "by hand". This was done by parametrizing the equation. The variables were selected so that the equation would predict an initial head array that resembled the steady-state freshwater heads, and would then be used to assign constant head boundary condition values. PEST++ was run in estimation mode for three iterations to reach stable parameter estimates. The primary function that generated the boundary files from Equation 1 was surface_02_extrapolate.

Table 1 presents the values for the seven parameters used to generate the initial head surface.

The parameter estimation that generated the values in Table 1 was performed prior to the calibration of the T-Fields performed in Task 7. These values were not allowed to vary during T-Field calibration.

Information Only

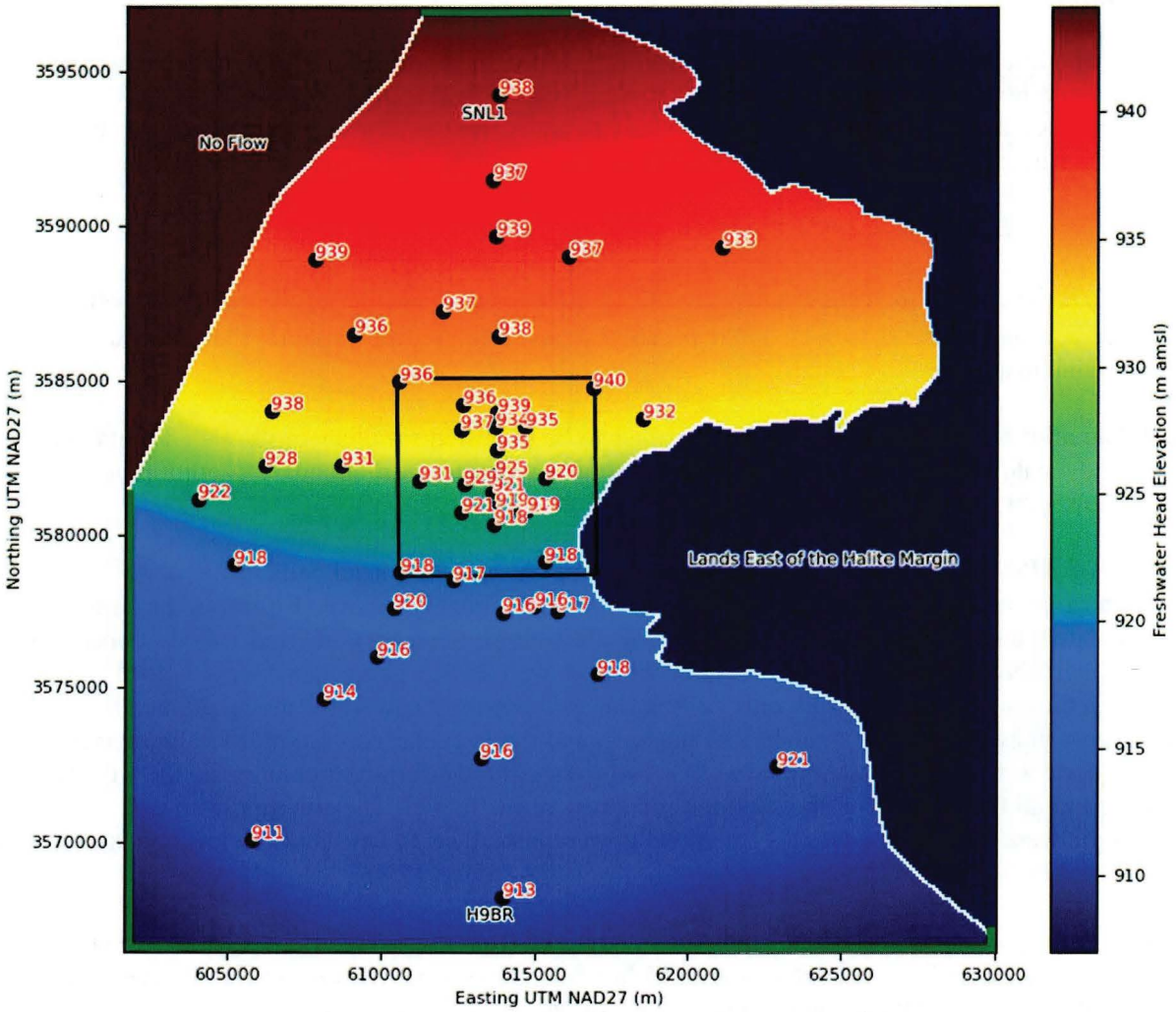

Figure 4. Map of Estimated Initial Heads Surface Used to Prescribe Fixed Head Boundary Conditions
(Values represent the mean, median, or mode freshwater heads, depending on distribution, from Table 1 of Farinacci & Bowman, 2022)

Table 1. Estimated Parameter Values Used to Generate Initial Head Surface and Assign Boundary Conditions

Parameter	Value
a	926.804
b	8.412
c	1.636
d	1.040
e	1.305
f	-1.389
exp	0.291

Information Only

3. Task 5 – Update Flow and Optimization Programs

The previous iteration of T-field calculations utilized the flow software MODFLOW 2000 (MF2K) and optimization software PEST 9.11. Continued development on MODFLOW and PEST since these versions were released have improved the capabilities of both tools. In this section, we describe the updates to the flow (MODFLOW) and optimization (PEST) programs. Note that the optimization application performed in this work is model calibration, so we use "calibration" rather than "optimization" in the discussion below.

3.1 MODFLOW6 Numerical Flow Model

Inverse calibration requires a forward numerical model which produces results that can be compared to observations. In this task, MODFLOW6 (Hughes et al., 2017) flow models were developed for the Culebra instead of MODFLOW-2000 (MF2K), which was used in Task 7 of AP-114 (Hart et al., 2008). In Task 5, the software qualification process was completed for MODFLOW6.

As mentioned in Task 5, MF2K and MODFLOW6 are numerical models used to simulate groundwater flow; MF2K is the version of the MODFLOW simulator used in Task 7 of AP-114 and is now no longer supported by the US Geological Survey (USGS), while MODFLOW6 is the most recent USGS version of MODFLOW.

The physics and underlying equations used in MODFLOW6 and MF2K are similar for the purposes of this application; however, MODFLOW6 has improved solver capabilities that increase the likelihood of model convergence. All the MODFLOW6 models were solved using the Iterative Model Solution (IMS) package, which offers more options than the Link Algebraic Multi-Grid (AMG) or Preconditioned Conjugate-Gradient (PCG) package used in MF2K.

MODFLOW6 has a significantly different input and output file structure than MF2K. The MODFLOW6 input files were converted from the MF2K format using the Python script `S03_Generate_MF6.py` which utilizes the open-source Python package FloPy (Bakker et al., 2016), of which there is a static version stored in the repository for this project.

3.2 PEST++ IES Parameter Estimator

In addition to advancements in MODFLOW, active development of PEST has migrated from the Fortran version to the refactored C++ software PEST++, which allows ensemble calibration capability of the iterative ensemble smoother (IES) algorithm for drastically faster optimization times.

Unlike older versions of PEST, PEST++ IES does not require the explicit construction of the Jacobian sensitivity matrix via finite differences, which requires one or two forward model calls for each parameter value estimated as part of the calibration. This equates to PEST having to run the entire forward model at least once for each parameter (roughly 1,100 to 1,700 in Task 7 AP-114) for each realization, which resulted in only 200 of the 1,000 base T-fields finishing the calibration process within the timeline of the project. PEST++ IES instead utilizes the concept of a prior ensemble where every parameter is defined probabilistically, e.g. by a gaussian distribution with a spatial correlation within a limit unique to a single realization. A single prior realization consists of parameter set sampled randomly from that set of prior parameter distributions. When PEST++ IES is launched, the prior parameter ensemble is evaluated first by running each of the one-thousand realizations and populating the prior observation file (`mf6.obs.0.csv`) with the simulated values produced by each forward model run.

Once the prior parameter ensemble has been evaluated, PEST++ IES performs the ensemble-based Gauss-Levenburg-Marquardt algorithm (GLMA) process using several candidate Marquardt-lambda values

Information Only

(White, 2018). The lambda value is a scaling parameter that controls the interpolation between linear and non-linear parameter upgrade strategies utilized by GLMA. Each lambda value yields a candidate parameter ensemble of 1,000 realizations, which collectively span the trust region between the Gauss-Newton search direction and the gradient descent direction. To provide additional support for non-linear inverse problems, PEST++ IES also uses backtracking factors, which effectively sample the search direction for each lambda. In total, this yields nine candidate parameter ensembles. PEST++ IES then randomly selects a small number of realizations from each of the nine candidate ensembles to evaluate which candidate ensemble yields the lowest relative objective function value. Based on the results of this randomized candidate testing, the candidate parameter ensemble that yields the lowest relative objective function value is selected, and the remaining realizations in that selected ensemble are evaluated. This workflow completes an iteration of the PEST++ IES algorithm.

After each PEST++ IES iteration, the selected ensemble is used as the basis for another ensemble-based GLMA iteration. Each iteration generally continues to minimize the overall objective function, until no more progress is made, and the iteration process is stopped, either by the analyst or automatically based on a minimum fractional progress made in objective function reduction. The final ensemble represents a set of probabilistically defined inputs and outputs, constrained by both the prior parameter distribution and the goal of improving the fit between observed and simulated values. The variability among the simulated values from each ensemble represents the uncertainty in the output predictions.

Information Only

4. Task 6 – Evaluation of Mills Ranch Pumping Data as Optimization Targets

In mid-2013, the SNL and Management and Operations Contractor (MOC) long-term, high-frequency monitoring programs began detecting significant decreases in water levels in many of the wells located southwest of the WIPP LWB screened in the Culebra. It was determined that these water level fluctuations were due to variable-rate pumping from a private well screened in the Culebra and located within the Mills Ranch property. This private well was not approved by the New Mexico Office of the State Engineer (OSE); therefore, pumping rate data were not documented nor provided to the OSE.

Task 6 involved developing a methodology to incorporate observation well data from the WIPP monitoring well network affected by Mills Ranch pumping in the optimization process of T-fields. As the observation well data are sound, the process focused on treating the variable Mills Ranch pumping rate as a fitting parameter.

The Culebra response to this long-term pumping was observed in high-frequency pressure and water level measurements from neighboring wells, which were used to estimate an average pumping rate for the Mills Ranch well, a key piece of data to inform the calibration process. Unlike intentional multi-pad pumping tests already used as calibration targets, the pumping rate was variable in time and unknown, but the pumping by Mills Ranch stressed the Culebra like no other hydraulic test. Historical pumping test rates were usually operated at lower and controlled constant pumping rates of approximately seven gallons per minute (gpm), and typically pumped for less than 30 days. **Figure 5** shows the location of the Mills Ranch pumping well, the surrounding wells, and the WIPP LWB.

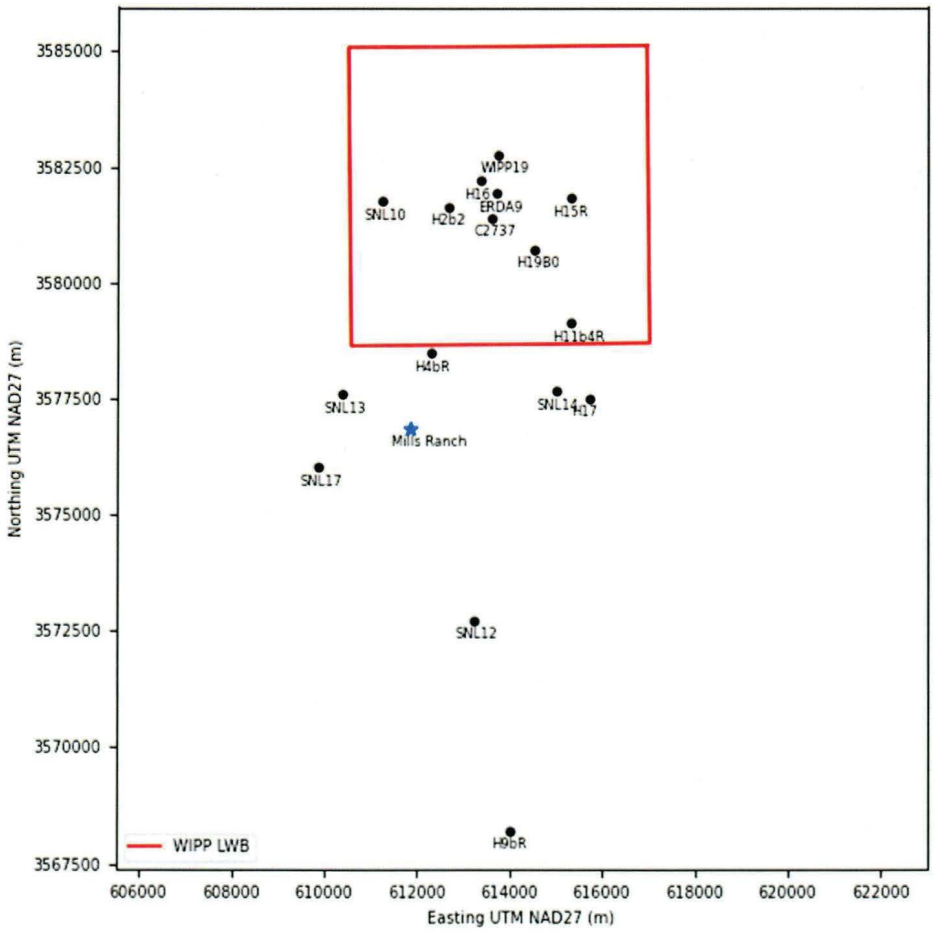

Figure 5. Location of Mills Ranch Culebra Well and Neighboring Culebra Wells

Information Only

4.1 Estimation of the Mills Ranch Pumping Rate

From late 2015 to early 2016, a recovery in water levels was observed in most of the wells affected by previous Mills Ranch pumping, due to an apparent temporary stop to pumping. At SNL-17, the water level recovery began on November 29, 2015, and ended on February 6, 2016, when increasing drawdown was observed again. The characteristic shape of the recovery event observed in SNL-17 was then used to estimate the relative pumping rate for the Mills Ranch well when it was actively pumping, compared to the pumping rate during recovery (Q_{rec}), assumed to be zero. Well SNL-17 was selected over the other wells that also responded to the anthropogenic pumping event because SNL-17 had the quickest response to pumping and recovery, even though it did not necessarily have the most significant response in drawdown magnitude (Kuhlman and Cobert, 2017). The water level in SNL-17 recovered about 15 feet (ft) (~4.57 meters) during the late 2015 to early 2016 recovery.

Figure 6 shows the recovery data plotted by Kuhlman and Corbet (2017), where the change in pressure transducer data for each well is plotted with colored dots and lines. The inset figure shows the spatial location of the private well as a red "X" and the monitoring network as colored circles. Recovery is computed as a change in head and time since November 29, 2015, at 2:00 PM, when the water level in well SNL-17 began to rise.

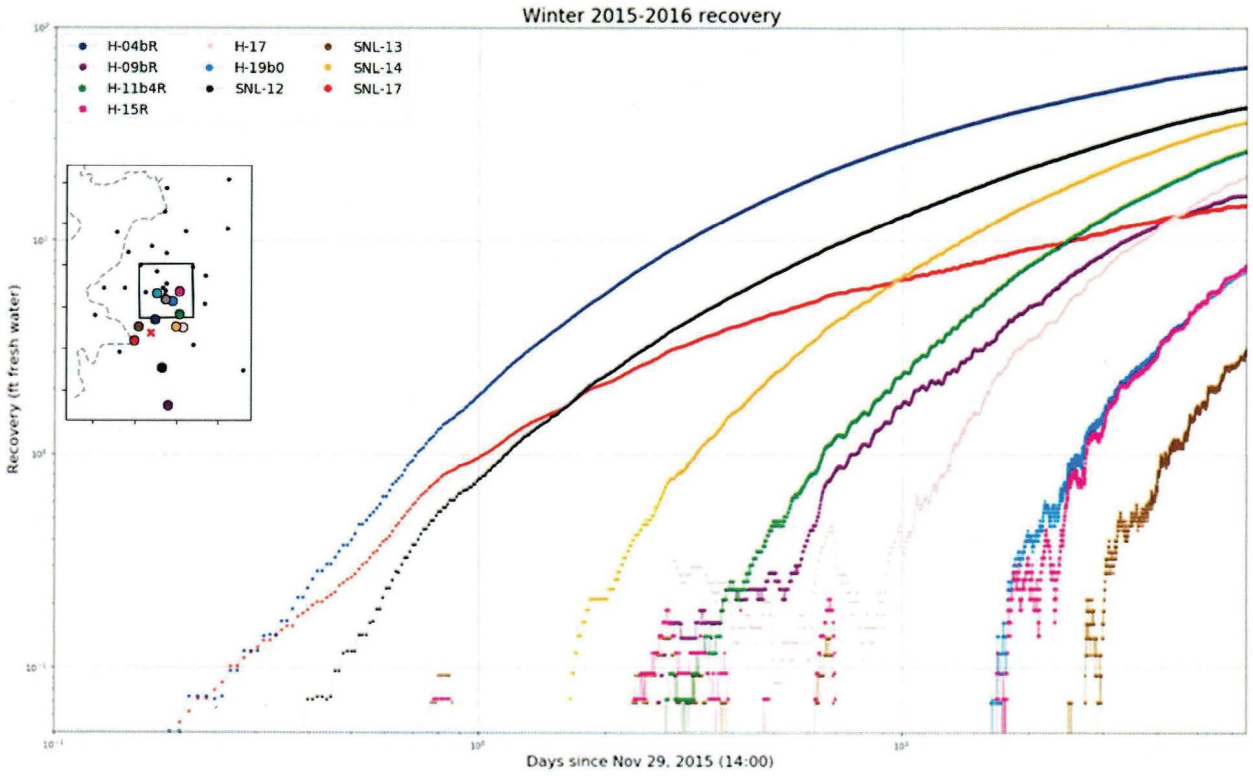

Figure 6. Recovery Data for Ten Wells from the Culebra Monitoring Network Located Near Mills Ranch Well (Kuhlman and Corbet, 2017)

The temporal data observed in SNL-17 (**Figure 7**, blue line) show many clear periods of increasing drawdown and periods of clear recovery. Wells further from the Mills Ranch pumping well have a more muted response, and may not clearly show a response to changes in pumping rate. Using the shape of the SNL-17 data, the "on" and "off" periods were determined through manual inspection of the data (i.e., concave up – recovery vs. concave down – pumping).

Information Only

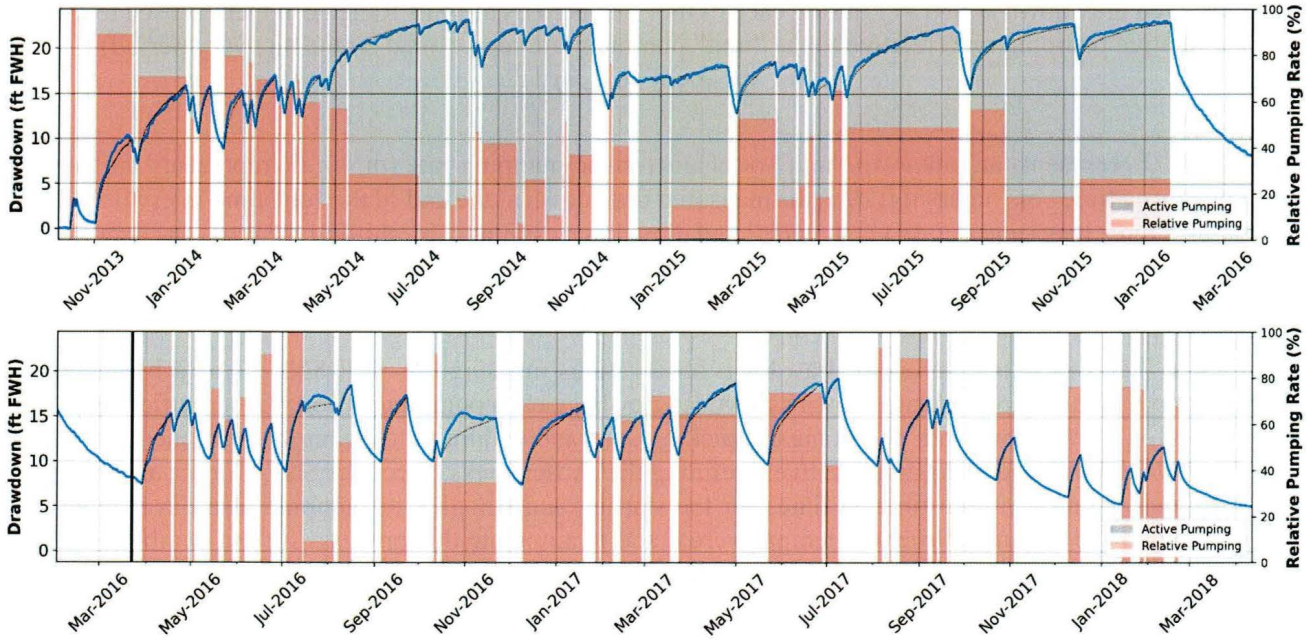

Figure 7. Drawdown Observations in Well SNL17 and Pumping Periods Selected for the Mills Ranch Pumping Well (vertical bars), Pink Fraction of Bar Represents Estimate Relative Pumping Rate

The long recovery period (late 2015 to early 2016) was used as a "characteristic response" which was first inverted (i.e., recovery converted to drawdown) then scaled in drawdown and shifted in time to estimate the relative pumping rate during each on cycle of pumping in the Mills Ranch well. This approach is analogous to the Theis (1935) theory behind "type curve" analysis. Essentially, drawdown is linearly proportional to the pumping rate. If drawdown is occurring at half the rate of a different time, the pumping rate is therefore half as large at the same relative time since pumping began.

While flow in the Culebra is not precisely represented by Theis (1935), the Theis solution provides a relatively good approximation. The Theis conceptualization of flow can be described as two-dimensional, confined, with an infinite radial extent and homogeneous material properties. The main difference between the Culebra and ideal Theis behavior is the double-porosity response of the Culebra. Rather than using a Theis response to fit the data, which would not account for double-porosity effects in the Culebra, the analysis used the characteristic recovery observed from December 2015 to January 2016.

Type curve analysis assumes a "typical" curve can be shifted up or down to estimate the transmissivity (T) and storativity (S), as long as the radial distance to the pumping well (r), the time since pumping began (t), and the volumetric flow rate (Q) are known. For well SNL-17, the Q for the pumping period (Q_i) was unknown, but it could be assumed that the well was not moving (constant r) and the formation properties were not changing with time (constant T and S). The Theis drawdown (d) response is defined as follows:

$$\textit{Equation 2.}\quad \boldsymbol{d = \frac{Q}{4\pi T} W(u)}, \textit{ where } \boldsymbol{u = \frac{r^2 S}{4Tt}}$$

If all other factors in the Theis drawdown equation remain the same (i.e., radial distance and formation properties), Q and d are linearly proportional to one another (**Equation 2**). This simple scaling is possible because $W(u)$ is not also a function of Q. It was assumed that this linear relationship between Q and d should remain valid for other linear non-Theis responses, as in this case. For this method to work, it was also assumed that Q remained linear; however, extreme pumping could potentially lead to turbulent losses or drying out of the formation, which could invalidate this linearity assumption.

Information Only

Observed drawdown at SNL-17 during each of the "on" periods at Mills Ranch can then be used to estimate the relative pumping rate (relative to the "unit" pumping rate represented by the recovery period).

$$\textit{Equation 3.}\quad \boldsymbol{Q_i = Q\frac{d_i}{d_{rec}(\tau)}}$$

Where Q represents an unknown "unit" or characteristic pumping rate (m^3/s); Q_i represents the pumping rate during time "on" interval i; d_i is the measured drawdown at the end of the "on" time interval i (interval being τ days long) and $d_{\mathrm{rec}}(\tau)$ is the predicted drawdown estimated by shifting the recovery data from the late 2015 to early 2016 period, at the same number of days. This is why the longest recovery period had to be used, as it had to be as long (or nearly as long) as all the pumping periods.

Figure 7 shows a time series of drawdown observations measured in well SNL-17 as a blue line. The individual pumping periods are shown as vertical grey bars; each pumping period was identified by plotting the SNL-17 drawdown data and manually picking start and ending times from the plot, then plotting the data with the selected picks and iteratively refining the chosen picks. Since the SNL-17 data are reported at 15-minute intervals, the estimated times for the starting and stopping of pumping also have a minimum accuracy of 15 minutes. Several attempts were made to automate this process, but the number of manual corrections necessary warranted manually selecting the pumping periods.

The analysis of the recovery data was performed by estimating the scale factor (shown as the pink fraction of the vertical bars in **Figure 7**) by determining the relative drawdown (d_i) between the beginning and end of the pumping interval. Task 7 of this AR describes how these relative rates were used to estimate an ensemble of temporal extraction rates for this private well.

The scaled and flipped characteristic recovery shape fits most of the pumping periods well. Some of the pumping periods deviate from this (e.g., July and November, 2016), possibly due to the operator changing the pumping rate during an individual pumping period, or other complications beyond the assumptions of this approach.

The estimated relative pumping rates make physical sense. The pumping rate was initially high (November 2014), and decayed with time until about July 2014. This might be explained by the increase in work required to lift water from greater depth, as drawdown was observed to increase in the area surrounding the Mills Ranch well. After the long break in pumping (late 2015 to early 2016), the character of pumping seemed to change (longer breaks between cycles when the pump was clearly "on"), which may be due to replacement of the pump, or changing in the scheduling or usage of pumping equipment. Because the periods before and after the long 2015-2016 break appear to be different, two different multipliers were estimated, one for the early pumping periods (before this break) and one for the late pumping periods after the break.

Information Only

5. Task 7 – Calibration of Revised T-fields

The T-field calibration process used the one-thousand "base" T-fields from Task 5 of AP-114 (Hart et al., 2008) as inputs. A parametrization was applied to calibrate the T-fields parameters: transmissivity (T), represented by hydraulic conductivity (K, m/sec), horizontal anisotropy (A), storativity (S), represented by specific storage (S_s, 1/m), and recharge (R). This parametrization includes a local scale parametrization based on grid-scale (each model cell in the model domain), a medium-scale parametrization based on a uniform grid of pilot points, and a large-scale parametrization based on zonal multipliers. The same transmissivity zones described in Task 7 of AP-114 were used in this task for transmissivity and anisotropy. Zones for storativity and recharge were based on other analyses completed in the area surrounding the WIPP site (see Section 5.2). Pilot points were selected for each parameter, and initial values were consistent with the conceptual model in Task 5 of AP-114 (see Section 5.2).

Additional parameters include the two Mills Ranch base pumping values, further explained in Section 4. Since the pumping rates during each pumping interval for Mills Ranch well were not documented (nor was the total pumped volume documented), it was decided to estimate them as "nuisance parameters", or parameters that are used in the calibration process to help estimate a plausible set of pumping rates throughout a multi-year long transient pumping event (see Section 4).

The steady-state freshwater head measurements and the drawdown data from the nine transient pumping tests were converted from MF2K files used in Task 7 of AP-114 to MODFLOW6 files using the Python script `S03_Generate_MF6.py`. Two additional transient models were added to the group of model runs that comprise a single forward run; the multi-pad pumping test at H-9bR and the Mills Ranch long-term transient pumping event for a total of twelve MODFLOW6 models, listed in **Table 2**.

Table 2. MODFLOW6 Model Runs

MODFLOW6 model simulation	Model Name
steady-state freshwater head measurements	mf6_head
transient pumping test 1	mf6_h19
transient pumping test 2	mf6_h3
transient pumping test 3	mf6_wqsp1
transient pumping test 4	mf6_h11
transient pumping test 5	mf6_wqsp2
transient pumping test 6	mf6_p14
transient pumping test 7	mf6_snl14
transient pumping test 8	mf6_wipp11
transient pumping test 9	mf6_wipp13
transient pumping test H-9bR	mf6_h9br
Mills Ranch long-term transient pumping event	mf6_mr

Once the MODFLOW6 models produced simulated drawdown and head results, the modeled results were compared to field data. An "actual" residual is the difference between the simulated and observed value, while a "measured" residual includes noise representing measurement and model error.

The residuals were then used as inputs by PEST++ IES to construct a randomized approximate Jacobian matrix, which was used to optimize every parameter value. The optimization goal was to minimize the objective function value (also known as phi, or ϕ), which is the sum of the weighted square residuals

Information Only

(**Equation 4**). Residuals are the difference between measured data and modeled predictions. The objective function is a model's prediction compared to measured data (see Section 5.1.5).

$$\textit{Equation 4.}\quad \boldsymbol{\phi} = \sum(\boldsymbol{residual_i} * \boldsymbol{weight_i})^2,$$

where the index, i, goes over all observations and weights.

While both the measured and actual phi values are provided by PEST++ IES for each iteration (PEST++ IES uses measured phi as the metric for choosing the best ensemble), the actual phi values are reported here. Because the weights were constant throughout the iterations of PEST++ IES, the weights provide a counterbalance to bring the calibration back into balance if one type of test (steady-state or transient) started to have an overly large contribution to the overall phi, and therefore overwhelm the calibration. In this document, the term "observation" defines a field measurement but does not define the value of that measurement.

After a few iterations of PEST++ IES, the realizations in the prior parameter ensemble have been "warped" such that, when evaluated with the model, each of these parameter realizations yield simulation results that reproduce the historical observations to varying degrees. The modeling workflow described herein was performed under quality-assurance (QA) run control (RC), and the inputs were stored in a git repository during the performance of the tasks. The T-field files have been archived in the version control system at – /data/cvs/CVSLIB/WIPP_EXTERNAL/ap203/.

The calibrations required approximately two days of continuous run-time on a total of 200 processors (see Section 5.5). **Figure 8** summarizes the workflow in the calibration briefly described above, and which will be discussed in detail in this section. The calibrated T, A, S, and R fields, the MODFLOW steady-state water budget, and the DTRKMF particle track results were placed in a single Results module in the git repository (see directory tree structure in Appendix A Section 7.6).

Information Only

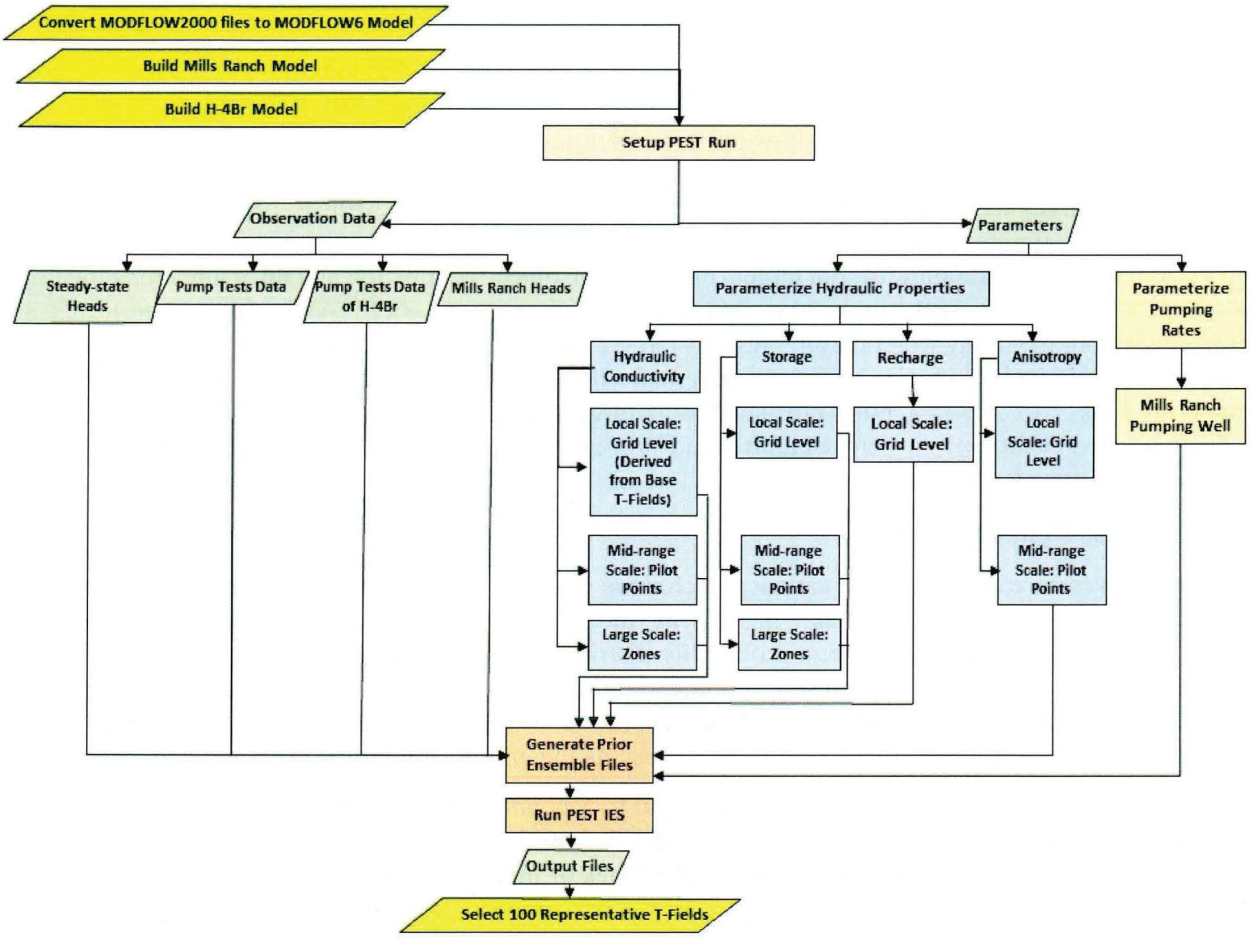

Figure 8. Flowchart of Calibration Workflow

5.1 Observations

In addition to the model output quantities corresponding to observations (used in history matching), several other important datasets were included as "observations" in the PEST-model interface. These observations include the values of the horizontal hydraulic conductivity array used by MODFLOW6 and summary statistics for hydraulic conductivity and storage. These observations were given a weight of zero (i.e., they do not contribute to the objective function) as these quantities simply monitor qualitative aspects of model behavior within the ensemble-based workflow.

5.1.1 Non-Weighted Observations

As mentioned earlier, any simulation output quantity with zero weight does not contribute to the objective function and therefore does not influence any parameter adjustments. In total, there were eleven zero-weighted observation groups containing 457,850 observations that do not affect the calibration process in PEST++ IES, including the observation groups for the four final T-field files; "hk", "aniso", "ss", and "rch" (`mf6_head.npf_k.txt`, `mf6_head.npf_k22.txt`, `mf6_head.sto_ss.txt` and `mf6_head.rcha_recharge_1.txt`, respectively). After the calibration process was complete and the final one-hundred realizations were selected, the final observation ensemble file `mf6.5.obs.csv` was read using a Python script to generate plots and rewrite each T-field file (S06_Plot_Results.py).

Information Only

5.1.2 Weighted Observations (Targets)

The non-zero weighted observations (referred to as targets) that affect the calibration process are split into four general observation categories: steady-state freshwater heads, multi-well pumping test drawdowns, Mills Ranch multi-well pumping test drawdown, and single-well formation performance test transmissivity estimates. Each of the ten multi-well pumping test drawdowns were given a unique observation group for weighting and tracking purposes, while the steady-state freshwater heads, Mills Ranch test, and single-well transmissivity estimates were assigned to one group each. This resulted in thirteen non-zero weighted observation groups containing 24,368 targets impacted the objective function and the parameter adjustment performed in PEST++ IES. Task 7 of AP-114 only incorporated steady-state freshwater heads and drawdown from the multi-well pumping tests as targets because pumping at Mills Ranch did not start until 2013. The single-well formation performance tests for transmissivity were originally handled as fixed pilot points in Task 7 of AP-114, but were handled as targets in this analysis owing to the ensemble-based workflow used herein. Both zero-weighted and non-zero-weighted observations are stored in the pest observation file `mf6.obs_data.csv`.

5.1.3 Measurement Noise

PEST++ Bayesian calibration is a statistical technique used to help estimate the uncertainty of a model's predictions. It is based on Bayesian probability theory, a mathematical framework for representing uncertainty. In Bayesian calibration, a probability distribution (rather than a single value or a value and a confidence interval) is used to represent the uncertainty in a model's predictions, and this distribution is updated as new data are included as part of the calibration. This calibration process updates the prior with data and produces a posterior distribution that represents the effects of both the prior and data.

In a Bayesian calibration problem, it is fundamental to account for the contribution of measurement noise in the prior parameter ensemble. In the ensemble-based workflow, an explicit representation of measurement noise was included by adding realizations of measurement noise to the observation values. Thus, each target is "paired" with a unique set of noisy observation values. Conceptually, these noisy observations have the effect of yielding a (slightly) different residual vector and, ultimately, objective function for each parameter realization. Including noisy observations within the PEST++ IES workflow results in each parameter realization being adjusted toward reproducing slightly different observation values rather than all realizations targeting an identical set of observation values. Ideally this helps maintain variance in the final parameter ensemble so that not every parameter trends to a single answer.

Noise was created for all non-zero weighted observations in the function `get_obs_noise` in the Python script `S00_Generate_Ensemble.py`. Noise was randomly distributed normally for each non-zero weighted observation so that the "obsval" column represents the mean of the distribution and the "standard_deviation" column determines the standard deviation of the distribution, both defined in the csv file `mf6.obs_data.csv`. Additionally, upper and lower limits were added to several of these observations using the columns "upper_bound" and "lower_bound" in the same csv file. This made it possible to represent other types of distributions such as truncated-normal distributions.

5.1.4 Calibration Targets

When different types of observations are used for history matching, it is important to balance the contribution of each observation type to the measurement objective function so the information contained in each observation type can be readily assimilated and tradeoff can exist between observation types can be mitigated (e.g., Doherty and Welter, 2010). Algorithmically, this balancing is accomplished by adjusting the weight value for each observation; these weights adjust the magnitude of the innovation/residual associated with each (noisy) observation (see White et al., 2020). For the workflow described herein, observations were separated into several general observation groups, namely steady-state freshwater heads, drawdowns measured from multi-well pumping tests, Mills Ranch pumping observations, and direct

Information Only

transmissivity estimates derived from single-well formation performance tests. Each of these general observation types is now described in detail, followed by a description of the selected weighting scheme.

5.1.4.1 Steady-state Fresh Water Heads

The steady-state freshwater heads (FWH) or ambient non-pumping heads were calculated freshwater heads at multiple wells screened in the Culebra near the WIPP site as described in Farinacci and Bowman (2022). Unlike the steady-state freshwater heads used as calibration targets in Task 7 of AP-114, these freshwater head measurements include a statistical distribution of the heads data for each well. Histograms and continuous distributions were generated, and the distributions were qualified by type to choose an appropriate centralization representation for each well's representative head value. For wells with normally distributed head values, the mean was used as the representative centralization. For wells with skewed distributions, the median was used. Finally, for wells with bimodal distributions, the mode was used. Table 3 shows the statistics for each well, with wells categorized by the type of distribution most representative of the associated head measurements. The representative centralization for each well is highlighted by blue, red, and green font colors, for the normal/mean, skewed/median, and bimodal/mode distributions.

As previously discussed, explicit realizations of measurement noise were included through a standard deviation calculated for each observation well in Task 1 of this AR. The minimum and maximum values were applied to the upper and lower limit values shown in **Table 3,** below, from Farinacci and Bowman (2022). The initial weight for these thirty-three wells was set to 1 over the standard deviation so that wells with a lower range of observed conditions were assigned a higher weight, implying higher confidence in the calculated steady-state.

The steady-state forward model contains a single stress period model with no time-varying boundary conditions. This model represents the Culebra with no pumping. After MODFLOW6 completes, the heads for each model cell are written to the MODFLOW binary output file (`mf6_head.hds`). The simulated heads at each well location are extracted from this file using function `mod2obs` in the Python script `forward_run.py` and are saved as observations.

Table 3. Fresh Water Heads (FWH) and Calculations for Selected Wells

Well*	FWH Minimum (m amsl)	FWH Maximum (m amsl)	FWH Mean (m amsl)	FWH Median (m amsl)	FWH Mode (m amsl)	Standard Deviation (m)	Data Point Count	May 2007 FWH (m amsl)	Change (m)
Normal Distributions									
ERDA-9	924.35	925.74	**925.14**	925.16	925.33	0.32	87	924.88	0.26
H-3b2	918.42	919.49	**919.00**	919.04	919.06	0.20	85	918.68	0.32
SNL-2	933.96	938.67	**936.31**	936.23	935.71	0.93	349	937.65	-1.34
SNL-9	929.60	932.05	**930.76**	930.71	930.63	0.64	273	932.05	-1.29
USGS-4	910.98	911.31	**911.13**	911.10	911.08	0.10	13	911.11	0.02
WQSP-2	937.17	941.85	**939.39**	939.21	937.81	1.02	294	939.87	-0.48
Skewed Distributions									
C-2737	919.99	921.94	921.24	**921.32**	921.63	0.40	80	921.23	0.09
H-4bR	915.83	917.21	916.75	**916.78**	917.01	0.29	92	916.34	0.44

Information Only

Well*	FWH Minimum (m amsl)	FWH Maximum (m amsl)	FWH Mean (m amsl)	FWH Median (m amsl)	FWH Mode (m amsl)	Standard Deviation (m)	Data Point Count	May 2007 FWH (m amsl)	Change (m)
H-5b	938.79	940.30	939.70	939.76	939.90	0.40	146	939.12	0.64
H-9c	911.23	913.39	912.88	912.97	912.98	0.40	63	912.80	0.17
H-10cR	920.28	923.37	921.30	921.07	921.04	0.52	76	922.02	-0.95
H-15R	919.10	920.04	919.78	919.86	919.86	0.21	58	920.32	-0.46
H-17	915.79	916.89	916.61	916.66	916.64	0.21	83	916.24	0.42
H-19b0	917.84	919.13	918.70	918.73	918.70	0.28	101	918.84	-0.11
SNL-12	915.29	916.24	915.87	915.87	915.76	0.20	193	915.24	0.63
SNL-13	919.58	920.62	920.26	920.37	920.50	0.26	109	918.19	2.18
SNL-14	915.24	916.31	915.93	915.94	916.12	0.22	152	916.33	-0.39
SNL-16	916.99	918.68	917.70	917.63	917.63	0.36	258	918.68	-1.05
SNL-19	938.10	941.79	939.50	939.25	938.47	0.83	274	937.58	1.67
WIPP-13	933.95	938.39	936.14	936.35	937.23	1.23	678	939.78	-3.43
WQSP-1	935.09	939.31	936.69	936.57	935.35	1.13	301	938.28	-1.71
WQSP-4	915.78	919.49	918.49	918.67	919.21	0.83	186	919.50	-0.83
WQSP-5	915.18	918.92	917.94	918.17	918.63	0.79	187	918.18	-0.01
WQSP-6	917.99	922.33	921.17	921.34	922.05	0.99	185	921.96	-0.62
AEC-7R	**931.79**	**933.49**	**933.34**	**933.37**	**933.37**	**0.19**	**79**	**NA**	**NA**
P-15	**917.51**	**918.20**	**917.67**	**917.61**	**917.55**	**0.17**	**64**	**NA**	**NA**
P-17	**915.28**	**915.65**	**915.51**	**915.55**	**NA**	**0.16**	**4**	**NA**	**NA**
WIPP-12	**933.80**	**934.72**	**934.08**	**933.99**	**934.23**	**0.21**	**18**	**NA**	**NA**
WIPP-25	**933.45**	**934.46**	**933.76**	**933.65**	**933.65**	**0.30**	**20**	**NA**	**NA**
WIPP-26	**922.19**	**923.21**	**922.41**	**922.36**	**922.36**	**0.32**	**9**	**NA**	**NA**
WIPP-30	**937.81**	**939.47**	**938.64**	**938.66**	**937.82**	**0.57**	**25**	**NA**	**NA**
Bimodal Distributions									
H-2b2	927.90	928.73	928.44	928.56	928.61	0.25	59	929.62	-1.01
H-6bR	935.14	937.28	936.11	935.99	935.63	0.57	131	936.44	-0.81
H-7b1	913.75	914.85	914.24	914.08	914.04	0.34	95	914.58	-0.54
H-11b4R	916.04	919.25	918.04	918.37	918.42	0.74	92	917.09	1.33
H-12R	917.43	918.29	917.90	917.91	917.91	0.16	101	916.53	1.38
IMC-461	925.80	929.37	927.57	927.64	927.52	0.90	153	928.95	-1.43
SNL-1	937.63	942.27	939.56	939.58	938.46	1.15	333	941.86	-3.40

Information Only

Well*	FWH Minimum (m amsl)	FWH Maximum (m amsl)	FWH Mean (m amsl)	FWH Median (m amsl)	FWH Mode (m amsl)	Standard Deviation (m)	Data Point Count	May 2007 FWH (m amsl)	Change (m)
SNL-3	936.58	940.28	938.27	938.25	**937.45**	0.91	324	939.81	-2.36
SNL-5	935.85	939.29	937.39	937.24	**936.57**	0.91	321	938.59	-2.02
SNL-8	930.84	932.69	931.75	931.66	**931.70**	0.57	238	929.94	1.76
SNL-10	928.79	931.86	930.40	930.72	**930.74**	0.98	263	931.54	-0.80
SNL-17a	915.68	916.89	916.40	916.38	**916.26**	0.31	174	916.78	-0.52
SNL-18	935.83	938.94	937.37	937.21	**936.60**	0.82	282	939.87	-3.27
WIPP-11	937.76	940.85	939.14	939.08	**938.29**	0.81	308	940.65	-2.36
WIPP-19	931.20	935.43	933.41	933.44	**934.64**	1.28	376	933.66	0.98
WQSP-3	934.62	937.94	935.85	935.55	**934.80**	0.92	218	936.43	-1.63

Notes –

*Rev 1 add wells are in bold (Farinacci & Bowman, 2022)

5.1.4.2 Multi-well Pumping Tests

The multi-well pumping tests consist of observations of drawdown taken during several pumping tests over the past thirty years. The same nine multi-well pumping tests used in Task 7 of AP-114 were included in this process, in addition to a newer test at well H-9bR (Bowman, 2014). The total observation data points are a subset of the possible observation data selected to accurately represent the individual pumping test responses. The subset consists of the drawdown and recovery portions of the tests, and the observations consist of the change in head after starting (drawdown) and stopping (recovery) the pump, rather than the absolute head elevation. The pumping tests used and their references are presented below.

- H-3 Pumping Test (Beauheim, 1987a)
  - 4 Observation Wells
  - 69 total observation data points
- WIPP-13 Pumping Test (Beauheim, 1987b)
  - 9 Observation Wells
  - 167 total observation data points
- H-11 Pumping Test (Beauheim, 1989)
  - 10 Observation Wells
  - 130 total observation data points
- P-14 Pumping Test (Beauheim & Ruskauff, 1998)
  - 5 Observation Wells
  - 69 total observation data points
- H-19/H-11 Multi-well Pumping Test (Beauheim & Ruskauff, 1998)
  - 7 Observation Wells
  - 143 total observation data points
- WQSP-1 Pumping Test (Beauheim & Ruskauff, 1998)

Information Only

  - 2 Observation Wells
  - 36 total observation data points
- WQSP-2 Pumping Test (Beauheim & Ruskauff, 1998)
  - 4 Observation Wells
  - 77 total observation data points
- WIPP-11 Pumping Test (Toll & Johnson, 2006b) (Roberts, 2006)
  - 12 Observation Wells
  - 250 total observation data points
- SNL-14 Pumping Test (Toll & Johnson, 2006a) (Roberts, 2006)
  - 12 Observation Wells
  - 252 total observation data points
- H-9bR Pumping Test (Bowman, 2014)
  - 5 Observation Wells
  - 220 total observation data points

Each of these pumping tests was represented in the forward model with its own transient MODFLOW6 model with varying time discretization based on the duration of the individual pumping tests. Each model was initialized with the same steady-state heads (`mf6_head.hds`). The MODFLOW6 models were converted from the MF2K model input formats using the `mf2k_to_mf6` function in the `S03_Generate_MF6.py` Python script. The same measurements of drawdown used in Task 7 of AP-114 were used in this analysis for the nine original pumping test wells.

The simulated values of drawdown for these models were extracted from the MODFLOW6 binary output files using the function `mod2obs` in the Python script `forward_run.py`. This function interpolates drawdown spatially (by bilinear interpolation using the four nearest grid cell centers) and temporally from the cell-centered model results and saves results into ASCII format files. The initial weights for all ten observation groups (one for each transient pumping test) were set to 1. A standard deviation of 0.5 meters was assigned to all drawdown measurements in these observation groups to generate measurement noise in each realization. Additionally, a lower limit of 0 was enforced on the observation noise for drawdown measurements so that drawdown could not be negative.

Inclusion of the H-9bR Multi-Well Pumping Test

The H-9bR multi-well pumping test began in August 2012 and included five observations wells. The data for these observations were sampled on a 15-minute interval, which was re-sampled to better align with the temporal discretization of the simulation and the observations from the other pumping tests. Specifically, the 15-minute drawdown data were aggregated to daily average water levels for the first two weeks of the pumping test and then weekly averages for the remainder of the data. This data smoothing resulted in 220 data points for history matching.

Although well H-9bR was included in this analysis, it is expected that the ability of the model to simulate this pumping test may be limited since the well is located near the southern constant-head boundary condition of the model.

5.1.4.3 Mills Ranch Pumping Event

Generation of the MODFLOW6 Model for the Mills Ranch Pumping Event

The MODFLOW6 model (`mf6_mr`) was generated by the function `gen_millsranch_model` in the Python script `S03_Generate_MF6.py`. This transient model was created based on the 76 time periods

Information Only

when the Mills Ranch pumping well was considered to be actively pumping. Refer to Section 4.1 for more detail on how these times were determined. The model contained 152 stress periods with varying lengths that started on August 8th, 2013, at 0:00 and ended on December 31st, 2017, at 24:00. The pumping well was represented by the use of the WEL package and placed in row 203, column 102 of the model. In MODFLOW, the WEL boundary condition acts at the center of the assigned grid cell. The model was initialized with the steady-state heads file (`mf6_head.hds`), similar to the multi-well pumping test models mentioned in the previous section.

Mills Ranch Pumping Event Observations

The Mills Ranch pumping event generated the largest stress (i.e., change in freshwater head) observed in the Culebra since continuous water level monitoring began in the network, in approximately the mid-1990s, in the vicinity of the WIPP. Water level declines as significant as 20 meters of drawdown were measured in several wells (Thomas et al., 2017; Kuhlman and Corbet, 2017). For this analysis, the Mills Ranch pumping is considered to be a large-scale, multi-year multi-well pumping test and, in this analysis, was handled similarly to the previously mentioned pumping tests. The fifteen wells that saw significant responses to the Mills Ranch pumping were included as calibration targets in this analysis in the form of drawdown from the static water level measured just before the private pumping well started extracting water from the Culebra on August 22nd, 2013. The 15-minute data was smoothed out by applying a 30-day rolling average to reduce the high-density dataset while preserving the main features from the response to the pumping event.

The observation group "mr" contains a 30-day rolling average drawdown for the fifteen wells listed in Table 4 (also shown spatially in **Figure 5**). The weighting and noise schemes were handled the same way as the multi-well pumping tests, where the standard deviation was set to 0.5 meters with a lower limit of 0 so observation noise could not cause a negative drawdown. All observations in this group were given an initial weight of 1, except for drawdown observations at well SNL-17, which was given a weight of 3. This was done because most of the observation wells are located north of the private pumping well, whereas SNL-17 is the only well west of the pumping well. This effectively meant that wells located north of the pumping well would contribute more to the calibration, so it was decided that SNL-17 should have more weight in the calibration process to address this potential issue.

Table 4. Wells with Drawdown Observations Impacted by Mills Ranch Pumping

Wells		
C-2737	H-15R	SNL-13
ERDA-9	H-16	SNL-14
H-2b2	H-17	SNL-17
H-4bR	H-19b0	WIPP-19
H-9bR	SNL-12	SNL-10

5.1.4.4 Single-Well Formation Performance Measurements of Transmissivity

In Task 7 of AP-114, single-well formation performance tests were included in the calibration process by fixing a pilot point at the model cells where each well was located to the transmissivity calculated at every single performance test, effectively conditioning the parameter realizations to match the single-well transmissivity estimates. The single-well formation performance tests may not be representative of the entire 100-m square element the well falls within, so the value of transmissivity assigned to the element that includes the well was allowed to differ from the value determined from the test. The single-well

Information Only

transmissivity estimates were treated as "noisy" observations of the transmissivity in the 100-m elements within the ensemble-based workflow. In this way, as with other observations, each parameter realization is paired with noisy single-well transmissivity estimates. The history-matching process aims to find parameter realizations that match historical water levels, drawdown observations, and noisy single-well transmissivity estimates. The noise of these observations was normally distributed around the log transform of the transmissivity targets with one standard deviation set to 0.25 ($\log_{10}(m^2/s)$), so most observations would settle within half of a log cycle of the measured values. **Table 5** and **Figure 9** show the transmissivity targets for the 63 observations in the observation group "meastrans". The transmissivity was calculated by sampling the hydraulic conductivity at the location of each well and multiplying it by the constant model thickness of 7.75 meters in the function `estimate_geo_trans` in the Python script `forward_run.py`

Information Only

Table 5. Single Well Performance Transmissivity Measurements

Well	$\log_{10}$ (m^2/s)	Well	$\log_{10}$ (m^2/s)	Well	$\log_{10}$ (m^2/s)
AEC-7R	-6.19	H-5c	-6.7	SNL-6	-11.06
C-2737	-6.2	H-6c	-4.4	SNL-8	-6.6
CB-1	-6.5	H-7c	-2.8	SNL-9	-4.4
D-268	-5.7	H-9bR	-3.84	USGS-1	-3.3
DOE-1	-4.9	IMC-461	-3.82	WIPP-11	-3.4
DOE-2	-4	P-14	-3.5	WIPP-12	-7
ENGLE	-4.3	P-15	-7	WIPP-13	-4.1
ERDA-9	-6.3	P-17	-6	WIPP-18	-6.5
H-1	-6	SNL-1	-3.2	WIPP-19	-6.2
H-10cR	-7.13	SNL-10	-6.5	WIPP-21	-6.6
H-11b4R	-4.49	SNL-12	-3.3	WIPP-22	-6.4
H-12R	-6.82	SNL-13	-6.4	WIPP-25	-3.6
H-14	-6.5	SNL-14	-4.3	WIPP-26	-2.9
H-15R	-6.91	SNL-15	-12.9	WIPP-28	-3.6
H-16	-6.1	SNL-16	-2.9	WIPP-30	-6.7
H-17	-6.6	SNL-17	-3.5	WQSP-1	-4.5
H-18	-5.7	SNL-18	-3.9	WQSP-2	-4.7
H-19b0	-5.2	SNL-19	-3.4	WQSP-3	-6.8
H-2c	-6.2	SNL-2	-3.8	WQSP-4	-4.9
H-3b1	-4.7	SNL-3	-3	WQSP-5	-5.9
H-4c	-6.1	SNL-5	-5.3	WQSP-6	-6.6

Information Only

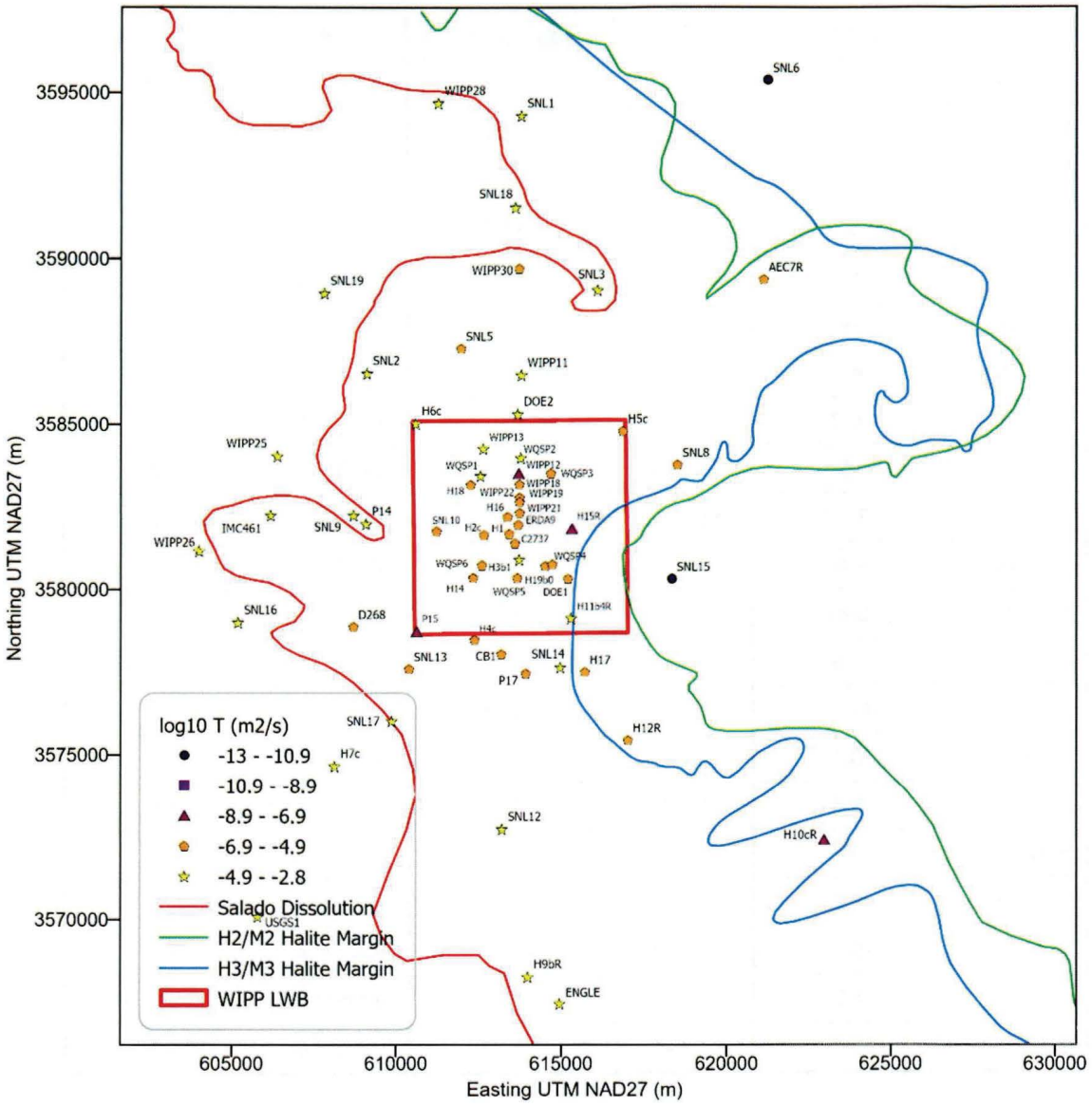

Figure 9. Map of Single Well Performance Transmissivity Measurements

5.1.5 Observation Weighting Scheme

All observations that were selected to comprise the measurement objective function were assigned initial weights of 1, except for the steady-state freshwater measurements and the drawdown observed at well SNL-17 in the Mills Ranch model (refer to Section 5.1.4.3 for more details). These weights were used in the evaluation of prior parameter ensemble to generate an initial ensemble of residual values. Then the weights were adjusted, as described below, so each general observation type contributed the desired amount to the measured objective function.

The weight adjustment process begins by evaluating the prior parameter ensemble using PEST++ IES with NOPTMAX option set to −1. Effectively, this option makes PEST++ IES only run the one-thousand

Information Only

realizations using the parameters provided by the prior ensemble file (`pe.csv`) and stop before the first iteration of optimization. This generates the prior simulated results in the observation ensemble file (`mf6.0.obs.csv`). By differencing the prior simulated results ensemble and the data, the initial residual vector is calculated for each of the one-thousand realizations. Using this residual vector, the weight of each observation group can be adjusted so that the contribution from each general observation type to the initial measured objective function (ϕ) matches the desired contribution shown in **Table 6**. By providing a desired ϕ percentage to each observation group, the weight required to change that observation group to represent the desired ϕ percentage was calculated for every realization. This weighting process yields an ensemble of weight values, one weight vector for each realization. The median weight value for each observation was then calculated and used in the PEST++ IES solution process by replacing the "weight" column of the observation file (`mf6.obs_data.csv`).

Table 6. General Observation Groups, Desired Objective Function Percentages, and Weight Multipliers

General Observation Group	Observation Group Name	Desired ϕ Percentage	Weight Multiplier
Steady-state Freshwater Heads	head	25%	19.34
Multi-well Pumping Tests	H-11	2.5%	8.54
	H-19	2.5%	2.24
	H-3	2.5%	8.10
	H-9bR	2.5%	4.44
	P-14	2.5%	104.90
	SNL-14	2.5%	4.59
	WIPP-11	2.5%	5.00
	WIPP-13	2.5%	4.85
	WQSP-1	2.5%	49.71
	WQSP-2	2.5%	45.45
Single Well Measured Transmissivity	meastrans	25%	113.03
Mills Ranch Pumping Test	mr	25%	0.54

Many numerical experiments were performed to explore the effect of varying the desired objective function percentages of each general observation type to improve history-matching. This ultimately led to splitting the desired objective function evenly amongst the four general observation groups (25% each), which yielded results that best fit the conceptual understanding of the system and gave equal importance to each general observation type.

There was much discussion about the decision to allow the Mills Ranch pumping event to represent such a large portion of the objective function when the pumping rate at the Mills Ranch was unknown. However, the WIPP water level monitoring network observed more than five years of water level measurements documenting the response due to the pumping event, so the Mills Ranch pumping rate could be confidently estimated as a nuisance parameter, as mentioned in Section 5.

Information Only

5.2 Parameters

Conceptually, "parameters" are used to explicitly represent recognized sources of model input uncertainty in the modeling workflow. Within the PEST++ IES algorithm, virtually an unlimited number of parameters can be used owing to the derivative-free ensemble-method algorithm. Additionally, parameters can be constructed to explicitly represent multiple spatial and/or temporal scales of model input uncertainty, facilitated by the non-intrusive design of PEST++ IES. In this workflow, 214,335 non-fixed parameters were estimated using PEST++ IES, compared to 1,100 to 1,700 parameters estimated in Task 7 of AP-114.

In this section, the parameterization design used for the five main groups of parameters, namely transmissivity, storage, horizontal anisotropy, recharge, and the Mills Ranch pumping event, is described in detail.

5.2.1 Setting Up the Prior Ensemble File and PEST++ IES Inputs

The prior ensemble file (`pe.csv`) is a stochastic PEST++ IES file generated using the Python script `S04_GenerateForwardRun.py`. This file contains the initial values for every parameter being estimated, for each of the one-thousand realizations. The parameters were drawn using a static version of the open-source Python package `pyemu` (White et al., 2016) and other methods described in this section. PEST++ IES uses the prior ensemble file as input to initialize the parameters.

Files used by PEST++ IES were generated by the same Python script `S04_GenerateForwardRun.py` used to create instruction files, template files, the control file, and the forward run Python script `forward_run.py`.

5.2.2 Transmissivity Parameters

Transmissivity was subjected to three spatial scales of parameterization: grid-scale parameters, pilot points multipliers, and zonal multipliers (refer to **Figure 8**).

Grid-scale parameters allowed for the direct inclusion of geostatistical realizations within the inversion process and allowed PEST++ IES to assimilate information during history matching directly at a model-grid scale. The pilot point multipliers were included to "warp" the transmissivity field at a broader scale than the grid-scale parameters, but the natural flexibility of the pilot point approach induced heterogeneity outside of the subspace spanned by the geostatistical realizations. Lastly, the zonal multiplier parameters adjusted the transmissivity fields at the spatial scales identified in the model's regional conceptualization.

5.2.2.1 Grid Scale Hydraulic Conductivity

The base T-fields geostatistical realizations for transmissivity from Task 5 of AP-114 were used directly as grid-scale parameters to populate the grid-scale elements of transmissivity. Given that the model has a constant thickness ($b = 7.75$ meters), and transmissivity is directly proportional to hydraulic conductivity (**Equation 5**), the parametrization of hydraulic conductivity (K) in the model input files was performed.

Equation 5. $T = K * b$

Initial hydraulic conductivity values for each model cell were based on the corresponding transmissivity value from the base T-fields from Task 5 of AP-114. The upper and lower limit of each grid-scale K cell was allowed to vary between the minimum and maximum values across the entire one-thousand transmissivity realizations (2.57E-25 m/s and 4.6E-3 m/s).

This process was performed by the function `generate_ensemble` in the Python script `S00_Generate_Ensamble.py` and is called in the function `setup_model` in `S04_GenerateForwardRun.py`. These values are also included in a spatial correlation defined by a

Information Only

similar variogram described in Task 7 of AP-114; the variogram parameters used in this analysis are shown in **Table 7.** This parameter group was named "hk" and contained 87,188 (nrow × ncol) free parameters.

Table 7. Variogram Parameters for Grid-Scale

Parameters	Value
Model Type	Exponential
Nugget	0.0
Range	9,500 m

The variogram used for the grid-scale parameters is not based on field measurements, but rather enforces spatial correlation on any variation at the grid-scale. This has the effect of preventing sharp transmissivity contrasts over short distances. Keeping the nugget at zero avoids adding "noise" unnecessarily at the grid-scale.

5.2.2.2 Transmissivity Pilot Point Multipliers

A set of pilot point multipliers were also used so that PEST++ IES would have some ability to explore potential uncertainty in hydraulic conductivity (and therefore transmissivity) outside of the spatial patterns present in the base T-field geostatistical realizations. As shown in **Figure 10**, pilot points were spaced evenly, 500 by 500 meters across the model domain, excluding the northwestern portion of the model (red region in figure). While pilot points were included in the constant-head area (blue region in figure), the effect of adding pilot points in this area was negligible because the value was held constant. The pilot points were set to a value of 1, and given a range of 0.01 to 100.

These initial stochastic realizations for the pilot point multiplier parameters were drawn from a $\log_{10}$ multivariate normal distribution with a mean of unity and a covariance matrix described by an exponential variogram shown in **Table 8.** This parameter group was named "k_pp", and contains 3,232 free parameters.

Information Only

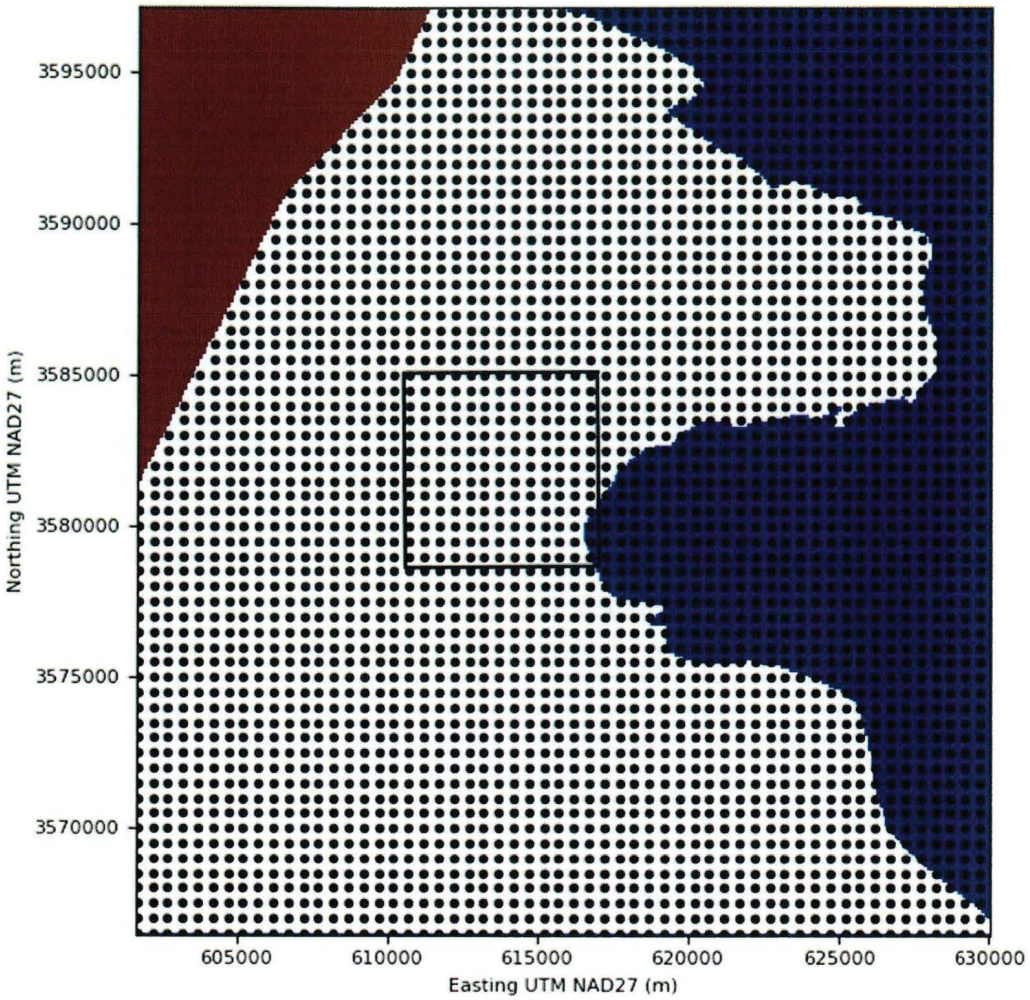

Figure 10. Pilot Point Multipliers in the Model Domain

Table 8. Variogram Parameters for Pilot Point Multipliers

Parameters	Value
Model Type	Exponential
Nugget	0.0
Range	30,000 m

5.2.2.3 Transmissivity Zonal Multipliers

Zone-based multiplier parameters were defined to represent regional-scale transmissivity based on the conceptual model for the analysis. These zones were consistent with the conceptual Culebra flow model defined in Task 5 of AP-114 and Task 7 of AP-114, except for the T and A parameter zones. In previous work, these two parameters used stochastic zones (zones 0 and 1) to represent a mixture of higher and lower transmissivity values across the one-thousand realizations. However, in this task, both zones were combined

Information Only

into a single zone (zone 1) since incorporating these stochastic zones would not likely result in more variation in the parameter fields than the current methodology.

As shown in **Figure 11**, there is a high-transmissivity zone to the west (zone 2), corresponding to the area of Salado dissolution, and a mixture of higher and lower transmissivity values corresponding to the stochastic zone (zone 1) provided in the base fields that defined the center of the model domain. This parameter group, named "t_mult", contained two free-moving parameters (zones 1 and 2) centered around 1 and given a range of 0.01 to 100. Model cells in these two zones were multiplied by these zonal multipliers after the grid-scale and pilot point parameters were applied.

Figure 11 also depicts two parameter multipliers in the halite sandwich zone to the east (zone 3) and the no-flow boundary to the north-west (zone 4). These two multipliers were also included in the workflow but fixed to a value of 1, so they did not affect the final transmissivity field.

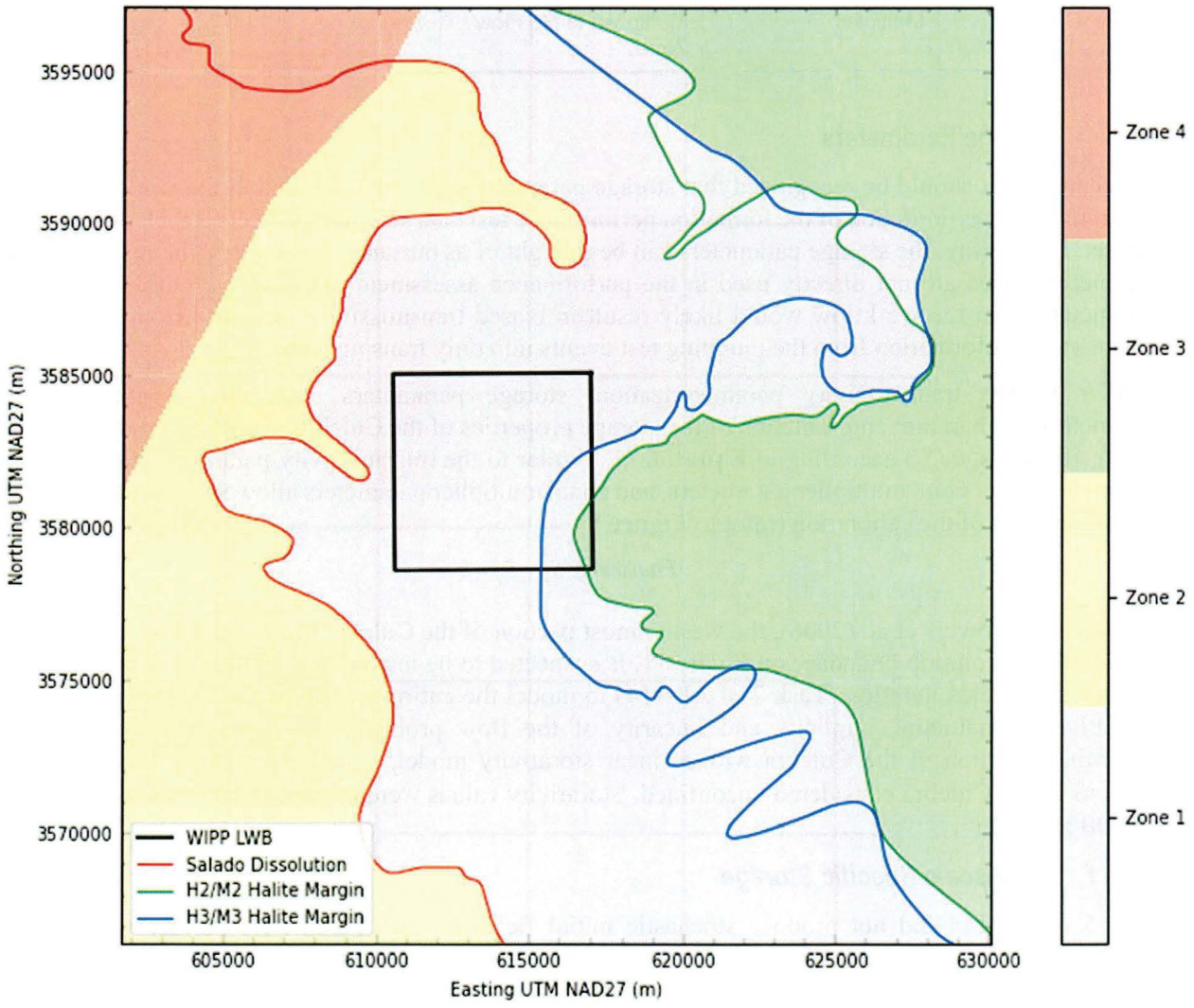

Figure 11. Transmissivity Zones

A summary table for the parameter specifications described above is provided below in **Table 9.**

Information Only

Table 9. Summary Table of Hydraulic Conductivity Parameters

Parameter	Type	Description	Hydraulic Conductivity (m/s)		
			Initial Value	Lower Limit	Upper Limit
Grid-Scale	Direct	Applied directly to model cells	Task 5 of AP-114	2.57E-25	4.6E3
Pilot Point	Multiplier	Multiplied to K field	1.00	0.01	100.00
Zone 1	Multiplier	Multiplied to Stochastic Zone	1.00	0.01	100.00
Zone 2	Multiplier	Multiplied to Salado Dissolution Zone	1.00	0.01	100.00
Zone 3	Multiplier	Multiplied to Halite Sandwich Zone	1.00	1.00	1.00
Zone 4	Multiplier	Multiplied to No Flow Zone	1.00	1.00	1.00

5.2.3 Storage Parameters

Conceptually, it should be recognized that storage parameters are only included in the workflow to allow for more robust assimilation of the formation performance test data sets and the Mills Ranch pumping event dataset. In this way, the storage parameters can be thought of as nuisance parameters: the resulting storage parameter values are not directly used in the performance assessment calculations, but excluding these parameters from the workflow would likely result in biased transmissivity estimates from attempting to assimilate all information from the pumping test events into only transmissivity.

Similar to the transmissivity parameterization, storage parameters used three spatial scales of parameterization in the representation of the storage properties of the Culebra, which input into the models as specific storage (S_s) according to **Equation 6**. Similar to the transmissivity parametrization, grid-scale parameters, pilot point multiplier parameters, and zonal multiplier parameters allowed for better exploration and adjustment of the calibration (refer to **Figure 8**).

$$\textit{Equation 6. } S = S_s * b$$

According to Powers et al. (2006), the westernmost portion of the Culebra in the Nash Draw area, west of the Salado Dissolution boundary on Figure 11, is suspected to be unconfined. However, it was decided in a previous T-fields iteration (Task 7 of AP-114) to model the entire domain of the Culebra as a confined formation to maintain simplicity and linearity of the flow problem. To approximately account the unconfined portion of the Culebra with a linear storativity model, storativity was set much higher for portions of the Culebra considered unconfined. Storativity values were capped at 10^5 or a specific storage of 4.08×10^2 m^{-1}.

5.2.3.1 Grid-scale Specific Storage

Task 5 of AP-114 did not produce stochastic initial fields for any parameters besides transmissivity; therefore, the grid-scale storage parameters were not populated from the base T-fields, as was the case with grid-scale transmissivity. Instead, the grid-scale storage parameters were allowed to vary according to the values assigned to the different storativity zones defined in Task 7 of AP-114. Initial parameter values and ranges for specific storage are shown in **Table 10**. The variogram for these grid-scale parameters was the same as for the grid-scale transmissivity parameter (see **Table 7**). This process was performed by the function `generate_ensemble` in the Python script `S00_Generate_Ensamble.py` and is called in

Information Only

the function `setup_model` in `S04_GenerateForwardRun.py`. These parameter groups were named "s_z1", "s_z2", "s_z3", "s_z4" and contained 58,516 free parameters ("s_z3" and "s_z4" were fixed due to being in the halite sandwich zone to the east and the no-flow boundary to the north-west.)

5.2.3.2 Specific Storage Pilot Point Multipliers

The same 500 by 500 m grid of pilot points used for K was applied to specific storage (see **Figure 10**). Pilot points were allowed to range between 0.01 and 10 and were drawn using the same pilot point variogram scheme as K (see **Table 8**). Pilot point multipliers were the only parameters used to modify storativity in the constant head zone to include some variance in this portion of the model domain.

5.2.3.3 Specific Storage Zonal Multipliers

Model cells in zone 0 were located in portions of the Culebra considered fully confined. The initial distribution of storativity values for these model cells had an average of 10^{-5} or a specific storage of 1.29×10^{-6} m^{-1}, which is the same values used for storativity in AP-088 (McKenna and Hart, 2003). Model cells in zone 1 were located in the transition zone from a confined to an unconfined unit in the western region of the Culebra. These cells were given an initial value of storativity of 10^{-4} or a specific storage of 1.29×10^{-5} m^{-1}. Model cells in zone 2 were located in the unconfined portion of the Culebra and were assigned much larger values of storativity to better represent an unconfined Culebra in the flow model: an initial value of $10^{-1.5}$ or a specific storage of 4.08×10^{-3} m^{-1}. Model cells in zone 3 were allowed to adjust by pilot point multipliers in the forward model, however, these model cells were located in constant head areas and therefore had a fixed storativity value of 10^{-5} for each realization. Model cells in zone 4 were located in no-flow areas. Each storativity zone was allowed to vary between the parameter limits of 0.1 and 10, centered around the initial value of 1, except for the constant and no-flow zones (zones 3 and 4).

Each storativity zone was multiplied by the values mentioned above after the application of grid-scale and pilot point parameters. These parameters grouped as "s_mult" were each multiplied by their respective specific storage cells.

A map of the storativity zones is shown in **Figure 12**, and **Table 10** provides a summary for the specific storage parameter specifications.

Information Only

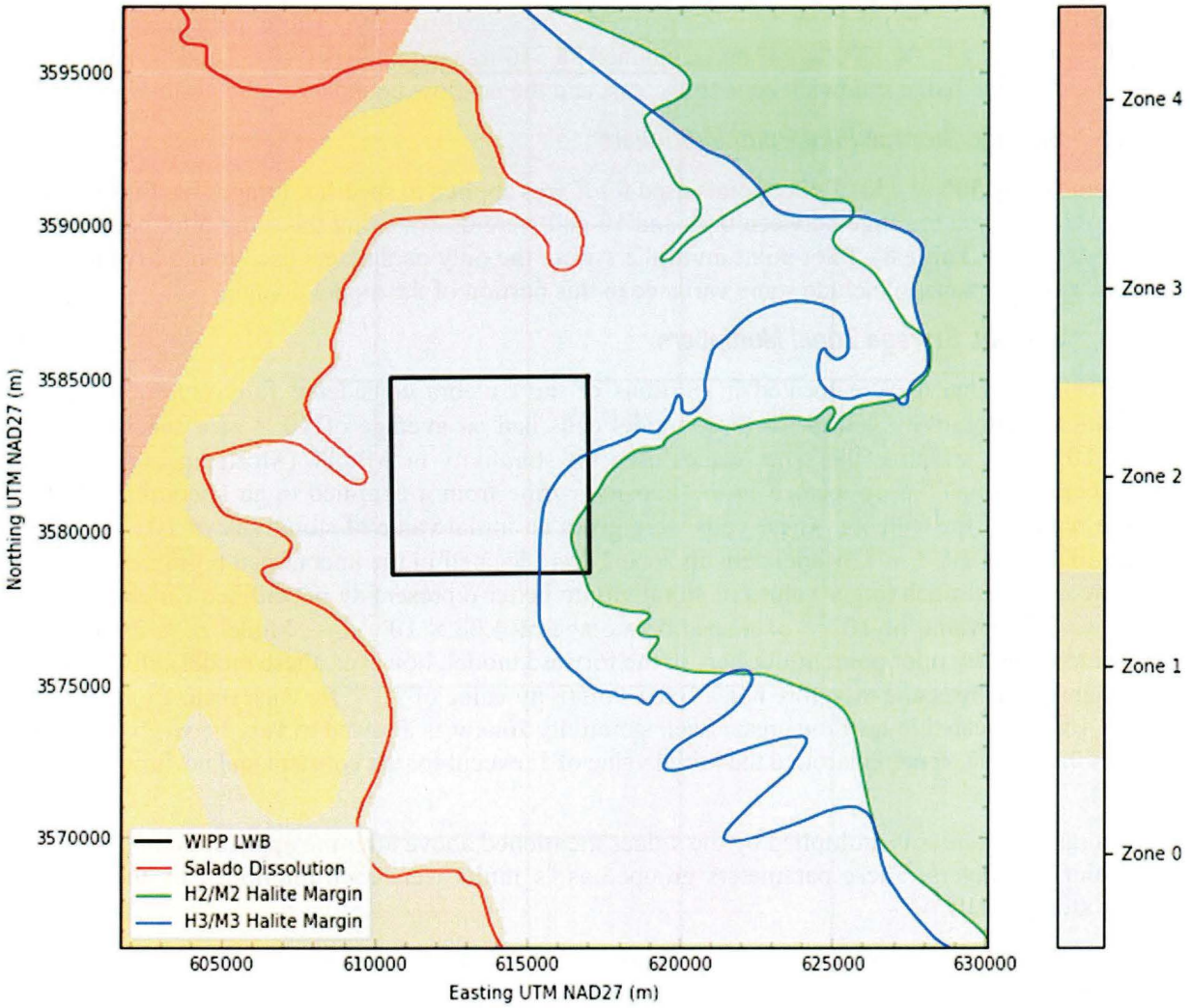

Figure 12. Storativity Zones

Table 10. Summary Table of Specific Storage Parameters

Parameter	Type	Description	Specific Storage (m^{-1})		
			Initial Value	Lower Limit	Upper Limit
Pilot Point	Multiplier	Multiplied to S_s field	1.00	0.01	100.00
Zone 0	Direct	Applied to Confined Zone	1.3E-6	4.1E-09	4.1E-06
Zone 1	Direct	Applied to Transition Zone	1.3E-05	1.3E-09	4.1E-02
Zone 2	Direct	Applied to Unconfined Zone	4.1E-03	4.1E-06	4.1E-02
Zone 3	Direct	Applied to Constant Zone	1.3E-06	1.3E-08	1.6E-06
Zone 4	Direct	Applied to No-Flow Zone	N/A	N/A	N/A

Information Only

5.2.4 Horizontal Anisotropy Parameters

The anisotropy fields were subjected to the same three levels of parameterization as transmissivity and storativity.

5.2.4.1 Grid-scale Horizontal Anisotropy

The grid-scale parameters of anisotropy were set to start at isotropic conditions of 1 and were allowed to move between 0.25 and 3.98 using the same variogram method as for the grid-scale transmissivity parameters. This process was performed by the function `generate_ensemble` in the Python script `S00_Generate_Ensamble.py` and is called in the function `setup_model` in `S04_GenerateForwardRun.py`. These values are also included in a spatial correlation defined by a similar variogram described in Task 7 of AP-114; the variogram parameters used in this analysis are shown in **Table 7.** This parameter group was named "a_z1", "a_z2", "a_z3", "a_z4" and contained 87,188 (nrow × ncol) free parameters.

5.2.4.2 Horizontal Anisotropy Zonal Multipliers

Because the anisotropy fields used in this task contain cell-by-cell anisotropy values for transmissivity (and only transmissivity), the same zones defined for transmissivity were used for anisotropy zonation (see **Figure 11**). Consequently, anisotropy parameters were also fixed to a value of 1 in both the constant and no-flow zones (zones 3 and 4).

5.2.4.3 Horizontal Anisotropy Pilot Point Multipliers

As with transmissivity, the same pilot point multiplier parameters were applied to anisotropy. Pilot points comprised an evenly spaced 500 by 500 m grid across the model domain. The pilot points were allowed to vary, excluding the no-flow portion of the model, and using the same variogram as for the pilot points for transmissivity (Table 8). Pilot points were the only method of adjustment for anisotropy values in zone 3. Pilot points were centered around the initial value of 1, and were allowed to vary between 0.01 and 100. The parameters were grouped as "a_pp"; a summary table of the parameter specifications is provided in **Table 11** below.

Information Only

Table 11. Summary Table of Anisotropy Parameters

Parameter	Type	Description	Anisotropy		
			Initial Value	Lower Limit	Upper Limit
Grid-Scale	Direct	Applied to A field	1.00	0.25	3.98
Pilot Point	Multiplier	Multiplied to A field	1.00	0.01	100.00
Zone 1	Multiplier	Multiplied to Stochastic Zone	1.00	0.32	3.2
Zone 2	Multiplier	Multiplied to Salado Dissolution Zone	1.00	0.32	3.2
Zone 3	Multiplier	Multiplied to Constant Zone	1.00	1.00	1.00
Zone 4	Multiplier	Multiplied to No Flow Zone	1.00	1.00	1.00

5.2.5 Recharge Parameters

As discussed in Task 7 of AP-114, the conceptual model presented in Holt (1997) and later Hart et al. (2008) indicates that a groundwater divide exists southwest of the WIPP site. Hart et al. (2008) represented this possible groundwater divide (which was the same location as a no-flow boundary in CRA-2004) by a simple line of recharge cells extending northwest to the southeast in the southwestern-most portion of the model domain. Consistent with this representation, model cells in the groundwater divide line were considered zone 1, while all the other model cells were considered zone 0 (see **Figure 13**). Given that the purpose of including recharge parameters in the T-fields was to evaluate the effect of a groundwater divide in the Culebra, the recharge parameters only contained grid-scale parametrization.

Information Only

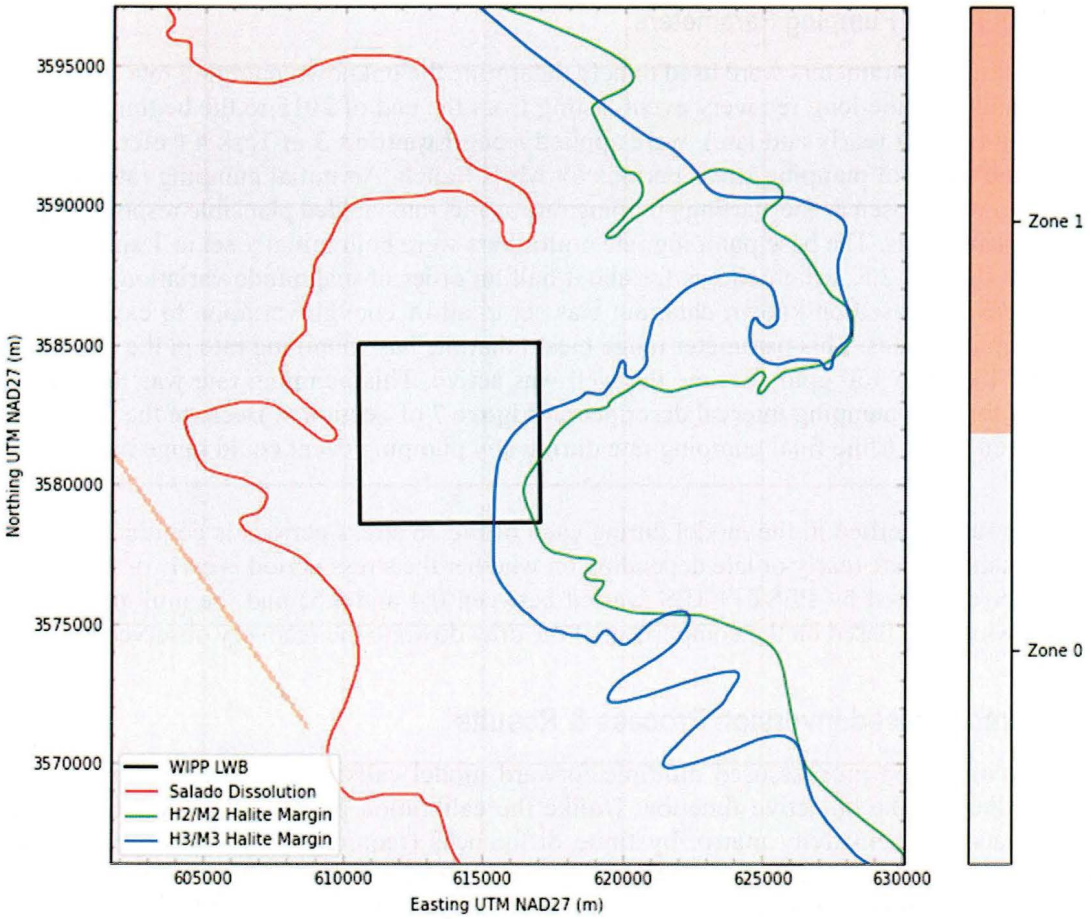

Figure 13. Recharge Zonation

5.2.5.1 Grid-Scale Recharge

Model cells in zone 0 were fixed at 10^{-30} m/s (effectively 0), while model cells in zone 1 were set to a very small initial recharge value of 10^{-15} m/s, and were allowed to vary between 10^{-19} and 10^{-10} m/s. Only three model cells in zone 1 to the far West were fixed at 10^{-19} m/s, so recharge could only increase towards the east.

These parameters were grouped as "r_z0" and "r_z1" for zones 0 and 1 in **Table 12**

Table 12. Summary Table of Recharge Parameters

Parameter	Type	Description	Recharge (m^3/s)		
			Initial Value	Lower Limit	Upper Limit
Zone 0	Direct	Applied directly to cells not in groundwater divide	1E-30	1E-30	1E-30
Zone 1	Direct	Applied directly to cells in groundwater divide	1E-15	1E-19	1E-10
Three cells in Zone 1	Direct	Applied to three cells in groundwater divide	1E-19	1E-19	1E-10

Information Only

5.2.6 Mills Ranch Pumping Parameters

Only two multiplier parameters were used to help determine the unknown pumping rate at the Mills Ranch well before and after the long recovery event lasting from the end of 2015 to the beginning of 2016. Two base pumping rates, Q (early and late), were applied using **Equation 3** in Task 4 (refer to Section 4.1) to produce a time series of pumping stress periods for Mills Ranch. An initial pumping rate of 60 gpm (both early and late) was chosen as the starting pumping rate as this rate yielded plausible responses of drawdown in the monitoring wells. The base pumping rate multipliers were both initially set to 1 and were allowed to vary between 0.4 and 2.5, which allows for about half an order of magnitude variation in each direction. This range was not based on known data, but was set to allow enough variation to explore a reasonable range of pumping values. This parameter range meant that the base pumping rate in the private well could range from 24 gpm to 150 gpm anytime the well was active. This pumping rate was then applied to the relative rates for each pumping interval described in **Figure 7** of Section 4. Because the relative multiplier ranges between 0 and 1, the final pumping rate during any pumping event could range between 0 gpm and 150 gpm.

The pumping rate specified in the model during each of the 76 stress periods is computed by multiplying by the base pumping rate (early or late depending on whether the stress period is early or late), the pumping rate multiplier estimated by PEST++ IES (varied between 0.4 and 2.5) and the multipliers described in Section 7.1, which are based on the comparison of the drawdown to the recovery observed during late 2015 to early 2016.

5.3 Ensemble-based Inversion Process & Results

The inverse calibration process used multiple forward model calls to evaluate the impact of changing parameter values on the objective function. Unlike the calibration process in Task 7 of AP-114, which created the Jacobian sensitivity matrix by finite differences (required the inversion process to run the forward model at least once per parameter and resulted in a six-month-long calibration for only two hundred of the original one-thousand base T-fields), this analysis used the PEST++ IES approach that saw the calibration of 973 of the one-thousand T-fields process reduced to two and a half days. The calibration process was spread across 10 cluster nodes, each with 20 processors utilizing the SLURM management software on the Fleetwood Mac (FWM) Linux cluster at Sandia National Laboratories in Carlsbad, New Mexico.

Of the 1,000 realizations, 27 realizations did not complete and therefore were not included in the final ensemble. These realizations were removed from the calibration because their objective function was greater than 4 standard deviations larger than the objective function average across all realizations.

5.3.1 PEST++ IES Calibration Process

The ensemble-based inverse process was performed using PEST++ IES and a series of functions in the Python script `forward_run.py` located in the folder `model_ws/mf6_template`. The master PEST++ control file and calibrated ensemble output are saved to the folder `master/`. The ensemble method encoded in PEST++ IES is based on the regularized Gauss-Levenburg-Marquardt algorithm or GLM (Doherty, 2004) using a Monte Carlo approximation to the first-order Jacobian sensitivity matrix (Chen and Oliver, 2013). With this algorithm, the entire parameter ensemble is iteratively adjusted towards a minimum of the weighted sum-of-squares objective function. Iterations are needed to resolve nonlinearities in the parameter-observation relation through repeated linearization. Because PEST++ IES does not explicitly compute a finite-difference based Jacobian matrix, the number of model runs required to approximate the Jacobian matrix is independent of the number of parameters and is controlled more by the number of realizations in the ensemble.

Information Only

5.3.2 Selection of IES iteration

Selecting the final one hundred calibrated fields for additional analyses consisted of two steps: selecting the final PEST++ IES iteration and identifying the subset of 100 fields from the full ensemble. The term "iteration" in PEST++ IES refers to running all realizations for a specific parameter set. For example, the first iteration of PEST++ IES is referred to as either iteration 0 or the "prior" iteration and uses the parameters established in the prior ensemble file (`pe.csv`), as mentioned in Section 5.

The parameter adjustment algorithm that PEST++ IES implements is referred to as an "iterative ensemble smoother". This means that the process through which a prior ensemble becomes a posterior ensemble requires a number of iterations of parameter field adjustment, these iterations being necessary to deal with the non-linearity of the parameter-to-model output relationship. During each iteration, a new approximation of the Jacobian matrix is calculated based on the latest ensemble. Upgrades to parameter sets are then calculated using this approximate Jacobian matrix. The process is repeated for the number of iterations defined in the pest control file (`mf6.pst`).

PEST++ IES seeks to improve the fit between observed groundwater levels and the corresponding simulated equivalent values. However, because the underlying groundwater model is an imperfect representation of the physical system, this fit cannot be the only metric by which we decide whether the model is "calibrated". Freyburg (1988) first reported the potential dangers in "overfitting" a model, because the model with the best fit may not produce the best predictions. Hunt et al. (2020) provided a new perspective on Freyburg's findings in the context of the highly parameterized approach used in this current work. The highly parameterized approach provides the flexibility to better capture the complexity of the physical system and can thus improve forecasting, but it does not eliminate the potential for "overfitting" and potentially biasing the model predictions.

The optimization process must be stopped when the fit to observations has been improved significantly and the model is doing a good job of representing the system as observed, but before introducing potential bias from fitting to noise or other intrinsic errors. The decision of which iteration to choose was based on three factors: standard practice, favoring conservatism, and evaluation of the probabilistic forecasts.

In practice, the modeler typically looks at how fit is improving with each iteration and stops the process when the downward trend in the objective function starts to flatten. **Figure 14** to **Figure 17** show how the overall objective function, and the objective function associated with each observation group vary with each iteration. **Figure 14** shows that the mean value of the overall objective function declines consistently in log space from iterations 2 to 5, but then has a slight inflection in the slope from Iteration 5 to 6. This inflection is most pronounced in the freshwater heads observation group (**Figure 15**). This suggests that Iteration 5 could be a defensible stopping point based on best practice.

The argument for ending the process prior to achieving "minimum" phi, is that this strategy maintains conservatism. This is because the initial set of parameters represented by the uncalibrated base T-fields provided in Task 5 of AP-114, conceptually should represent the maximum plausible uncertainty in the hydraulic conductivity field, and ultimately, the particle travel time. The apparent uncertainty in particle travel time is generally reduced by improving the match to groundwater levels. This leads to a tradeoff between reducing variance by (appropriately) assimilating groundwater levels, but avoiding potentially damaging biases that occur when trying to match the groundwater levels too well. Within this tradeoff, retaining excess variance in the simulated particle travel time distribution is a more conservative and robust approach since we have accounted for and estimated this variance in the simulated particle travel time distribution.

The conservatism in the strategy is shown in the probabilistic forecasts for this study, which are focused on particle travel times. A comparison of basic statistics for particle travel times by iteration is shown in **Figure 18** to **Figure 21** for different candidate release points (CRP). The same statistics are reported in

Information Only

Table 15 to **Table 18** in Section 5.4.9. The central tendency (mean/median) in each case stabilizes in Iteration 5, while maintaining a significant range in the travel time outcomes. Maintaining the variance in this ensemble of realizations is crucial for providing a robust assessment of the uncertainty associated with a system or process and helps to ensure that important factors are not overlooked or underestimated.

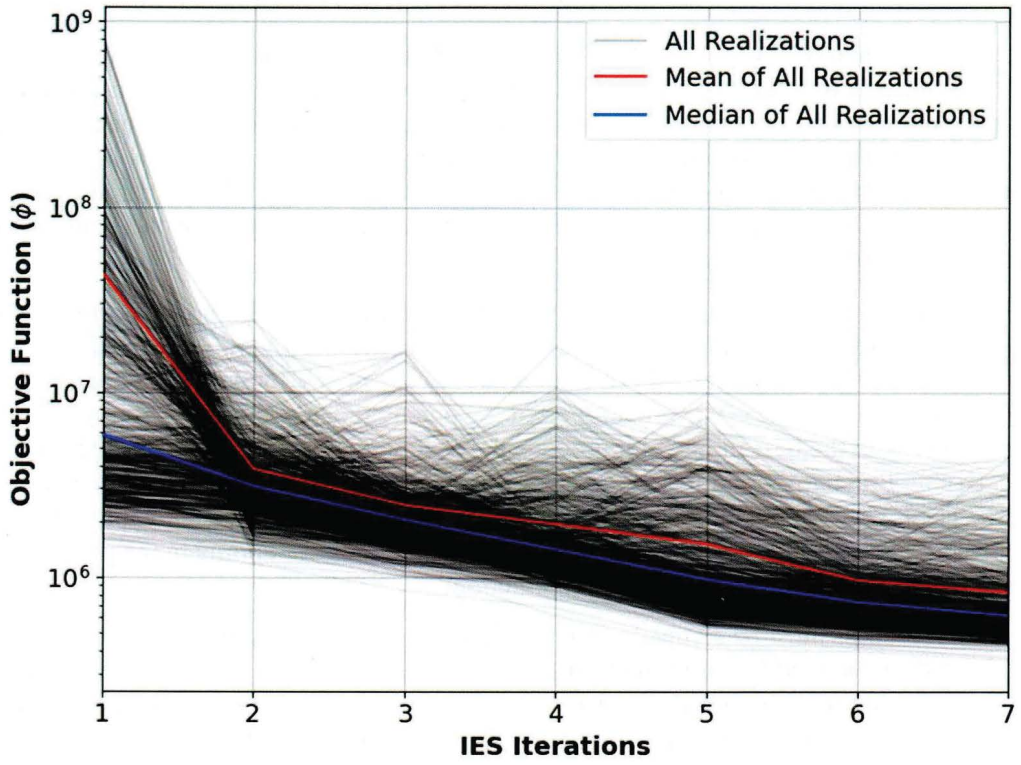

Figure 14. Evolution of Total Objective Function with IES Iteration

Information Only

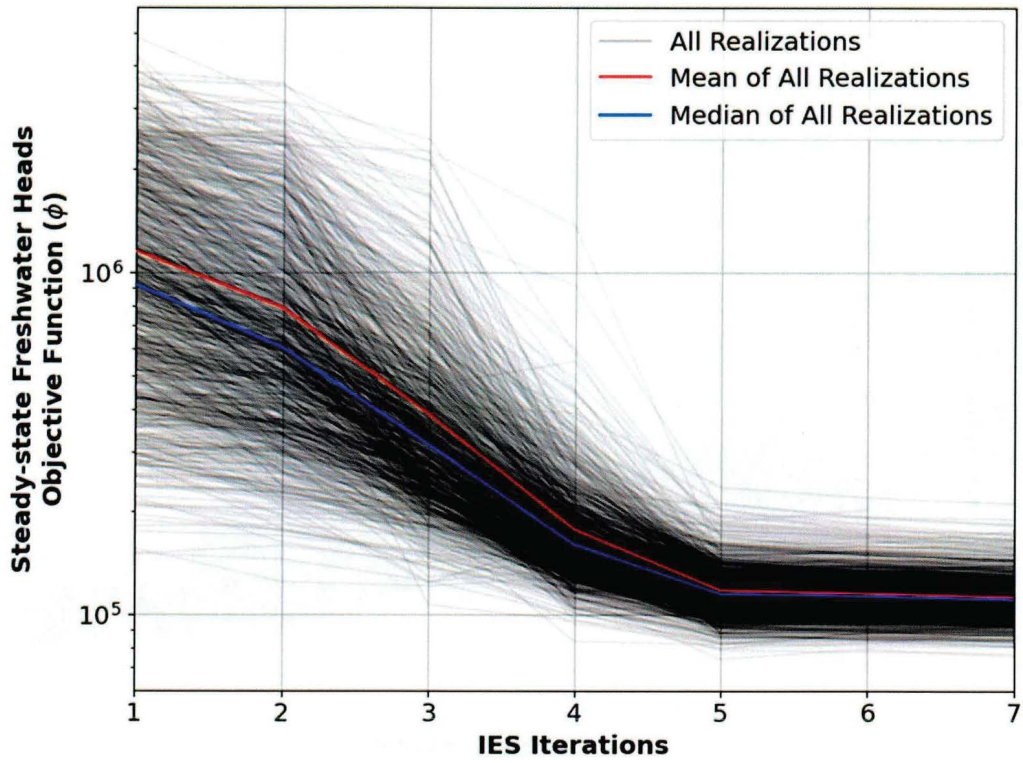

Figure 15. Evolution of Objective Function with IES Iteration for Steady-state Freshwater Heads Observation Group

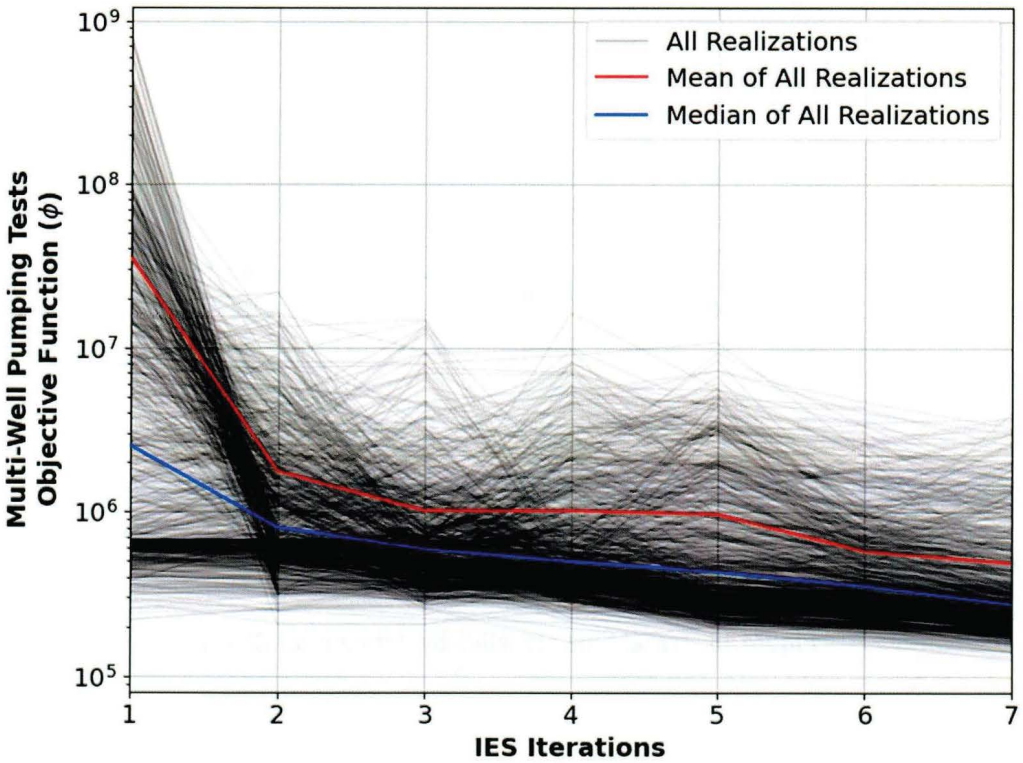

Figure 16. Evolution of Total Objective Function with IES Iteration for Multi-Well Pumping Tests

Information Only

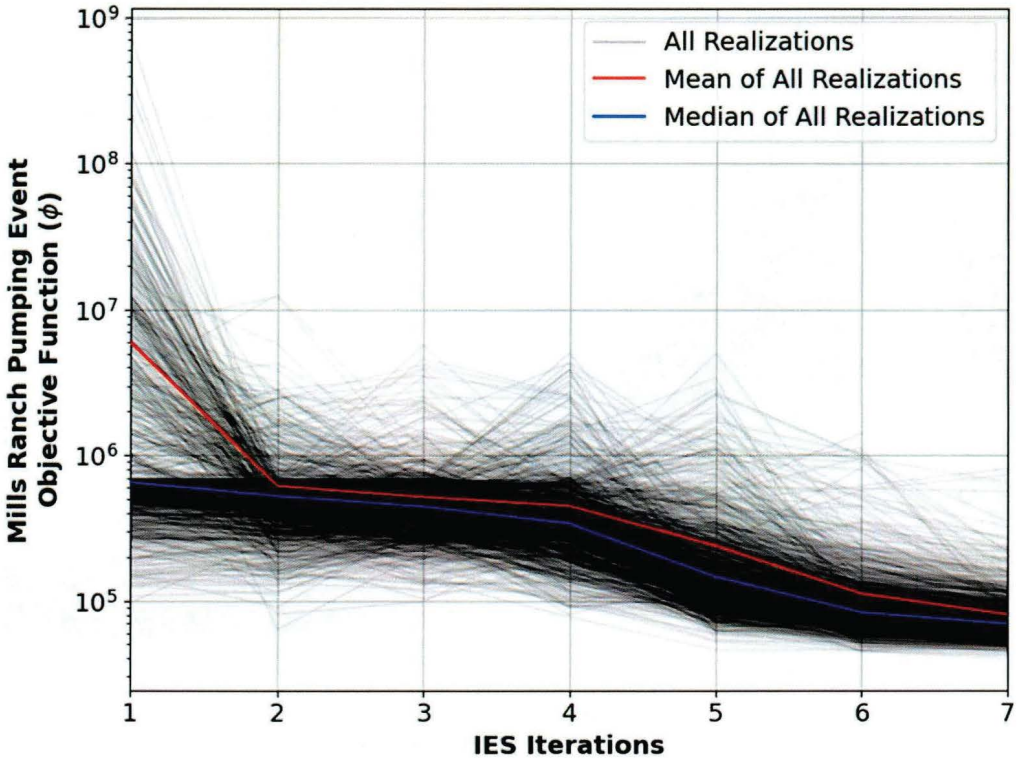

Figure 17. Evolution of Total Objective Function with IES Iteration for Mills Ranch Pumping Event

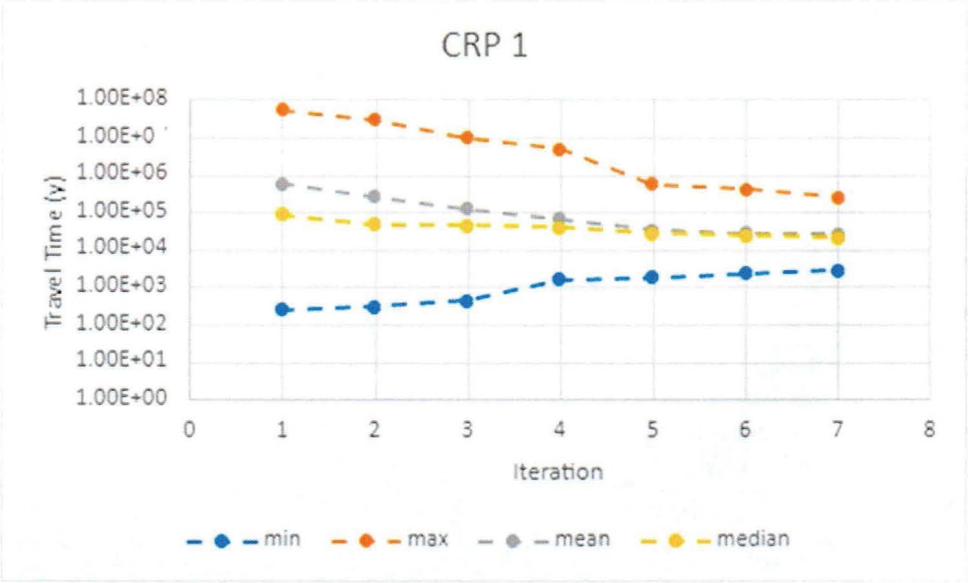

Figure 18. Travel time statistics by iteration for CRP 1

Information Only

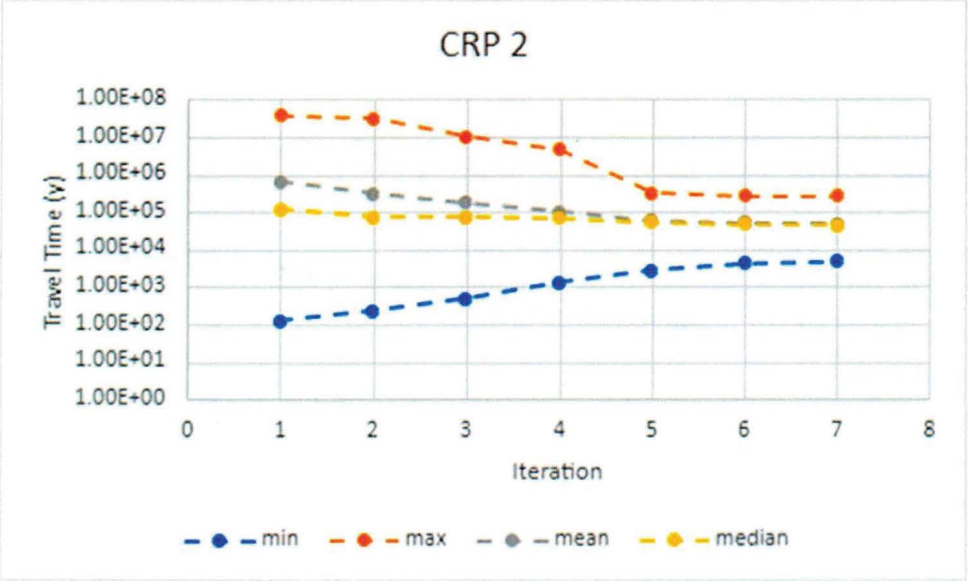

Figure 19. Travel time statistics by iteration for CRP 2

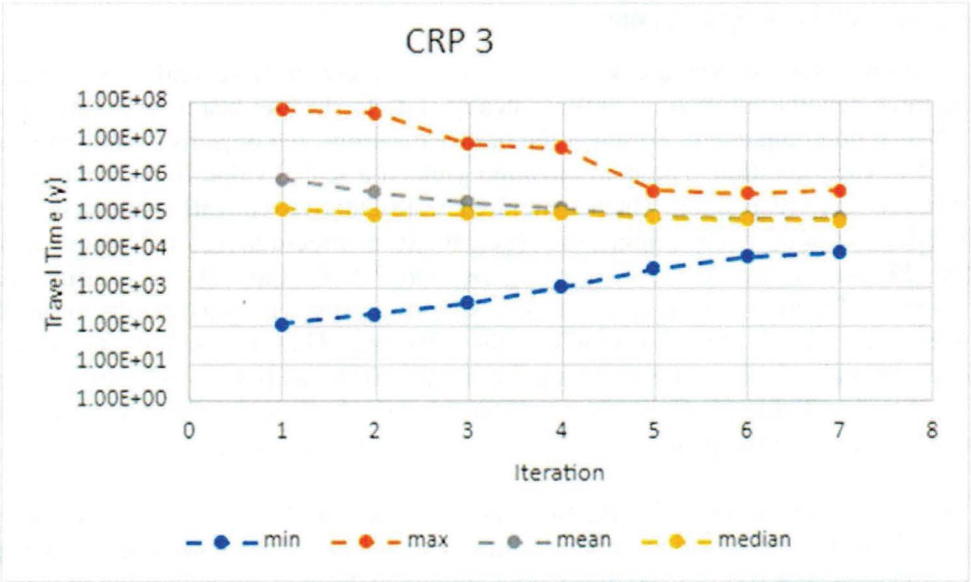

Figure 20. Travel time statistics by iteration for CRP 3

Information Only

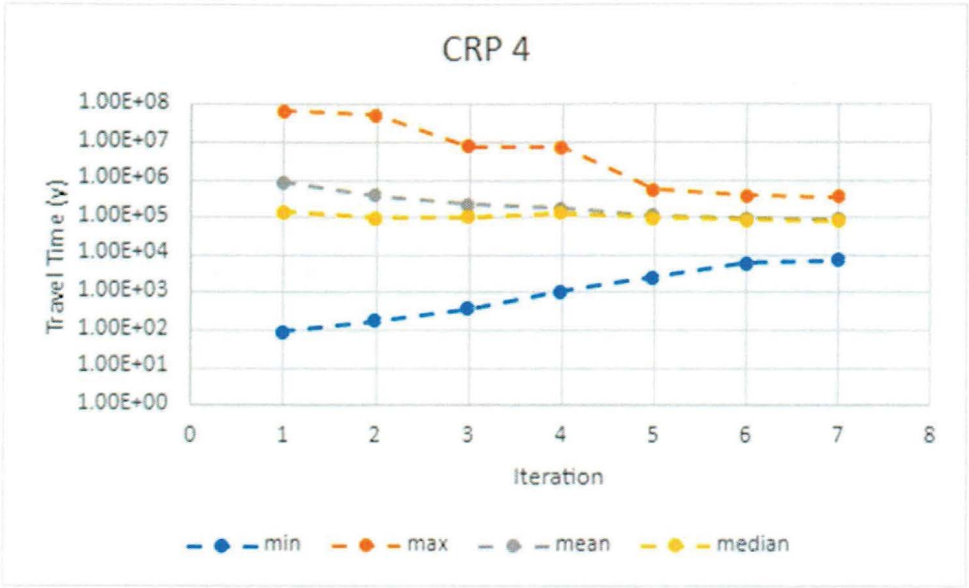

Figure 21. Travel time statistics by iteration for CRP 4

5.3.3 Choosing 100 Final Realizations

To support additional downstream analyses, one hundred representative realizations were chosen by comparing the three general observation groups: steady-state freshwater heads, multi-well pumping tests, and the Mills Ranch pumping event. To select the best realizations, the objective function was normalized between 0 and 1 at each iteration. The normalization yielded a scaled value for each of the three general observation types for each realization. The one hundred representative realizations were selected as the one hundred realizations closest to the origin point (i.e., 0,0,0 in three-dimensional space) in a Euclidean-distance sense (**Figure 22** and Table comprising Section 7.1 in Appendix A). **Figure 23** shows the normalized objective function for the general observation groups. The gray results show the final 973 realization ensemble, while the blue results indicate the 100 selected best realizations. The final one hundred selected realizations maintain the same identification number from the base T-fields produced in Task 5 of AP-114 and are listed in **Table 13**. Collectively, the one hundred selected realizations span an appropriate range of variability shown in the particle travel time figures and tables in Section 5.4.9

It should be noted that the single-well formation performance tests transmissivity observations were not included when selecting the realizations because these measurements were included in the generation of the base T-fields in Task 5 of AP-114 and thus were maintained through the calibration process (see Section 5.4).

Information Only

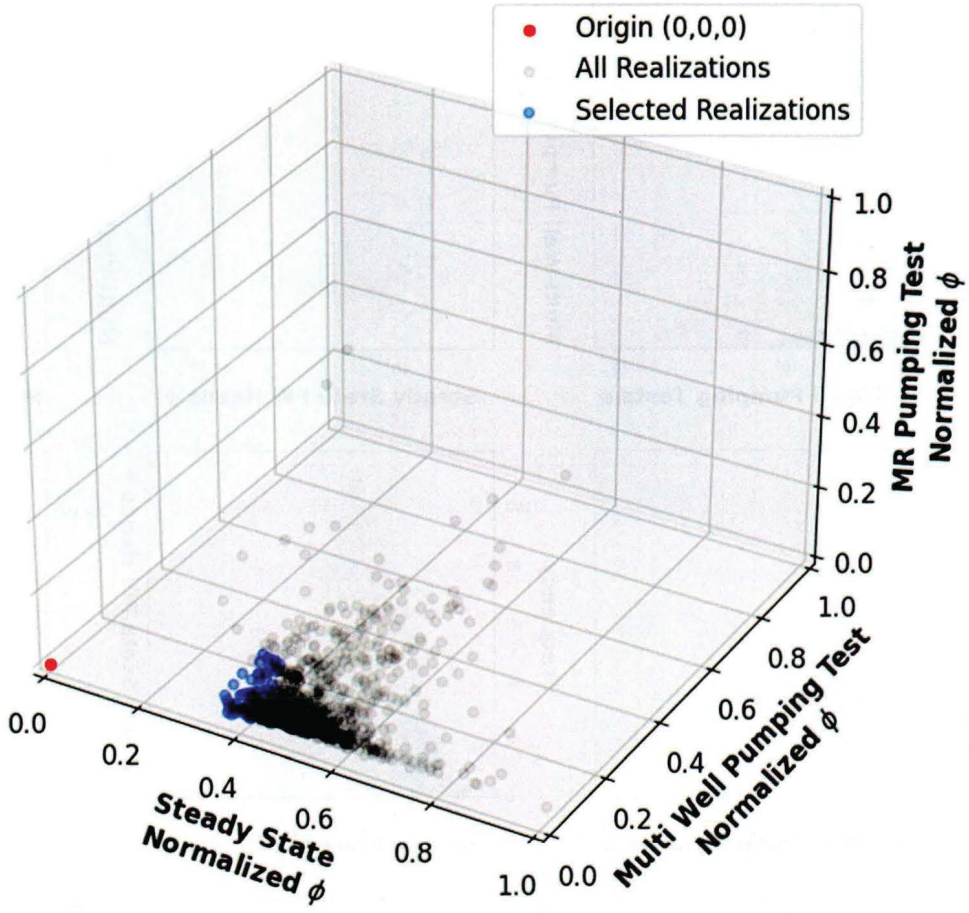

Figure 22. Normalized Objective Function for Observation Groups at Iteration 5

Information Only

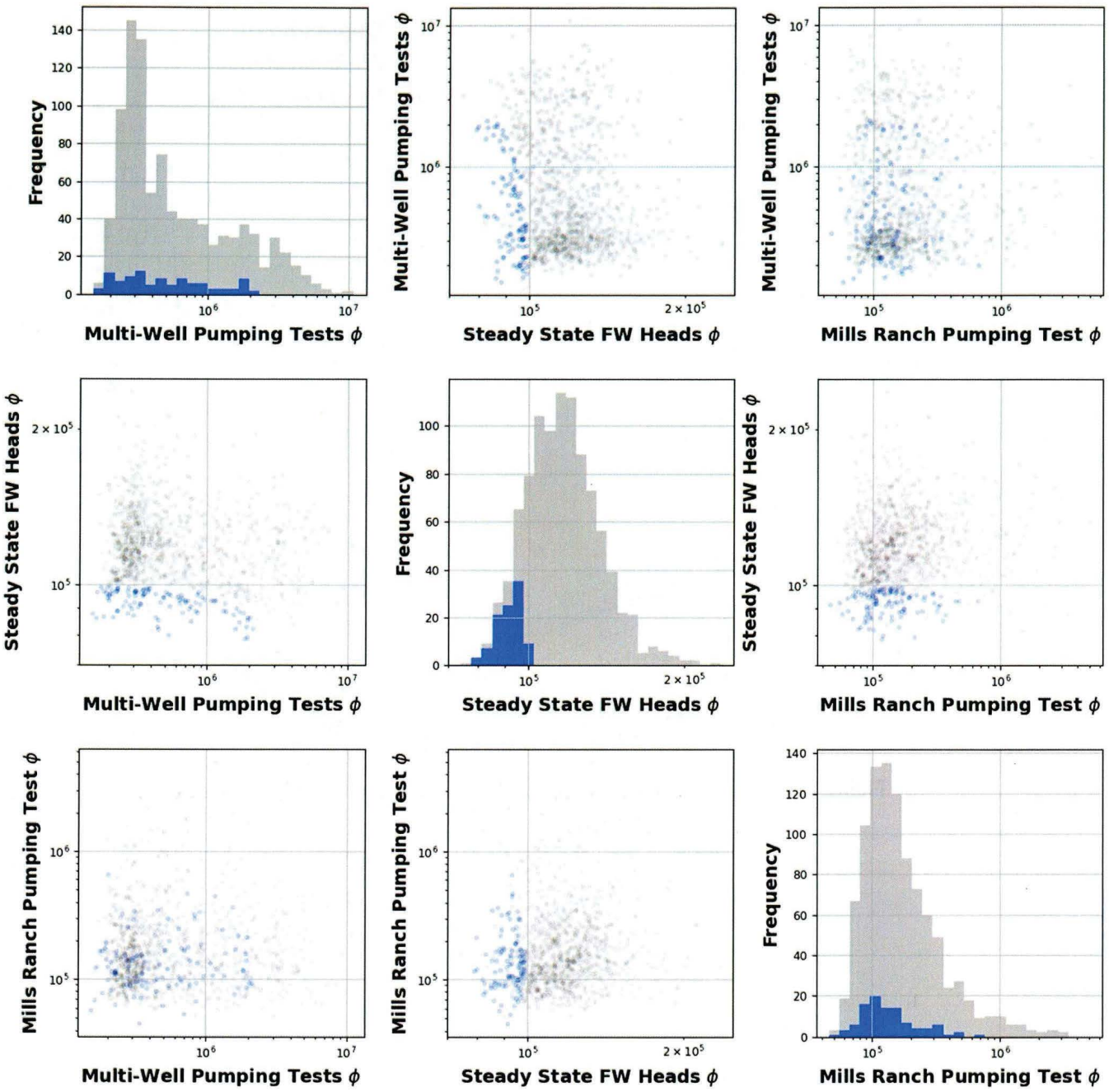

Figure 23. Histograms and Scatter Plots of Normalized Objective Function for Primary Observation Groups

Information Only

Table 13. 100 Selected T-Field Realizations

100 Selected Realizations									
5	150	320	434	511	590	660	728	807	856
12	173	325	441	517	614	664	729	808	869
27	194	338	455	519	619	672	736	810	892
71	213	344	456	530	620	675	737	811	895
73	219	345	473	531	638	700	744	820	909
92	247	351	487	536	641	705	759	822	914
97	255	358	488	541	642	713	760	825	929
119	269	362	492	563	649	714	780	826	970
129	298	393	494	570	651	723	786	837	983
146	304	430	496	572	654	724	803	841	988

5.4 Calibrated Results

The results of the above-described modeling workflow indicate that the history matching analysis using PEST++ IES successfully assimilated a wide range of historical water table shape and pumping test data towards conditioning the base T-field geostatistical realizations to best re-create observations. The results related to simulating each general observation type are discussed in detail below; generally, the history-matching process successfully adjusted the parameters coherently so that the simulation results appropriately reproduce the historical observations.

5.4.1 Steady-state Freshwater Heads

The steady-state freshwater heads overall fit relatively well, especially at wells located near or within the LWB (see location of wells in **Figure 2** in Task 2). Some wells near the model boundaries had a harder time fitting; as mentioned in Task 4 of this AP. Figures in Section 7.2 show histograms of each well's simulated freshwater head distribution and the noise applied to each observation. **Figure 24** shows the median steady-state head calculated from MODFLOW6 for the selected one-hundred realizations as contours across the model boundary and the observed steady-state freshwater heads for each of the 47 wells.

Information Only

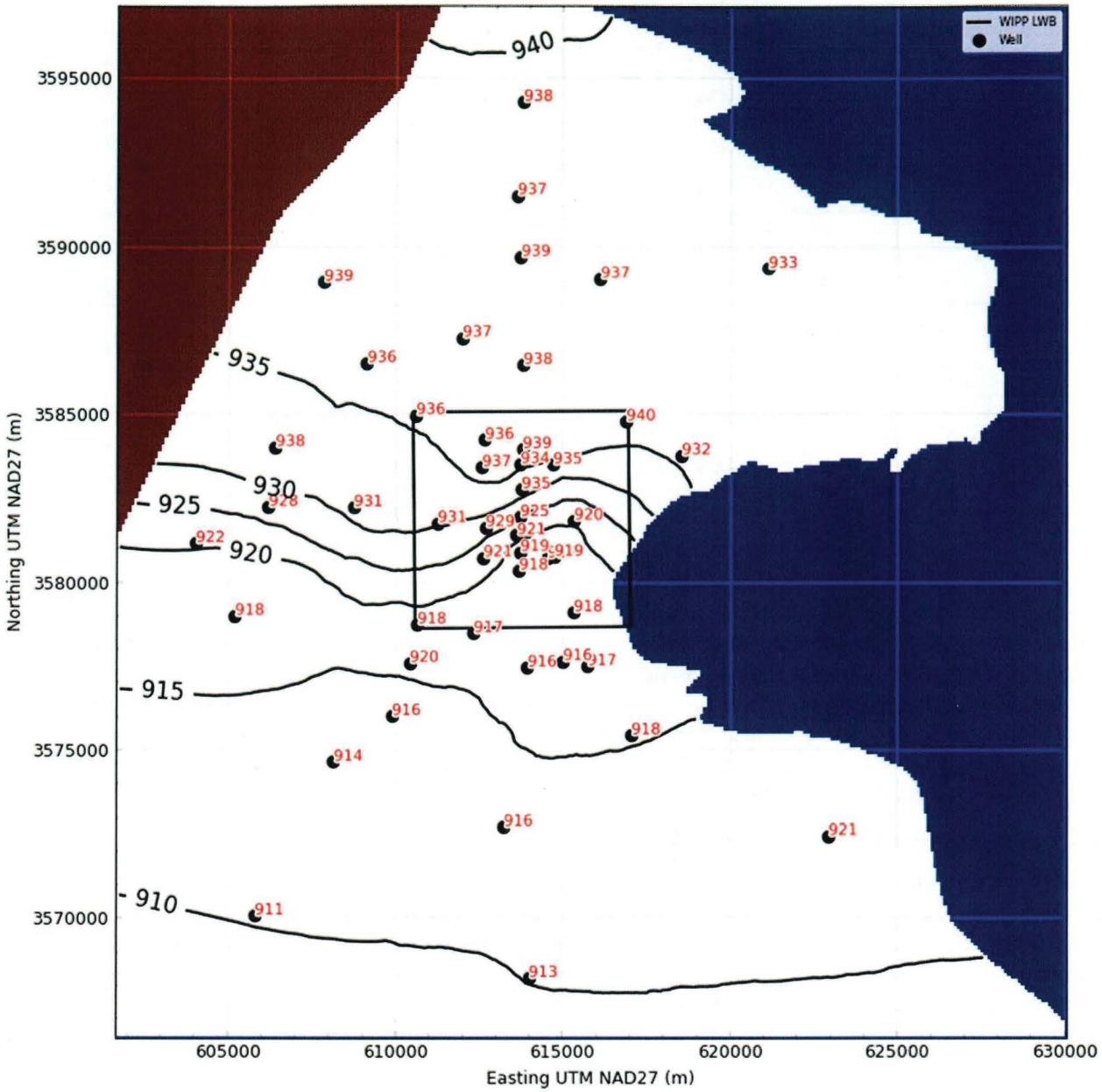

Figure 24. Contour of median steady-state freshwater head in meters above sea level in black. Mean, median, or mode of observed steady-state freshwater heads for each well are in red.

5.4.2 Simulated Multi-Well Pumping Tests

The one hundred selected realizations generally reproduced the observed spatial and temporal drawdown patterns for each multi-well pumping test. **Figure 94** through **Figure 130** in Appendix A Section 7.3 shows the observed vs. simulated drawdown for the ten multi-well pumping tests, where the distribution of simulated drawdown across the one hundred selected realizations are illustrated using violin plots.

5.4.3 Simulated Mills Ranch Pumping Event

As previously discussed, Mills Ranch pumping represents a previously unseen stress on the Culebra in its spatial distribution and drawdown magnitude. Hence, the observations associated with this event were

Information Only

assigned a high proportion of the measured objective function to give the observations a (consequently) significant importance during the history matching. In general, the analysis results, as represented by the one hundred selected realizations, have captured the observed system response to Mills Ranch pumping shown in **Figure 131** to **Figure 145** in Appendix A Section 7.4. Furthermore, the estimated groundwater extraction rate is consistent with prior expectations, and the magnitude is within the range of physically plausible values. **Figure 25** is a violin plot that represent the distribution of pumping for each pumping interval, and the width of each violin represents the length of time the well was actively pumping. The pumping rates before the winter 2015-2016 recovery event show, on average, a larger amount of pumping than the rates after the event, which would be consistent with the Mills Ranch wells' pump failing after pumping too hard.

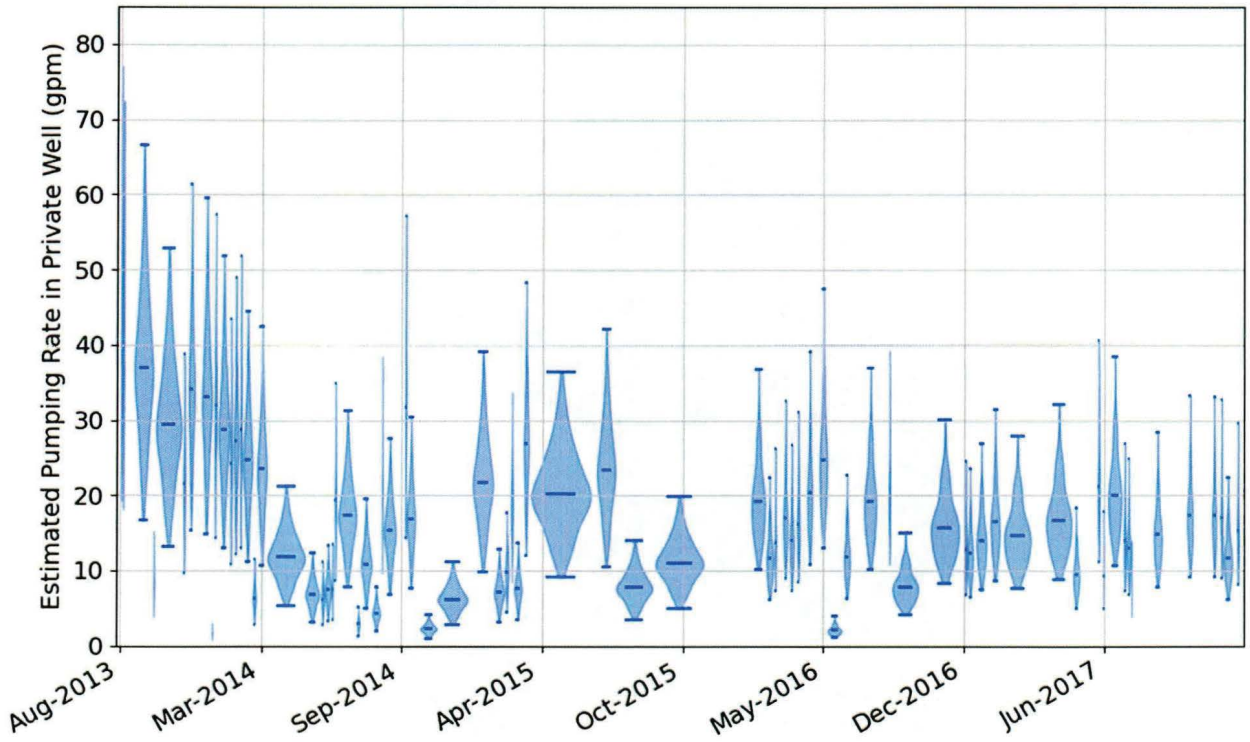

Figure 25. Distributions of Estimated Mills Ranch Pumping Rates for the 100 Selected Realizations

5.4.4 Final Transmissivity Fields

In general, the estimated transmissivity fields for the one hundred selected realizations present a spatially coherent and expected pattern of heterogeneity. The one hundred selected realizations also reproduce the single-well transmissivity estimates within the measurement noise caused by scaling effects resulting from the 100 m by 100 m grid size as shown in Section 5.4.8. The figures shown in this section describe the transmissivity, which is derived from the hydraulic conductivity (m/s) used by MODFLOW through multiplication by a thickness of 7.75 m. In Task 7 of AP-114 effective transmissivity or transmissivity in the X-direction as a product of transmissivity and horizontal anisotropy was reported rather than the "bulk transmissivity". In this report transmissivity and anisotropy are reported separately.

Figure 26 shows the standard deviation of transmissivity across the one hundred selected realizations. Zone 1 shows the most variability, as expected; however, the standard deviation in cells around the southwest portion of the LWB is much lower than most of this zone. This decrease in variability is due to the larger number of observations in this location, where well locations contain observations for both Mills Ranch

Information Only

and the steady-state heads. Small bullseyes of low variability also show up in this figure that are artifacts of the generation of the base T-fields produced in Task 5 of AP-114, for example, along the high-T channel extending south of the LWB. The low values of the mean transmissivity (**Figure 27**) around the same area of low variability shown in **Figure 26** indicate that the transmissivity in this area is predicted to be low with higher confidence.

Figure 28 and **Figure 29** show the number of high-T cells in the prior and Iteration 5 for the one hundred selected realizations. The cutoff value for "high-T" was set in Hart et al. (2008) to be the bulk transmissivity value of the base fields: -5.41 $\log_{10}$ m^2/s. **Figure 30** shows the change from the number of high-T cells in the prior to low-T cells in Iteration 5, and **Figure 31** shows the reverse. This analysis was calculated for each cell.

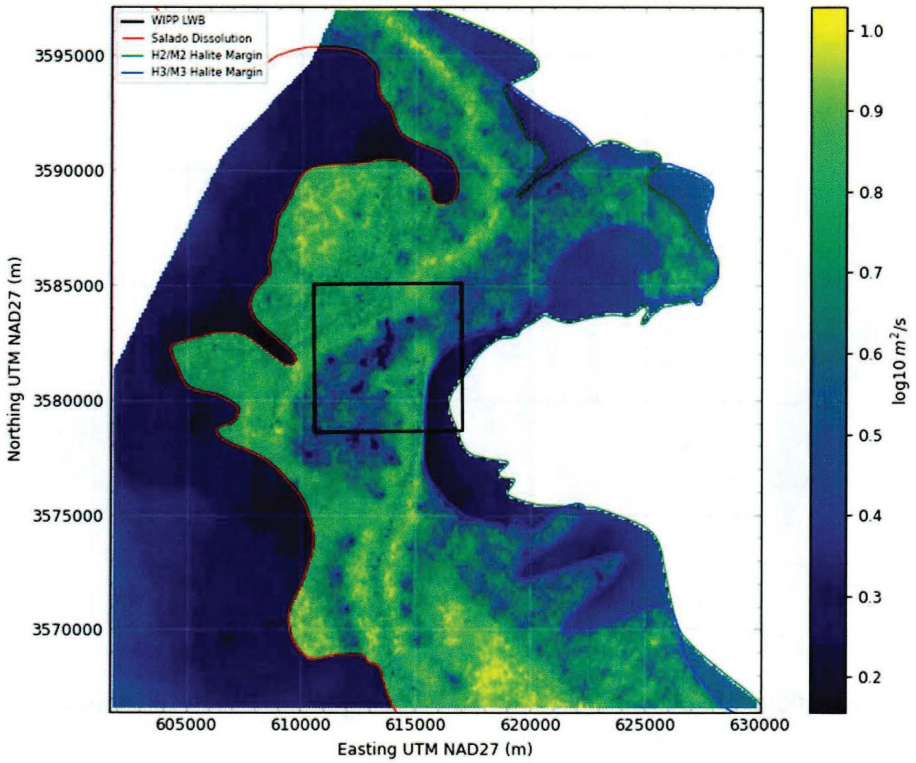

Figure 26. Standard Deviation of Transmissivity Across 100 Selected Realizations at Iteration 5

Information Only

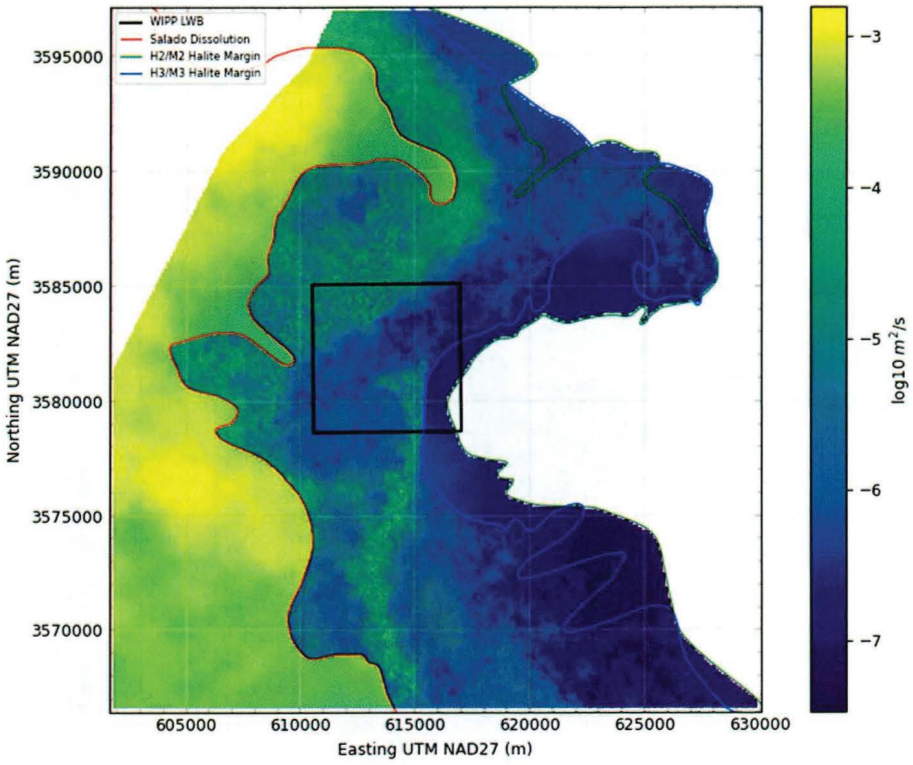

Figure 27. Mean Transmissivity Across 100 Selected Realizations at Iteration 5

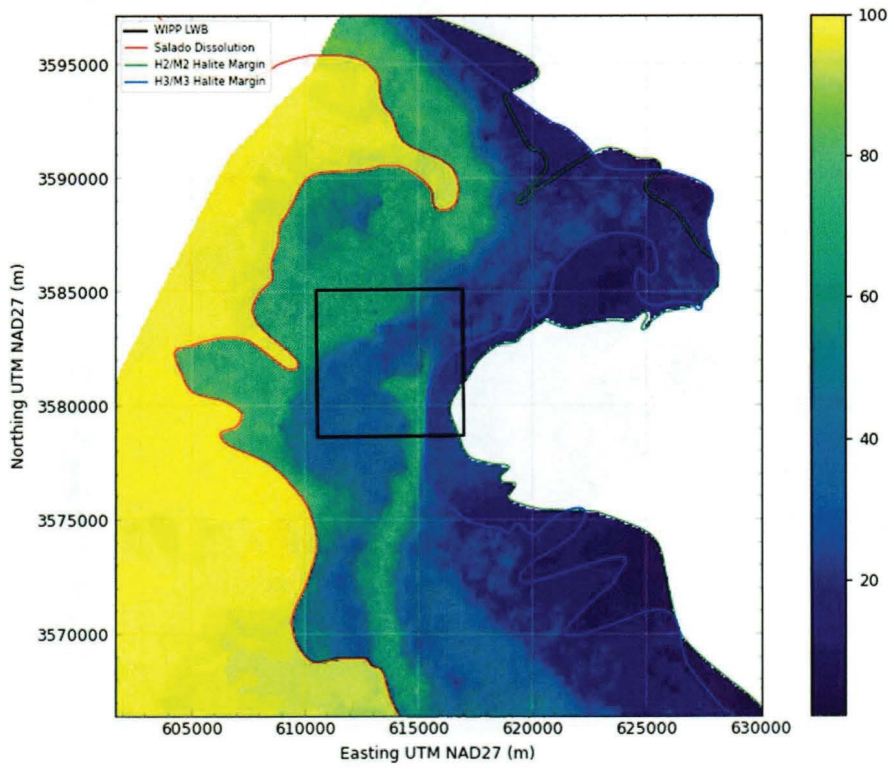

Figure 28. Count of "High-T" Zone Membership at Iteration 0

Information Only

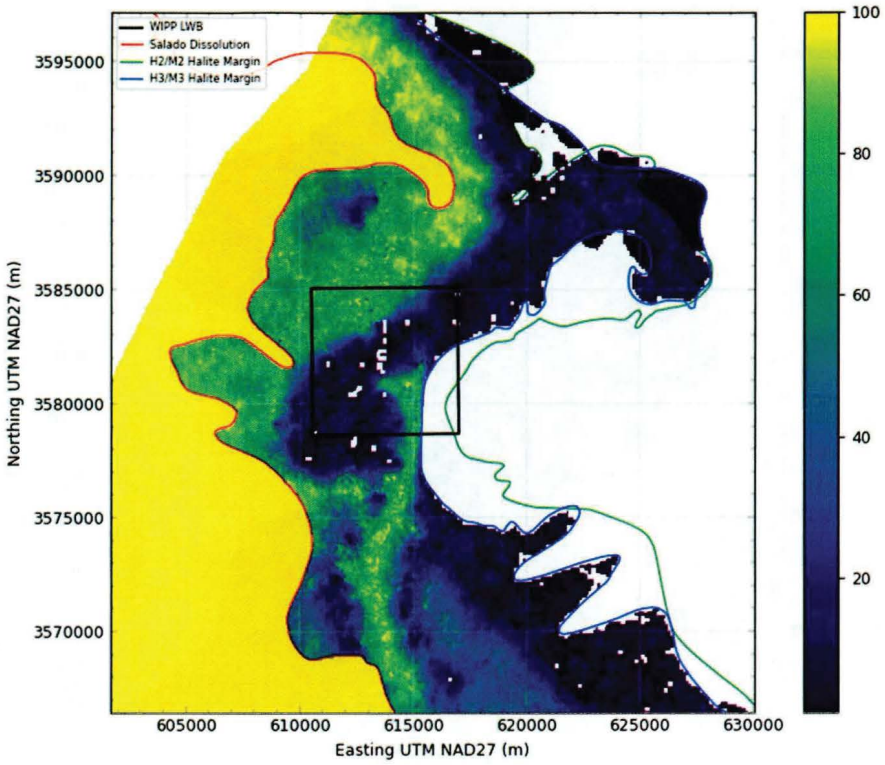

Figure 29. Count of "High-T" Zone Membership at Iteration 5

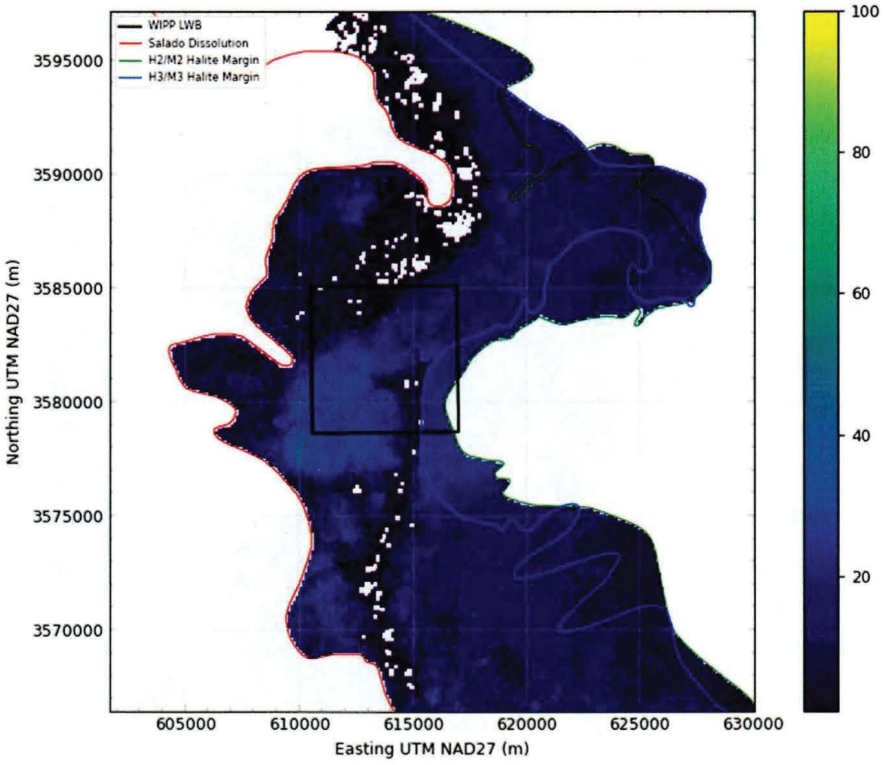

Figure 30. Change from High-T to Low-T Membership Between Iterations 0 and 5

Information Only

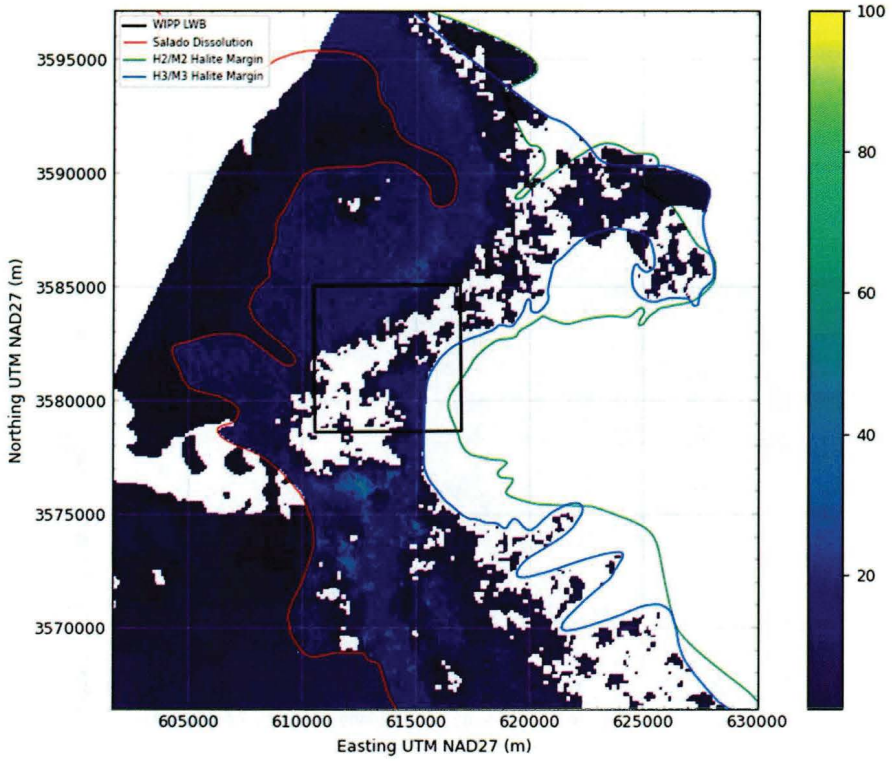

Figure 31. Change from Low-T to High-T Membership Between Iterations 0 and 5

5.4.5 Final Storativity Fields

The standard deviation and mean of the one hundred selected realizations for storativity are presented in **Figure 32** and **Figure 33**. The transition zone shows the largest variability of storativity across the 100 realizations, while the confined portion maintains the smallest variability across realizations (**Figure 32**). The mean storativity values indicate that the overall storativity values in the confined, transitional, and unconfined zones did not change much from the initial (i.e., central) values (**Figure 33**). Because the model was run as confined for all cells, including the unconfined zone, storativity is simply represented by specific storage (m^{-1}) multiplied by the thickness of 7.75 m.

Information Only

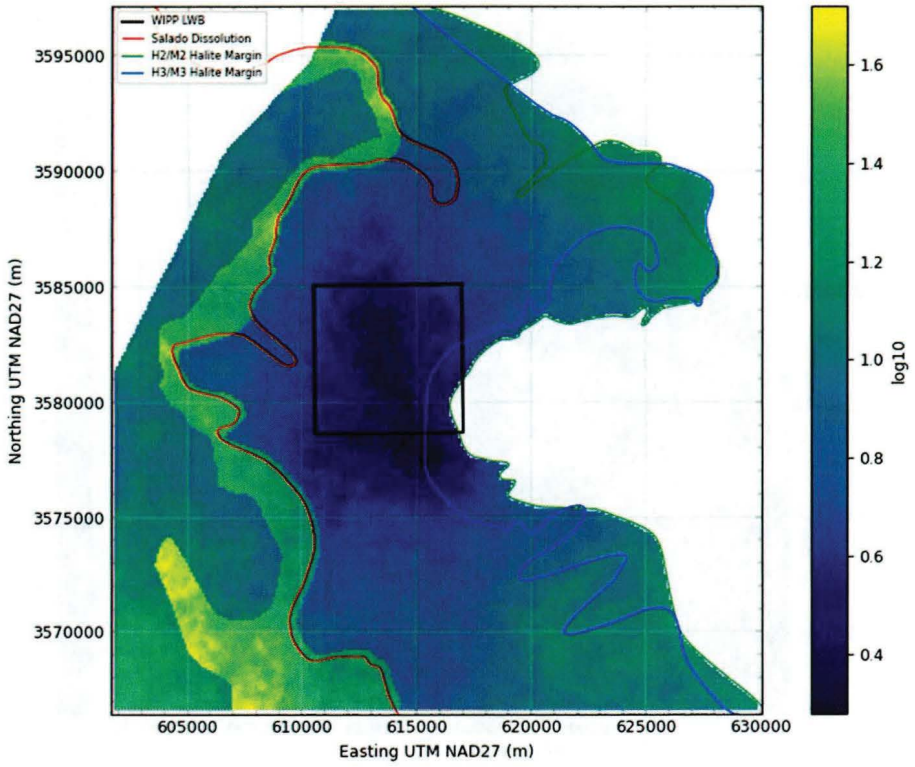

Figure 32. Standard Deviation of Storativity Across 100 Selected Realizations at Iteration 5

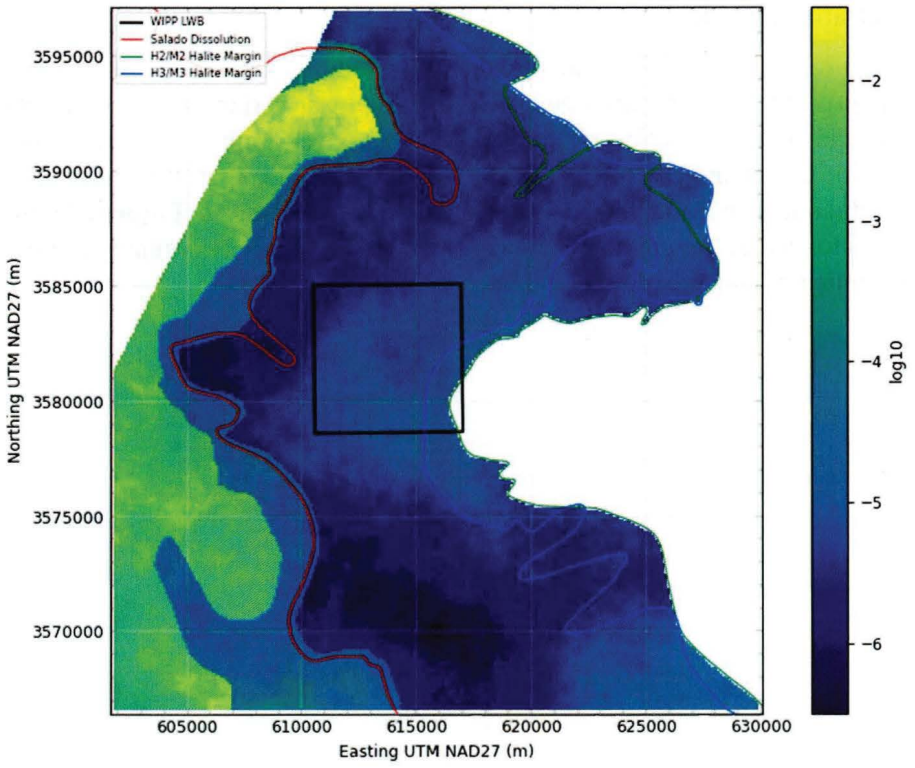

Figure 33. Mean Storativity Across 100 Selected Realizations at Iteration 5

Information Only

5.4.6 Final Anisotropy Fields

The standard deviation and mean of horizontal anisotropy for the final one hundred selected realizations are presented in **Figure 34** and **Figure 35**. In general, positive values of $\log_{10}$ horizontal anisotropy indicate a strong north-south anisotropy, while negative values of $\log_{10}$ anisotropy indicate strong east-west anisotropy. These maps show that in the high-T area (zone 1), there is generally a stronger north-south anisotropy.

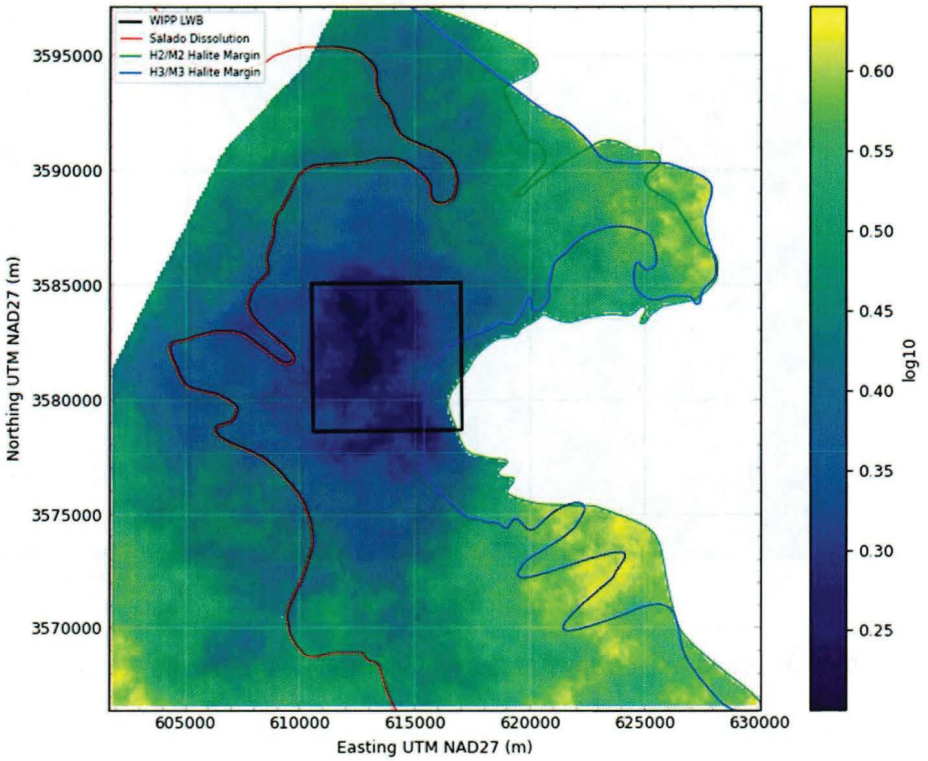

Figure 34. Standard Deviation of Anisotropy Across 100 Selected Realizations at Iteration 5

Information Only

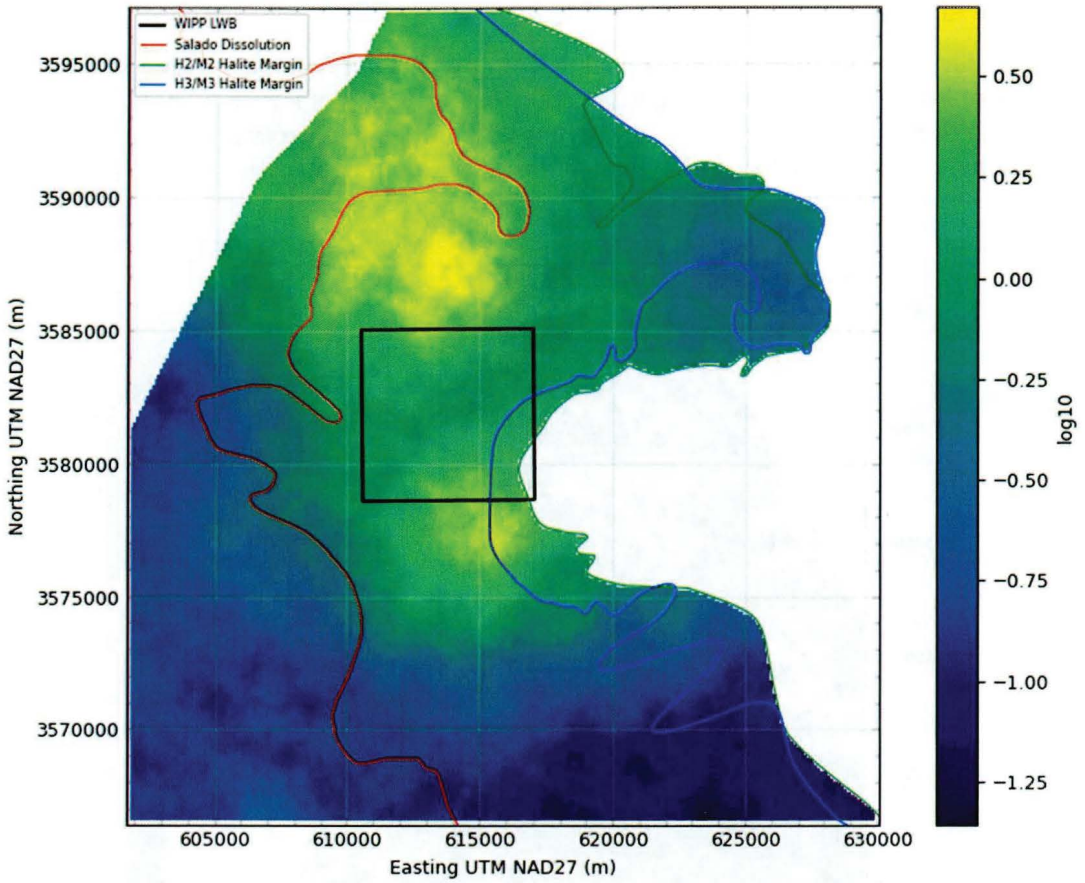

Figure 35. Mean Anisotropy Across 100 Selected Realizations at Iteration 5

5.4.7 Final Recharge fields

The final recharge values were all very small and with a maximum of 10^{-10} m/s (3.2×10^{-3} m/yr), as shown in **Figure 36**. Compared to other parameters, recharge was not allowed to vary as much, because it is known that there is not significant recharge to the Culebra. **Figure 37** and **Figure 38** show maps of the mean and standard deviation of recharge across the 100 selected realizations, where all the white cells represent no recharge.

Information Only

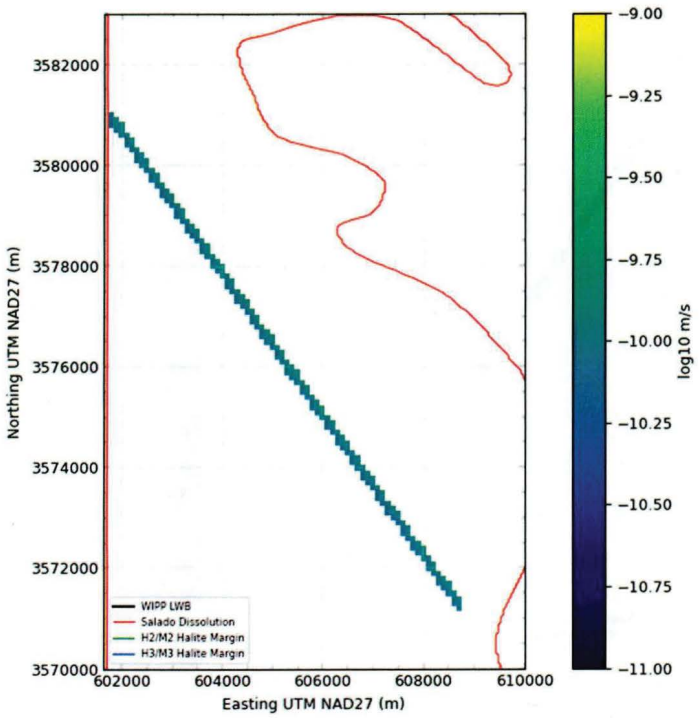

Figure 36. Maximum Recharge Across Final 100 Selected Realizations at Iteration 5

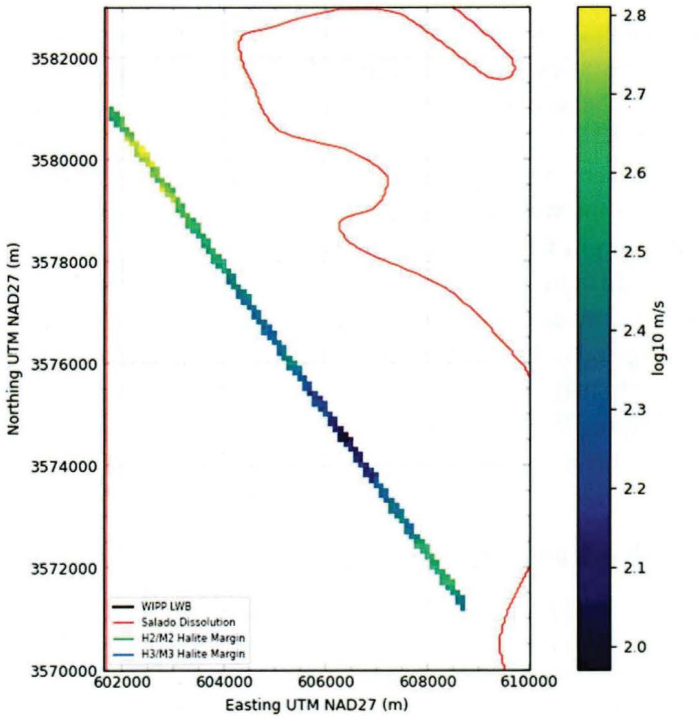

Figure 37. Standard Deviation of Recharge Across Final 100 Selected Realizations at Iteration 5

Information Only

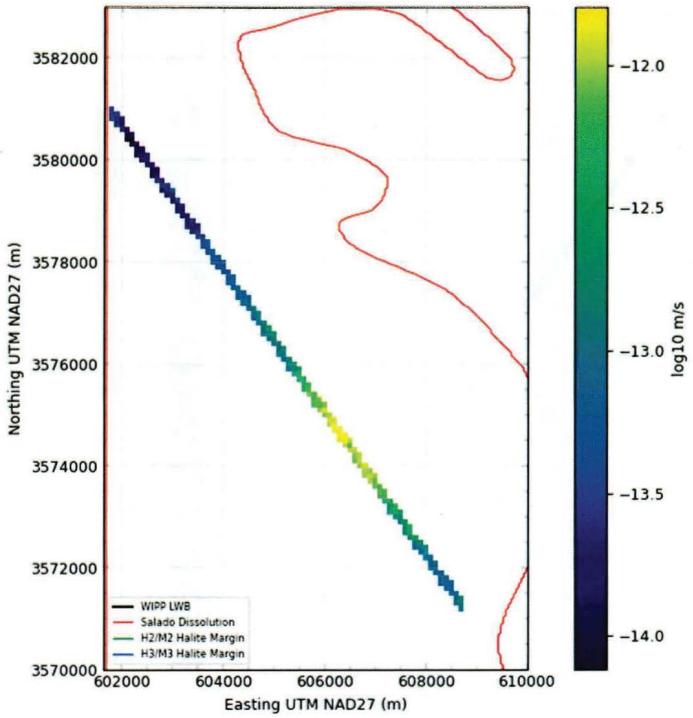

Figure 38. Mean Recharge Across Final 100 Selected Realizations at Iteration 5

5.4.8 Single Well Formation Performance Transmissivities

Overall, transmissivities sampled at the single well formation performance well locations did a good job at matching the estimated transmissivities shown in **Table** 5. The overall quality of the fit is due to the inclusion of transmissivity values incorporated in the generation of the base geostatistical transmissivity fields described in Task 5 of AP-114. PEST++ IES was therefore able to condition the realizations to maintain the measured transmissivity values in most wells, as shown in **Figure 146** to **Figure 208** in Appendix A Section 7.5. A few of the wells that were difficult to match such as H-15R, H-17, and SNL-15 were located close to the halite margin where the transmissivities were low, such as 1.0E-6 m^2/s and as low as 1.0E-13 m^2/s. WIPP-30 was difficult to match (as can be seen in **Figure 202**), however, this well is located in the Salado Dissolution Zone and far from the LWB, and was not included in the CRA-2009PABC calibration. As can be seen in **Figure 121** in Appendix A Section 7.3, high drawdown is being simulated in some cases of WIPP-30. It is likely that the low transmissivity estimate was causing too large of a response at the multi well pumping test from WIPP-11 which could have caused a conflict with the transmissivity value. This could also have been caused by the proximity of WIPP-30 to the no-flow boundary in the north-western portion of the model.

5.4.9 Calculation of Advective Transport Travel Time CDF

Particle tracking from a release point to the WIPP LWB is only done for flow field visualization and does not influence or create data used in the final performance assessment. Similar to Task 7 of AP-114, particle tracks were implemented in the forward model using the particle tracking code DTRKMF v1.02 DD/UM (Bowman, 2020b) to estimate the time required for a particle to reach the LWB. However, four starting points were used rather than a single point located at the center of the original WIPP panel footprint used in PABC09. These four Culebra Release Points (CRPs) are mapped out in **Figure 39** for reference (Bethune, 2022c). CRP1 is very close the PABC09 release point located at the center of panels 1-8. It was moved about 15 meters to the south to make it consistent with the input to the SECOTP2D transport model.

Information Only

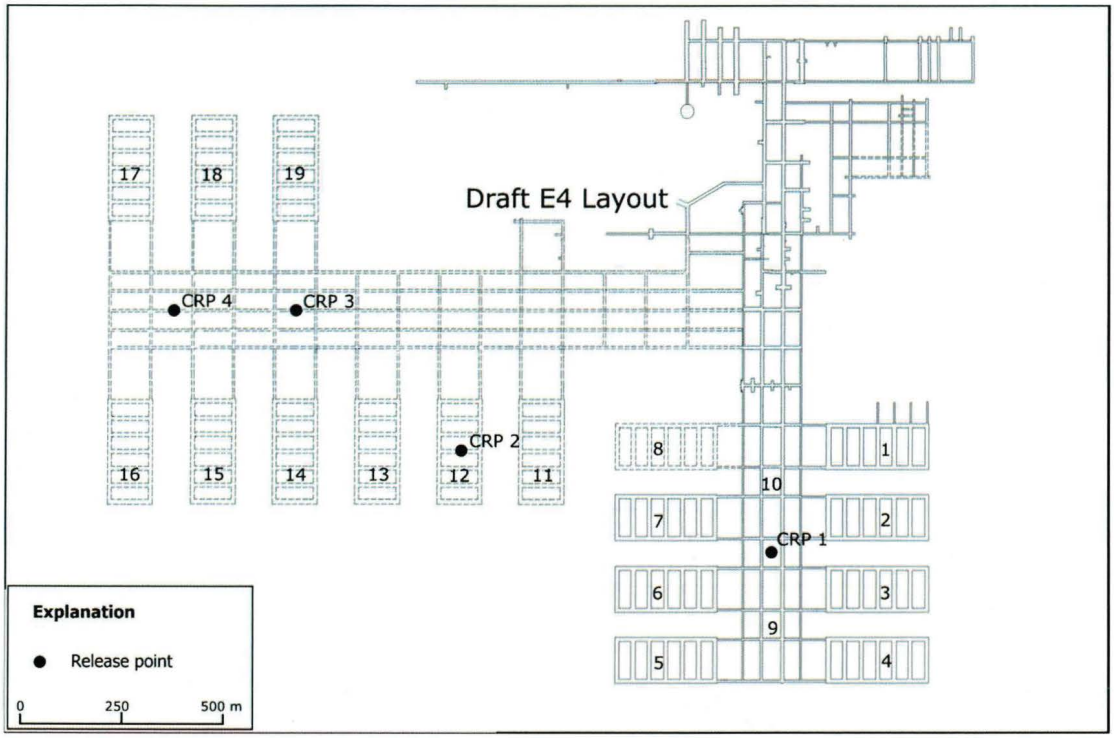

Figure 39. Four CRP Starting Point Locations on WIPP Layout (Figure from Bethune, 2022c)

Because DTRKMF was initially designed to work with MF2K output files, a Python script `cbb2dtrkmf.py` was written to convert the steady-state binary budget file (`mf6_head.cbb`) to the same MF2K style format DTRKMF expects to read. This process was included in the forward model, so the final particle travel time for each of the four release points was tracked for each realization.

The travel time calculation assumes a Culebra thickness of 4 m, and the porosity was held constant at 0.16 (mean value of the WIPP parameter CULEBRA:DPOROS). Because transport is mostly believed to occur in the lower 4-m of the Culebra, travel times were then scaled to a 4-m-thick Culebra (i.e., assuming all flux through the entire 7.75-m Culebra thickness was instead focused through only the lower 4 m of Culebra.), as discussed in the CCA Appendix MASS (MASS Attachment 15-6). Travel times were recorded as zero-weighted observations, so they have no effect on the calibration process. **Table 14** shows particle travel time statistics for each CRP for the 100 selected realizations in Iteration 5, while **Table 15** to **Table 18** show particle travel time statistics for all the realizations and iterations, grouped by CRP.

Table 14. Particle Travel Times to the LWB for 100 Selected Realizations at Iteration 5

	Particle Travel Time (Years)			
CRP	**Min**	**Max**	**Mean**	**Median**
CRP 1	1,806	103,974	26,510	20,276
CRP 2	4,409	158,675	48,943	42,600
CRP 3	11,596	284,218	71,858	62,784
CRP 4	10,325	224,211	92,304	83,945

Information Only

Table 15. Particle Travel Times to the LWB for All the Realizations for CRP1

Iteration	Particle Travel Time for All Realizations (Years)			
	min	max	mean	Median
1	2.42E+02	5.30E+07	5.81E+05	8.10E+04
2	2.91E+02	2.81E+07	2.61E+05	4.62E+04
3	4.20E+02	9.42E+06	1.20E+05	4.10E+04
4	1.62E+03	4.54E+06	6.56E+04	3.74E+04
5	1.81E+03	5.28E+05	3.32E+04	2.50E+04
6	2.24E+03	3.81E+05	2.76E+04	2.21E+04
7	2.69E+03	2.41E+05	2.54E+04	2.04E+04

Table 16. Particle Travel Times to the LWB for All the Realizations for CRP2

Iteration	Particle Travel Time for All Realizations (Years)			
	min	max	mean	median
1	1.23E+02	3.65E+07	6.56E+05	1.16E+05
2	2.40E+02	2.95E+07	3.05E+05	7.00E+04
3	4.84E+02	9.58E+06	1.73E+05	7.06E+04
4	1.30E+03	4.46E+06	9.81E+04	6.68E+04
5	2.79E+03	3.00E+05	5.78E+04	4.93E+04
6	4.27E+03	2.60E+05	5.08E+04	4.37E+04
7	4.93E+03	2.51E+05	4.82E+04	4.12E+04

Table 17. Particle Travel Times to the LWB for All the Realizations for CRP3

Iteration	Particle Travel Time for All Realizations (Years)			
	min	max	mean	median
1	1.11E+02	5.74E+07	8.26E+05	1.30E+05
2	2.09E+02	4.97E+07	3.68E+05	8.69E+04
3	4.17E+02	7.13E+06	2.01E+05	9.23E+04
4	1.11E+03	5.52E+06	1.40E+05	9.75E+04
5	3.33E+03	4.02E+05	8.44E+04	7.22E+04
6	7.01E+03	3.35E+05	7.45E+04	6.46E+04
7	8.99E+03	3.80E+05	7.15E+04	6.15E+04

Information Only

Table 18. Particle Travel Times to the LWB for All the Realizations for CRP4

Iteration	Particle Travel Time for All Realizations (Years)			
	min	max	mean	median
1	8.83E+01	6.29E+07	8.46E+05	1.30E+05
2	1.71E+02	4.96E+07	3.78E+05	8.77E+04
3	3.61E+02	7.16E+06	2.15E+05	9.68E+04
4	1.02E+03	6.94E+06	1.68E+05	1.22E+05
5	2.52E+03	5.13E+05	1.04E+05	9.02E+04
6	5.67E+03	3.49E+05	8.72E+04	7.76E+04
7	7.02E+03	3.33E+05	8.24E+04	7.25E+04

The cumulative distribution of particle travel time for the four CRPs for the 100 selected realizations and for all the realizations in Iteration 5 are shown respectively in **Figure 40** and **Figure 41**. The cumulative distributions of particle travel time for all the realizations and for each iteration, grouped by CRP, are shown in **Figure 42** to **Figure 45**.

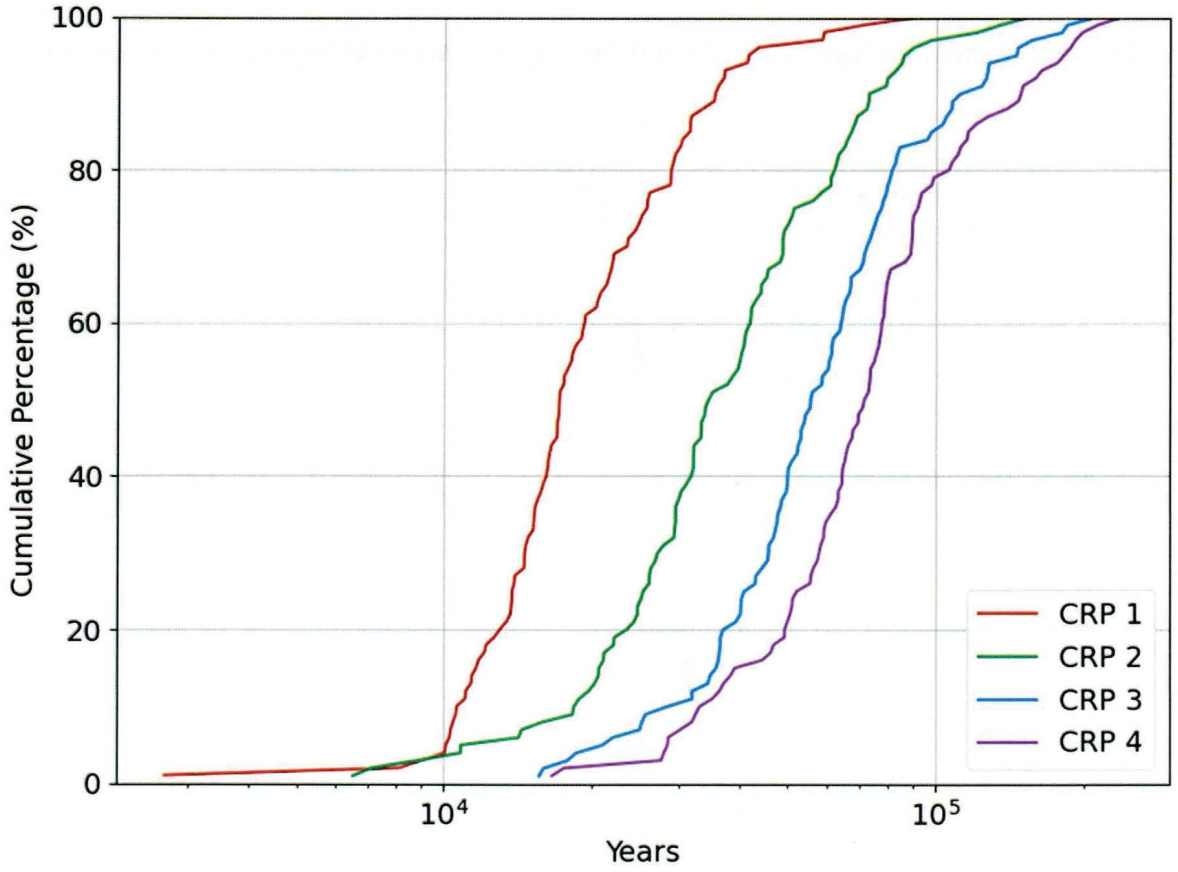

Figure 40. Cumulative Distribution of Travel Times to the LWB for 100 Selected Realizations at Iteration 5

Information Only

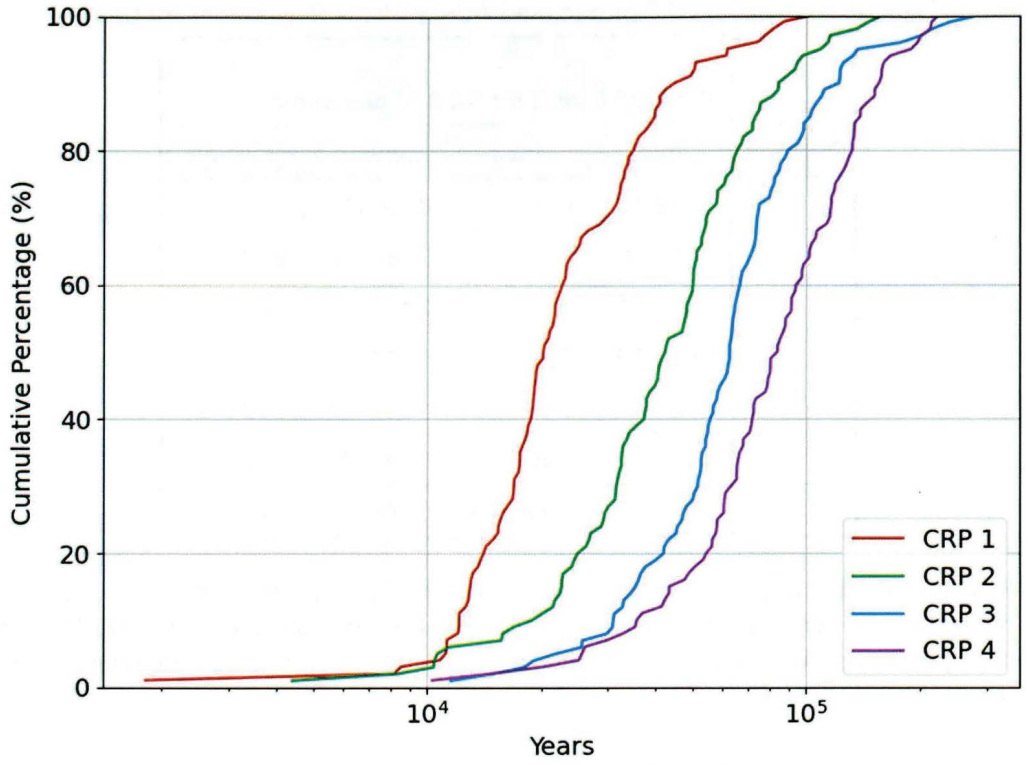

Figure 41. Cumulative Distribution of Travel Times to the LWB for All Realizations at Iteration 5

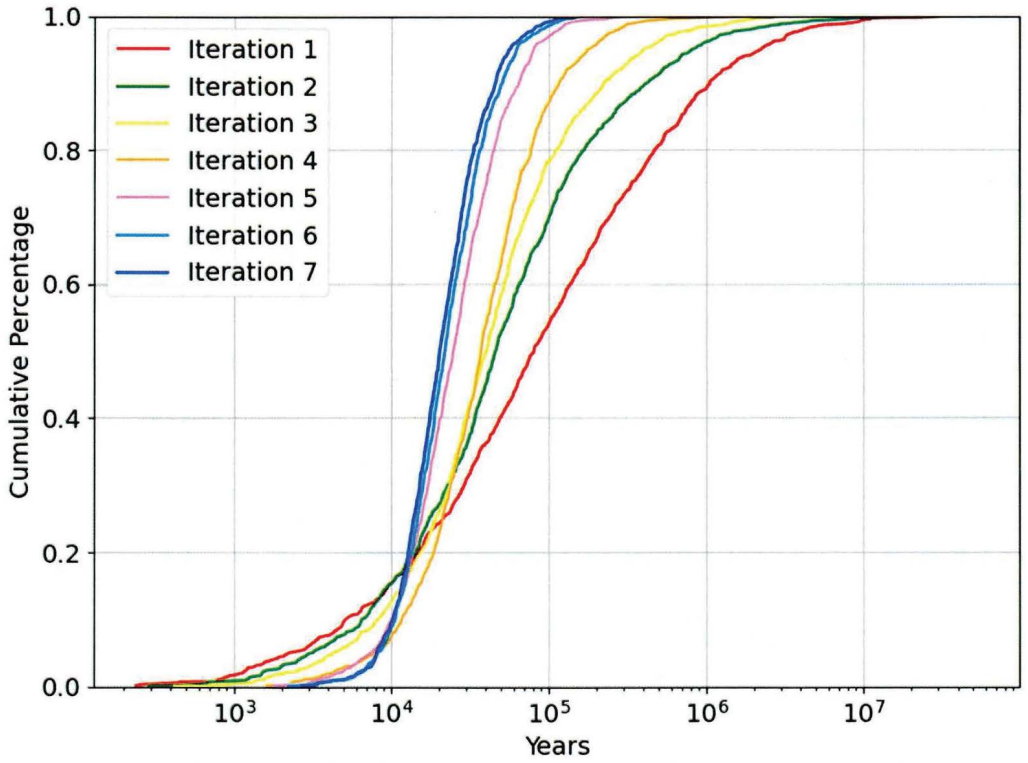

Figure 42. Cumulative Distribution of Travel Times to the LWB for All Realizations for CRP 1

Information Only

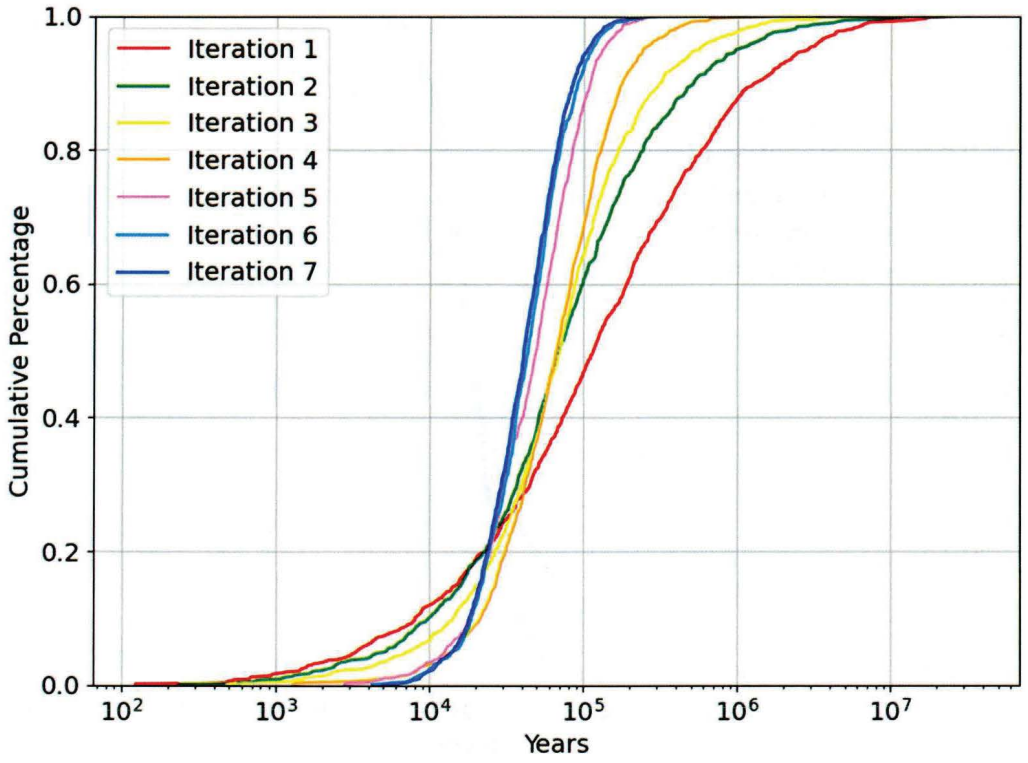

Figure 43. Cumulative Distribution of Travel Times to the LWB for All Realizations for CRP 2

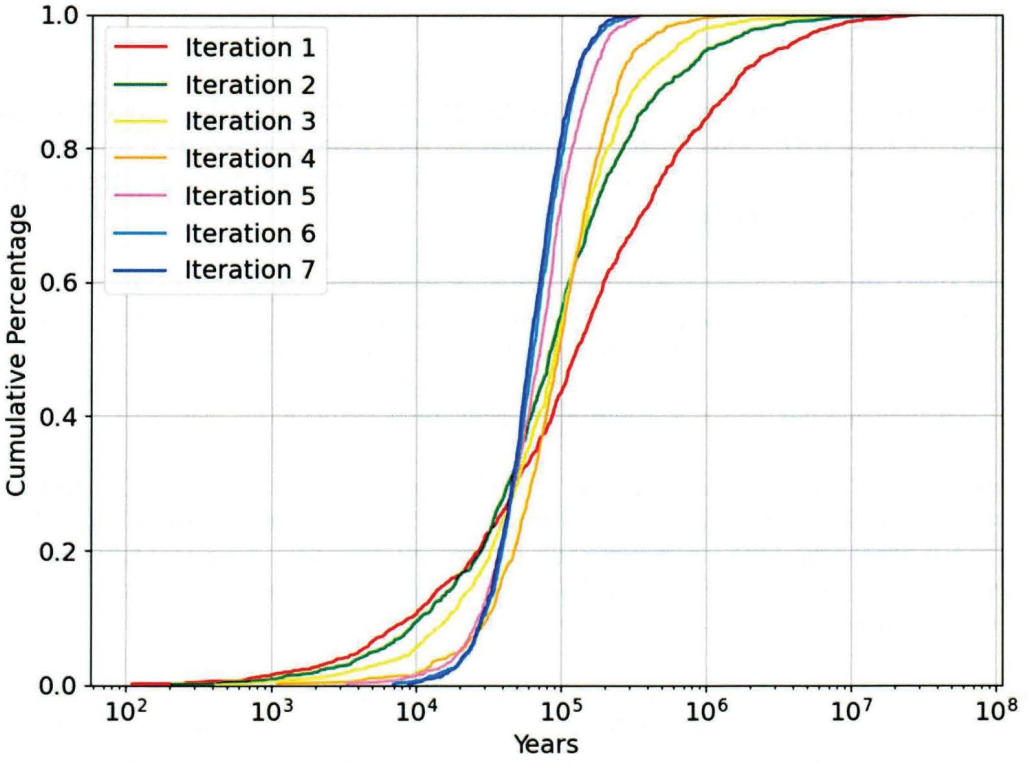

Figure 44. Cumulative Distribution of Travel Times to the LWB for All Realizations for CRP 3

Information Only

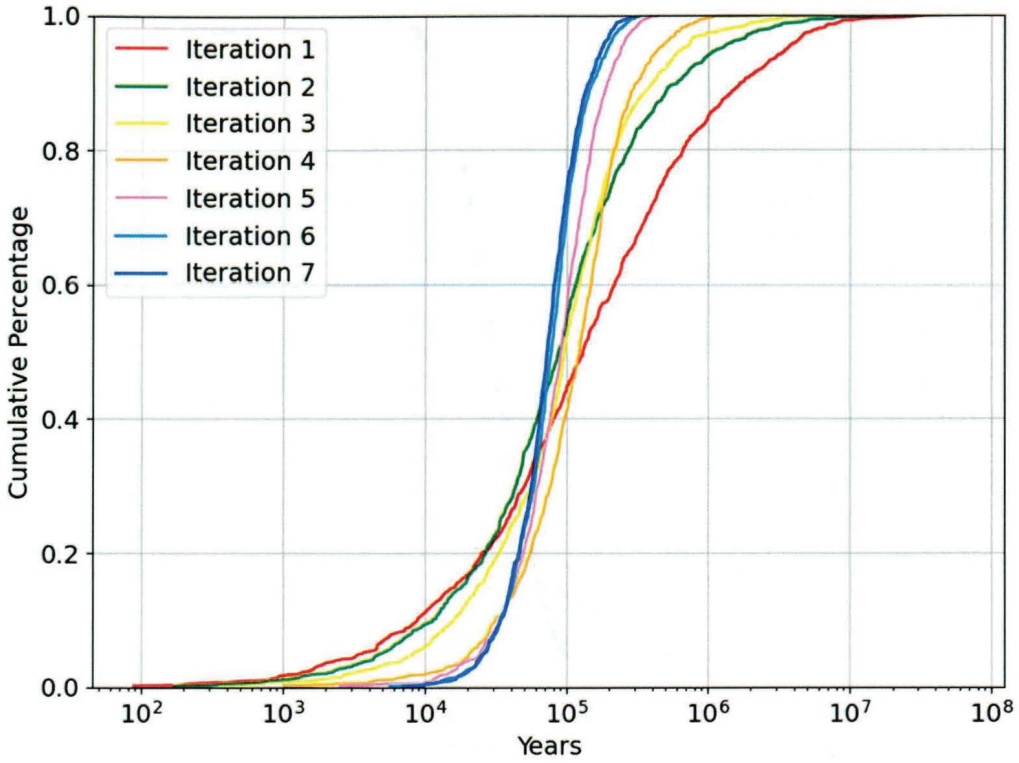

Figure 45. Cumulative Distribution of Travel Times to the LWB for All Realizations for CRP 4

Figure 46 compares the CRP1 results to CRA-2009PABC (CRA 2010 in the legend), CRA-2004, and CCA results. In brief, the CRP1 travel times are similar in range to the CRA-2004 travel times, and slower than both CRA-2014 and CCA travel times. To add some historical context to these differences, DOE (2009) notes that the travel times are:

"two to three times as long in the CRA-2004 fields as in the CCA fields. Considering the degree of uncertainty involved in characterizing a geologic medium on the scale of the T fields, a factor of two or three difference in travel-time CDFs represents excellent agreement."

DOE (2014), when discussing the CRA-2009PABC travel time results notes that:

"The non-mined travel times from the center of the WIPP waste panels to the WIPP LWB are similar to those computed for the CCA and therefore faster than those computed for the CRA-2004 PABC. The decrease in travel time to the LWB can be attributed to the presence of a consistent high-transmissivity pathway leaving the south-east portion of the LWB. The presence of this pathway is supported by observed drawdown data from the SNL-14 pumping test."

As discussed in Section 5.4.4 of the current report, the final calibrated transmissivity fields for CRA-2024 retained the high-transmissivity pathway referenced in DOE (2014) and reproduced in the base transmissivity fields from Task 5 of AP-114. So, the increase in travel time to LWB in CRA-2024 was more likely due to the influence of the calibration to the Mills Ranch pumping event on transmissivities inside and near the LWB, as well as calibration to additional steady-state head calibration targets. While

Information Only

the updated software (newer versions of MODFLOW and PEST) made the process of calibration and uncertainty propagation more efficient, these updates alone should not significantly affect the overall results.

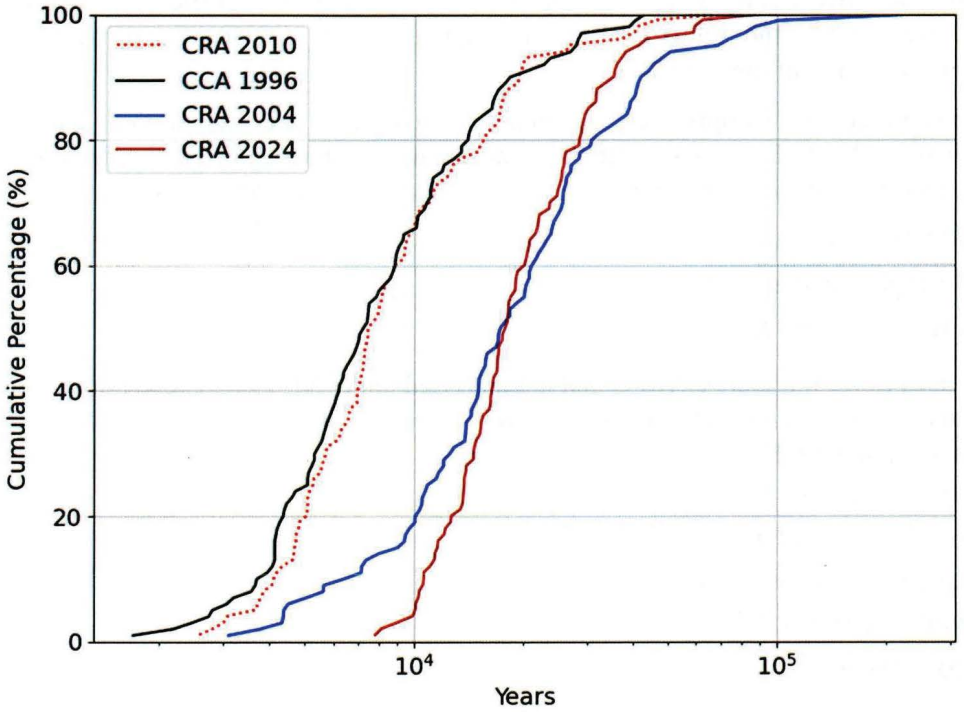

Figure 46. Cumulative Distribution of Travel Times to the LWB for CRP1 for Previous and Current Work

Information Only

5.5 Run Control, Software, and Hardware

This analysis was performed on multiple computers and operating systems before the final QA runs were executed and required that the workflow was general enough to use on any system. This run control was performed by using two elements. The first was to use a repository for all files that were part of this task. The second was to use the run-control shell script `launch_master_slurm.sh` to execute the calibration and selection of the final T-fields.

Pre- and post-processing scripts were written for this task, and the source codes are stored at /data/cvs/CVSLIB/WIPP_EXTERNAL/ap203/. The acquired and developed software programs used in the calibration process were qualified under NP 19-1, and can be found below:

- MODFLOW6 – version 6.2.2
- PEST++ IES – version 5.1.6
- DTRKMF – version 1.02

Python was used as off the shelf software and not qualified under NP 19-1. The version number for Python and Python packages used for this analysis are listed below:

- Python – version 3.6.8
  - Pandas – version 1.1.4
  - Numpy – version 1.19.4
  - Matplotlib - version 3.3.3
  - Pyemu – version 1.2.0
  - Flopy – version 3.3.5

5.5.1 Repository

The repository that was used for this task is located at /data/cvs/CVSLIB/WIPP_EXTERNAL/ap203/. This repository contains several static and predefined input files used by the calibration and previous tasks.

5.5.2 Hardware Systems Used

A single Linux cluster was used in the calibration process: the FWM Linux cluster in Carlsbad, New Mexico.

5.5.3 Run Control

A thorough description of how to launch the calibration process is described in the README.md file on the main page of the repository - /data/cvs/CVSLIB/WIPP_EXTERNAL/ap203/.

Information Only

6. References

Bakker, M., Post, V., Langevin, C.D., Hughes, J.D., White, J.T., Starn, J.J. and Fienen, M.N., 2016, Scripting MODFLOW Model Development Using Python and FloPy: Groundwater, v. 54, p. 733–739, doi:10.1111/gwat.12413.

Beauheim, R.L., 1987a, "Analysis of Pumping Tests of the Culebra Dolomite Conducted at the H-3 Hydropad at the Waste Isolation Pilot Plant (WIPP) Site", SAND86-2311, Sandia National Laboratories.

Beauheim, R.L., 1987b, "Interpretation of the WIPP-13 Multipad Pumping Test of the Culebra Dolomite at the Waste Isolation Pilot Plant (WIPP) Site", SAND87-2456, Sandia National Laboratories.

Beauheim, R.L., 1989, "Interpretation of H-11b4 Hydraulic Tests and the H-11 Multipad Pumping Test of the Culebra Dolomite at the Waste Isolation Pilot Plant (WIPP) Site", SAND89-0536, Sandia National Laboratories.

Beauheim, R.L. & Ruskauff, G.J., 1998, "Analysis of Hydraulic Tests of the Culebra and Magenta Dolomites and Dewey Lake Redbeds Conducted at the Waste Isolation Pilot Plant Site", SAND98-0049, Sandia National Laboratories.

Beauheim, R.L., 2002, "Analysis Plan for Evaluation of the Effects of Head Changes on Calibration of Culebra Transmissivity Fields, AP-088, Revision 1". December 6, 2002. Sandia National Laboratories.

Bethune, J.C. 2022a, "Addendum to the Design Document and User's Manual for PEST ++ Version 5.1.6". Sandia National Laboratories. Carlsbad, NM. ERMS 576753.

Bethune, J.C. 2022b, "Requirements Document, Verification and Validation Plan, and Validation Document for PEST++ Version 5.1.6". Sandia National Laboratories. Carlsbad, NM. ERMS 576751.

Bethune, J.C. 2022c, "Culebra Transport Analysis Report for the RPPA". Sandia National Laboratories, Carlsbad, NM. ERMS 577307.

Bowman, D.O., 2009, "Analysis of Culebra and Magenta Hydraulic Tests Performed Between January 2005 and August 2008," February 2009, ERMS 550906, Sandia National Laboratories.

Bowman, D.O., 2013, "Analysis of the H-11b4R Pumping Test Conducted From 6/11/12 to 6/14/12," September 13, 2013, ERMS 560942, Sandia National Laboratories.

Bowman, D.O., 2014, "Analysis of the H-9bR Pumping Test Conducted from 8/6/12 to 8/22/12," July 2, 2014, ERMS 562291, Sandia National Laboratories.

Bowman, D.O., 2015a, "Analysis of the AEC-7R Pumping Test Conducted from 3/9/15 to 3/13/15," September 2015, ERMS 564693, Sandia National Laboratories.

Bowman, D.O., 2015b, "Analysis of the H-12R Pumping Test Conducted from 4/20/15 to 4/22/15," September 2015, ERMS 564697, Sandia National Laboratories.

Bowman, D.O., 2016, "Analysis of the IMC-461 Sinusoidal Test Conducted from 6/6/16 to 6/9/16,"

Information Only

September 14, 2016, ERMS 566972, Sandia National Laboratories.

Bowman, D.O., 2017, "Analysis of the H-10cR Pumping Test Conducted from 7/24/17 to 7/27/17," September 26, 2017, ERMS 568762, Sandia National Laboratories.

Bowman, D.O., 2019. "Milestone Report for Calculated Steady-State Heads for the WIPP Monitoring Wells for Updated Freshwater Head Comparisons", September 23, 2019. Sandia National Laboratories.

Bowman, D.O., 2020a, "Analysis of the H-15R Pumping Test Conducted from 1/19/09 to 1/22/09," May 28, 2020, ERMS 573484, Sandia National Laboratories.

Bowman, D.O., 2020b, "DTRKMF Version 1.02 Design Document and User's Manual." Carlsbad, NM: Sandia National Laboratories. ERMS #574327.

Bowman, D.O., 2021, "Milestone HYDRO-21-01: Milestone report that reviews progress made on the WIPP Integrated Hydrology Program Plan in FY2020," March 19, 2021, Sandia National Laboratories.

Bowman, D.O., 2022, "Analysis Plan for Evaluation and Recalibration of Culebra Transmissivity Fields, AP-203, Revision 0." December 6, 2022. Sandia National Laboratories. ERMS 578663.

Brunell, S. 2022a, Addendum to the User's Manual for MODFLOW6 Version 6.2.2. Sandia National Laboratories. Carlsbad, NM. ERMS 576747.

Brunell, S. 2022b, Requirements Document, Verification and Validation Plan, and Validation Document for MODFLOW6 Version 6.2.2. Sandia National Laboratories. Carlsbad, NM. ERMS 576745.

Chen, Y. and Oliver, D.S., 2013, Levenberg–Marquardt forms of the iterative ensemble smoother for efficient history-matching and uncertainty quantification. Computational Geosciences. 17(4), 689–703.

Doherty, J, 2004, "PEST: Model Independent Parameter Estimation. User's Manual: 5th Edition", Watermark Numerical Computing.

Doherty, J., and D.E. Welter, 2010, A short exploration of structural noise. Water Resources Research 46, no. 5: W05525. https://doi.org/10.1029/2009WR008377

Farinacci, M. and Bowman, D.O., 2022, "Analysis Report Documenting Water Level Analysis, Revision 1, Analysis Report for AP-150, Analysis Plan for the Analysis of Observed Water Level Fluctuations." September 2022, Sandia National Laboratories.

Freyberg, D. L., 1988. An exercise in ground-water model calibration and prediction. Groundwater, 26(3), 350-360.

Hart, D.B., Holt, R.M., & McKenna, S.A., 2008, Analysis report for Task 5 of AP-114: Generation of revised base transmissivity fields (pp. 122). Carlsbad, NM: Sandia National Laboratories.

Hart, D.B., Beauheim, R.L., & McKenna, S.A., 2009, Analysis report for Task 7 of AP-114: Calibration of Culebra transmissivity fields (pp. 187). Carlsbad, NM: Sandia National Laboratories

Information Only

Holt, R.M., 1997, "Conceptual Model for Transport Processes in the Culebra Dolomite Member, Rustler Formation", SAND97-0194, Sandia National Laboratories, Albuquerque, NM.

Hughes, J.D., Langevin, C.D., and Banta, E.R., 2017, Documentation for the MODFLOW6 framework: U.S. Geological Survey Techniques and Methods, book 6, chap. A57, 40 p., https://doi.org/10.3133/tm6A57.

Hunt, R. J., Fienen, M. N., & White, J. T., 2020. Revisiting "an exercise in groundwater model calibration and prediction" after 30 years: Insights and new directions. Groundwater, 58(2), 168-182.

Kuhlman, K.L. 2009. AP-144 Analysis Plan for the Calculation of Culebra Flow and Transport for CRA2009PABC. Carlsbad, NM: Sandia National Laboratories. ERMS 551676.

Kuhlman, K.L. 2010. Analysis Report for the CRA-2009 PABC Culebra Flow and Transport Calculations (AP-144). Carlsbad, NM: Sandia National Laboratories. ERMS 552951.

Kuhlman, K.L., & Corbet, T.F., 2017, WIPP Milestone Report: 2016 Culebra Groundwater Level Fluctuations. 2017. Sandia National Laboratories.

Langevin, C.D., J.D. Hughes, E.R. Banta, R.G. Niswonger, S. Panday, and A.M. Provost, 2017, Documentation for the MODFLOW 6 Groundwater Flow Model. U.S. Geological Survey. Reston, VA. https://doi.org/10.3133/tm6A55.

McKenna, S.A. & Hart, D.B., 2003, "Analysis Report for Task 4 of AP-088: Conditioning of Base T fields to Transient Heads", ERMS# 531124, Sandia National Laboratories WIPP Records Center, Carlsbad, NM.

PEST++ Development Team, 2021. "Documentation for PEST++ Version 5.1.6". https://github.com/usgs/pestpp/blob/5.1.6/documentation/pestpp_users_guide_v5.1.6.docx

Powers, D.W., Holt, R.M., Beauheim, R.L., & Richardson, R.G., 2006, Advances in depositional models of the Permian Rustler Formation, southeastern New Mexico. In L. Land, V. W. Lueth, W. Raatz, P. Boston, & D. W. Love (Eds.), New Mexico geological society guidebook, 57th field conference, caves and karst of southeastern New Mexico (pp. 267–276). Albuquerque, NM: New Mexico Geological Society.

Powers, D.W., S.J. Lambert, S-E. Shaffer, L.R. Hill, and W.D. Weart, eds. 1978. Geological Characterization Report, Waste Isolation Pilot Plant (WIPP) Site, Southeastern New Mexico. SAND78-1596. Albuquerque, NM: Sandia National Laboratories. Vols. 1-2. WPO 5448-Vol. 1, WPO 26829-26530 (Vol. 2)

Roberts, R.M., 2006, "Analysis Report for AP-070, Analysis of Culebra Pumping Tests Performed Between December 2003 and August 2005", ERMS# 543901, Sandia National Laboratories WIPP Records Center, Carlsbad, NM.

Theis, C.V., 1935. The relation between the lowering of the piezometric surface and the rate and duration of discharge of a well using groundwater storage, Am. Geophys. Union Trans., vol. 16, pp. 519-524.

Information Only

Thomas M.A., Kuhlman K.L., Ward A.L., 2017. Anthropogenic influences on groundwater in the vicinity of a long-lived radioactive waste repository. Hydrological Processes, 31(41):2637–2647.

Toll, N.J. & Johnson, P.B., 2006a, "Routine Calculations Report In Support of Task 6 of AP-114, SNL-14 August 2005 Pumping Test Observation Well Data Processing, Summary of Files", ERMS# 543371, Sandia National Laboratories WIPP Records Center, Carlsbad, NM.

Toll, N.J. & Johnson, P.B., 2006b, "Routine Calculations Report In Support of Task 6 of AP-114, WIPP-11 February 2005 Pumping Test Observation Well Data Processing – Summary of Files", ERMS# 543651, Sandia National Laboratories WIPP Records Center, Carlsbad, NM.

U.S. Department of Energy (DOE), 1996. Title 40 CFR Part 191 Compliance Certification Application for the Waste Isolation Pilot, Appendix TFIELD. Carlsbad, NM: U.S. Department of Energy Waste Isolation Pilot Plant, Carlsbad Area Office. DOE/CAO-1996-2184.

U.S. Department of Energy (DOE), 2004. Title 40 CFR Part 191 Subparts B and C Compliance Recertification Application for the Waste Isolation Pilot Plant, Appendix TFIELD. Carlsbad, NM: US Department of Energy Carlsbad Field Office. DOE/WIPP 2004-3231.

U.S. Department of Energy (DOE). 2009. Title 40 CFR Part 191 Subparts B and C Compliance Recertification Application for the Waste Isolation Pilot Plant. Appendix TFIELD-2009, Transmissivity Fields. Carlsbad, NM: US Department of Energy Carlsbad Field Office. DOE/WIPP 2009-3424.

U.S. Department of Energy (DOE). 2014. Title 40 CFR Part 191 Subparts B and C Compliance Recertification Application 2014 for the Waste Isolation Pilot Plant. Appendix TFIELD-2014, Transmissivity Fields. Carlsbad, NM: US Department of Energy Carlsbad Field Office.

White, J.T., Fienen, M.N., and Doherty, J.E., 2016, A Python framework for environmental model uncertainty analysis. Environ. Modell. Software, 85 (2016), pp. 217-228.

White, J. T., 2018, A model-independent iterative ensemble smoother for efficient history-matching and uncertainty quantification in very high dimensions. Environmental Modelling & Software, 109, 191-201.

White, J.T., Hunt, R.J., Fienen, M.N., and Doherty, J.E., 2020, Approaches to Highly Parameterized Inversion: PEST++ Version 5, a Software Suite for Parameter Estimation, Uncertainty Analysis, Management Optimization and Sensitivity Analysis: U.S. Geological Survey Techniques and Methods 7C26, 52 p.

Information Only

7. Appendix A

7.1 Normalized Objective Function for Observation Groups at Iteration 5

Realization Number	Ranking Based on Dist. from Origin	Phi for Major Observation Groups			Normalized Phi for Major Observation Groups			Distance from Origin
		Pumping Tests	Steady-state Heads	Mills Ranch Pumping Test	Pumping Tests	Steady-state Heads	Mills Ranch Pumping Test	
0	903	293233	159438	153276	0.03	0.68	0.03	0.68
1	581	212710	124373	99861	0.02	0.53	0.02	0.53
2	814	451139	142189	209329	0.04	0.60	0.04	0.61
3	680	311629	130929	256548	0.03	0.56	0.05	0.56
4	733	204821	133133	540785	0.02	0.56	0.11	0.58
5	34	638187	92129	105187	0.06	0.39	0.02	0.40
6	689	249602	132011	110216	0.02	0.56	0.02	0.56
7	495	1183152	116834	242901	0.11	0.50	0.05	0.51
8	545	2964952	103502	80881	0.28	0.44	0.02	0.52
9	197	225147	104907	112117	0.02	0.44	0.02	0.45
10	720	276466	134359	68313	0.03	0.57	0.01	0.57
11	954	352856	188648	599662	0.03	0.80	0.12	0.81
12	32	464443	92329	131564	0.04	0.39	0.03	0.39
13	384	260251	114411	125392	0.02	0.49	0.03	0.49
14	612	444983	125806	72701	0.04	0.53	0.01	0.54
15	673	3588662	104447	127083	0.33	0.44	0.03	0.56
16	353	1766535	106399	74062	0.16	0.45	0.01	0.48
17	686	2280801	122060	144873	0.21	0.52	0.03	0.56
18	597	2593827	111413	201287	0.24	0.47	0.04	0.53
19	625	2451535	114896	171337	0.23	0.49	0.03	0.54
20	764	305196	137478	195902	0.03	0.58	0.04	0.59
21	923	2971352	153755	134308	0.28	0.65	0.03	0.71
22	350	1425874	101834	804088	0.13	0.43	0.16	0.48
23	200	222083	105174	110123	0.02	0.45	0.02	0.45
24	369	261416	113809	94082	0.02	0.48	0.02	0.48
26	316	1103176	109077	94585	0.10	0.46	0.02	0.47

Information Only

Realization Number	Ranking Based on Dist. from Origin	Phi for Major Observation Groups			Normalized Phi for Major Observation Groups			Distance from Origin
		Pumping Tests	Steady-state Heads	Mills Ranch Pumping Test	Pumping Tests	Steady-state Heads	Mills Ranch Pumping Test	
27	54	277860	95148	255846	0.03	0.40	0.05	0.41
28	661	1286829	126969	97398	0.12	0.54	0.02	0.55
29	905	334571	160665	226405	0.03	0.68	0.05	0.68
30	617	402387	126129	62331	0.04	0.53	0.01	0.54
31	198	1296347	99853	358642	0.12	0.42	0.07	0.45
32	811	1637519	137716	181373	0.15	0.58	0.04	0.60
33	667	428419	129747	235710	0.04	0.55	0.05	0.55
34	130	573812	101263	95371	0.05	0.43	0.02	0.43
35	115	984547	98701	172797	0.09	0.42	0.03	0.43
36	273	553140	107642	291895	0.05	0.46	0.06	0.46
37	815	744985	141614	208469	0.07	0.60	0.04	0.61
38	887	353796	155096	136820	0.03	0.66	0.03	0.66
39	165	454527	102813	182644	0.04	0.44	0.04	0.44
40	335	956522	110789	77505	0.09	0.47	0.02	0.48
41	586	405708	124454	89345	0.04	0.53	0.02	0.53
42	496	228797	120089	83622	0.02	0.51	0.02	0.51
43	428	918086	114717	184488	0.09	0.49	0.04	0.50
44	247	508471	104704	485020	0.05	0.44	0.10	0.46
45	399	210321	114348	318842	0.02	0.48	0.06	0.49
46	400	476732	114473	228023	0.04	0.49	0.05	0.49
47	196	1635076	98634	137029	0.15	0.42	0.03	0.45
48	486	312806	107715	1103340	0.03	0.46	0.22	0.51
49	516	228817	120798	97412	0.02	0.51	0.02	0.51
50	833	436249	144122	268216	0.04	0.61	0.05	0.61
51	825	448881	124828	1506970	0.04	0.53	0.30	0.61
52	869	289302	150922	192483	0.03	0.64	0.04	0.64
53	539	3884430	86571	261305	0.36	0.37	0.05	0.52
54	596	220256	125076	163579	0.02	0.53	0.03	0.53
55	702	1194310	130333	119819	0.11	0.55	0.02	0.56

Information Only

Realization Number	Ranking Based on Dist. from Origin	Phi for Major Observation Groups			Normalized Phi for Major Observation Groups			Distance from Origin
		Pumping Tests	Steady-state Heads	Mills Ranch Pumping Test	Pumping Tests	Steady-state Heads	Mills Ranch Pumping Test	
56	517	218298	120765	121510	0.02	0.51	0.02	0.51
57	110	803204	98370	66830	0.07	0.42	0.01	0.42
58	472	248170	118971	143248	0.02	0.50	0.03	0.51
59	879	309487	153482	174282	0.03	0.65	0.04	0.65
60	878	3788549	129137	78987	0.35	0.55	0.02	0.65
61	424	291848	116348	93992	0.03	0.49	0.02	0.49
62	847	4565345	106589	228007	0.42	0.45	0.05	0.62
63	442	584244	114496	487296	0.05	0.49	0.10	0.50
64	820	280745	142998	140639	0.03	0.61	0.03	0.61
65	791	268979	141008	73135	0.03	0.60	0.01	0.60
66	914	4928068	123166	147261	0.46	0.52	0.03	0.70
67	899	265763	158628	159911	0.02	0.67	0.03	0.67
68	220	263068	106040	119908	0.02	0.45	0.02	0.45
69	773	345195	138822	121289	0.03	0.59	0.02	0.59
70	917	4707126	128677	171066	0.44	0.55	0.03	0.70
71	31	302819	92582	146431	0.03	0.39	0.03	0.39
72	301	573245	110186	106240	0.05	0.47	0.02	0.47
73	6	772160	85063	90486	0.07	0.36	0.02	0.37
74	488	443790	119369	143249	0.04	0.51	0.03	0.51
75	244	2000212	97826	209923	0.19	0.41	0.04	0.46
76	236	590864	105999	155673	0.05	0.45	0.03	0.45
77	776	299515	138973	203806	0.03	0.59	0.04	0.59
78	710	536467	130674	537752	0.05	0.55	0.11	0.57
79	164	257762	103222	149203	0.02	0.44	0.03	0.44
81	103	207557	99416	69792	0.02	0.42	0.01	0.42
82	341	442050	112466	98924	0.04	0.48	0.02	0.48
83	790	4299337	104182	114826	0.40	0.44	0.02	0.60
84	543	236542	121902	139785	0.02	0.52	0.03	0.52
85	215	1956507	96912	111256	0.18	0.41	0.02	0.45

Information Only

Realization Number	Ranking Based on Dist. from Origin	Phi for Major Observation Groups			Normalized Phi for Major Observation Groups			Distance from Origin
		Pumping Tests	Steady-state Heads	Mills Ranch Pumping Test	Pumping Tests	Steady-state Heads	Mills Ranch Pumping Test	
86	762	249933	137075	256502	0.02	0.58	0.05	0.58
87	708	304563	132856	259410	0.03	0.56	0.05	0.57
88	397	648601	114180	189469	0.06	0.48	0.04	0.49
89	291	752612	109134	82820	0.07	0.46	0.02	0.47
91	608	955768	124285	95454	0.09	0.53	0.02	0.53
92	42	495517	94431	62801	0.05	0.40	0.01	0.40
93	852	3383014	127369	122105	0.31	0.54	0.02	0.63
94	795	278423	141174	145790	0.03	0.60	0.03	0.60
95	514	887840	118539	289086	0.08	0.50	0.06	0.51
97	14	226974	89116	63347	0.02	0.38	0.01	0.38
98	565	459237	122657	243651	0.04	0.52	0.05	0.52
99	361	288180	113205	105325	0.03	0.48	0.02	0.48
100	713	3123741	112084	538437	0.29	0.48	0.11	0.57
101	924	343908	112983	2596370	0.03	0.48	0.52	0.71
102	433	262034	116624	160968	0.02	0.49	0.03	0.50
103	844	3110235	128929	255974	0.29	0.55	0.05	0.62
104	724	3547096	109416	324866	0.33	0.46	0.07	0.57
105	266	1243452	104688	244531	0.12	0.44	0.05	0.46
106	752	230182	136257	344215	0.02	0.58	0.07	0.58
107	937	5166103	134494	243549	0.48	0.57	0.05	0.75
108	909	3456659	142935	136241	0.32	0.61	0.03	0.69
110	600	399703	124935	164047	0.04	0.53	0.03	0.53
111	915	311954	163907	86924	0.03	0.70	0.02	0.70
112	252	694512	106677	166597	0.06	0.45	0.03	0.46
113	861	343888	148729	164715	0.03	0.63	0.03	0.63
114	102	1284885	95204	151710	0.12	0.40	0.03	0.42
115	894	4160513	127882	113550	0.39	0.54	0.02	0.67
116	687	261532	130470	429775	0.02	0.55	0.09	0.56
117	191	316940	104738	83432	0.03	0.44	0.02	0.45

Information Only

Realization Number	Ranking Based on Dist. from Origin	Phi for Major Observation Groups			Normalized Phi for Major Observation Groups			Distance from Origin
		Pumping Tests	Steady-state Heads	Mills Ranch Pumping Test	Pumping Tests	Steady-state Heads	Mills Ranch Pumping Test	
118	227	1077179	104153	71183	0.10	0.44	0.01	0.45
119	50	1944971	85281	139766	0.18	0.36	0.03	0.41
120	946	344695	181321	129597	0.03	0.77	0.03	0.77
121	251	213376	107665	161935	0.02	0.46	0.03	0.46
122	129	869569	99997	161968	0.08	0.42	0.03	0.43
123	963	317147	202378	126734	0.03	0.86	0.03	0.86
124	706	618201	124002	994335	0.06	0.53	0.20	0.57
125	336	834311	110995	190041	0.08	0.47	0.04	0.48
126	162	1890618	94871	73096	0.18	0.40	0.01	0.44
127	789	513590	138028	499652	0.05	0.59	0.10	0.60
128	394	790347	112793	329506	0.07	0.48	0.07	0.49
129	10	296998	87155	139779	0.03	0.37	0.03	0.37
130	881	4956660	108739	205736	0.46	0.46	0.04	0.65
131	836	315089	145419	87795	0.03	0.62	0.02	0.62
132	566	2084903	113607	365667	0.19	0.48	0.07	0.52
133	410	2063337	106694	148960	0.19	0.45	0.03	0.49
134	253	352098	107725	74836	0.03	0.46	0.02	0.46
135	296	252206	110415	102829	0.02	0.47	0.02	0.47
136	512	349138	106027	1214220	0.03	0.45	0.24	0.51
137	452	1353405	114151	183413	0.13	0.48	0.04	0.50
138	225	208008	106370	76574	0.02	0.45	0.02	0.45
139	226	320134	105977	236518	0.03	0.45	0.05	0.45
140	657	244631	129001	233410	0.02	0.55	0.05	0.55
141	652	215200	129240	83845	0.02	0.55	0.02	0.55
142	886	324373	155021	138871	0.03	0.66	0.03	0.66
143	863	526139	147125	482105	0.05	0.62	0.10	0.63
144	958	817440	193795	84145	0.08	0.82	0.02	0.83
145	674	1265788	128195	112313	0.12	0.54	0.02	0.56
146	62	1344553	91875	107246	0.12	0.39	0.02	0.41

Information Only

Realization Number	Ranking Based on Dist. from Origin	Phi for Major Observation Groups			Normalized Phi for Major Observation Groups			Distance from Origin
		Pumping Tests	Steady-state Heads	Mills Ranch Pumping Test	Pumping Tests	Steady-state Heads	Mills Ranch Pumping Test	
147	451	342556	117696	118340	0.03	0.50	0.02	0.50
148	865	168794	149760	127396	0.02	0.64	0.03	0.64
149	416	493803	104840	1032520	0.05	0.44	0.21	0.49
150	12	153455	88141	57364	0.01	0.37	0.01	0.37
152	568	954233	121795	139098	0.09	0.52	0.03	0.52
153	530	2294828	110664	85112	0.21	0.47	0.02	0.52
154	106	2308118	85812	149520	0.21	0.36	0.03	0.42
155	455	261516	117284	339378	0.02	0.50	0.07	0.50
156	284	1212413	106178	117443	0.11	0.45	0.02	0.46
157	912	3750266	140489	173001	0.35	0.60	0.03	0.69
158	754	295543	136790	253972	0.03	0.58	0.05	0.58
159	213	334085	105479	182944	0.03	0.45	0.04	0.45
160	311	344447	110231	335654	0.03	0.47	0.07	0.47
161	380	712731	113134	194218	0.07	0.48	0.04	0.49
162	233	242839	106786	76516	0.02	0.45	0.02	0.45
163	157	366723	102993	71505	0.03	0.44	0.01	0.44
164	170	497601	103172	100707	0.05	0.44	0.02	0.44
165	727	376128	134681	189214	0.03	0.57	0.04	0.57
166	563	399136	122997	134950	0.04	0.52	0.03	0.52
167	571	273143	123540	174878	0.03	0.52	0.04	0.53
168	897	5558859	100811	199749	0.52	0.43	0.04	0.67
169	933	354742	173105	127242	0.03	0.73	0.03	0.74
170	970	9344267	98924	156830	0.87	0.42	0.03	0.97
171	502	582268	119701	125009	0.05	0.51	0.03	0.51
172	111	803923	98659	75862	0.07	0.42	0.02	0.43
173	100	176107	98718	166619	0.02	0.42	0.03	0.42
174	848	4953119	96191	450246	0.46	0.41	0.09	0.62
175	245	919018	97537	863873	0.09	0.41	0.17	0.46
176	155	222504	101438	376224	0.02	0.43	0.08	0.44

Information Only

Realization Number	Ranking Based on Dist. from Origin	Phi for Major Observation Groups			Normalized Phi for Major Observation Groups			Distance from Origin
		Pumping Tests	Steady-state Heads	Mills Ranch Pumping Test	Pumping Tests	Steady-state Heads	Mills Ranch Pumping Test	
178	648	350924	126411	530555	0.03	0.54	0.11	0.55
179	654	197768	114990	1251760	0.02	0.49	0.25	0.55
180	324	473211	110816	314984	0.04	0.47	0.06	0.48
181	857	4853747	103648	65338	0.45	0.44	0.01	0.63
182	337	1296482	104377	680321	0.12	0.44	0.14	0.48
183	740	335719	135621	248380	0.03	0.58	0.05	0.58
184	944	5221068	138748	83130	0.49	0.59	0.02	0.76
185	969	521219	212047	271242	0.05	0.90	0.05	0.90
186	841	350093	145829	110019	0.03	0.62	0.02	0.62
187	171	299404	103594	83645	0.03	0.44	0.02	0.44
188	176	1293914	100266	81066	0.12	0.43	0.02	0.44
189	169	500297	102924	168086	0.05	0.44	0.03	0.44
191	509	449003	118484	452847	0.04	0.50	0.09	0.51
192	819	1156588	140465	232818	0.11	0.60	0.05	0.61
193	124	914187	99748	81847	0.08	0.42	0.02	0.43
194	87	209414	97649	136705	0.02	0.41	0.03	0.42
195	275	207825	106598	499907	0.02	0.45	0.10	0.46
196	359	240974	113127	127868	0.02	0.48	0.03	0.48
197	892	281760	156708	140585	0.03	0.66	0.03	0.67
198	635	374722	126433	414534	0.03	0.54	0.08	0.54
199	232	227033	106683	117646	0.02	0.45	0.02	0.45
200	723	1130956	132525	150302	0.11	0.56	0.03	0.57
201	739	321805	135199	337904	0.03	0.57	0.07	0.58
202	132	349422	101812	97758	0.03	0.43	0.02	0.43
203	474	334563	119133	142807	0.03	0.51	0.03	0.51
204	942	720935	176711	226666	0.07	0.75	0.05	0.75
205	413	405599	115155	263953	0.04	0.49	0.05	0.49
206	719	637242	133160	258143	0.06	0.56	0.05	0.57
207	934	5487287	125644	73913	0.51	0.53	0.01	0.74

Information Only

Realization Number	Ranking Based on Dist. from Origin	Phi for Major Observation Groups			Normalized Phi for Major Observation Groups			Distance from Origin
		Pumping Tests	Steady-state Heads	Mills Ranch Pumping Test	Pumping Tests	Steady-state Heads	Mills Ranch Pumping Test	
208	218	272892	105860	144923	0.03	0.45	0.03	0.45
209	190	259647	103889	303192	0.02	0.44	0.06	0.45
210	133	221830	102029	100753	0.02	0.43	0.02	0.43
211	898	3136055	142657	127975	0.29	0.61	0.03	0.67
212	745	216019	135928	297134	0.02	0.58	0.06	0.58
213	16	229924	88954	166124	0.02	0.38	0.03	0.38
214	249	692344	105853	315425	0.06	0.45	0.06	0.46
215	421	289067	116270	84561	0.03	0.49	0.02	0.49
216	250	293743	106724	319963	0.03	0.45	0.06	0.46
217	405	247357	115474	146222	0.02	0.49	0.03	0.49
218	866	422467	150206	110244	0.04	0.64	0.02	0.64
219	1	532665	79806	120259	0.05	0.34	0.02	0.34
220	649	1911909	122193	74569	0.18	0.52	0.01	0.55
221	362	337170	113224	64398	0.03	0.48	0.01	0.48
222	178	283766	104136	84303	0.03	0.44	0.02	0.44
223	264	538715	108066	85078	0.05	0.46	0.02	0.46
224	670	367279	129841	291143	0.03	0.55	0.06	0.55
225	210	260266	105111	220093	0.02	0.45	0.04	0.45
226	810	326626	141872	257325	0.03	0.60	0.05	0.60
227	538	3574085	93516	71884	0.33	0.40	0.01	0.52
228	422	322404	116236	94209	0.03	0.49	0.02	0.49
229	794	752045	140223	181560	0.07	0.59	0.04	0.60
230	614	253106	126009	129069	0.02	0.53	0.03	0.54
231	935	791800	118755	2664420	0.07	0.50	0.54	0.74
232	216	213869	105950	72052	0.02	0.45	0.01	0.45
233	479	1169141	116563	188238	0.11	0.49	0.04	0.51
234	700	360038	132572	126457	0.03	0.56	0.03	0.56
235	913	1962292	157955	78917	0.18	0.67	0.02	0.69
236	528	259312	121191	88608	0.02	0.51	0.02	0.51

Information Only

Realization Number	Ranking Based on Dist. from Origin	Phi for Major Observation Groups			Normalized Phi for Major Observation Groups			Distance from Origin
		Pumping Tests	Steady-state Heads	Mills Ranch Pumping Test	Pumping Tests	Steady-state Heads	Mills Ranch Pumping Test	
237	365	495915	112746	204593	0.05	0.48	0.04	0.48
238	728	2331340	123775	398556	0.22	0.52	0.08	0.57
239	471	470797	118793	62439	0.04	0.50	0.01	0.51
240	112	254241	100493	92686	0.02	0.43	0.02	0.43
241	298	218574	108637	445066	0.02	0.46	0.09	0.47
242	807	1975088	135331	113006	0.18	0.57	0.02	0.60
243	120	352684	101061	149708	0.03	0.43	0.03	0.43
244	389	554185	113859	221983	0.05	0.48	0.04	0.49
245	481	389419	118946	234736	0.04	0.50	0.05	0.51
246	957	614182	193382	66977	0.06	0.82	0.01	0.82
247	92	864978	96566	134032	0.08	0.41	0.03	0.42
248	854	4192305	115376	156069	0.39	0.49	0.03	0.63
249	916	462254	158161	916163	0.04	0.67	0.18	0.70
250	907	246675	161174	105813	0.02	0.68	0.02	0.68
251	348	1870630	105114	162911	0.17	0.45	0.03	0.48
252	867	338170	150337	174400	0.03	0.64	0.04	0.64
253	953	652001	132813	2852570	0.06	0.56	0.57	0.81
254	800	4480174	101931	127128	0.42	0.43	0.03	0.60
255	83	270396	97209	141228	0.03	0.41	0.03	0.41
256	391	254185	114787	86885	0.02	0.49	0.02	0.49
257	402	335822	115149	149911	0.03	0.49	0.03	0.49
258	947	585727	181395	81158	0.05	0.77	0.02	0.77
259	125	235165	101609	99987	0.02	0.43	0.02	0.43
260	549	3466307	95725	166000	0.32	0.41	0.03	0.52
261	527	613910	120465	136640	0.06	0.51	0.03	0.51
262	651	196451	129042	168768	0.02	0.55	0.03	0.55
263	114	755634	99715	86724	0.07	0.42	0.02	0.43
264	246	434103	107240	75481	0.04	0.45	0.02	0.46
265	223	295193	106081	109701	0.03	0.45	0.02	0.45

Information Only

Realization Number	Ranking Based on Dist. from Origin	Phi for Major Observation Groups			Normalized Phi for Major Observation Groups			Distance from Origin
		Pumping Tests	Steady-state Heads	Mills Ranch Pumping Test	Pumping Tests	Steady-state Heads	Mills Ranch Pumping Test	
266	212	278666	105706	114348	0.03	0.45	0.02	0.45
267	426	1581222	111300	130073	0.15	0.47	0.03	0.50
268	960	619558	153777	2608230	0.06	0.65	0.52	0.84
269	89	379534	97906	94433	0.04	0.42	0.02	0.42
270	945	3380134	163070	429185	0.31	0.69	0.09	0.76
271	466	2145645	108361	298882	0.20	0.46	0.06	0.50
272	461	1569234	113520	87279	0.15	0.48	0.02	0.50
273	555	397067	122388	137881	0.04	0.52	0.03	0.52
274	888	230257	155430	110450	0.02	0.66	0.02	0.66
275	195	281011	104782	129741	0.03	0.44	0.03	0.45
276	128	1587909	95565	166441	0.15	0.41	0.03	0.43
277	623	344212	126509	156196	0.03	0.54	0.03	0.54
278	526	521919	120791	63003	0.05	0.51	0.01	0.51
279	423	233619	112595	629950	0.02	0.48	0.13	0.49
280	158	225831	103170	99343	0.02	0.44	0.02	0.44
281	593	212494	125127	106080	0.02	0.53	0.02	0.53
282	371	244228	113766	148888	0.02	0.48	0.03	0.48
283	826	363888	143849	123139	0.03	0.61	0.02	0.61
284	626	3346295	100194	590103	0.31	0.42	0.12	0.54
285	331	703034	111132	202712	0.07	0.47	0.04	0.48
286	830	285578	144150	181659	0.03	0.61	0.04	0.61
287	524	322311	117850	590605	0.03	0.50	0.12	0.51
288	379	361363	113659	252697	0.03	0.48	0.05	0.49
289	544	1094798	119707	106947	0.10	0.51	0.02	0.52
290	261	270348	106230	448014	0.03	0.45	0.09	0.46
291	843	247954	145976	132387	0.02	0.62	0.03	0.62
292	386	248540	114532	86672	0.02	0.49	0.02	0.49
293	304	252283	110433	227129	0.02	0.47	0.05	0.47
294	546	450050	121846	79951	0.04	0.52	0.02	0.52

Information Only

Realization Number	Ranking Based on Dist. from Origin	Phi for Major Observation Groups			Normalized Phi for Major Observation Groups			Distance from Origin
		Pumping Tests	Steady-state Heads	Mills Ranch Pumping Test	Pumping Tests	Steady-state Heads	Mills Ranch Pumping Test	
295	875	669717	148890	601639	0.06	0.63	0.12	0.65
296	470	554027	118457	84817	0.05	0.50	0.02	0.51
297	270	1513080	103424	210653	0.14	0.44	0.04	0.46
298	26	825432	88887	319444	0.08	0.38	0.06	0.39
299	540	313166	121481	202050	0.03	0.52	0.04	0.52
300	258	2442268	94083	83321	0.23	0.40	0.02	0.46
301	558	258798	122927	74984	0.02	0.52	0.02	0.52
302	497	284007	120082	91669	0.03	0.51	0.02	0.51
303	615	1433121	121335	336649	0.13	0.51	0.07	0.54
304	57	1937165	86353	86649	0.18	0.37	0.02	0.41
305	510	704890	119734	104927	0.07	0.51	0.02	0.51
306	104	1276197	95452	130461	0.12	0.40	0.03	0.42
307	621	373945	126377	155495	0.03	0.54	0.03	0.54
308	395	284040	114970	98544	0.03	0.49	0.02	0.49
309	475	1766280	105288	875262	0.16	0.45	0.18	0.51
310	664	255314	130061	176255	0.02	0.55	0.04	0.55
311	908	5141887	115833	102279	0.48	0.49	0.02	0.69
312	352	727193	111933	146197	0.07	0.47	0.03	0.48
313	387	324425	114448	111136	0.03	0.49	0.02	0.49
314	396	463041	114466	215650	0.04	0.49	0.04	0.49
315	217	680295	105032	83974	0.06	0.45	0.02	0.45
316	260	284913	108146	93138	0.03	0.46	0.02	0.46
317	553	552399	121952	96712	0.05	0.52	0.02	0.52
318	606	226969	124610	355194	0.02	0.53	0.07	0.53
319	152	223459	102734	114643	0.02	0.44	0.02	0.44
320	88	346818	97407	153996	0.03	0.41	0.03	0.42
321	829	2045736	137271	101192	0.19	0.58	0.02	0.61
322	669	625599	129911	138181	0.06	0.55	0.03	0.55
323	672	348912	129828	304216	0.03	0.55	0.06	0.55

Information Only

Realization Number	Ranking Based on Dist. from Origin	Phi for Major Observation Groups			Normalized Phi for Major Observation Groups			Distance from Origin
		Pumping Tests	Steady-state Heads	Mills Ranch Pumping Test	Pumping Tests	Steady-state Heads	Mills Ranch Pumping Test	
324	955	1523014	186458	521842	0.14	0.79	0.10	0.81
325	94	231621	98421	151478	0.02	0.42	0.03	0.42
326	859	1643274	144540	114723	0.15	0.61	0.02	0.63
327	180	670204	103336	130905	0.06	0.44	0.03	0.44
328	374	1838128	105710	342327	0.17	0.45	0.07	0.48
329	573	312796	123327	227415	0.03	0.52	0.05	0.53
330	339	2454945	99204	82142	0.23	0.42	0.02	0.48
331	287	249831	103829	757780	0.02	0.44	0.15	0.47
332	116	244784	101110	108774	0.02	0.43	0.02	0.43
333	806	273977	136194	852694	0.03	0.58	0.17	0.60
334	663	327808	129863	184241	0.03	0.55	0.04	0.55
335	381	724699	112883	247155	0.07	0.48	0.05	0.49
336	855	790409	147256	136104	0.07	0.62	0.03	0.63
337	435	263048	116852	93229	0.02	0.50	0.02	0.50
338	36	1363601	88591	160068	0.13	0.38	0.03	0.40
339	610	333980	125683	177116	0.03	0.53	0.04	0.54
340	822	3185552	125360	152988	0.30	0.53	0.03	0.61
341	175	714315	102926	105067	0.07	0.44	0.02	0.44
343	308	290550	111094	121103	0.03	0.47	0.02	0.47
344	22	740517	89709	176559	0.07	0.38	0.04	0.39
345	3	439927	82968	80557	0.04	0.35	0.02	0.35
346	340	350591	112550	128676	0.03	0.48	0.03	0.48
347	697	254086	132037	264118	0.02	0.56	0.05	0.56
348	925	2004790	140488	1691880	0.19	0.60	0.34	0.71
349	536	1303273	115477	571418	0.12	0.49	0.11	0.52
350	799	304534	141340	88556	0.03	0.60	0.02	0.60
351	44	831554	92331	298910	0.08	0.39	0.06	0.40
352	772	3142067	120130	269146	0.29	0.51	0.05	0.59
353	828	1036061	142379	137149	0.10	0.60	0.03	0.61

Information Only

Realization Number	Ranking Based on Dist. from Origin	Phi for Major Observation Groups			Normalized Phi for Major Observation Groups			Distance from Origin
		Pumping Tests	Steady-state Heads	Mills Ranch Pumping Test	Pumping Tests	Steady-state Heads	Mills Ranch Pumping Test	
354	896	2266922	149777	229449	0.21	0.64	0.05	0.67
355	293	1035161	107545	230100	0.10	0.46	0.05	0.47
356	404	1244207	112486	71769	0.12	0.48	0.01	0.49
357	393	279145	114745	138241	0.03	0.49	0.03	0.49
358	60	351321	96062	89925	0.03	0.41	0.02	0.41
359	712	1424235	129959	126437	0.13	0.55	0.03	0.57
360	827	332090	143921	105415	0.03	0.61	0.02	0.61
361	796	224366	140862	263644	0.02	0.60	0.05	0.60
362	74	308118	97010	72536	0.03	0.41	0.01	0.41
363	851	755510	146326	96017	0.07	0.62	0.02	0.62
364	760	1094196	135428	135513	0.10	0.57	0.03	0.58
365	295	188136	110228	178088	0.02	0.47	0.04	0.47
366	408	327025	115557	126311	0.03	0.49	0.03	0.49
367	766	321559	138041	150007	0.03	0.59	0.03	0.59
369	583	671336	123311	226002	0.06	0.52	0.05	0.53
370	650	430516	128908	59771	0.04	0.55	0.01	0.55
371	647	288320	114453	1251720	0.03	0.49	0.25	0.55
372	784	3151749	120642	347535	0.29	0.51	0.07	0.59
373	118	196936	101104	160434	0.02	0.43	0.03	0.43
374	299	387241	110268	181187	0.04	0.47	0.04	0.47
375	753	2023730	129872	118621	0.19	0.55	0.02	0.58
376	518	263067	120807	79638	0.02	0.51	0.02	0.51
377	679	472861	130859	197461	0.04	0.55	0.04	0.56
378	936	2984876	161218	316114	0.28	0.68	0.06	0.74
379	183	1684828	97798	113556	0.16	0.41	0.02	0.44
380	490	388978	118771	313662	0.04	0.50	0.06	0.51
381	403	637211	113262	397303	0.06	0.48	0.08	0.49
382	458	2509682	105052	61115	0.23	0.45	0.01	0.50
383	849	912700	145157	137994	0.08	0.62	0.03	0.62

Information Only

Realization Number	Ranking Based on Dist. from Origin	Phi for Major Observation Groups			Normalized Phi for Major Observation Groups			Distance from Origin
		Pumping Tests	Steady-state Heads	Mills Ranch Pumping Test	Pumping Tests	Steady-state Heads	Mills Ranch Pumping Test	
384	432	319673	115811	302072	0.03	0.49	0.06	0.50
385	463	2045085	109875	101442	0.19	0.47	0.02	0.50
387	638	3054152	109160	216269	0.28	0.46	0.04	0.54
388	904	253750	159790	149451	0.02	0.68	0.03	0.68
389	779	255882	139349	167648	0.02	0.59	0.03	0.59
390	480	357443	118943	231569	0.03	0.50	0.05	0.51
391	375	940543	109913	508157	0.09	0.47	0.10	0.49
392	552	288618	122239	96659	0.03	0.52	0.02	0.52
393	82	228494	97306	109130	0.02	0.41	0.02	0.41
394	703	309540	132865	91183	0.03	0.56	0.02	0.56
395	268	929303	106685	174177	0.09	0.45	0.03	0.46
396	184	262856	104452	80778	0.02	0.44	0.02	0.44
397	542	537030	120043	405309	0.05	0.51	0.08	0.52
398	717	261438	133859	79495	0.02	0.57	0.02	0.57
399	319	914880	108734	389952	0.09	0.46	0.08	0.48
400	449	868899	116208	141478	0.08	0.49	0.03	0.50
401	201	221244	105259	82282	0.02	0.45	0.02	0.45
402	604	591001	124861	116929	0.05	0.53	0.02	0.53
403	414	323109	115844	111214	0.03	0.49	0.02	0.49
404	134	764725	100795	87603	0.07	0.43	0.02	0.43
405	972	10758006	118779	223093	1.00	0.50	0.04	1.12
407	464	1166332	115368	263149	0.11	0.49	0.05	0.50
408	272	310947	108805	110776	0.03	0.46	0.02	0.46
409	591	2951872	106927	124622	0.27	0.45	0.03	0.53
410	354	324440	111603	383549	0.03	0.47	0.08	0.48
411	297	1102879	107903	92782	0.10	0.46	0.02	0.47
412	592	1020052	123200	71690	0.09	0.52	0.01	0.53
413	320	263001	111835	108969	0.02	0.47	0.02	0.48
414	193	310223	96978	842885	0.03	0.41	0.17	0.45

Information Only

Realization Number	Ranking Based on Dist. from Origin	Phi for Major Observation Groups			Normalized Phi for Major Observation Groups			Distance from Origin
		Pumping Tests	Steady-state Heads	Mills Ranch Pumping Test	Pumping Tests	Steady-state Heads	Mills Ranch Pumping Test	
416	177	266272	103868	153726	0.02	0.44	0.03	0.44
417	577	3157606	102322	243988	0.29	0.43	0.05	0.53
418	143	1436699	97294	156954	0.13	0.41	0.03	0.43
419	732	4556354	91606	114272	0.42	0.39	0.02	0.58
420	902	5618531	101512	80848	0.52	0.43	0.02	0.68
421	575	220810	112793	1084910	0.02	0.48	0.22	0.53
422	922	288790	166629	183773	0.03	0.71	0.04	0.71
423	554	4084023	83627	127950	0.38	0.35	0.03	0.52
424	441	278005	116489	292325	0.03	0.49	0.06	0.50
425	792	4583077	99106	119550	0.43	0.42	0.02	0.60
426	968	226073	210530	267193	0.02	0.89	0.05	0.89
427	641	250821	128100	203723	0.02	0.54	0.04	0.55
428	759	479756	128736	1005080	0.04	0.55	0.20	0.58
429	616	327048	126011	145664	0.03	0.53	0.03	0.54
430	53	963642	93431	105660	0.09	0.40	0.02	0.41
431	930	710092	150421	1765350	0.07	0.64	0.35	0.73
432	755	4462352	96502	119137	0.41	0.41	0.02	0.58
433	364	314125	113337	116723	0.03	0.48	0.02	0.48
434	95	1160429	93166	444257	0.11	0.40	0.09	0.42
435	541	1773792	115019	272459	0.16	0.49	0.05	0.52
436	484	1823557	112934	89545	0.17	0.48	0.02	0.51
437	325	303488	111697	206086	0.03	0.47	0.04	0.48
438	742	270079	126195	1086720	0.03	0.54	0.22	0.58
439	492	306834	119759	124320	0.03	0.51	0.02	0.51
440	557	349052	122739	88330	0.03	0.52	0.02	0.52
441	37	694573	92598	54064	0.06	0.39	0.01	0.40
442	302	288596	110194	254095	0.03	0.47	0.05	0.47
443	910	220645	161039	504572	0.02	0.68	0.10	0.69
444	312	2735602	93856	169474	0.25	0.40	0.03	0.47

Information Only

Realization Number	Ranking Based on Dist. from Origin	Phi for Major Observation Groups			Normalized Phi for Major Observation Groups			Distance from Origin
		Pumping Tests	Steady-state Heads	Mills Ranch Pumping Test	Pumping Tests	Steady-state Heads	Mills Ranch Pumping Test	
445	323	272951	111884	157988	0.03	0.47	0.03	0.48
446	440	240250	117199	124143	0.02	0.50	0.02	0.50
447	473	471108	118794	127396	0.04	0.50	0.03	0.51
448	289	312762	109954	96081	0.03	0.47	0.02	0.47
449	747	4344417	98083	126190	0.40	0.42	0.03	0.58
450	785	3196299	121213	96891	0.30	0.51	0.02	0.59
451	101	310398	98695	223819	0.03	0.42	0.04	0.42
452	952	305430	185433	116234	0.03	0.79	0.02	0.79
453	551	288799	122223	96706	0.03	0.52	0.02	0.52
454	446	317041	117394	135275	0.03	0.50	0.03	0.50
455	40	2122563	82437	93369	0.20	0.35	0.02	0.40
456	67	193158	96491	175684	0.02	0.41	0.04	0.41
457	805	1832677	135971	203053	0.17	0.58	0.04	0.60
458	613	446782	125625	167213	0.04	0.53	0.03	0.54
459	793	280820	141012	121279	0.03	0.60	0.02	0.60
460	300	512740	110368	79892	0.05	0.47	0.02	0.47
461	560	457576	122715	138094	0.04	0.52	0.03	0.52
462	715	2963701	117036	115819	0.28	0.50	0.02	0.57
463	322	321627	111835	98491	0.03	0.47	0.02	0.48
464	140	281161	101922	174969	0.03	0.43	0.04	0.43
465	135	226667	102071	85908	0.02	0.43	0.02	0.43
466	189	286567	103897	295269	0.03	0.44	0.06	0.45
467	906	386356	160931	71762	0.04	0.68	0.01	0.68
468	345	932883	110939	153407	0.09	0.47	0.03	0.48
469	457	1373487	114306	199085	0.13	0.48	0.04	0.50
471	259	412440	106975	316301	0.04	0.45	0.06	0.46
472	640	445095	128147	59744	0.04	0.54	0.01	0.55
473	35	265585	92859	155080	0.02	0.39	0.03	0.40
474	434	2644542	91188	951409	0.25	0.39	0.19	0.50

Information Only

Realization Number	Ranking Based on Dist. from Origin	Phi for Major Observation Groups			Normalized Phi for Major Observation Groups			Distance from Origin
		Pumping Tests	Steady-state Heads	Mills Ranch Pumping Test	Pumping Tests	Steady-state Heads	Mills Ranch Pumping Test	
475	358	294514	110252	543043	0.03	0.47	0.11	0.48
476	748	279230	136578	149158	0.03	0.58	0.03	0.58
477	812	2856503	127909	205030	0.27	0.54	0.04	0.61
478	281	901233	107607	110029	0.08	0.46	0.02	0.46
479	499	292976	114828	749833	0.03	0.49	0.15	0.51
480	373	355991	113822	135695	0.03	0.48	0.03	0.48
481	609	269244	125716	175647	0.03	0.53	0.04	0.53
482	877	548764	150492	515882	0.05	0.64	0.10	0.65
483	430	226796	116627	115144	0.02	0.49	0.02	0.50
484	932	4875715	134591	398517	0.45	0.57	0.08	0.73
485	500	243186	119409	305006	0.02	0.51	0.06	0.51
486	279	542700	99953	909668	0.05	0.42	0.18	0.46
487	61	1121832	93278	106467	0.10	0.40	0.02	0.41
488	23	279120	91251	125508	0.03	0.39	0.03	0.39
489	774	1323206	136235	131659	0.12	0.58	0.03	0.59
490	182	1027553	102025	117854	0.10	0.43	0.02	0.44
491	206	229254	105457	109171	0.02	0.45	0.02	0.45
492	11	271591	87940	90613	0.03	0.37	0.02	0.37
493	256	311775	107920	102704	0.03	0.46	0.02	0.46
494	49	199890	95303	98972	0.02	0.40	0.02	0.41
495	962	2177986	195575	87293	0.20	0.83	0.02	0.85
496	38	1311980	89023	243169	0.12	0.38	0.05	0.40
497	584	227468	124419	139357	0.02	0.53	0.03	0.53
498	788	3121716	122383	106858	0.29	0.52	0.02	0.60
499	166	586026	102762	129711	0.05	0.44	0.03	0.44
501	501	877962	118627	163741	0.08	0.50	0.03	0.51
502	443	2933862	98340	69452	0.27	0.42	0.01	0.50
503	444	311290	117332	95796	0.03	0.50	0.02	0.50
504	928	4423632	138143	440179	0.41	0.59	0.09	0.72

Information Only

Realization Number	Ranking Based on Dist. from Origin	Phi for Major Observation Groups			Normalized Phi for Major Observation Groups			Distance from Origin
		Pumping Tests	Steady-state Heads	Mills Ranch Pumping Test	Pumping Tests	Steady-state Heads	Mills Ranch Pumping Test	
505	920	5013056	123218	345211	0.47	0.52	0.07	0.70
506	777	502598	138197	324542	0.05	0.59	0.07	0.59
507	580	303421	118129	809516	0.03	0.50	0.16	0.53
508	525	477728	120629	173155	0.04	0.51	0.03	0.51
509	204	248302	103988	360055	0.02	0.44	0.07	0.45
510	283	301462	109034	184943	0.03	0.46	0.04	0.46
511	97	367373	98359	137959	0.03	0.42	0.03	0.42
512	569	398741	123191	187813	0.04	0.52	0.04	0.53
513	254	401831	81777	1484390	0.04	0.35	0.30	0.46
514	802	322103	141501	85435	0.03	0.60	0.02	0.60
515	230	574885	105254	284152	0.05	0.45	0.06	0.45
516	818	298986	142769	112378	0.03	0.61	0.02	0.61
517	29	1687240	84899	85589	0.16	0.36	0.02	0.39
518	771	434442	136383	491549	0.04	0.58	0.10	0.59
519	39	699428	93140	167548	0.07	0.40	0.03	0.40
520	756	497904	119656	1412750	0.05	0.51	0.28	0.58
521	948	232740	183149	146090	0.02	0.78	0.03	0.78
522	757	1419860	133630	212595	0.13	0.57	0.04	0.58
523	931	278422	172721	71930	0.03	0.73	0.01	0.73
524	628	676413	115253	1110840	0.06	0.49	0.22	0.54
525	491	521866	119198	169457	0.05	0.51	0.03	0.51
526	842	324516	143518	568216	0.03	0.61	0.11	0.62
527	688	319759	131323	284308	0.03	0.56	0.06	0.56
528	489	284585	119610	143777	0.03	0.51	0.03	0.51
529	454	275149	117677	253210	0.03	0.50	0.05	0.50
530	68	428580	95990	220821	0.04	0.41	0.04	0.41
531	27	330425	91942	101484	0.03	0.39	0.02	0.39
532	388	476032	113235	346786	0.04	0.48	0.07	0.49
533	425	260766	116446	65137	0.02	0.49	0.01	0.49

Information Only

Realization Number	Ranking Based on Dist. from Origin	Phi for Major Observation Groups			Normalized Phi for Major Observation Groups			Distance from Origin
		Pumping Tests	Steady-state Heads	Mills Ranch Pumping Test	Pumping Tests	Steady-state Heads	Mills Ranch Pumping Test	
534	599	345452	124154	345731	0.03	0.53	0.07	0.53
535	450	1973279	109672	84585	0.18	0.47	0.02	0.50
536	66	309570	95337	341755	0.03	0.40	0.07	0.41
537	407	258427	115661	98071	0.02	0.49	0.02	0.49
538	202	2048377	95340	88606	0.19	0.40	0.02	0.45
539	941	339463	177467	99399	0.03	0.75	0.02	0.75
540	315	439726	111323	74234	0.04	0.47	0.01	0.47
541	46	633733	93506	250474	0.06	0.40	0.05	0.40
542	797	285920	141080	193457	0.03	0.60	0.04	0.60
543	900	504897	158500	231546	0.05	0.67	0.05	0.68
544	367	437033	113358	107041	0.04	0.48	0.02	0.48
545	678	313739	131159	119583	0.03	0.56	0.02	0.56
546	366	1847439	106256	99669	0.17	0.45	0.02	0.48
547	817	238971	142857	76361	0.02	0.61	0.02	0.61
548	564	328403	123187	113352	0.03	0.52	0.02	0.52
549	515	1136358	118328	81143	0.11	0.50	0.02	0.51
550	294	738922	109284	75998	0.07	0.46	0.02	0.47
551	782	312341	139426	202325	0.03	0.59	0.04	0.59
552	971	286150	235783	127747	0.03	1.00	0.03	1.00
553	346	581282	112203	110256	0.05	0.48	0.02	0.48
554	280	933836	106907	250871	0.09	0.45	0.05	0.46
555	476	247248	119264	160111	0.02	0.51	0.03	0.51
556	885	294227	155042	131034	0.03	0.66	0.03	0.66
557	690	2916112	115576	159269	0.27	0.49	0.03	0.56
558	234	430365	106404	124577	0.04	0.45	0.03	0.45
559	508	321462	120507	79726	0.03	0.51	0.02	0.51
560	633	1669873	120867	443373	0.16	0.51	0.09	0.54
561	637	264189	128173	86338	0.02	0.54	0.02	0.54
562	572	379409	123248	222678	0.04	0.52	0.04	0.53

Information Only

Realization Number	Ranking Based on Dist. from Origin	Phi for Major Observation Groups			Normalized Phi for Major Observation Groups			Distance from Origin
		Pumping Tests	Steady-state Heads	Mills Ranch Pumping Test	Pumping Tests	Steady-state Heads	Mills Ranch Pumping Test	
563	7	431705	86577	97142	0.04	0.37	0.02	0.37
564	163	901859	101095	229997	0.08	0.43	0.05	0.44
565	203	1742389	98123	136568	0.16	0.42	0.03	0.45
566	620	1794469	120400	143706	0.17	0.51	0.03	0.54
567	427	295274	116463	102991	0.03	0.49	0.02	0.50
568	714	2802673	118940	105364	0.26	0.50	0.02	0.57
569	482	433621	119358	70205	0.04	0.51	0.01	0.51
570	30	764711	91036	139410	0.07	0.39	0.03	0.39
571	786	967533	137749	336070	0.09	0.58	0.07	0.59
572	5	212616	86373	113936	0.02	0.37	0.02	0.37
573	503	1974121	112441	97236	0.18	0.48	0.02	0.51
574	117	225213	101223	108870	0.02	0.43	0.02	0.43
575	477	267542	119358	129492	0.02	0.51	0.03	0.51
576	274	2350255	96173	136435	0.22	0.41	0.03	0.46
577	778	488609	139093	77330	0.05	0.59	0.02	0.59
578	816	584256	142220	120959	0.05	0.60	0.02	0.61
579	145	239007	102286	110587	0.02	0.43	0.02	0.43
580	559	262218	122893	136521	0.02	0.52	0.03	0.52
581	731	3246823	114891	203755	0.30	0.49	0.04	0.57
582	356	230108	112794	206354	0.02	0.48	0.04	0.48
583	194	1424732	100336	60310	0.13	0.43	0.01	0.45
584	823	237341	143539	76680	0.02	0.61	0.02	0.61
585	415	303340	109510	807510	0.03	0.46	0.16	0.49
586	831	4385468	107975	110204	0.41	0.46	0.02	0.61
587	603	315780	125180	152762	0.03	0.53	0.03	0.53
588	267	392063	108387	95173	0.04	0.46	0.02	0.46
589	601	213231	125272	133788	0.02	0.53	0.03	0.53
590	18	291277	89617	89436	0.03	0.38	0.02	0.38
591	420	204196	116271	111115	0.02	0.49	0.02	0.49

Information Only

Realization Number	Ranking Based on Dist. from Origin	Phi for Major Observation Groups			Normalized Phi for Major Observation Groups			Distance from Origin
		Pumping Tests	Steady-state Heads	Mills Ranch Pumping Test	Pumping Tests	Steady-state Heads	Mills Ranch Pumping Test	
592	437	671147	116295	72903	0.06	0.49	0.01	0.50
593	939	427358	176613	122333	0.04	0.75	0.02	0.75
594	478	215300	119218	195706	0.02	0.51	0.04	0.51
595	918	740613	161036	721091	0.07	0.68	0.14	0.70
596	276	395771	108613	189252	0.04	0.46	0.04	0.46
597	734	310064	135422	103684	0.03	0.57	0.02	0.58
599	683	173062	131129	279435	0.02	0.56	0.06	0.56
600	582	1135219	121976	119857	0.11	0.52	0.02	0.53
601	853	761174	146609	112586	0.07	0.62	0.02	0.63
602	419	1588523	111099	66273	0.15	0.47	0.01	0.49
603	589	478978	123451	345235	0.04	0.52	0.07	0.53
604	522	229221	120511	264808	0.02	0.51	0.05	0.51
605	142	205058	99891	478443	0.02	0.42	0.10	0.43
606	372	409179	112057	420697	0.04	0.48	0.08	0.48
607	263	769754	107316	111915	0.07	0.46	0.02	0.46
608	240	835472	104240	365609	0.08	0.44	0.07	0.45
609	161	215046	103366	89896	0.02	0.44	0.02	0.44
610	965	253771	204171	151306	0.02	0.87	0.03	0.87
611	736	307953	135724	78565	0.03	0.58	0.02	0.58
612	173	1971754	93111	370071	0.18	0.39	0.07	0.44
613	148	228000	102343	138633	0.02	0.43	0.03	0.44
614	9	450048	85293	349352	0.04	0.36	0.07	0.37
615	840	3258461	127305	121676	0.30	0.54	0.02	0.62
616	237	2231857	94977	149934	0.21	0.40	0.03	0.45
617	349	243163	112275	265353	0.02	0.48	0.05	0.48
618	248	184061	107313	198956	0.02	0.46	0.04	0.46
619	17	666591	88243	175303	0.06	0.37	0.04	0.38
620	19	852924	88356	94197	0.08	0.37	0.02	0.38
621	327	254353	112131	88465	0.02	0.48	0.02	0.48

Information Only

Realization Number	Ranking Based on Dist. from Origin	Phi for Major Observation Groups			Normalized Phi for Major Observation Groups			Distance from Origin
		Pumping Tests	Steady-state Heads	Mills Ranch Pumping Test	Pumping Tests	Steady-state Heads	Mills Ranch Pumping Test	
622	883	515559	147627	951872	0.05	0.63	0.19	0.66
623	548	531949	121699	121632	0.05	0.52	0.02	0.52
624	658	282781	129332	139792	0.03	0.55	0.03	0.55
625	459	619552	116578	362903	0.06	0.49	0.07	0.50
626	141	3210891	74158	157466	0.30	0.31	0.03	0.43
627	627	1164280	124712	156618	0.11	0.53	0.03	0.54
628	406	309437	103011	1110000	0.03	0.44	0.22	0.49
629	159	604132	101836	259504	0.06	0.43	0.05	0.44
630	758	896145	135904	178117	0.08	0.58	0.04	0.58
631	973	1174192	132351	4978470	0.11	0.56	1.00	1.15
633	579	3267216	101306	98571	0.30	0.43	0.02	0.53
634	436	234825	116892	93395	0.02	0.50	0.02	0.50
635	696	443587	124895	911986	0.04	0.53	0.18	0.56
636	333	1109382	108521	389946	0.10	0.46	0.08	0.48
637	398	178851	115119	152929	0.02	0.49	0.03	0.49
638	58	200951	96036	124390	0.02	0.41	0.02	0.41
639	513	348203	120507	112242	0.03	0.51	0.02	0.51
640	136	357055	101848	115191	0.03	0.43	0.02	0.43
641	93	393467	98184	121394	0.04	0.42	0.02	0.42
642	21	321271	90439	95224	0.03	0.38	0.02	0.39
643	438	432892	116754	156364	0.04	0.50	0.03	0.50
644	487	232583	119597	151981	0.02	0.51	0.03	0.51
645	804	543532	141366	141777	0.05	0.60	0.03	0.60
646	744	630606	135175	304625	0.06	0.57	0.06	0.58
647	576	227344	122075	455426	0.02	0.52	0.09	0.53
648	950	715962	162179	1835720	0.07	0.69	0.37	0.78
649	2	452214	81944	100947	0.04	0.35	0.02	0.35
650	305	253951	110887	105397	0.02	0.47	0.02	0.47
651	59	360879	95921	98600	0.03	0.41	0.02	0.41

Information Only

Realization Number	Ranking Based on Dist. from Origin	Phi for Major Observation Groups			Normalized Phi for Major Observation Groups			Distance from Origin
		Pumping Tests	Steady-state Heads	Mills Ranch Pumping Test	Pumping Tests	Steady-state Heads	Mills Ranch Pumping Test	
652	668	273557	129010	423486	0.03	0.55	0.09	0.55
653	850	414408	144834	529100	0.04	0.61	0.11	0.62
654	28	253186	91083	322382	0.02	0.39	0.06	0.39
655	709	3940800	101855	90135	0.37	0.43	0.02	0.57
656	684	1160153	128426	338757	0.11	0.54	0.07	0.56
657	588	265819	124325	231148	0.02	0.53	0.05	0.53
658	108	229013	99539	159334	0.02	0.42	0.03	0.42
659	738	743267	135135	67183	0.07	0.57	0.01	0.58
660	25	335370	91535	45750	0.03	0.39	0.01	0.39
661	824	3566037	120565	84792	0.33	0.51	0.02	0.61
662	639	2727452	113340	195504	0.25	0.48	0.04	0.54
663	587	347401	124046	256180	0.03	0.53	0.05	0.53
664	33	1903172	83043	159176	0.18	0.35	0.03	0.40
665	595	894631	123577	176343	0.08	0.52	0.04	0.53
666	927	323815	169179	133028	0.03	0.72	0.03	0.72
667	417	2451191	103097	104580	0.23	0.44	0.02	0.49
668	730	295300	135202	112342	0.03	0.57	0.02	0.57
669	392	780379	113680	108333	0.07	0.48	0.02	0.49
670	685	426596	131451	161833	0.04	0.56	0.03	0.56
671	636	289364	126539	431817	0.03	0.54	0.09	0.54
672	80	226465	97182	113412	0.02	0.41	0.02	0.41
673	681	328831	131452	138962	0.03	0.56	0.03	0.56
674	940	5611502	127820	138959	0.52	0.54	0.03	0.75
675	64	1686695	88775	221140	0.16	0.38	0.04	0.41
676	653	315785	128293	332908	0.03	0.54	0.07	0.55
677	224	353379	106049	122758	0.03	0.45	0.02	0.45
678	959	6692279	129504	64301	0.62	0.55	0.01	0.83
679	257	2770704	88797	256082	0.26	0.38	0.05	0.46
680	520	1238274	117223	291090	0.12	0.50	0.06	0.51

Information Only

Realization Number	Ranking Based on Dist. from Origin	Phi for Major Observation Groups			Normalized Phi for Major Observation Groups			Distance from Origin
		Pumping Tests	Steady-state Heads	Mills Ranch Pumping Test	Pumping Tests	Steady-state Heads	Mills Ranch Pumping Test	
681	483	598102	118942	128905	0.06	0.50	0.03	0.51
682	876	276637	152318	121447	0.03	0.65	0.02	0.65
683	901	259114	159205	90776	0.02	0.68	0.02	0.68
684	321	264660	111570	195844	0.02	0.47	0.04	0.48
686	961	3728470	88214	3408540	0.35	0.37	0.68	0.85
687	919	1722078	160758	314483	0.16	0.68	0.06	0.70
688	656	377834	129046	162601	0.04	0.55	0.03	0.55
689	746	395990	136357	152992	0.04	0.58	0.03	0.58
690	351	279867	112798	136498	0.03	0.48	0.03	0.48
691	532	283943	121296	139316	0.03	0.51	0.03	0.52
692	338	254946	112659	107312	0.02	0.48	0.02	0.48
693	873	267814	151441	240426	0.02	0.64	0.05	0.64
694	385	2170438	104307	88867	0.20	0.44	0.02	0.49
695	550	232202	120379	463079	0.02	0.51	0.09	0.52
696	645	1877243	119934	484175	0.17	0.51	0.10	0.55
697	303	471100	109816	275439	0.04	0.47	0.06	0.47
698	839	3281535	126962	115985	0.31	0.54	0.02	0.62
699	439	235461	117222	99301	0.02	0.50	0.02	0.50
700	52	622746	94757	91202	0.06	0.40	0.02	0.41
701	519	1412148	112923	651911	0.13	0.48	0.13	0.51
702	493	363243	119773	134849	0.03	0.51	0.03	0.51
703	966	7262358	128215	373606	0.68	0.54	0.08	0.87
704	368	287658	113651	96929	0.03	0.48	0.02	0.48
705	73	321492	96765	151776	0.03	0.41	0.03	0.41
706	911	297653	162577	163266	0.03	0.69	0.03	0.69
707	677	206386	130404	321428	0.02	0.55	0.06	0.56
708	168	1005326	101294	108060	0.09	0.43	0.02	0.44
709	891	437050	156143	119979	0.04	0.66	0.02	0.66
710	109	385333	99430	129464	0.04	0.42	0.03	0.42

Information Only

Realization Number	Ranking Based on Dist. from Origin	Phi for Major Observation Groups			Normalized Phi for Major Observation Groups			Distance from Origin
		Pumping Tests	Steady-state Heads	Mills Ranch Pumping Test	Pumping Tests	Steady-state Heads	Mills Ranch Pumping Test	
711	377	447499	111554	508527	0.04	0.47	0.10	0.49
712	286	699388	108681	103947	0.07	0.46	0.02	0.47
713	20	1925019	79450	212442	0.18	0.34	0.04	0.38
714	48	1542091	87559	366829	0.14	0.37	0.07	0.40
715	292	615089	106083	583353	0.06	0.45	0.12	0.47
716	675	3331639	109135	77169	0.31	0.46	0.02	0.56
717	344	470332	112211	184655	0.04	0.48	0.04	0.48
718	138	1228774	98600	124842	0.11	0.42	0.03	0.43
719	185	318134	104282	134480	0.03	0.44	0.03	0.44
720	309	275267	111280	115613	0.03	0.47	0.02	0.47
721	691	306656	131310	309678	0.03	0.56	0.06	0.56
722	154	237100	102552	186125	0.02	0.43	0.04	0.44
723	45	892842	91853	335225	0.08	0.39	0.07	0.40
724	24	536245	91003	88707	0.05	0.39	0.02	0.39
725	174	272300	103942	70564	0.03	0.44	0.01	0.44
726	660	293799	129559	220604	0.03	0.55	0.04	0.55
728	71	163875	96948	122422	0.02	0.41	0.02	0.41
729	96	231385	98568	116561	0.02	0.42	0.02	0.42
730	630	740030	126701	144141	0.07	0.54	0.03	0.54
732	314	1618859	100495	712029	0.15	0.43	0.14	0.47
733	498	341822	120063	79145	0.03	0.51	0.02	0.51
734	469	263589	118764	141773	0.02	0.50	0.03	0.51
735	743	278139	134866	441921	0.03	0.57	0.09	0.58
736	81	847706	95718	68664	0.08	0.41	0.01	0.41
737	63	552134	95405	198661	0.05	0.40	0.04	0.41
738	147	1556245	96683	102240	0.14	0.41	0.02	0.44
739	137	1945635	92956	76690	0.18	0.39	0.02	0.43
740	787	344715	140002	95000	0.03	0.59	0.02	0.59
741	122	408054	101290	93715	0.04	0.43	0.02	0.43

Information Only

Realization Number	Ranking Based on Dist. from Origin	Phi for Major Observation Groups			Normalized Phi for Major Observation Groups			Distance from Origin
		Pumping Tests	Steady-state Heads	Mills Ranch Pumping Test	Pumping Tests	Steady-state Heads	Mills Ranch Pumping Test	
742	956	5729328	143342	464360	0.53	0.61	0.09	0.81
743	722	474624	133422	369244	0.04	0.57	0.07	0.57
744	47	350073	95040	71773	0.03	0.40	0.01	0.40
745	269	262592	108731	133829	0.02	0.46	0.03	0.46
746	967	8376255	92243	92601	0.78	0.39	0.02	0.87
747	507	290939	120437	90046	0.03	0.51	0.02	0.51
748	562	282029	123224	66789	0.03	0.52	0.01	0.52
749	121	555995	100819	88375	0.05	0.43	0.02	0.43
750	529	291373	121150	179226	0.03	0.51	0.04	0.52
751	567	535055	122623	233943	0.05	0.52	0.05	0.52
752	494	1456684	104352	1065380	0.14	0.44	0.21	0.51
753	390	273058	114802	62229	0.03	0.49	0.01	0.49
754	255	1926929	99500	106875	0.18	0.42	0.02	0.46
755	460	408384	118213	107141	0.04	0.50	0.02	0.50
756	809	361172	141986	182938	0.03	0.60	0.04	0.60
757	209	1841257	97635	105811	0.17	0.41	0.02	0.45
758	363	1262221	109986	127068	0.12	0.47	0.03	0.48
759	99	275235	98663	102666	0.03	0.42	0.02	0.42
760	77	383196	96902	85460	0.04	0.41	0.02	0.41
761	448	274141	117698	75663	0.03	0.50	0.02	0.50
762	666	293051	129994	208652	0.03	0.55	0.04	0.55
763	342	700030	111639	173724	0.07	0.47	0.03	0.48
764	221	789698	104800	126096	0.07	0.44	0.03	0.45
765	803	359004	141217	196442	0.03	0.60	0.04	0.60
766	207	544656	104970	84451	0.05	0.45	0.02	0.45
767	222	207665	105457	280642	0.02	0.45	0.06	0.45
768	277	278692	109080	117363	0.03	0.46	0.02	0.46
769	769	293266	138101	194445	0.03	0.59	0.04	0.59
770	926	442084	168310	241764	0.04	0.71	0.05	0.72

Information Only

Realization Number	Ranking Based on Dist. from Origin	Phi for Major Observation Groups			Normalized Phi for Major Observation Groups			Distance from Origin
		Pumping Tests	Steady-state Heads	Mills Ranch Pumping Test	Pumping Tests	Steady-state Heads	Mills Ranch Pumping Test	
771	750	422354	136718	126865	0.04	0.58	0.03	0.58
772	411	945646	113693	237183	0.09	0.48	0.05	0.49
774	119	1593080	94655	241148	0.15	0.40	0.05	0.43
775	737	263608	125000	1125690	0.02	0.53	0.23	0.58
776	676	932362	129676	100594	0.09	0.55	0.02	0.56
777	160	996687	100709	189562	0.09	0.43	0.04	0.44
778	655	250236	129329	89401	0.02	0.55	0.02	0.55
779	711	705409	132488	202175	0.07	0.56	0.04	0.57
780	84	535692	95906	298229	0.05	0.41	0.06	0.41
781	858	502851	147972	184295	0.05	0.63	0.04	0.63
782	834	217556	144357	270515	0.02	0.61	0.05	0.61
783	860	245516	148290	304617	0.02	0.63	0.06	0.63
784	765	216951	136966	375760	0.02	0.58	0.08	0.59
785	692	328336	132072	72877	0.03	0.56	0.01	0.56
786	65	658395	95737	100050	0.06	0.41	0.02	0.41
787	531	424614	120292	325811	0.04	0.51	0.07	0.52
788	181	473670	103291	269751	0.04	0.44	0.05	0.44
789	378	1206861	111415	58440	0.11	0.47	0.01	0.49
790	938	508552	175885	159903	0.05	0.75	0.03	0.75
791	721	316807	134420	105231	0.03	0.57	0.02	0.57
792	228	253664	106590	104445	0.02	0.45	0.02	0.45
793	357	393614	112764	158209	0.04	0.48	0.03	0.48
794	594	280887	125032	151209	0.03	0.53	0.03	0.53
795	219	283231	105907	131332	0.03	0.45	0.03	0.45
796	238	1698101	100518	62428	0.16	0.43	0.01	0.45
797	149	305683	102268	169612	0.03	0.43	0.03	0.44
798	535	393982	120986	256229	0.04	0.51	0.05	0.52
799	505	344753	120150	162819	0.03	0.51	0.03	0.51
800	285	329673	109388	96165	0.03	0.46	0.02	0.47

Information Only

Realization Number	Ranking Based on Dist. from Origin	Phi for Major Observation Groups			Normalized Phi for Major Observation Groups			Distance from Origin
		Pumping Tests	Steady-state Heads	Mills Ranch Pumping Test	Pumping Tests	Steady-state Heads	Mills Ranch Pumping Test	
802	187	501031	104131	99454	0.05	0.44	0.02	0.44
803	98	194951	98641	141787	0.02	0.42	0.03	0.42
804	964	7262564	125882	91245	0.68	0.53	0.02	0.86
805	921	3751282	143547	329502	0.35	0.61	0.07	0.70
806	453	239857	118097	89915	0.02	0.50	0.02	0.50
807	4	162070	86242	69330	0.02	0.37	0.01	0.37
808	55	210631	96027	81859	0.02	0.41	0.02	0.41
809	949	499109	170764	1391550	0.05	0.72	0.28	0.78
810	69	183514	96963	77572	0.02	0.41	0.02	0.41
811	8	183817	86798	165831	0.02	0.37	0.03	0.37
812	698	1951596	125329	240338	0.18	0.53	0.05	0.56
813	718	1428433	130392	68966	0.13	0.55	0.01	0.57
814	798	3524301	117474	346469	0.33	0.50	0.07	0.60
815	871	3450925	131003	244767	0.32	0.56	0.05	0.64
816	707	1371310	129813	104008	0.13	0.55	0.02	0.57
817	156	385005	102682	163293	0.04	0.44	0.03	0.44
818	199	1403865	100585	82624	0.13	0.43	0.02	0.45
819	123	221762	101540	107198	0.02	0.43	0.02	0.43
820	70	1607468	90149	172561	0.15	0.38	0.03	0.41
821	821	3531590	120895	92284	0.33	0.51	0.02	0.61
822	43	671254	93904	97125	0.06	0.40	0.02	0.40
823	242	2208615	92258	556749	0.21	0.39	0.11	0.46
824	598	1200206	122526	121550	0.11	0.52	0.02	0.53
825	15	1589237	82278	76658	0.15	0.35	0.02	0.38
826	76	308993	96983	102065	0.03	0.41	0.02	0.41
827	607	290046	123440	512162	0.03	0.52	0.10	0.53
828	643	2820949	112864	99756	0.26	0.48	0.02	0.55
829	288	286664	109623	170393	0.03	0.46	0.03	0.47
830	317	353548	110983	268081	0.03	0.47	0.05	0.47

Information Only

Realization Number	Ranking Based on Dist. from Origin	Phi for Major Observation Groups			Normalized Phi for Major Observation Groups			Distance from Origin
		Pumping Tests	Steady-state Heads	Mills Ranch Pumping Test	Pumping Tests	Steady-state Heads	Mills Ranch Pumping Test	
831	307	257379	110614	253956	0.02	0.47	0.05	0.47
832	150	241300	102424	182034	0.02	0.43	0.04	0.44
833	241	258346	107049	122720	0.02	0.45	0.02	0.46
834	332	297136	112327	144252	0.03	0.48	0.03	0.48
835	127	321074	101534	109170	0.03	0.43	0.02	0.43
836	770	379340	91783	2186740	0.04	0.39	0.44	0.59
837	86	303698	96704	292891	0.03	0.41	0.06	0.42
838	334	261027	112437	131731	0.02	0.48	0.03	0.48
839	671	276542	128405	515250	0.03	0.54	0.10	0.55
840	893	3819244	132555	223644	0.36	0.56	0.04	0.67
841	41	194240	94520	191893	0.02	0.40	0.04	0.40
842	895	404234	156780	207676	0.04	0.66	0.04	0.67
843	146	1200915	99075	71288	0.11	0.42	0.01	0.44
844	884	301871	154686	96516	0.03	0.66	0.02	0.66
845	701	456345	132433	126445	0.04	0.56	0.03	0.56
846	290	351179	109545	226832	0.03	0.46	0.05	0.47
847	605	349546	125420	109528	0.03	0.53	0.02	0.53
848	874	200963	152011	75674	0.02	0.64	0.02	0.65
849	504	3360608	95047	187412	0.31	0.40	0.04	0.51
850	144	1686669	95065	220980	0.16	0.40	0.04	0.43
851	868	1200247	146456	527841	0.11	0.62	0.11	0.64
852	151	1589018	96658	148873	0.15	0.41	0.03	0.44
853	872	749121	135224	1417350	0.07	0.57	0.28	0.64
854	355	255821	112749	209643	0.02	0.48	0.04	0.48
855	172	316417	103520	107870	0.03	0.44	0.02	0.44
856	78	734893	93400	470929	0.07	0.40	0.09	0.41
857	838	287289	144260	430849	0.03	0.61	0.09	0.62
858	856	2688035	135943	213120	0.25	0.58	0.04	0.63
859	729	2169102	126701	105094	0.20	0.54	0.02	0.57

Information Only

Realization Number	Ranking Based on Dist. from Origin	Phi for Major Observation Groups			Normalized Phi for Major Observation Groups			Distance from Origin
		Pumping Tests	Steady-state Heads	Mills Ranch Pumping Test	Pumping Tests	Steady-state Heads	Mills Ranch Pumping Test	
860	662	1467737	125541	286120	0.14	0.53	0.06	0.55
861	880	1201985	151584	84690	0.11	0.64	0.02	0.65
862	835	3041084	128683	218769	0.28	0.55	0.04	0.62
863	813	245191	142568	142813	0.02	0.60	0.03	0.61
864	808	2235857	132966	307351	0.21	0.56	0.06	0.60
865	694	747761	127058	707557	0.07	0.54	0.14	0.56
866	313	718979	109748	281416	0.07	0.47	0.06	0.47
867	465	221547	118366	201266	0.02	0.50	0.04	0.50
868	561	346571	122917	155098	0.03	0.52	0.03	0.52
869	90	200781	93250	660650	0.02	0.40	0.13	0.42
870	131	1393263	96370	308763	0.13	0.41	0.06	0.43
871	282	741343	108159	129875	0.07	0.46	0.03	0.46
872	429	313968	116150	226382	0.03	0.49	0.05	0.50
873	211	217941	105555	146198	0.02	0.45	0.03	0.45
874	347	251587	112815	100140	0.02	0.48	0.02	0.48
875	186	383797	88585	1166840	0.04	0.38	0.23	0.44
876	278	285523	109149	97698	0.03	0.46	0.02	0.46
878	382	2095458	104719	174172	0.19	0.44	0.03	0.49
879	107	1731596	92117	155726	0.16	0.39	0.03	0.42
880	556	350656	122568	149880	0.03	0.52	0.03	0.52
881	418	307732	116000	144451	0.03	0.49	0.03	0.49
882	570	309431	123572	139937	0.03	0.52	0.03	0.53
883	705	968216	131587	62103	0.09	0.56	0.01	0.57
884	235	312918	106455	182449	0.03	0.45	0.04	0.45
885	761	355059	137298	148996	0.03	0.58	0.03	0.58
886	578	935334	121961	209277	0.09	0.52	0.04	0.53
887	768	273268	138364	74419	0.03	0.59	0.01	0.59
888	695	278470	132209	105487	0.03	0.56	0.02	0.56
889	682	319557	131421	158767	0.03	0.56	0.03	0.56

Information Only

Realization Number	Ranking Based on Dist. from Origin	Phi for Major Observation Groups			Normalized Phi for Major Observation Groups			Distance from Origin
		Pumping Tests	Steady-state Heads	Mills Ranch Pumping Test	Pumping Tests	Steady-state Heads	Mills Ranch Pumping Test	
891	629	274936	127117	260109	0.03	0.54	0.05	0.54
892	56	1076427	93138	134225	0.10	0.40	0.03	0.41
893	775	845357	138132	105226	0.08	0.59	0.02	0.59
894	634	294881	127731	157779	0.03	0.54	0.03	0.54
895	51	486636	94956	103826	0.05	0.40	0.02	0.41
896	329	277183	112230	113484	0.03	0.48	0.02	0.48
897	468	475782	118099	237545	0.04	0.50	0.05	0.51
898	412	474745	115652	72139	0.04	0.49	0.01	0.49
899	574	289280	123754	89898	0.03	0.52	0.02	0.53
900	704	721399	132200	82120	0.07	0.56	0.02	0.56
901	624	306795	126618	179609	0.03	0.54	0.04	0.54
902	889	193417	155571	190934	0.02	0.66	0.04	0.66
903	749	1679969	131733	201562	0.16	0.56	0.04	0.58
904	741	2033153	128458	218287	0.19	0.54	0.04	0.58
905	456	1024063	116202	145068	0.10	0.49	0.03	0.50
906	485	299683	119550	132977	0.03	0.51	0.03	0.51
907	882	2057501	147175	132507	0.19	0.62	0.03	0.65
908	642	1335169	124889	213258	0.12	0.53	0.04	0.55
909	85	509261	96897	169340	0.05	0.41	0.03	0.42
910	585	243024	124184	245412	0.02	0.53	0.05	0.53
911	467	2118319	109297	168414	0.20	0.46	0.03	0.50
912	646	406006	128381	198705	0.04	0.54	0.04	0.55
913	243	267824	107186	160724	0.02	0.45	0.03	0.46
914	79	2036295	86436	94420	0.19	0.37	0.02	0.41
915	105	202333	99469	151817	0.02	0.42	0.03	0.42
916	632	586609	127256	72547	0.05	0.54	0.01	0.54
917	401	624641	114227	209693	0.06	0.48	0.04	0.49
918	659	688780	128922	150935	0.06	0.55	0.03	0.55
919	271	278394	108824	115329	0.03	0.46	0.02	0.46

Information Only

Realization Number	Ranking Based on Dist. from Origin	Phi for Major Observation Groups			Normalized Phi for Major Observation Groups			Distance from Origin
		Pumping Tests	Steady-state Heads	Mills Ranch Pumping Test	Pumping Tests	Steady-state Heads	Mills Ranch Pumping Test	
920	506	2469185	107659	130341	0.23	0.46	0.03	0.51
921	845	225847	145742	269787	0.02	0.62	0.05	0.62
922	139	621903	95469	728947	0.06	0.40	0.15	0.43
923	523	504273	120640	133842	0.05	0.51	0.03	0.51
924	229	690811	105194	233167	0.06	0.45	0.05	0.45
925	929	313823	170911	164919	0.03	0.72	0.03	0.73
926	725	297014	134793	179952	0.03	0.57	0.04	0.57
927	837	2617566	133841	128968	0.24	0.57	0.03	0.62
928	360	455815	112628	191664	0.04	0.48	0.04	0.48
929	13	1863013	78789	116873	0.17	0.33	0.02	0.38
930	602	3385139	101093	141841	0.31	0.43	0.03	0.53
931	376	902226	112562	126765	0.08	0.48	0.03	0.49
932	534	346120	121457	116059	0.03	0.52	0.02	0.52
933	326	366942	111955	96921	0.03	0.47	0.02	0.48
934	832	1533893	106271	1951770	0.14	0.45	0.39	0.61
935	619	3113356	106582	160401	0.29	0.45	0.03	0.54
936	735	519688	134703	262942	0.05	0.57	0.05	0.58
937	262	254096	108494	79416	0.02	0.46	0.02	0.46
938	537	190918	121077	304950	0.02	0.51	0.06	0.52
939	113	301942	100183	237933	0.03	0.42	0.05	0.43
940	330	325488	112129	129613	0.03	0.48	0.03	0.48
941	188	468003	104342	81735	0.04	0.44	0.02	0.44
942	214	442808	105487	122650	0.04	0.45	0.02	0.45
943	231	229997	106697	72059	0.02	0.45	0.01	0.45
944	870	297974	150015	402701	0.03	0.64	0.08	0.64
945	547	842002	120890	52909	0.08	0.51	0.01	0.52
946	862	1967373	142635	161427	0.18	0.60	0.03	0.63
947	431	265561	116646	85540	0.02	0.49	0.02	0.50
948	781	2240932	130688	160054	0.21	0.55	0.03	0.59

Information Only

Realization Number	Ranking Based on Dist. from Origin	Phi for Major Observation Groups			Normalized Phi for Major Observation Groups			Distance from Origin
		Pumping Tests	Steady-state Heads	Mills Ranch Pumping Test	Pumping Tests	Steady-state Heads	Mills Ranch Pumping Test	
949	383	320815	113687	277213	0.03	0.48	0.06	0.49
950	318	3036855	90165	51783	0.28	0.38	0.01	0.48
951	310	955355	109436	125061	0.09	0.46	0.03	0.47
952	631	459558	126940	261503	0.04	0.54	0.05	0.54
953	763	934082	136112	166051	0.09	0.58	0.03	0.58
954	153	301942	102728	95869	0.03	0.44	0.02	0.44
955	780	2095212	131348	288845	0.19	0.56	0.06	0.59
956	726	462158	134641	156549	0.04	0.57	0.03	0.57
957	783	3256624	120261	127098	0.30	0.51	0.03	0.59
959	767	236948	138294	100207	0.02	0.59	0.02	0.59
960	618	516474	125911	167922	0.05	0.53	0.03	0.54
961	192	1485386	99108	260326	0.14	0.42	0.05	0.45
962	167	1935697	94550	103869	0.18	0.40	0.02	0.44
963	644	4083535	92242	174939	0.38	0.39	0.04	0.55
964	590	364837	122046	545367	0.03	0.52	0.11	0.53
965	751	696348	135960	213099	0.06	0.58	0.04	0.58
966	205	1161939	102342	127177	0.11	0.43	0.03	0.45
967	126	208802	101695	76758	0.02	0.43	0.02	0.43
968	890	198327	155633	207172	0.02	0.66	0.04	0.66
969	693	560669	131570	149433	0.05	0.56	0.03	0.56
970	72	1819347	88487	118404	0.17	0.38	0.02	0.41
971	328	327314	111984	125309	0.03	0.47	0.03	0.48
972	716	348065	133644	111617	0.03	0.57	0.02	0.57
974	265	282596	107997	243220	0.03	0.46	0.05	0.46
975	445	301375	117478	82966	0.03	0.50	0.02	0.50
976	611	210615	125771	193150	0.02	0.53	0.04	0.54
977	943	6074916	120110	66873	0.56	0.51	0.01	0.76
978	462	1581056	112888	257180	0.15	0.48	0.05	0.50
979	533	3359907	96834	99449	0.31	0.41	0.02	0.52

Information Only

Realization Number	Ranking Based on Dist. from Origin	Phi for Major Observation Groups			Normalized Phi for Major Observation Groups			Distance from Origin
		Pumping Tests	Steady-state Heads	Mills Ranch Pumping Test	Pumping Tests	Steady-state Heads	Mills Ranch Pumping Test	
980	447	438375	117410	80827	0.04	0.50	0.02	0.50
981	864	269945	130311	1556000	0.03	0.55	0.31	0.64
982	511	384814	120507	72377	0.04	0.51	0.01	0.51
983	91	350540	98143	111779	0.03	0.42	0.02	0.42
984	306	293207	110710	212987	0.03	0.47	0.04	0.47
986	951	469390	184274	160997	0.04	0.78	0.03	0.78
987	409	323691	115673	102965	0.03	0.49	0.02	0.49
988	75	926943	94731	191165	0.09	0.40	0.04	0.41
989	179	405770	103380	249317	0.04	0.44	0.05	0.44
990	665	465857	127528	544000	0.04	0.54	0.11	0.55
991	622	431525	126260	183076	0.04	0.54	0.04	0.54
992	343	1290031	109215	134865	0.12	0.46	0.03	0.48
993	846	381421	146082	172761	0.04	0.62	0.03	0.62
994	370	366003	113662	124012	0.03	0.48	0.02	0.48
995	801	256537	141217	225170	0.02	0.60	0.05	0.60
996	521	306673	120726	177357	0.03	0.51	0.04	0.51
997	208	1872726	97135	167910	0.17	0.41	0.03	0.45
998	239	1734391	100197	79910	0.16	0.42	0.02	0.45
999	699	3222375	111827	278121	0.30	0.47	0.06	0.56

Information Only

7.2 Distribution of Steady-State Freshwater Heads

Figure 47 through **Figure 93** present plots of the steady-state freshwater head distributions for each of the wells, for the 100 selected realizations. Heads are bi-linearly interpolated from the cell-centered mesh values predicted by MODFLOW6 to the well's coordinates. Observations are described in Task 1 of the AR.

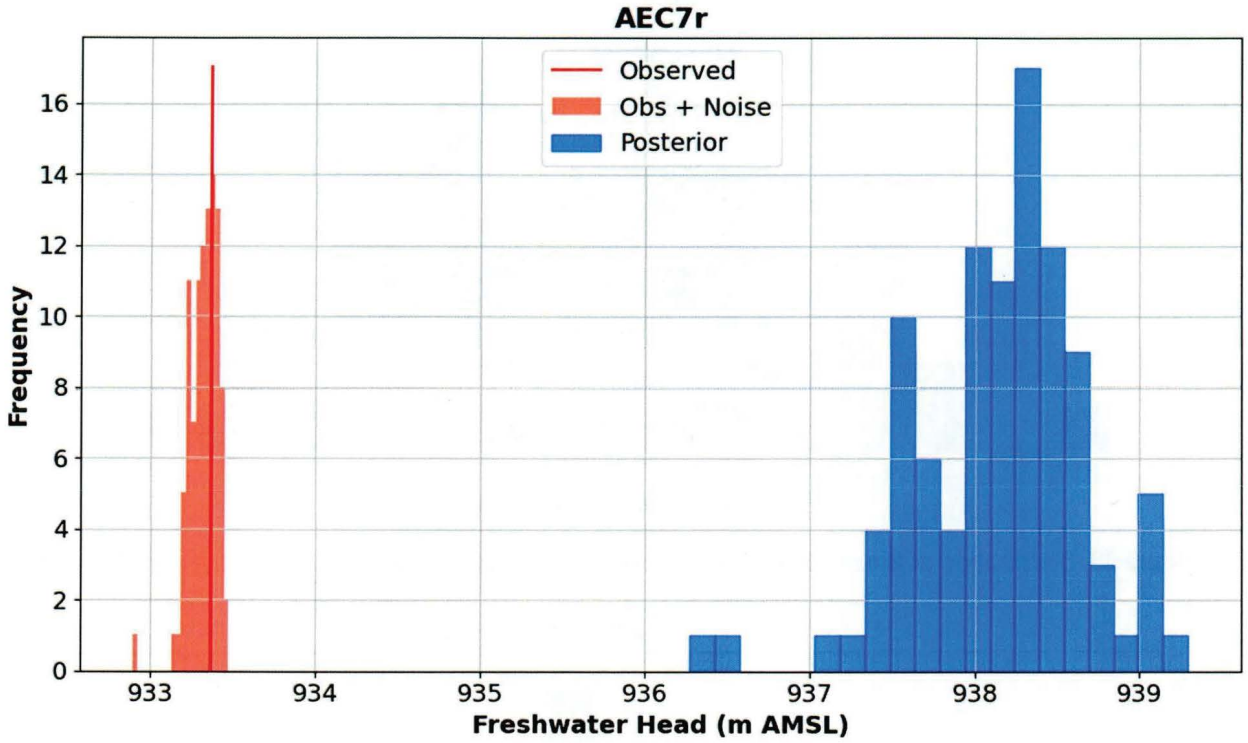

Figure 47. Distribution of Steady-State Freshwater Heads in AEC-7R for 100 Realizations at Iteration 5

Information Only

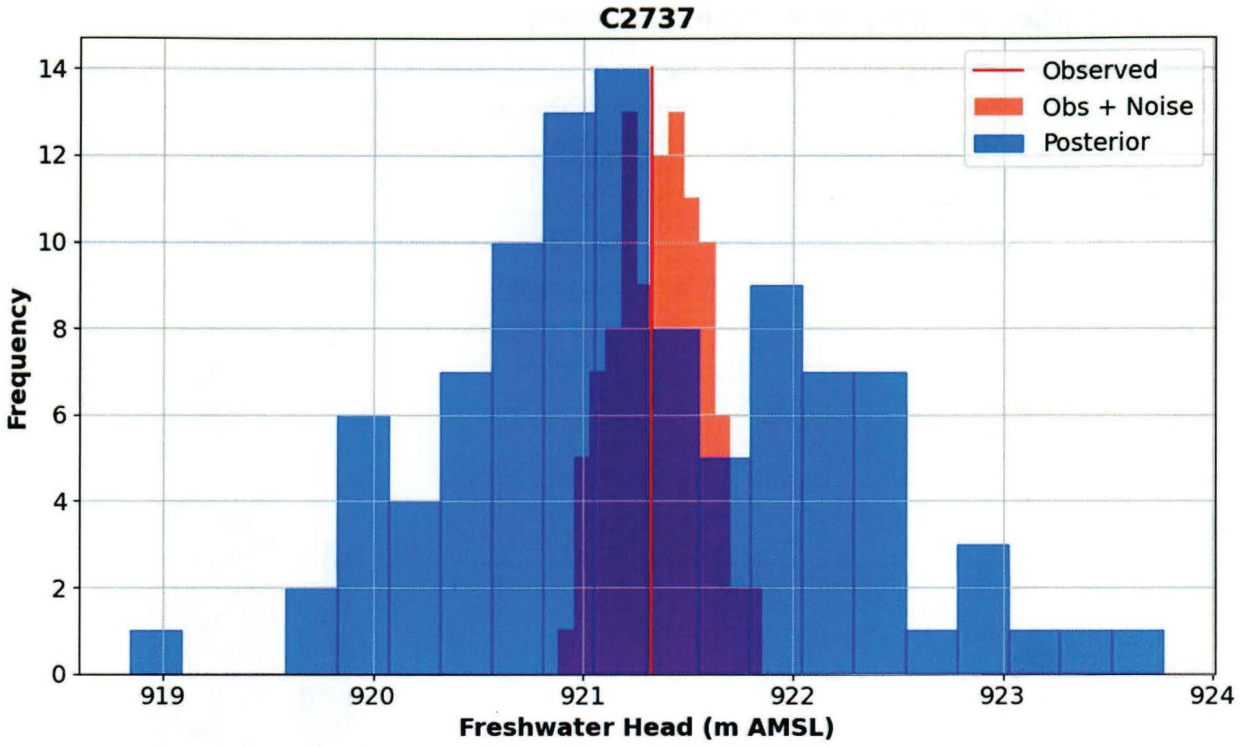

Figure 48. Distribution of Steady-State Freshwater Heads in C-2737 for 100 Realizations at Iteration 5

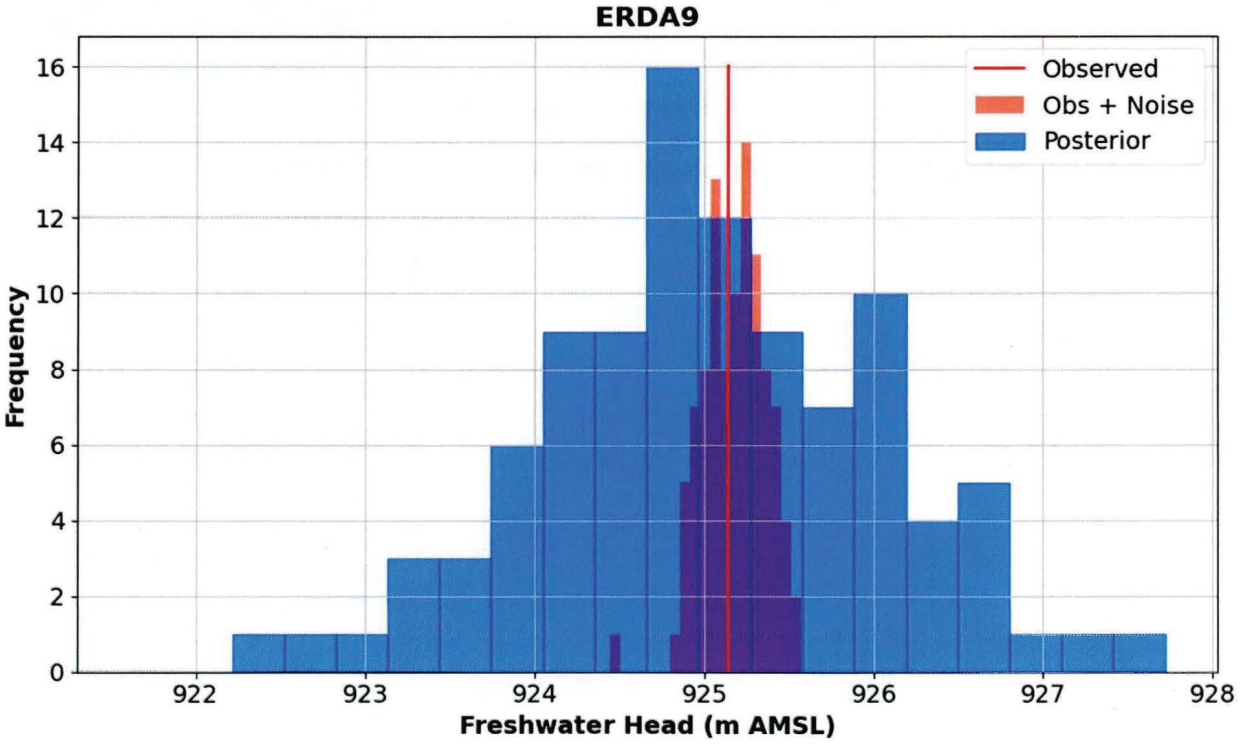

Figure 49. Distribution of Steady-State Freshwater Heads in ERDA-9 for 100 Realizations at Iteration 5

Information Only

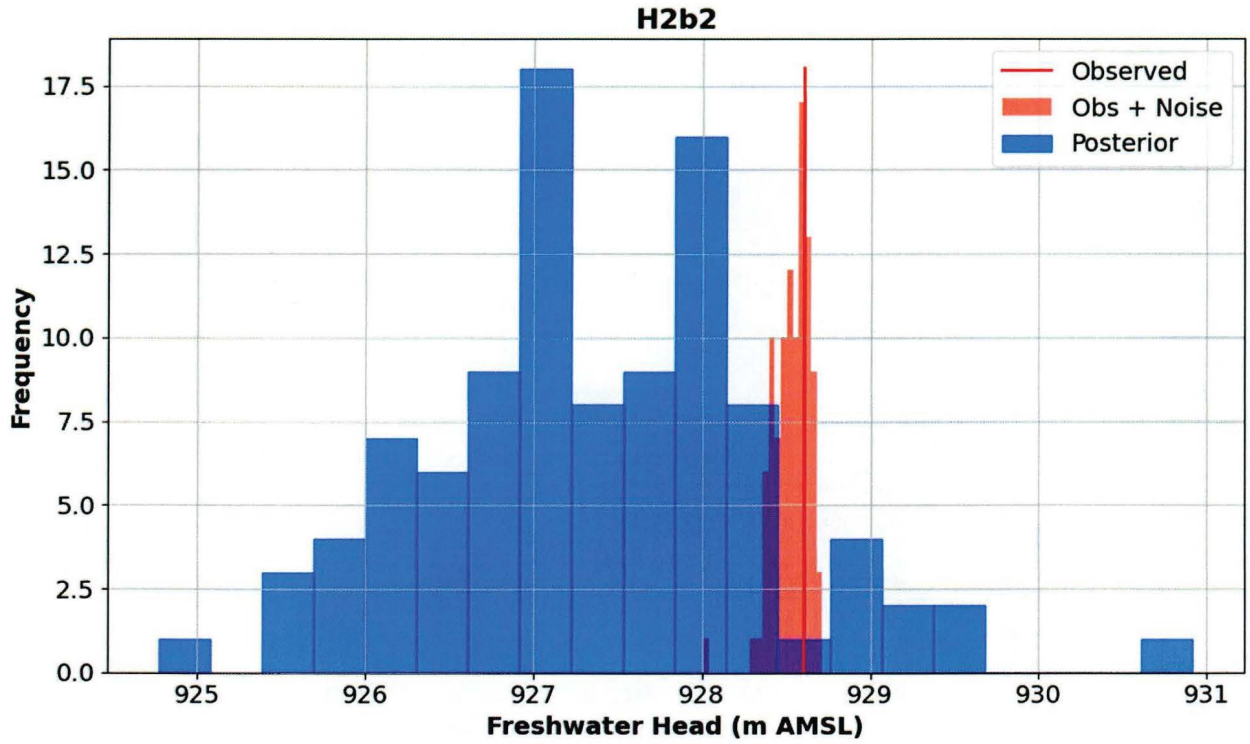

Figure 50. Distribution of Steady-State Freshwater Heads in H-2b2 for 100 Realizations at Iteration 5

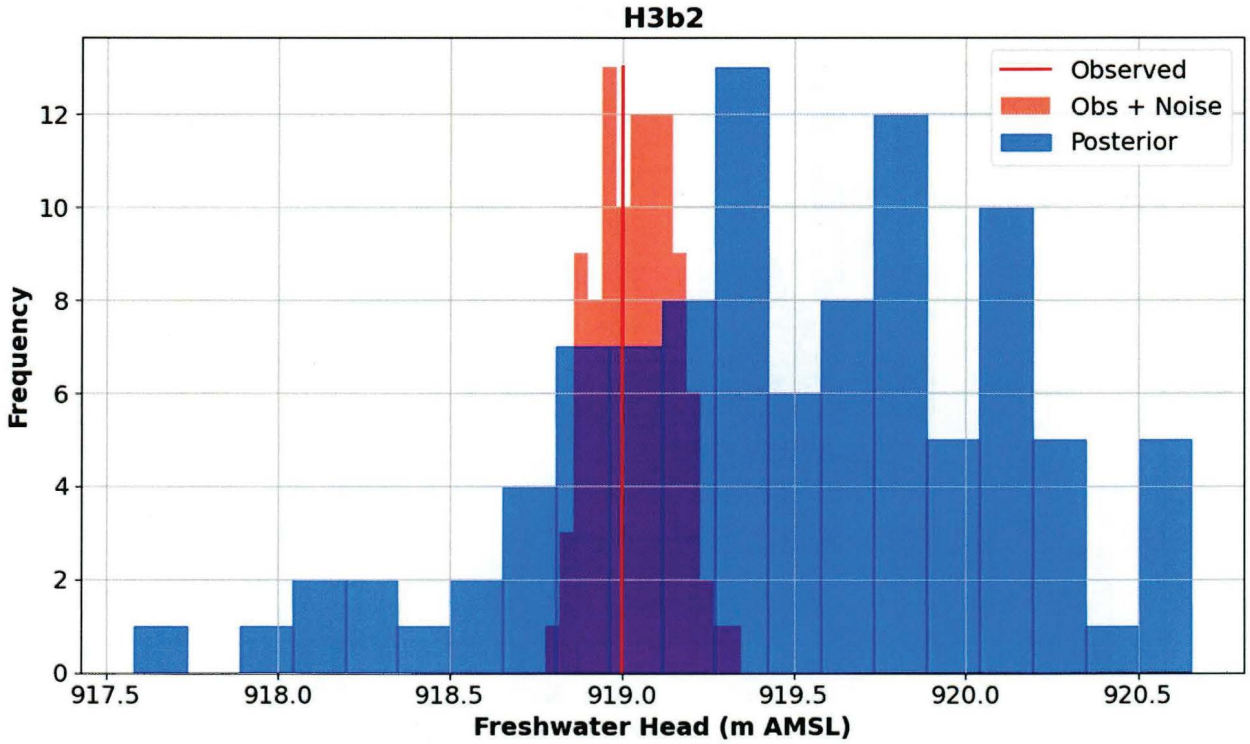

Figure 51. Distribution of Steady-State Freshwater Heads in H-3b2 for 100 Realizations at Iteration 5

Information Only

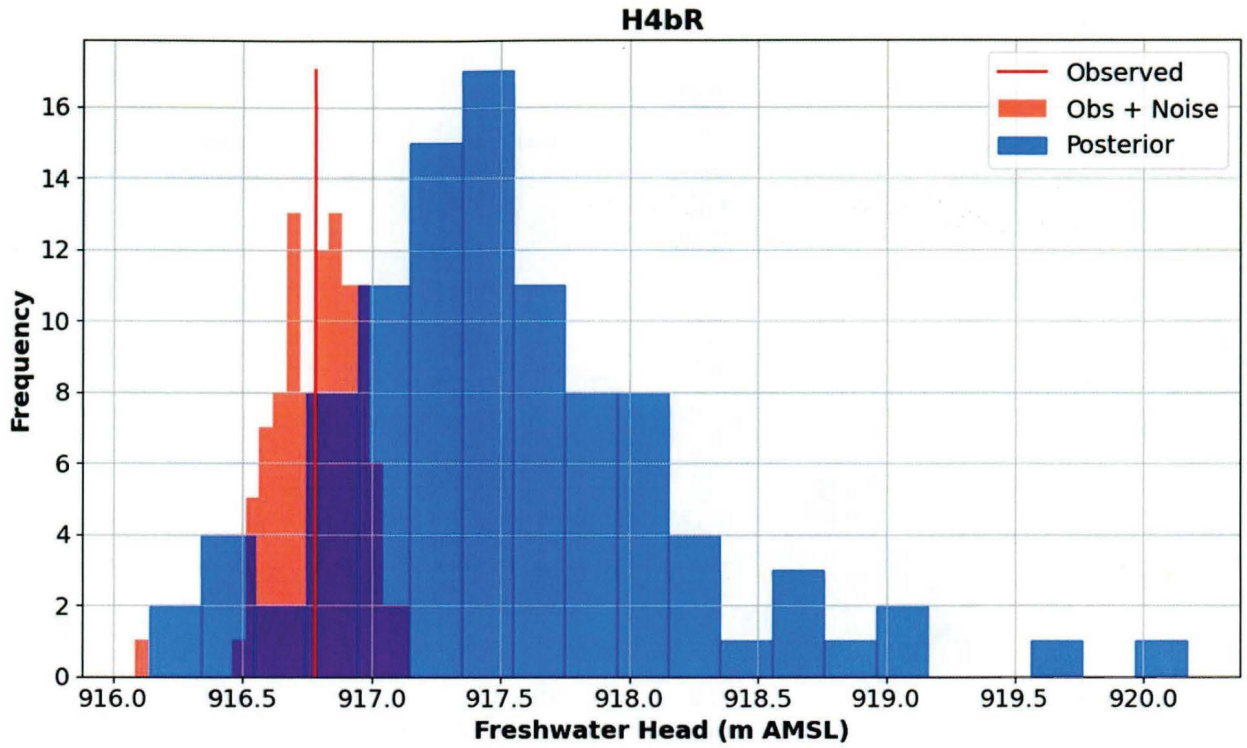

Figure 52. Distribution of Steady-State Freshwater Heads in H-4bR for 100 Realizations at Iteration 5

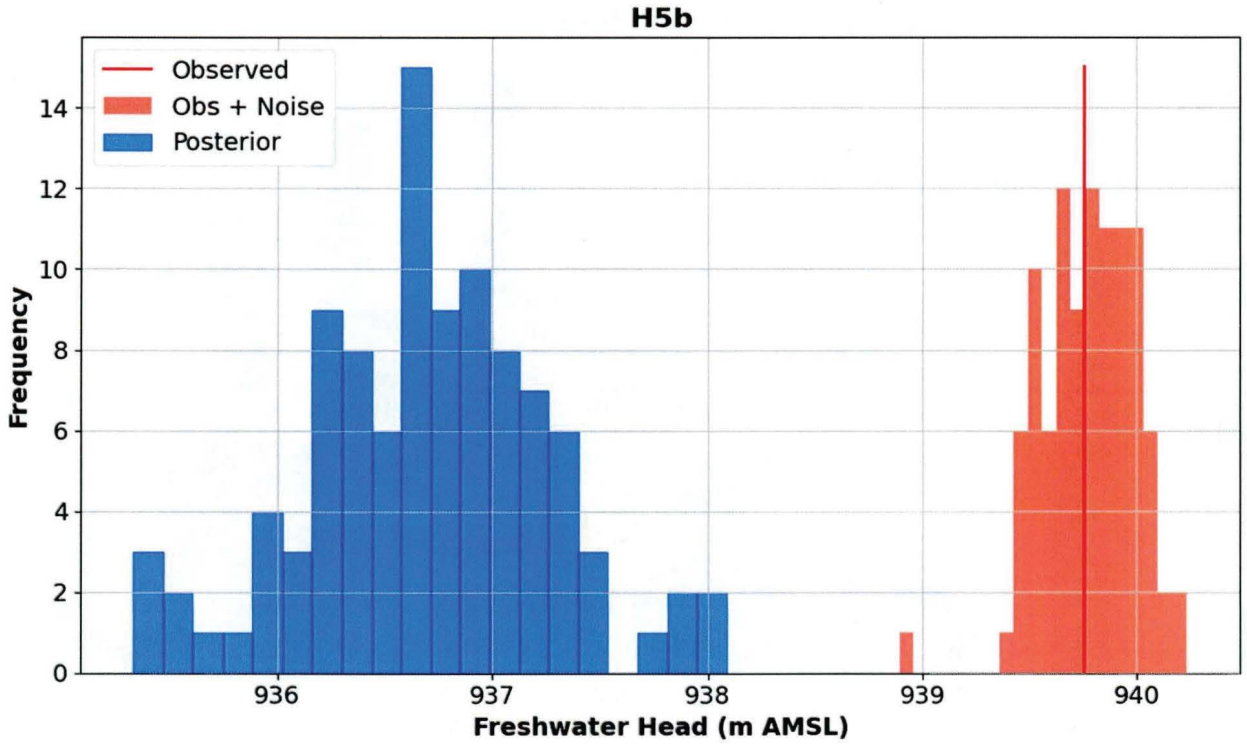

Figure 53. Distribution of Steady-State Freshwater Heads in H-5b for 100 Realizations at Iteration 5

Information Only

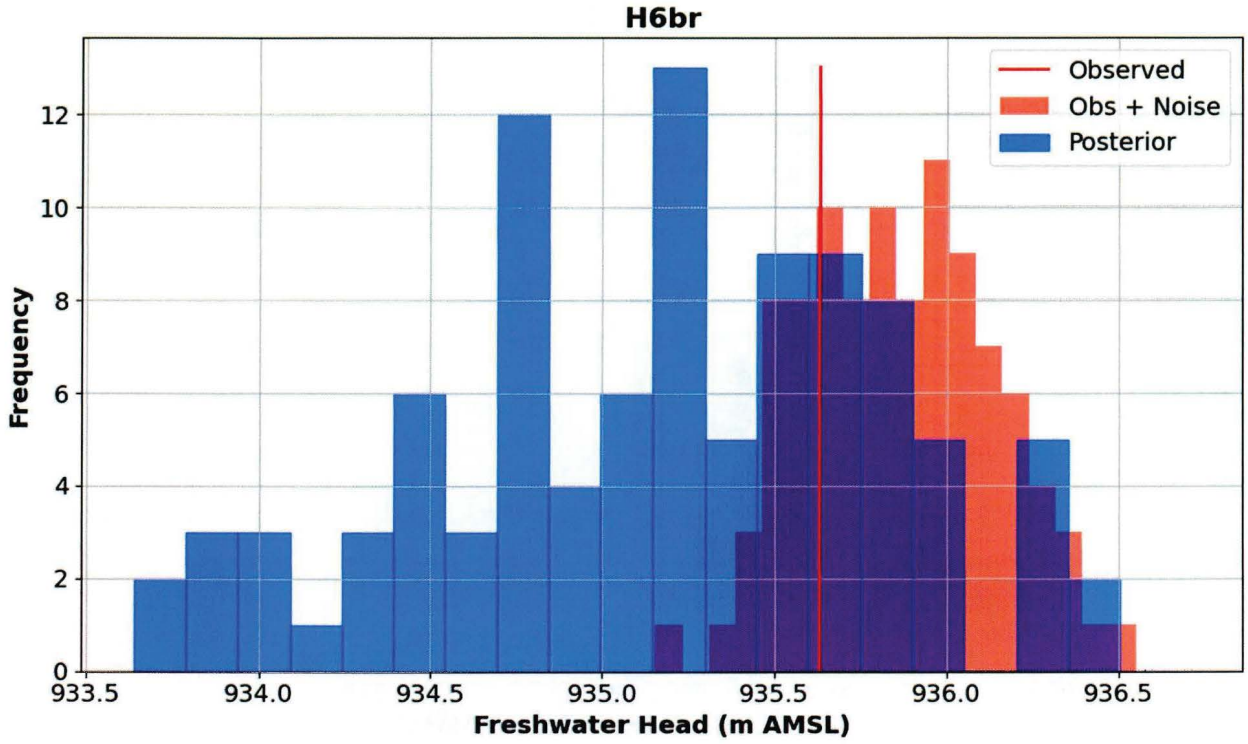

Figure 54. Distribution of Steady-State Freshwater Heads in H-6bR for 100 Realizations from Iteration 5

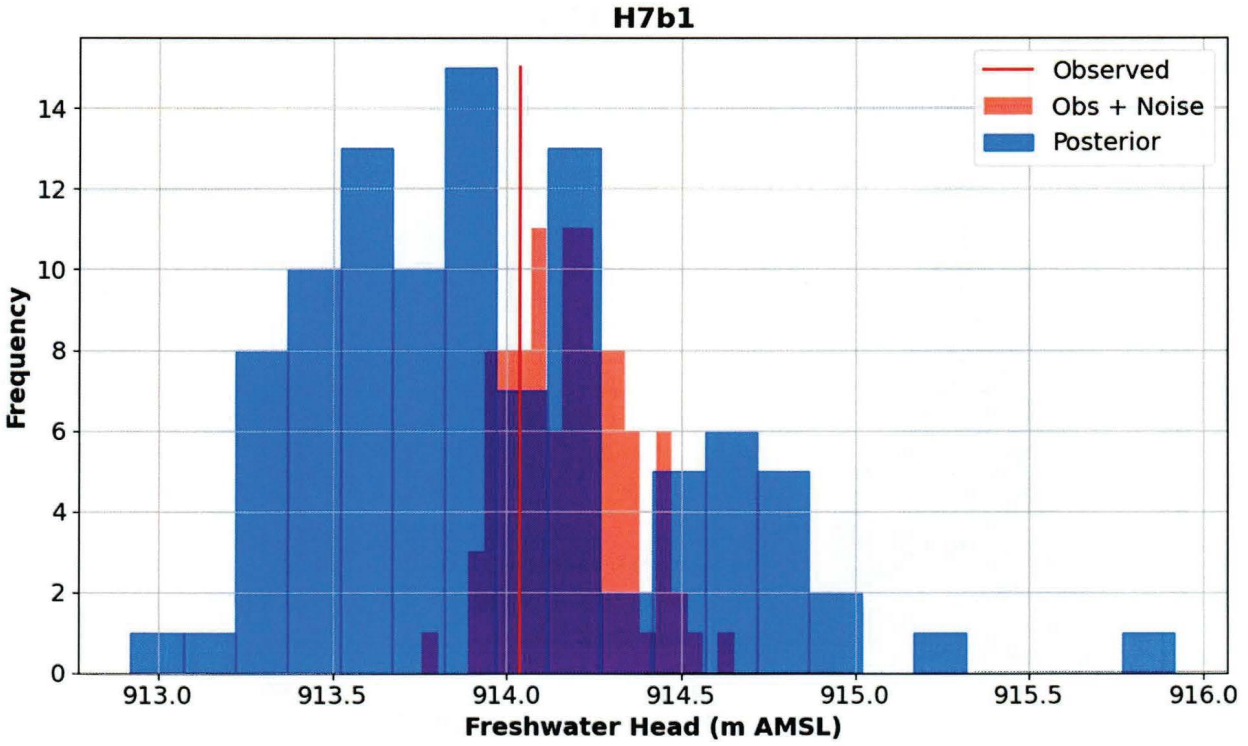

Figure 55. Distribution of Steady-State Freshwater Heads in H-7b1 for 100 Realizations at Iteration 5

Information Only

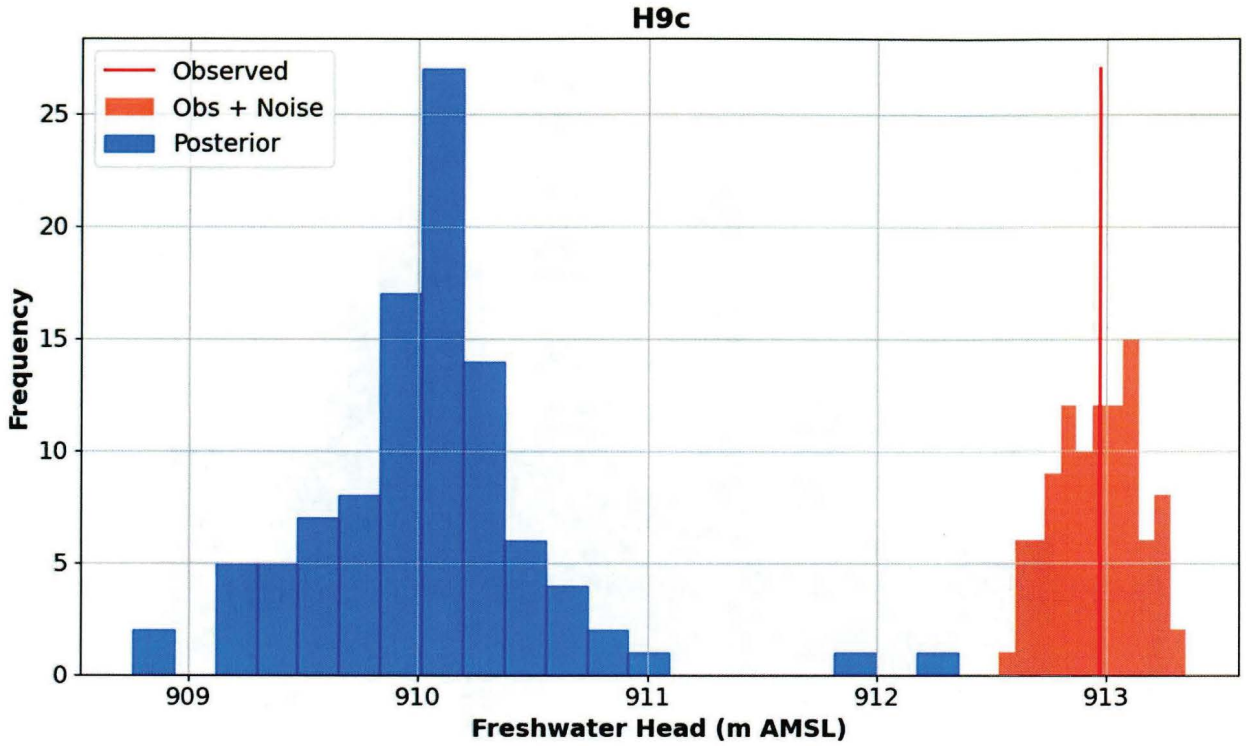

Figure 56. Distribution of Steady-State Freshwater Heads in H-9c for 100 Realizations at Iteration 5

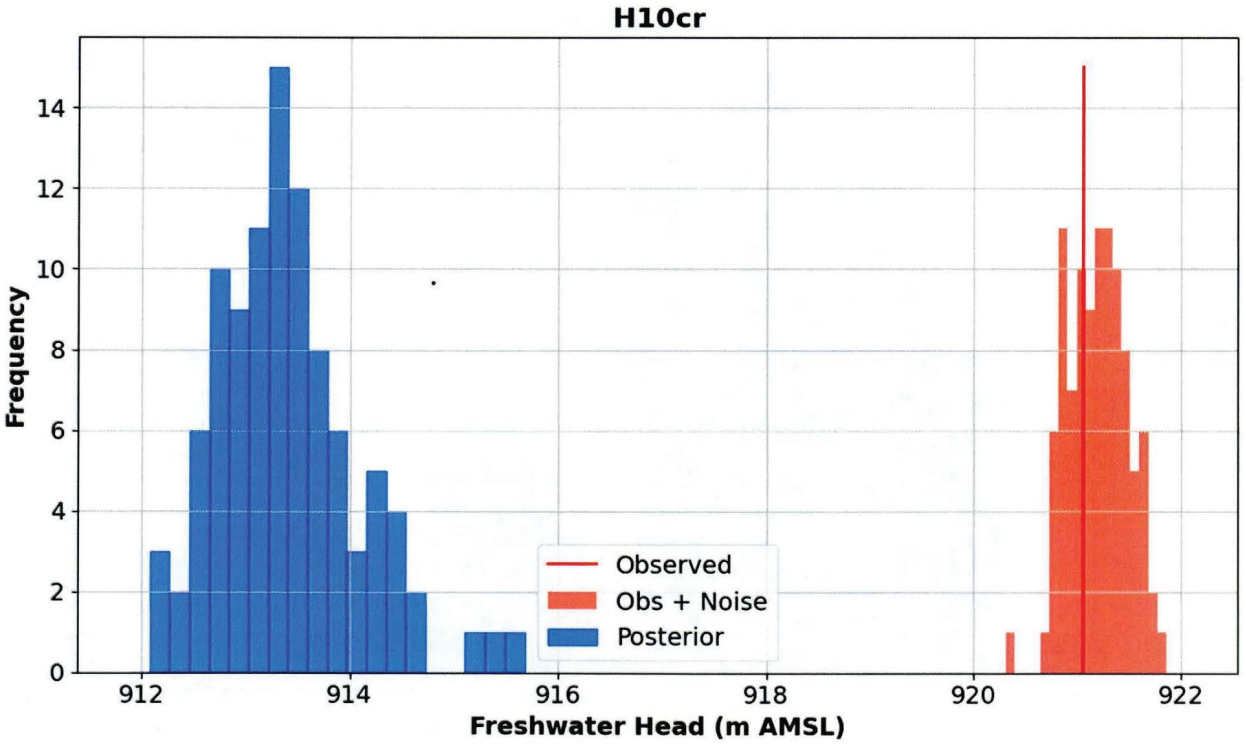

Figure 57. Distribution of Steady-State Freshwater Heads in H-10cR for 100 Realizations from Iteration 5

Information Only

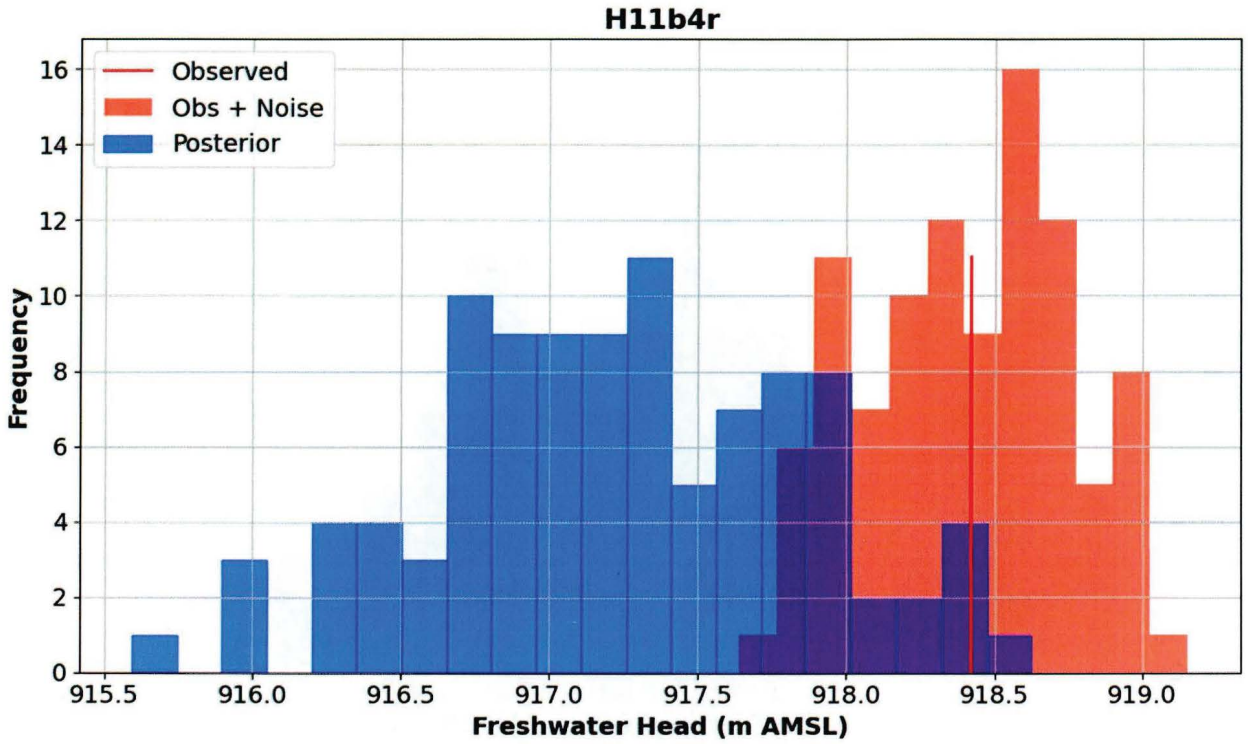

Figure 58. Distribution of Steady-State Freshwater Heads in H-11b4R for 100 Realizations at Iteration 5

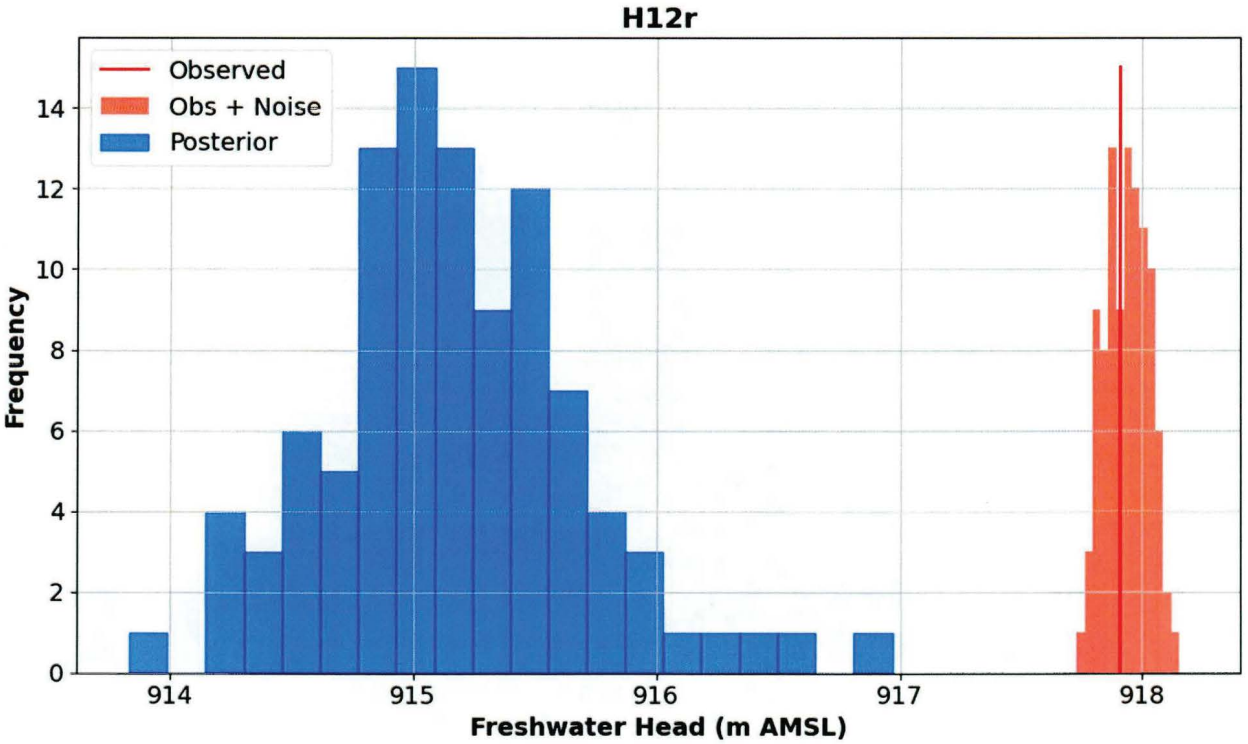

Figure 59. Distribution of Steady-State Freshwater Heads in H-12R for 100 Realizations at Iteration 5

Information Only

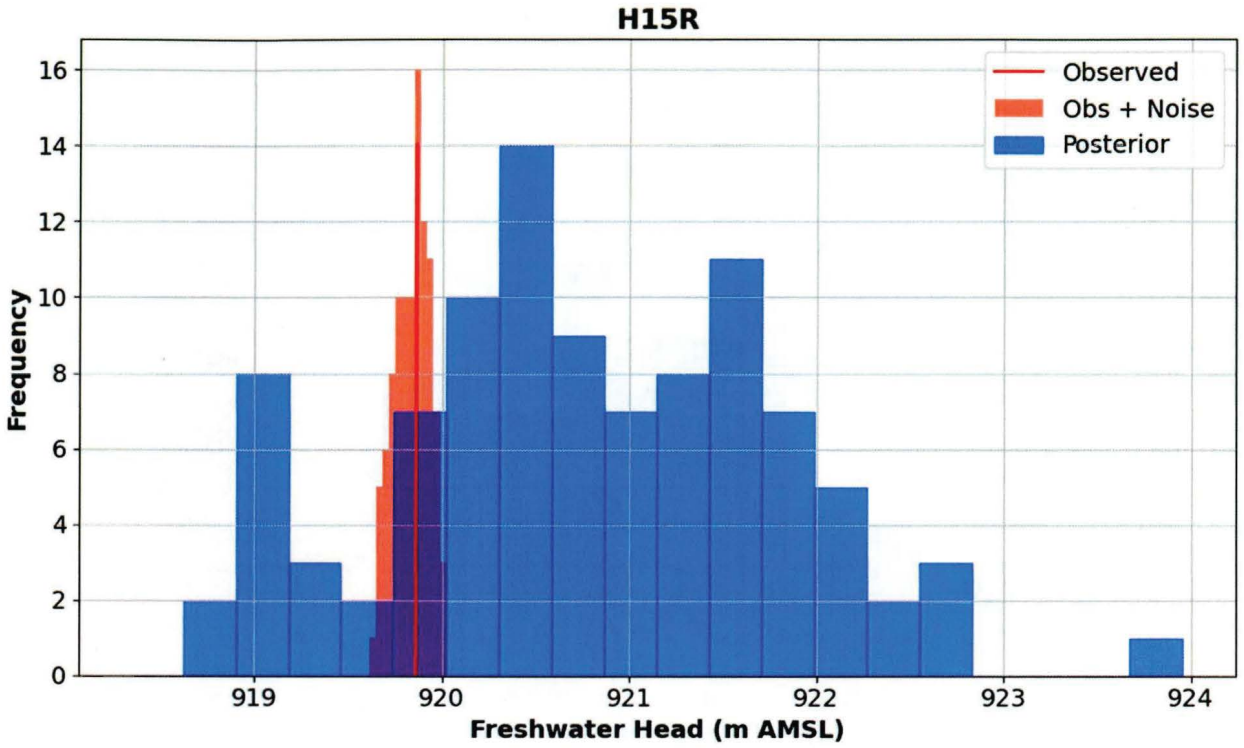

Figure 60. Distribution of Steady-State Freshwater Heads in H-15R for 100 Realizations at Iteration 5

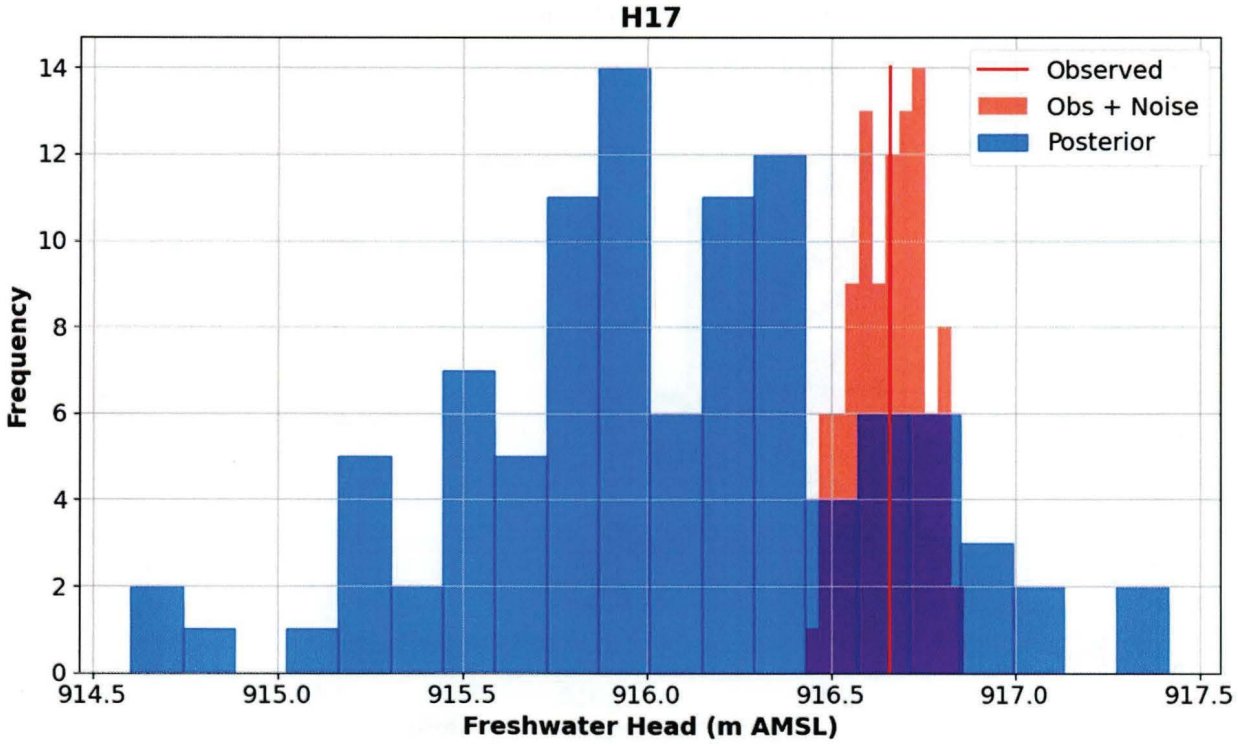

Figure 61. Distribution of Steady-State Freshwater Heads in H-17 for 100 Realizations at Iteration 5

Information Only

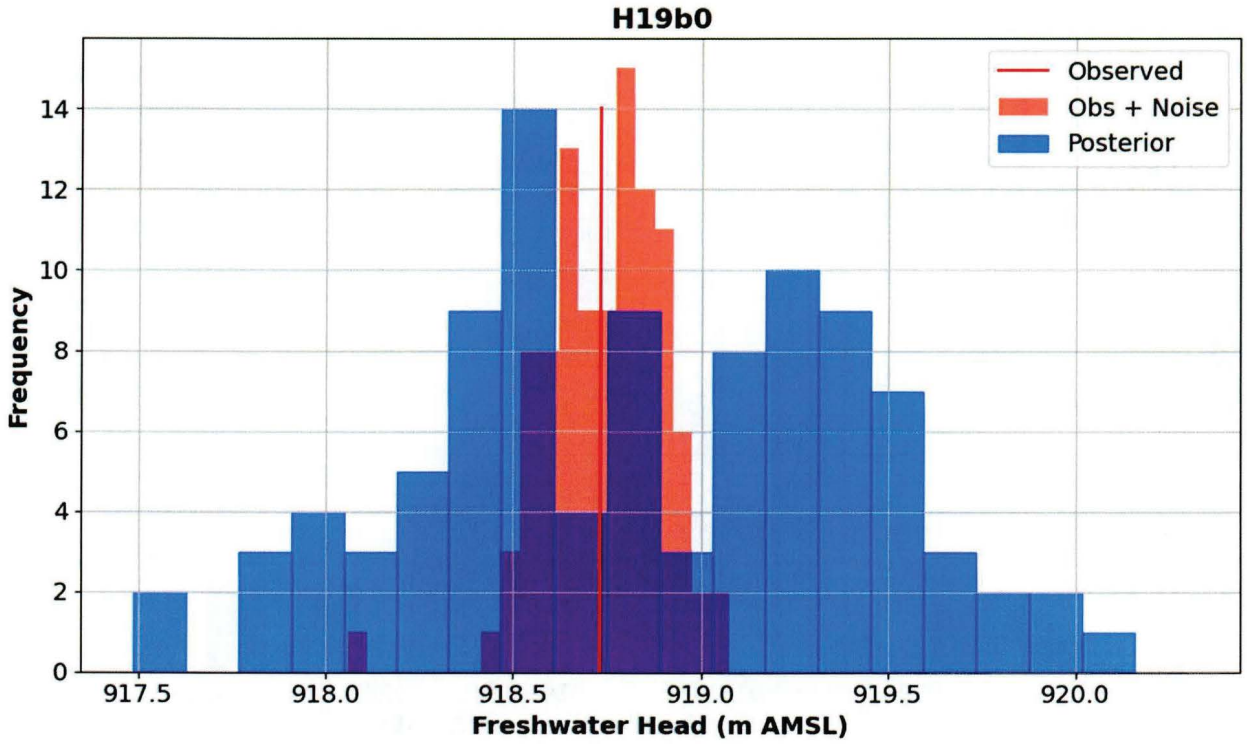

Figure 62. Distribution of Steady-State Freshwater Heads in H-19b0 for 100 Realizations at Iteration 5

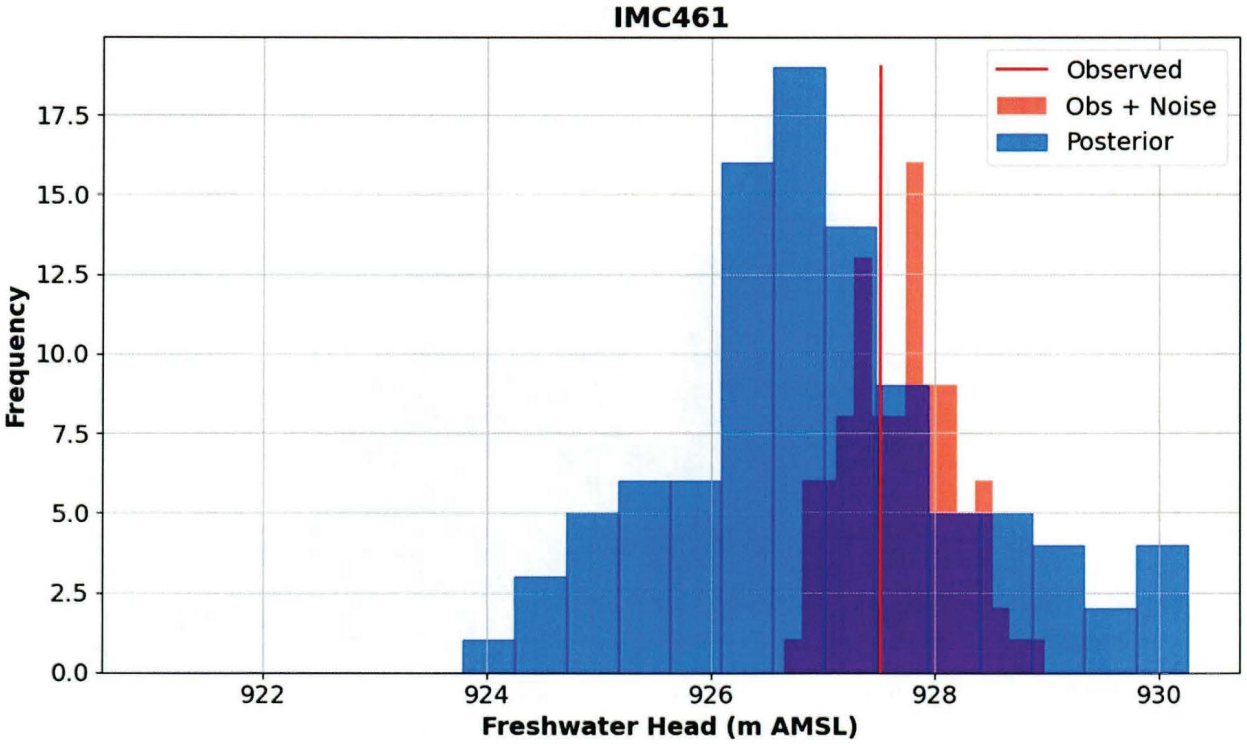

Figure 63. Distribution of Steady-State Freshwater Heads in IMC-461 for 100 Realizations at Iteration 5

Information Only

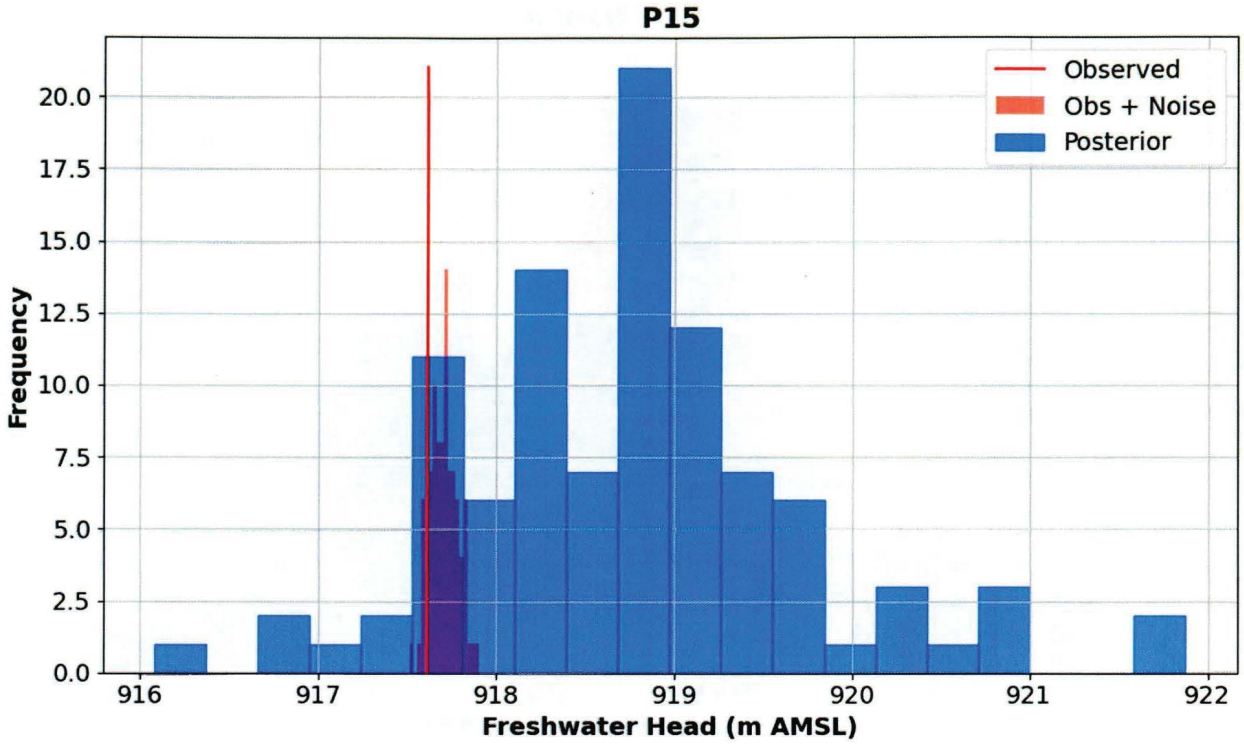

Figure 64. Distribution of Steady-State Freshwater Heads in P-15 for 100 Realizations at Iteration 5

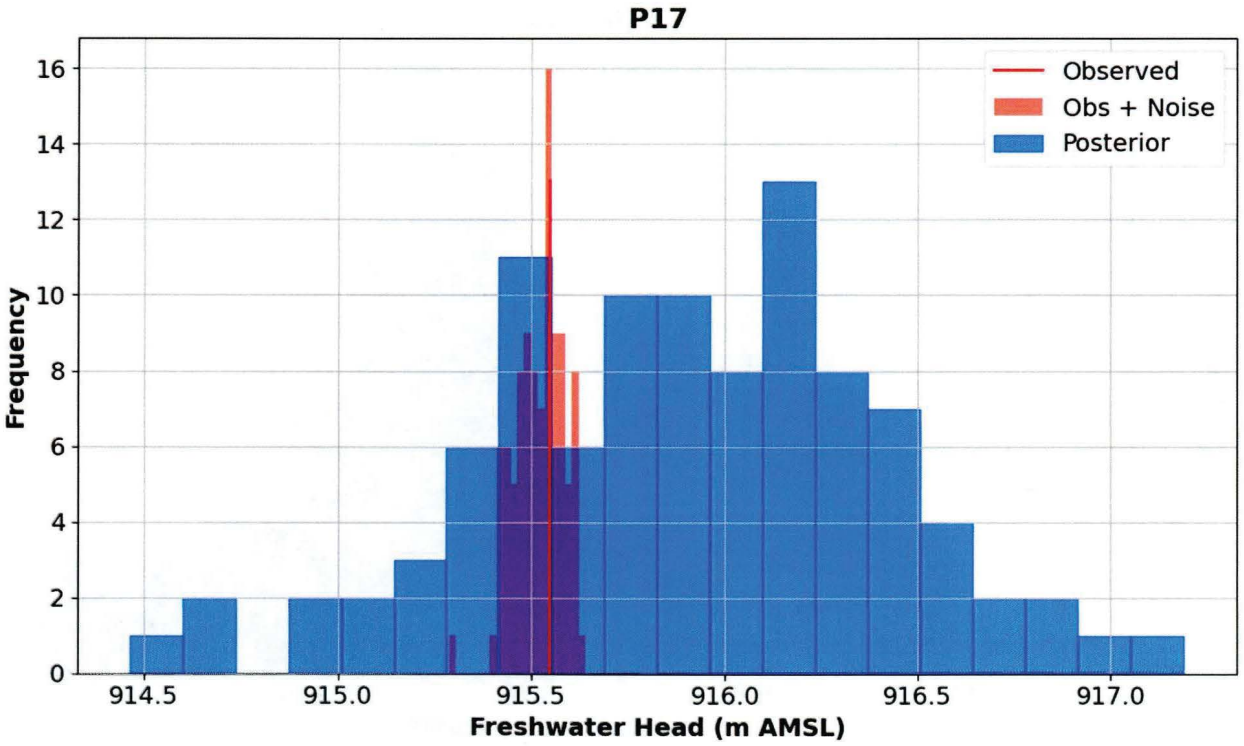

Figure 65. Distribution of Steady-State Freshwater Heads in P-17 for 100 Realizations at Iteration 5

Information Only

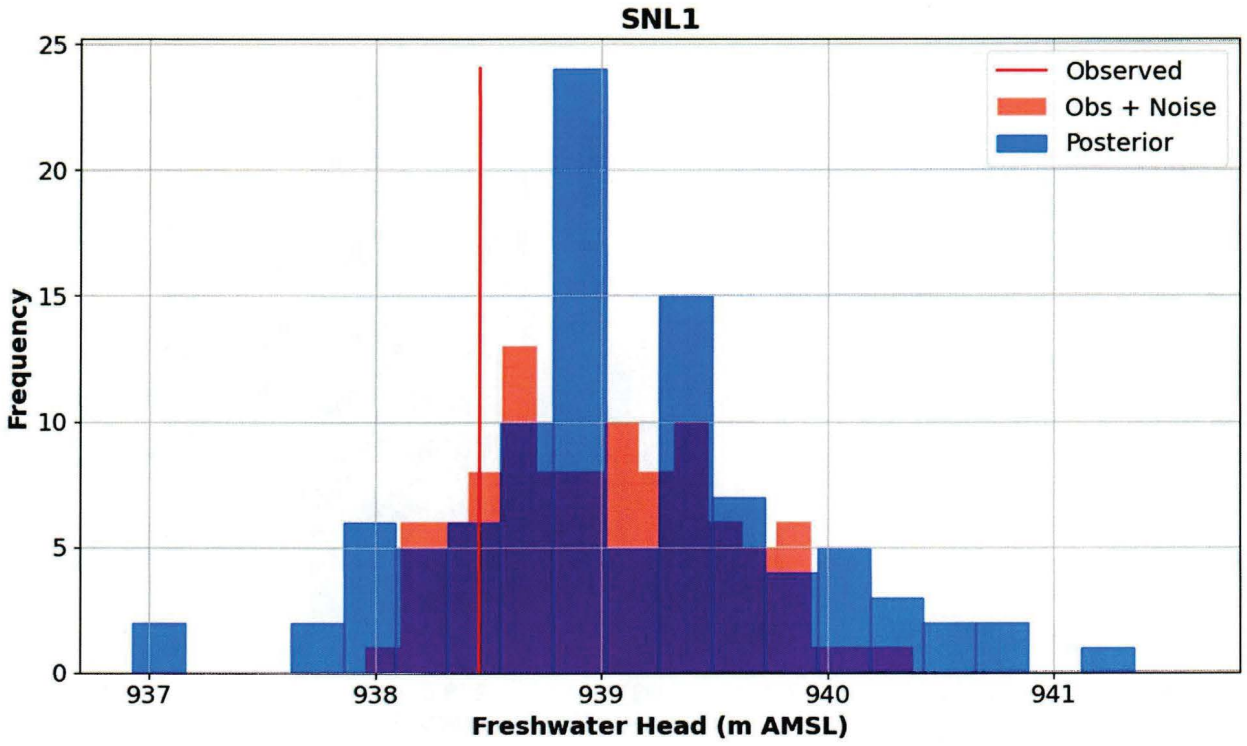

Figure 66. Distribution of Steady-State Freshwater Heads in SNL-1 for 100 Realizations at Iteration 5

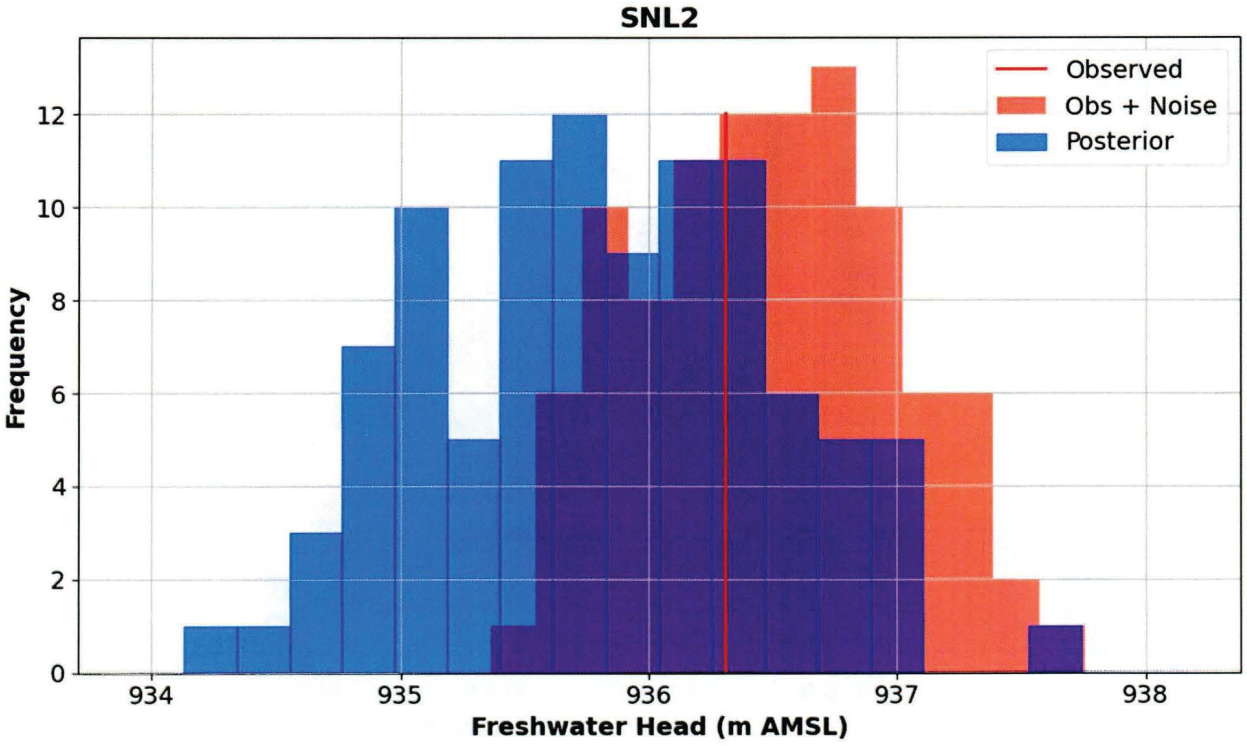

Figure 67. Distribution of Steady-State Freshwater Heads in SNL-2 for 100 Realizations at Iteration 5

Information Only

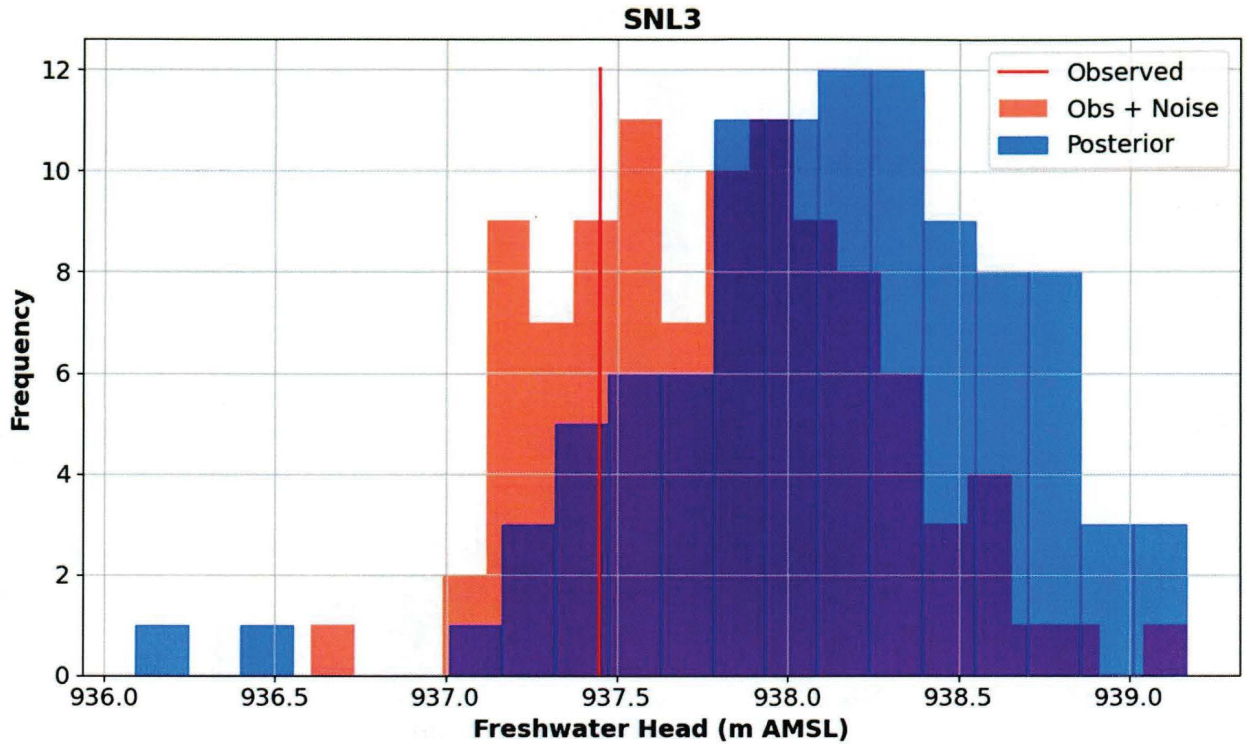

Figure 68. Distribution of Steady-State Freshwater Heads in SNL-3 for 100 Realizations at Iteration 5

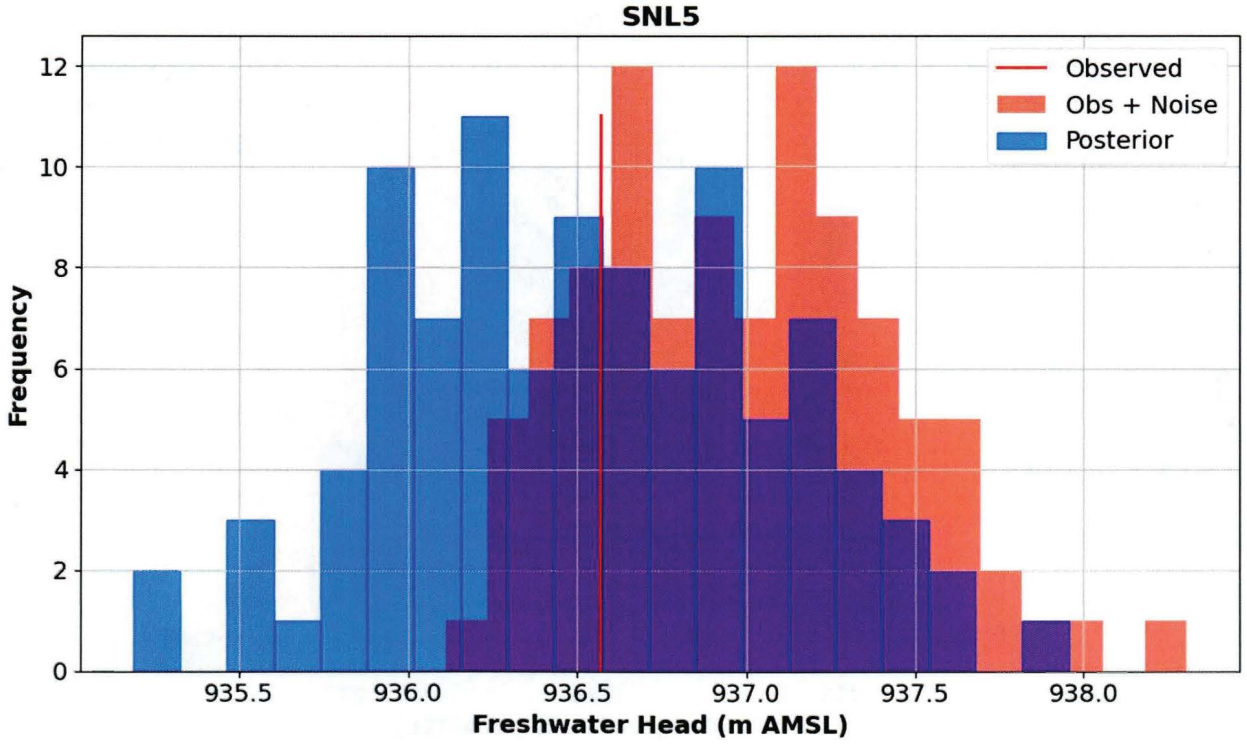

Figure 69. Distribution of Steady-State Freshwater Heads in SNL-5 for 100 Realizations at Iteration 5

Information Only

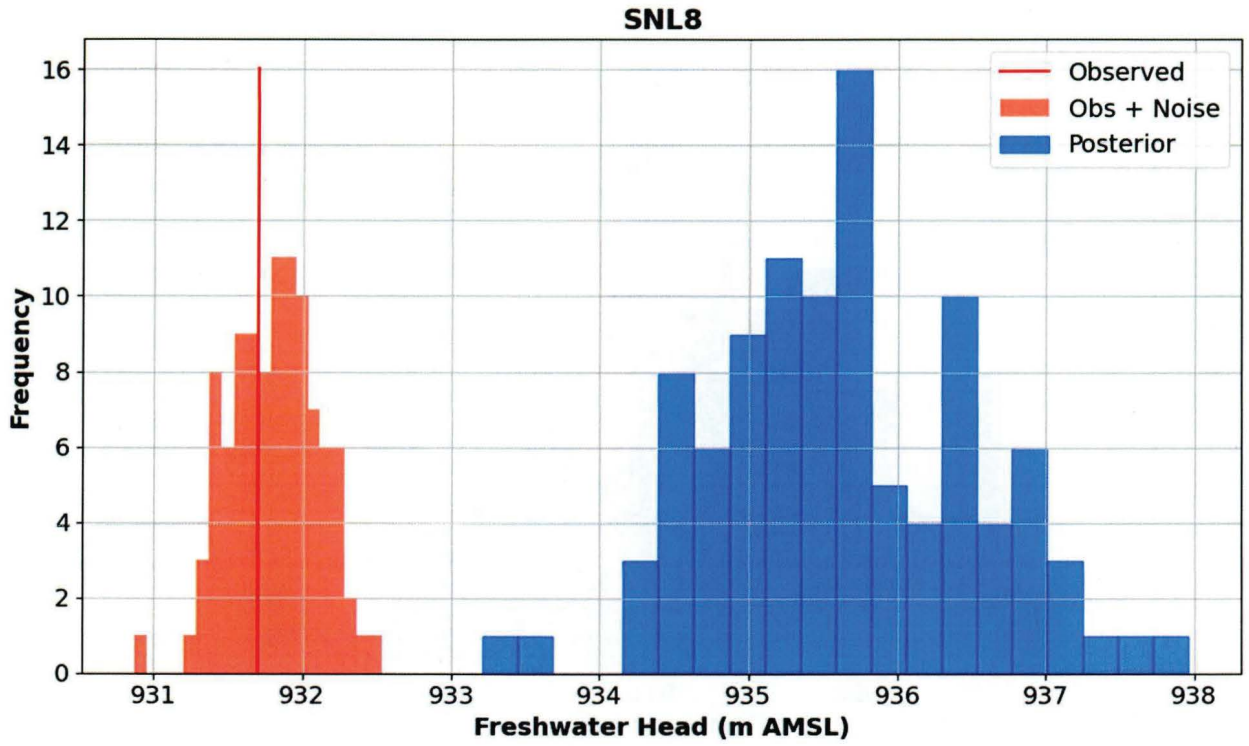

Figure 70. Distribution of Steady-State Freshwater Heads in SNL-8 for 100 Realizations at Iteration 5

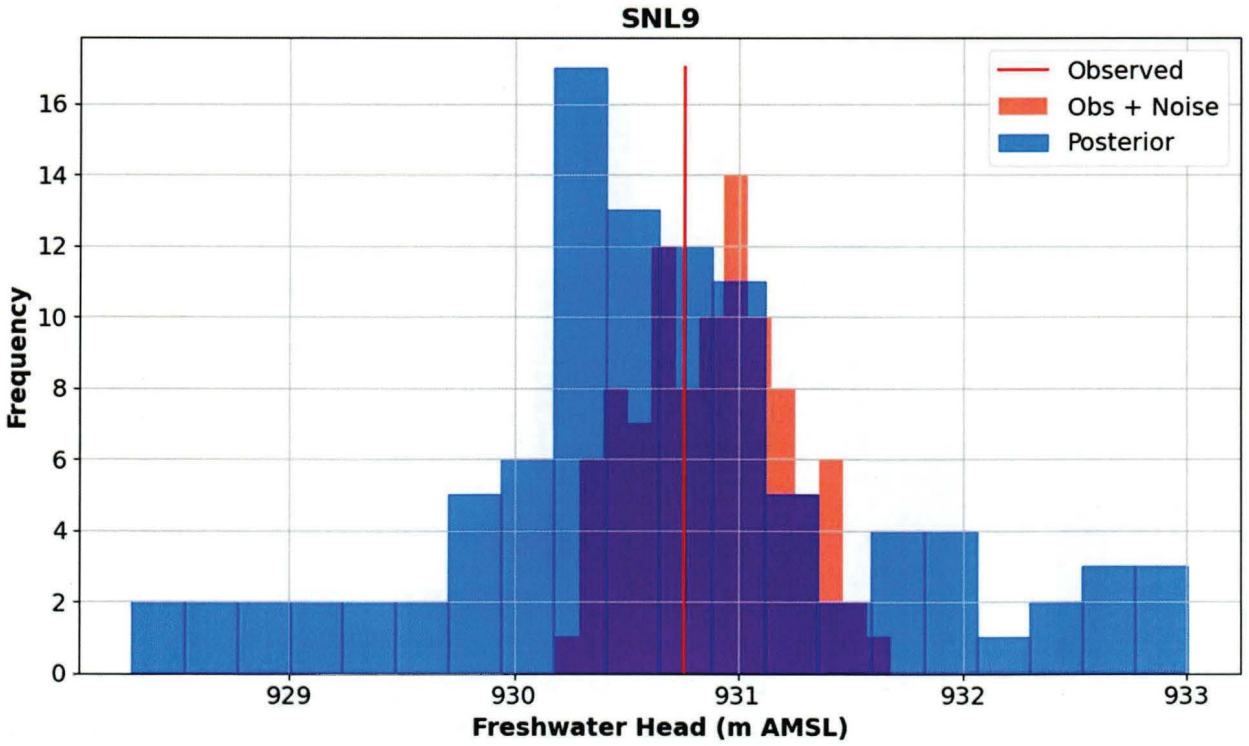

Figure 71. Distribution of Steady-State Freshwater Heads in SNL-9 for 100 Realizations at Iteration 5

Information Only

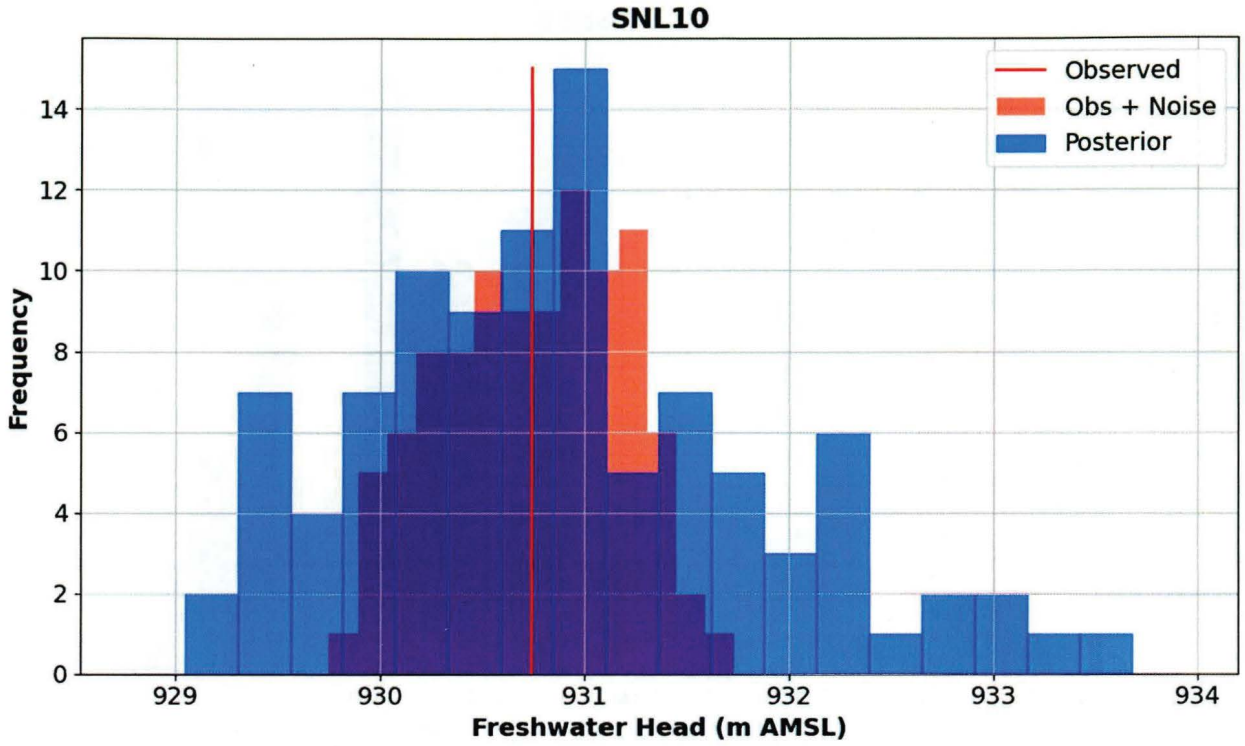

Figure 72. Distribution of Steady-State Freshwater Heads in SNL-10 for 100 Realizations at Iteration 5

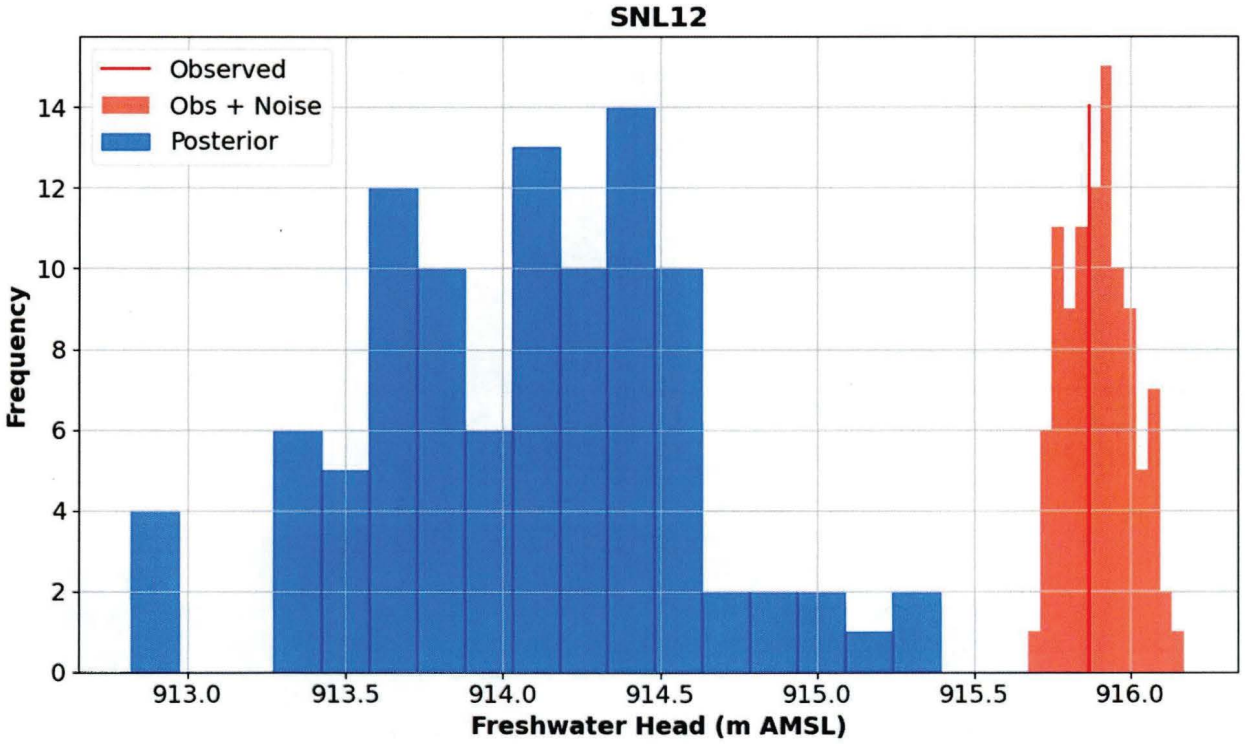

Figure 73. Distribution of Steady-State Freshwater Heads in SNL-12 for 100 Realizations at Iteration 5

Information Only

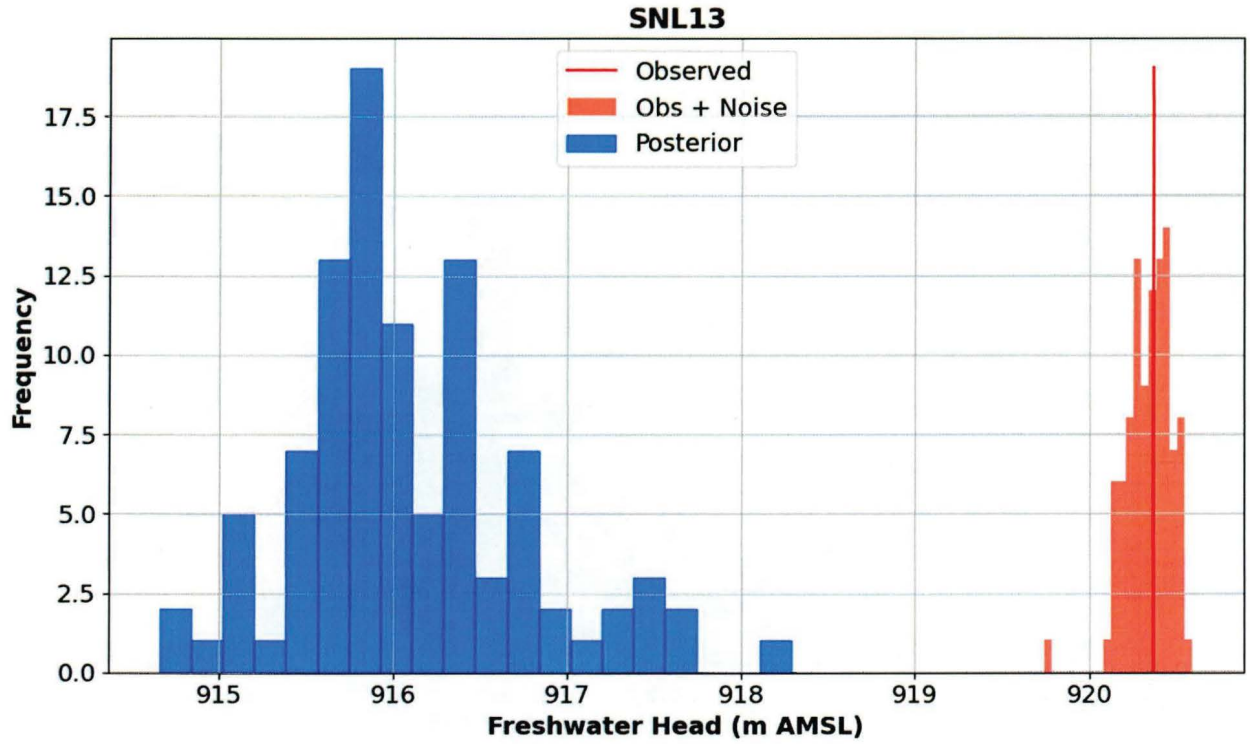

Figure 74. Distribution of Steady-State Freshwater Heads in SNL-13 for 100 Realizations at Iteration 5

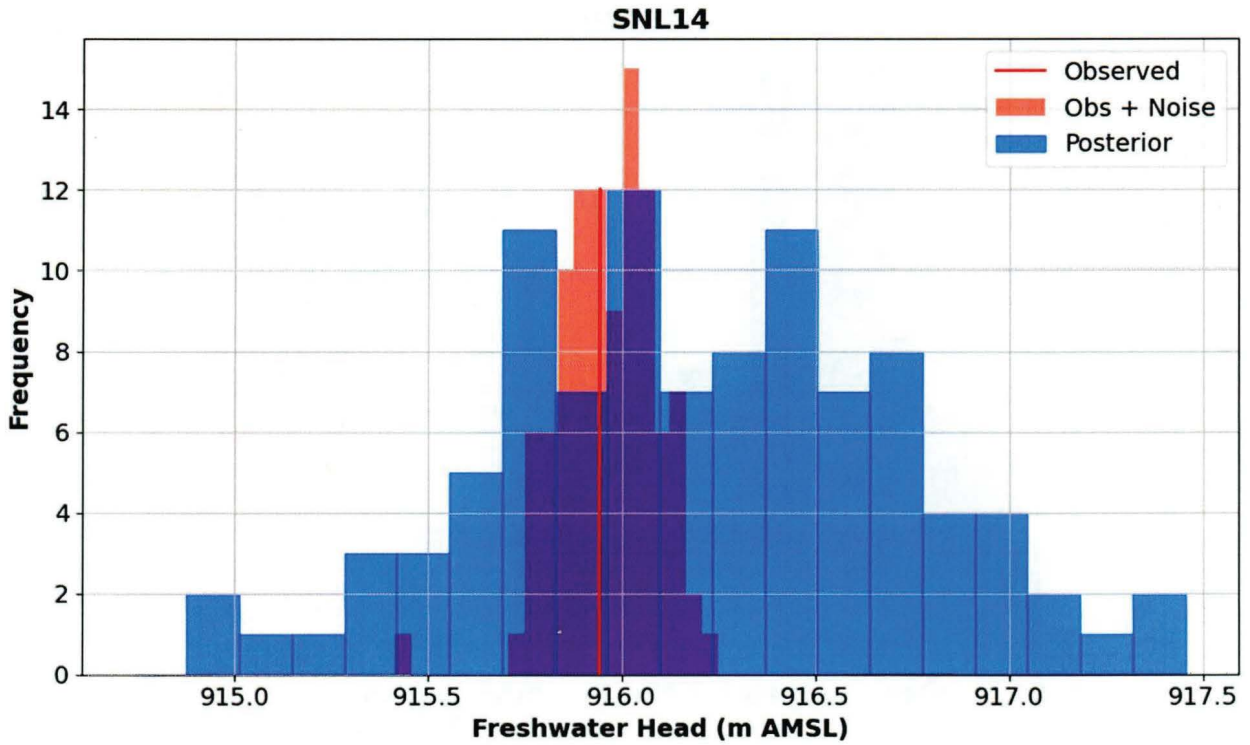

Figure 75. Distribution of Steady-State Freshwater Heads in SNL-14 for 100 Realizations at Iteration 5

Information Only

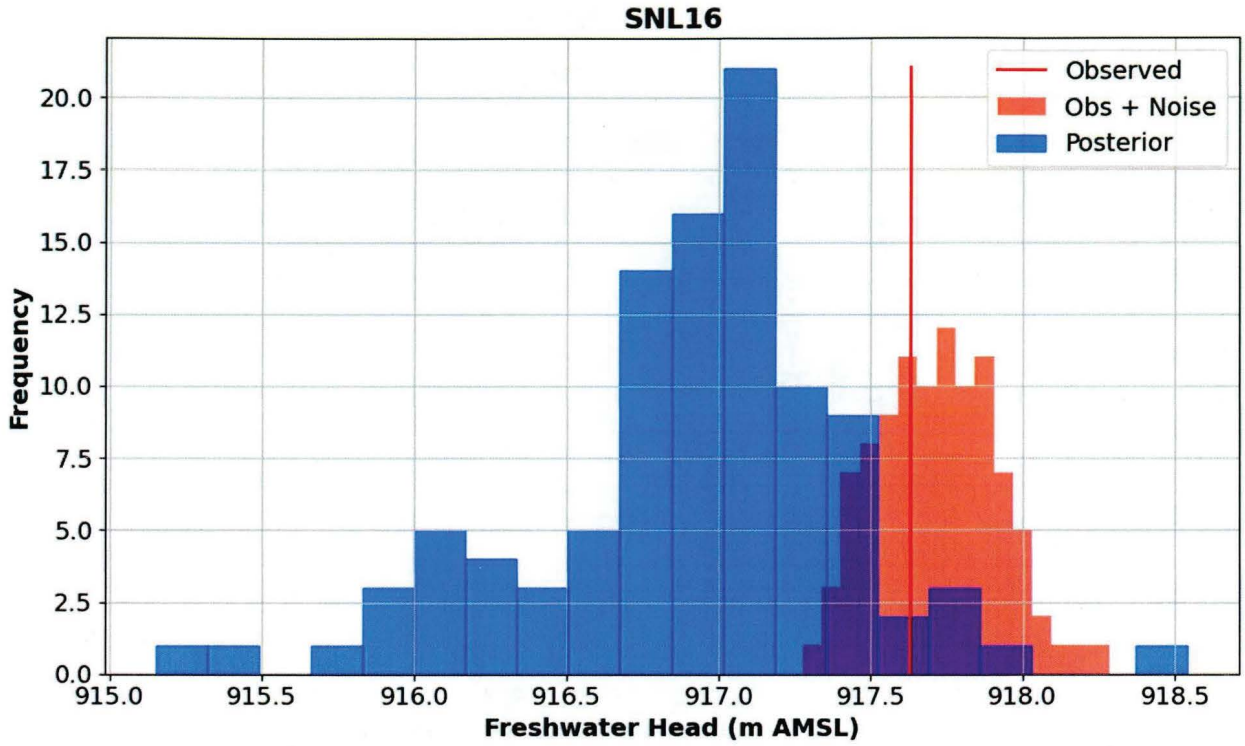

Figure 76. Distribution of Steady-State Freshwater Heads in SNL-16 for 100 Realizations at Iteration 5

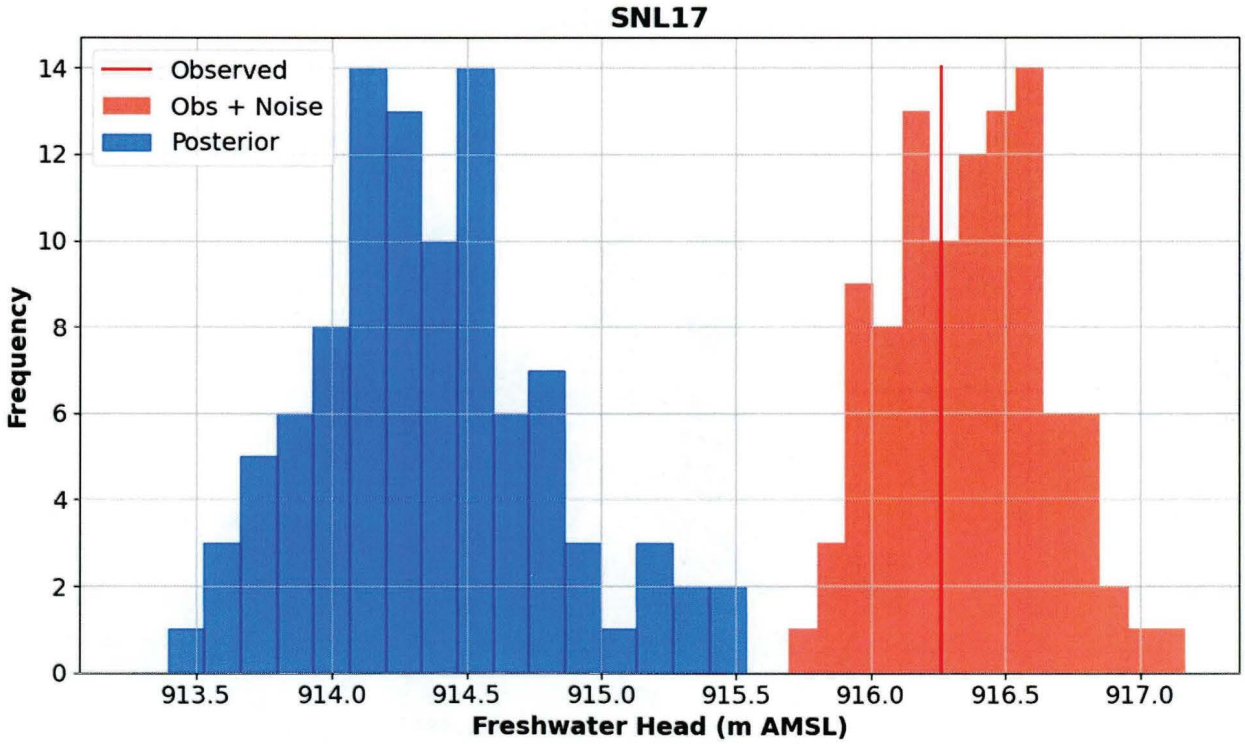

Figure 77. Distribution of Steady-State Freshwater Heads in SNL-17 for 100 Realizations at Iteration 5

Information Only

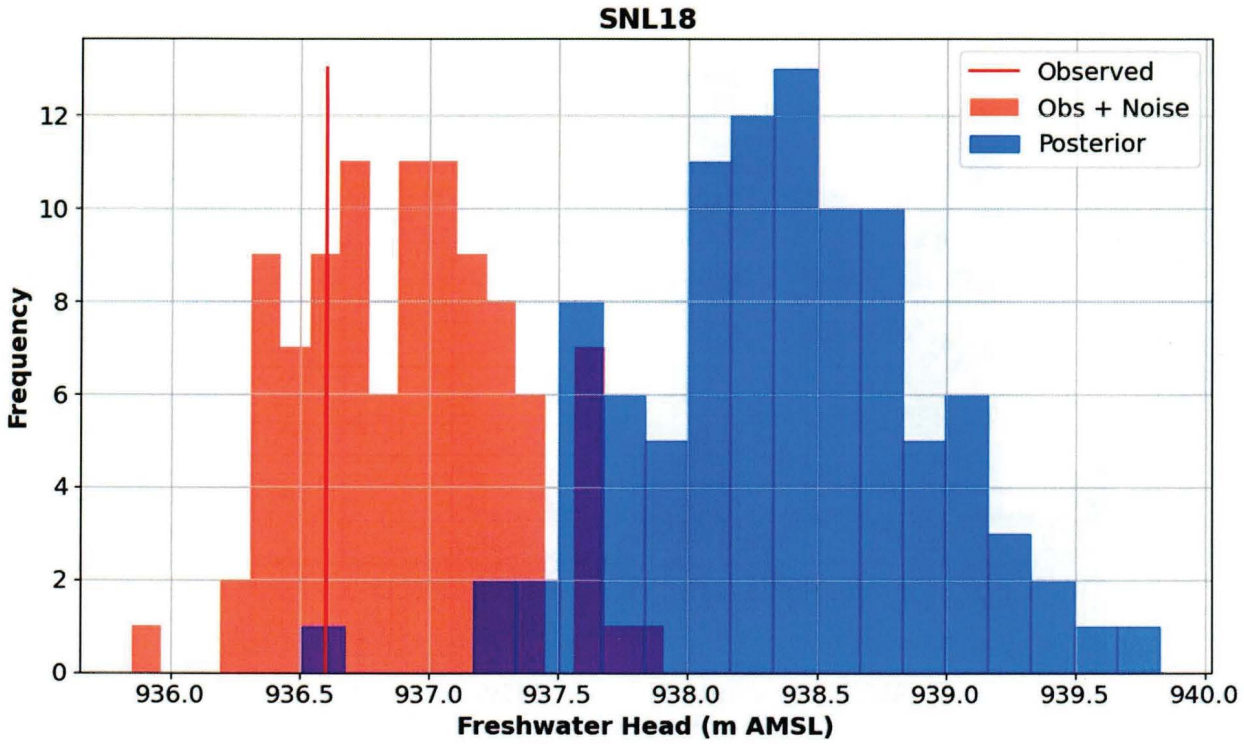

Figure 78. Distribution of Steady-State Freshwater Heads in SNL-18 for 100 Realizations at Iteration 5

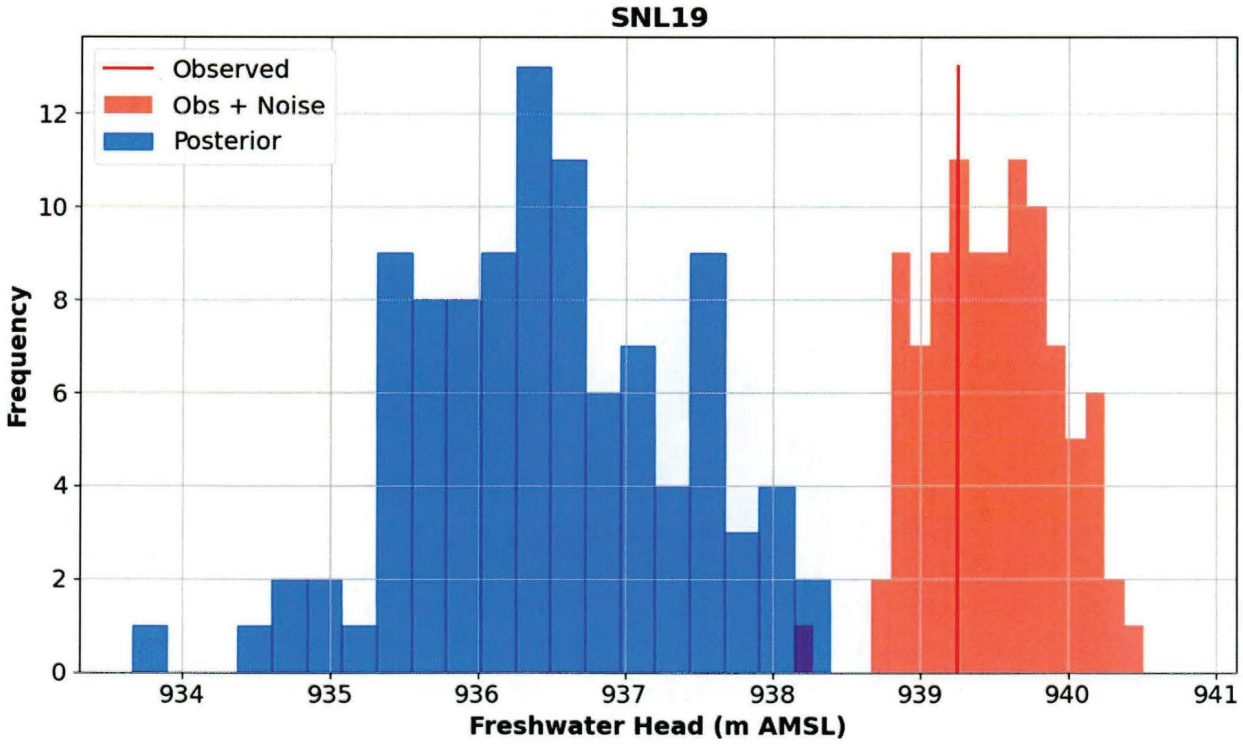

Figure 79. Distribution of Steady-State Freshwater Heads in SNL-19 for 100 Realizations at Iteration 5

Information Only

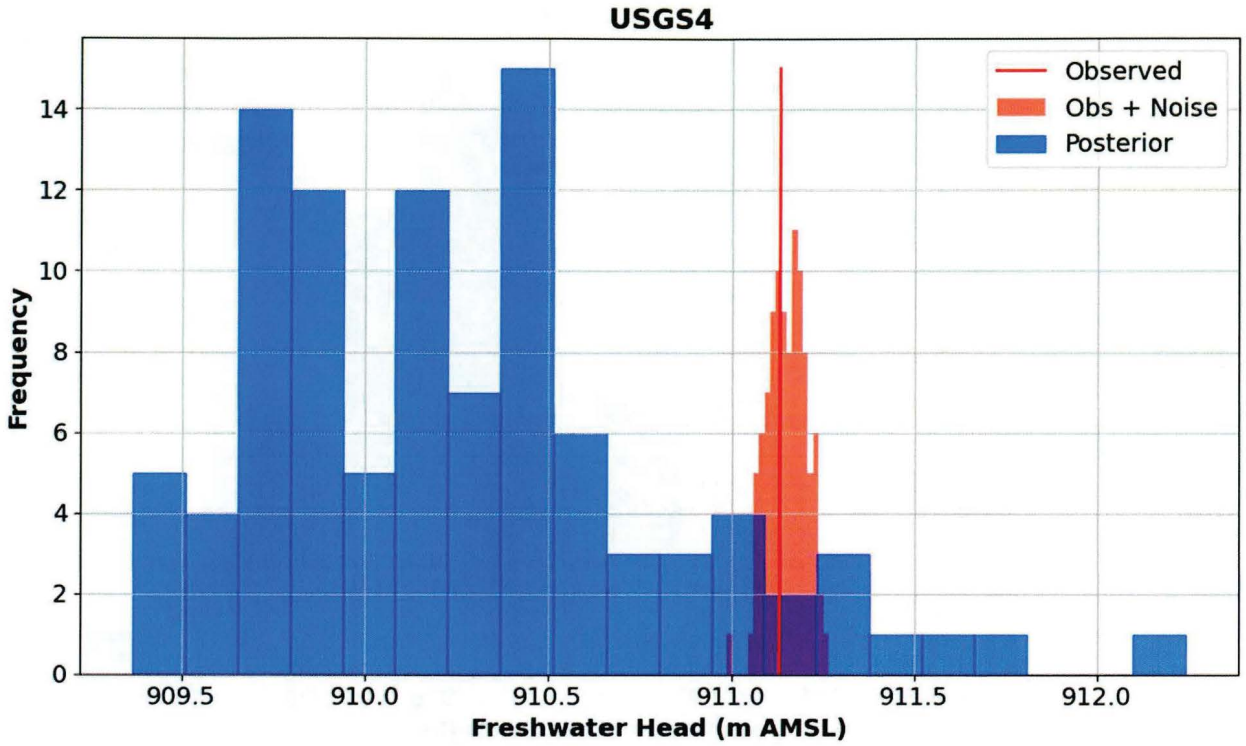

Figure 80. Distribution of Steady-State Freshwater Heads in USGS-4 for 100 Realizations at Iteration 5

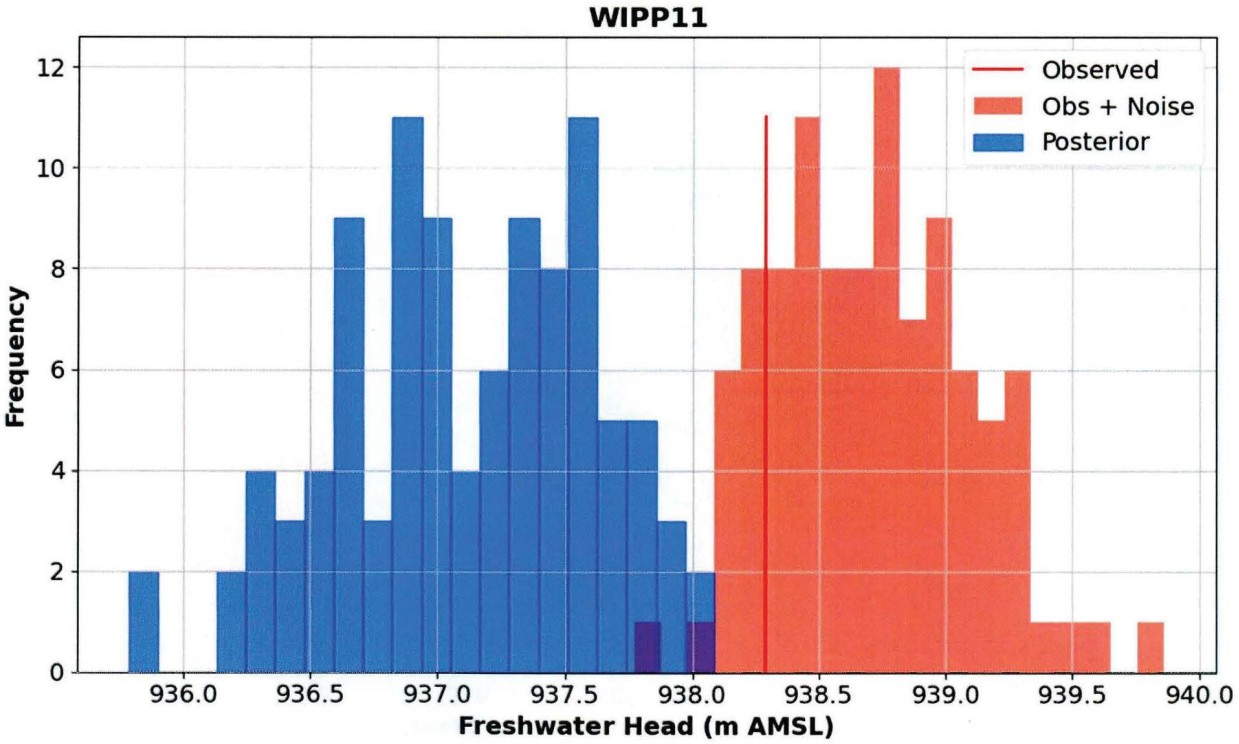

Figure 81. Distribution of Steady-State Freshwater Heads in WIPP-11 for 100 Realizations at Iteration 5

Information Only

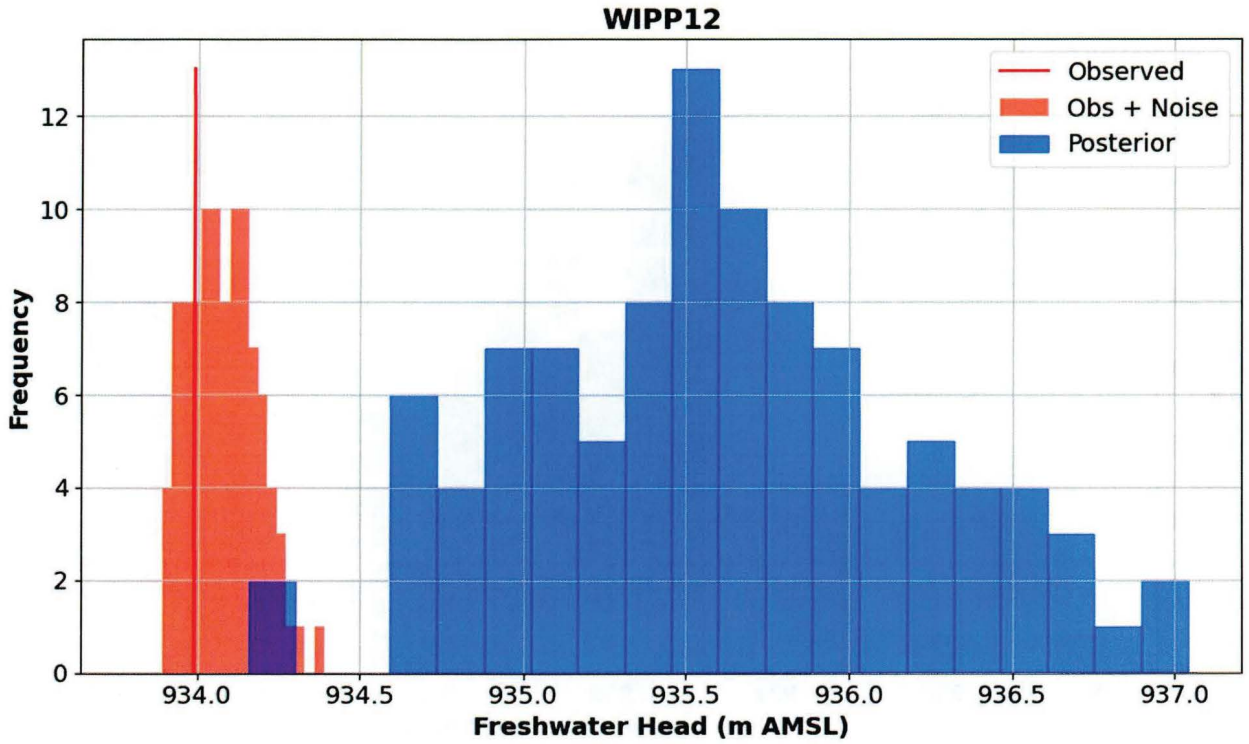

Figure 82. Distribution of Steady-State Freshwater Heads in WIPP-12 for 100 Realizations at Iteration 5

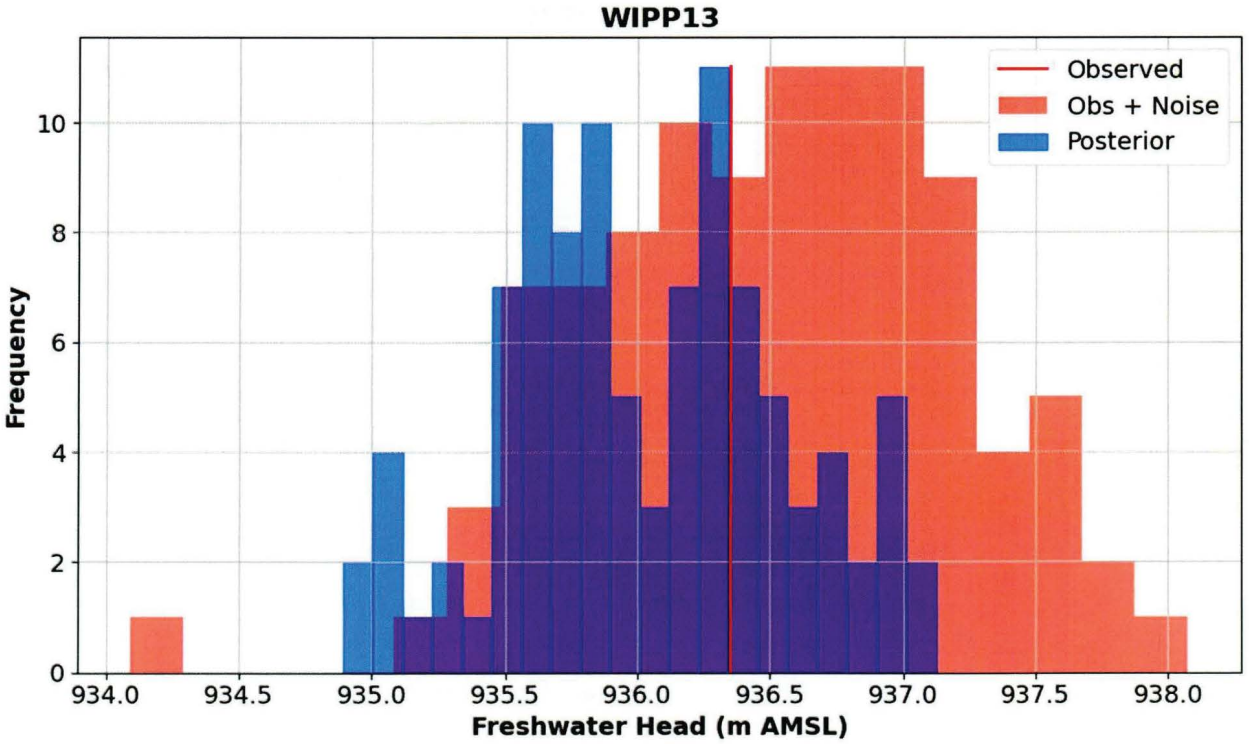

Figure 83. Distribution of Steady-State Freshwater Heads in WIPP-13 for 100 Realizations at Iteration 5

Information Only

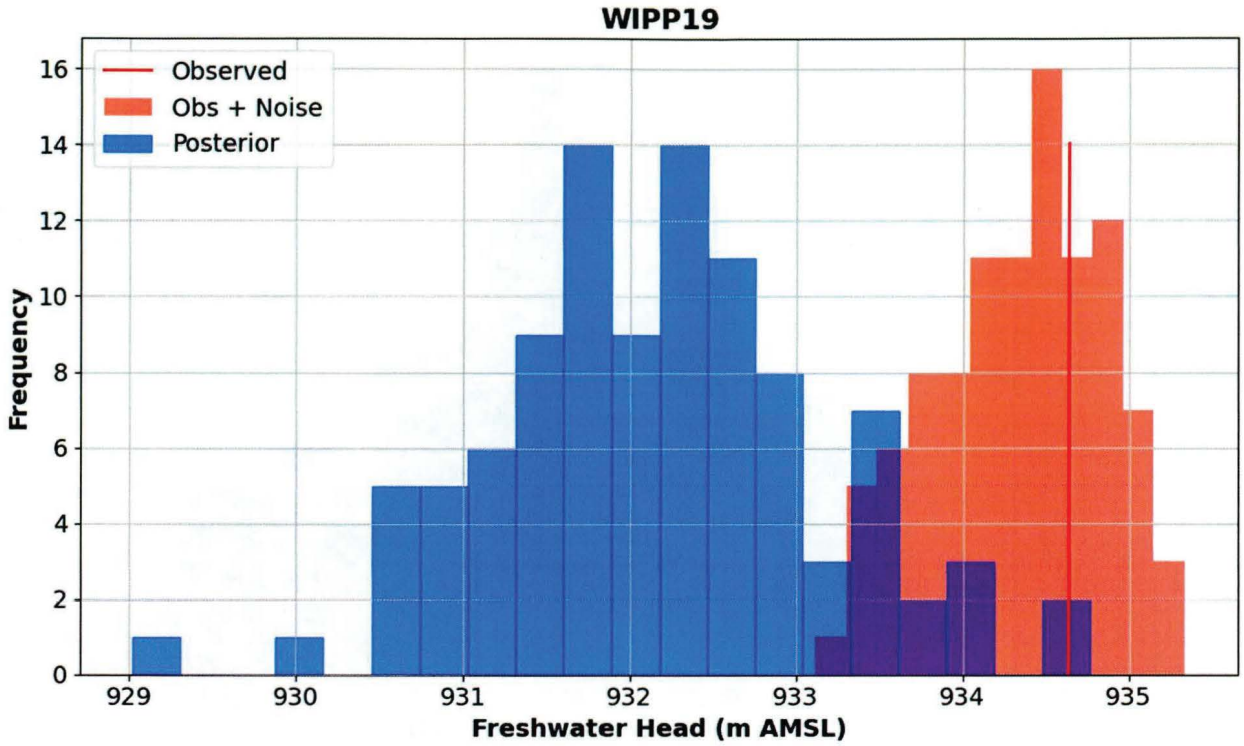

Figure 84. Distribution of Steady-State Freshwater Heads in WIPP-19 for 100 Realizations at Iteration 5

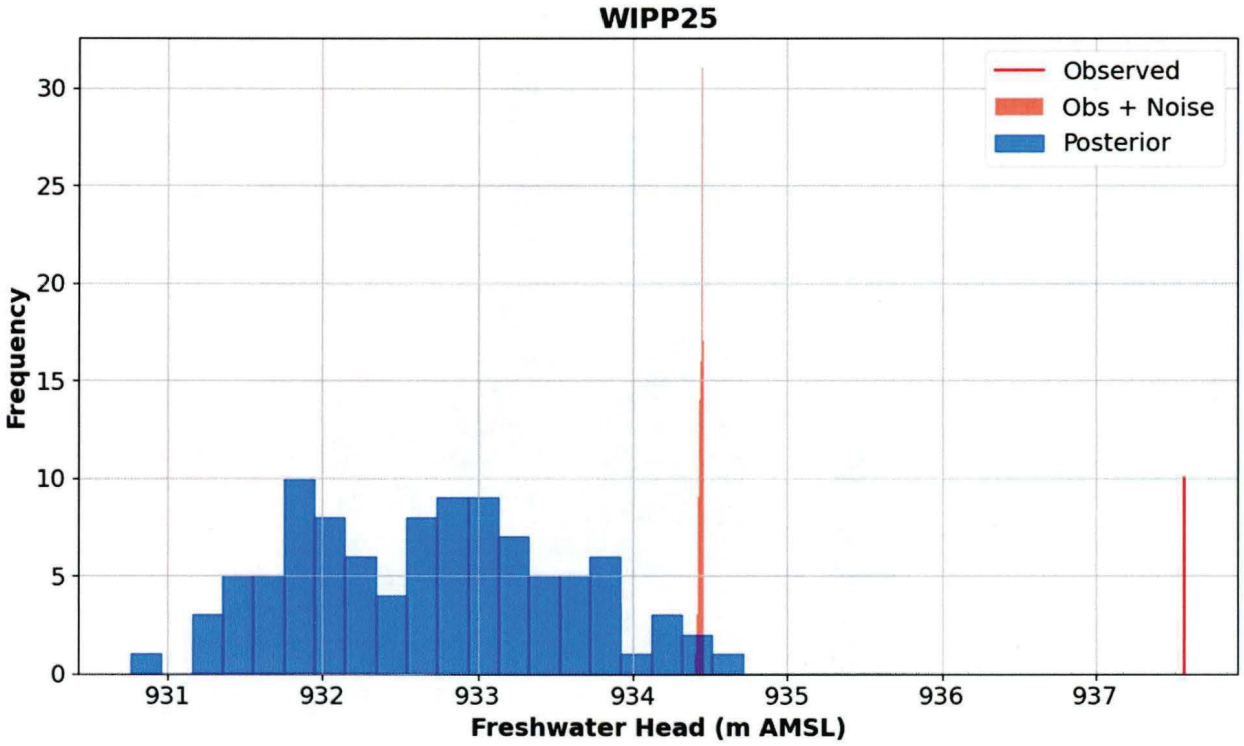

Figure 85. Distribution of Steady-State Freshwater Heads in WIPP-25 for 100 Realizations at Iteration 5

Information Only

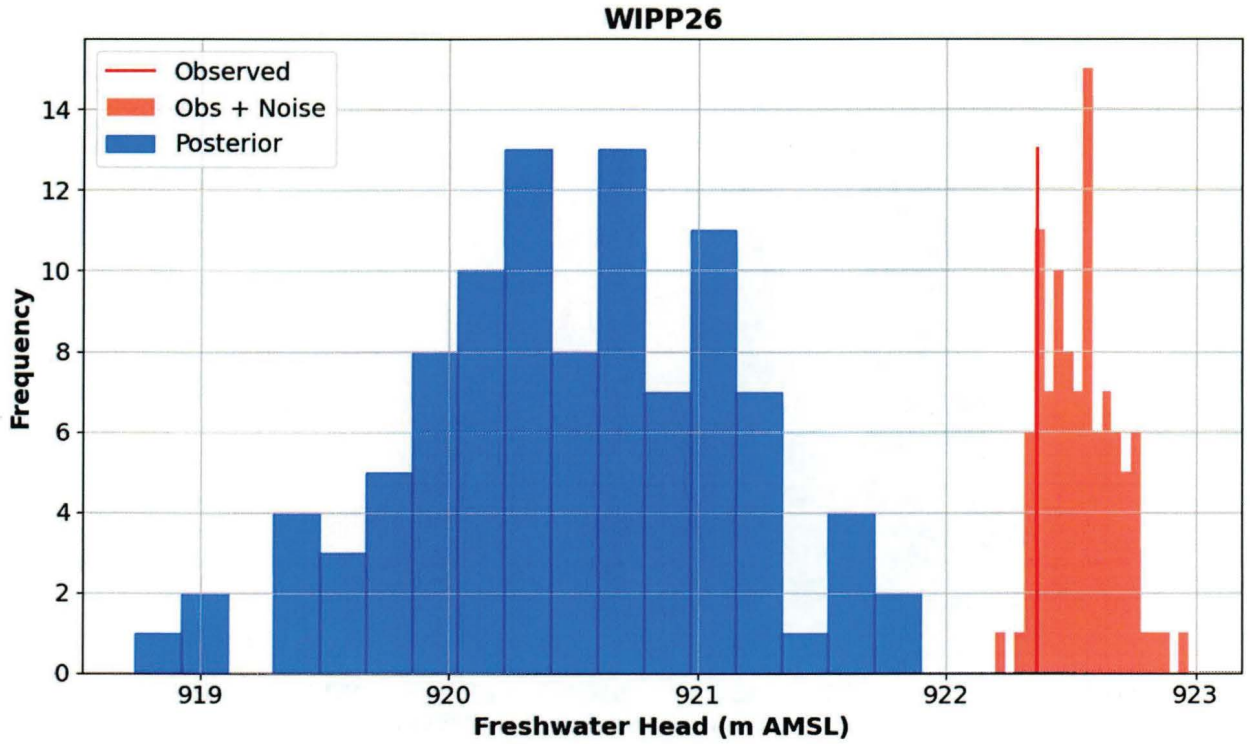

Figure 86. Distribution of Steady-State Freshwater Heads in WIPP-26 for 100 Realizations at Iteration 5

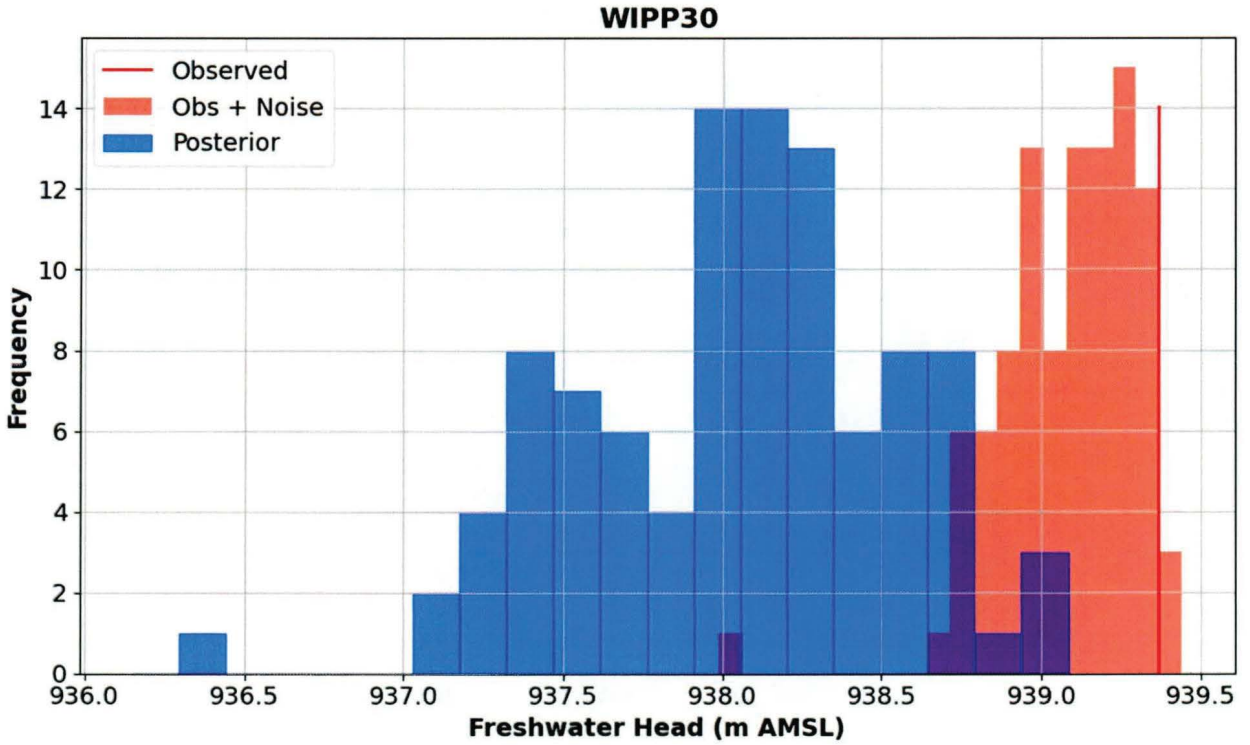

Figure 87. Distribution of Steady-State Freshwater Heads in WIPP-30 for 100 Realizations at Iteration 5

Information Only

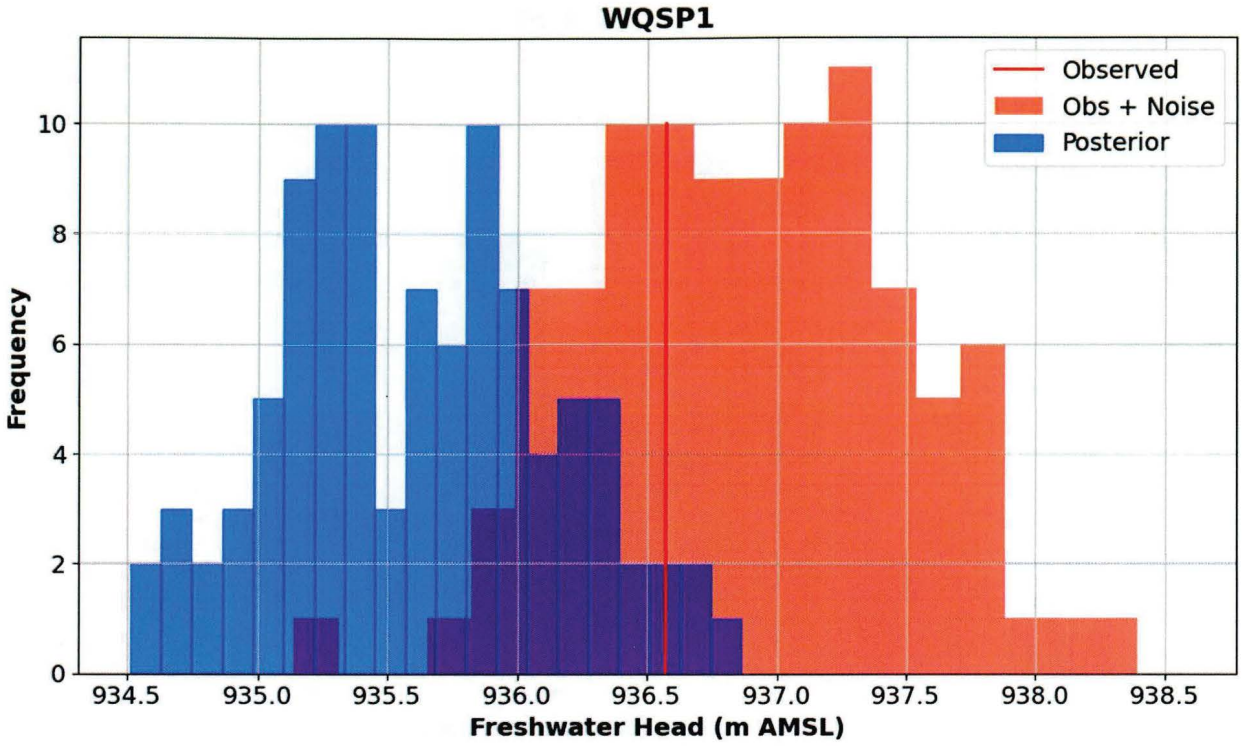

Figure 88. Distribution of Steady-State Freshwater Heads in WQSP-1 for 100 Realizations at Iteration 5

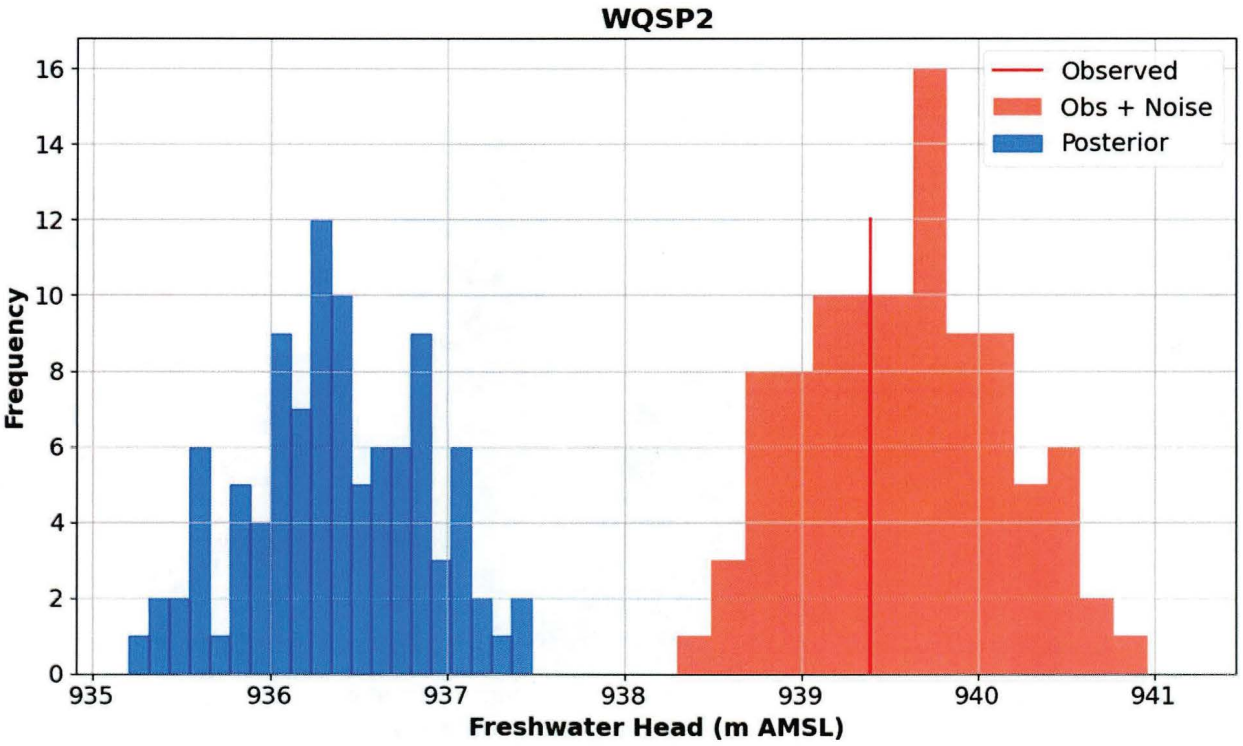

Figure 89. Distribution of Steady-State Freshwater Heads in WQSP-2 for 100 Realizations at Iteration 5

Information Only

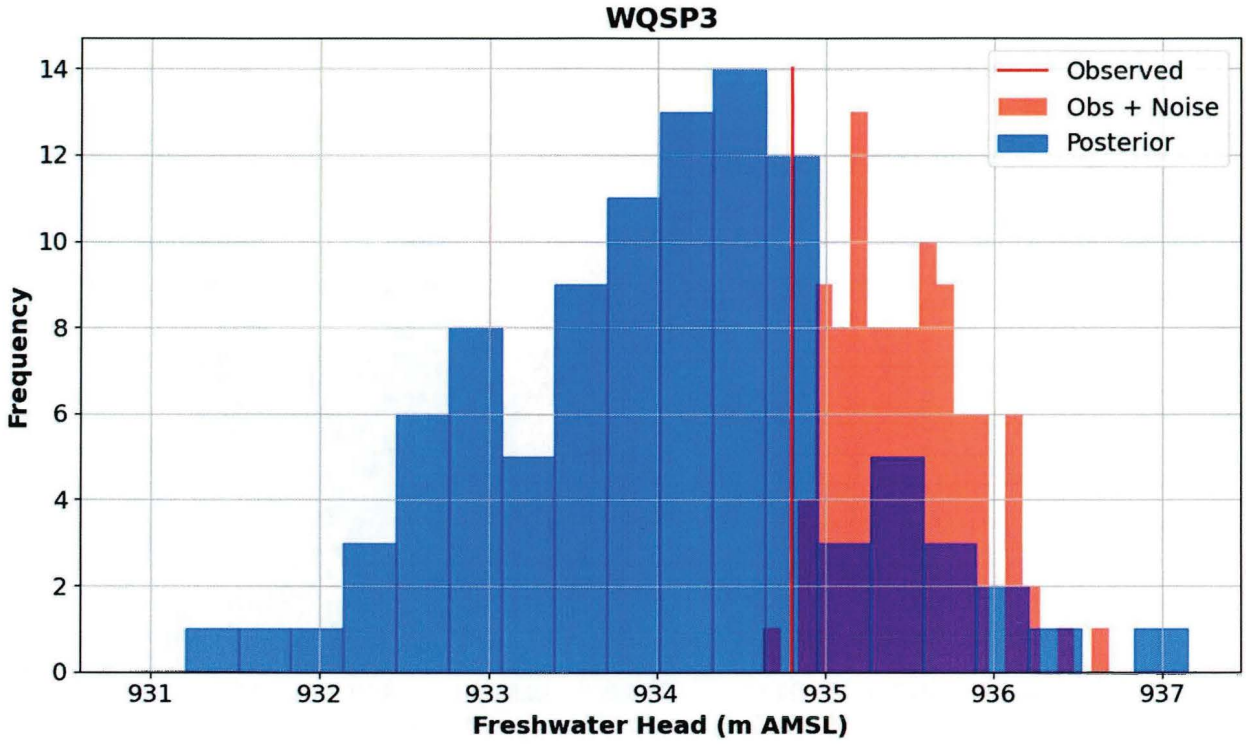

Figure 90. Distribution of Steady-State Freshwater Heads in WQSP-3 for 100 Realizations at Iteration 5

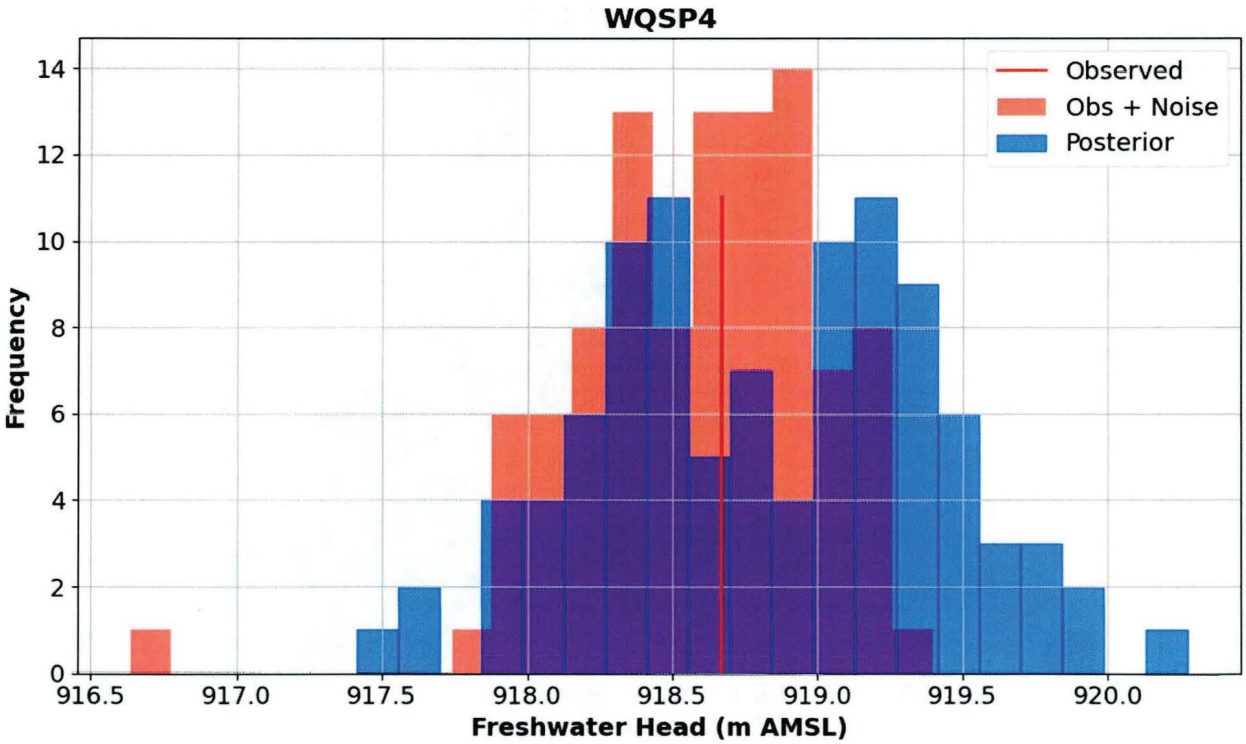

Figure 91. Distribution of Steady-State Freshwater Heads in WQSP-4 for 100 Realizations at Iteration 5

Information Only

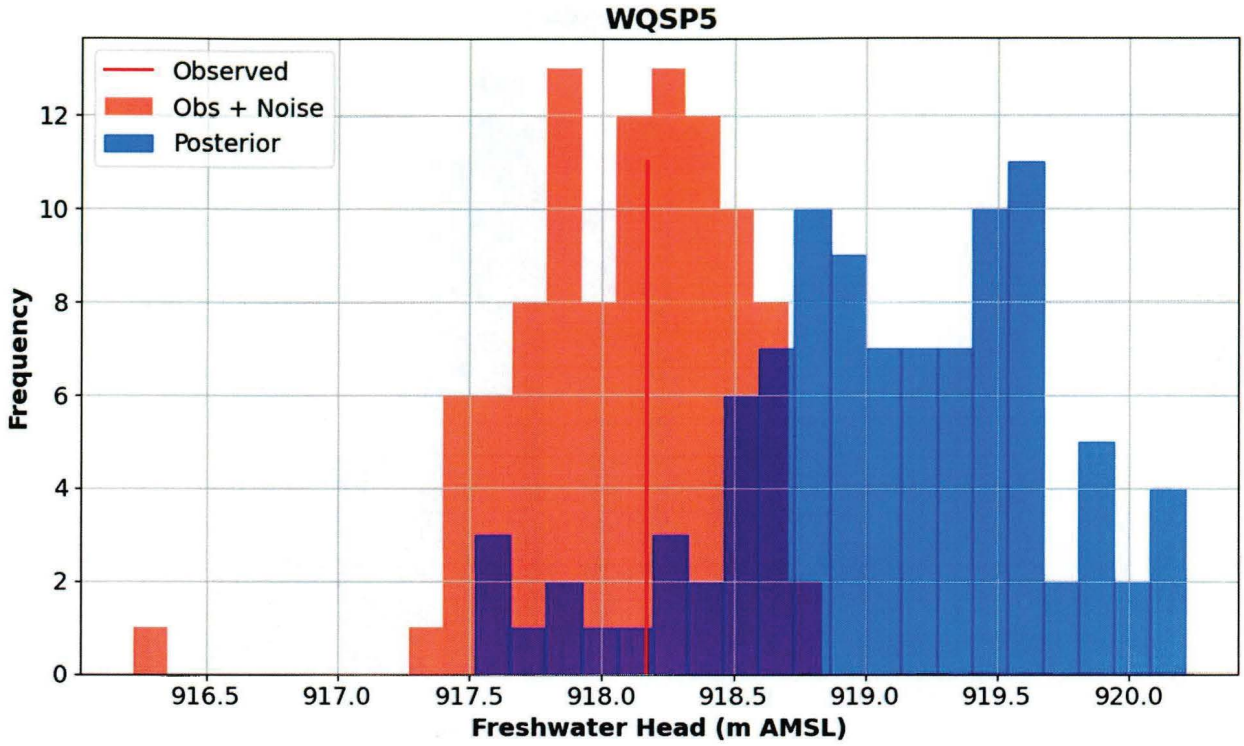

Figure 92. Distribution of Steady-State Freshwater Heads in WQSP-5 for 100 Realizations at Iteration 5

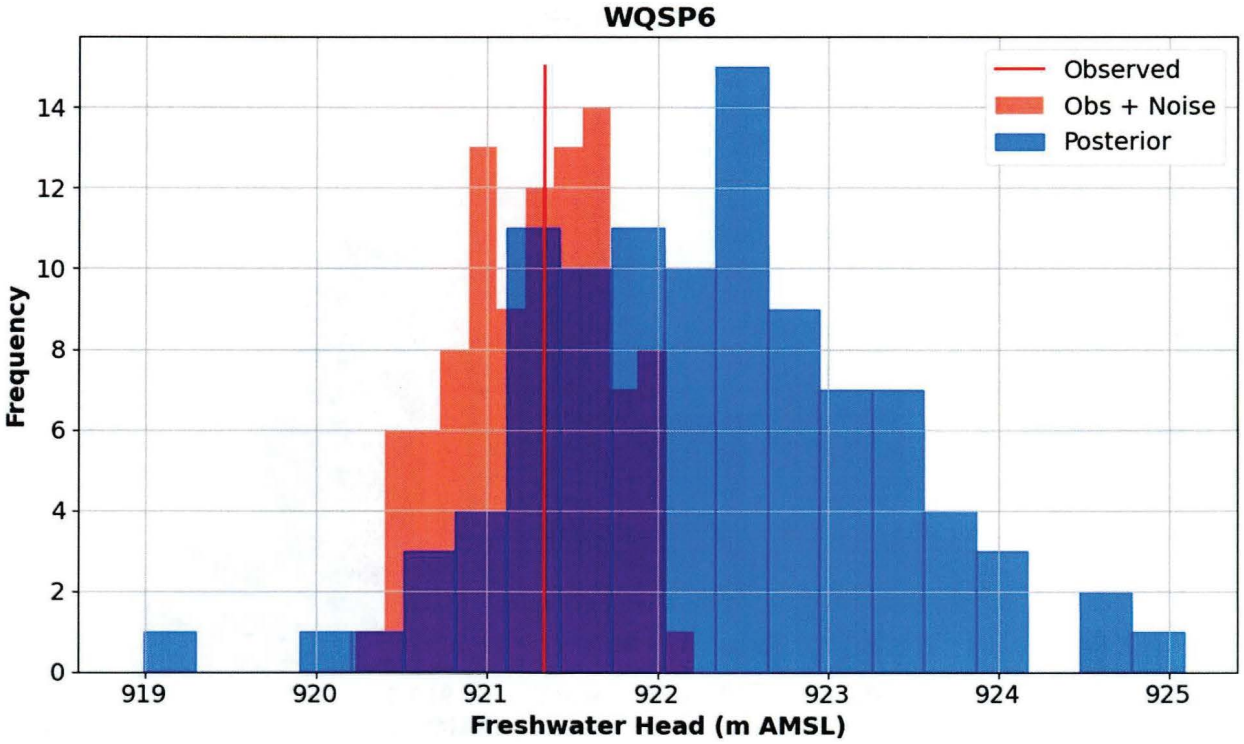

Figure 93. Distribution of Steady-State Freshwater Heads in WQSP-6 for 100 Realizations at Iteration 5

Information Only

7.3 Distribution of Observed vs Simulated Drawdown at Monitoring Locations for the Multi-Well Pumping Tests

Figure 94 through **Figure 145** present violin plots of the observed versus simulated drawdown responses in the observation wells for long-term pumping tests. Model results were bi-linearly interpolated in space and linearly interpolated in time to the observation locations and times.

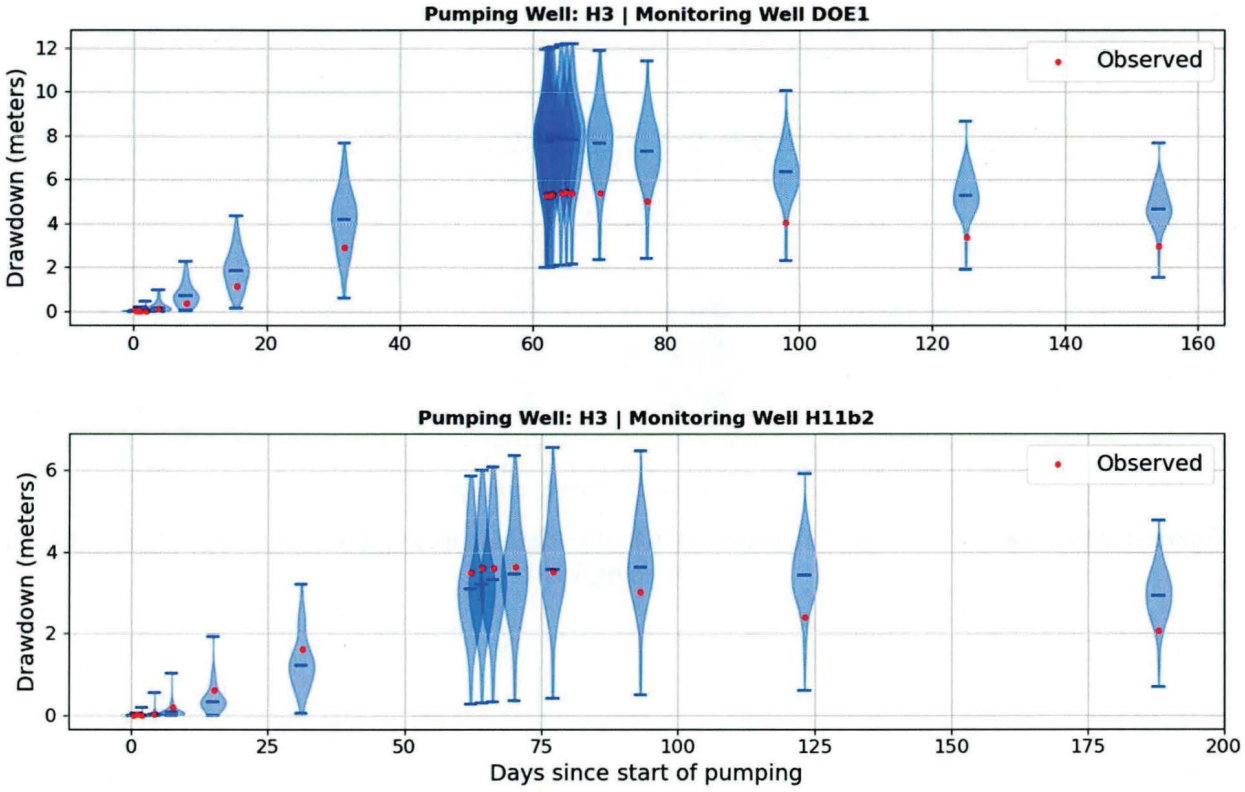

Figure 94. Observed vs Simulated Drawdown at DOE-1 And H11-b2 Monitoring Locations for the H-3 Multi-Well Pumping Test

Information Only

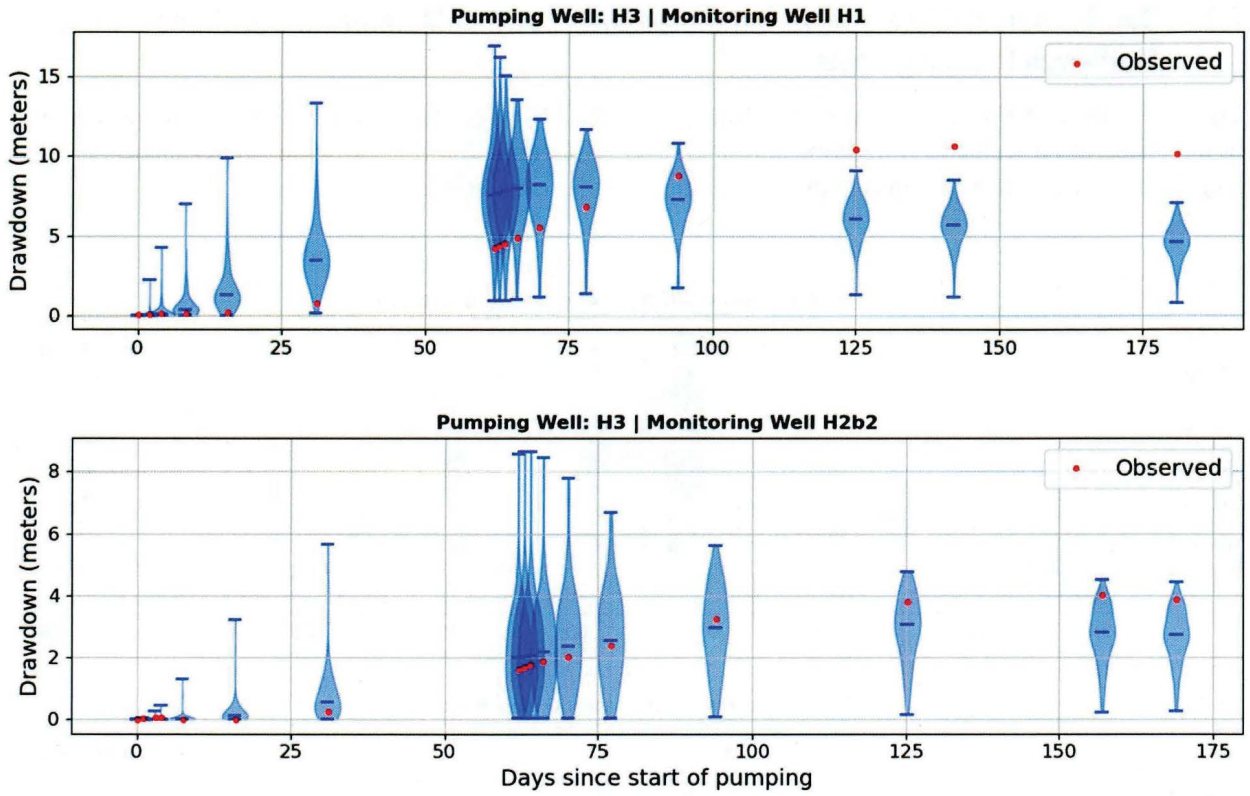

Figure 95. Observed vs Simulated Drawdown at H-1 and H-2b2 Monitoring Locations for the H-3 Multi-Well Pumping Test

Information Only

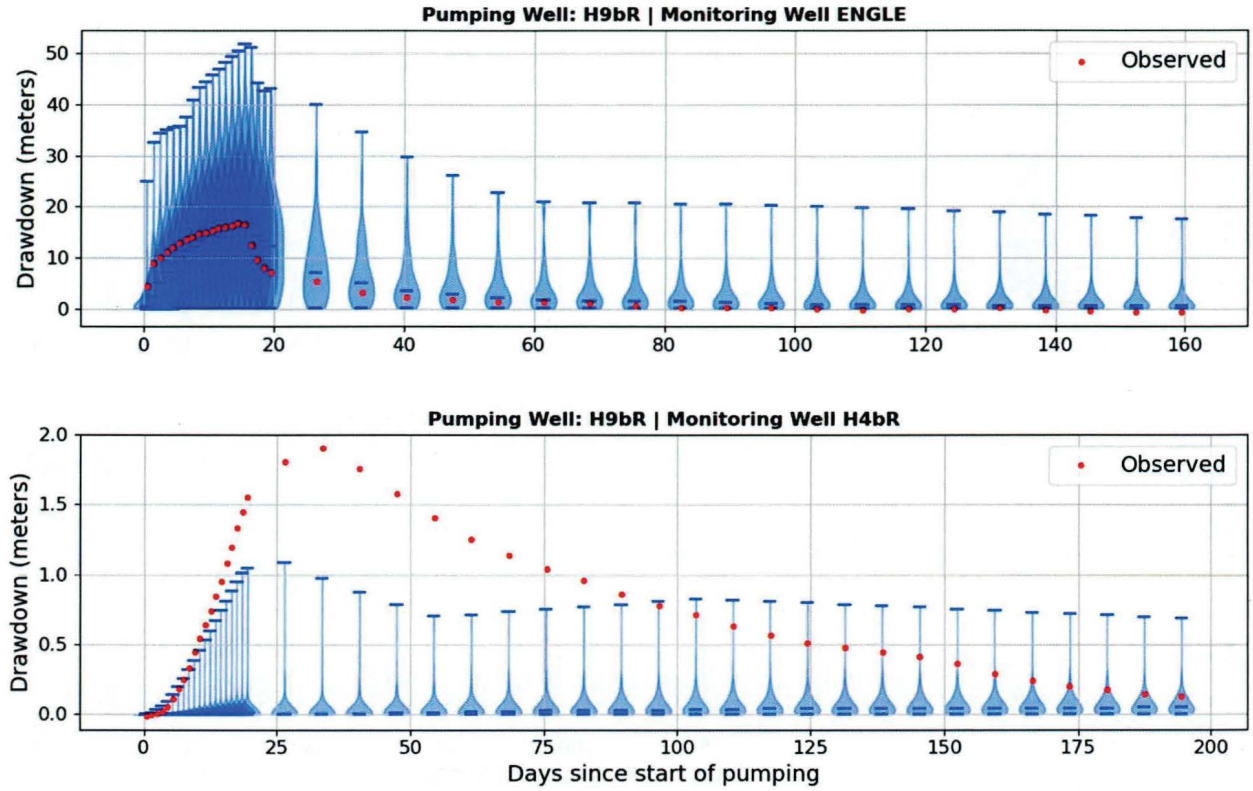

Figure 96. Observed vs Simulated Drawdown at ENGLE and H-4bR Monitoring Locations for the H-9bR Multi-Well Pumping Test

Information Only

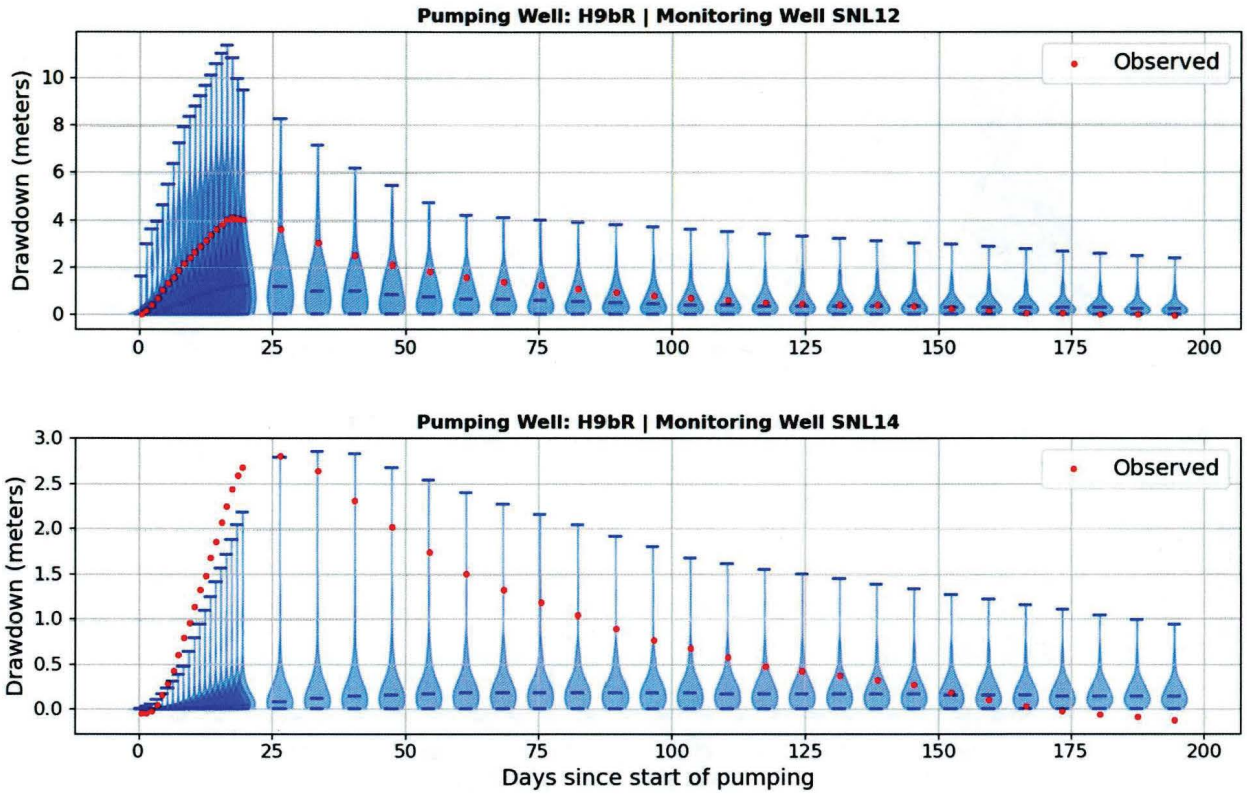

Figure 97. Observed vs Simulated Drawdown at SNL-12 and SNL-14 Monitoring Locations for the H-9bR Multi-Well Pumping Test

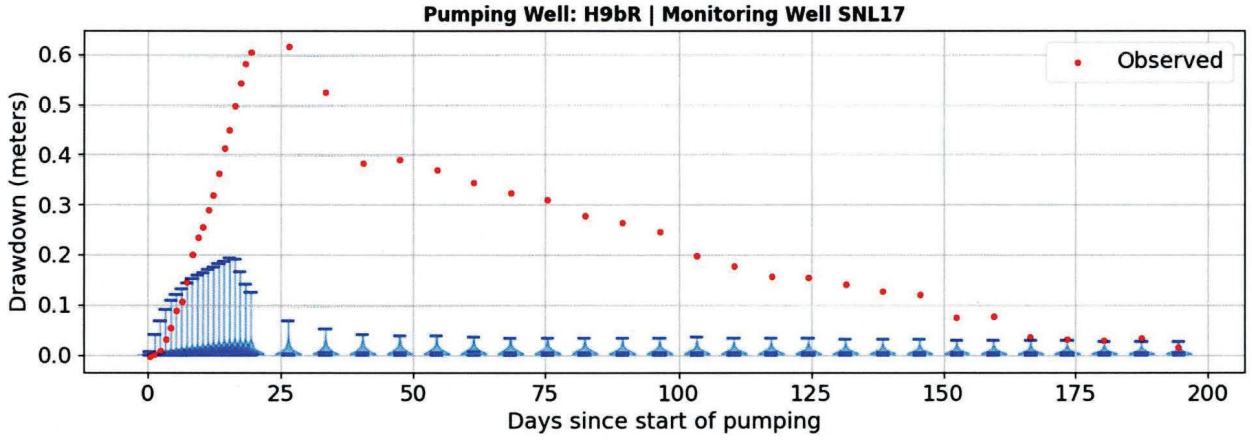

Information Only

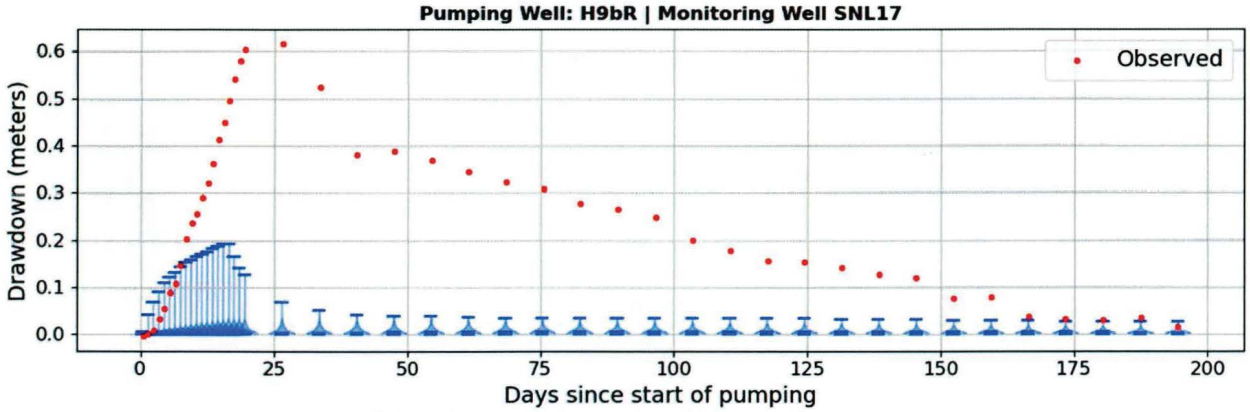

Figure 98. Observed vs Simulated Drawdown at SNL-17 Monitoring Location for the H-9bR Multi-Well Pumping Test

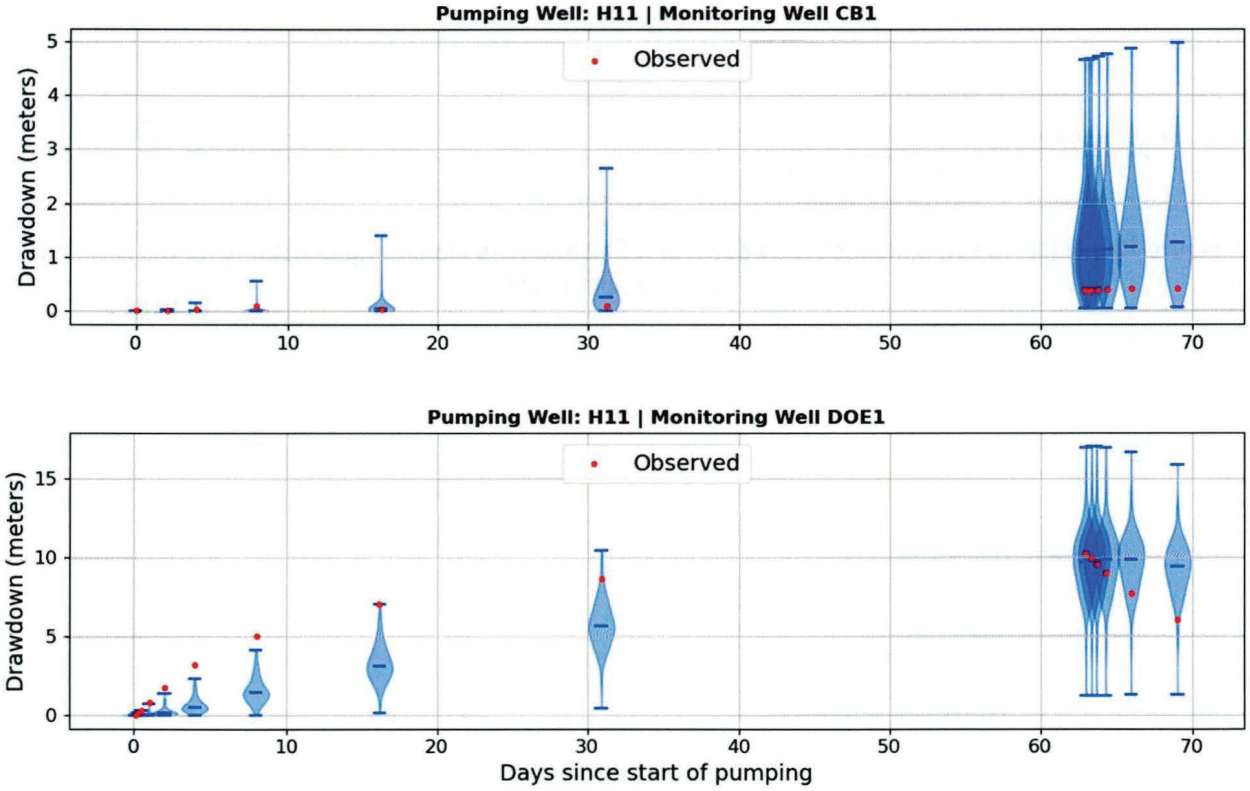

Figure 99. Observed vs Simulated Drawdown at CB-1 and DOE-1 Monitoring Locations for the H-11 Multi-Well Pumping Test

Information Only

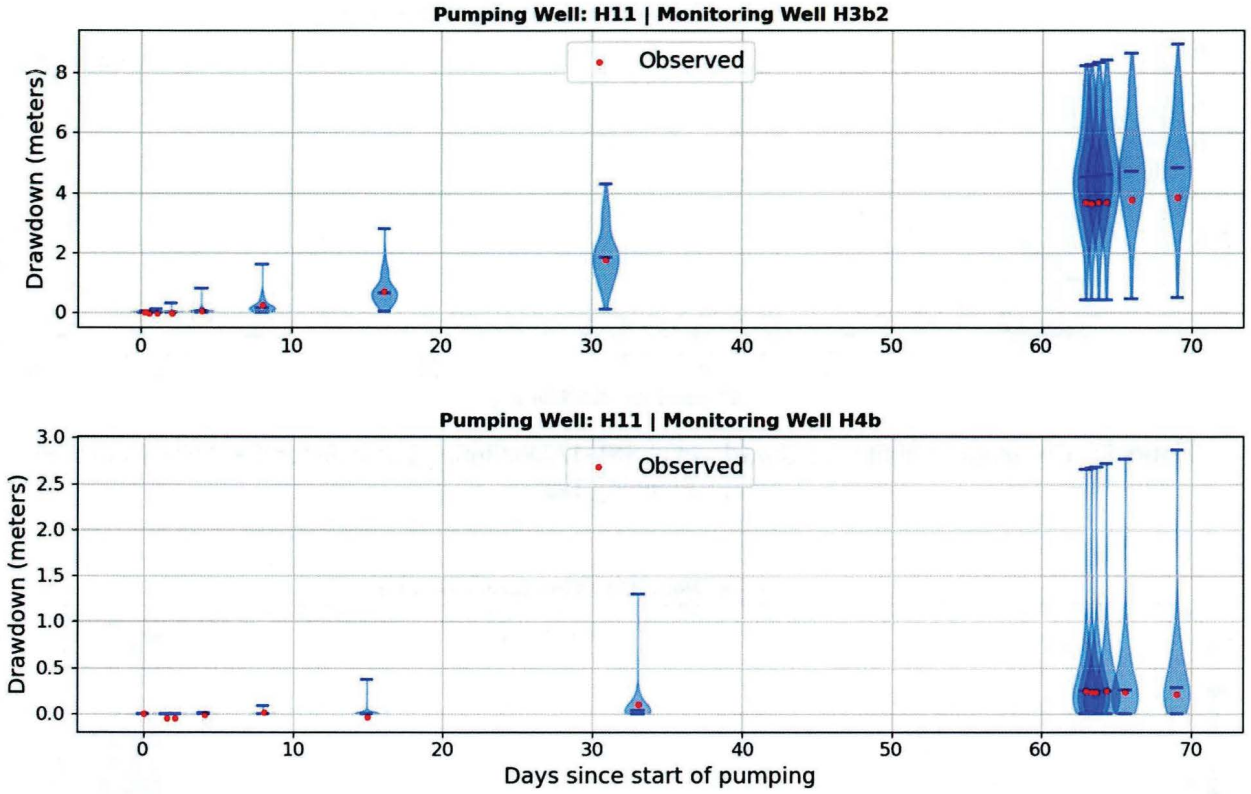

Figure 100. Observed vs Simulated Drawdown at H-3b2 and H-4b Monitoring Locations for the H-11 Multi-Well Pumping Test

Information Only

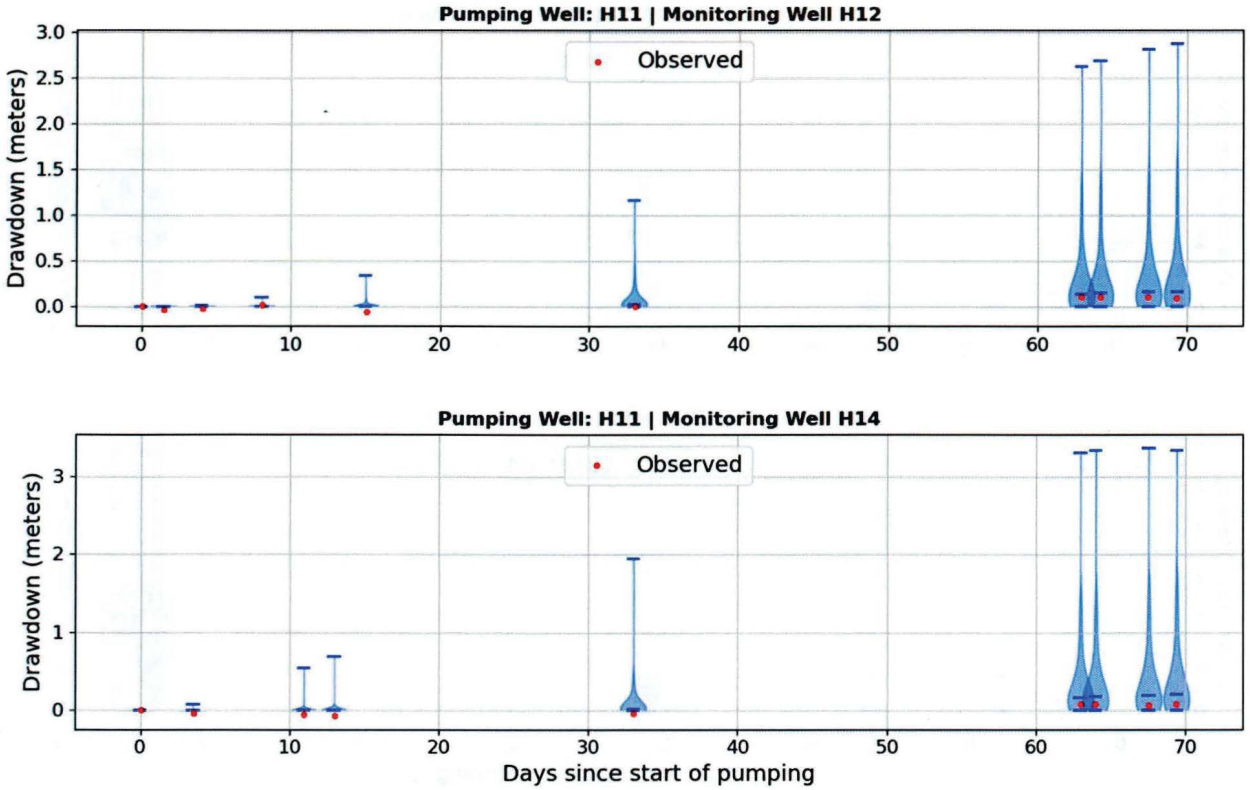

Figure 101. Observed vs Simulated Drawdown at H-12 and H-14 Monitoring Locations for the H-11 Multi-Well Pumping Test

Information Only

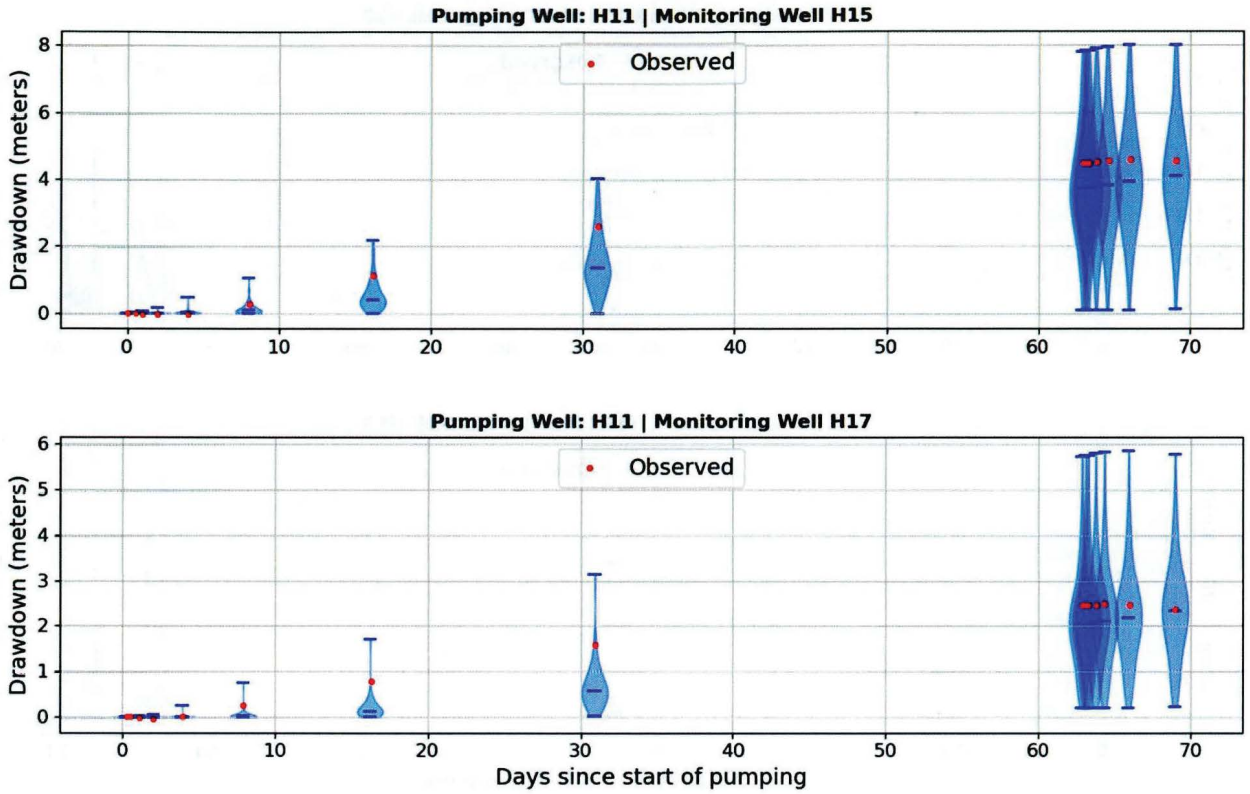

Figure 102. Observed vs Simulated Drawdown at H-15 and H-17 Monitoring Locations for the H-11 Multi-Well Pumping Test

Information Only

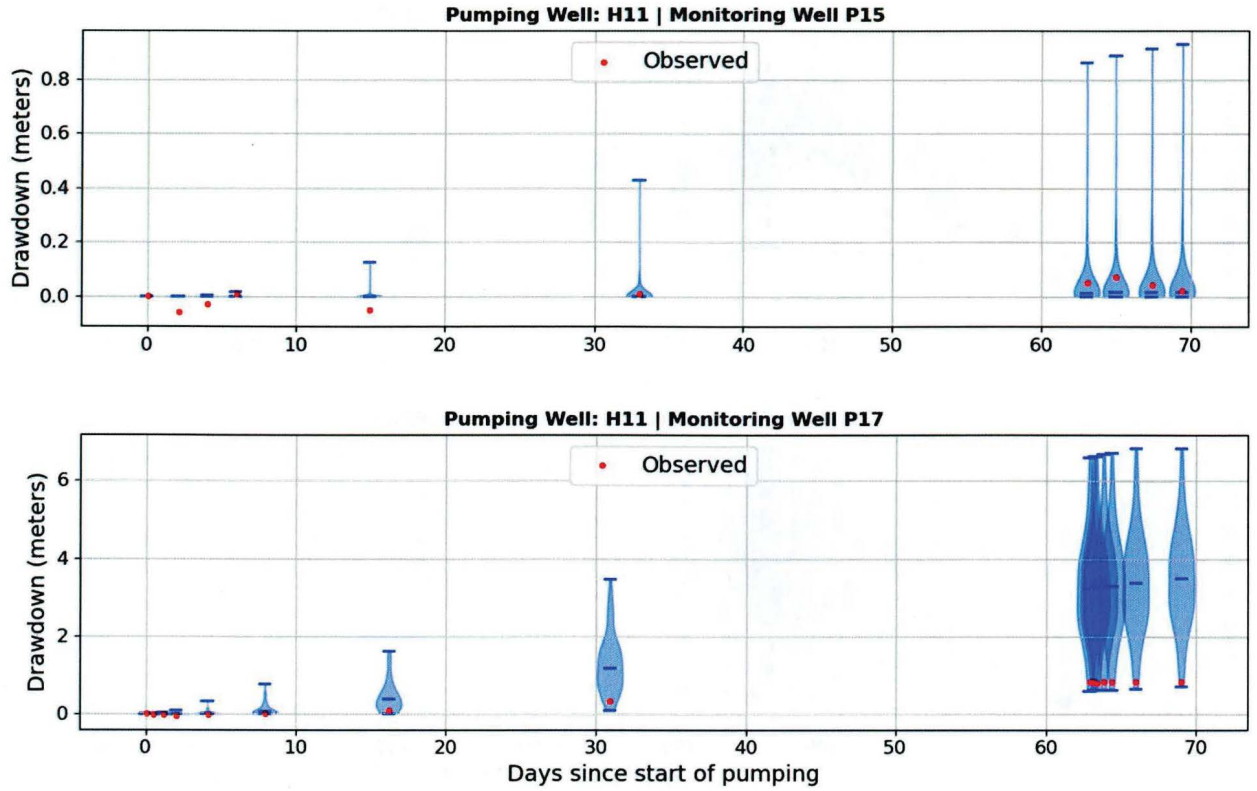

Figure 103. Observed vs Simulated Drawdown at P-15 and P-17 Monitoring Locations for the H-11 Multi-Well Pumping Test

Information Only

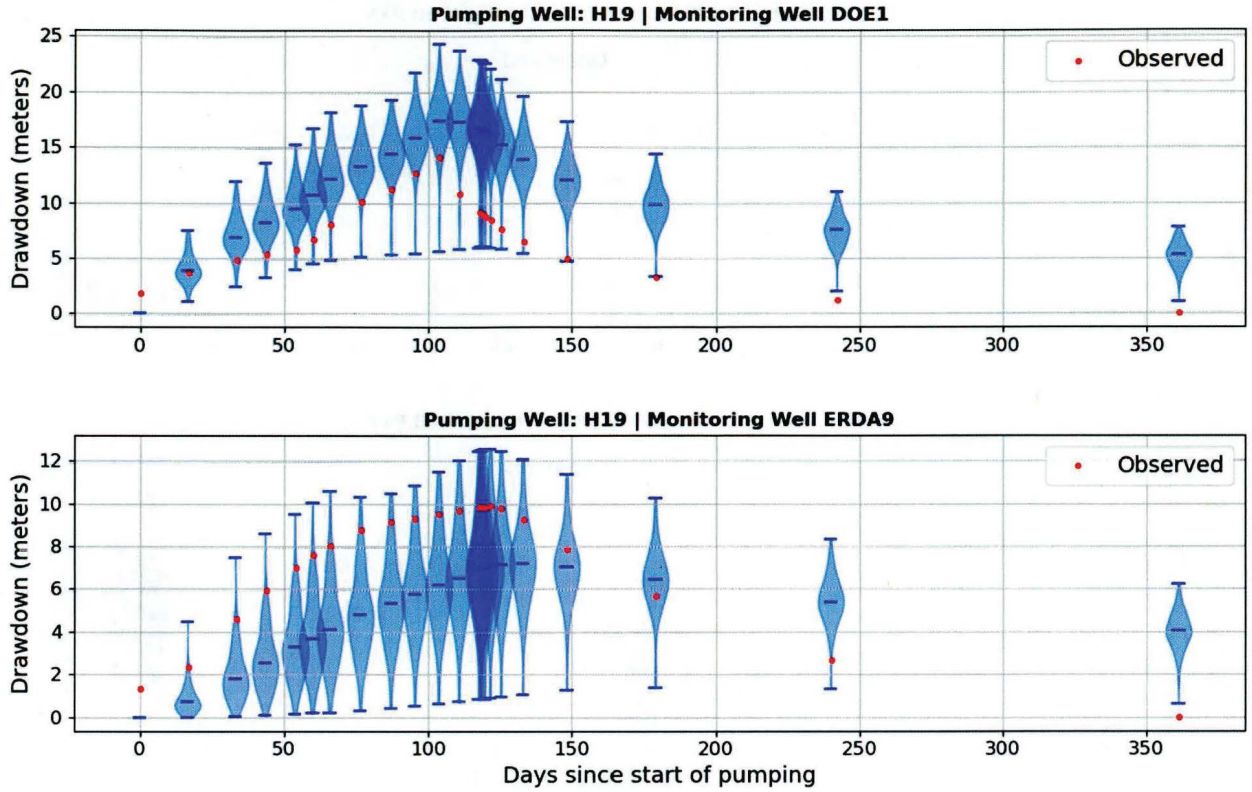

Figure 104. Observed vs Simulated Drawdown at DOE-1 and ERDA-9 Monitoring Locations for the H-19 Multi-Well Pumping Test

Information Only

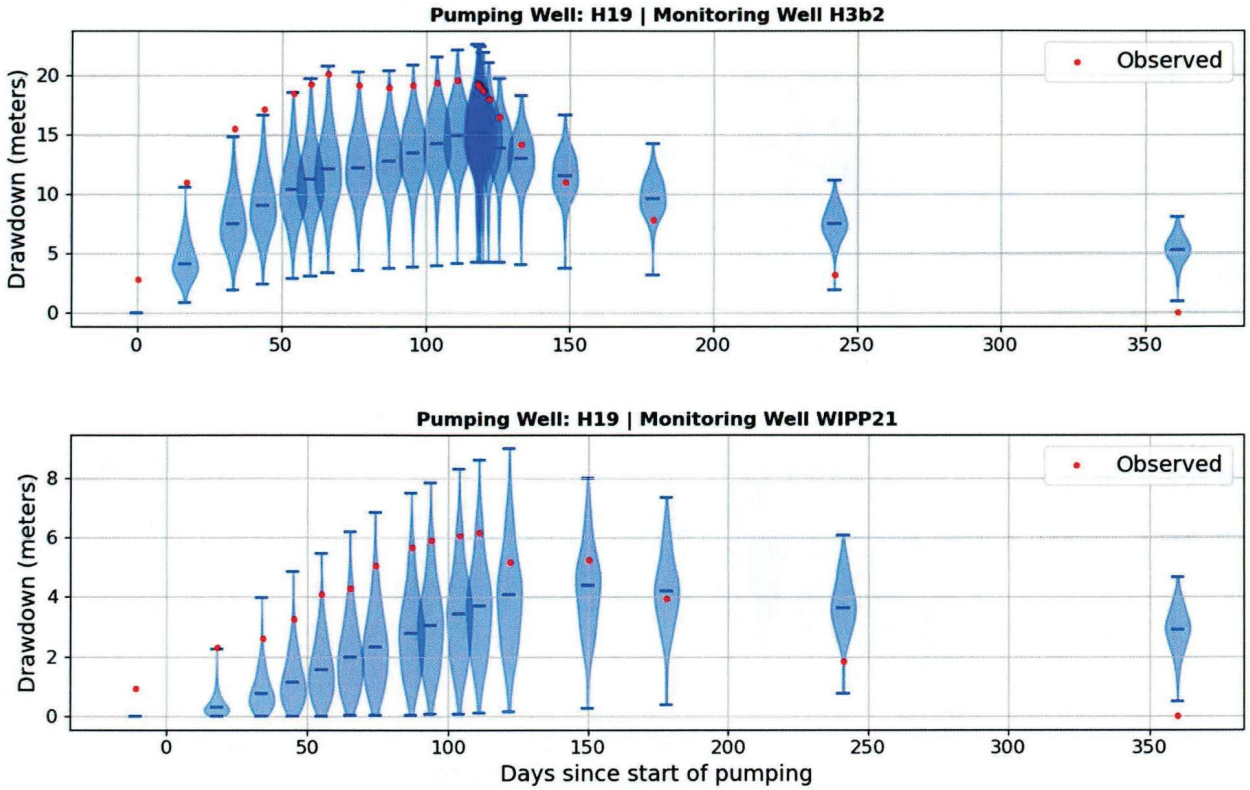

Figure 105. Observed vs Simulated Drawdown at H-3b2 and WIPP-21 Monitoring Locations for the H-19 Multi-Well Pumping Test

Information Only

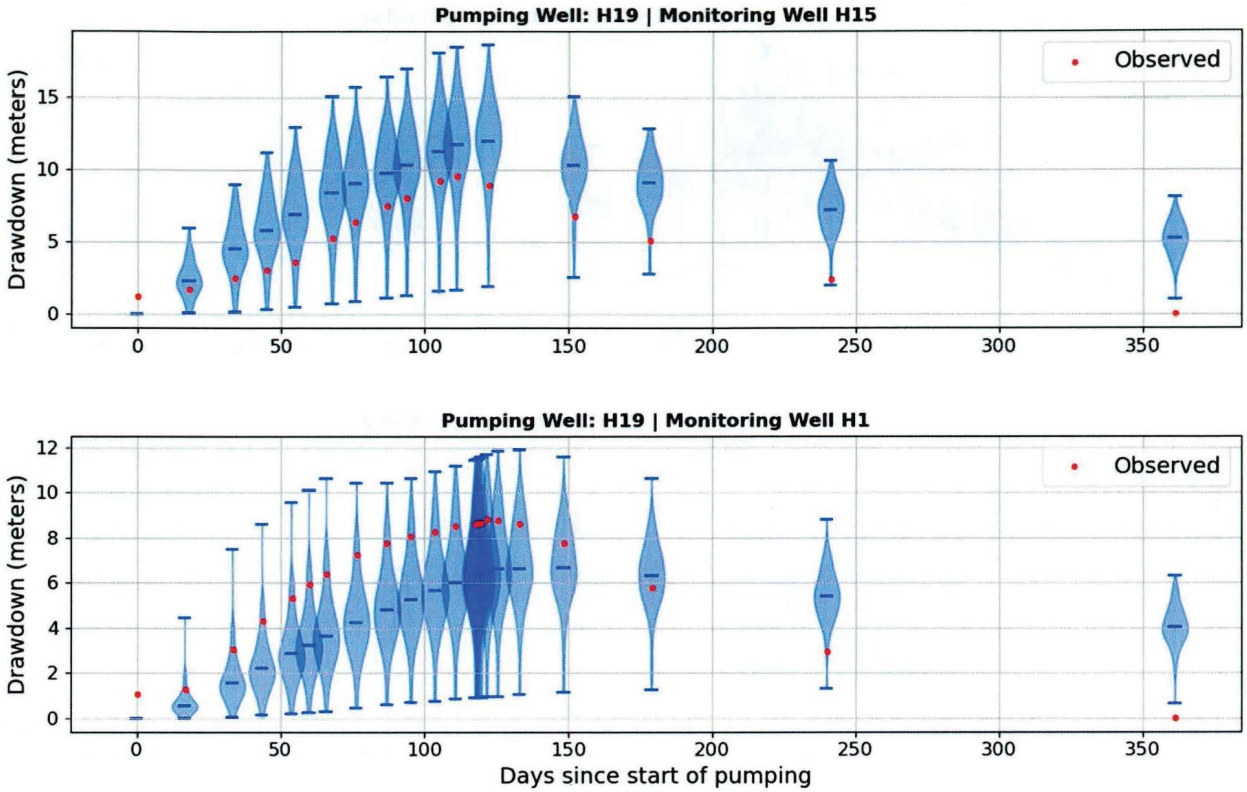

Figure 106. Observed vs Simulated Drawdown at H-15 and H-1 Monitoring Locations for the H-19 Multi-Well Pumping Test

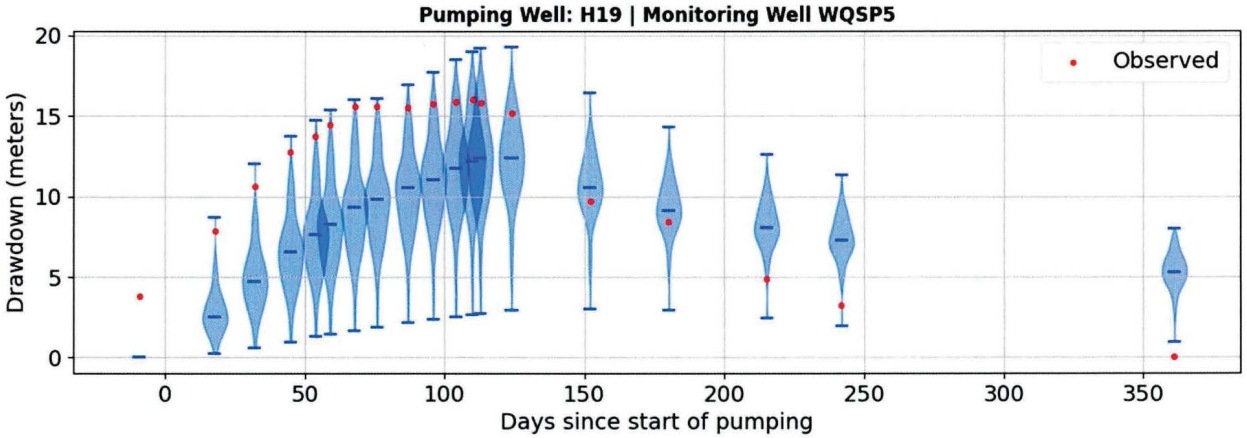

Figure 107. Observed vs Simulated Drawdown at WQSP-5 Monitoring Location for the H-19 Multi-Well Pumping Test

Information Only

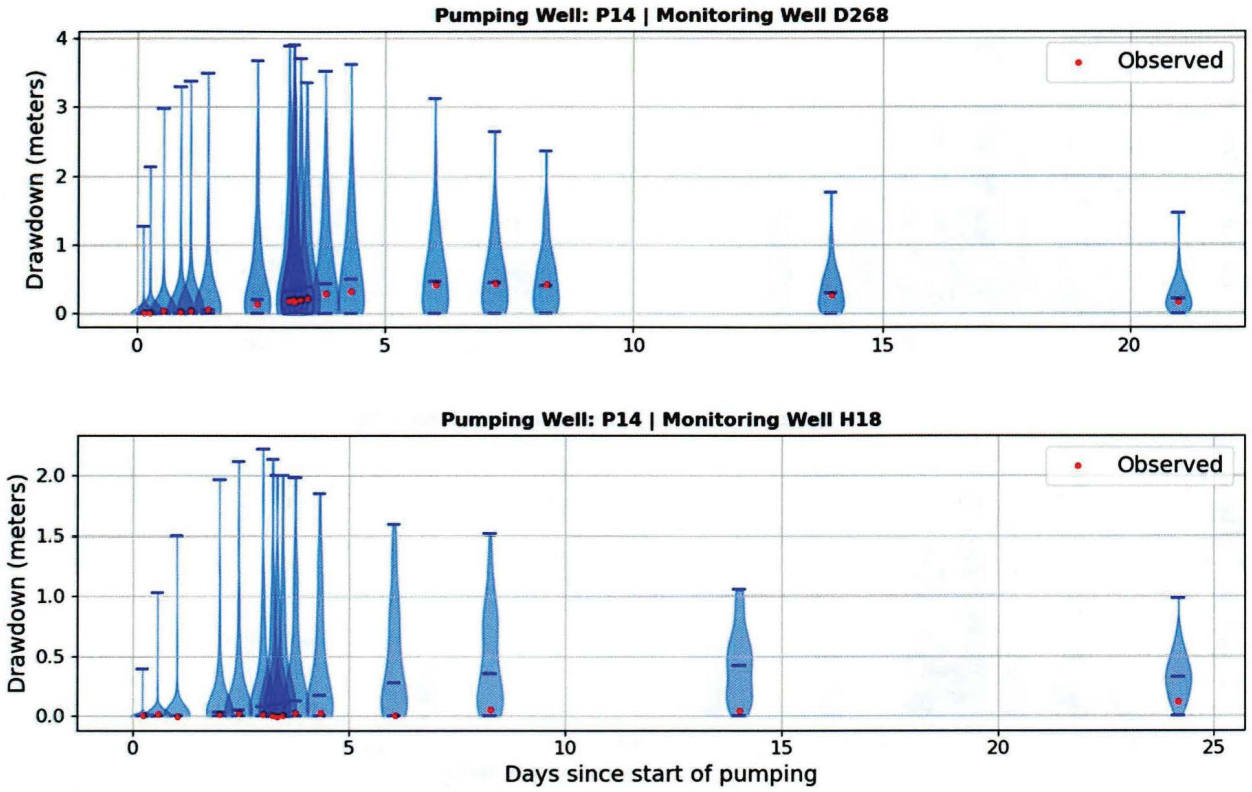

Figure 108. Observed vs Simulated Drawdown at D-268 and H-18 Monitoring Locations for the P-14 Multi-Well Pumping Test

Information Only

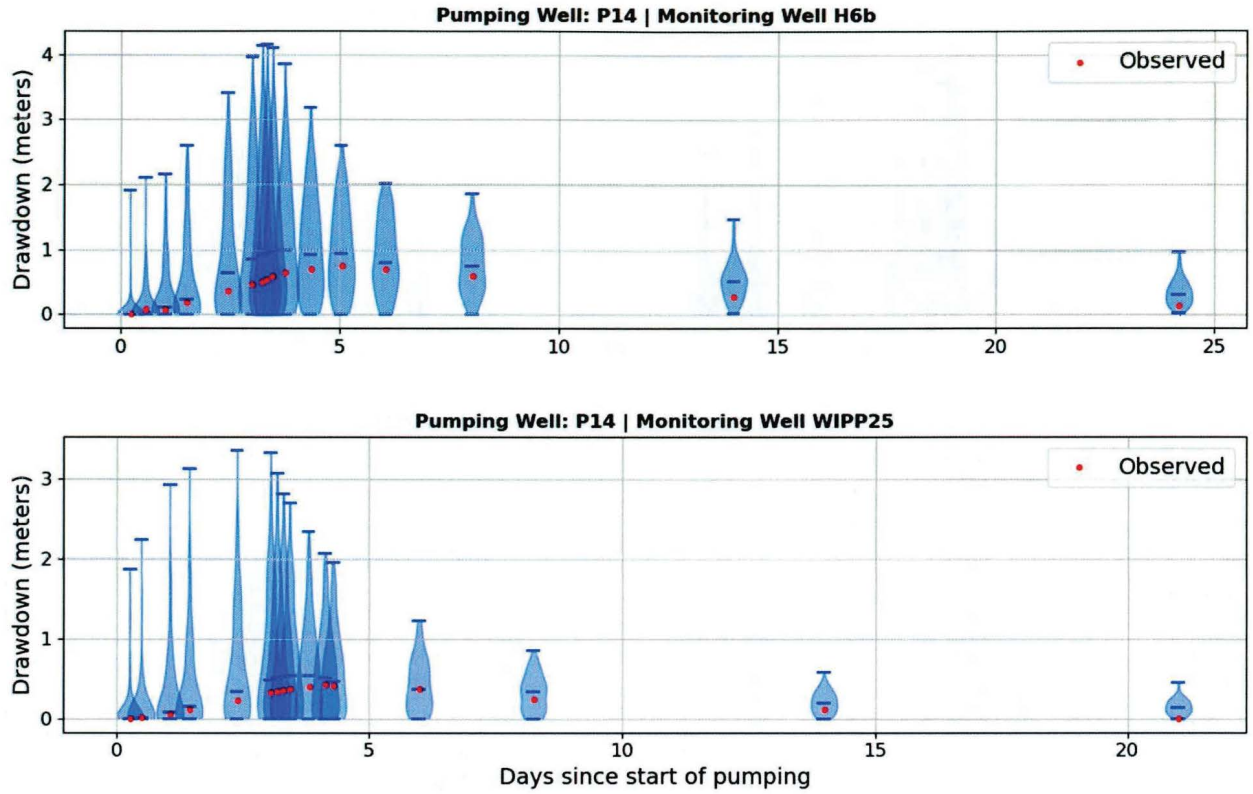

Figure 109. Observed vs Simulated Drawdown at H-6b and WIPP-25 Monitoring Locations for the P-14 Multi-Well Pumping Test

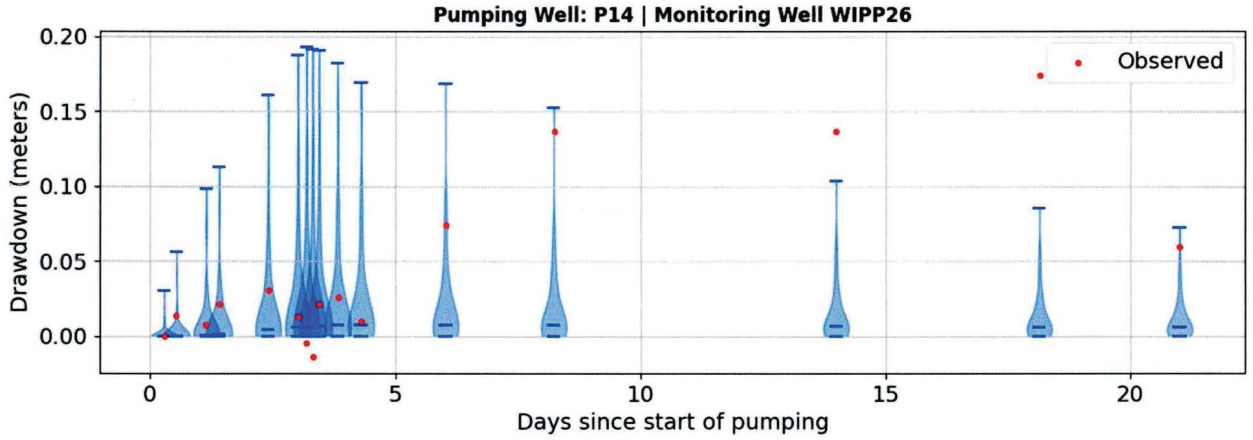

Figure 110. Observed vs Simulated Drawdown at WIPP-26 Monitoring Locations for the P-14 Multi-Well Pumping Test

Information Only

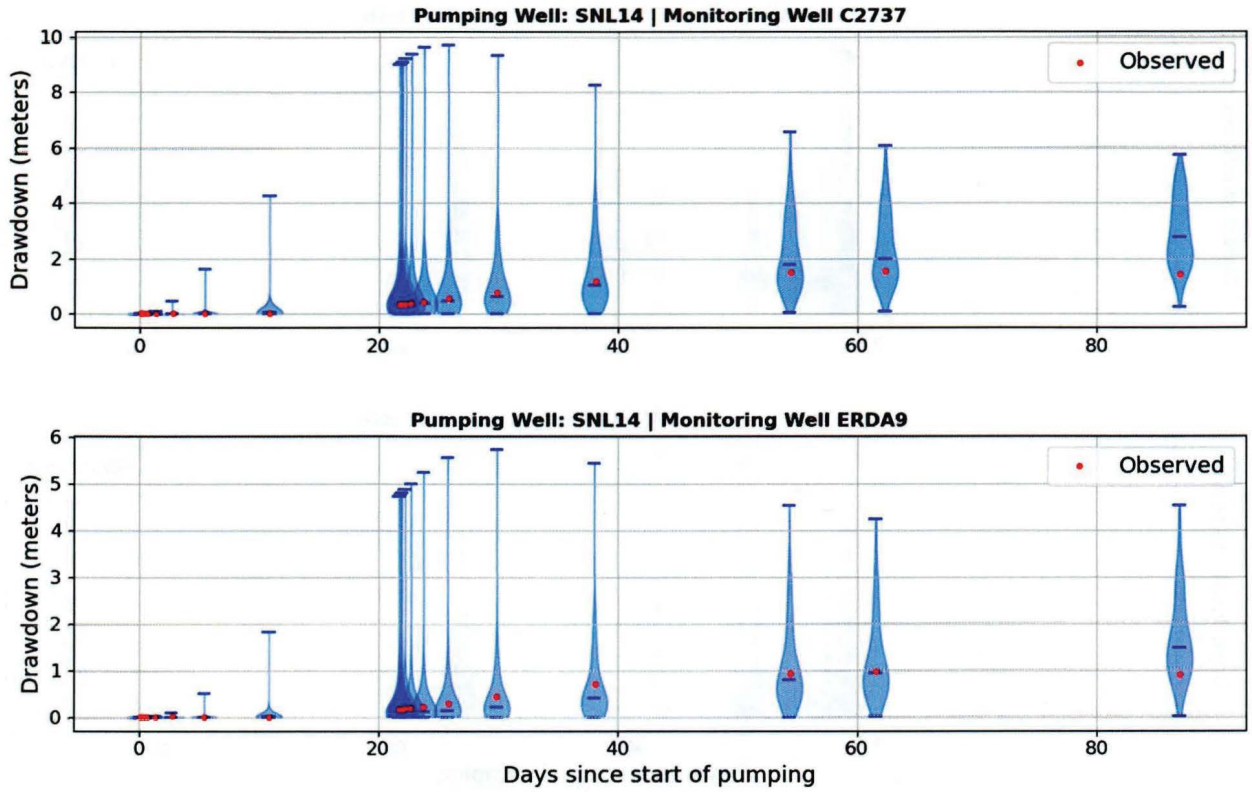

Figure 111. Observed vs Simulated Drawdown at C-2737 and ERDA-9 Monitoring Locations for the SNL-14 Multi-Well Pumping Test

Information Only

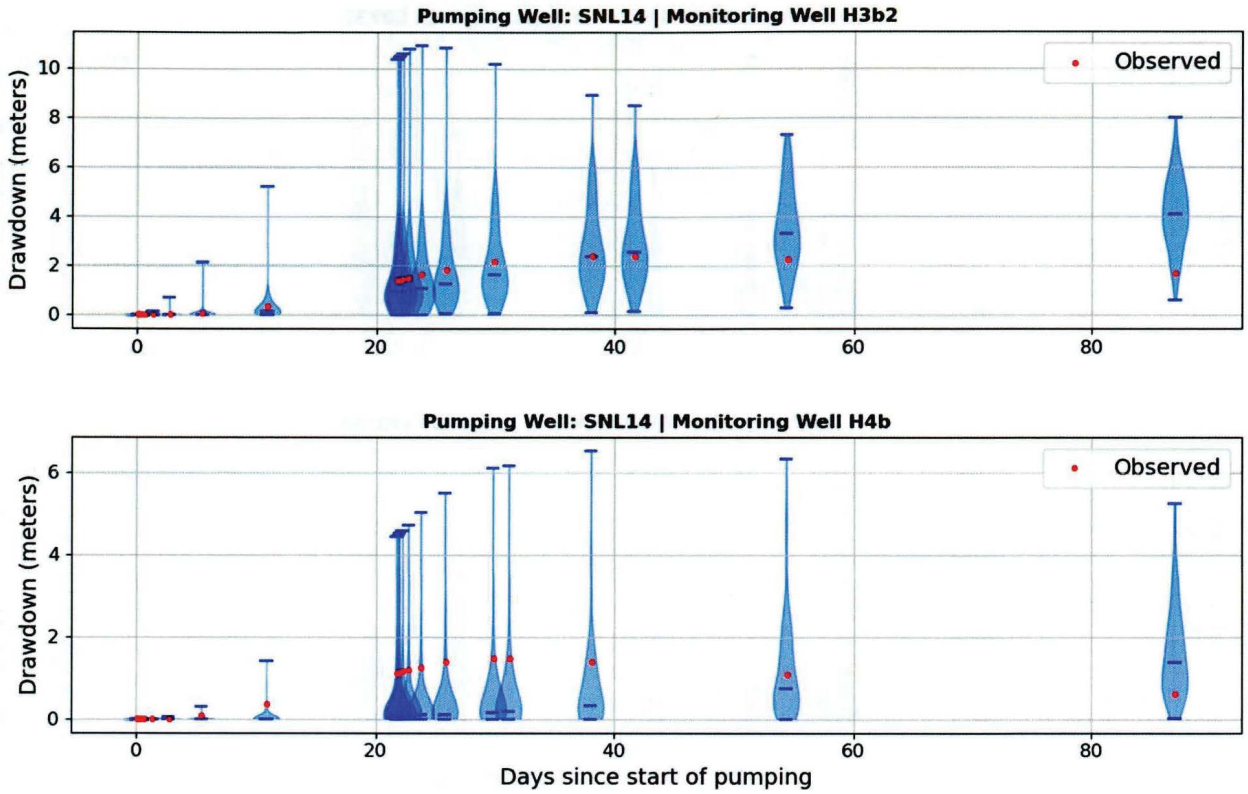

Figure 112. Observed vs Simulated Drawdown at H-3b2 and H-4b Monitoring Locations for the SNL-14 Multi-Well Pumping Test

Information Only

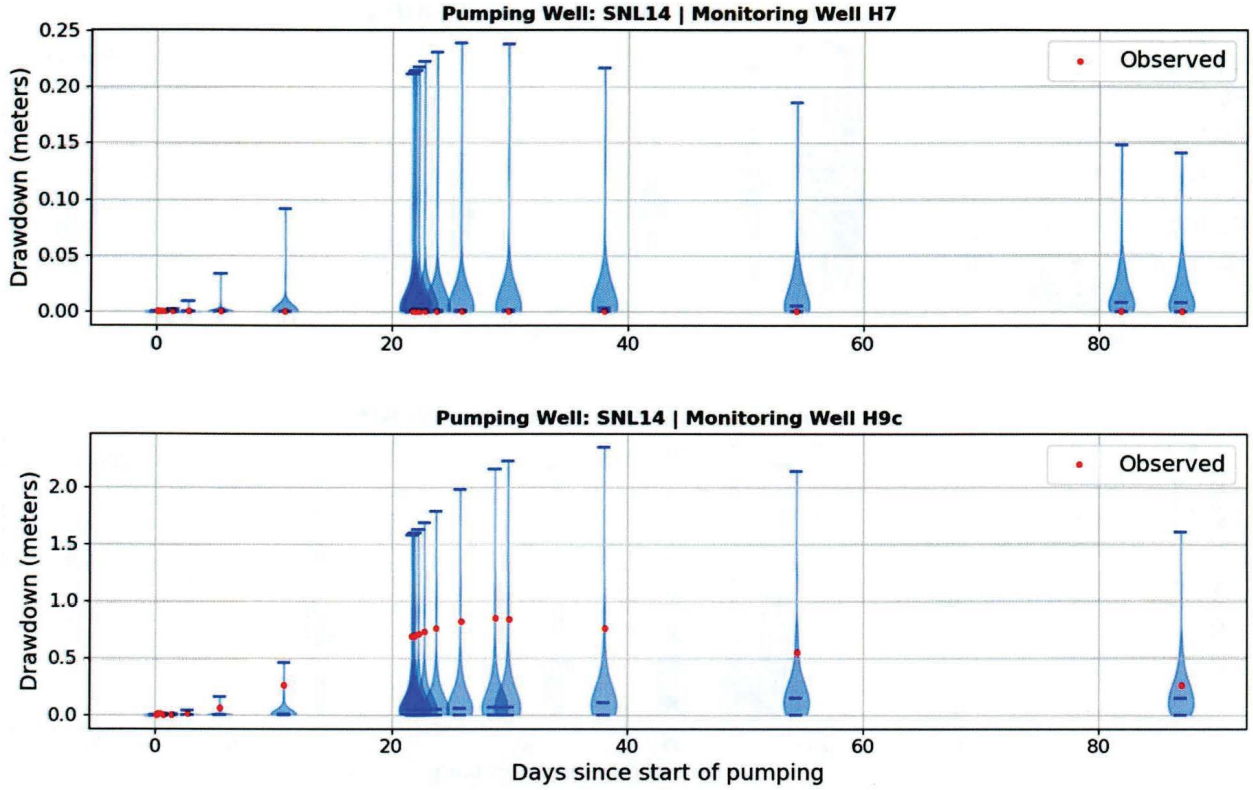

Figure 113. Observed vs Simulated Drawdown at H-7 and H-9c Monitoring Locations for the SNL-14 Multi-Well Pumping Test

Information Only

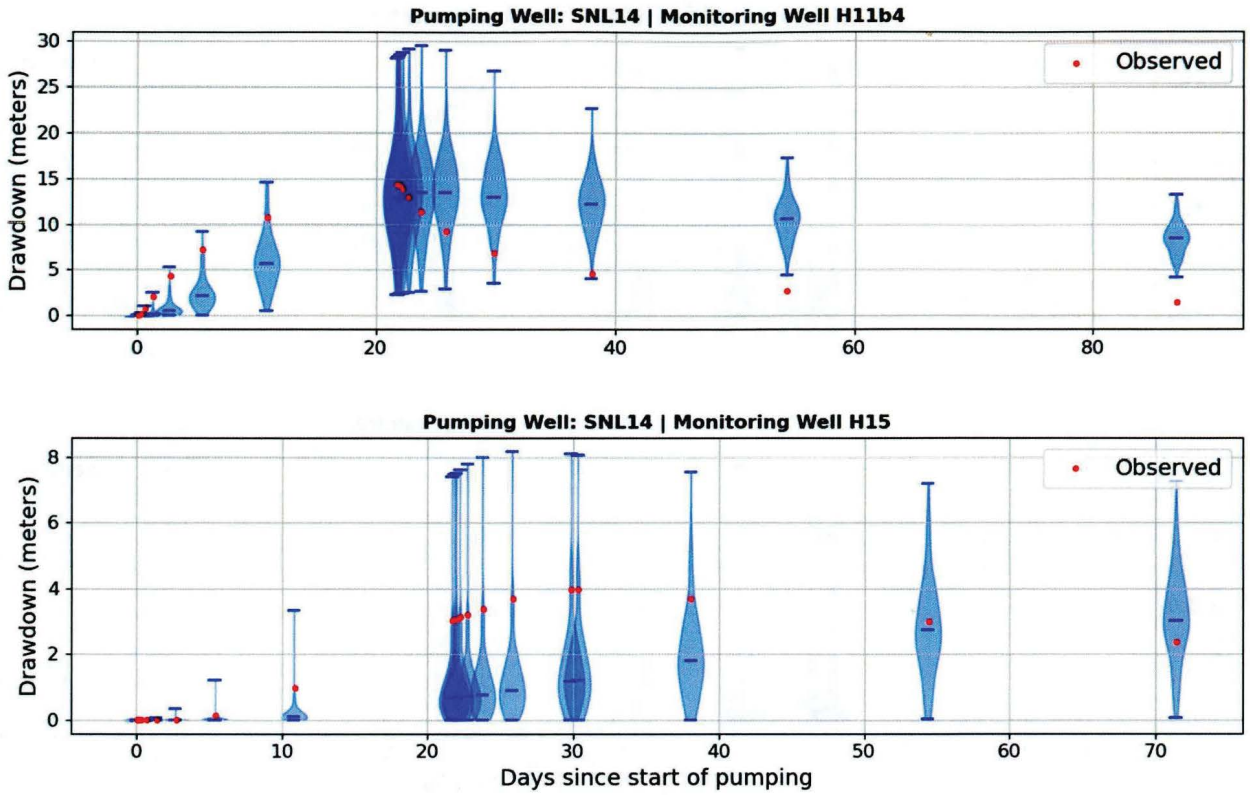

Figure 114. Observed vs Simulated Drawdown at H-11b4 and H-15 Monitoring Locations for the SNL-14 Multi-Well Pumping Test

Information Only

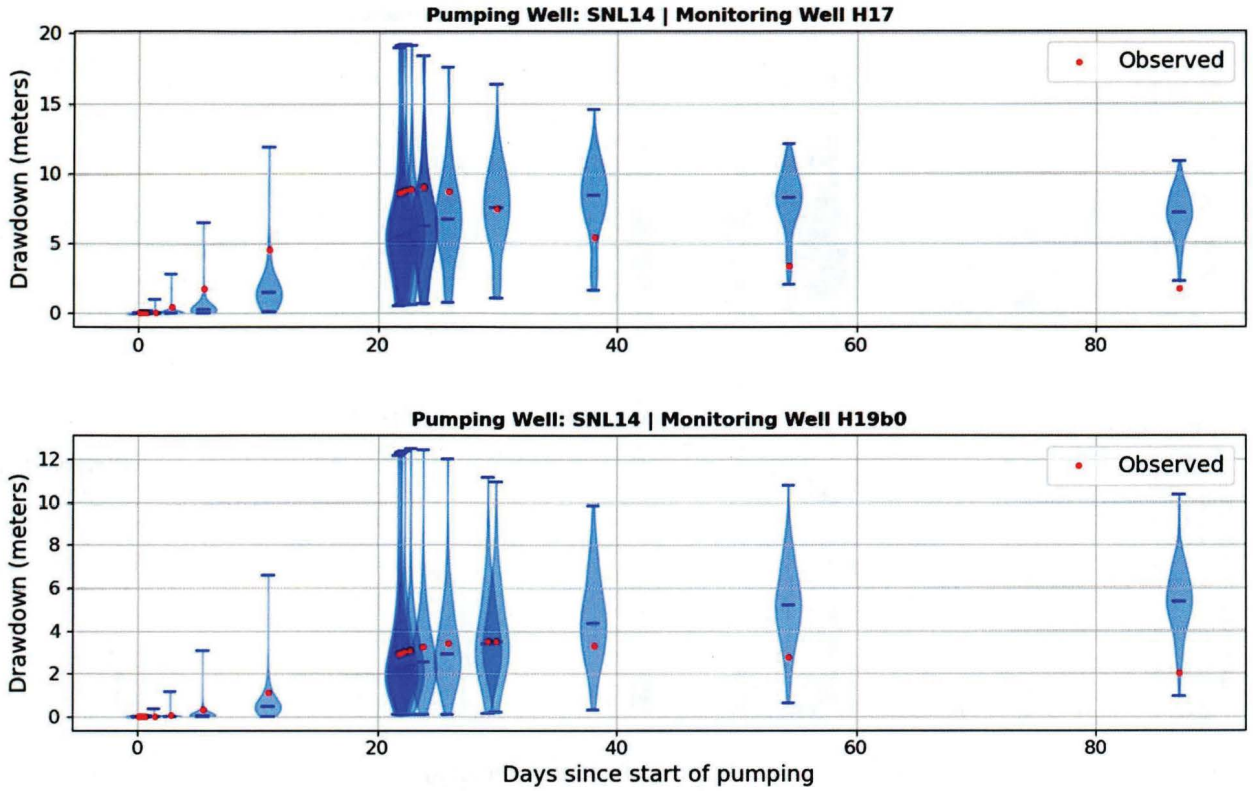

Figure 115. Observed vs Simulated Drawdown at H-17 and H-19b0 Monitoring Locations for the SNL-14 Multi-Well Pumping Test

Information Only

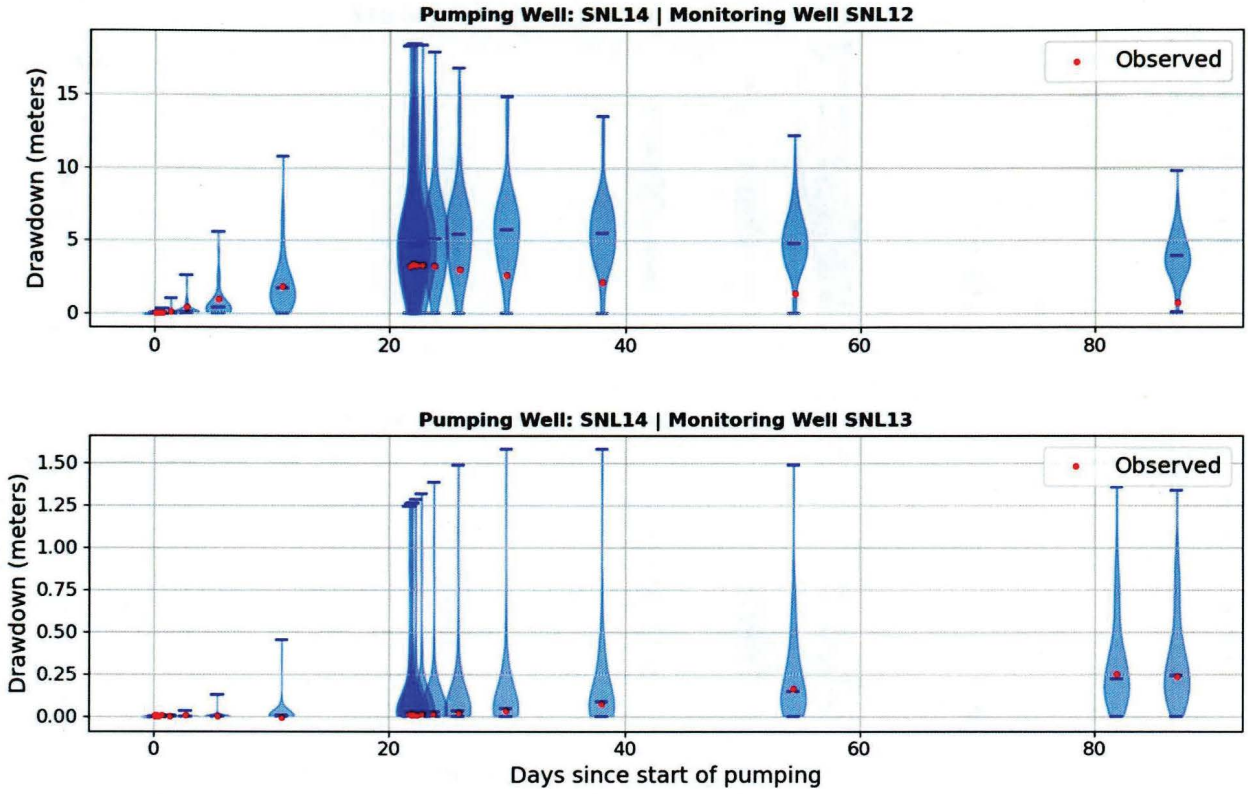

Figure 116. Observed vs Simulated Drawdown at SNL-12 and SNL-13 Monitoring Locations for the SNL-14 Multi-Well Pumping Test

Information Only

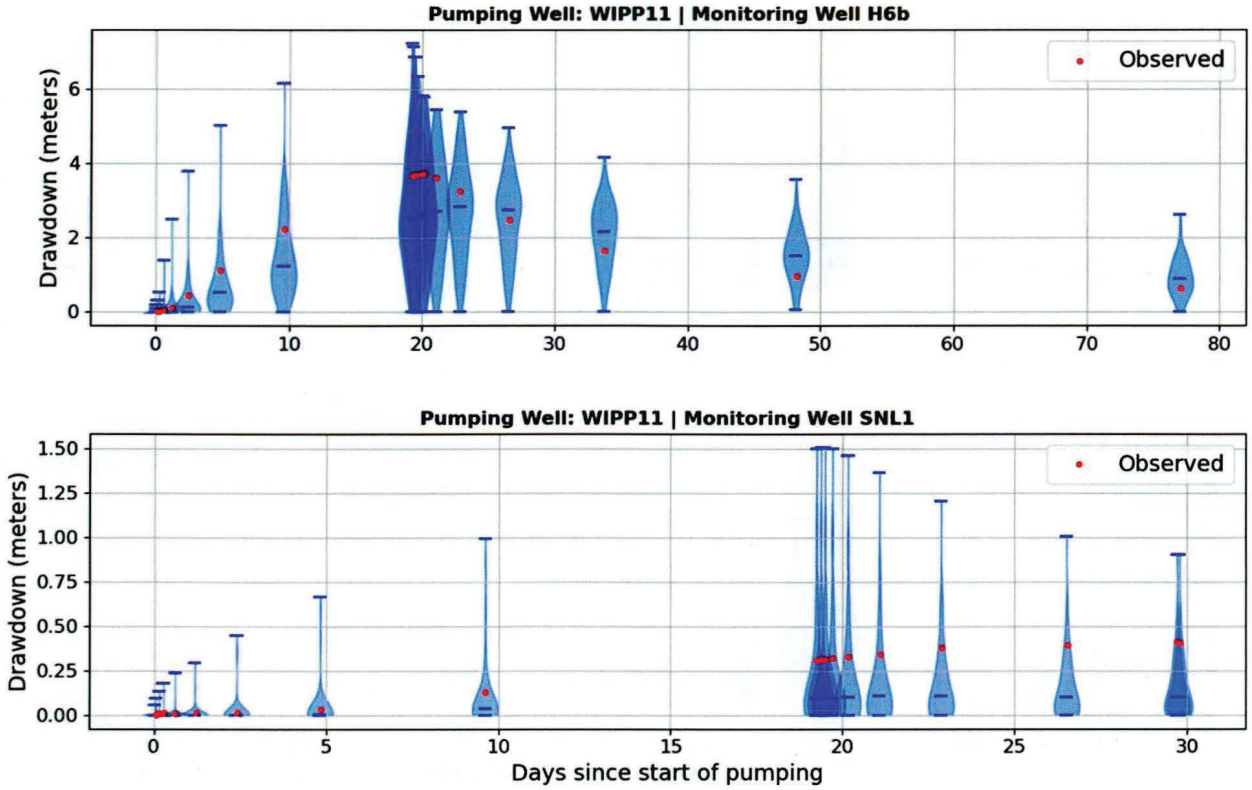

Figure 117. Observed vs Simulated Drawdown at H-6b and SNL-1 Monitoring Locations for the WIPP-11 Multi-Well Pumping Test

Information Only

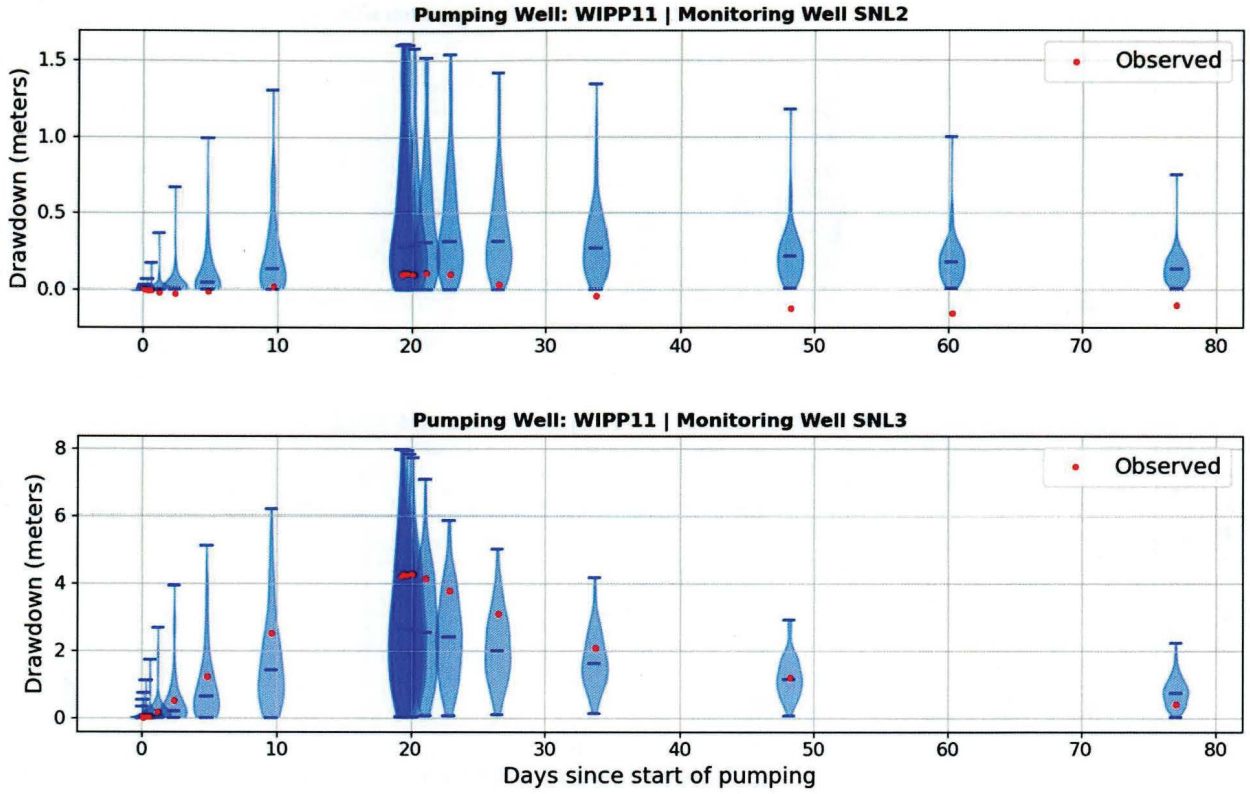

Figure 118. Observed vs Simulated Drawdown at SNL-2 and SNL-3 Monitoring Locations for the WIPP-11 Multi-Well Pumping Test

Information Only

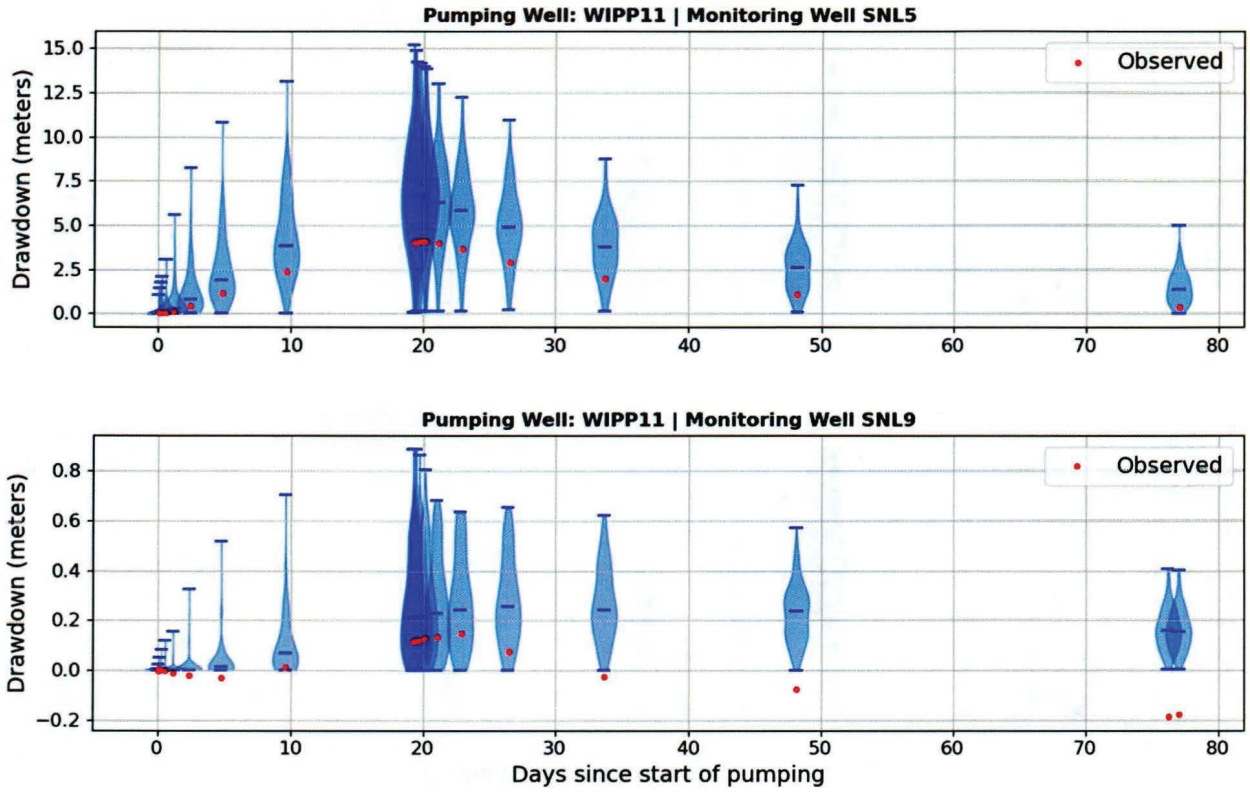

Figure 119. Observed vs Simulated Drawdown at SNL-5 and SNL-9 Monitoring Locations for the WIPP-11 Multi-Well Pumping Test

Information Only

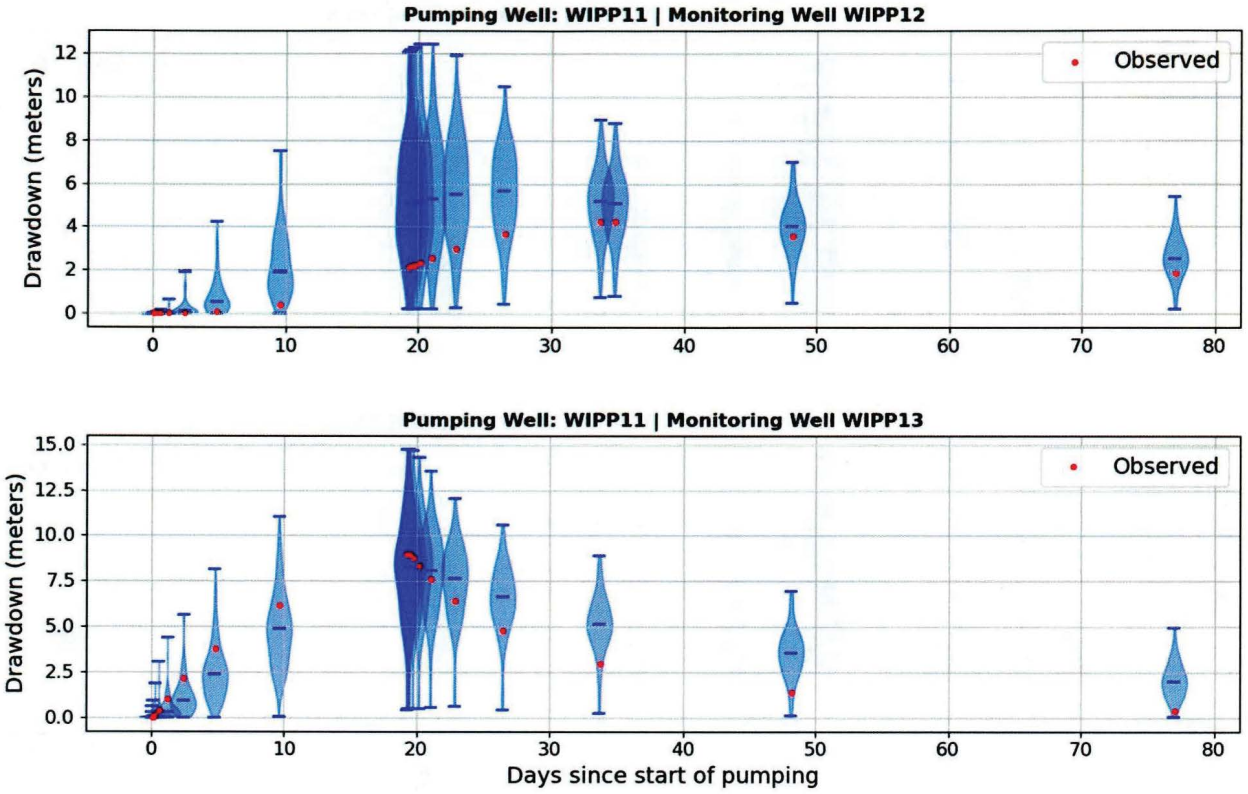

Figure 120. Observed vs Simulated Drawdown at WIPP-12 and WIPP-13 Monitoring Locations for the WIPP-11 Multi-Well Pumping Test

Information Only

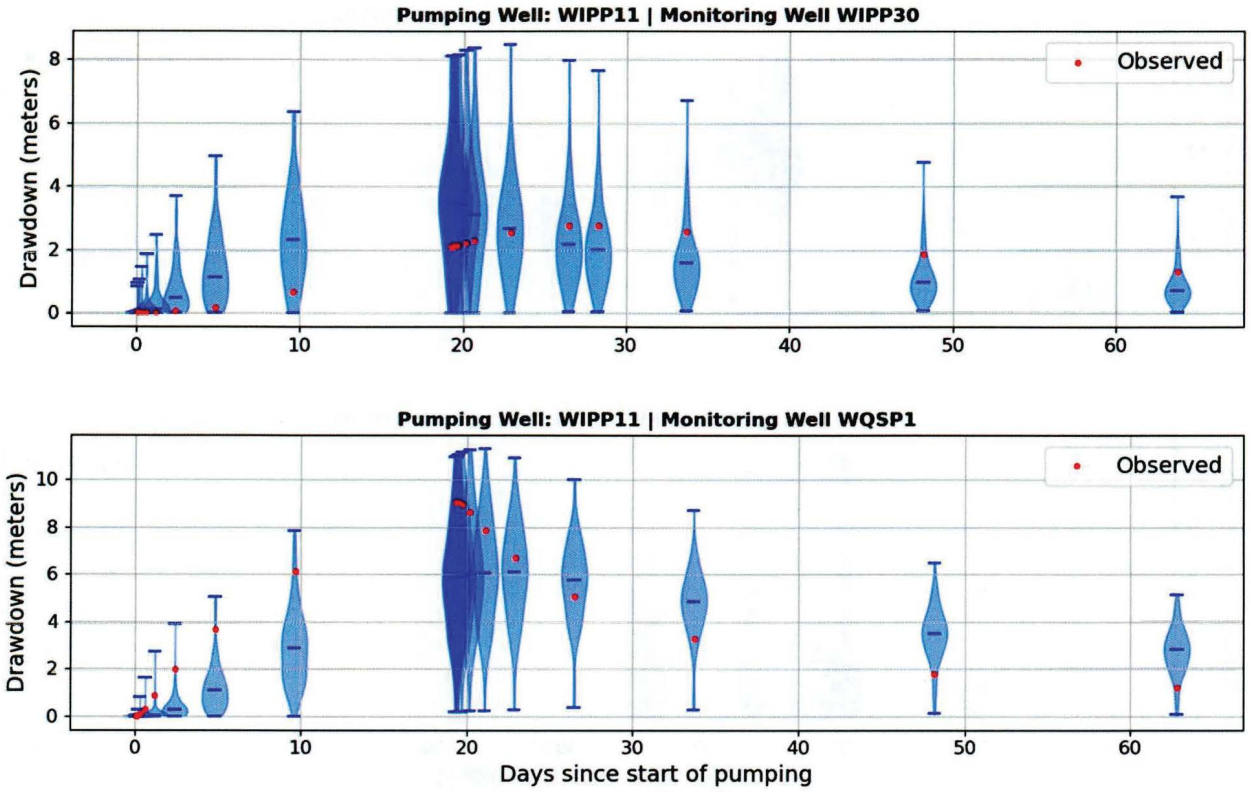

Figure 121. Observed vs Simulated Drawdown at WIPP-30 and WQSP-1 Monitoring Locations for the WIPP-11 Multi-Well Pumping Test

Information Only

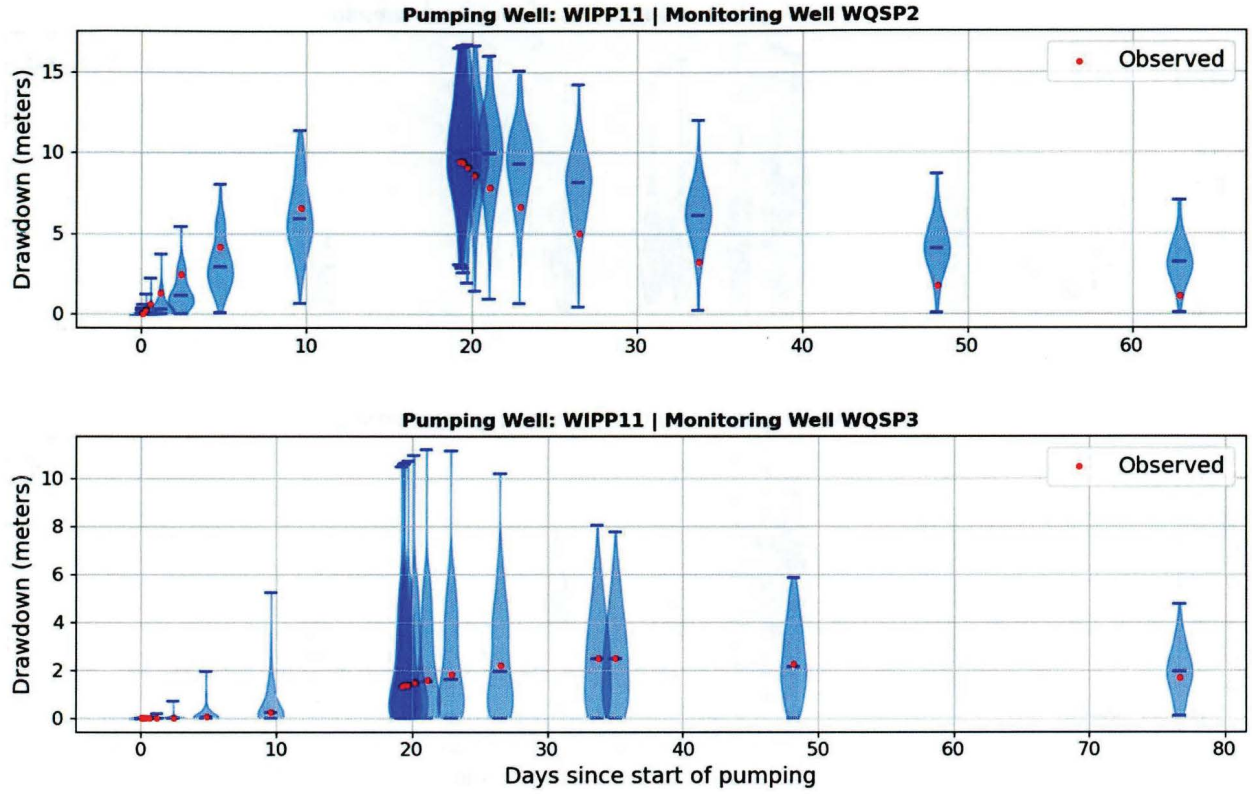

Figure 122. Observed vs Simulated Drawdown at WQSP-2 and WQSP-3 Monitoring Locations for the WIPP-11 Multi-Well Pumping Test

Information Only

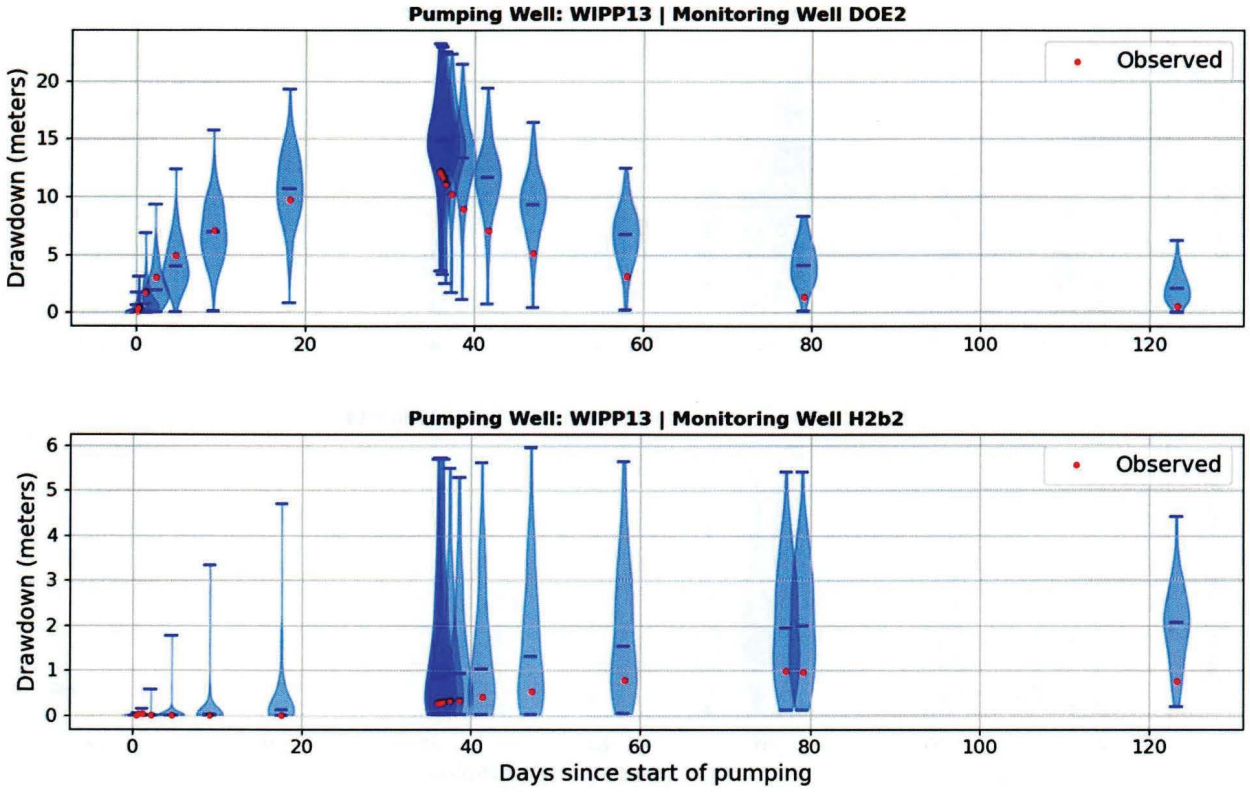

Figure 123. Observed vs Simulated Drawdown at DOE-2 and H-2b2 Monitoring Locations for the WIPP-13 Multi-Well Pumping Test

Information Only

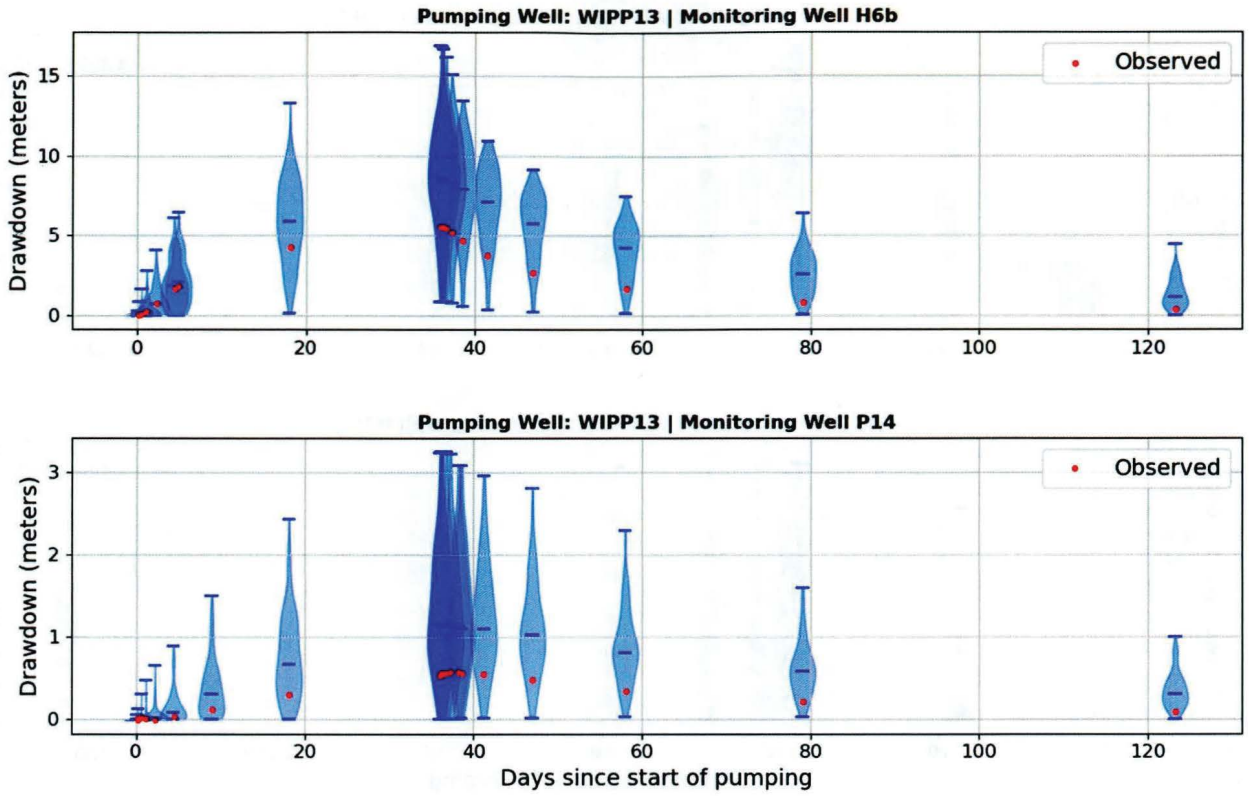

Figure 124. Observed vs Simulated Drawdown at H-6b and P-14 Monitoring Locations for the WIPP-13 Multi-Well Pumping Test

Information Only

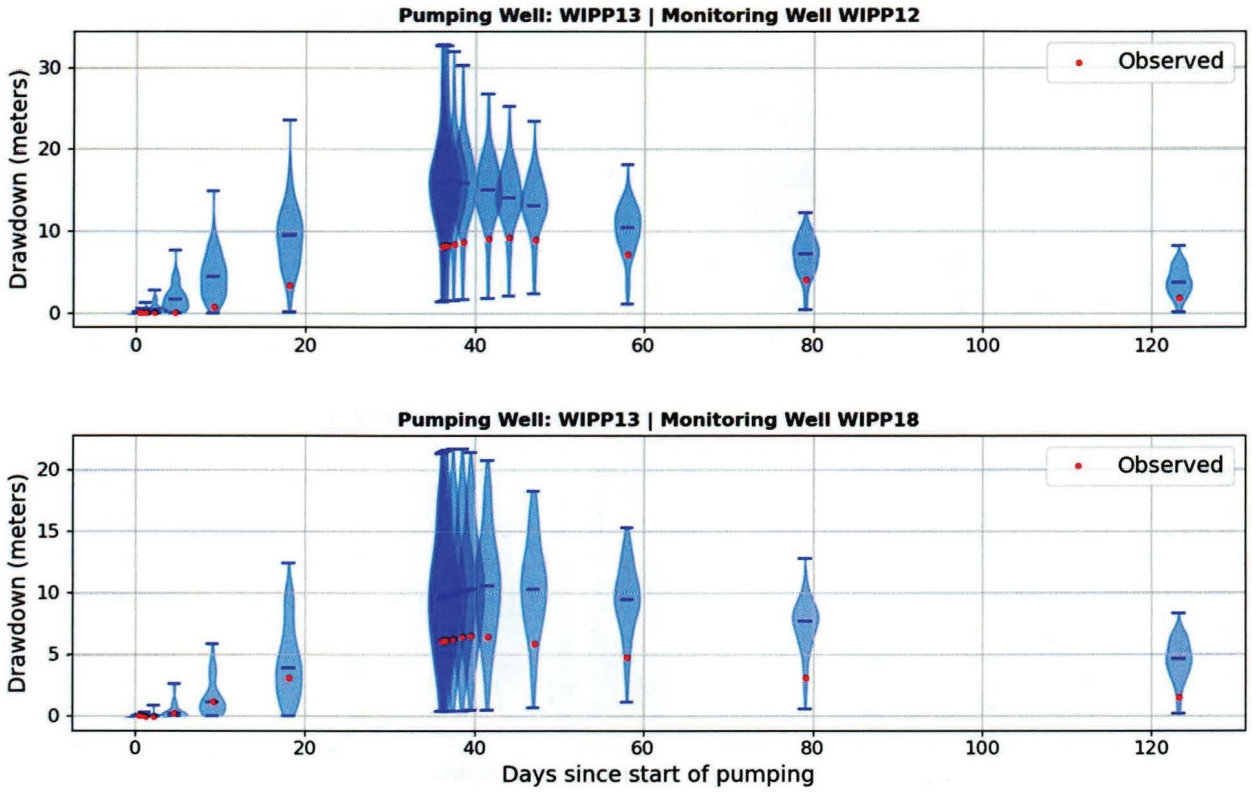

Figure 125. Observed vs Simulated Drawdown at WIPP-12 and WIPP-18 Monitoring Locations for the WIPP-13 Multi-Well Pumping Test

Information Only

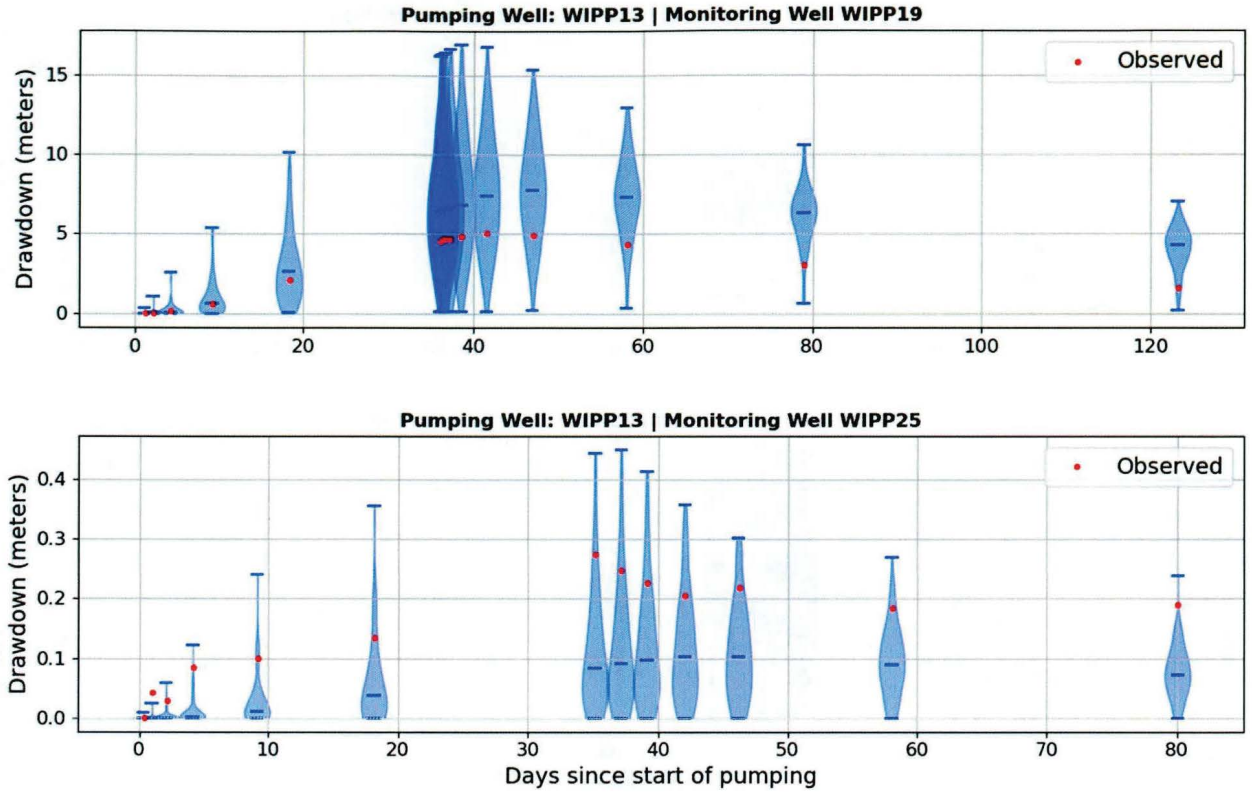

Figure 126. Observed vs Simulated Drawdown at WIPP-19 and WIPP-25 Monitoring Locations for the WIPP-13 Multi-Well Pumping Test

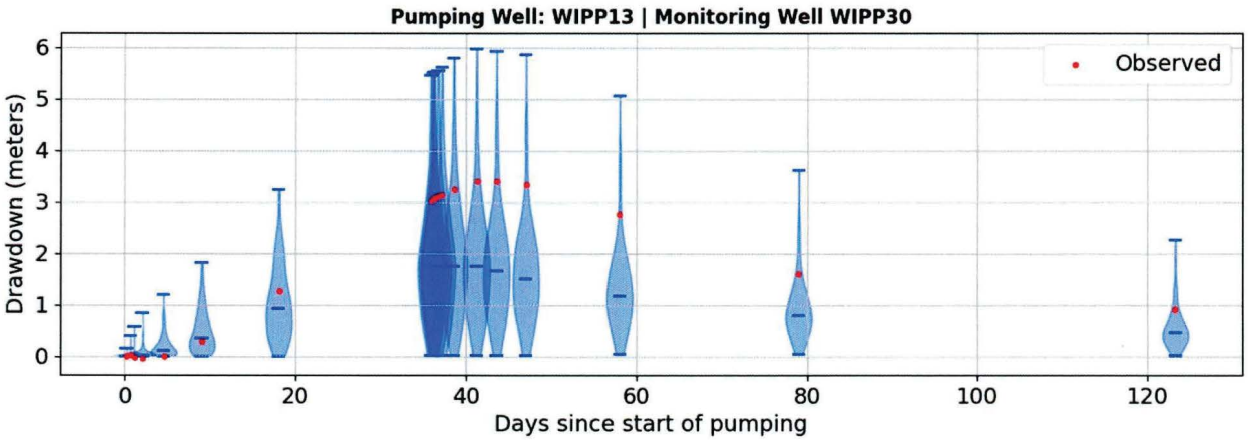

Figure 127. Observed vs Simulated Drawdown at WIPP-30 Monitoring Location for the WIPP-13 Multi-Well Pumping Test

Information Only

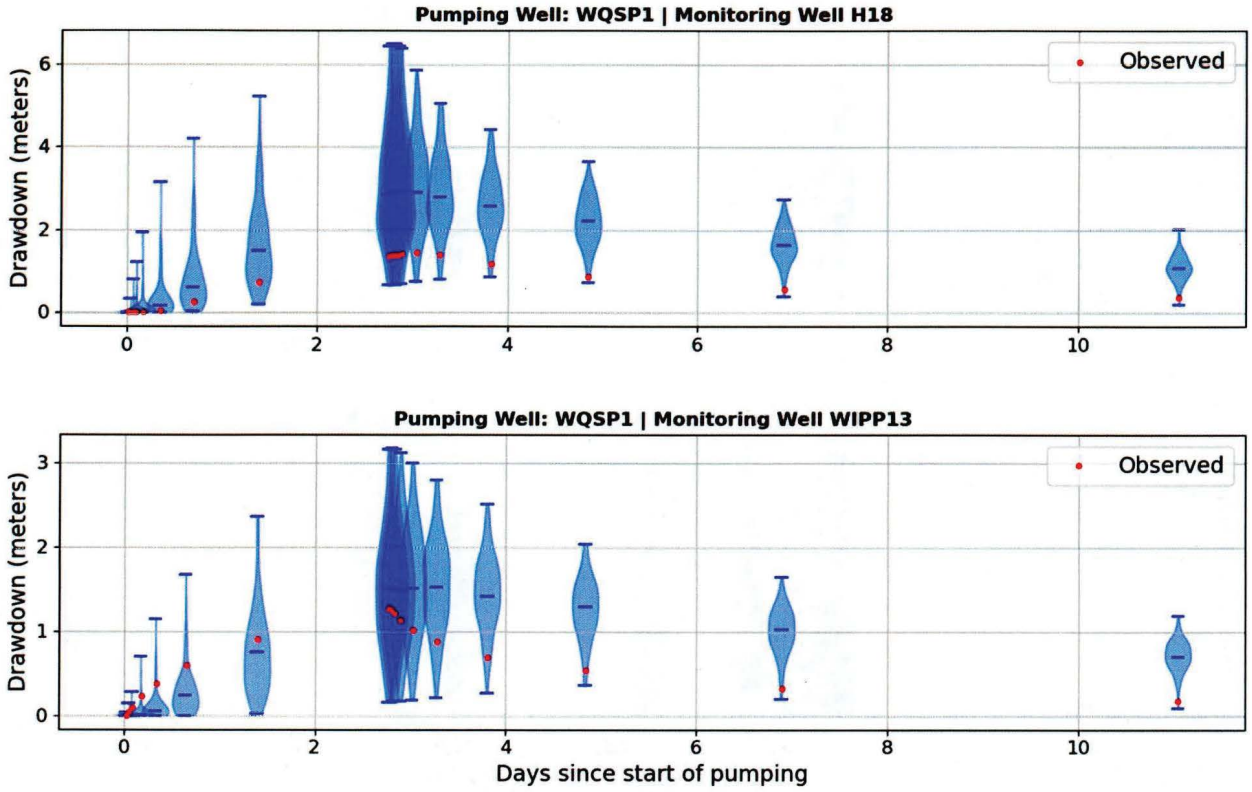

Figure 128. Observed vs Simulated Drawdown at H-18 and WIPP-13 Monitoring Locations for the WQSP-1 Multi-Well Pumping Test

Information Only

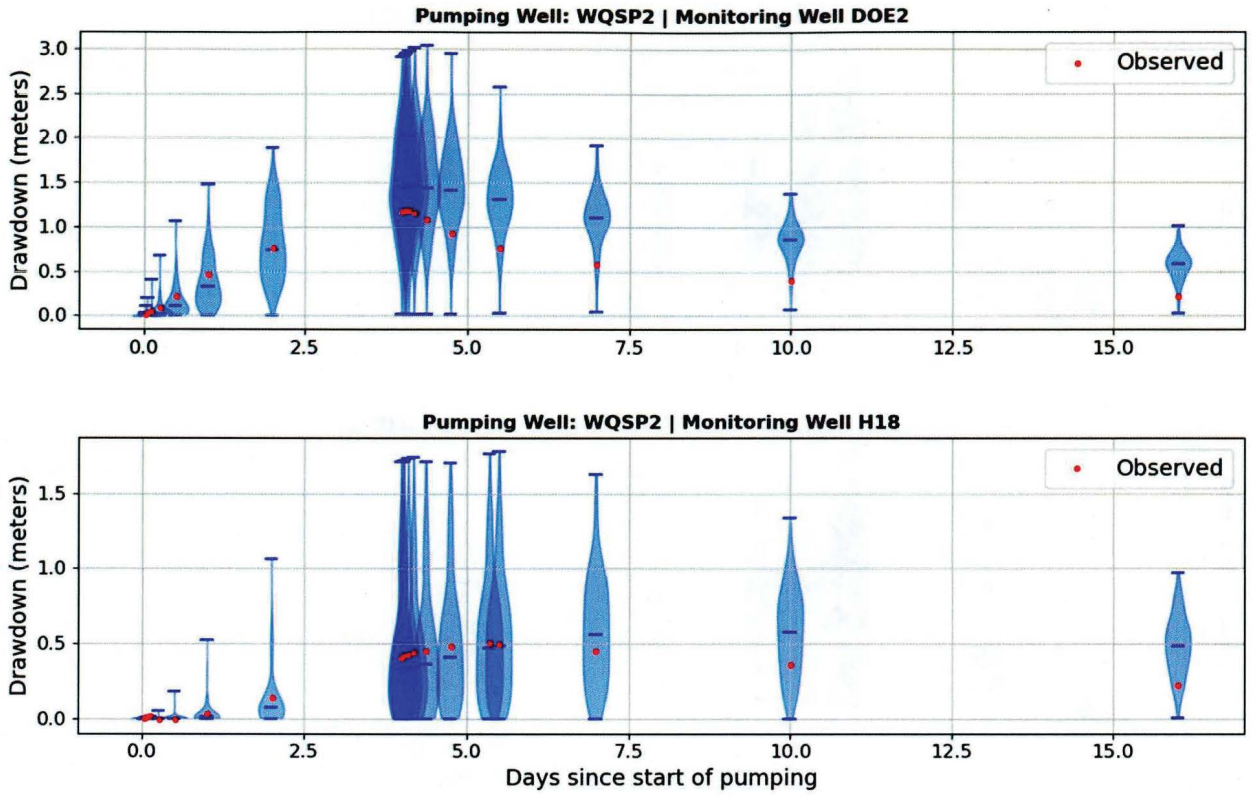

Figure 129. Observed vs Simulated Drawdown at DOE-2 and H-18 Monitoring Locations for the WQSP-2 Multi-Well Pumping Test

Information Only

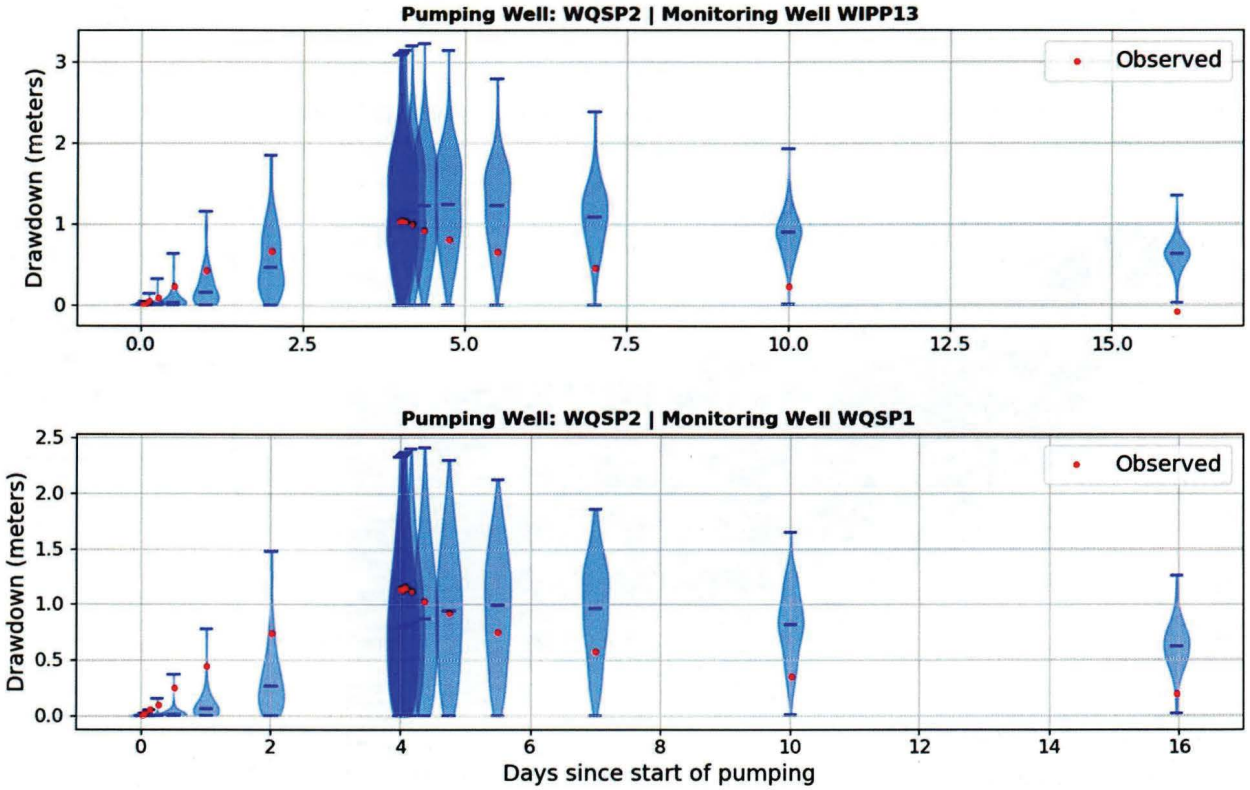

Figure 130. Observed vs Simulated Drawdown at WIPP-13 and WQSP-1 Monitoring Locations for the WQSP-2 Multi-Well Pumping Test

Information Only

7.4 Observed vs Simulated Drawdown at Monitoring Locations during Mills Ranch Pumping

Figure 131 through **Figure 145** present plots of observed versus simulated drawdown responses at monitoring well locations influenced by Mills Ranch pumping.

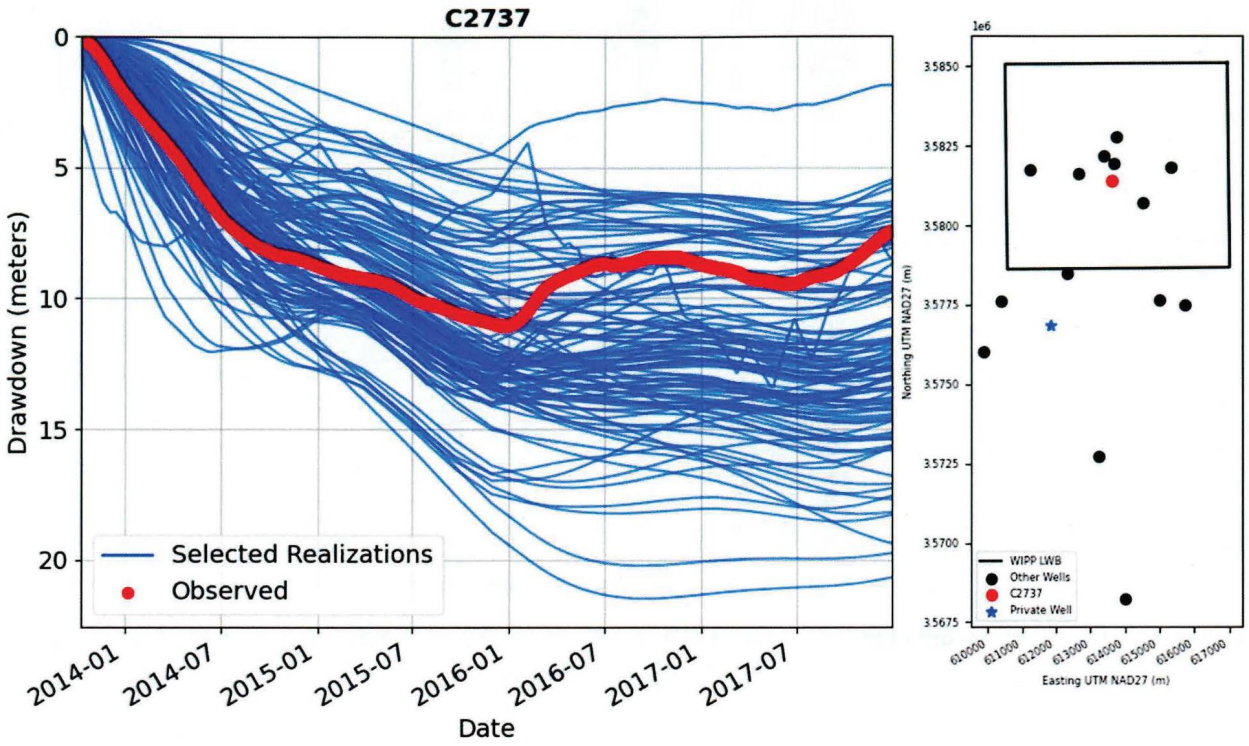

Figure 131. Observed vs Simulated Drawdown at Monitoring Location C-2737 during Mills Ranch Pumping for 100 Selected Realizations from Iteration 5

Information Only

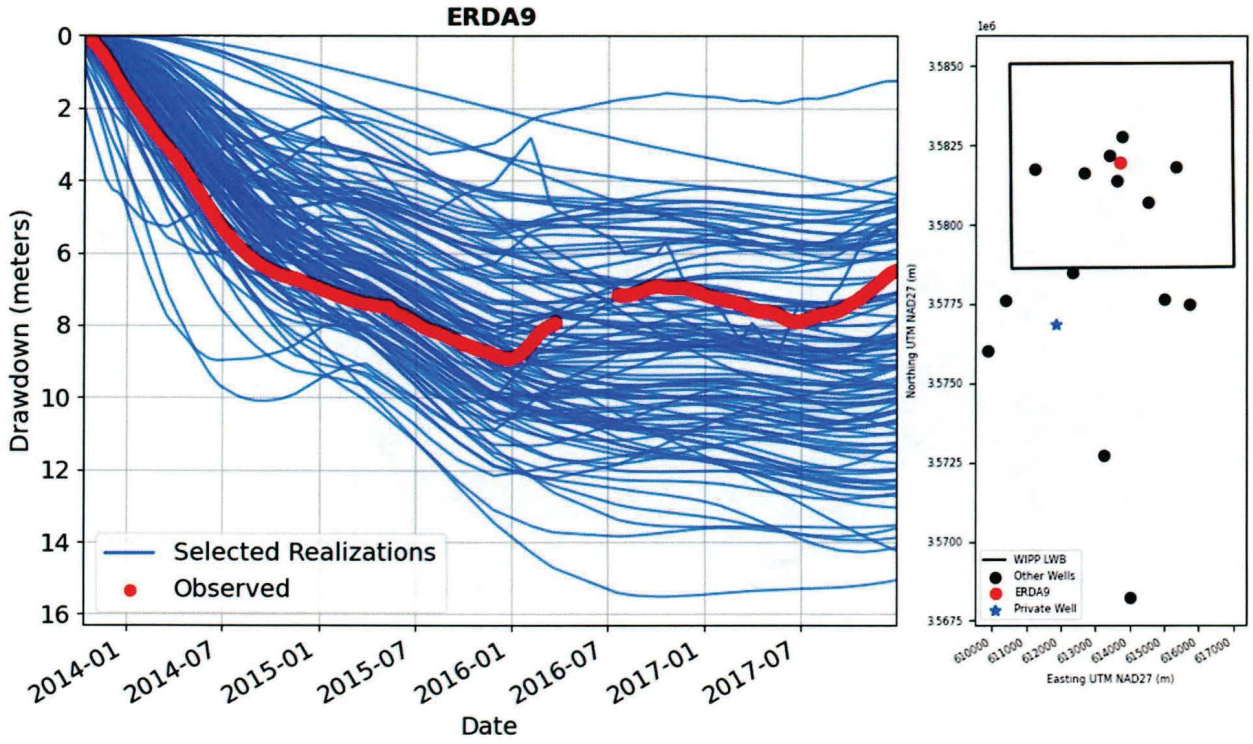

Figure 132. Observed vs Simulated Drawdown at Monitoring Location ERDA-9 during Mills Ranch Pumping for 100 Selected Realizations from Iteration 5

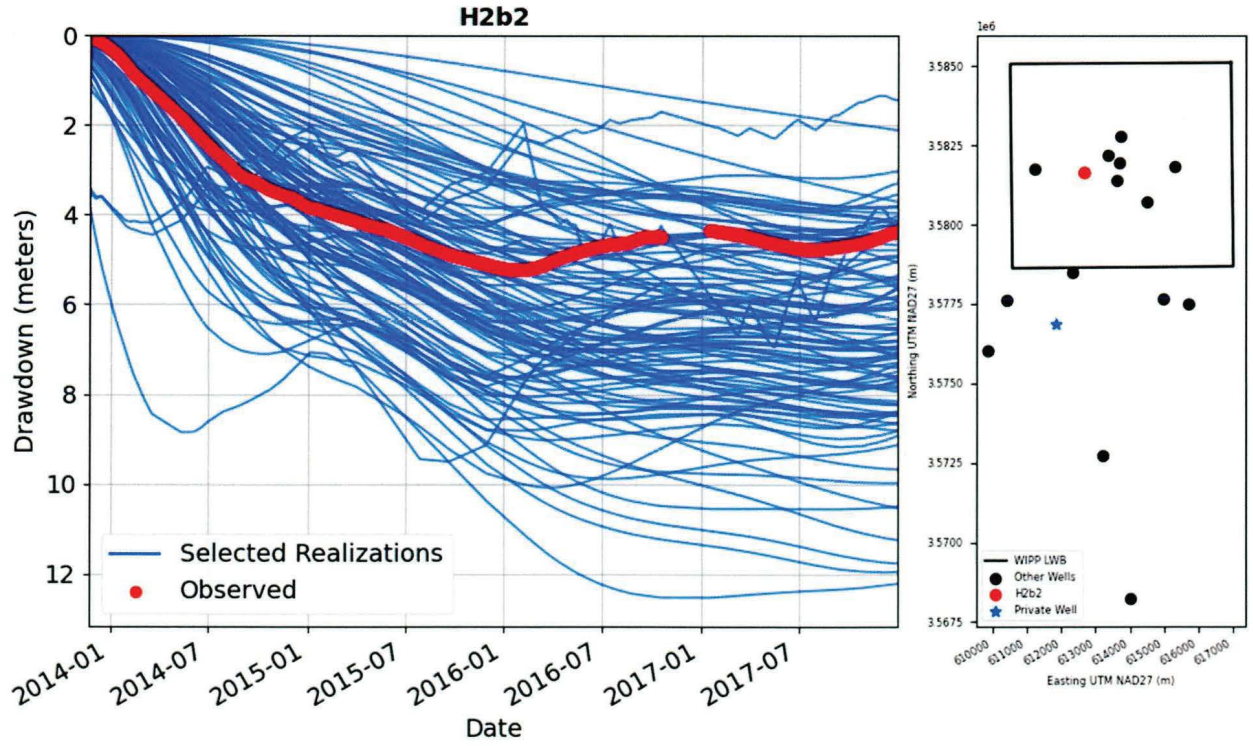

Figure 133. Observed vs Simulated Drawdown at Monitoring Location H-2b2 during the Mills Ranch Pumping Event for 100 Selected Realizations from Iteration 5

Information Only

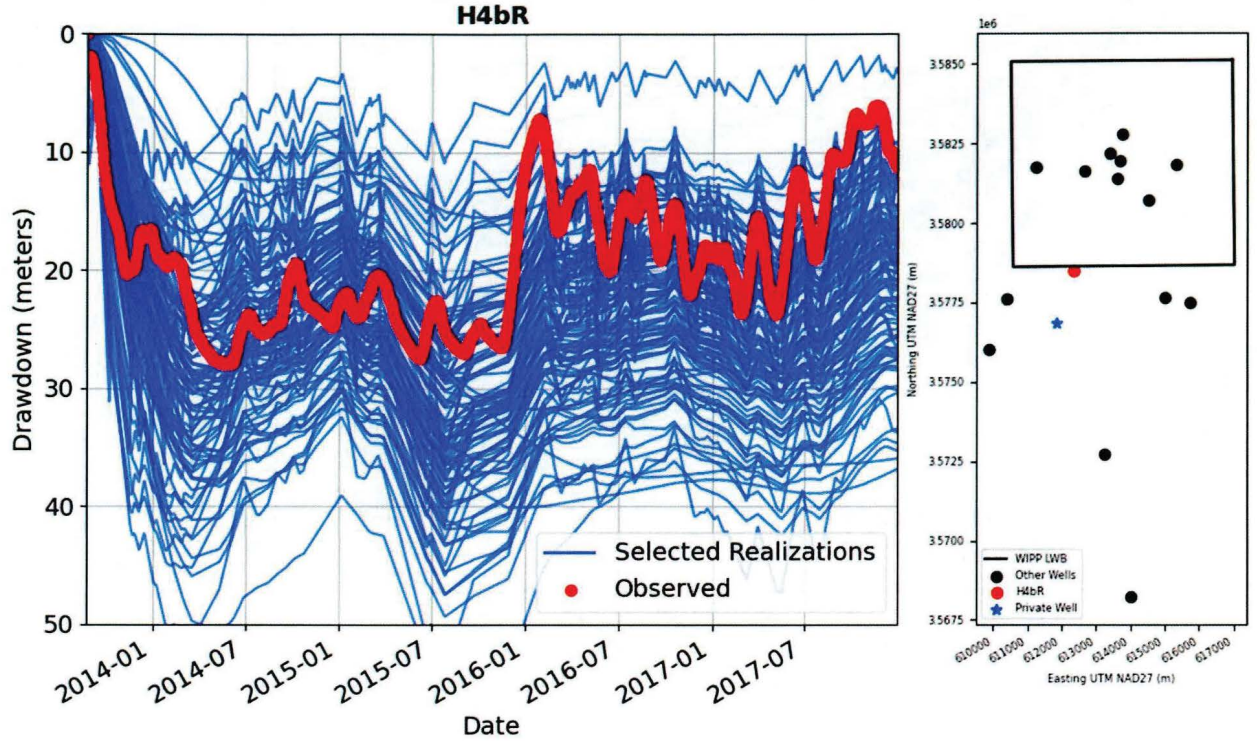

Figure 134. Observed vs Simulated Drawdown at Monitoring Location H-4bR during the Mills Ranch Pumping Event for 100 Selected Realizations from Iteration 5

Information Only

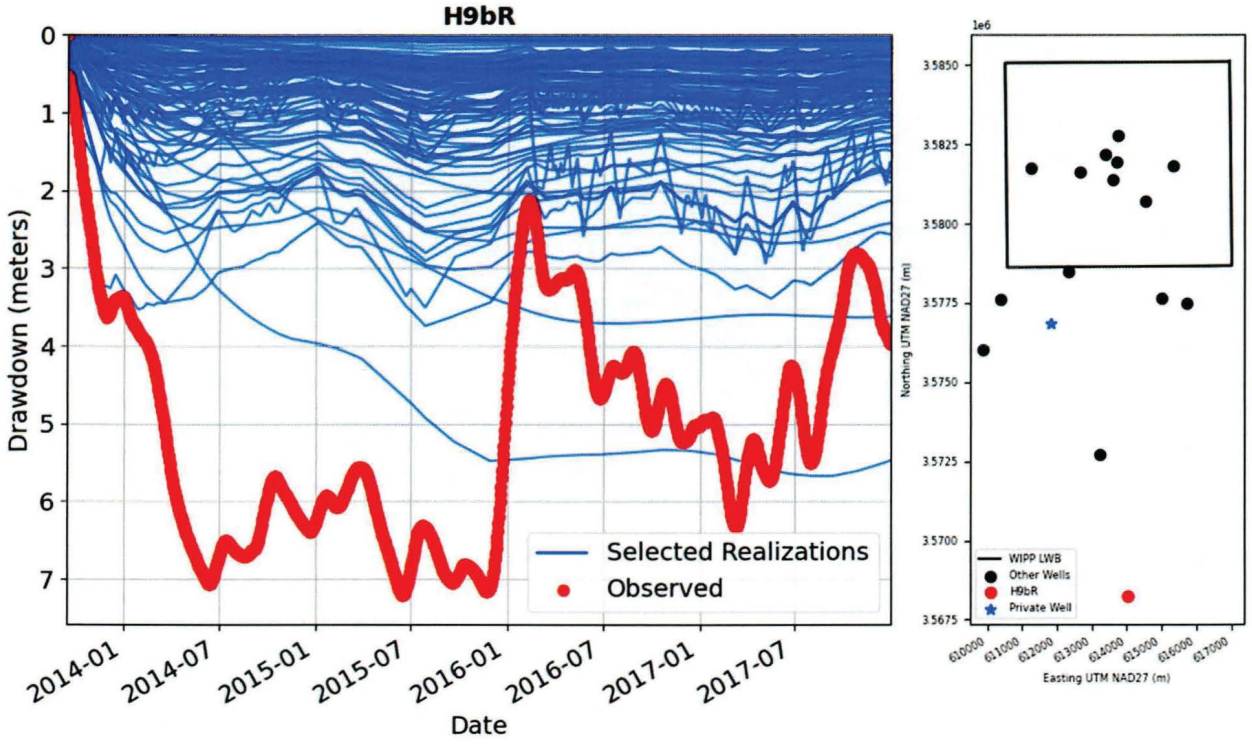

Figure 135. Observed vs Simulated Drawdown at Monitoring Location H-9bR during Mills Ranch Pumping for 100 Selected Realizations from Iteration 5

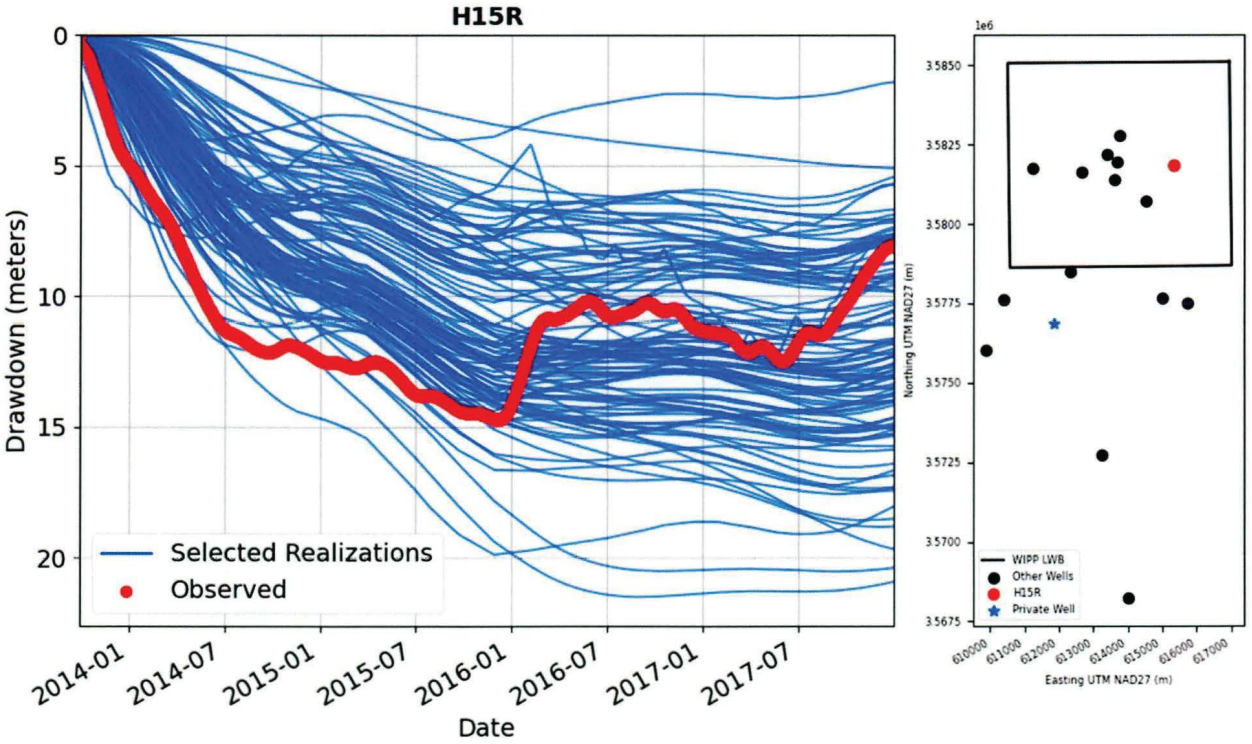

Figure 136. Observed vs Simulated Drawdown at Monitoring Location H-15R during Mills Ranch Event for 100 Selected Realizations from Iteration 5

Information Only

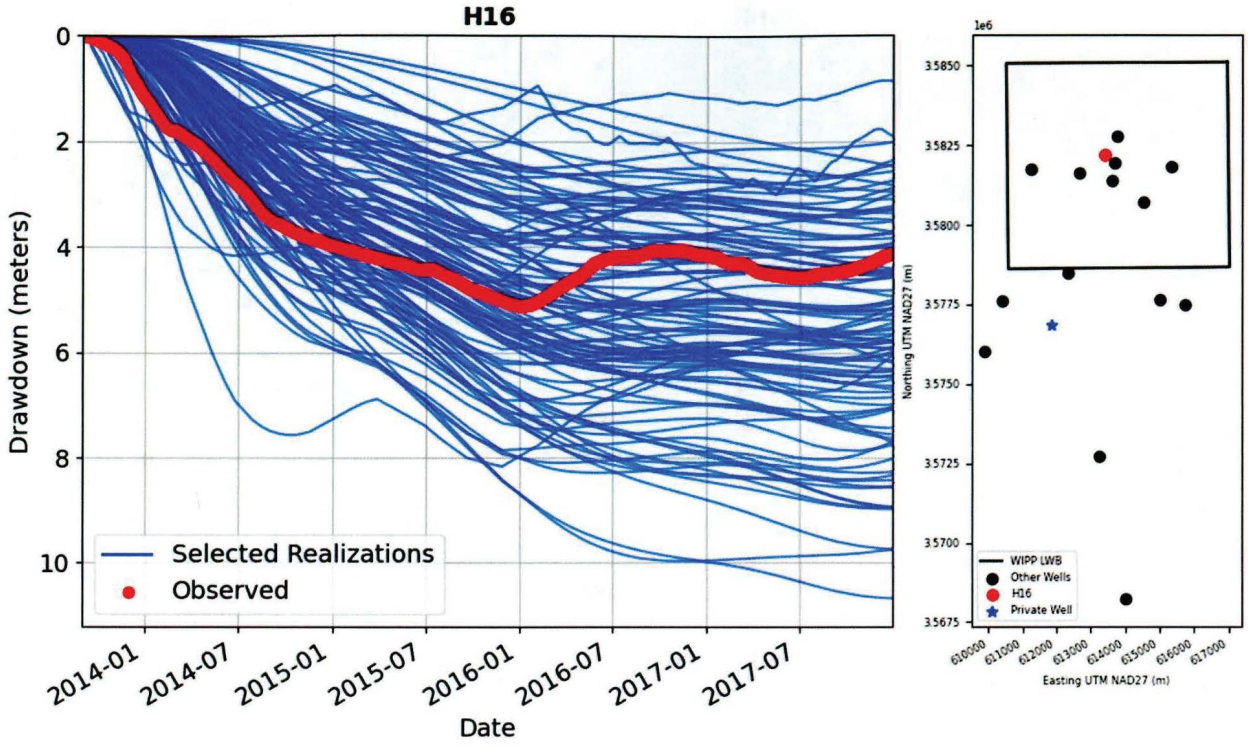

Figure 137. Observed vs Simulated Drawdown at Monitoring Location H-16 during Mills Ranch Pumping for 100 Selected Realizations from Iteration 5

Information Only

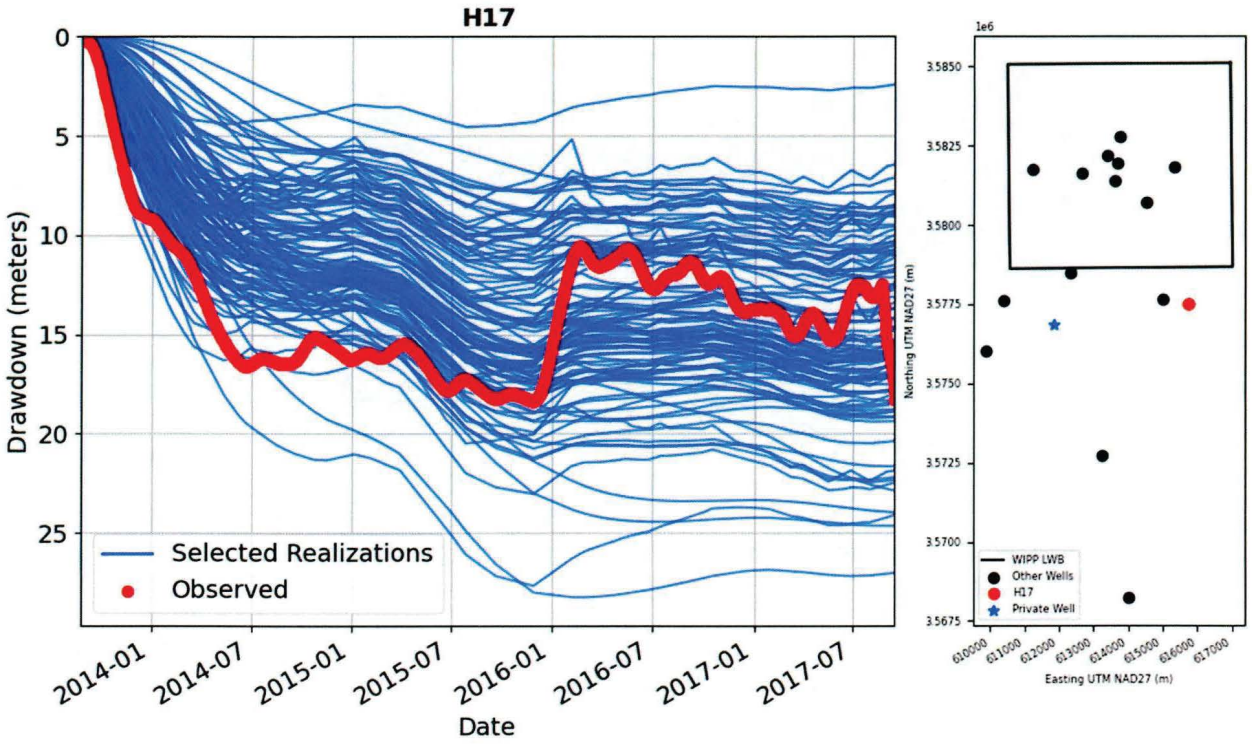

Figure 138. Observed vs Simulated Drawdown at Monitoring Location H-17 during Mills Ranch Pumping for 100 Selected Realizations from Iteration 5

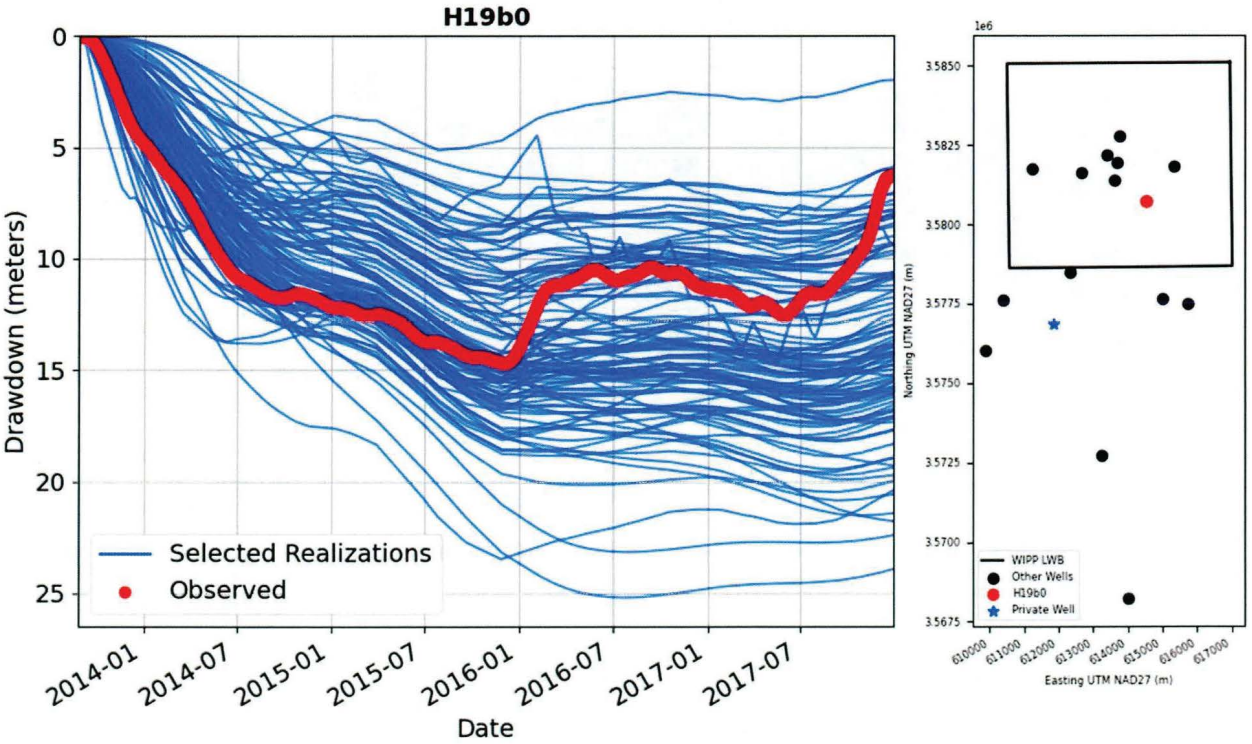

Figure 139. Observed vs Simulated Drawdown at Monitoring Location H-19b0 during Mills Ranch Pumping for 100 Selected Realizations from Iteration 5

Information Only

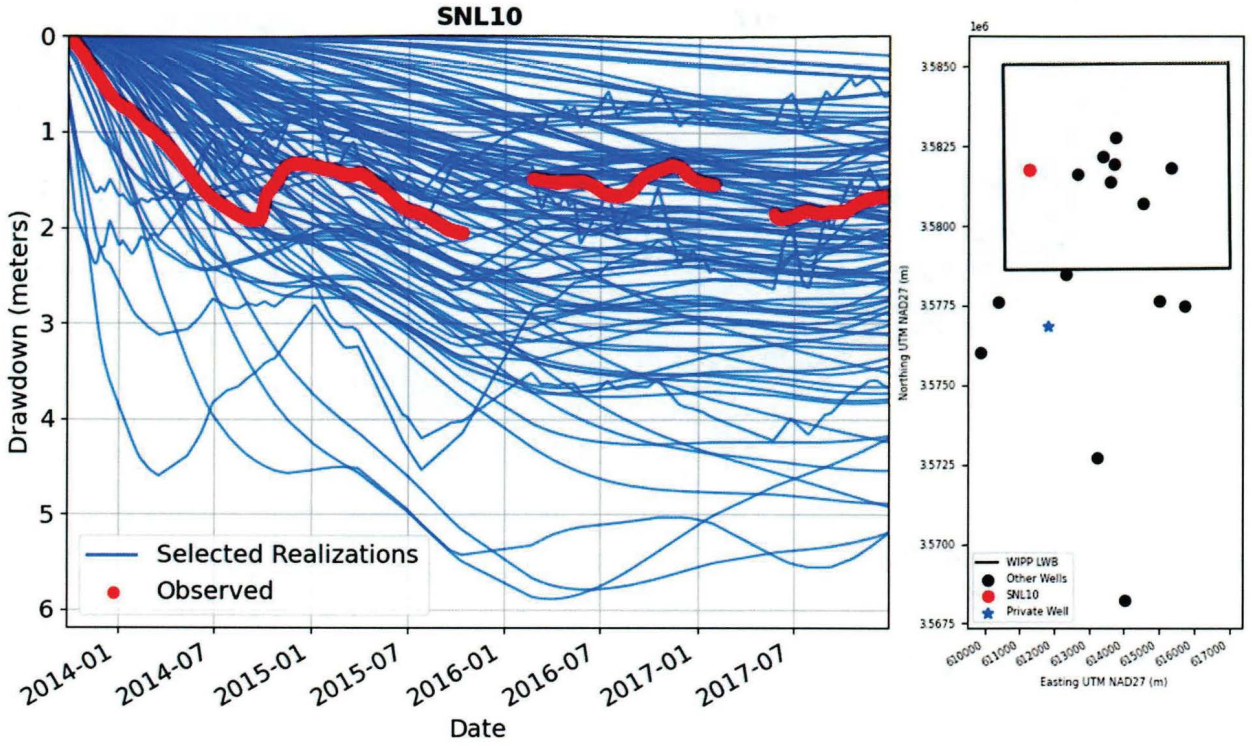

Figure 140. Observed vs Simulated Drawdown at Monitoring Location SNL-10 during Mills Ranch Pumping for 100 Selected Realizations from Iteration 5

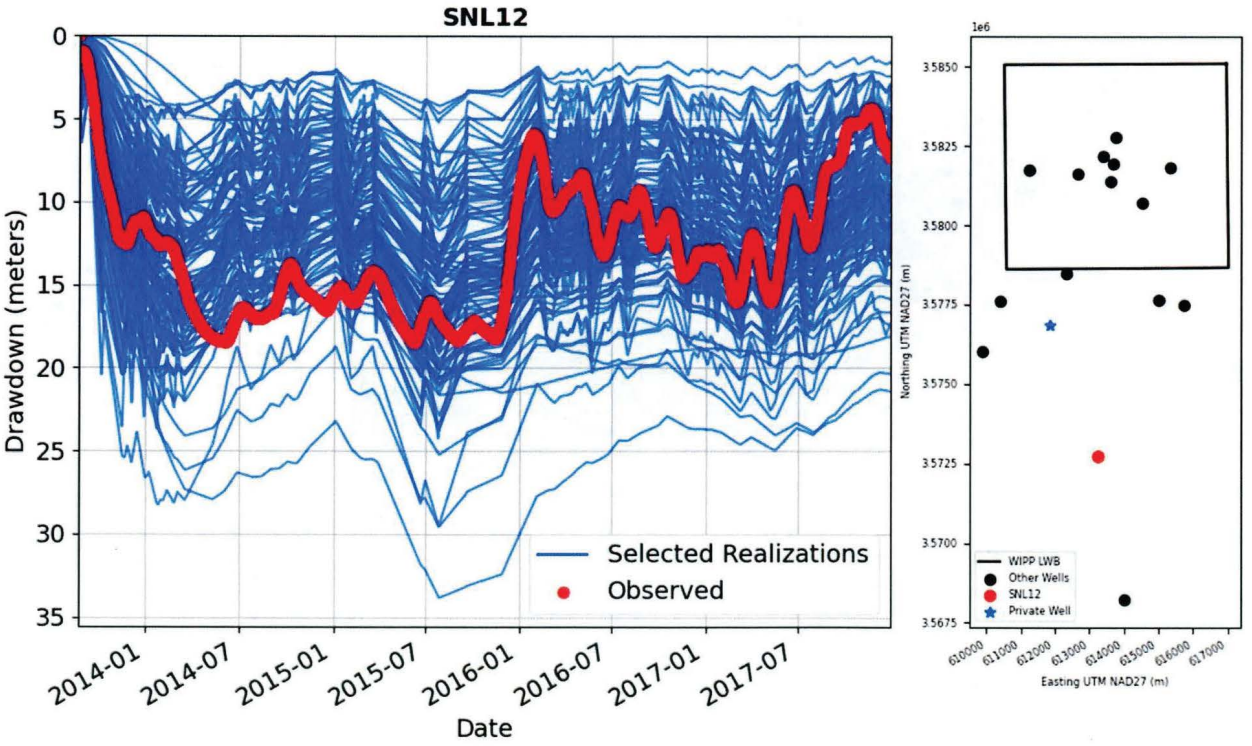

Figure 141. Observed vs Simulated Drawdown at Monitoring Location SNL-12 during Mills Ranch Pumping for 100 Selected Realizations from Iteration 5

Information Only

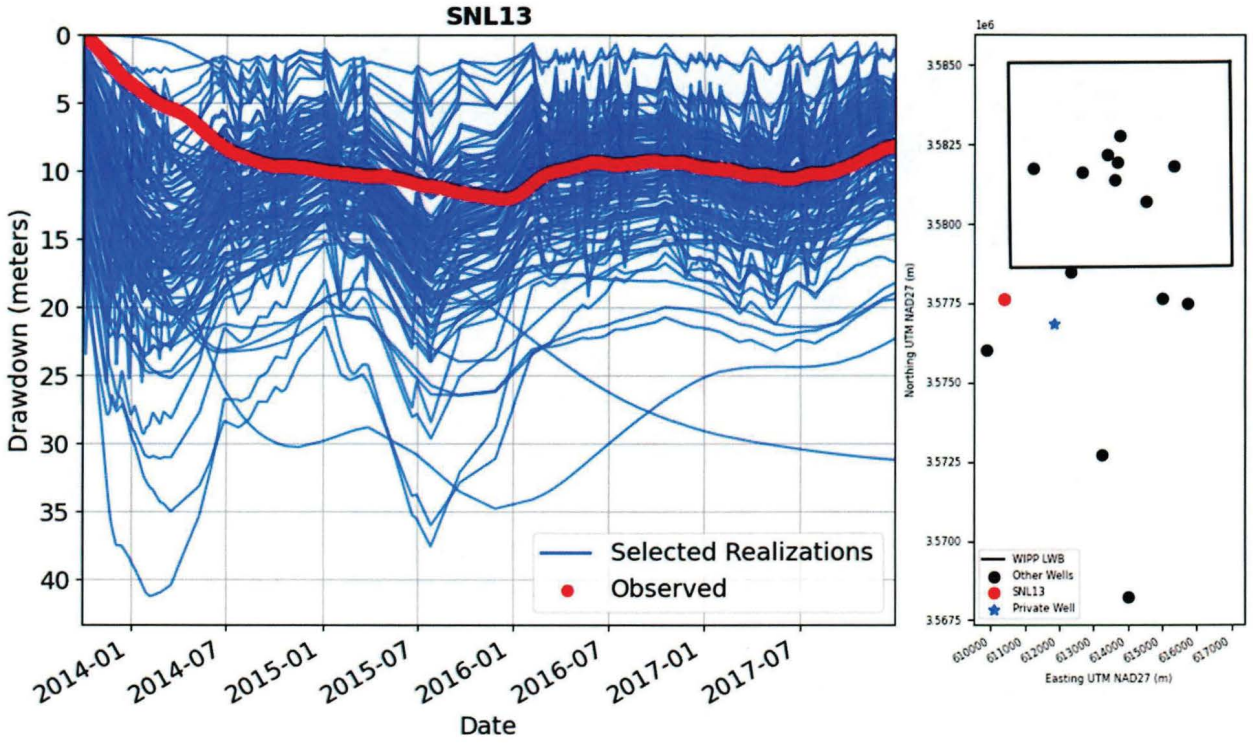

Figure 142. Observed vs Simulated Drawdown at Monitoring Location SNL-13 during Mills Ranch Pumping for 100 Selected Realizations from Iteration 5

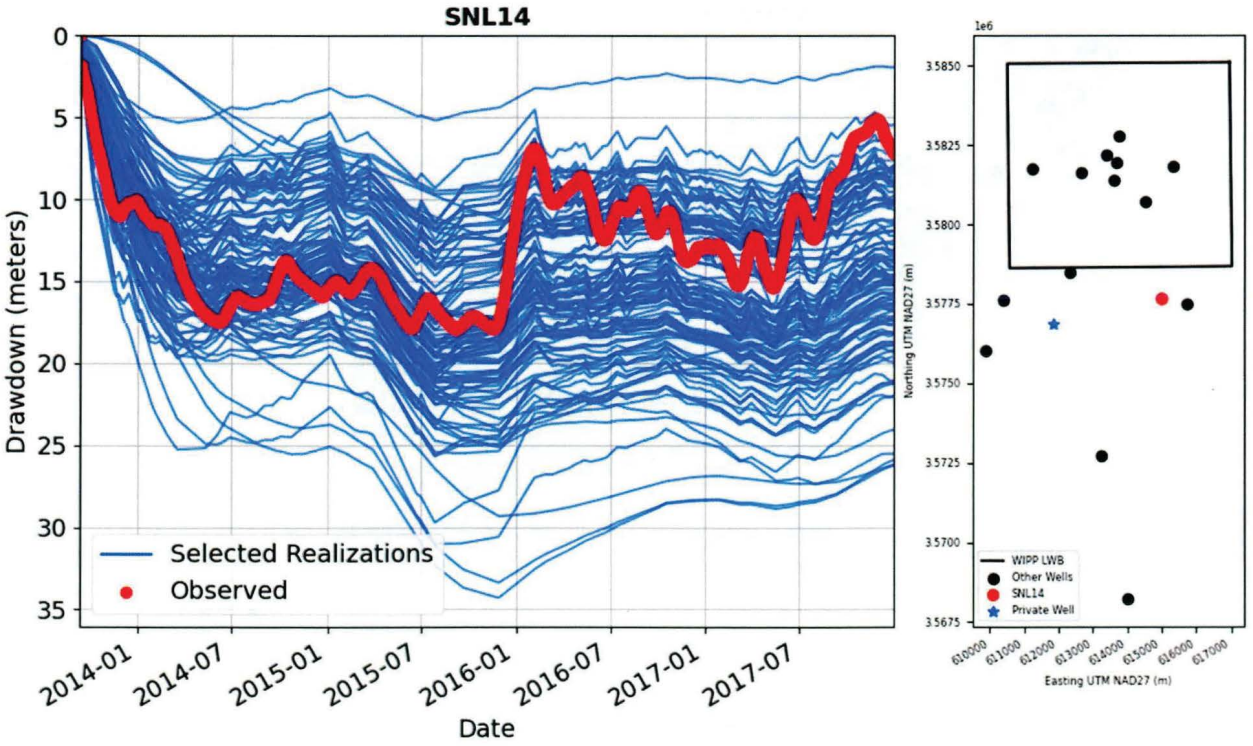

Figure 143. Observed vs Simulated Drawdown at Monitoring Location SNL-14 during Mills Ranch Pumping for 100 Selected Realizations from Iteration 5

Information Only

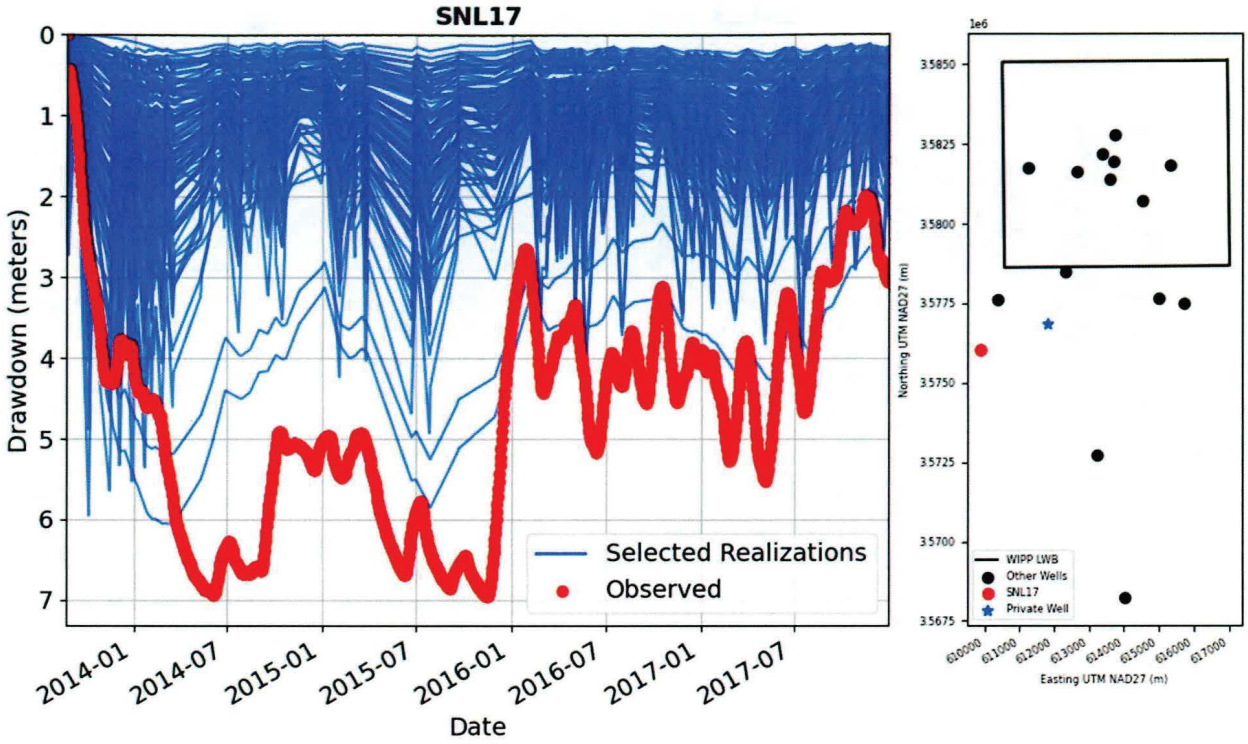

Figure 144. Observed vs Simulated Drawdown at Monitoring Location SNL-17 during Mills Ranch Pumping for 100 Selected Realizations from Iteration 5

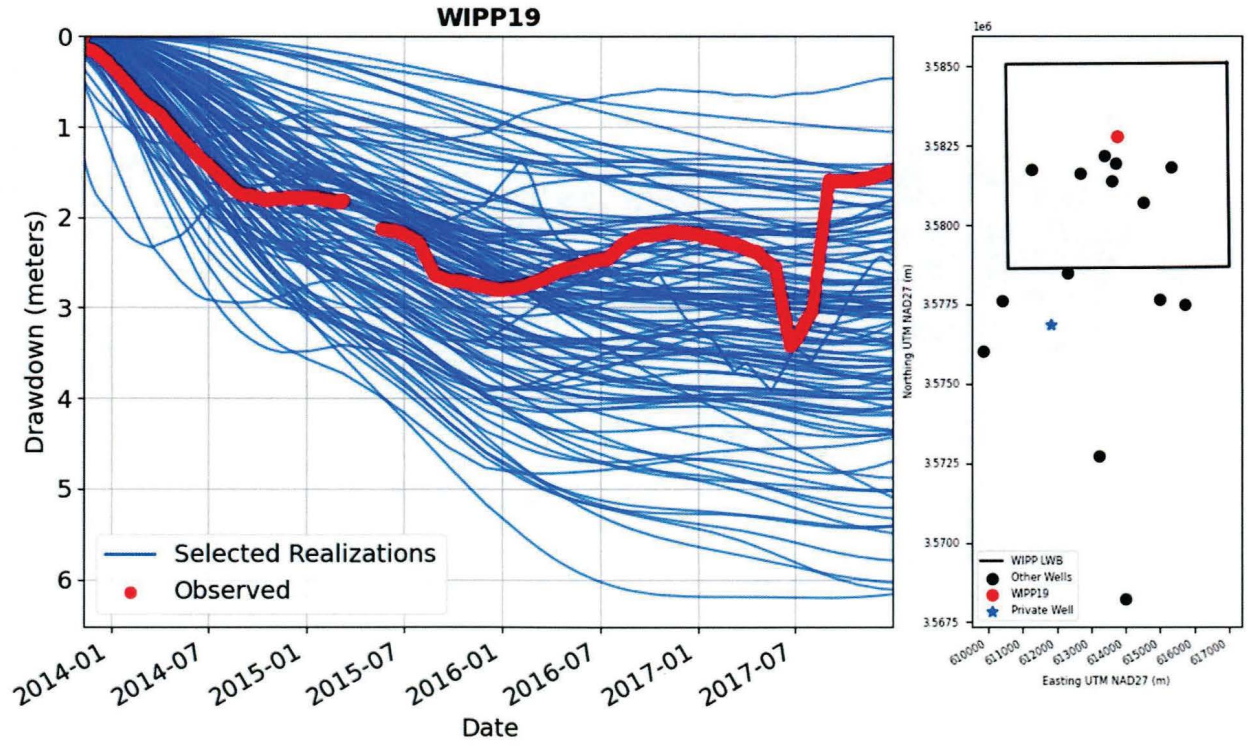

Figure 145. Observed vs Simulated Drawdown at Monitoring Location WIPP-19 during Mills Ranch Pumping for 100 Selected Realizations from Iteration 5

Information Only

7.5 Distribution of Estimated Transmissivity Values with Single-Well Performance Test Data

Figure 146 through **Figure 208** present distribution plots of estimated transmissivity values from single-well formation performance tests (i.e., observed), compared to the transmissivity value estimated for the 100 m × 100 m element the well is located in for each well for 100 selected realizations. The histogram listed as observed shows samples from a lognormal distribution with the mean at the best-estimate of transmissivity from the single-well formation performance test, assuming a standard deviation of ½ log-cycle of transmissivity (m^2/s).

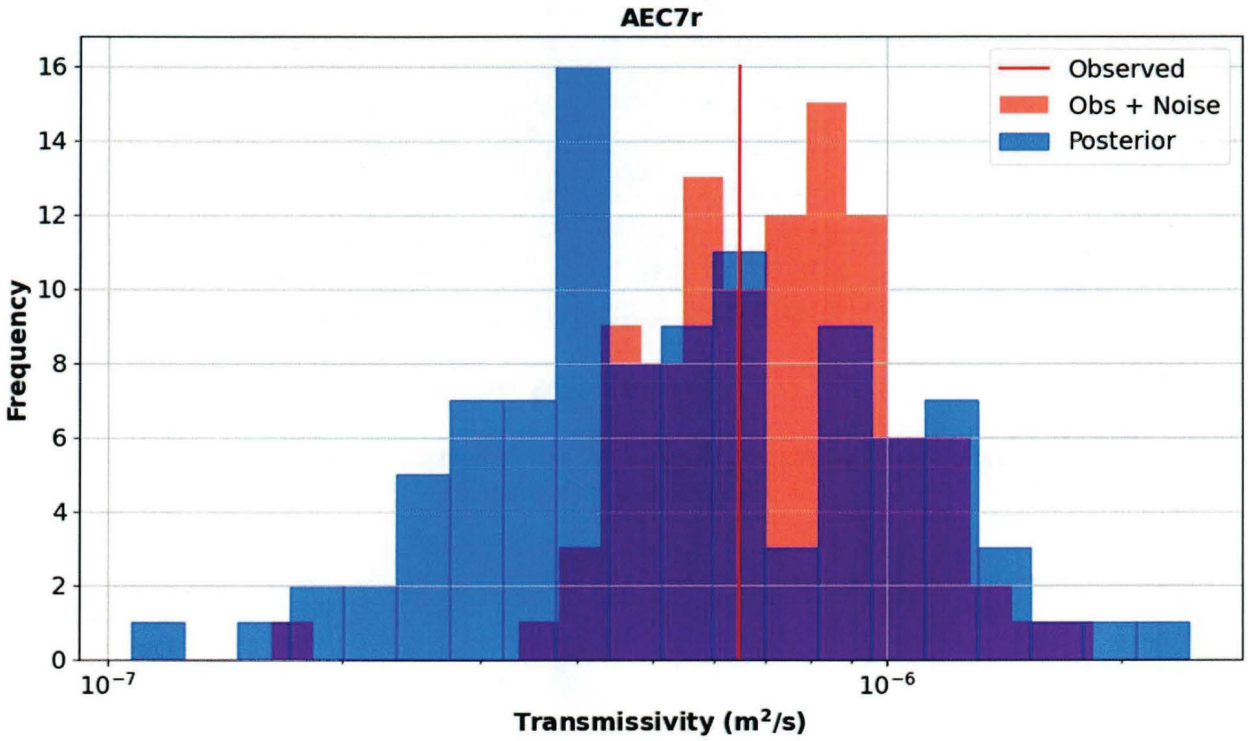

Figure 146. Distribution of Transmissivity Values in Model Element Containing AEC-7R for 100 Selected Realizations from Iteration 5

Information Only

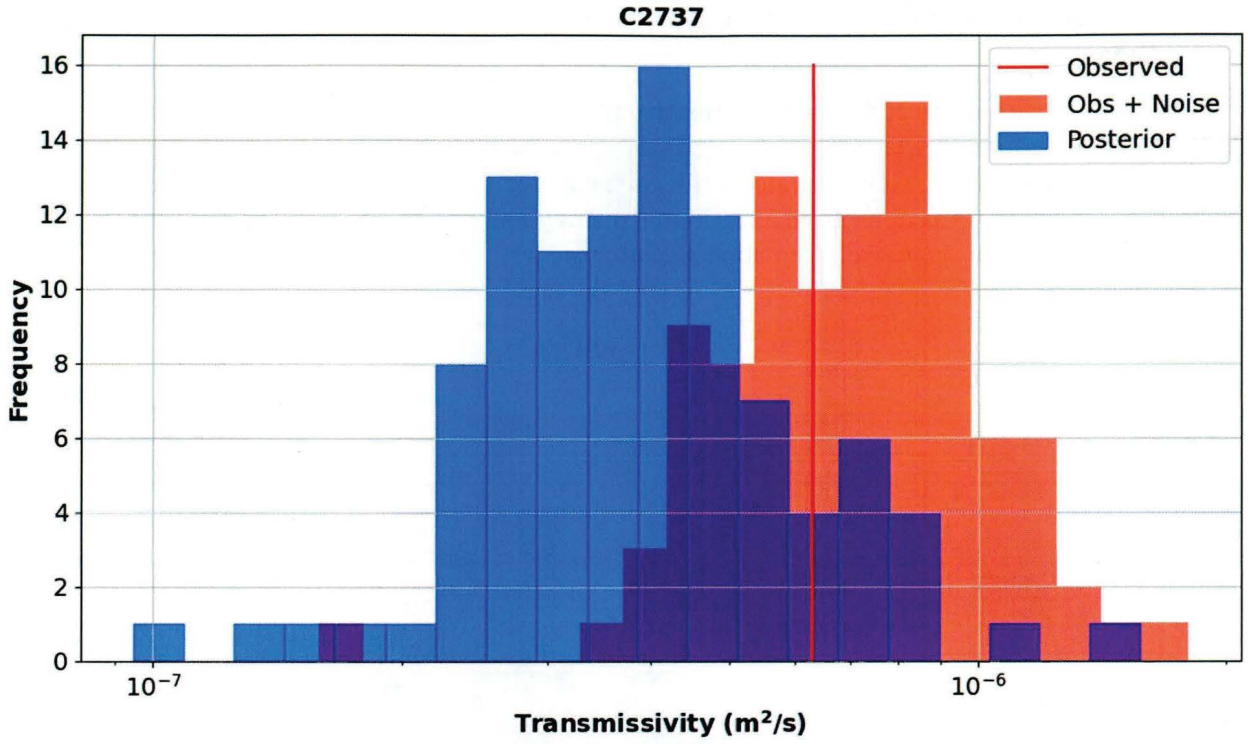

Figure 147. Distribution of Transmissivity Values in Model Element Containing C-2737 for 100 Selected Realizations from Iteration 5

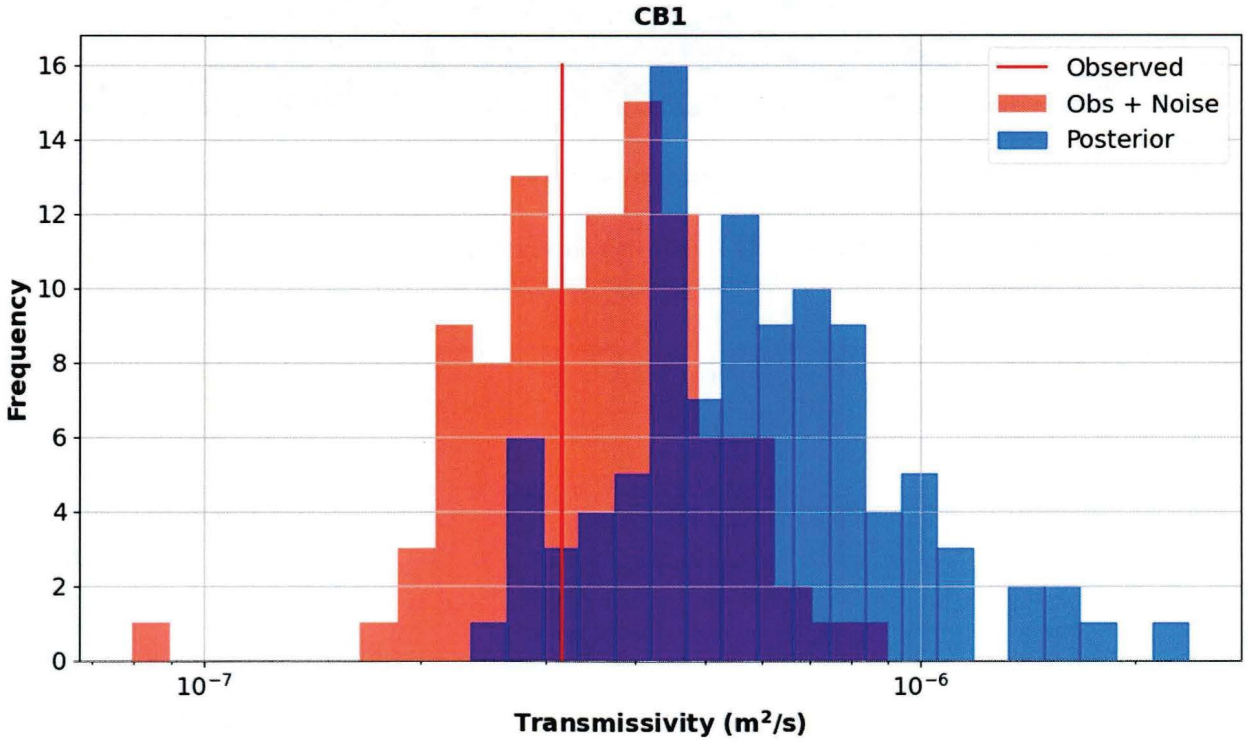

Figure 148. Distribution of Transmissivity Values in Model Element Containing CB-1 for 100 Selected Realizations from Iteration 5

Information Only

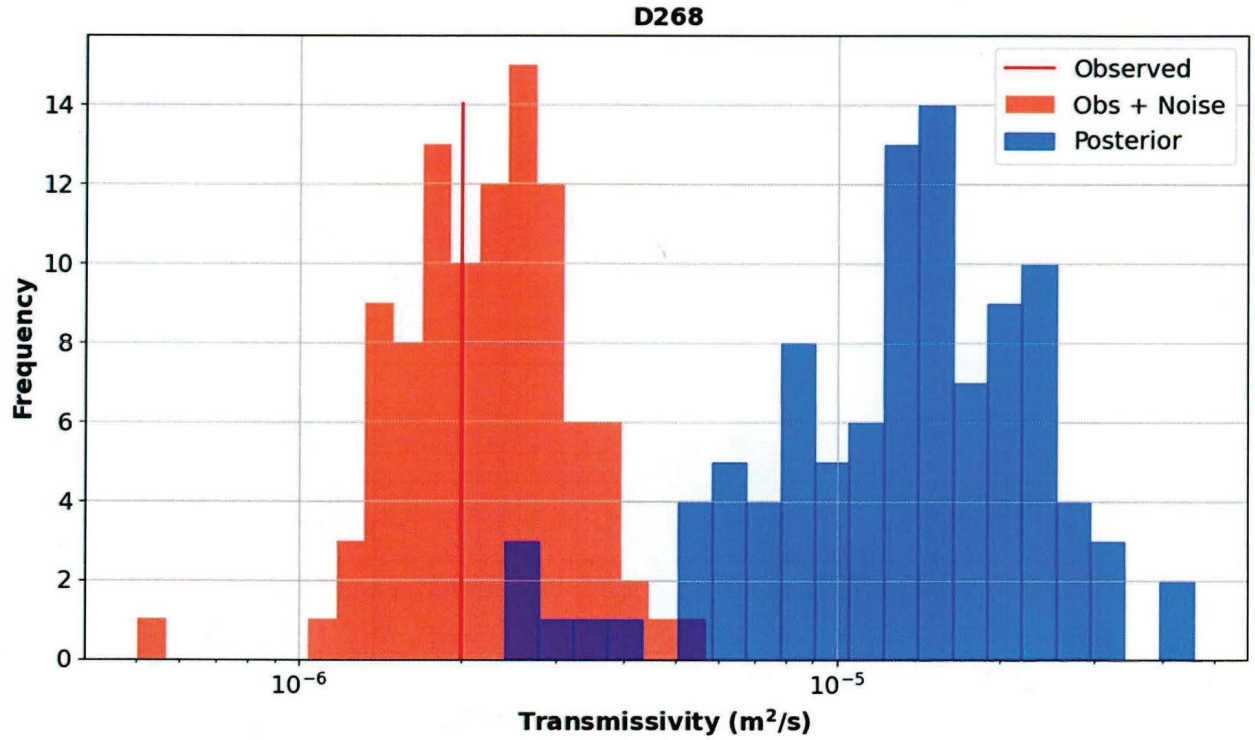

Figure 149. Distribution of Transmissivity Values in Model Element Containing D-268 for 100 Selected Realizations from Iteration 5

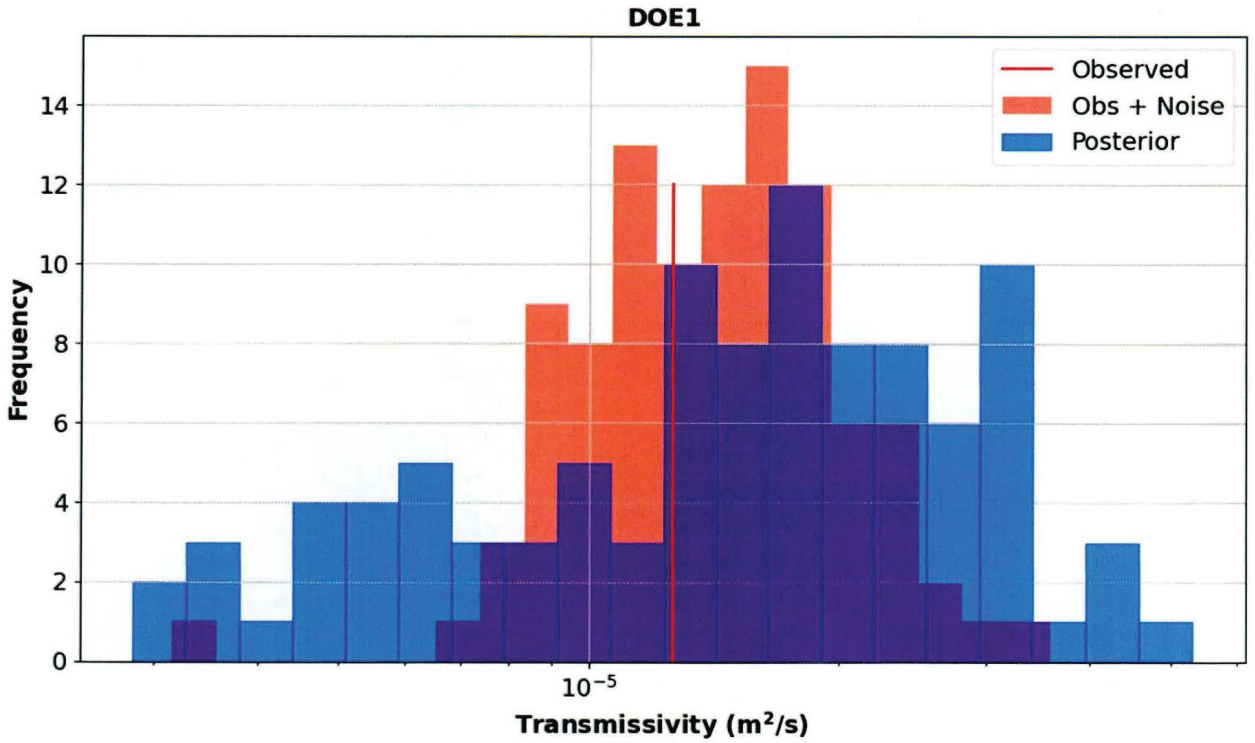

Figure 150. Distribution of Transmissivity Values in Model Element Containing DOE-1 for 100 Selected Realizations from Iteration 5

Information Only

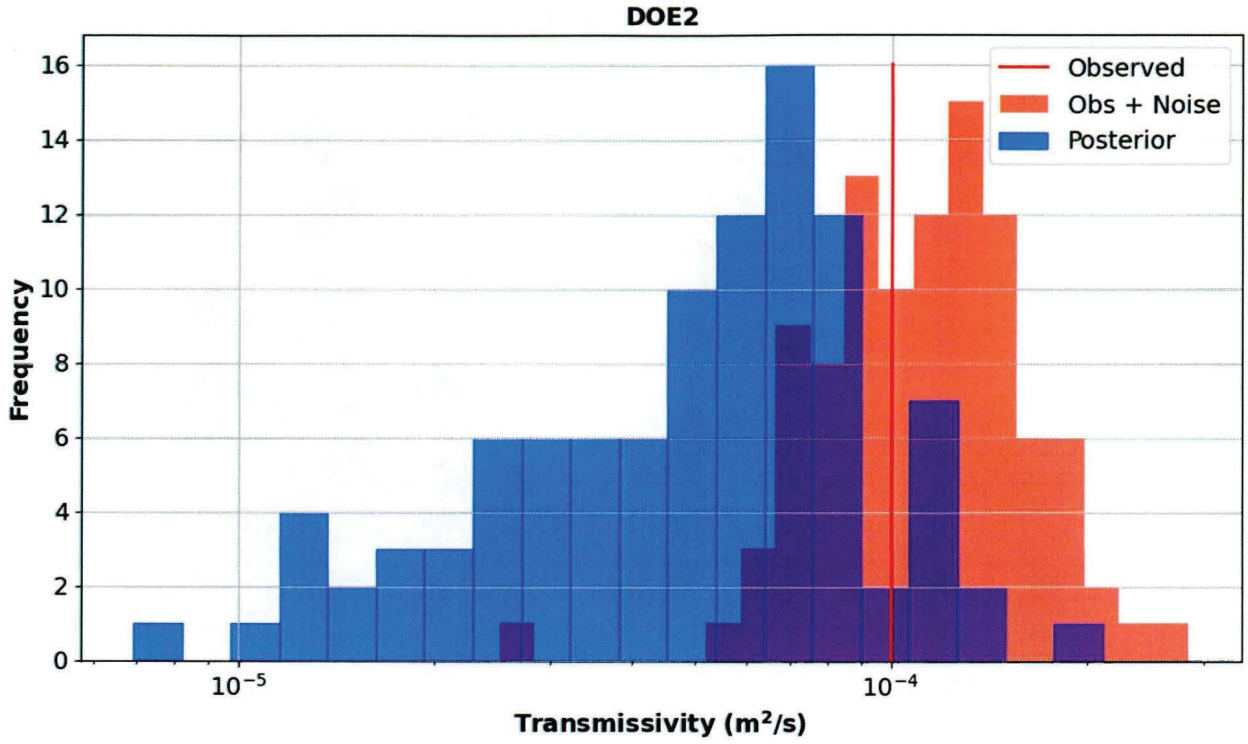

Figure 151. Distribution of Transmissivity Values in Model Element Containing DOE-2 for 100 Selected Realizations from Iteration 5

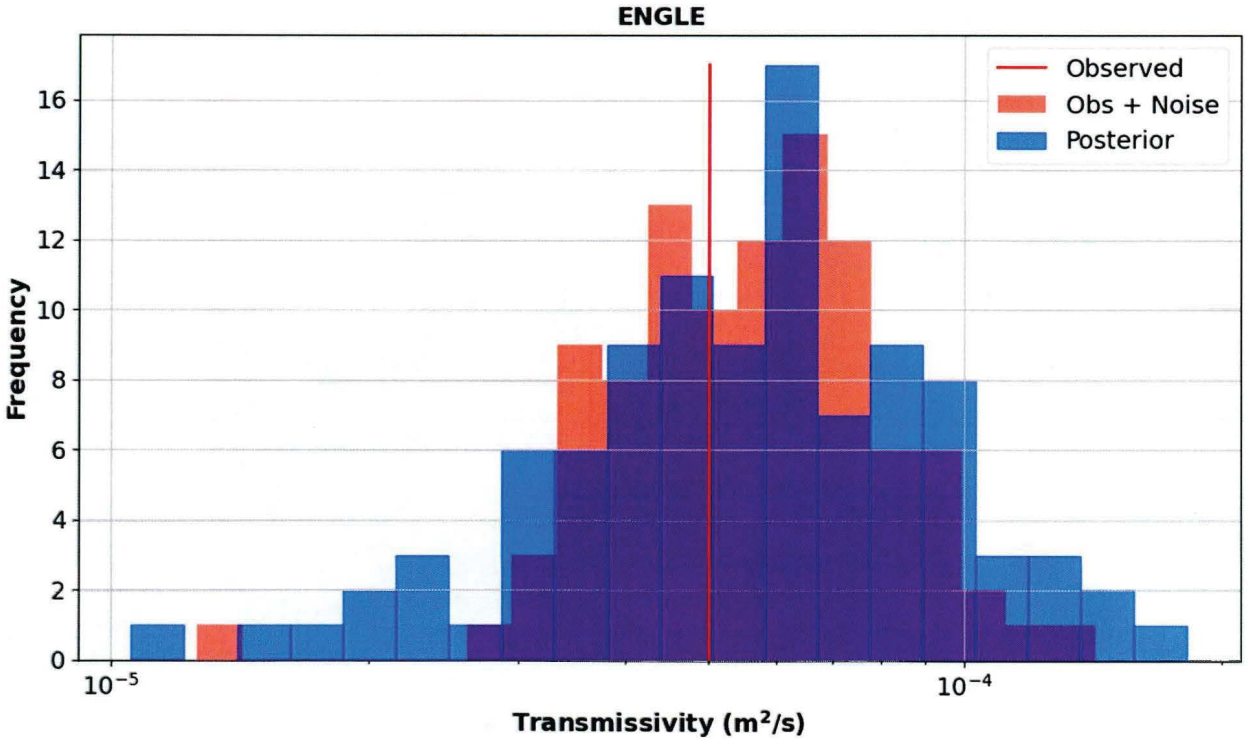

Figure 152. Distribution of Transmissivity Values in Model Element Containing ENGLE Well for 100 Selected Realizations from Iteration 5

Information Only

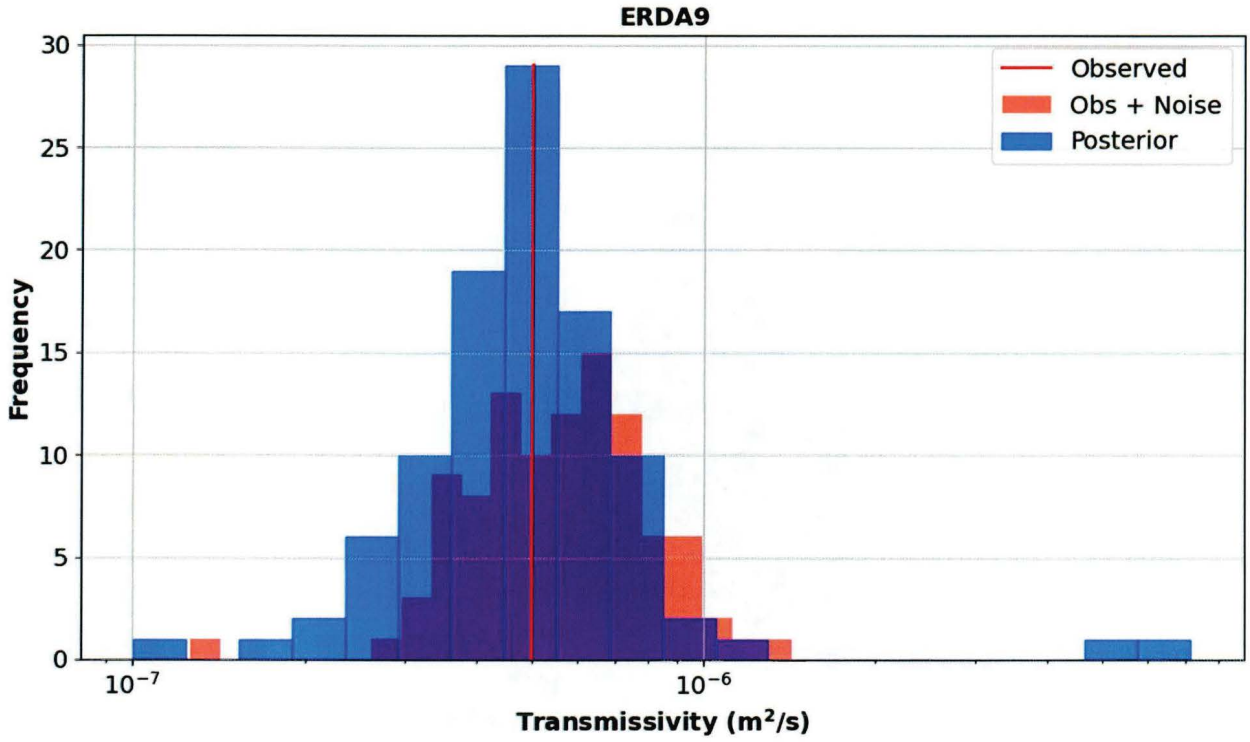

Figure 153. Distribution of Transmissivity Values in Model Element Containing ERDA-9 for 100 Selected Realizations from Iteration 5

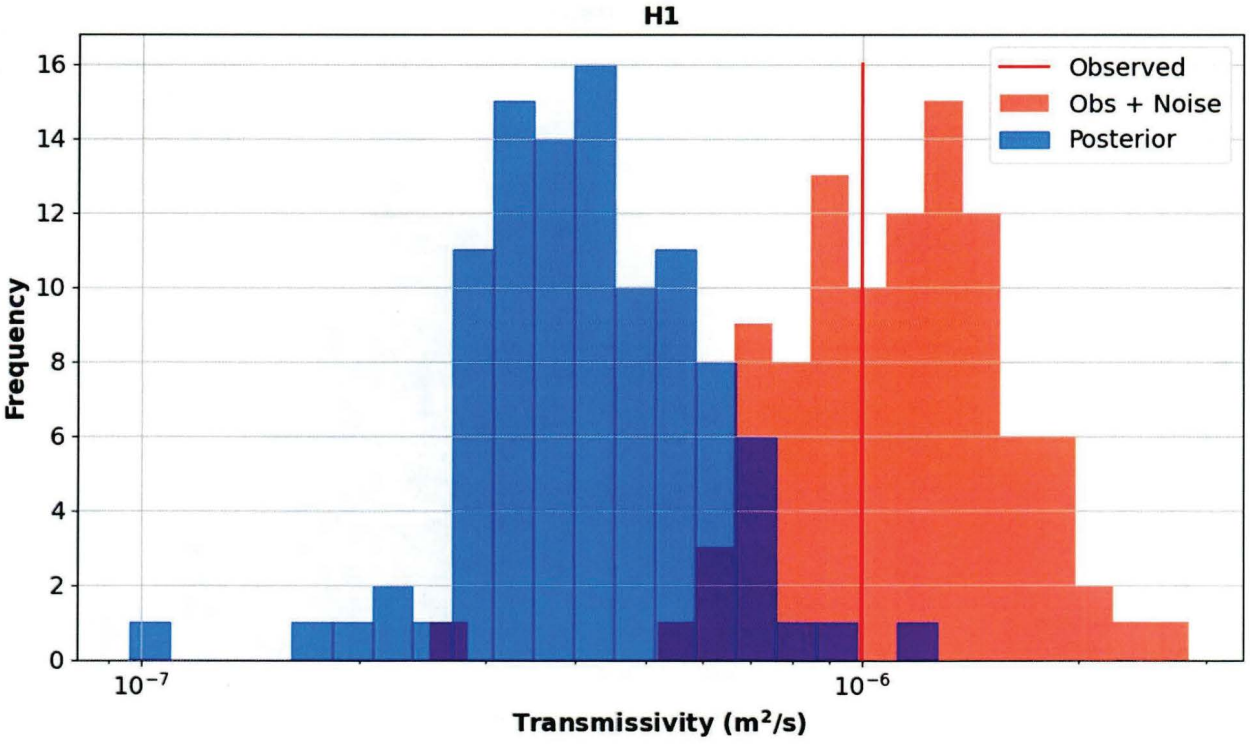

Figure 154. Distribution of Transmissivity Values in Model Element Containing H-1 for 100 Selected Realizations from Iteration 5

Information Only

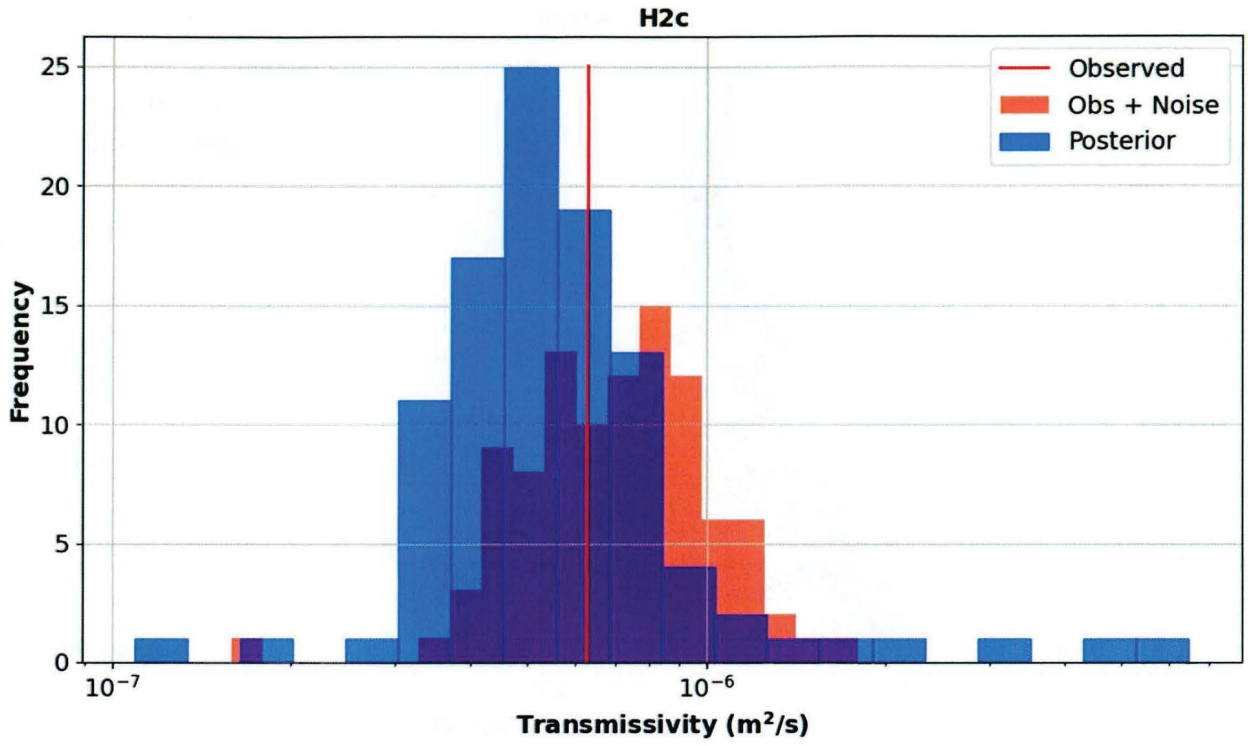

Figure 155. Distribution of Transmissivity Values in Model Element Containing H-2c for 100 Selected Realizations from Iteration 5

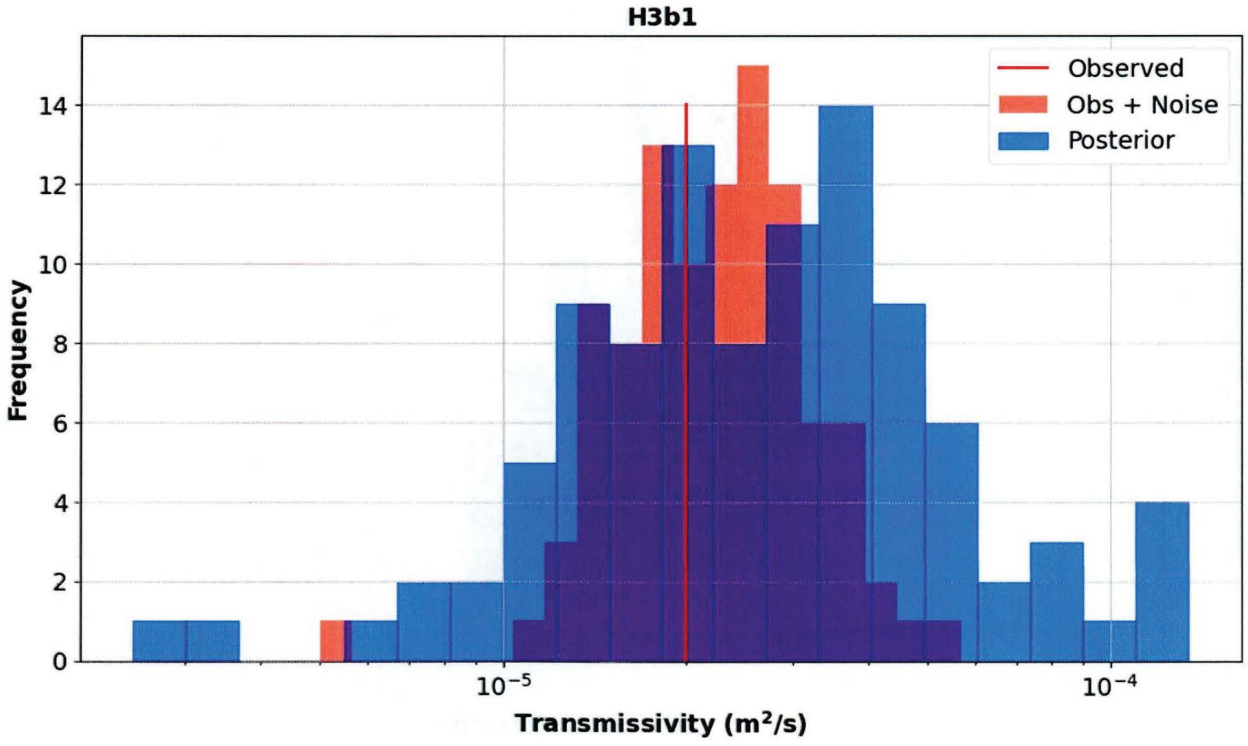

Figure 156. Distribution of Transmissivity Values in Model Element Containing H-3b1 for 100 Selected Realizations from Iteration 5

Information Only

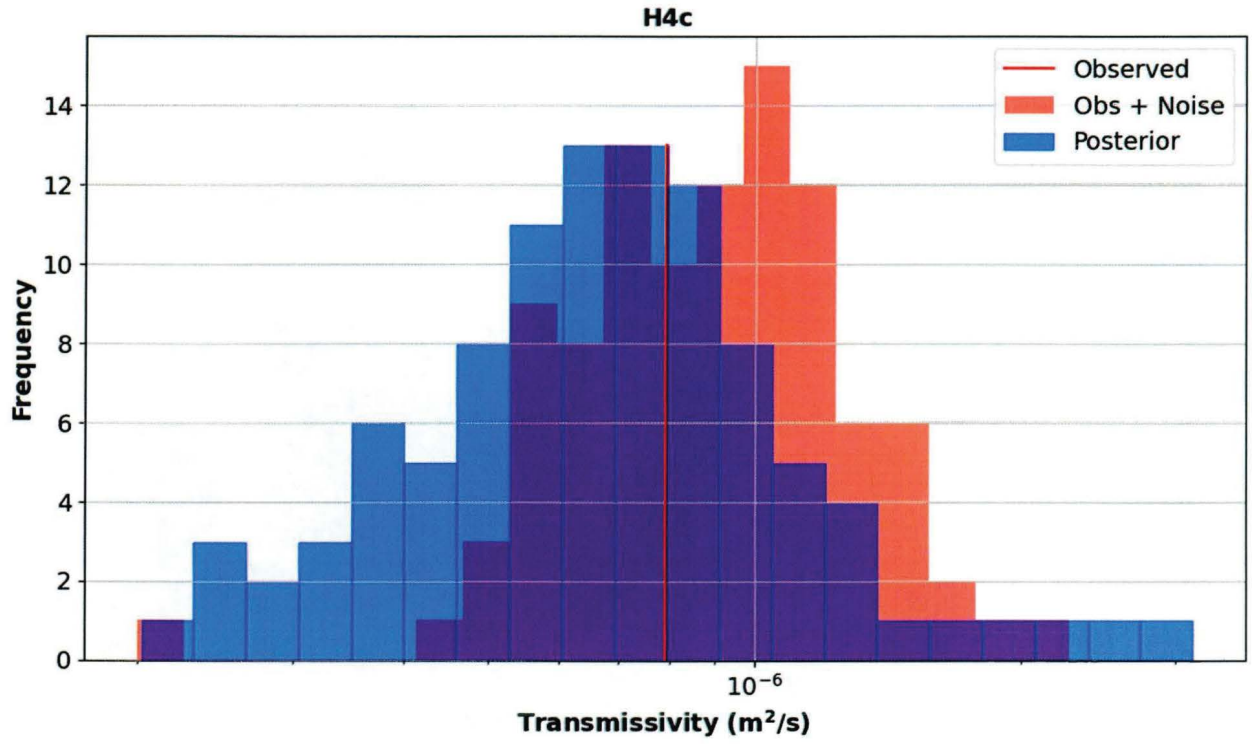

Figure 157. Distribution of Transmissivity Values in Model Element Containing H-4c for 100 Selected Realizations from Iteration 5

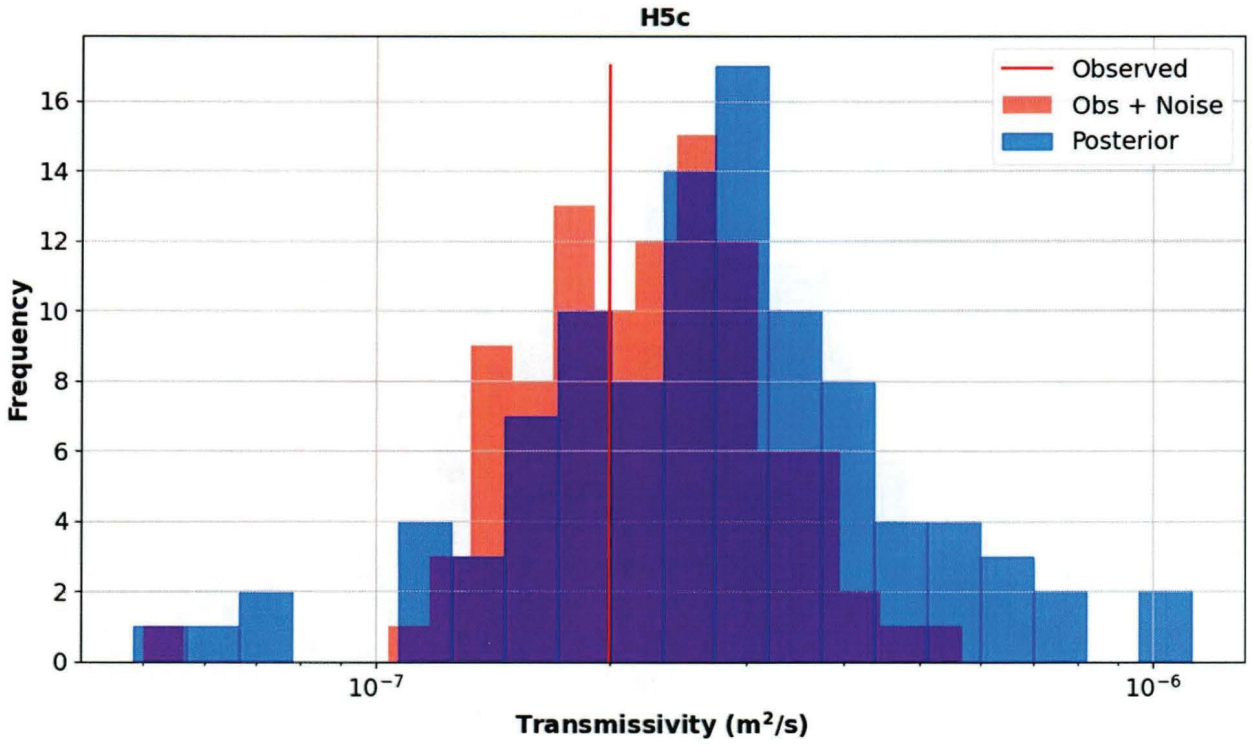

Figure 158. Distribution of Transmissivity Values in Model Element Containing H-5c for 100 Selected Realizations from Iteration 5

Information Only

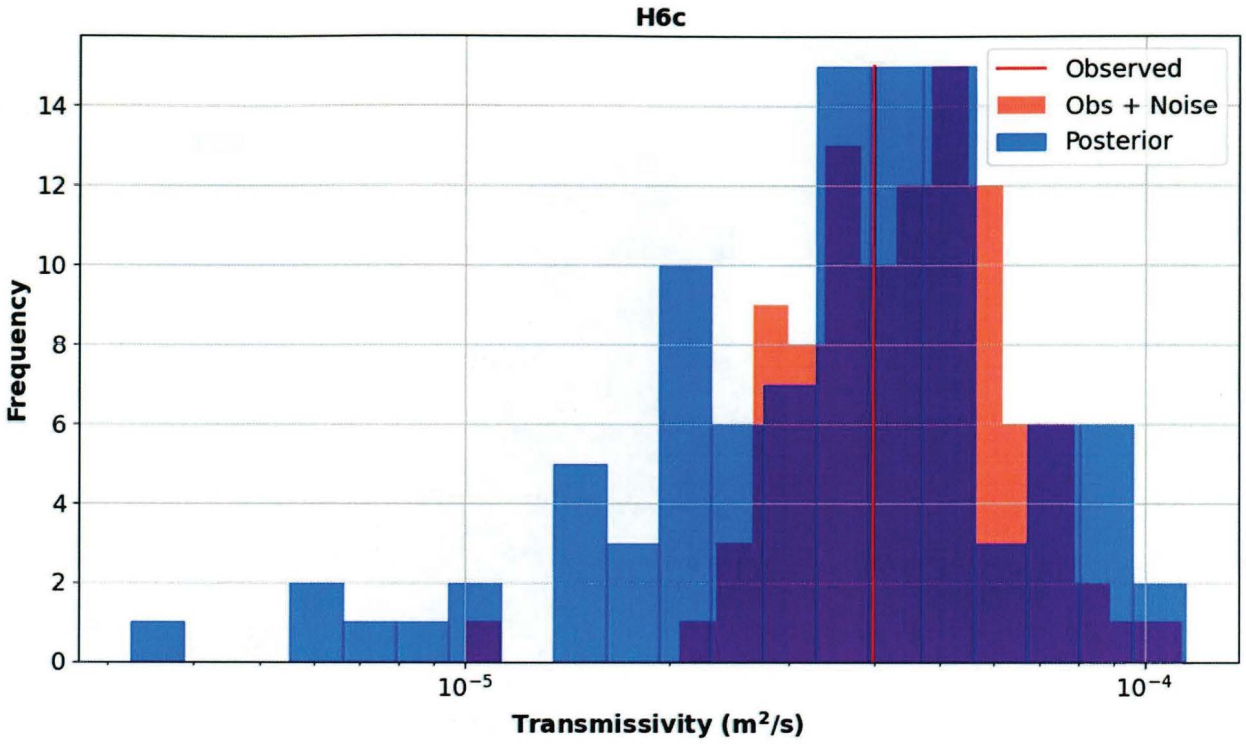

Figure 159. Distribution of Transmissivity Values in Model Element Containing H-6c for 100 Selected Realizations from Iteration 5

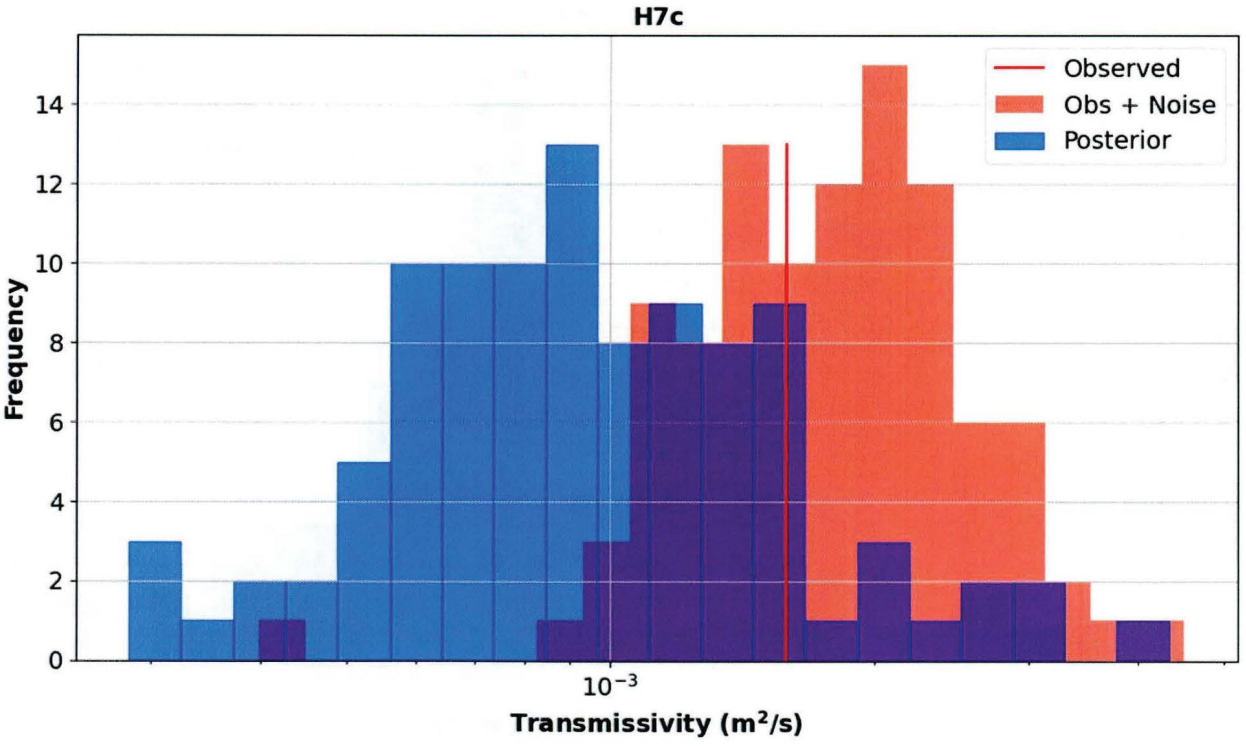

Figure 160. Distribution of Transmissivity Values in Model Element Containing H-7c for 100 Selected Realizations from Iteration 5

Information Only

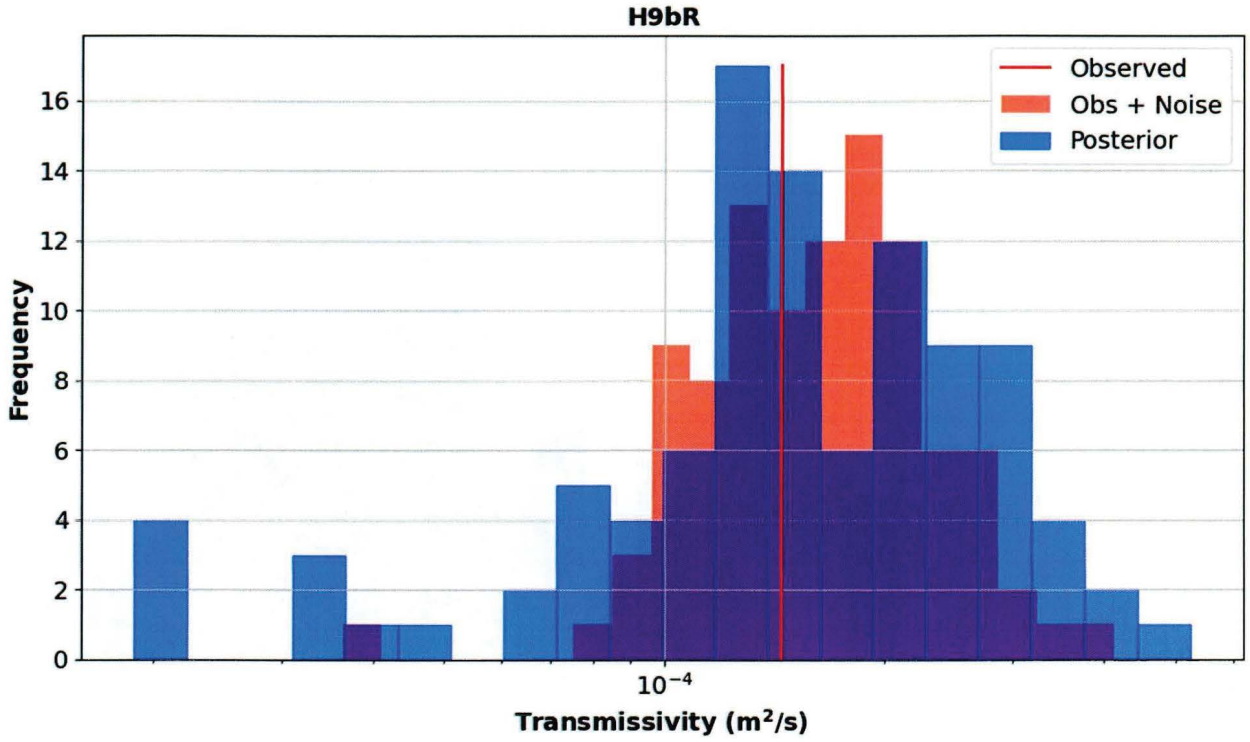

Figure 161. Distribution of Transmissivity Values in Model Element Containing H-9bR for 100 Selected Realizations from Iteration 5

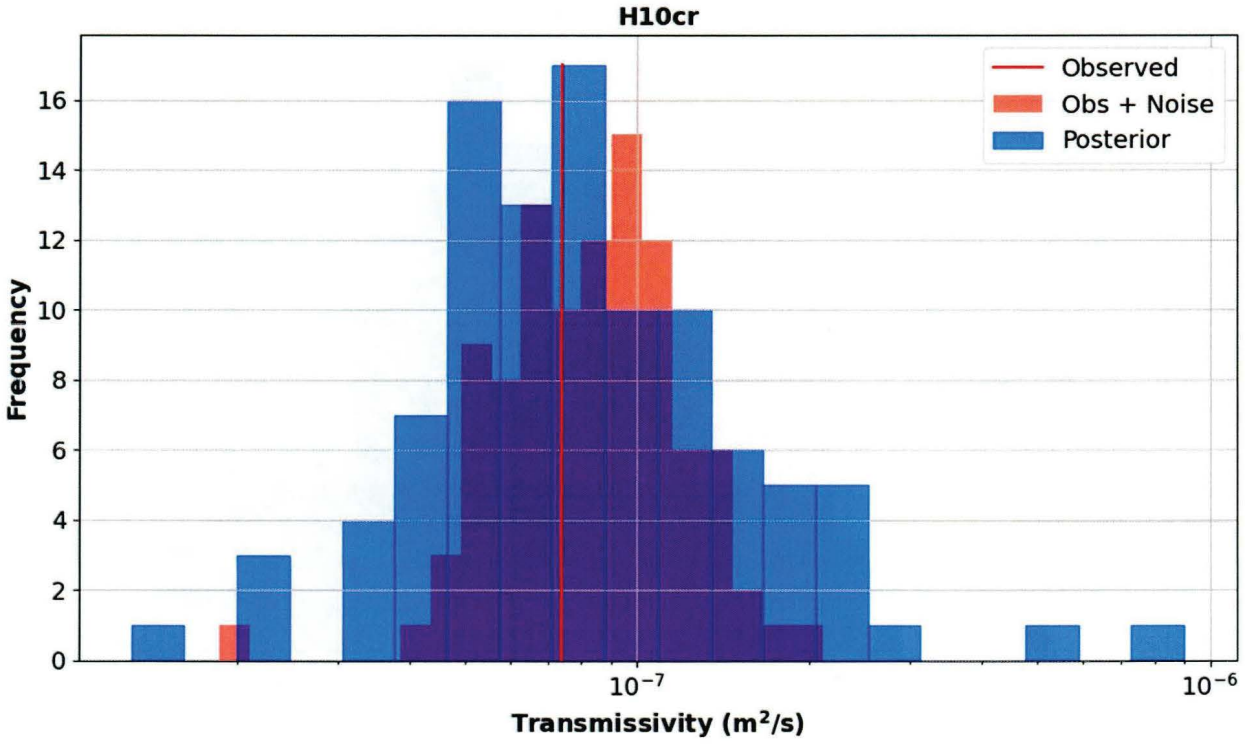

Figure 162. Distribution of Transmissivity Values in Model Element Containing H-10cR for 100 Selected Realizations from Iteration 5

Information Only

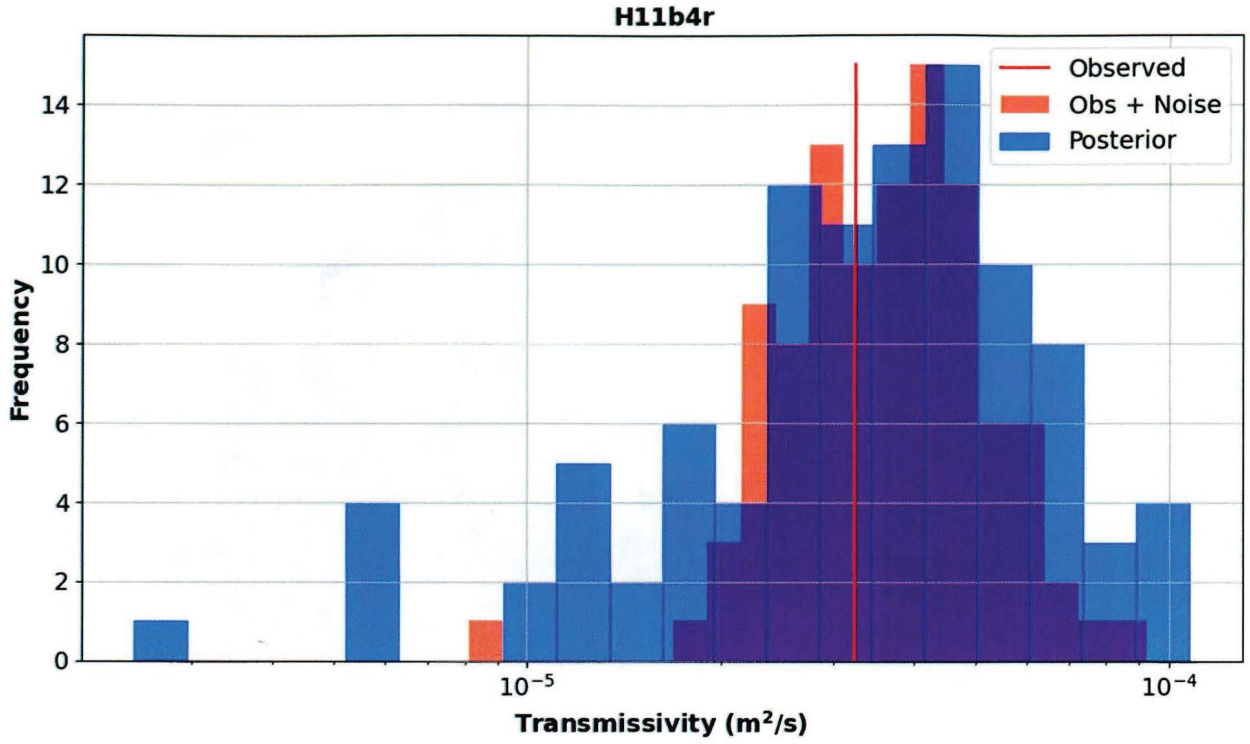

Figure 163. Distribution of Transmissivity Values in Model Element Containing H-11b4R for 100 Selected Realizations from Iteration 5

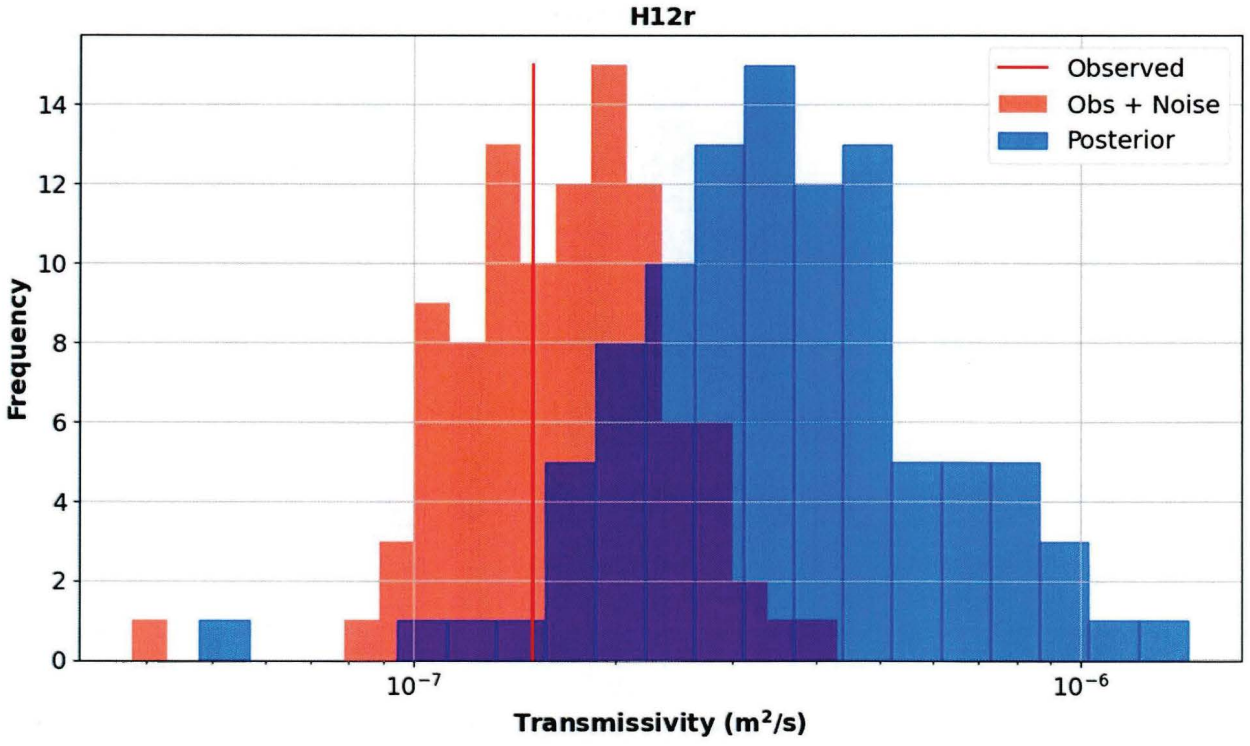

Figure 164. Distribution of Transmissivity Values in Model Element Containing H-12R for 100 Selected Realizations from Iteration 5

Information Only

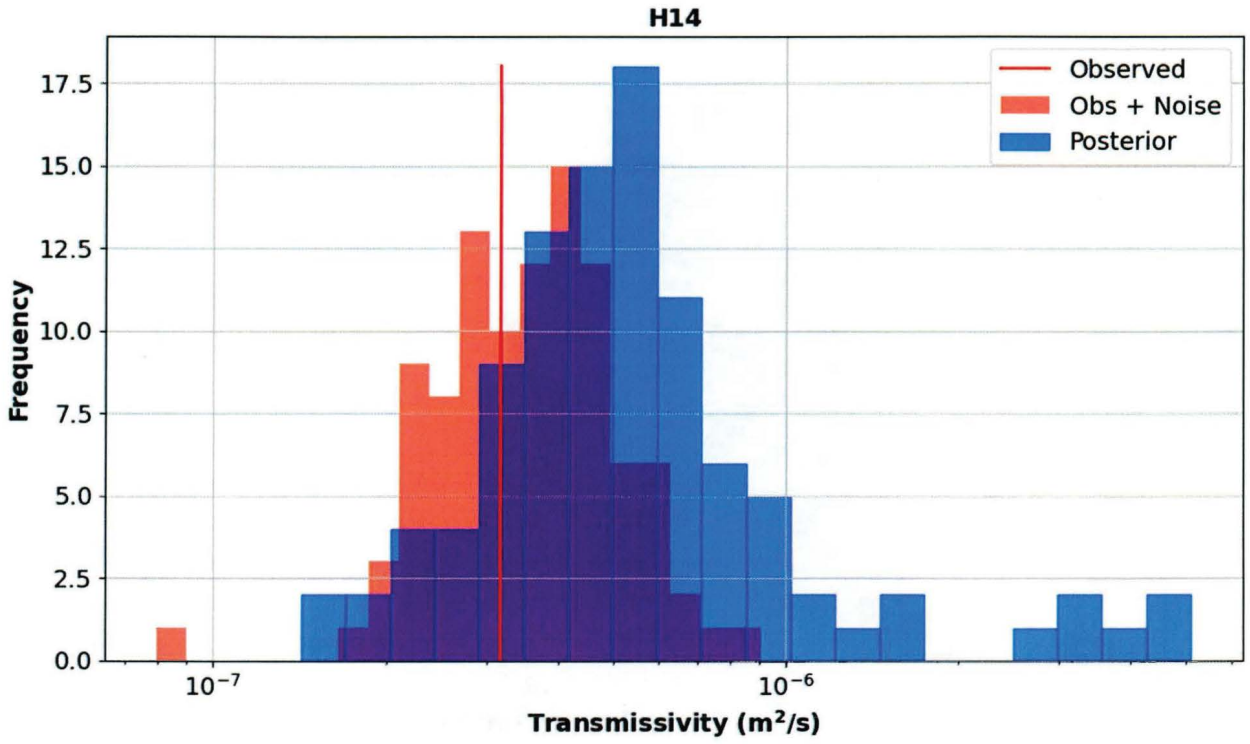

Figure 165. Distribution of Transmissivity Values in Model Element Containing H-14 for 100 Selected Realizations from Iteration 5

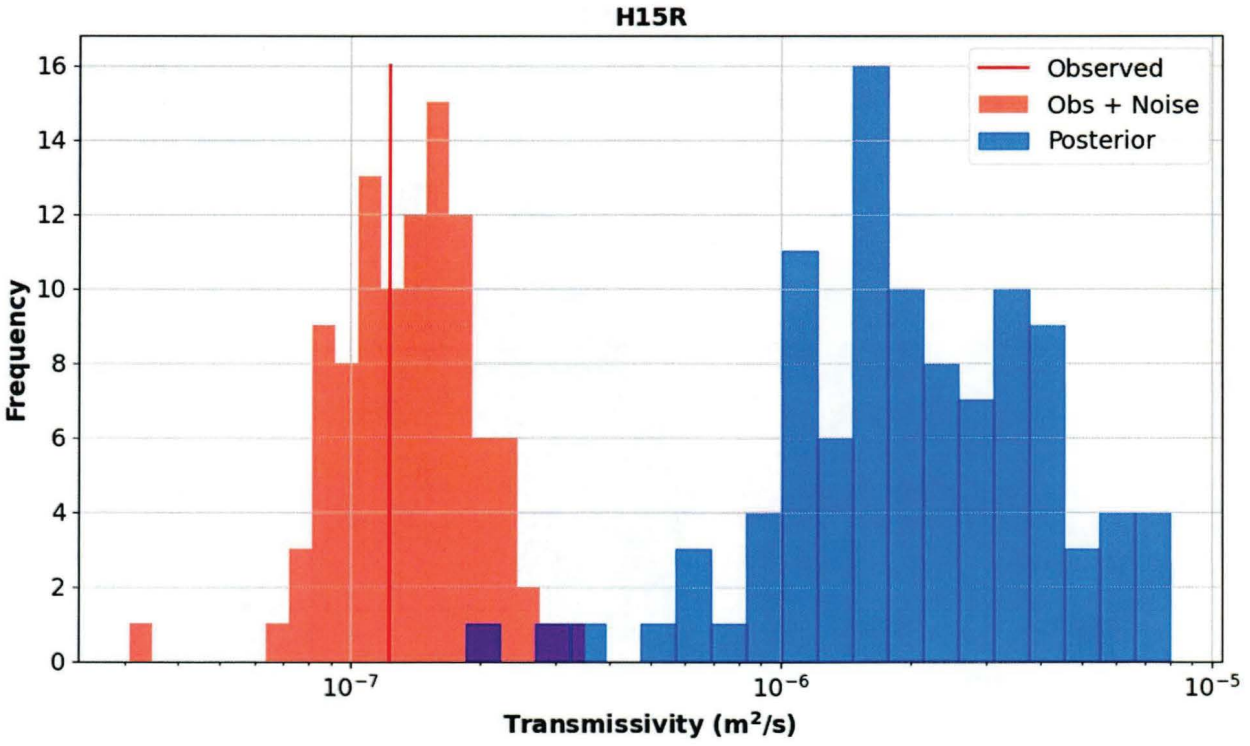

Figure 166. Distribution of Transmissivity Values in Model Element Containing H-15R for 100 Selected Realizations from Iteration 5

Information Only

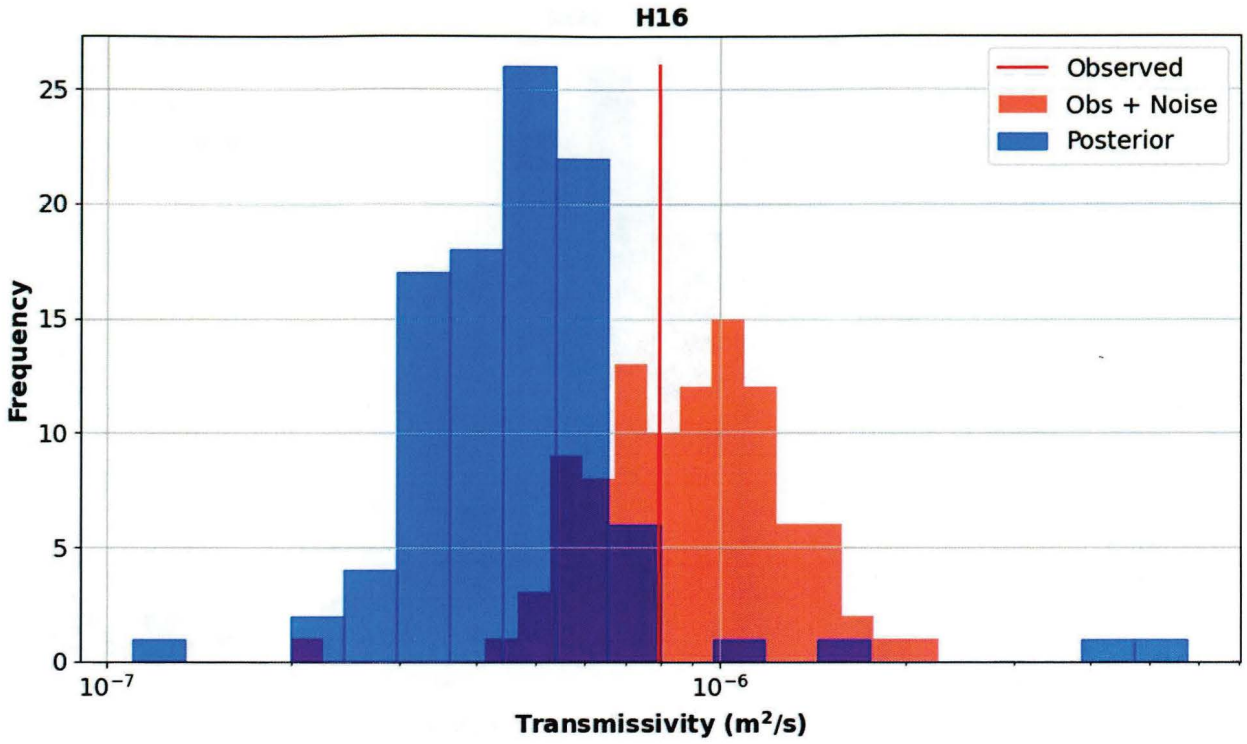

Figure 167. Distribution of Transmissivity Values in Model Element Containing H-16 for 100 Selected Realizations from Iteration 5

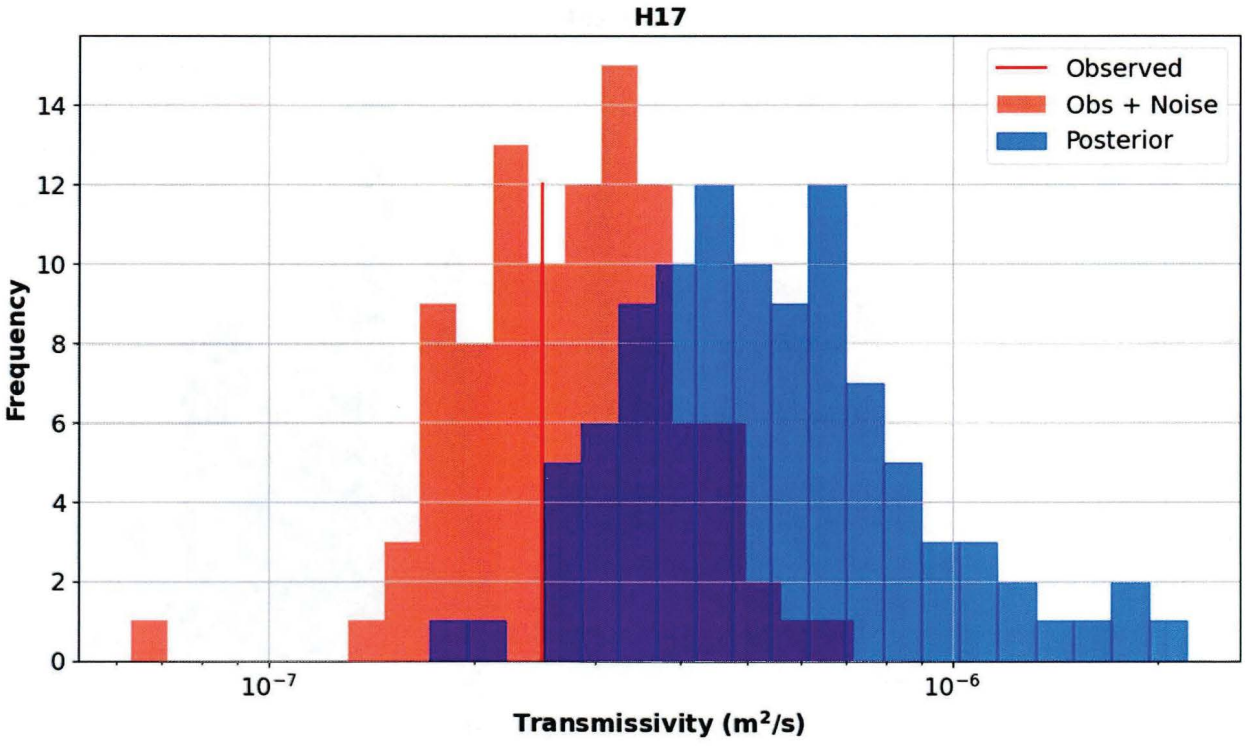

Figure 168. Distribution of Transmissivity Values in Model Element Containing H-17 for 100 Selected Realizations from Iteration 5

Information Only

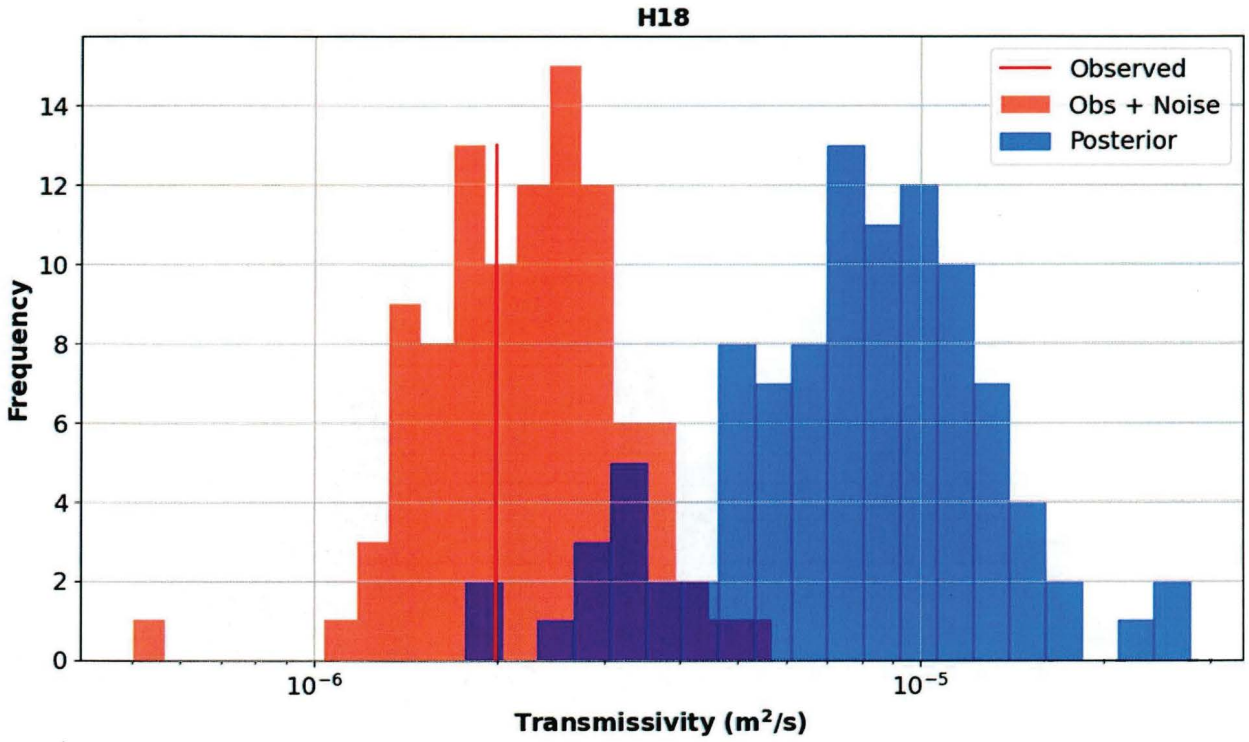

Figure 169. Distribution of Transmissivity Values in Model Element Containing H-18 for 100 Selected Realizations from Iteration 5

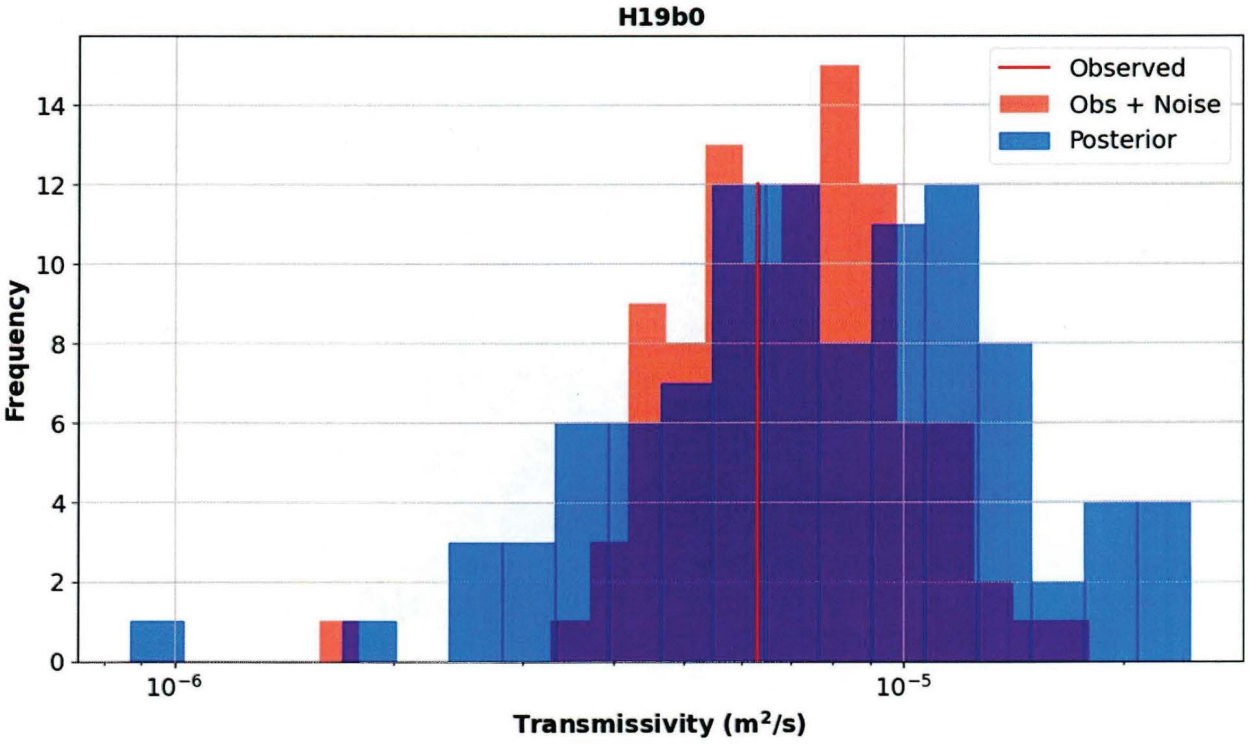

Figure 170. Distribution of Transmissivity Values in Model Element Containing H-19b0 for 100 Selected Realizations from Iteration 5

Information Only

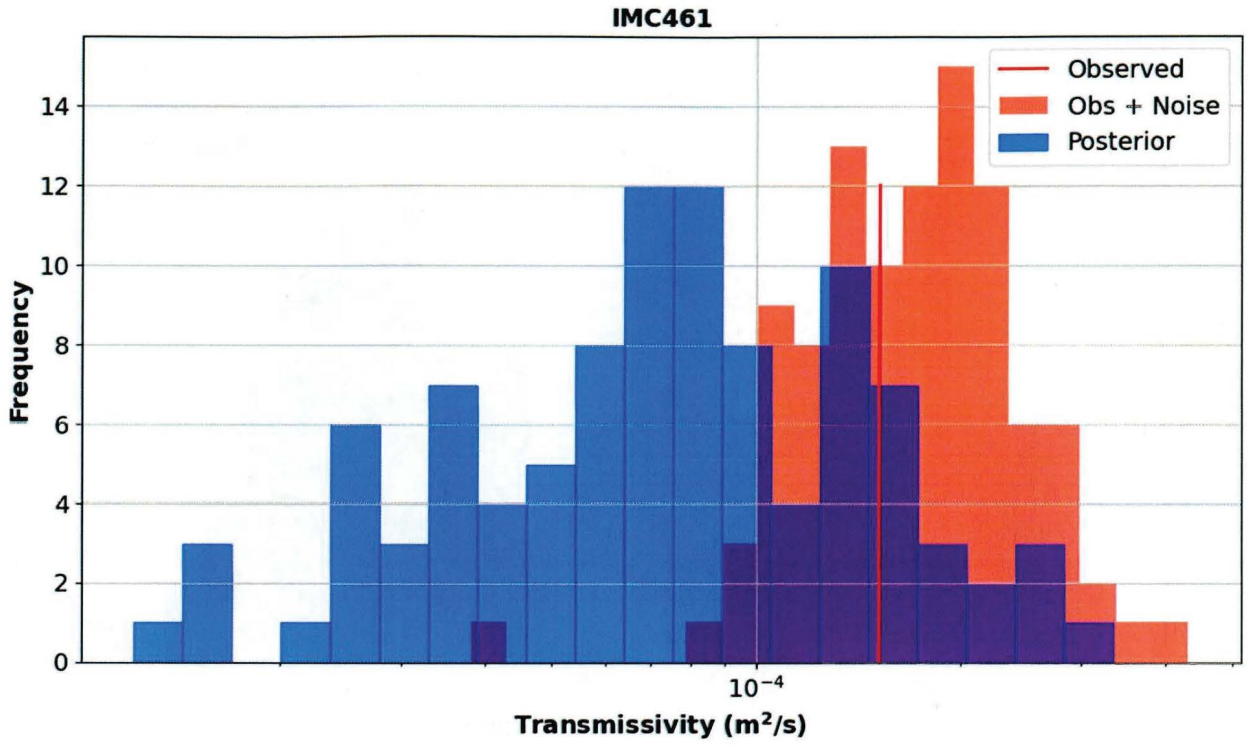

Figure 171. Distribution of Transmissivity Values in Model Element Containing IMC-461 for 100 Selected Realizations from Iteration 5

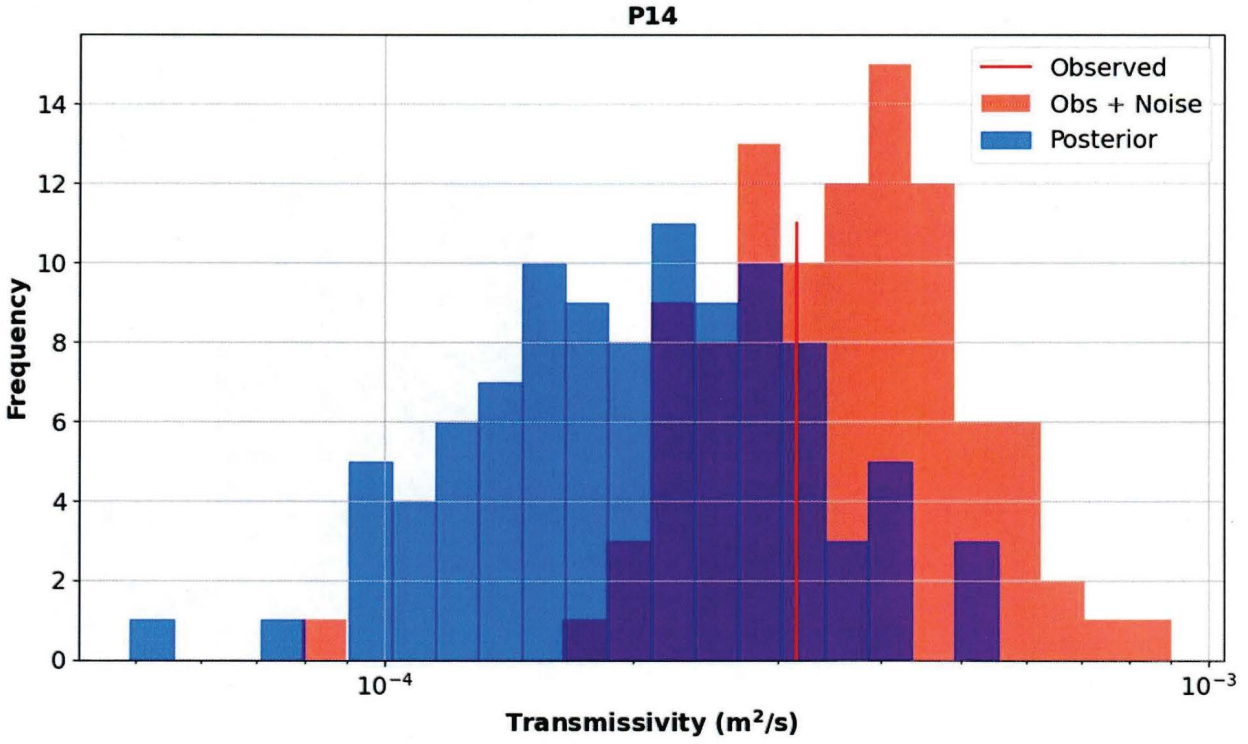

Figure 172. Distribution of Transmissivity Values in Model Element Containing P-14 for 100 Selected Realizations from Iteration 5

Information Only

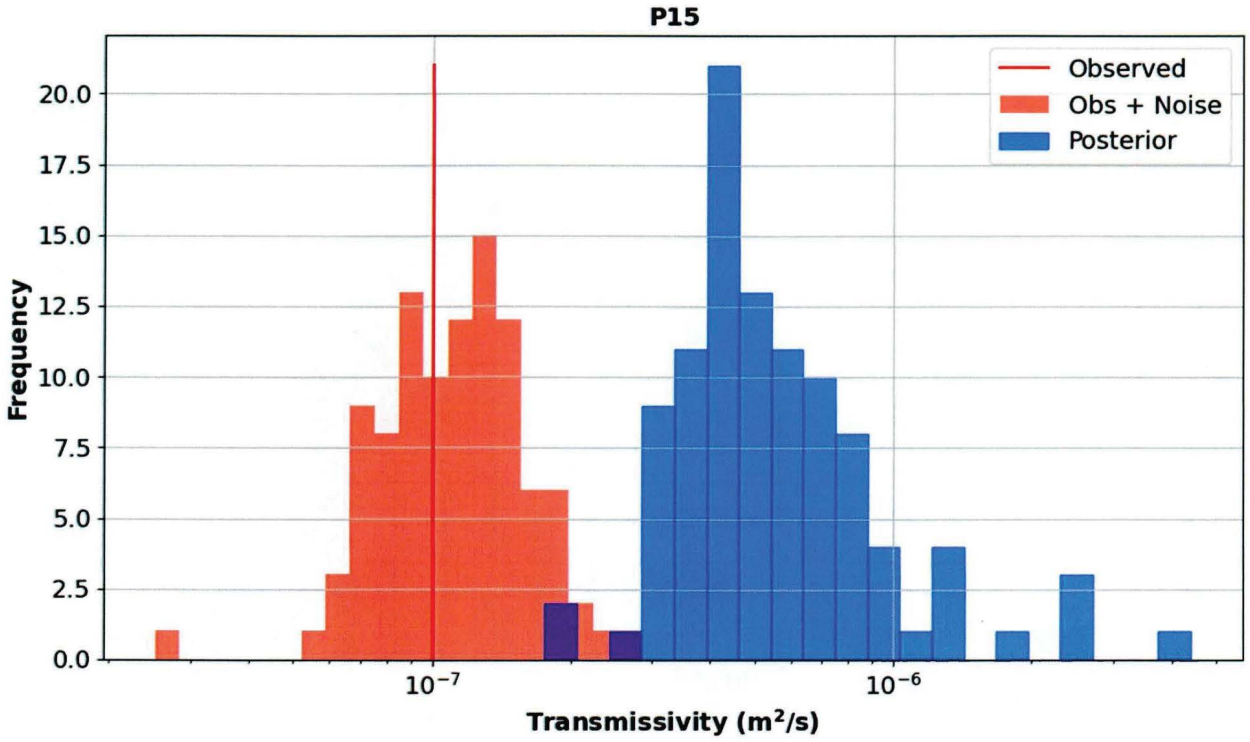

Figure 173. Distribution of Transmissivity Values in Model Element Containing P-15 for 100 Selected Realizations from Iteration 5

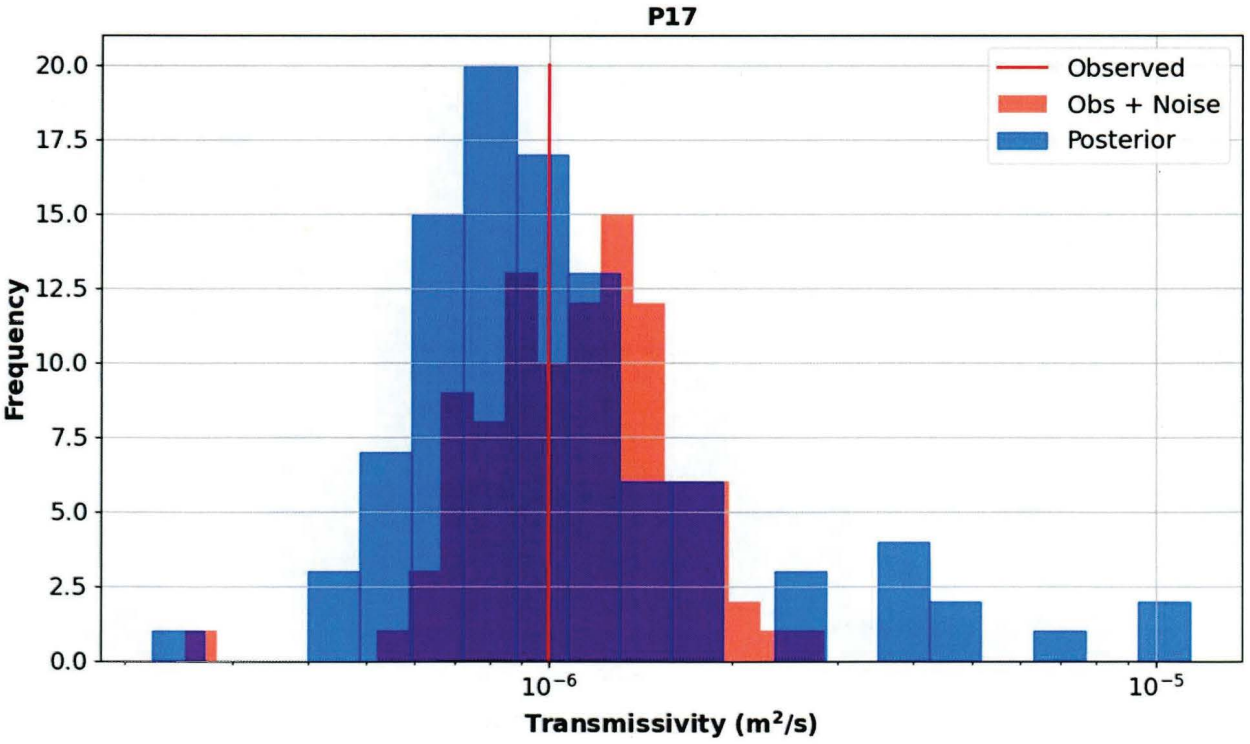

Figure 174. Distribution of Transmissivity Values in Model Element Containing P-17 for 100 Selected Realizations from Iteration 5

Information Only

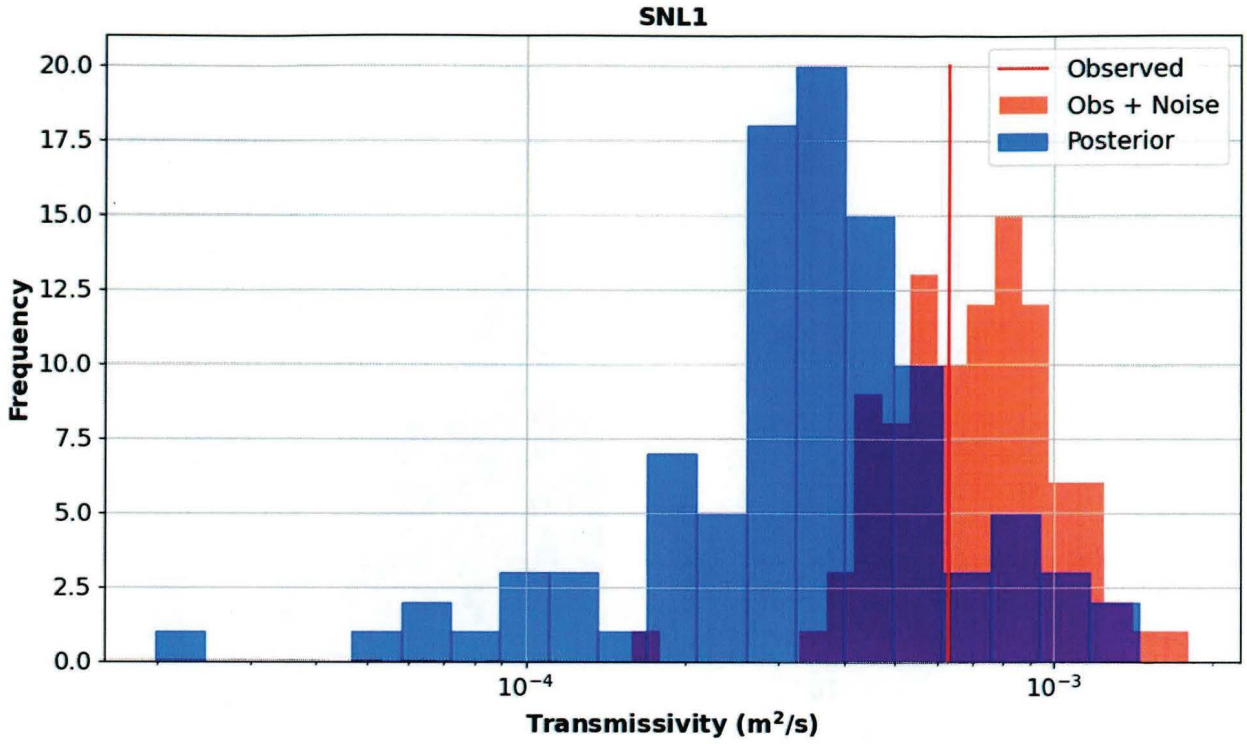

Figure 175. Distribution of Transmissivity Values in Model Element Containing SNL-1 for 100 Selected Realizations from Iteration 5

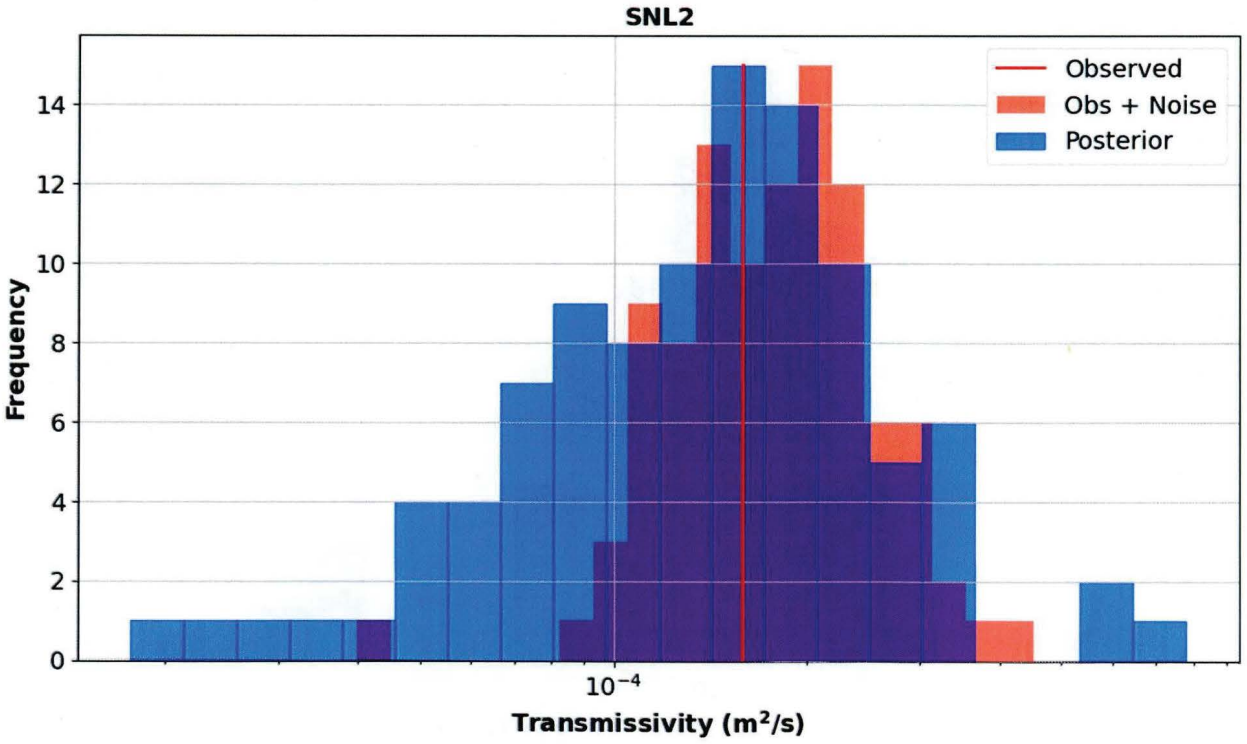

Figure 176. Distribution of Transmissivity Values in Model Element Containing SNL-2 for 100 Selected Realizations from Iteration 5

Information Only

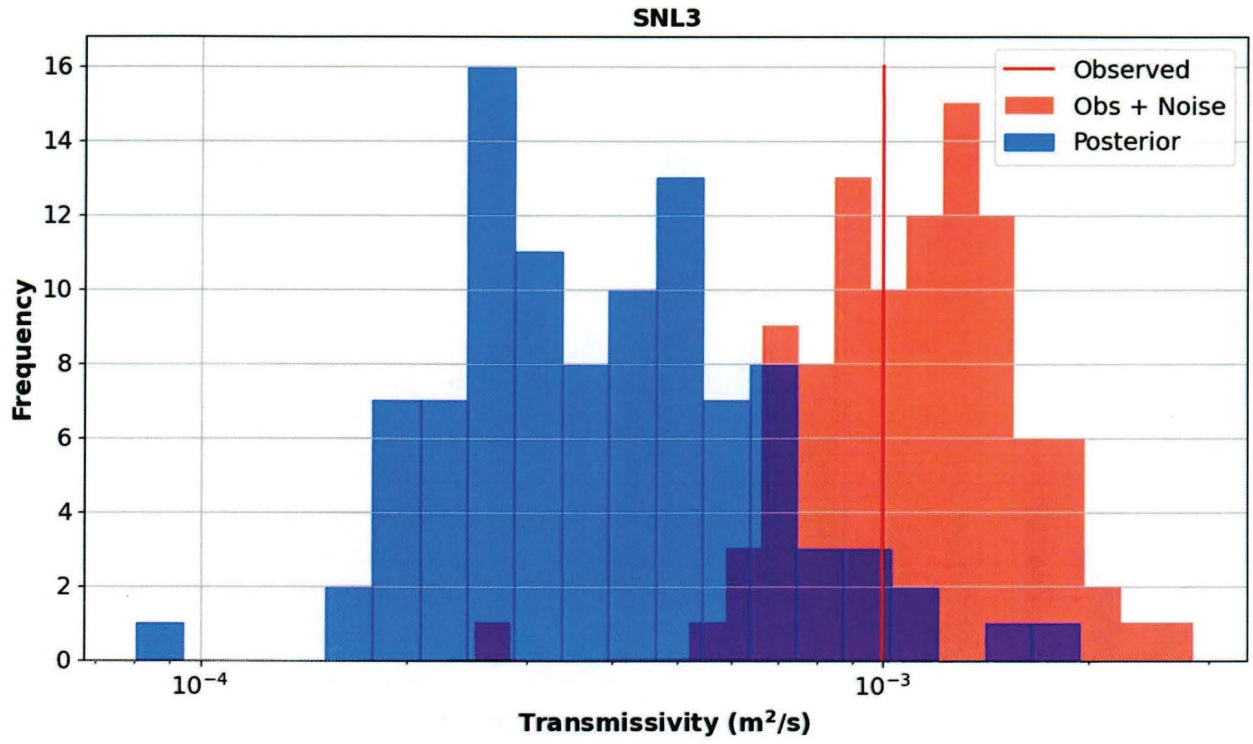

Figure 177. Distribution of Transmissivity Values in Model Element Containing SNL-3 for 100 Selected Realizations from Iteration 5

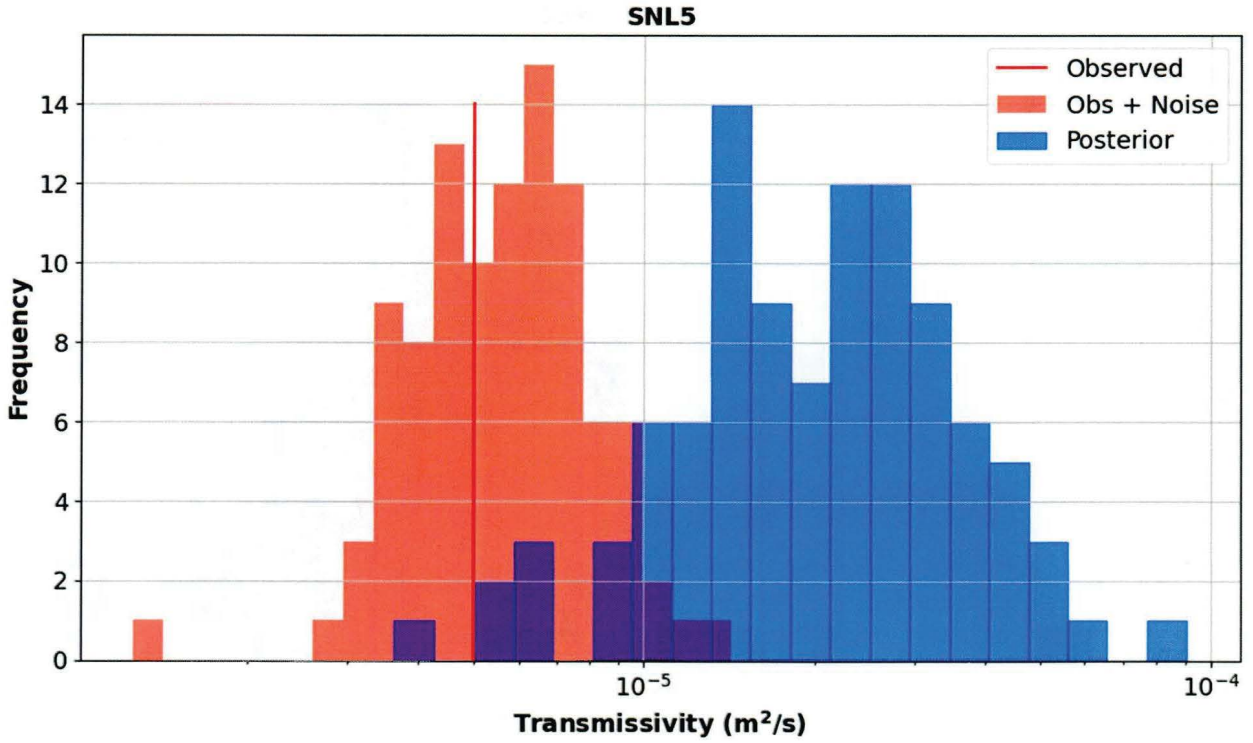

Figure 178. Distribution of Transmissivity Values in Model Element Containing SNL-5 for 100 Selected Realizations from Iteration 5

Information Only

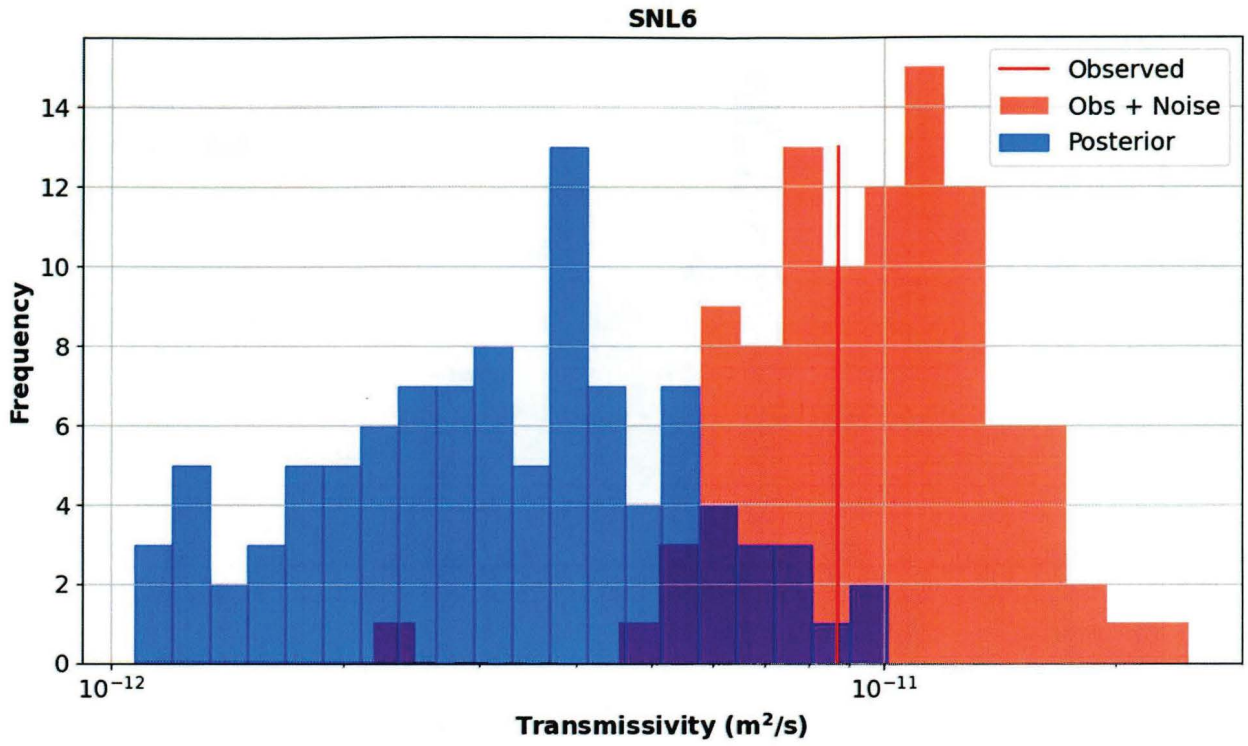

Figure 179. Distribution of Transmissivity Values in Model Element Containing SNL-6 for 100 Selected Realizations from Iteration 5

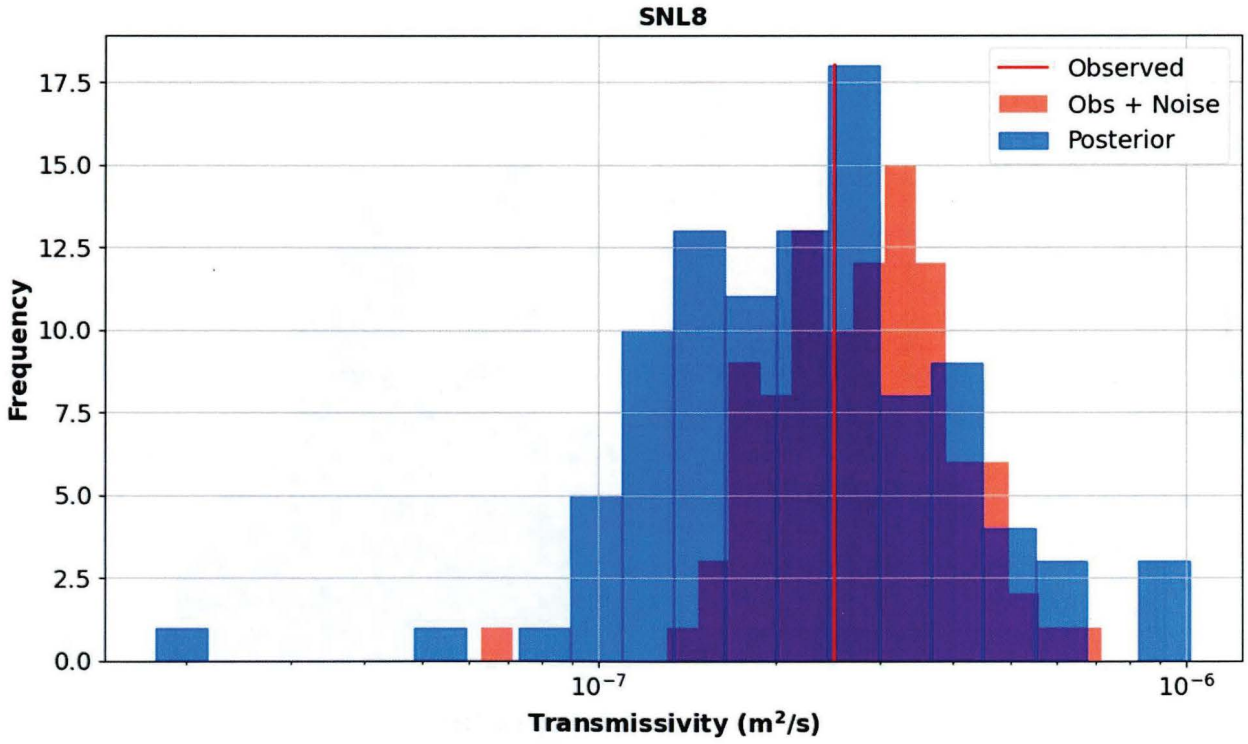

Figure 180. Distribution of Transmissivity Values in Model Element Containing SNL-8 for 100 Selected Realizations from Iteration 5

Information Only

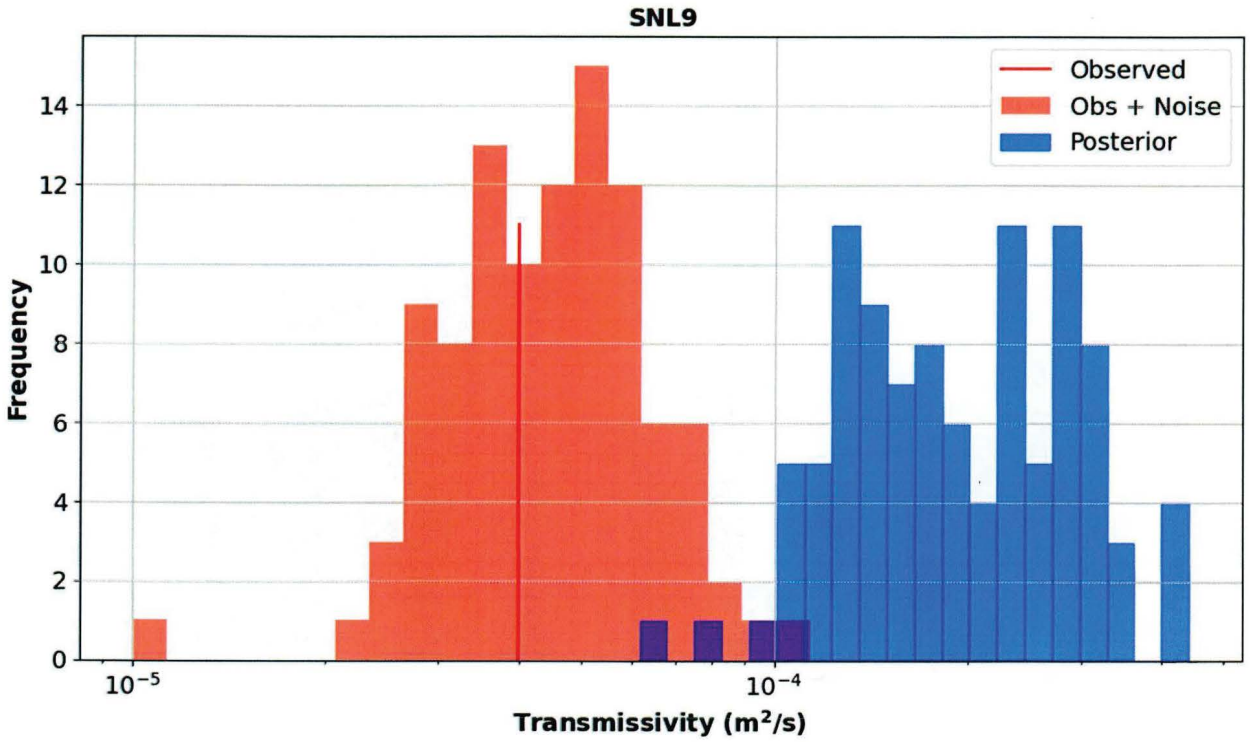

Figure 181. Distribution of Transmissivity Values in Model Element Containing SNL-9 for 100 Selected Realizations from Iteration 5

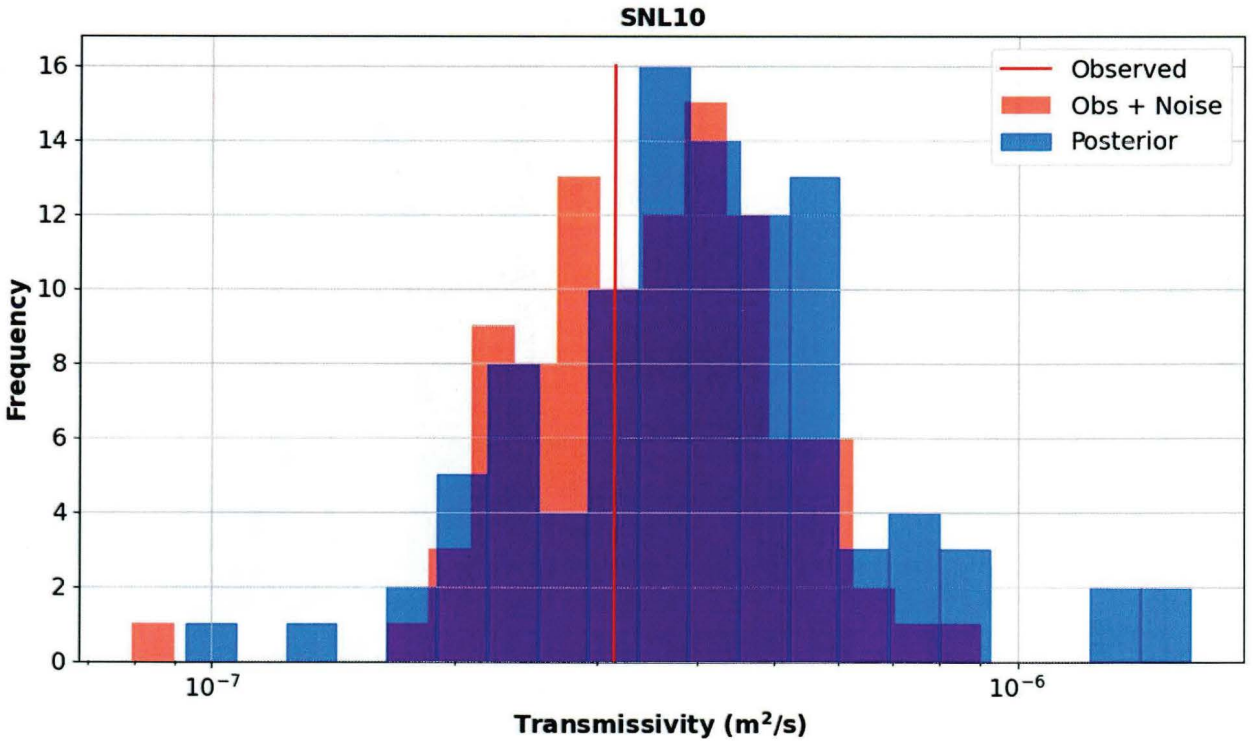

Figure 182. Distribution of Transmissivity Values in Model Element Containing SNL-10 for 100 Selected Realizations from Iteration 5

Information Only

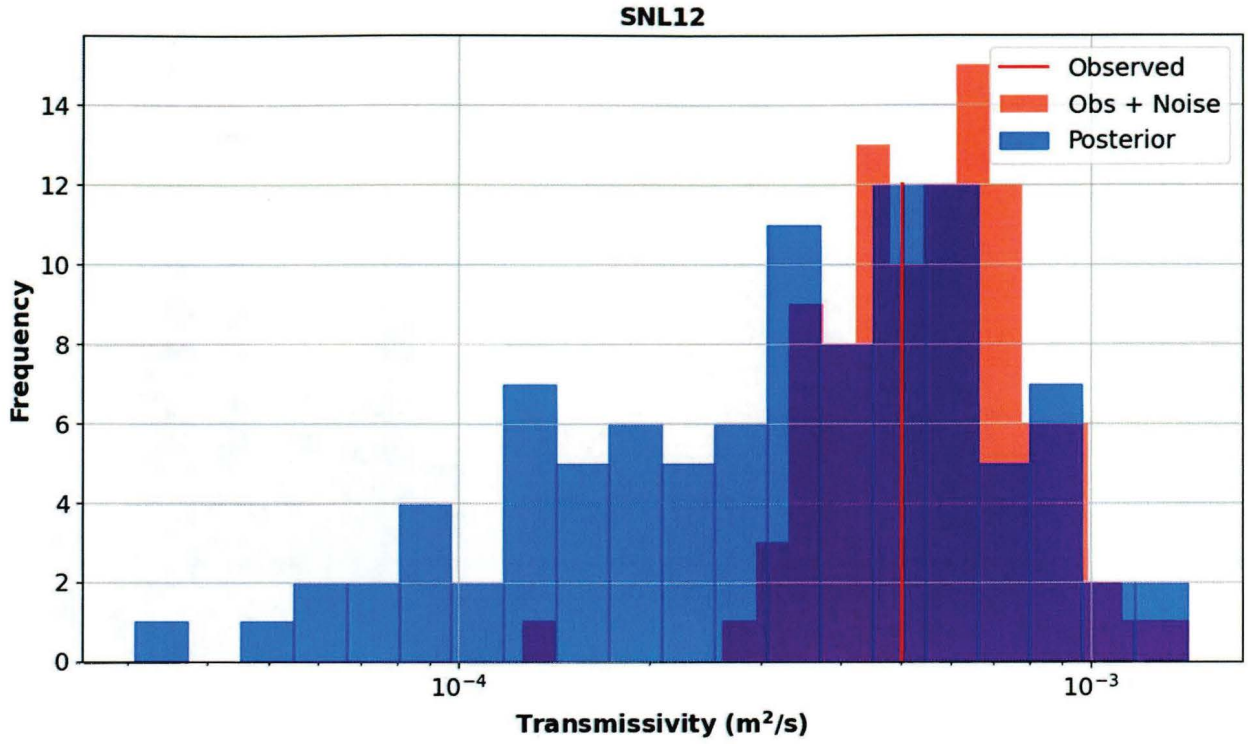

Figure 183. Distribution of Transmissivity Values in Model Element Containing SNL-12 for 100 Selected Realizations from Iteration 5

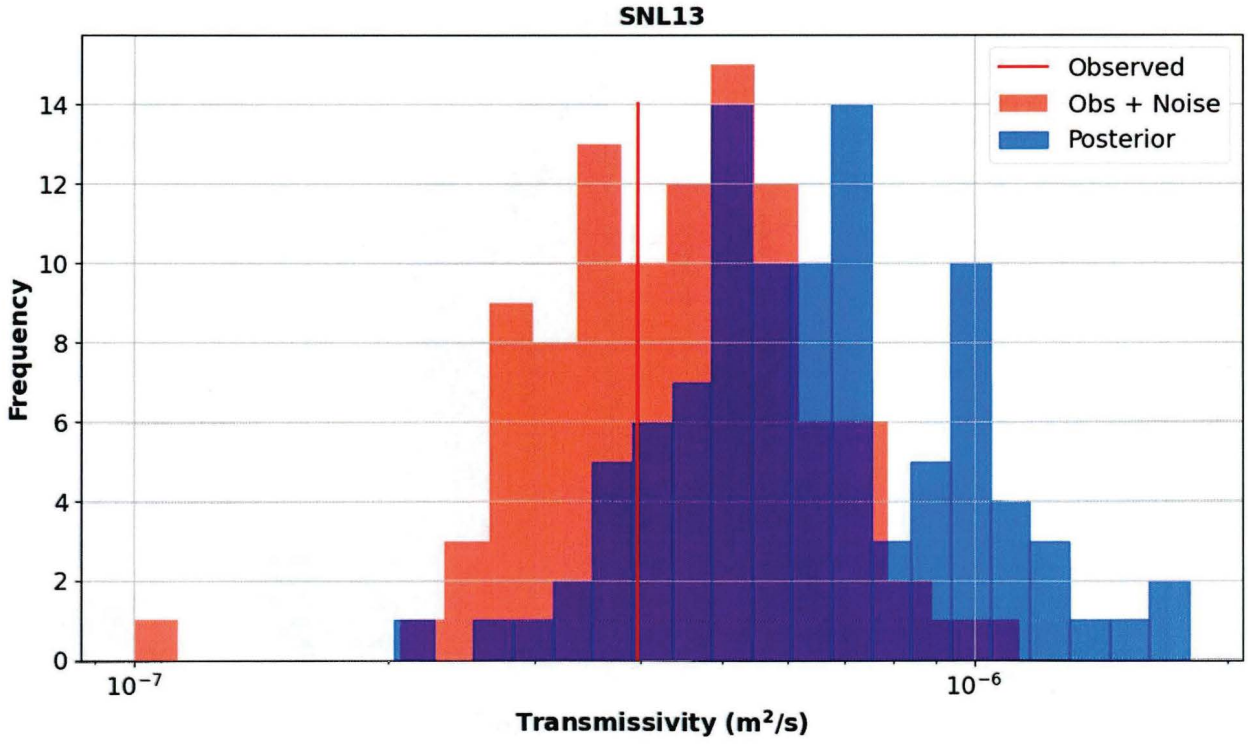

Figure 184. Distribution of Transmissivity Values in Model Element Containing SNL-13 for 100 Selected Realizations from Iteration 5

Information Only

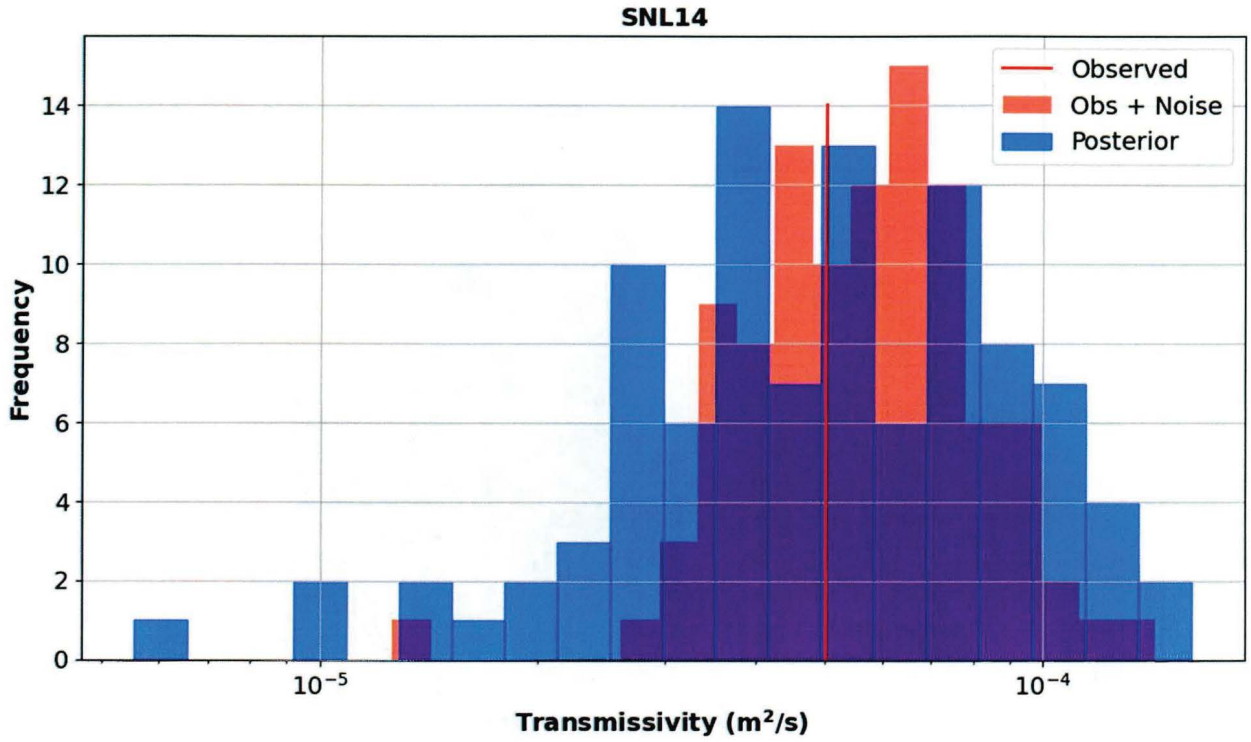

Figure 185. Distribution of Transmissivity Values in Model Element Containing SNL-14 for 100 Selected Realizations from Iteration 5

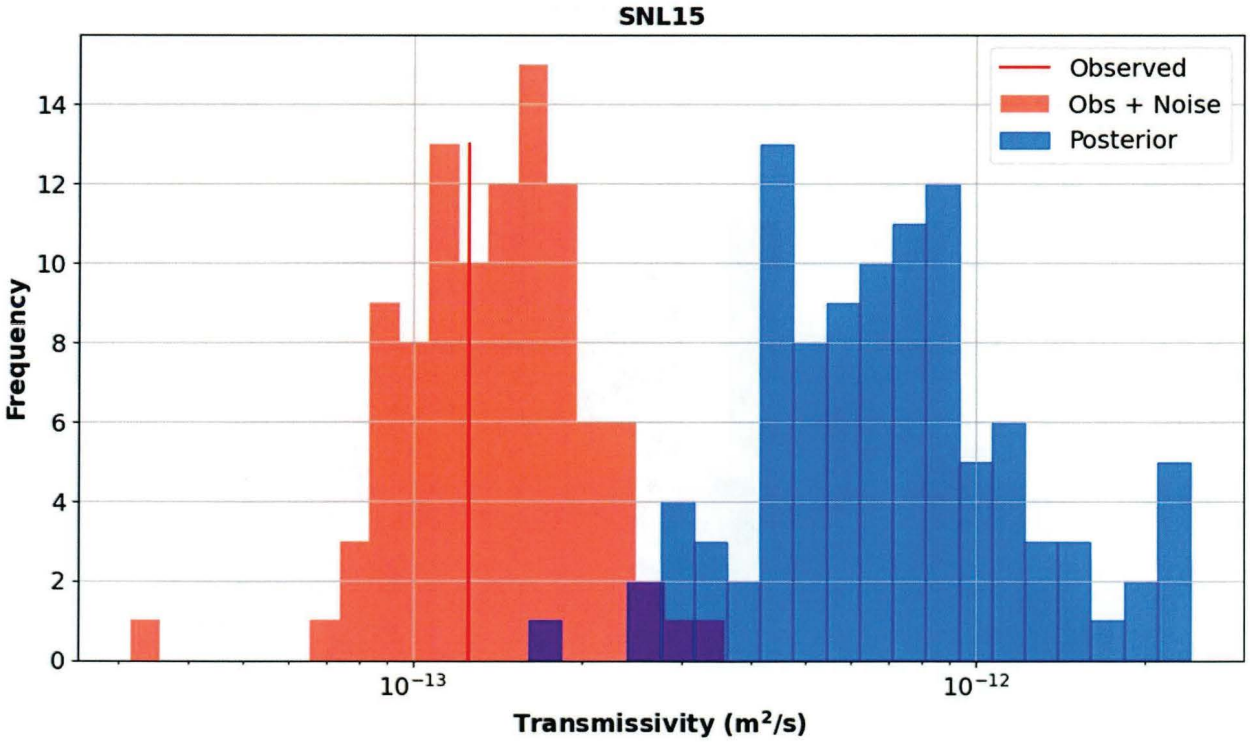

Figure 186. Distribution of Transmissivity Values in Model Element Containing SNL-15 for 100 Selected Realizations from Iteration 5

Information Only

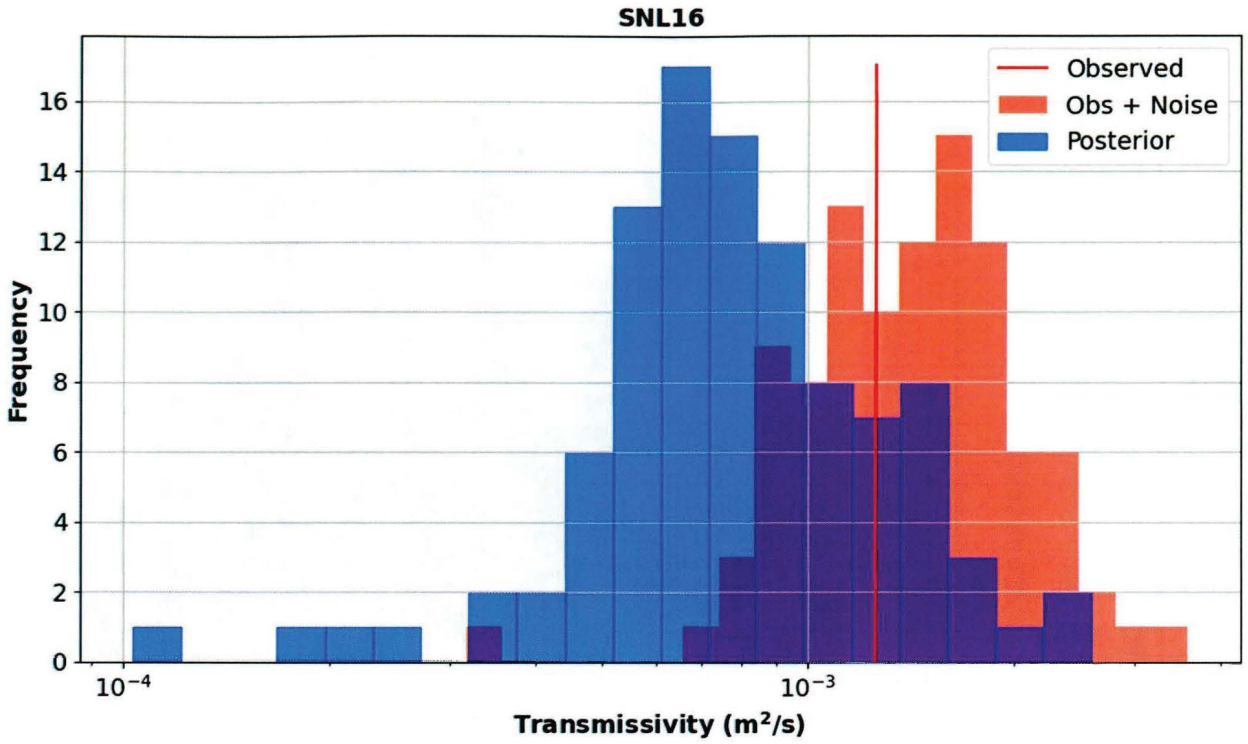

Figure 187. Distribution of Transmissivity Values in Model Element Containing SNL-16 for 100 Selected Realizations from Iteration 5

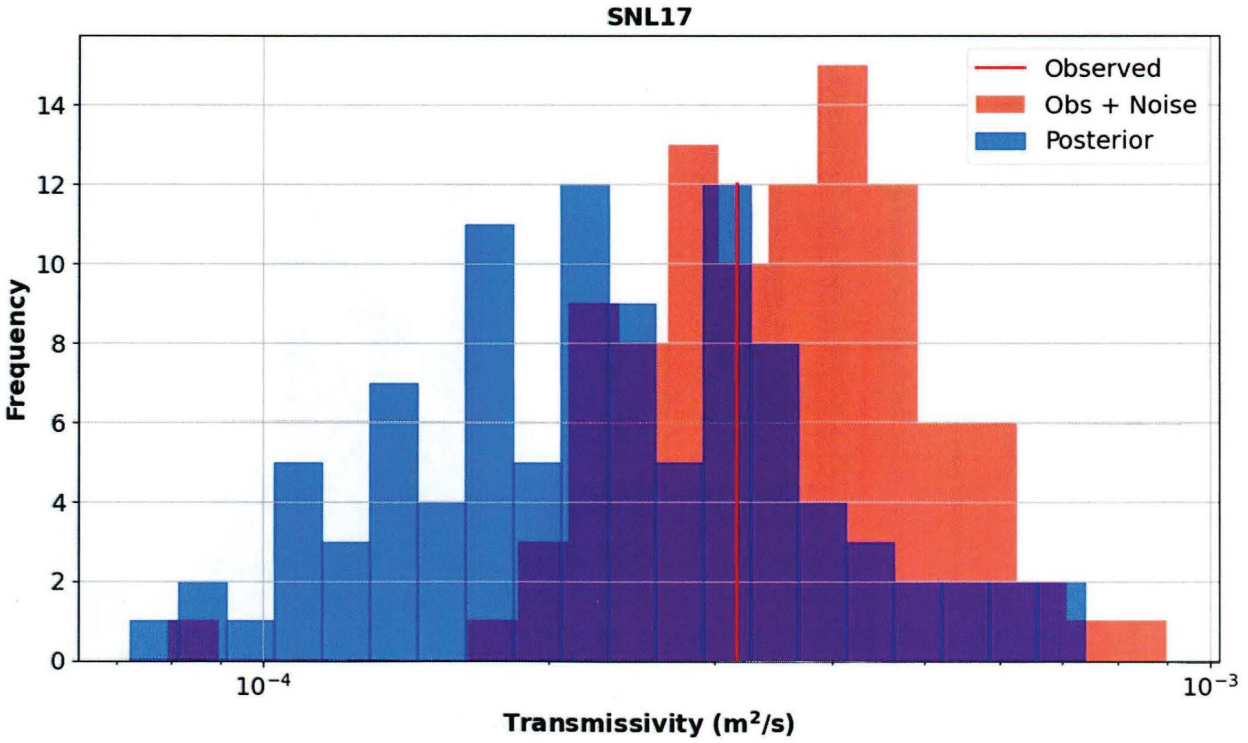

Figure 188. Distribution of Transmissivity Values in Model Element Containing SNL-17 for 100 Selected Realizations from Iteration 5

Information Only

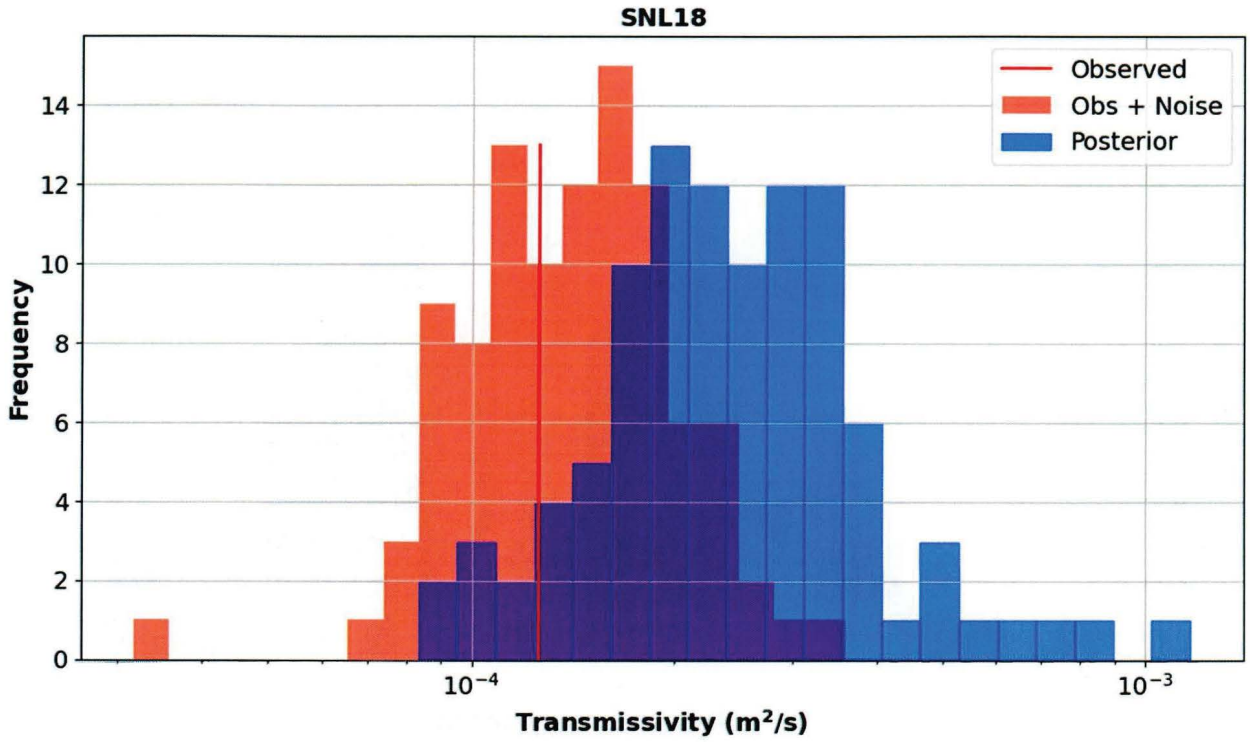

Figure 189. Distribution of Transmissivity Values in Model Element Containing SNL-18 for 100 Selected Realizations from Iteration 5

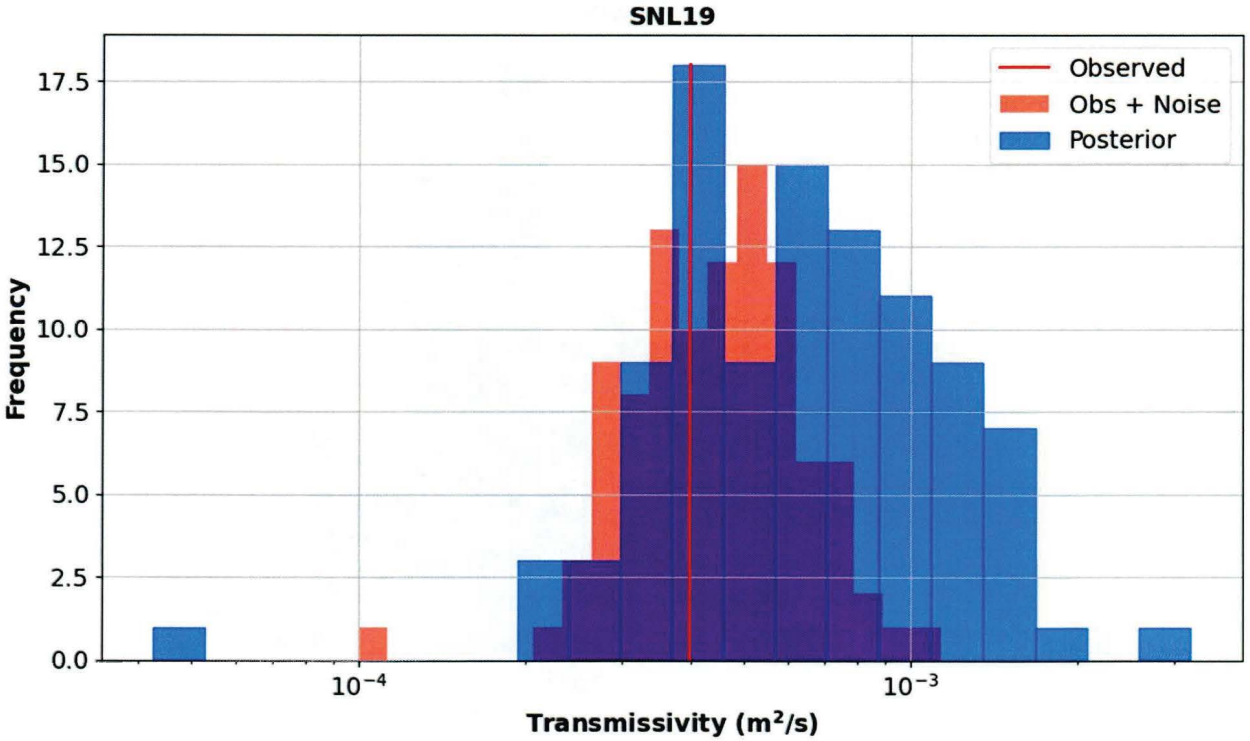

Figure 190. Distribution of Transmissivity Values in Model Element Containing SNL-19 for 100 Selected Realizations from Iteration 5

Information Only

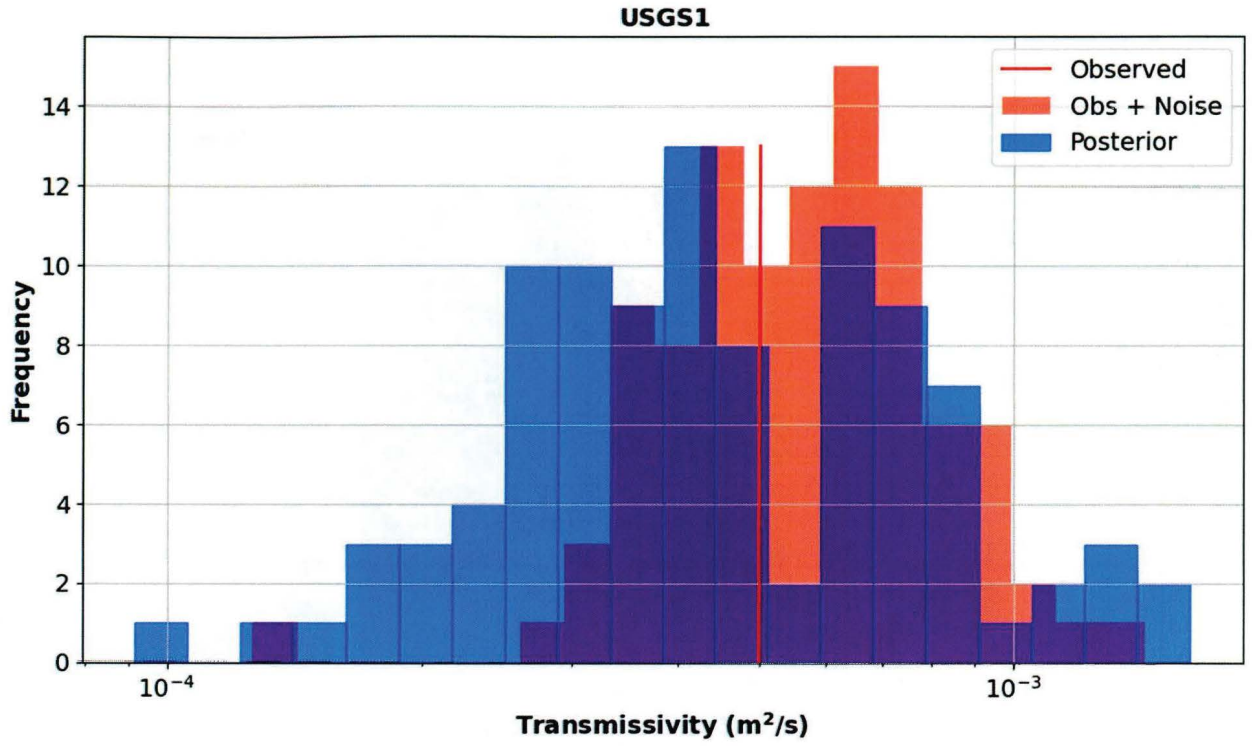

Figure 191. Distribution of Transmissivity Values in Model Element Containing USGS-1 for 100 Selected Realizations from Iteration 5

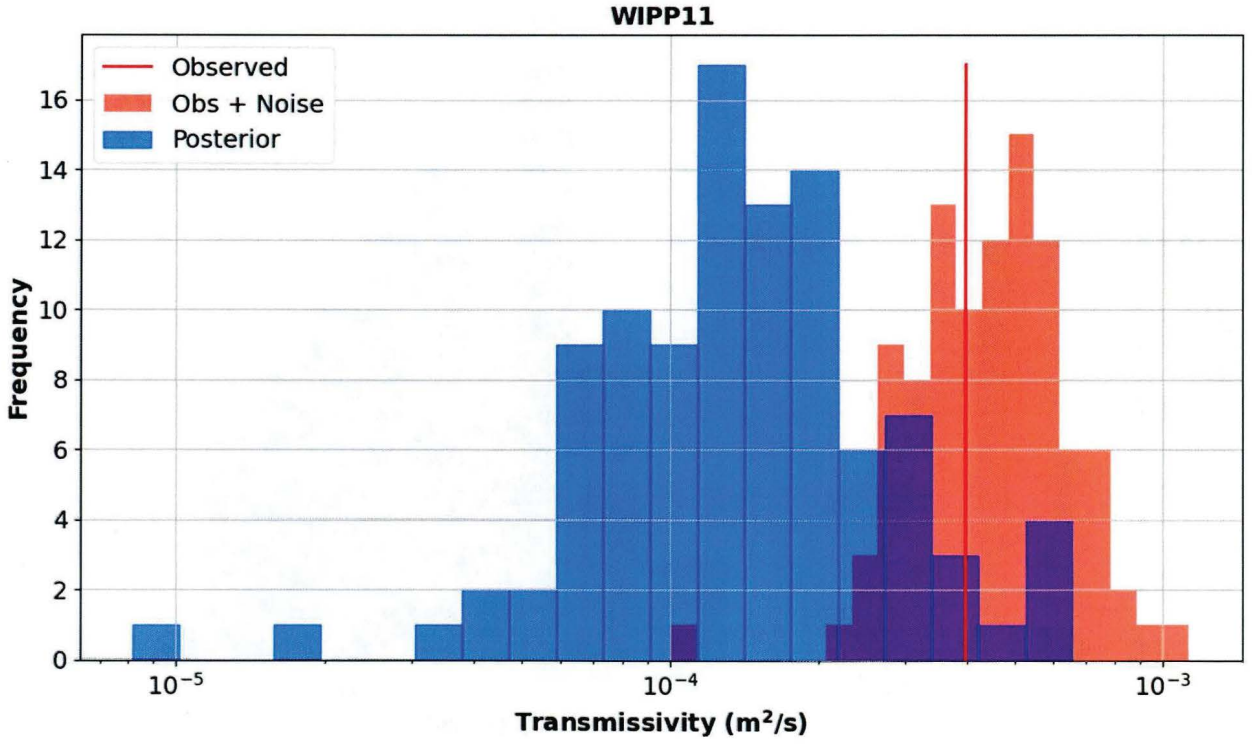

Figure 192. Distribution of Transmissivity Values in Model Element Containing WIPP-11 for 100 Selected Realizations from Iteration 5

Information Only

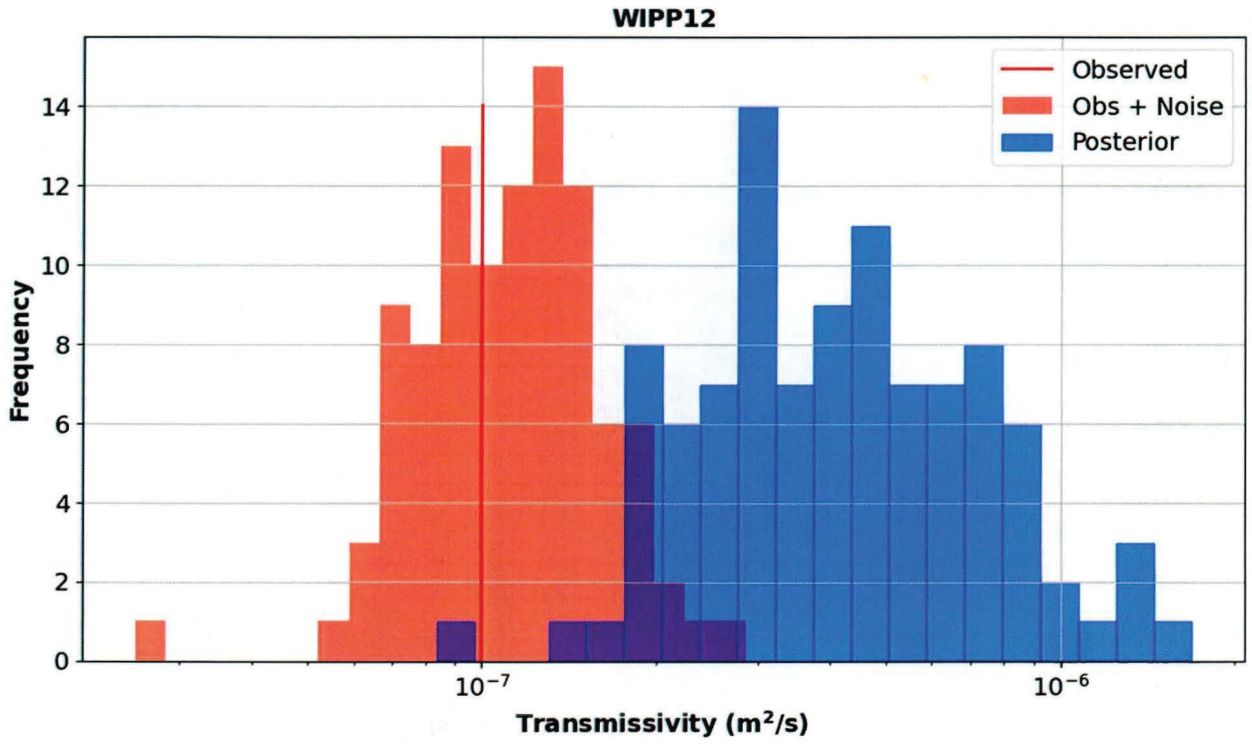

Figure 193. Distribution of Transmissivity Values in Model Element Containing WIPP-12 for 100 Selected Realizations from Iteration 5

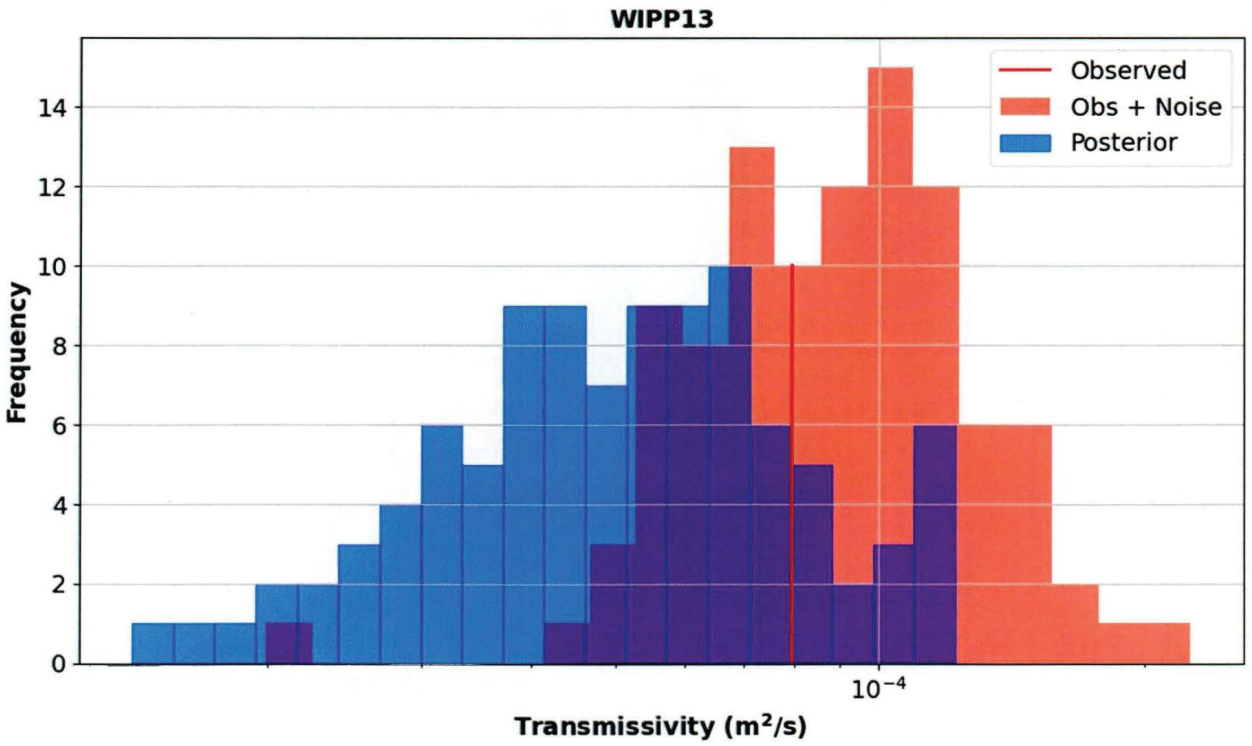

Figure 194. Distribution of Transmissivity Values in Model Element Containing WIPP-13 for 100 Selected Realizations from Iteration 5

Information Only

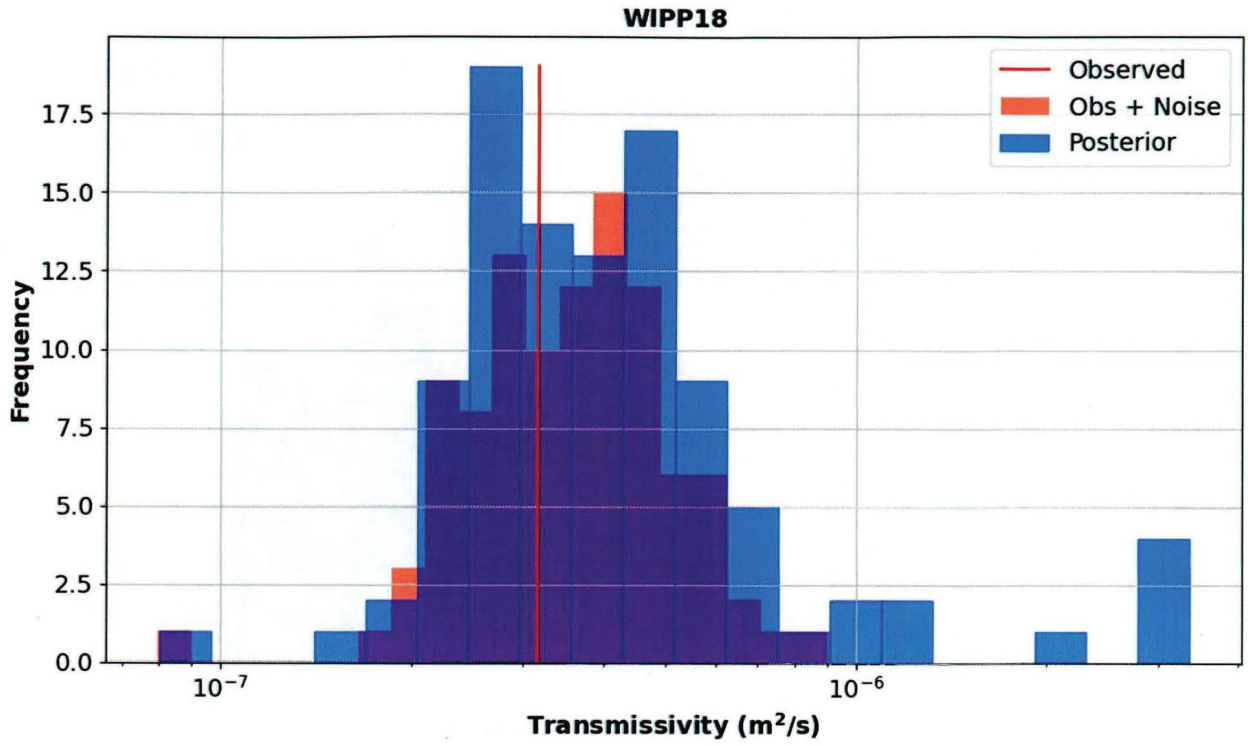

Figure 195. Distribution of Transmissivity Values in Model Element Containing WIPP-18 for 100 Selected Realizations from Iteration 5

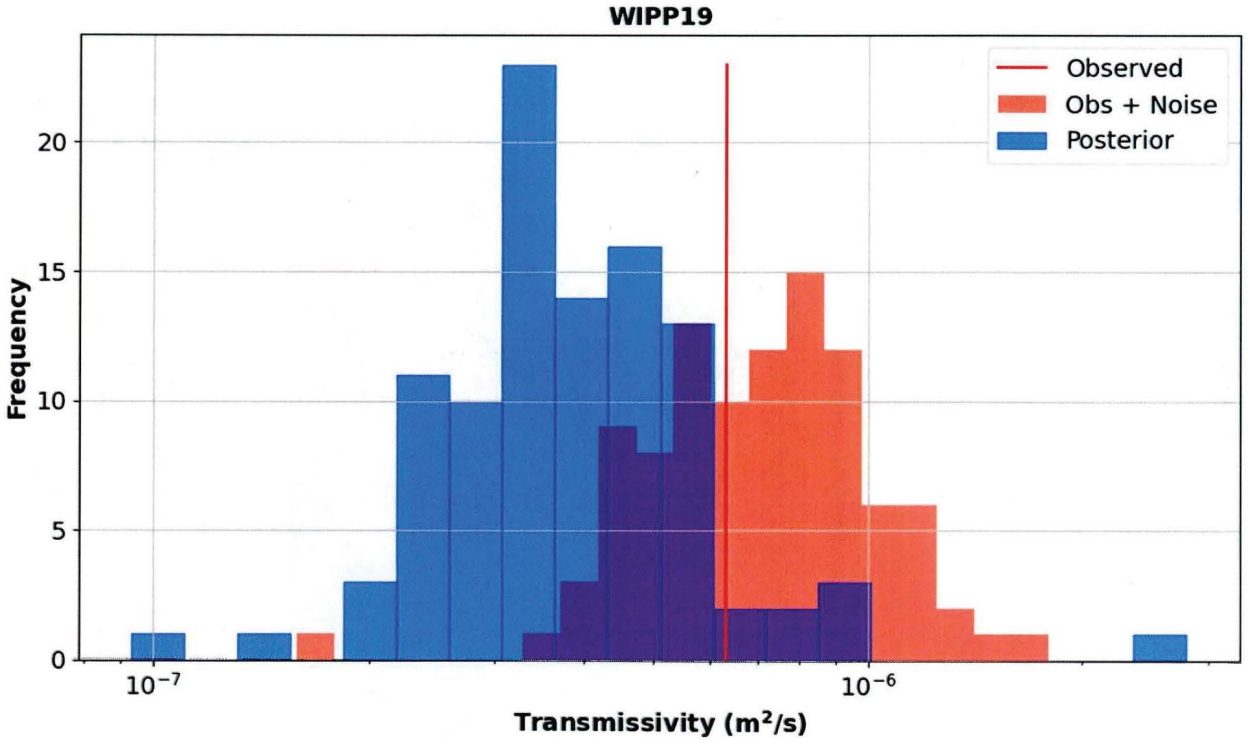

Figure 196. Distribution of Transmissivity Values in Model Element Containing WIPP-19 for 100 Selected Realizations from Iteration 5

Information Only

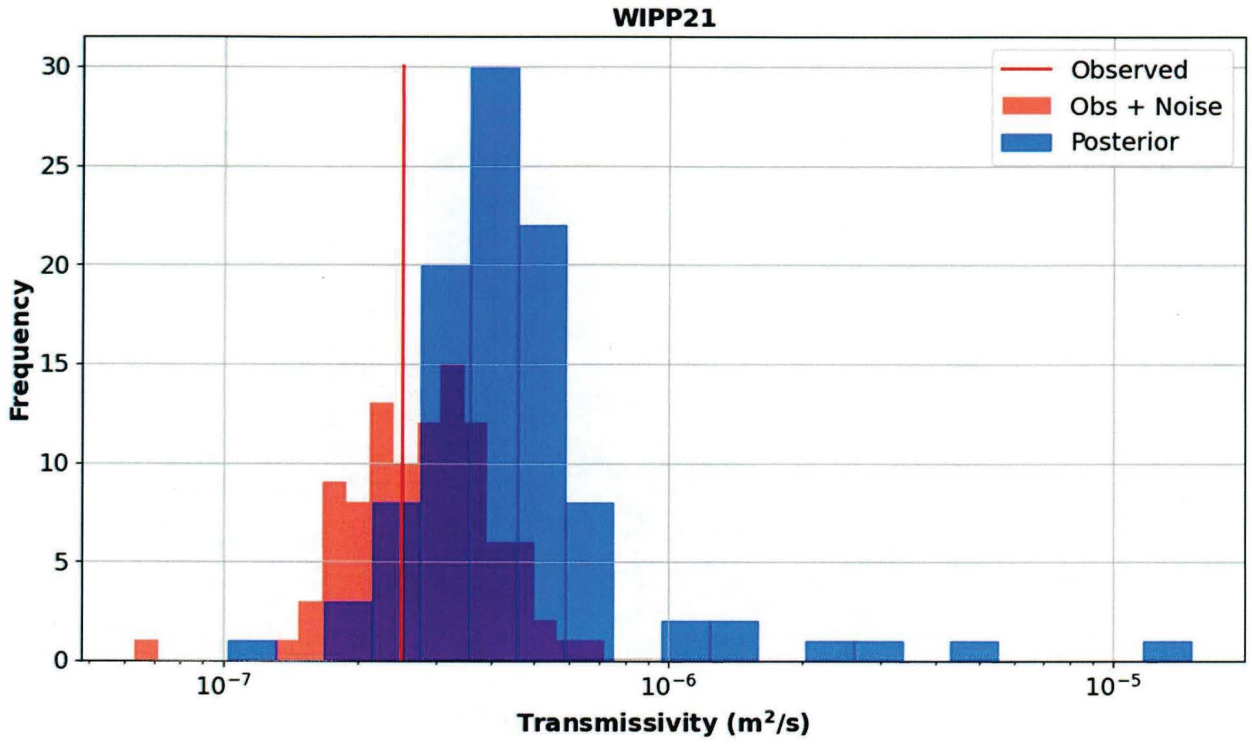

Figure 197. Distribution of Transmissivity Values in Model Element Containing WIPP-21 for 100 Selected Realizations from Iteration 5

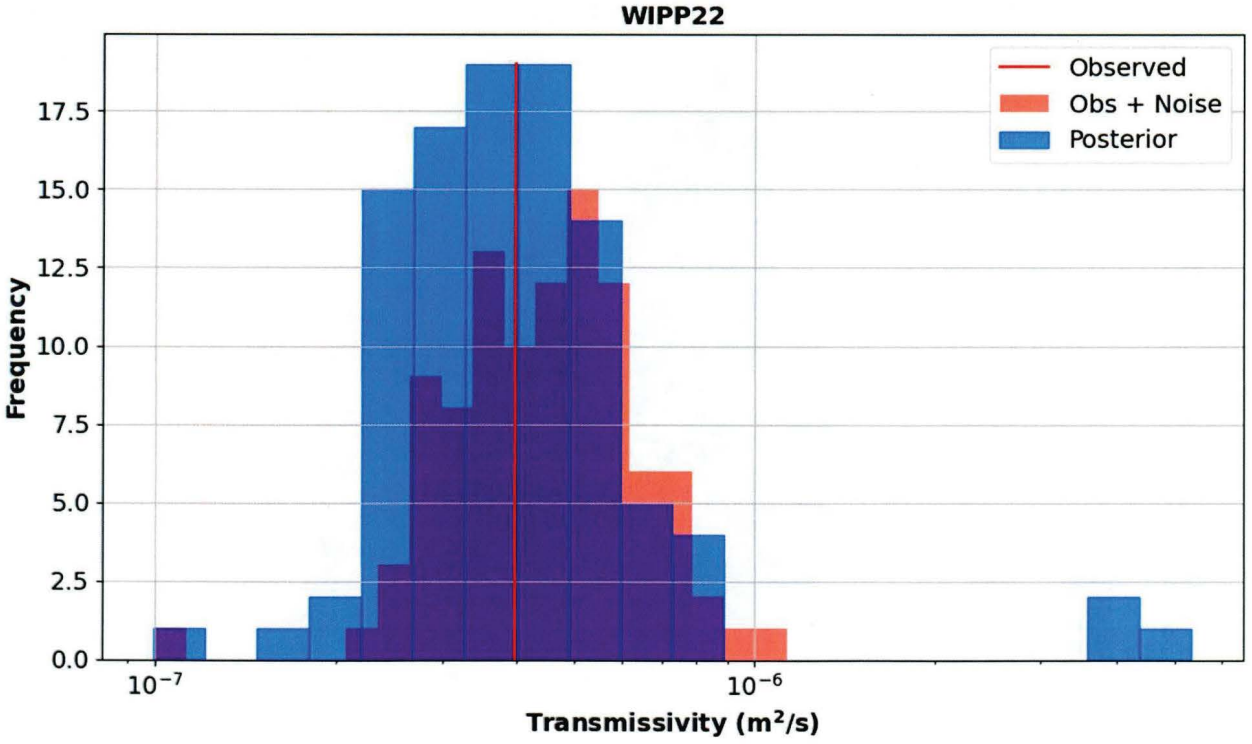

Figure 198. Distribution of Transmissivity Values in Model Element Containing WIPP-22 for 100 Selected Realizations from Iteration 5

Information Only

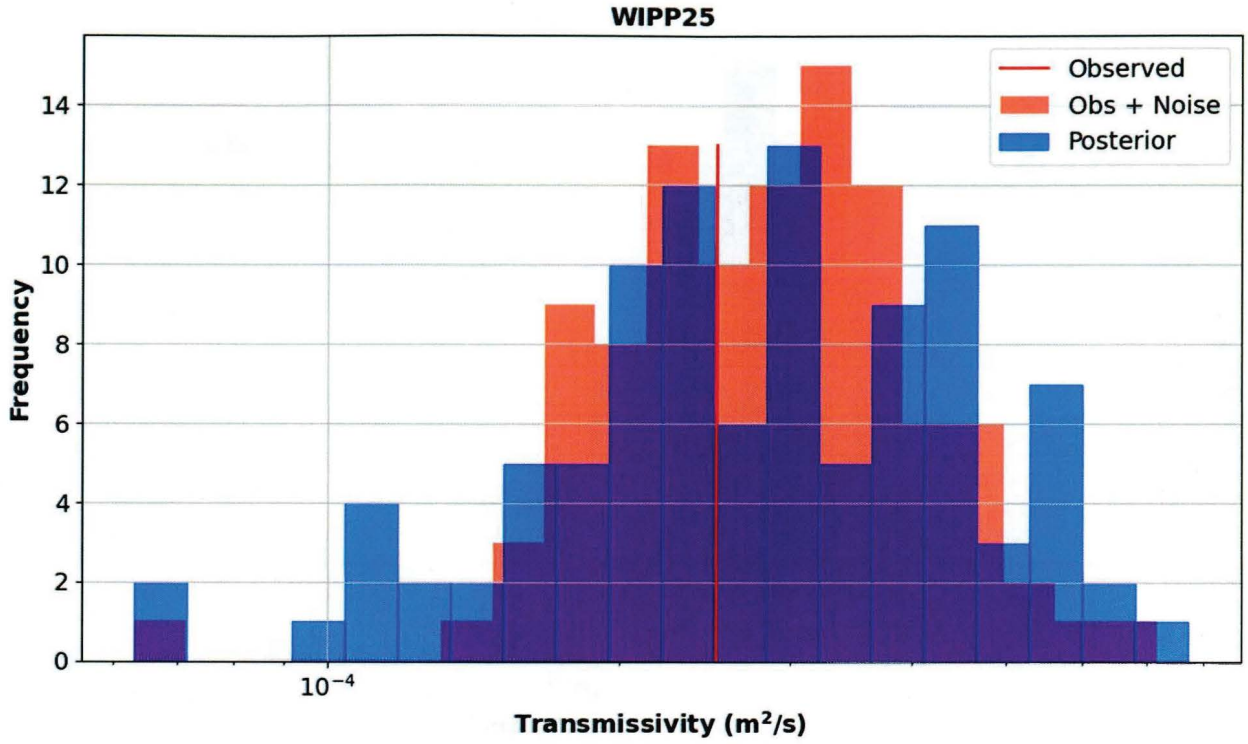

Figure 199. Distribution of Transmissivity Values in Model Element Containing WIPP-25 for 100 Selected Realizations from Iteration 5

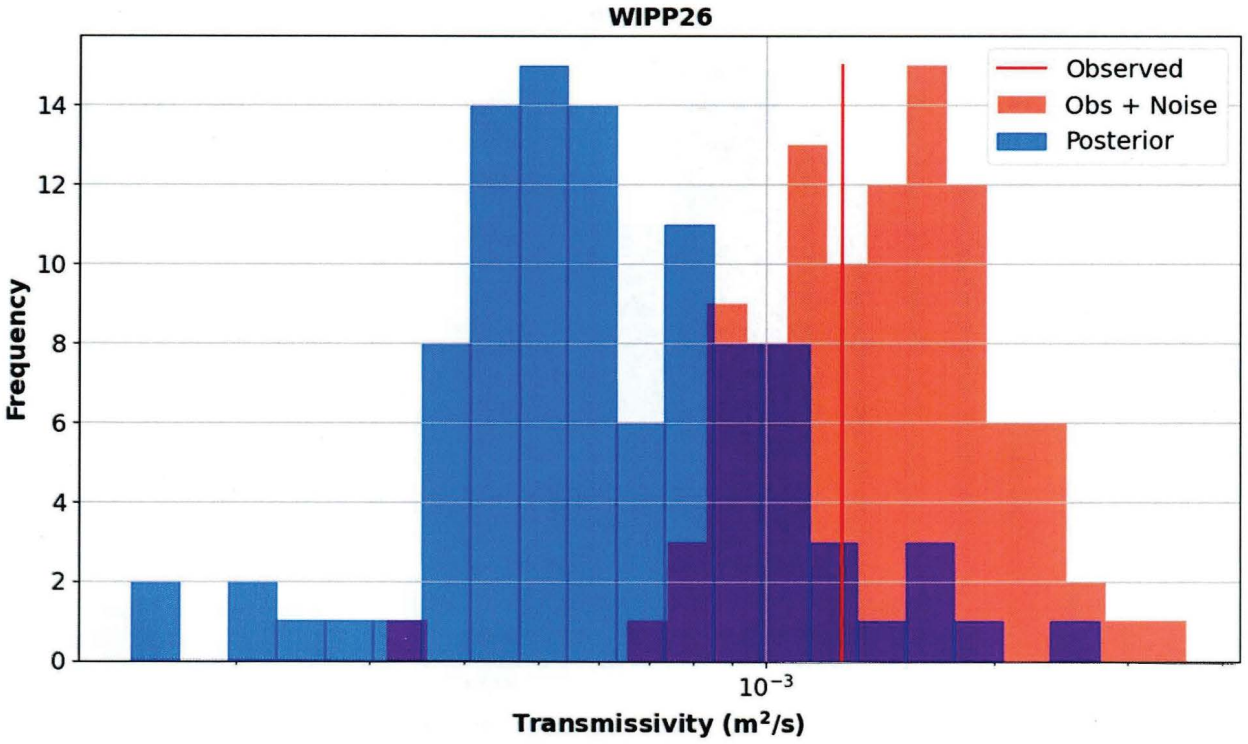

Figure 200. Distribution of Transmissivity Values in Model Element Containing WIPP-26 for 100 Selected Realizations from Iteration 5

Information Only

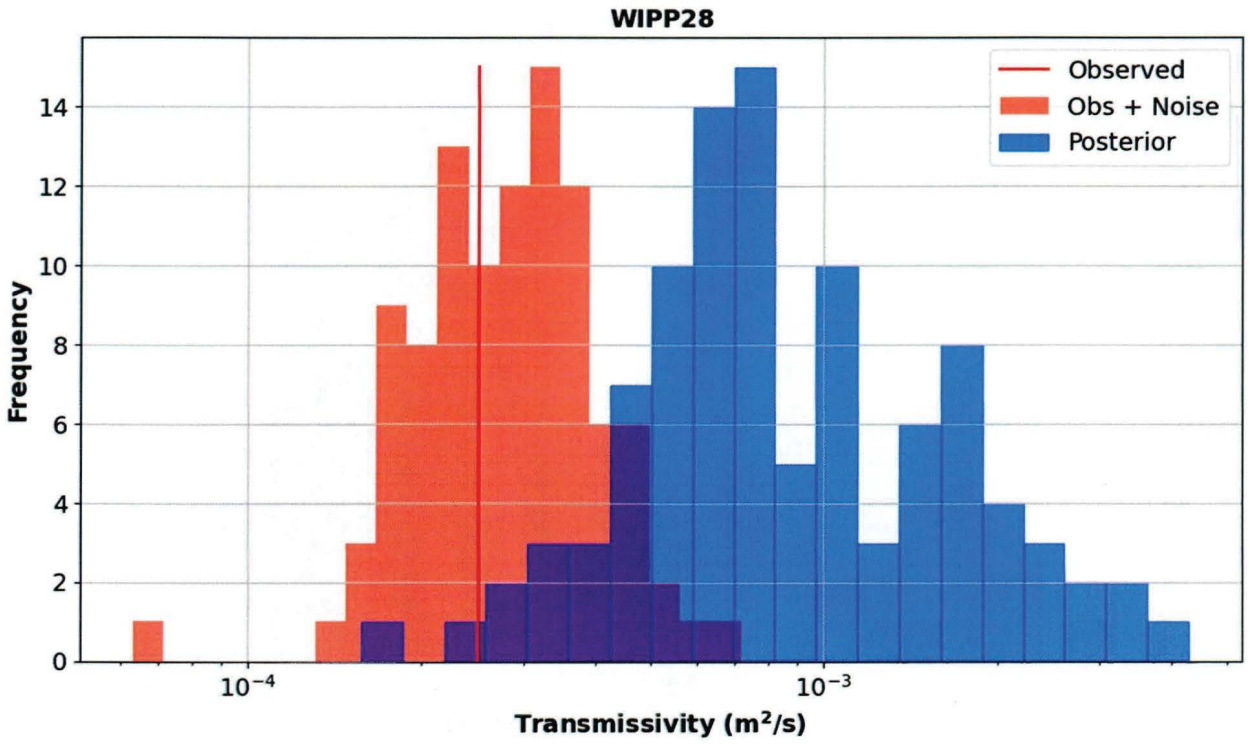

Figure 201. Distribution of Transmissivity Values in Model Element Containing WIPP-28 for 100 Selected Realizations from Iteration 5

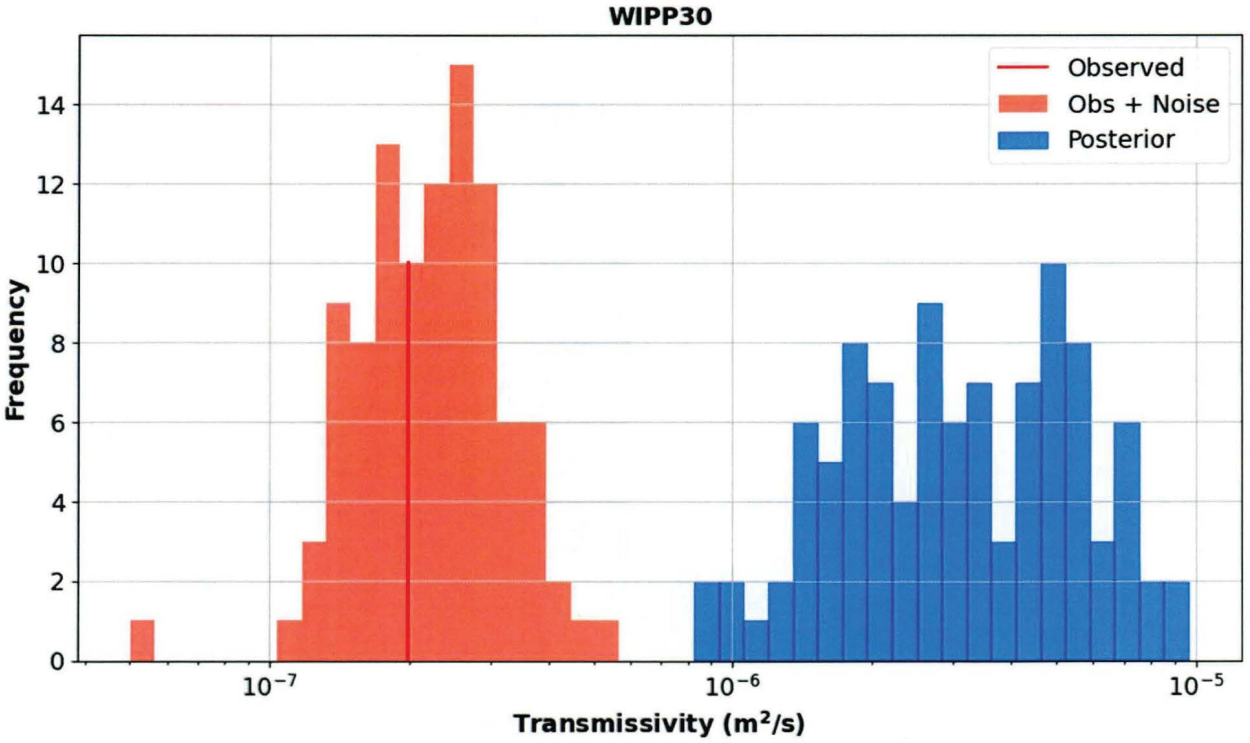

Figure 202. Distribution of Transmissivity Values in Model Element Containing WIPP-30 for 100 Selected Realizations from Iteration 5

Information Only

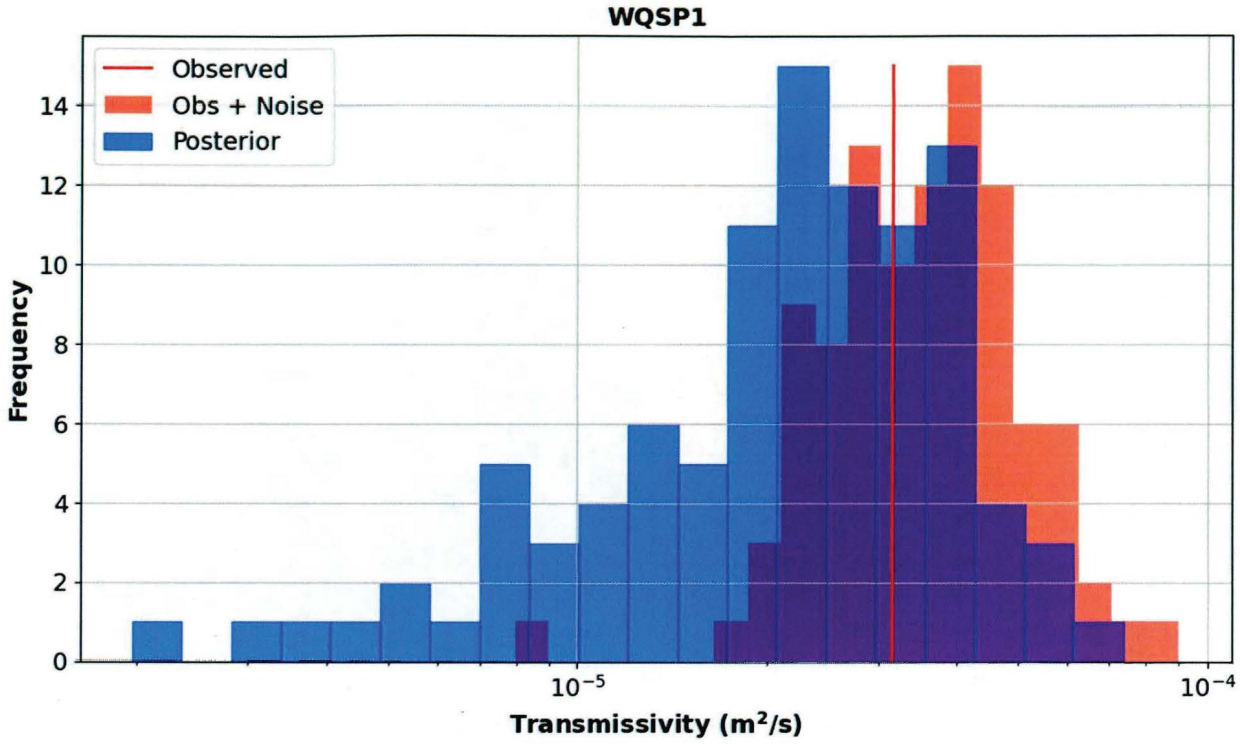

Figure 203. Distribution of Transmissivity Values in Model Element Containing WQSP-1 for 100 Selected Realizations from Iteration 5

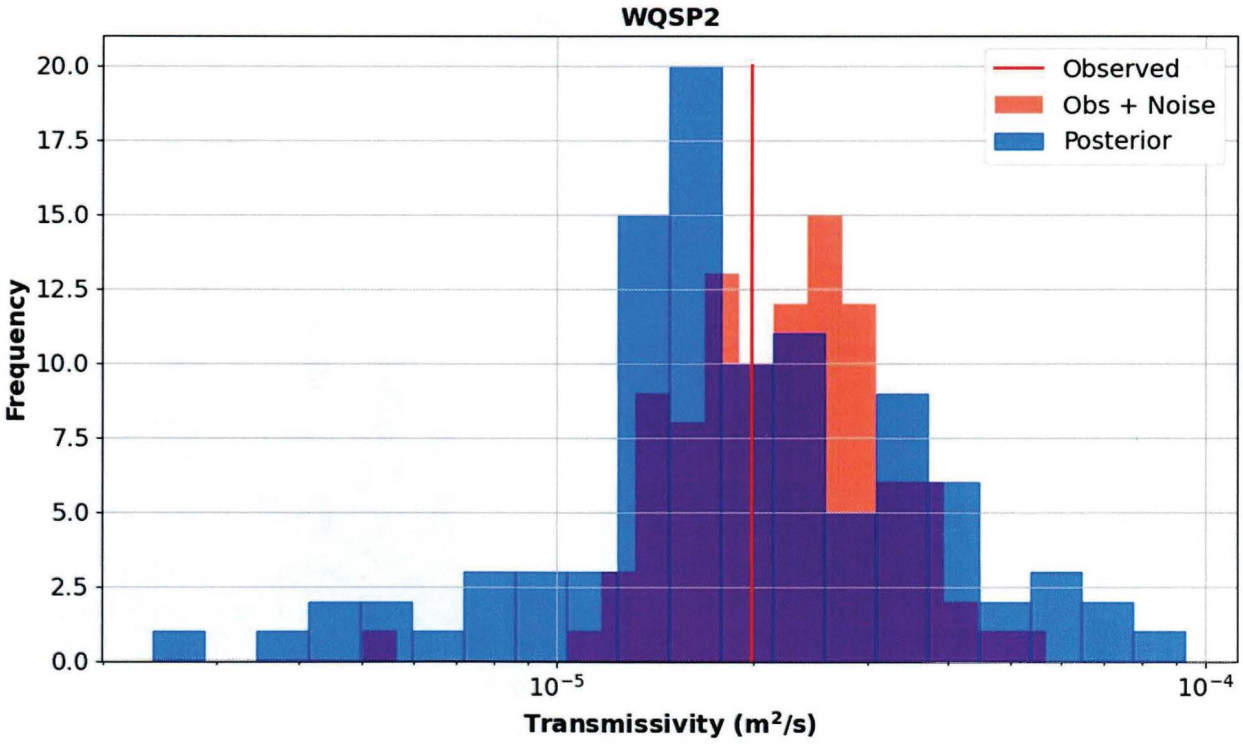

Figure 204. Distribution of Transmissivity Values in Model Element Containing WQSP-2 for 100 Selected Realizations from Iteration 5

Information Only

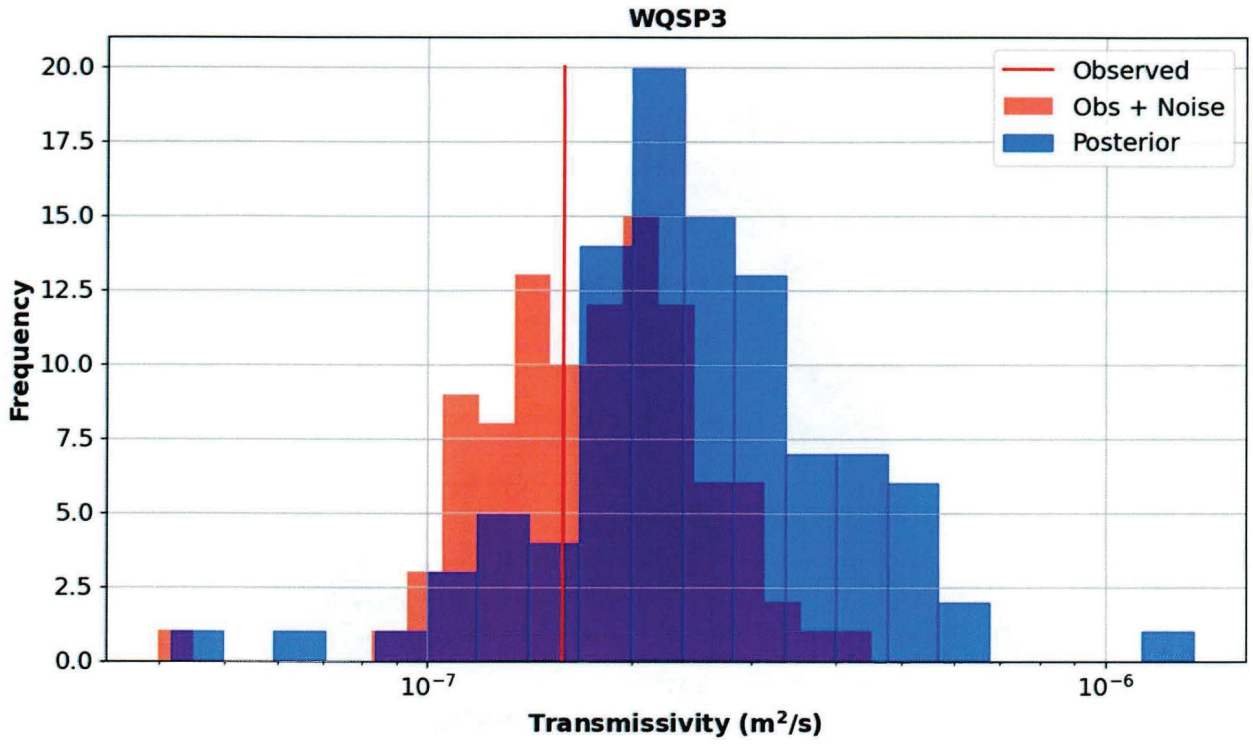

Figure 205. Distribution of Transmissivity Values in Model Element Containing WQSP-3 for 100 Selected Realizations from Iteration 5

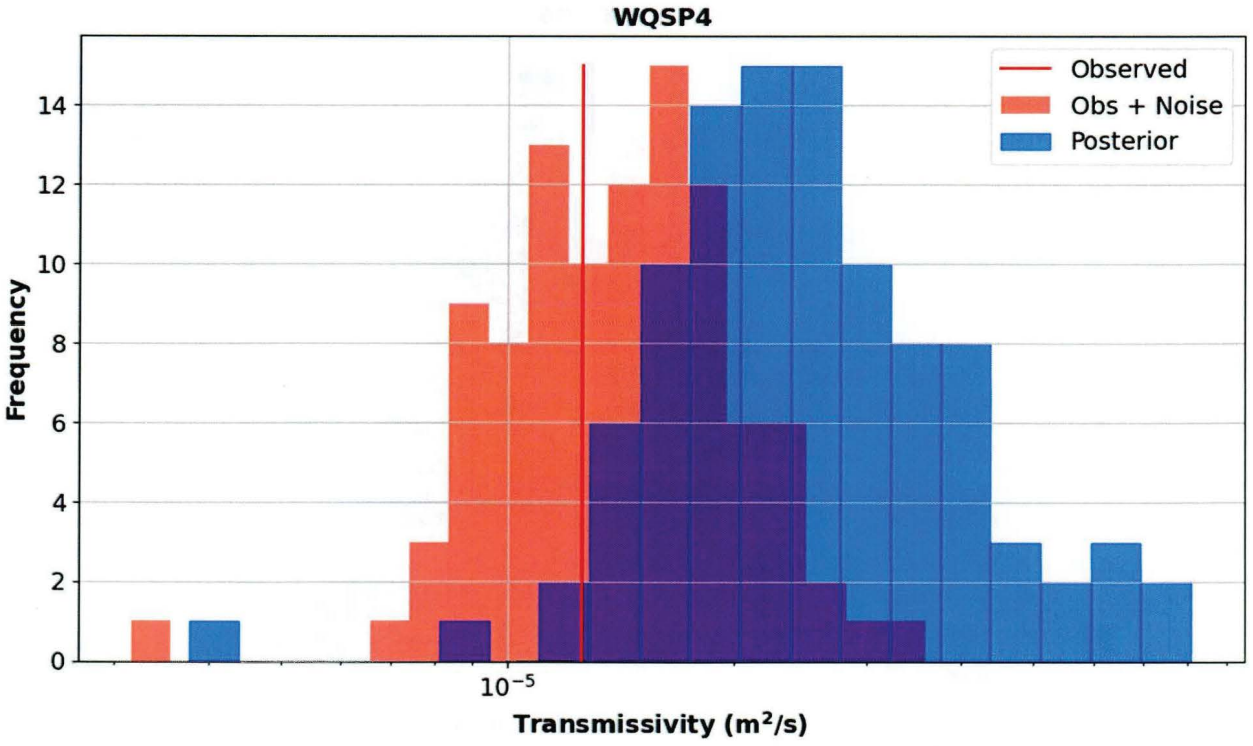

Figure 206. Distribution of Transmissivity Values in Model Element Containing WQSP-4 for 100 Selected Realizations from Iteration 5

Information Only

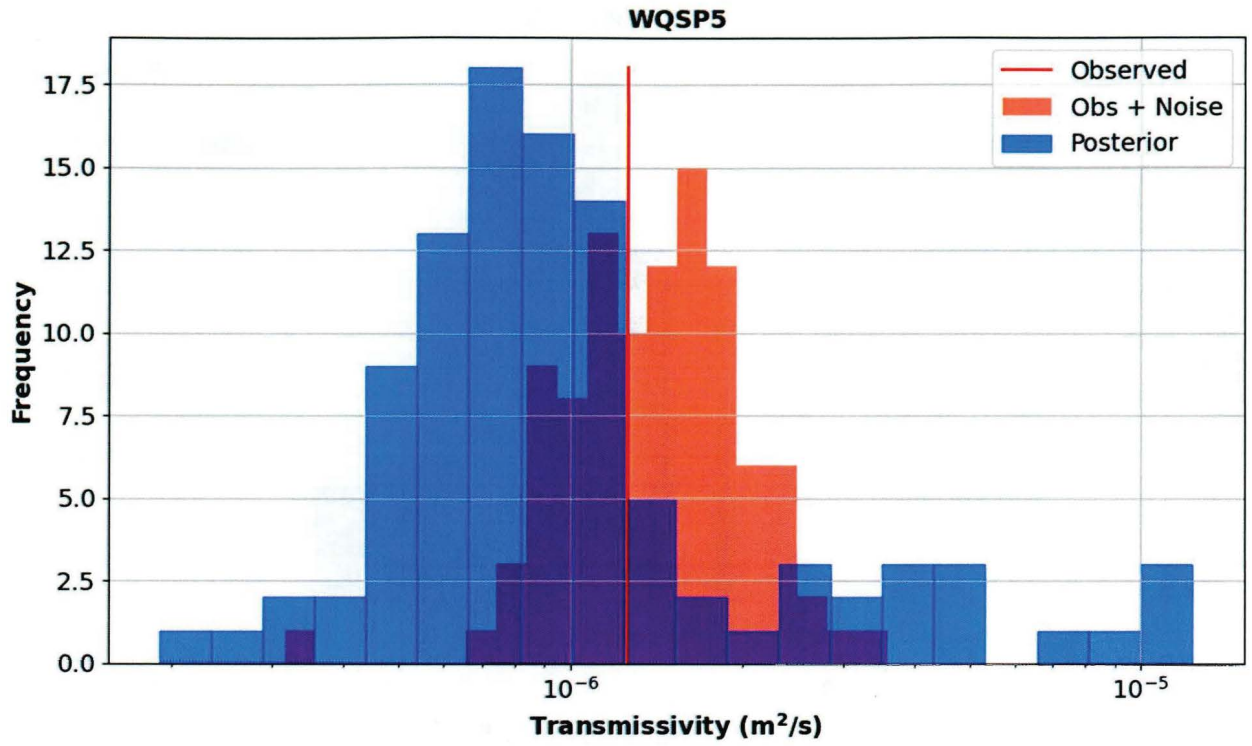

Figure 207. Distribution of Transmissivity Values in Model Element Containing WQSP-5 for 100 Selected Realizations from Iteration 5

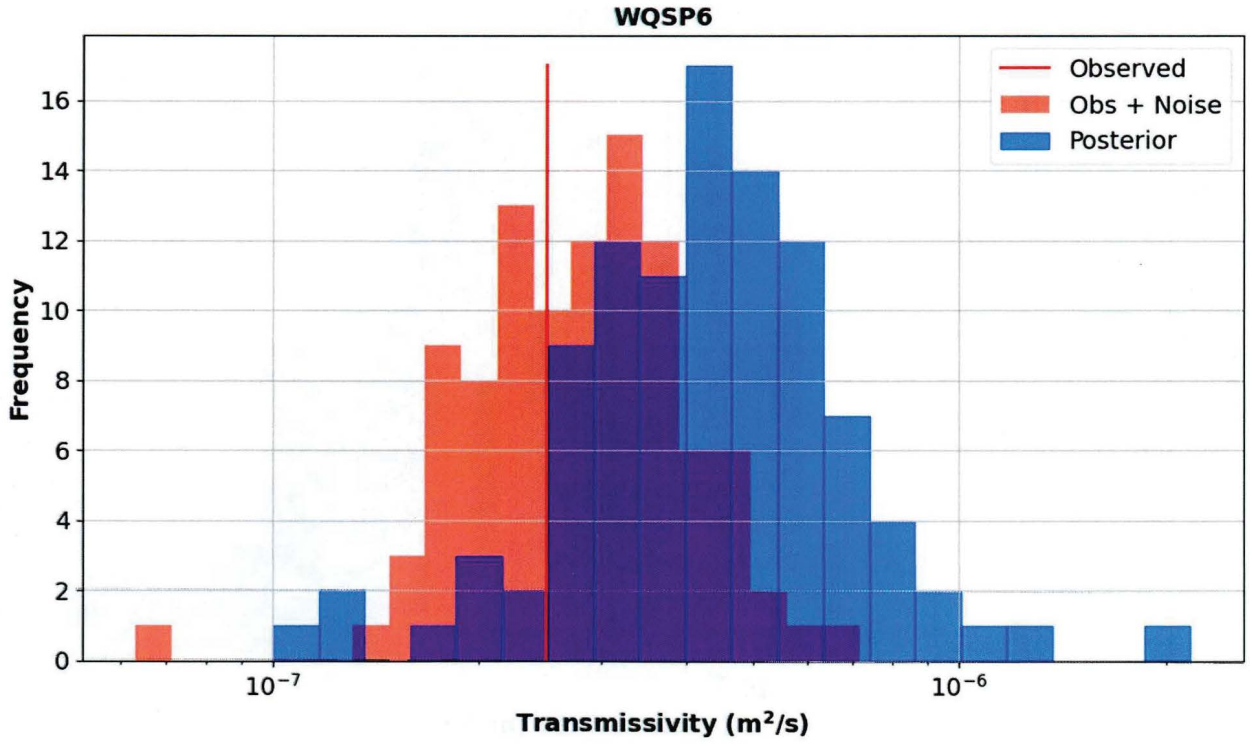

Figure 208. Distribution of Transmissivity Values in Model Element Containing WQSP-6 for 100 Selected Realizations from Iteration 5

Information Only

7.6 Directory Tree Structure

The main output files are archived in the folder noted below, and the directory tree structure for the original files (/data/home/run_mast/work/tfields/wipp_tfields_2021/) and the archived files is provided below –

/data/cvs/CVSLIB/WIPP_EXTERNAL/ap203/wipp_tfields_2021/Outputs/Results_02.21.23/r[rrr*]/

```
├── aser
├── bestguess.millsranch.wel
├── bin
│   ├── CVS
│   │   └── CVS
│   ├── linux
│   │   └── bin
│   ├── mac
│   └── win
│       └── gwutils
│           └── documentation
├── config
│   ├── flopy
│   │   ├── discretization
│   │   ├── export
│   │   ├── mf6
│   │   │   ├── coordinates
│   │   │   ├── data
│   │   │   │   └── dfn
│   │   │   ├── modflow
│   │   │   └── utils
│   │   ├── modflow
│   │   ├── modflowlgr
│   │   ├── modpath
│   │   ├── mt3d
│   │   ├── pest
│   │   ├── plot
│   │   │   └── mplstyle
│   │   ├── seawat
│   │   └── utils
│   └── pyemu
│       ├── mat
│       ├── plot
│       ├── prototypes
│       ├── pst
│       └── utils
├── dtrkmf
├── flopy
│   ├── discretization
│   │   └── __pycache__
│   ├── export
│   │   └── __pycache__
│   ├── mf6
│   │   ├── coordinates
│   │   │   └── __pycache__
│   │   ├── data
│   │   │   ├── dfn
│   │   │   └── __pycache__
│   │   ├── modflow
```

Information Only



Information Only

```
│   │   ├── pest
│   │   │   └── __pycache__
│   │   ├── plot
│   │   │   ├── mplstyle
│   │   │   └── __pycache__
│   │   ├── __pycache__
│   │   ├── seawat
│   │   │   └── __pycache__
│   │   └── utils
│   │       └── __pycache__
│   ├── input_data
│   │   └── meas
│   ├── mf6_h11
│   ├── mf6_h19
│   ├── mf6_h3
│   ├── mf6_h9br
│   ├── mf6_head
│   ├── mf6_mr
│   ├── mf6_p14
│   ├── mf6_sn114
│   ├── mf6_wipp11
│   ├── mf6_wipp13
│   ├── mf6_wqsp1
│   ├── mf6_wqsp2
│   ├── mult
│   ├── org
│   ├── prelim_figs.2023.02.21
│   │   ├── 3D.NormPhi.Scatter
│   │   ├── Iteration.1
│   │   │   ├── Afield.plots.v2
│   │   │   ├── ASER.pars
│   │   │   ├── meas.trans.hist
│   │   │   ├── mr.hydrographs
│   │   │   ├── mr.pumping
│   │   │   ├── Rfield.plots.v2
│   │   │   ├── Sfield.plots.v2
│   │   │   ├── steadystate.contour.maps
│   │   │   ├── steadystate.noise.hist
│   │   │   ├── steady.state.obs
│   │   │   ├── tfield.plots.v2
│   │   │   ├── well.obs
│   │   │   └── well.obs.best
│   │   ├── Iteration.2
│   │   │   ├── Afield.plots.v2
│   │   │   ├── ASER.pars
│   │   │   ├── meas.trans.hist
│   │   │   ├── mr.hydrographs
│   │   │   ├── mr.pumping
│   │   │   ├── Rfield.plots.v2
│   │   │   ├── Sfield.plots.v2
│   │   │   ├── steadystate.contour.maps
│   │   │   ├── steadystate.noise.hist
│   │   │   ├── steady.state.obs
│   │   │   ├── tfield.plots.v2
│   │   │   ├── well.obs
│   │   │   └── well.obs.best
```

Information Only

```
├── Iteration.3
│   ├── Afield.plots.v2
│   ├── ASER.pars
│   ├── meas.trans.hist
│   ├── mr.hydrographs
│   ├── mr.pumping
│   ├── Rfield.plots.v2
│   ├── Sfield.plots.v2
│   ├── steadystate.contour.maps
│   ├── steadystate.noise.hist
│   ├── steady.state.obs
│   ├── tfield.plots.v2
│   ├── well.obs
│   └── well.obs.best
├── Iteration.4
│   ├── Afield.plots.v2
│   ├── ASER.pars
│   ├── meas.trans.hist
│   ├── mr.hydrographs
│   ├── mr.pumping
│   ├── Rfield.plots.v2
│   ├── Sfield.plots.v2
│   ├── steadystate.contour.maps
│   ├── steadystate.noise.hist
│   ├── steady.state.obs
│   ├── tfield.plots.v2
│   ├── well.obs
│   └── well.obs.best
├── Iteration.5
│   ├── Afield.plots.v2
│   ├── ASER.pars
│   ├── meas.trans.hist
│   ├── mr.hydrographs
│   ├── mr.pumping
│   ├── particle_track_maps
│   ├── Rfield.plots.v2
│   ├── Sfield.plots.v2
│   ├── steadystate.contour.maps
│   ├── steadystate.noise.hist
│   ├── steady.state.obs
│   ├── tfield.plots.v2
│   ├── well.obs
│   └── well.obs.best
├── Iteration.6
│   ├── Afield.plots.v2
│   ├── ASER.pars
│   ├── meas.trans.hist
│   ├── mr.hydrographs
│   ├── mr.pumping
│   ├── Rfield.plots.v2
│   ├── Sfield.plots.v2
│   ├── steadystate.contour.maps
│   ├── steadystate.noise.hist
│   ├── steady.state.obs
│   ├── tfield.plots.v2
│   ├── well.obs
```

Information Only

```
│   │   │   └── well.obs.best
│   │   ├── Iteration.7
│   │   │   ├── Afield.plots.v2
│   │   │   ├── ASER.pars
│   │   │   ├── meas.trans.hist
│   │   │   ├── mr.hydrographs
│   │   │   ├── mr.pumping
│   │   │   ├── Rfield.plots.v2
│   │   │   ├── Sfield.plots.v2
│   │   │   ├── steadystate.contour.maps
│   │   │   ├── steadystate.noise.hist
│   │   │   ├── steady.state.obs
│   │   │   ├── tfield.plots.v2
│   │   │   ├── well.obs
│   │   │   └── well.obs.best
│   │   ├── ParticleTrackCDFs
│   │   ├── Phi.Histograms
│   │   ├── Phi.Horsetail
│   │   └── Phi.Matrix
│   └── pyemu
│       ├── mat
│       │   └── __pycache__
│       ├── plot
│       │   └── __pycache__
│       ├── prototypes
│       │   └── __pycache__
│       ├── pst
│       │   └── __pycache__
│       ├── __pycache__
│       └── utils
│           └── __pycache__
├── master.prior
│   ├── flopy
│   │   ├── discretization
│   │   ├── export
│   │   ├── mf6
│   │   │   ├── coordinates
│   │   │   ├── data
│   │   │   │   └── dfn
│   │   │   ├── modflow
│   │   │   └── utils
│   │   ├── modflow
│   │   ├── modflowlgr
│   │   ├── modpath
│   │   ├── mt3d
│   │   ├── pest
│   │   ├── plot
│   │   │   └── mplstyle
│   │   ├── seawat
│   │   └── utils
│   ├── input_data
│   │   └── meas
│   ├── mf6_h11
│   ├── mf6_h19
│   ├── mf6_h3
│   ├── mf6_h9br
```

Information Only

```
    ├── mf6_head
    ├── mf6_mr
    ├── mf6_p14
    ├── mf6_snl14
    ├── mf6_wipp11
    ├── mf6_wipp13
    ├── mf6_wqsp1
    ├── mf6_wqsp2
    ├── mult
    ├── org
    └── pyemu
        ├── mat
        ├── plot
        ├── prototypes
        ├── pst
        └── utils
├── mf2k
├── MF_prelim_figs
    ├── A_field2010_plots
    ├── R_tfield2010_plots
    ├── S_field2010_plots
    └── tfield2010_plots
├── mills_ranch_data
    ├── Mills_Ranch_Obs_files
    │   └── dd_out
    └── MillsRanch.Resampled.Drawdowns
├── model_ws
    ├── 2010_tfields
    │   ├── r000
    │   │   └── CVS
    │   ├── r001
    │   │   └── CVS
    │   └── r001_template
    ├── mf2k_h9br
    ├── mf6_clean_template
    │   ├── flopy
    │   │   ├── discretization
    │   │   │   └── __pycache__
    │   │   ├── export
    │   │   │   └── __pycache__
    │   │   ├── mf6
    │   │   │   ├── coordinates
    │   │   │   │   └── __pycache__
    │   │   │   ├── data
    │   │   │   │   ├── dfn
    │   │   │   │   └── __pycache__
    │   │   │   ├── modflow
    │   │   │   │   └── __pycache__
    │   │   │   ├── __pycache__
    │   │   │   └── utils
    │   │   │       └── __pycache__
    │   │   ├── modflow
    │   │   │   └── __pycache__
    │   │   ├── modflowlgr
    │   │   │   └── __pycache__
    │   │   ├── modpath
```

Information Only

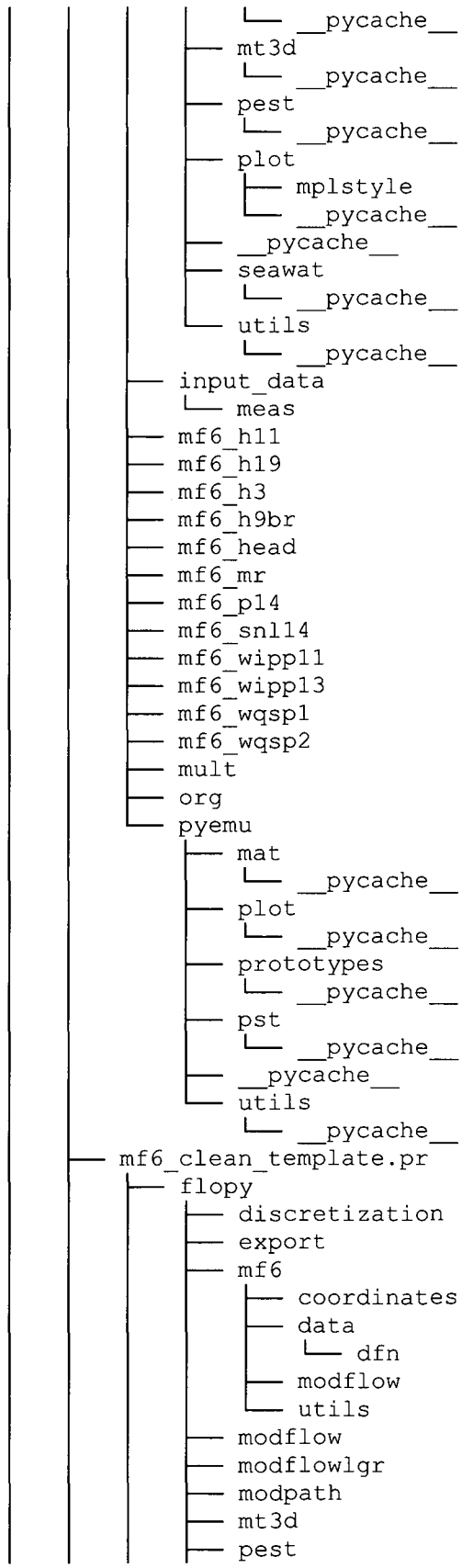

Information Only

```
│   │   │   ├── plot
│   │   │   │   └── mplstyle
│   │   │   ├── seawat
│   │   │   └── utils
│   │   ├── input_data
│   │   │   └── meas
│   │   ├── mf6_h11
│   │   ├── mf6_h19
│   │   ├── mf6_h3
│   │   ├── mf6_h9br
│   │   ├── mf6_head
│   │   ├── mf6_mr
│   │   ├── mf6_p14
│   │   ├── mf6_snl14
│   │   ├── mf6_wipp11
│   │   ├── mf6_wipp13
│   │   ├── mf6_wqsp1
│   │   ├── mf6_wqsp2
│   │   ├── mult
│   │   ├── org
│   │   └── pyemu
│   │       ├── mat
│   │       ├── plot
│   │       ├── prototypes
│   │       ├── pst
│   │       └── utils
│   ├── mf6_template
│   │   ├── flopy
│   │   │   ├── discretization
│   │   │   │   └── __pycache__
│   │   │   ├── export
│   │   │   │   └── __pycache__
│   │   │   ├── mf6
│   │   │   │   ├── coordinates
│   │   │   │   │   └── __pycache__
│   │   │   │   ├── data
│   │   │   │   │   ├── dfn
│   │   │   │   │   └── __pycache__
│   │   │   │   ├── modflow
│   │   │   │   │   └── __pycache__
│   │   │   │   ├── __pycache__
│   │   │   │   └── utils
│   │   │   │       └── __pycache__
│   │   │   ├── modflow
│   │   │   │   └── __pycache__
│   │   │   ├── modflowlgr
│   │   │   │   └── __pycache__
│   │   │   ├── modpath
│   │   │   │   └── __pycache__
│   │   │   ├── mt3d
│   │   │   │   └── __pycache__
│   │   │   ├── pest
│   │   │   │   └── __pycache__
│   │   │   ├── plot
│   │   │   │   ├── mplstyle
│   │   │   │   └── __pycache__
```

Information Only

```
│   │   │   ├── __pycache__
│   │   │   ├── seawat
│   │   │   │   └── __pycache__
│   │   │   └── utils
│   │   │       └── __pycache__
│   │   ├── input_data
│   │   │   └── meas
│   │   ├── mf6_h11
│   │   ├── mf6_h19
│   │   ├── mf6_h3
│   │   ├── mf6_h9br
│   │   ├── mf6_head
│   │   ├── mf6_mr
│   │   ├── mf6_p14
│   │   ├── mf6_snl14
│   │   ├── mf6_wipp11
│   │   ├── mf6_wipp13
│   │   ├── mf6_wqsp1
│   │   ├── mf6_wqsp2
│   │   ├── mult
│   │   ├── org
│   │   └── pyemu
│   │       ├── mat
│   │       │   └── __pycache__
│   │       ├── plot
│   │       │   └── __pycache__
│   │       ├── prototypes
│   │       │   └── __pycache__
│   │       ├── pst
│   │       │   └── __pycache__
│   │       ├── __pycache__
│   │       └── utils
│   │           └── __pycache__
│   └── mf6_ws_r001
│       ├── mf6_h11
│       ├── mf6_h19
│       ├── mf6_h3
│       ├── mf6_h9br
│       ├── mf6_head
│       ├── mf6_mr
│       ├── mf6_p14
│       ├── mf6_snl14
│       ├── mf6_wipp11
│       ├── mf6_wipp13
│       ├── mf6_wqsp1
│       └── mf6_wqsp2
├── obs_data
├── Outputs
│   ├── result_2023.02.21.itr5
│   │   ├── rYYY*
│   │   └── mf6_head
├── prelim_figs
│   ├── MillsRanch.Resampled.Drawdowns
│   └── MillsRanch.Resampled.Drawdowns.Peaks
├── presentations
└── PreviousWork
```

Information Only

```
    ├── PEST
    │   └── Builds
    │       ├── CVS
    │       ├── Linux
    │       └── Solaris
    │           └── CVS
    ├── Task5
    │   └── Outputs
    │       └── runs
    │           └── subtask5
    └── tfields
        ├── inputs
        │   ├── config
        │   ├── data
        │   ├── modflow
        │   └── scripts
        └── outputs
            └── r001
                └── CVS
├── __pycache__
└── pyemu
    ├── mat
    │   └── __pycache__
    ├── plot
    │   └── __pycache__
    ├── prototypes
    │   └── __pycache__
    ├── pst
    │   └── __pycache__
    ├── __pycache__
    └── utils
        └── __pycache__
```

- rYYY folders exist in the results and archived files for each of the selected T Field realizations included in Table 13.

Information Only

8. Appendix B – Routine Calculations

to: Records Center

from: Ross Kushnereit, Michelle Pedrazas, James Pinkard, INTERA Inc

subject: Calculations in Python scripts

The following calculations are part of the AR-203 *Recalibration of T-Fields*. The derivation of the data is explained in the following sections and supporting data are attached.

1. Calculation Process:
Script: S04_GenerateForwardRun.py
Function: balance_weights()

This function is used to balance the weights for a PEST++ IES run. PESTPP-IES is an iterative ensemble smoother (IES) that is part of the PEST++ suite.
This function takes in the following arguments as inputs:

- **template_ws=** path to the forward model folder directory that holds all the modflow6 model runs and PEST template and instruction files.
- **balanced_groups_perc={},** this is a dictionary with the assigned percentages of desired phi contribution for each observation group.
- **run_ext_prior=False**, boolean, if true, run prior ensemble in external folder. The prior run is run independently of the forward pest run. If false, the prior gets run in its own folder and copied to the next run.
- **prior_dir='master.prior'**, path to master directory where prior is run
- **usebin=True**, boolean, that if true, use .jcb binary files, and if false, use .csv text-based files

A PEST utility is used to load '**mf6.pst**' after PEST is run once in forward mode. '**mf6.pst**' is the pest control file which is built in the script. This function extracts the residual information, named '**res**' as a pandas dataframe object. The non-zero weighted observation groups are loaded in, as well as the simulated observations from the prior. A "**residual**" column in the '**res**' dataframe is calculated as the product of the "**modeled**" values in the '**res**' dataframe minus the "measured" values in the '**res**' dataframe. A new column "**phi**" is then calculated as the squared product of the "residual" column multiplied by the "**weight**" column. Total phi is calculated as the sum of the "**phi**" column in the '**res**' dataframe.

2. Identification/Listing of Input, Input sources, and Output:

- **Input**
  - **template_ws=** path to the forward model folder directory that holds all the modflow6 model runs and PEST template and instruction files.
  - **balanced_groups_perc={}** this is a dictionary with the assigned percentages of desired phi contribution for each observation group.
  - **run_ext_prior=False**, boolean, if true, run prior ensemble in external folder. The prior run is run independently of the forward pest run. If false, the prior gets run in its own folder and copied to the next run.
  - **prior_dir='master.prior'**, path to master directory where prior is ran

Information Only

- **usebin=True**, boolean, that if true, use .jcb binary files, and if false, use csv files

- **Output**
  - **mf6.pst-** Control file of the pest simulation with balanced weights

3. Data Qualification for Compliance Decision Analysis:

Data sources are documented in the References Section of this memorandum.

4. Software Used:

This is a Python script, run as part of the calibration process. A single Linux cluster was used in the calibration process: the FWM Linux cluster in Carlsbad, New Mexico.

5. References:

- The scripts and functions described in this memorandum, as well as several static and predefined input files, are saved in the final results repository - /data/cvs/CVSLIB/WIPP_EXTERNAL/ap203/wipp_tfields_2021/

6. List of Attachments:

- All files are archived at – /data/cvs/CVSLIB/WIPP_EXTERNAL/ap203/wipp_tfields_2021/

Information Only

1. Calculation Process:
Script: S06_Plot_Results.py
Function: get_best_phi_norm3D()

To support additional downstream analyses, one hundred representative realizations were chosen by comparing the three general observation groups: steady-state freshwater heads, multi-well pumping tests, and the Mills Ranch pumping event. To select the best 100 realizations, the objective function was normalized between 0 and 1 at each iteration. The normalization yielded a scaled value for each of the three general observation groups for each realization. The one hundred representative realizations were selected as the one hundred realizations closest to the origin point (i.e., 0,0,0 in three-dimensional space) in a Euclidean-distance sense.

This function takes in the following arguments as inputs:

- **master_dir**= path to master directory
- **itrs=[1]**, iterations to be analyzed
- **n=10**, number of selected realizations to choose, in this case 100
- **use_date=''**, to find a post-processing directory with a specific timestamp
- **plot=False**, boolean, if true, plot results.

The following input file is read in using pandas: '**mf6.phi.group.csv**'. This pandas dataframe named "**phi_df**" contains the following columns: **[iteration, total_runs, obs_realization, par_realization, aniso, bc, chd, pexit, h11, h19, h3, h9br, head, hk, meastrans, shds, mr, mr_flux, p14, rch, s_zone, snl14, ss, t_zone, wipp11,wipp13,wqsp1,wqsp2]**. "**Iteration**" represents the iteration number, "**obs_realization**" represents the realization number, and the rest of the columns represent observation groups recorded by PEST++ies.

To obtain the total phi for the three major observation groups, certain columns that represent observations for members of the three major observation groups are added together, using the following dictionary:

- **phi_groups** = {'ptests': ['h11', 'h19', 'h3', 'h9br','p14','snl14','wipp11', 'wipp13', 'wqsp1', 'wqsp2'], 'ss_head': ['head'], 'mr_ptest': ['mr']}

Where "**ptests**", "**ss_head**" and "**mr_ptests**" represent the three major observation groups and their respective values in the dictionary represent the names of the individual observation groups.

The iteration to work with, in our case iteration 5, is chosen by selecting it from the "**iteration**" column. The dataframe is now closer to 1000 rows (957), where each row represents the information collected from each realization in the iteration at hand. The next step is to normalize the three main observation groups from the "**phi_groups**" dictionary by the maximum value of phi for said iteration. A column "**dist**" is calculated as the closest distance to the origin point (i.e., 0,0,0 in three-dimensional space) in a Euclidean-distance sense. The dataframe is then sorted by the column "**dist**", and the 100 realizations with the closest distances to the origin point are chosen as the selected 100 realizations. The output file that includes all iterations with these calculations can be found here: **/master_dir/prelim_figs.{use_date}/best.realizations.itr{itr}.csv**

The function outputs a variable **best_phi** that is a dictionary with the selected 100 best realizations for the iterations of interest.

Information Only

2. Identification/Listing of Input, Input sources, and Output:

- **Input**
  - **master_dir=** path to master directory
  - **itrs=[1]**, iterations to be analyzed
  - **n=10**, number of selected realizations to choose, in this case 100
  - **use_date=''**, to find a post-processing directory with a specific timestamp
  - **plot=False**, boolean, if true, plot results.
- **Output**
  - **best_phi –** dictionary with the selected 100 best realizations for the selected iterations and their distances from the origin point in 3-d space (0,0,0)
  - **/master_dir/prelim_figs.{use_date}/best.realizations.itr{itr}.csv –** csv that stores the best phi values
  - **/fig_dir/3D.Normphi.{use_date}.itr{itr}.png -** Plot of 3d Normalized Phi

3. Data Qualification for Compliance Decision Analysis:

Data sources are documented in the References Section of this memorandum.

4. Software Used:

This is a Python script, run as part of the calibration process. A single Linux cluster was used in the calibration process: the FWM Linux cluster in Carlsbad, New Mexico.

5. References:

- The scripts and functions described in this memorandum, as well as several static and predefined input files, are saved in the final results repository - /data/cvs/CVSLIB/WIPP_EXTERNAL/ap203/wipp_tfields_2021/

6. List of Attachments:

- All files are archived at – /data/cvs/CVSLIB/WIPP_EXTERNAL/ap203/wipp_tfields_2021/

Information Only

1. Calculation Process:
Script: S06_Plot_Results.py
Function: plot_particle_time_cdfs()

This function is used to calculate particle travel time for each candidate release point for the 100 selected realizations in the chosen iteration, in this case iteration 5.

This function takes in the following arguments as inputs:

- **master_dir=** path to master directory
- **itr=5,** this is the iteration number of interest to analyze
- **obs_df_dict={},** this is a dictionary of the observed values for each iteration
- **use_date=** to find a post-processing directory with a specific timestamp
- **best_phi={},** dictionary with the selected 100 best realizations for the iteration of interest
- **pts=[1,2,3,4],** this is the number of particles of interest to analyze
- **pick_itr=5,** this is the iteration chosen to calculate the best 100 for

An **obs_df** dataframe is generated using an obs_df_dictionary, which was generated in the function **get_ies_obs_dict()** by loading either **'mf6.{i}.obs.jcb'** or **'mf6.{i}.obs.csv'**, and making a dictionary with the iterations as keys, and the resulting dataframe from the observations as the mapped values. For each particle of interest and for each iteration of interest the ensemble of particle travel time to the LWB is used to generate a CDF of the **obs_df** dataframe. From the ensemble of particle travel time, the min, max, mean, median and standard deviations are calculated from the particle travel times using NumPy. The statistics are saved here:
/{fig_dir}/All.Particle.crp{pt}/Exit.itr{i}/{use_date}.csv

2. Identification/Listing of Input, Input sources, and Output:

- **Input**
  - **master_dir=** path to master directory
  - **itr=5,** this is the iteration number of interest to analyze
  - **obs_df_dict={},** this is a dictionary of the observed values for each iteration
  - **use_date=** to find a post-processing directory with a specific timestamp
  - **best_phi={},** dictionary with the selected 100 best realizations for the iteration of interest
  - **pts=[1,2,3,4],** this is the number of particles of interest to analyze
  - **pick_itr=5,** this is the iteration chosen to calculate the best 100 for
- **Output**
  - **/{fig_dir}/All.Particle.crp{pt}/Exit.itr{i}/{use_date}.csv** – The csv that stores the statistics of ensemble of particle travel time which comprises of the min, max, mean, median and standard deviations.

3. Data Qualification for Compliance Decision Analysis:
Data sources are documented in the References Section of this memorandum.

4. Software Used:
This is a Python script, run as part of the calibration process. A single Linux cluster was used in the calibration process: the FWM Linux cluster in Carlsbad, New Mexico.

Information Only

5. References:

- The scripts and functions described in this memorandum, as well as several static and predefined input files, are saved in the final results repository - /data/cvs/CVSLIB/WIPP_EXTERNAL/ap203/wipp_tfields_2021/

6. List of Attachments:

- All files are archived at – /data/cvs/CVSLIB/WIPP_EXTERNAL/ap203/wipp_tfields_2021/

Information Only

1. Calculation Process:
Script: S00_Generate_Ensemble.py
Function: get_truncated_normal()

This function generates an ensemble of noise utilizing scipy's truncnorm function to draw a normal distribution while also limiting the upper and lower bounds.

This function takes in the following arguments as inputs:

- **mean=0,** this is the mean
- **sd=1,** this is the standard deviation
- **low=0,** this is the lower bound
- **upp=10,** this is the upper bound
- **nreal=10,** the number of realizations
- **fill_bound_mult=10,** the multiplier to fill bounds?

A random seed is chosen. Upper and lower bounds are calculated only for weighted observations. If the lower bound (**'low1'**) is not specified (type **'nan'**), then the lower bound is calculated as the mean plus the fill bound multiplier (**fill_bound_mult)** multiplied by the standard deviation (**'sd'**) [**mean + (fill_bound_mult * sd)**]. Similarly, the upper bound (**'upp1'**) is calculated as the mean minus the **fill_bound_mult** multiplied by the standard deviation (**'sd'**) [**mean - (fill_bound_mult * sd)**]. If the upper and lower bounds are specified, then that is the value used. Regardless of what the new calculated **'low1'** and **'upp1'** are, this function will make the lower bound be the smaller value between **'low1'** and **'upp1'**, and the upper bound be the larger value between **'low1'** and **'upp1'**. Now that the lower and upper bounds have been defined, the function returns a list of random variates from a set of truncated normal values **list(X.rvs(nreal))** .

2. Identification/Listing of Input, Input sources, and Output:

- **Input**
  - **mean=0,** this is the mean
  - **sd=1,** this is the standard deviation
  - **low=0,** this is the lower bound
  - **upp=10,** this is the upper bound
  - **nreal=10,** the number of realizations
  - **fill_bound_mult=10,** the multiplier to fill bounds?
- **Output**
  - **list(X.rvs(nreal))** – list of random variates from truncated normal values

3. Data Qualification for Compliance Decision Analysis:
Data sources are documented in the References Section of this memorandum.

4. Software Used:
This is a Python script, run as part of the calibration process. A single Linux cluster was used in the calibration process: the FWM Linux cluster in Carlsbad, New Mexico.

Information Only

5. References:

- The scripts and functions described in this memorandum, as well as several static and predefined input files, are saved in the final results repository - /data/cvs/CVSLIB/WIPP_EXTERNAL/ap203/wipp_tfields_2021/

6. List of Attachments:

- All files are archived at – /data/cvs/CVSLIB/WIPP_EXTERNAL/ap203/wipp_tfields_2021/

Information Only

1. Calculation Process:
Script: S00_Generate_Ensemble.py
Function: generate_ensemble()

This function is used to extract the initial transmissivity values from the Task5 of AP-114, converts them to hydraulic conductivity and populates them into the prior ensemble file as gridscale parameters.

This function takes in the following arguments as inputs:

- **nreals = 100,** the number of realizations to use (max 1000)
- **verbose = False,** boolean, if True, then a statement will be printed out on the screen when the function has finished building an ensemble data for testing.

Initial T-fields are read in from the following directory:
/PreviousWork/Task5/Outputs/runs/subtask5/
Model coordinates to iterate through each model cell is read in from here:
input_data/model.coord.info.csv/

This function will iterate through transmissivity values for each model cell for each realization (defined in 'nreals' argument) from the initial T-fields results from AP-114, and save this information as arrays with the same number of rows and columns as the model discretization in a pandas dataframe called **'df'**.

2. Identification/Listing of Input, Input sources, and Output:

- **Input**
  - **nreals = 100,** the number of realizations to use (max 1000)
  - **verbose = False,** boolean, if True, then a statement will be printed out on the screen when the function has finished building an ensemble data for testing.
- **Output**
  - **df –** pandas dataframe of transmissivity values for each model cell for each realization

3. Data Qualification for Compliance Decision Analysis:
Data sources are documented in the References Section of this memorandum.

4. Software Used:
This is a Python script, run as part of the calibration process. A single Linux cluster was used in the calibration process: the FWM Linux cluster in Carlsbad, New Mexico.

5. References:

- The scripts and functions described in this memorandum, as well as several static and predefined input files, are saved in the final results repository - /data/cvs/CVSLIB/WIPP_EXTERNAL/ap203/wipp_tfields_2021/

6. List of Attachments:

- All files are archived at – /data/cvs/CVSLIB/WIPP_EXTERNAL/ap203/wipp_tfields_2021/

Information Only

1. Calculation Process:
Script: model_functions.py
Function: multiply_zones()

This function is used to apply a multiplier to each property array based on zonation.

This function takes in the following arguments as inputs:

- **prop='t'** property of interest to apply multiplier on: t=transmissivity, s=specific storage, a=anisotropy
- **model_ws** = path to model workspace directory

For a given property, this function assigns a multiplier to each zone (**'zone_mult'**) This multiplier is read in from here: **/model_ws/{prop}_zone_mult.csv.** The function then loads in the zone assignments for the model cells (**'zone_arr'**) from the following input file: **/model_ws/{prop}_zones.txt.** The property arrays are loaded in from the following CSVs:

- Transmissivity: model_ws/mf6_head.npf_k.txt
- Specific storage: model_ws/mf6_head.sto_ss.txt
- Anisotropy: model_ws/mf6_head.npf_k22.txt

The multiplier is then multiplied to each model cell value depending on what zone each model cell is associated with for the property of interest. For specific storage, an upper-limit of 0.0408 is imposed for the array. This function then overwrites loaded csv file with the resulting property array (for example, transmissivity, specific storage or anisotropy) after applying the corresponding multiplier to the values for each zone.

2. Identification/Listing of Input, Input sources, and Output:

- **Input**
  - **prop='t'**, property of interest to apply multiplier on:- t=transmissivity, s=specific storage, a=anisotropy
  - **model_ws** = path to model workspace directory
- **Output**
  - Transmissivity: model_ws/mf6_head.npf_k.txt
  - Specific storage: model_ws/mf6_head.sto_ss.txt
  - Anisotropy: model_ws/mf6_head.npf_k22.txt

3. Data Qualification for Compliance Decision Analysis:
Data sources are documented in the References Section of this memorandum.

4. Software Used:
This is a Python script, run as part of the calibration process. A single Linux cluster was used in the calibration process: the FWM Linux cluster in Carlsbad, New Mexico.

5. References:

- The scripts and functions described in this memorandum, as well as several static and predefined input files, are saved in the final results repository - /data/cvs/CVSLIB/WIPP_EXTERNAL/ap203/wipp_tfields_2021/

Information Only

6. List of Attachments:

- All files are archived at –
  /data/cvs/CVSLIB/WIPP_EXTERNAL/ap203/wipp_tfields_2021/

Information Only

1. Calculation Process:
Script: model_functions.py
Function: surface_02_extrapolate()

This function was lifted from SP 9-9 (Kuhlman, 2009), the procedure to develop potentiometric surface maps for the Annual Site Environmental Reports (ASERs), ultimately for use as a boundary condition.

This function takes in the following arguments as inputs:

- **model_ws**: model workspace directory
- **plot=False,** boolean, if true, color plots of initial original head, new head and ibound will be generated.

The function surface_02_extrapolate() reads in data files containing information about the initial head, relative coordinates, and initial boundary conditions for a MODFLOW model. It applies an exponential surface and constant head value to the active cells (ibound=1) and non-geologic boundary conditions (ibound=-2), respectively. The resulting initial/boundary head is output to a file for the MODFLOW model to use.

Additionally, the function reads in a file with initial boundary conditions (ibound) for a MODFLOW model, replaces certain values in the ibound array with values of -2, and exports the modified ibound array to a file. The function then populates the MODFLOW constant head (chd) package file using the modified ibound array and the initial/boundary head file created earlier.

If plot parameter is set to True, the function will generate color plots of initial original head, freshwater head and ibound.

This function returns updated initial heads and chd files.

2. Identification/Listing of Input, Input sources, and Output:

- **Input**
  - **model_ws**: model workspace directory
  - **plot=False**: boolean, if true, color plots of initial original head, new head and ibound will be generated.
- **Output**
  - Constant head package data-Model_ws/mf6_head.chd_stress_period_data_1.txt
  - Plot of initial original initial head, new initial head, and ibound

3. Data Qualification for Compliance Decision Analysis:
Data sources are documented in the References Section of this memorandum.

4. Software Used:
This is a Python script, run as part of the calibration process. A single Linux cluster was used in the calibration process: the FWM Linux cluster in Carlsbad, New Mexico.

Information Only

5. References:

- The scripts and functions described in this memorandum, as well as several static and predefined input files, are saved in the final results repository - /data/cvs/CVSLIB/WIPP_EXTERNAL/ap203/wipp_tfields_2021/
- Kuhlman, K.L. 2009. Procedure SP 9-9, revision 0, Preparation of Culebra potentiometric surface contour maps. Carlsbad, NM: Sandia National Laboratories, ERMS 552306.

6. List of Attachments:

- All files are archived at – /data/cvs/CVSLIB/WIPP_EXTERNAL/ap203/wipp_tfields_2021/

Information Only

1. Calculation Process:
Script: model_functions.py
Function: save_ssheads()

This function is used to save the starting heads as a reference file using the flopy library.

This function takes in the following arguments as inputs:

- **model_ws**: model workspace directory
- **plot=False**: boolean, if true, generates a color plot of starting heads for quality control.

This Python function saves starting heads as a reference file using the **flopy** library. The starting heads are read from the steady-state modflow6 run (**mf6_head.hds)** file in the **model_ws** directory, and dry cells are displayed as -9999 instead of 1e30 values. The **ibound** variable is read from the **init_bnds.inf** file in the **model_ws** directory, and the **plot** boolean argument determines whether a color plot of the starting heads is generated for quality control.

It reads in the first stress period and saves it as an output file: **/{model_ws}/ mf6_head.ref**

2. Identification/Listing of Input, Input sources, and Output:

- **Input**
  - **model_ws**: model workspace directory
  - **plot=False**: boolean, if true, generates a color plot of starting heads for quality control.
- **Output**
  - First stress period - **/{model_ws}/ mf6_head.ref**
  - QA Plot of starting heads

3. Data Qualification for Compliance Decision Analysis:
Data sources are documented in the References Section of this memorandum.

4. Software Used:
This is a Python script, run as part of the calibration process. A single Linux cluster was used in the calibration process: the FWM Linux cluster in Carlsbad, New Mexico.

5. References:

- The scripts and functions described in this memorandum, as well as several static and predefined input files, are saved in the final results repository - /data/cvs/CVSLIB/WIPP_EXTERNAL/ap203/wipp_tfields_2021/

6. List of Attachments:

- All files are archived at – /data/cvs/CVSLIB/WIPP_EXTERNAL/ap203/wipp_tfields_2021/

Information Only

1. Calculation Process:
Script: model_functions.py
Function: chd2csv()

This function saves time-variant specified head boundaries for Stress Period 1.

This function takes in the following arguments as inputs:

- **model_ws**: model workspace directory

This function loads in the time-variant specified head boundaries ('**chd**') for Stress Period 1:
model_ws/mf6_head.chd_stress_period_data_1.txt
and saves this information as a comma-separated values (CSV) file, using the following column header:
['**layer**','**row**','**column**','**head**']).
This function saves the CSV file to the following location:
model_ws/mf6_head.chd_stress_period_data_1.csv

2. Identification/Listing of Input, Input sources, and Output:

- **Input**
  - **model_ws**: model workspace directory
- **Output**
  - **model_ws/mf6_head.chd_stress_period_data_1.csv** - Constant head data saved as csv

3. Data Qualification for Compliance Decision Analysis:
Data sources are documented in the References Section of this memorandum.

4. Software Used:
This is a Python script, run as part of the calibration process. A single Linux cluster was used in the calibration process: the FWM Linux cluster in Carlsbad, New Mexico.

5. References:

- The scripts and functions described in this memorandum, as well as several static and predefined input files, are saved in the final results repository - /data/cvs/CVSLIB/WIPP_EXTERNAL/ap203/wipp_tfields_2021/

6. List of Attachments:

- All files are archived at – /data/cvs/CVSLIB/WIPP_EXTERNAL/ap203/wipp_tfields_2021/

Information Only

1. Calculation Process:
Script: model_functions.py
Function: estimate_geo_trans()

This function updates the measured log10 transmissivity values based on updated hydraulic conductivity values. Hydraulic conductivity values are spatially interpolated.

This function takes in the following arguments as inputs:

- **model_ws='.'**: model workspace directory

The measured transmissivities are read in from: **{model_ws}/measured_trans.csv** and loaded into a pandas dataframe called meast_df.

Hydraulic conductivity values are read in from: **{model_ws}/mf6_head.npf_k csv.**
Well coordinates are read in from: **/input_data/well.coords.csv**

Transmissivity values are calculated by performing a spatially bilinear interpolation on the product of hydraulic conductivity values for each model cell and a constant model thickness of 7.75 m. Then, a logarithmic operation is applied to the values. The results are saved in the following output file:
{model_ws}/measured_transt.out.csv

2. Identification/Listing of Input, Input sources, and Output:

- **Input**
  - **model_ws='.'**: model workspace directory
- **Output**
  - **{model_ws}/measured_transt.out.csv –** updated transmissivity values

3. Data Qualification for Compliance Decision Analysis:
Data sources are documented in the References Section of this memorandum.

4. Software Used:
This is a Python script, run as part of the calibration process. A single Linux cluster was used in the calibration process: the FWM Linux cluster in Carlsbad, New Mexico.

5. References:

- The scripts and functions described in this memorandum, as well as several static and predefined input files, are saved in the final results repository - /data/cvs/CVSLIB/WIPP_EXTERNAL/ap203/wipp_tfields_2021/

6. List of Attachments:

- All files are archived at – /data/cvs/CVSLIB/WIPP_EXTERNAL/ap203/wipp_tfields_2021/

Information Only

1. Calculation Process:
Script: model_functions.py
Function: bilinear_interpolate()

This is a Python function that performs bilinear interpolation on a 2D NumPy array. Bilinear interpolation is a method used to estimate the value at a point in a 2D grid using the values in the element containing the point and its four nearest neighbors.

This function takes in the following arguments as inputs:

- **im**: 2D NumPy array representing the matrix to be used in the interpolation.
- **x**: the column plus the remainder of the x position
- **y**: the row plus the remainder of the y position

The function returns the interpolated value at the given (x,y) position.

The implementation of the function calculates the coordinates of the four nearest neighbors of the point using floor functions, and then calculates the weights to be applied to each of the neighbors to obtain the interpolated value.

2. Identification/Listing of Input, Input sources, and Output:

- **Input**
  - **im**: 2D NumPy array representing the matrix to be interpolated.
  - **x**: the column plus the remainder of the x position
  - **y**: the row plus the remainder of the y position
- **Output**
  - **{model_ws}/measured_transt.out.csv** – updated transmissivity values

3. Data Qualification for Compliance Decision Analysis:
Data sources are documented in the References Section of this memorandum.

4. Software Used:
This is a Python script, run as part of the calibration process. A single Linux cluster was used in the calibration process: the FWM Linux cluster in Carlsbad, New Mexico.

5. References:

- The scripts and functions described in this memorandum, as well as several static and predefined input files, are saved in the final results repository - /data/cvs/CVSLIB/WIPP_EXTERNAL/ap203/wipp_tfields_2021/

6. List of Attachments:

- All files are archived at – /data/cvs/CVSLIB/WIPP_EXTERNAL/ap203/wipp_tfields_2021/

Information Only

1. Calculation Process:
Script: get_heads.py
Function: mod2obs()

This function performs a spatial interpolation from the model grid discretization to the locations of wells of interest and a temporal interpolation from model output times to times of interest.

This Python function extracts simulated heads for wells of interest in a MODFLOW6 groundwater flow model, using spatial and temporal interpolation. The function takes the following parameters:

- **model_ws**: directory of the MODFLOW6 simulation
- **name**: MODFLOW6 simulation name
- **wells**: list of wells to extract heads from
- **forobs=False**: a boolean that determines whether to use initial values or extracted heads from the model for a given time. Default is False.
- **Freq=1**: frequency of the extracted data. If freq = 30, then a 30-day smoothed-average for mills ranch is read in. If freq = 1, data is passed. Default is 1.

The function first reads in the start times and well coordinates data from CSV files. It then reads in the measurement data and stores it in a Pandas dataframe. The function then calculates the model coordinates for each well, and extracts the head data from the model at the corresponding coordinates using bilinear interpolation.

If the **name** parameter is equal to **'head'**, the function interpolates the head data for each well at the initial simulation time and adds it to the final dataframe. If not, the function calculates the change in head data for each well over time and adds it to the final dataframe.

The function then saves the final dataframe to a CSV file in the simulation directory with a name depending on the **name** and **freq** parameters. If the **forobs** parameter is True, the function uses the measured values as the output values.

2. Identification/Listing of Input, Input sources, and Output:

- **Input**
  - **model_ws**: directory of the MODFLOW6 simulation
  - **name**: MODFLOW6 simulation name
  - **wells**: list of wells to extract heads from
  - **forobs=False**: a boolean that determines whether to use initial values or extracted heads from the model for a given time. Default is False.
  - **Freq=1**: frequency of the extracted data. If freq = 30, then a 30-day smoothed-average for mills ranch is read in. If freq = 1, data is passed. Default is 1.
- **Output**
  - **{model_ws}/{name}.obs.csv or {model_ws}/{name}.{freq}d.obs.csv** – table of simulated heads

3. Data Qualification for Compliance Decision Analysis:
Data sources are documented in the References Section of this memorandum.

Information Only

4. Software Used:

This is a Python script, run as part of the calibration process. A single Linux cluster was used in the calibration process: the FWM Linux cluster in Carlsbad, New Mexico.

5. References:

- The scripts and functions described in this memorandum, as well as several static and predefined input files, are saved in the final results repository - /data/cvs/CVSLIB/WIPP_EXTERNAL/ap203/wipp_tfields_2021/

6. List of Attachments:

- All files are archived at – /data/cvs/CVSLIB/WIPP_EXTERNAL/ap203/wipp_tfields_2021/

Information Only

1. Calculation Process:
Script: model_functions.py
Function: apply_pumping2mr()

This function generates well files per stress period to represent the Mills Ranch pumping rates.

This function takes in the following arguments as inputs:

- **model_ws='.'**, model workspace directory
- **mr_nper=152**, number of stress periods to apply mills ranch pumping rates to

This function uses ratio of drawdown to recovery (in recovery period) observed in well SNL-17 to derive pumping rate in Mills Ranch well. Unit conversions from cm/s to gallons/min and vice-versa are applied using the following two functions: Qcns2Qgpm() and Qgpm2Qcms().

The two initial fluxes with start and stop SPs are read in as **'mr_flux_df'** from: **/{model_ws}/mr_iflux.txt**
The relative pumping rates based on drawdown of nearby wells are read in as **realtiveQ_df** from: **/{model_ws}/snl17.relativeq.csv**.

For each stress period, the initial pumping rate is multiplied by the ratio of drawdown to recovery (in recovery period) observed in well SNL-17. This function then writes out a well file for every stress period (**mr_nper**) as follows: **/{model_ws}/mf6_mr.wel_stress_period_data_{sp+1}.txt**

2. Identification/Listing of Input, Input sources, and Output:

- **Input**
  - **model_ws='.'**, model workspace directory
  - **mr_nper=152**, number of stress periods to apply mills ranch pumping rates to
- **Output**
  - **{model_ws}/mf6_mr.wel_stress_period_data_{sp+1}.txt –** well file for every stress period where **{sp+1}** is the stress period number

3. Data Qualification for Compliance Decision Analysis:
Data sources are documented in the References Section of this memorandum.

4. Software Used:
This is a Python script, run as part of the calibration process. A single Linux cluster was used in the calibration process: the FWM Linux cluster in Carlsbad, New Mexico.

5. References:

- The scripts and functions described in this memorandum, as well as several static and predefined input files, are saved in the final results repository - /data/cvs/CVSLIB/WIPP_EXTERNAL/ap203/wipp_tfields_2021/

6. List of Attachments:

- All files are archived at – /data/cvs/CVSLIB/WIPP_EXTERNAL/ap203/wipp_tfields_2021/

Information Only

1. Calculation Process:
Script: get_heads.py
Function: get_mr_pumping ()

This function extracts flux rates for each stress period from well files, performs a unit conversion on the flux rates from meters per second to gallons per minute, and appends the information into one CSV file.

This function takes in the following arguments as inputs:

- **model_ws='.'**, model workspace directory
- **mr_nper=152**, number of stress periods to iterate through

This function iterates through stress periods of interest (**mr_nper**) and reads in the well files for each respective stress period to extract the flux at each stress period. These flux rates are then converted from m/s to gallons/minute. The information is then appended into a dataframe (**'df'**) with columns [**'sp','flux','gpm','weight'**].and exported as an output file: **model_ws/mr_pumping.csv**.

2. Identification/Listing of Input, Input sources, and Output:

- **Input**
  - **model_ws='.'**, model workspace directory
  - **mr_nper=152**, number of stress periods to iterate through
- **Output**
  - **{model_ws}/mr_pumping.csv** – csv file containing the stress period, flux in m/s, pumping rate in gpm, and a weight which is set to 0.

3. Data Qualification for Compliance Decision Analysis:
Data sources are documented in the References Section of this memorandum.

4. Software Used:
This is a Python script, run as part of the calibration process. A single Linux cluster was used in the calibration process: the FWM Linux cluster in Carlsbad, New Mexico.

5. References:

- The scripts and functions described in this memorandum, as well as several static and predefined input files, are saved in the final results repository - /data/cvs/CVSLIB/WIPP_EXTERNAL/ap203/wipp_tfields_2021/

6. List of Attachments:

- All files are archived at – /data/cvs/CVSLIB/WIPP_EXTERNAL/ap203/wipp_tfields_2021/

Information Only

1. Calculation Process:
Script: cbb2dtrkmf.py
Function: convert_budget2dtrkmf()

This function converts the modflow6 budget file (**mf6_head.cbb**) into a dtrkmf-compatible format.

This function takes in the following arguments as inputs:

- **model_ws='.'**, model workspace directory

This function loads in the modflow6 budget file from: **/{model_ws}/mf6_head.cbb**.
It then proceeds to load two more input files needed to re-format the budget file:
/{model_ws}/mf6.ja.txt – coordinate reference system (CRS) column pointers
/{model_ws}/mf6.ia.txt – CRS connection data row pointers

It loads the '**mf6.ja.txt**' and '**mf6.ia.txt**' files from the **model_ws** directory. It then loops over each stress period and time step in the input budget file and extracts the data for storage and flow face terms. For each term, it creates a binary output file in the DTRKMF format with the appropriate header and data structure. Finally, the function writes the output binary files to disk and prints a message indicating that it has finished.

The resulting output file that is now ready to be used with the dtrkmf particle tracking software is saved here: **/{model_ws}/'mf6_head.dtrkmf.cbb**

2. Identification/Listing of Input, Input sources, and Output:

- **Input**
  - **model_ws='.'**, model workspace directory
- **Output**
  - **{model_ws}/mf6_head.dtrkmf.cbb** – modflow 6 budget file converted to a dtrkmf format

3. Data Qualification for Compliance Decision Analysis:
Data sources are documented in the References Section of this memorandum.

4. Software Used:
This is a Python script, run as part of the calibration process. A single Linux cluster was used in the calibration process: the FWM Linux cluster in Carlsbad, New Mexico.

5. References:

- The scripts and functions described in this memorandum, as well as several static and predefined input files, are saved in the final results repository - /data/cvs/CVSLIB/WIPP_EXTERNAL/ap203/wipp_tfields_2021/

6. List of Attachments:

- All files are archived at – /data/cvs/CVSLIB/WIPP_EXTERNAL/ap203/wipp_tfields_2021/

Information Only

1. Calculation Process:
Script: model_functions.py
Function: read_dtrkmf_out()

This function reads in the DTRKMF version of particle tracking output files, and outputs a CSV for each particle with exit data (times and coordinates).

This function takes in the following arguments as inputs:

- **model_ws='.'**, model workspace directory
- **pts=[1,2,3,4]**, number of particles to be released
- **plot_particle=False**, boolean, if true, plots particle tracks.

The function reads in data from a CSV file named**/{model_ws}/dtrk_crp{pt}.out**, where {pt} is the particle number. It then extracts the exit times and coordinates for each particle with exit data and writes it to a new CSV file named **dtrkmf_crp{pt}.exit.csv**.

The function also performs some coordinate transformations and corrections for the Culebra aquifer. Since the travel time calculation was done with a Culebra thickness of 4 m, a correction is needed for the higher T portion of the Culebra. This correction is performed by dividing the travel time by 4 and multiplying by 7.75 m (model thickness).

This function returns an output file for every particle: **/{model_ws}/dtrkmf_crp{pt}.exit.csv**

2. Identification/Listing of Input, Input sources, and Output:

- **Input**
  - **model_ws='.',** model workspace directory
  - **pts=[1,2,3,4]**, number of particles to be released
  - **plot_particle=False**, boolean, if true, plots particle tracks.
- **Output**
  - **/{model_ws}/dtrkmf_crp{pt}.exit.csv –** csv file of exit times and coordinates for every particle with exit data

3. Data Qualification for Compliance Decision Analysis:
Data sources are documented in the References Section of this memorandum.

4. Software Used:
A single Linux cluster was used in the calibration process: the FWM Linux cluster in Carlsbad, New Mexico.

5. References:

- The scripts and functions described in this memorandum, as well as several static and predefined input files, are saved in the final results repository - /data/cvs/CVSLIB/WIPP_EXTERNAL/ap203/wipp_tfields_2021/

6. List of Attachments:

- All files are archived at – /data/cvs/CVSLIB/WIPP_EXTERNAL/ap203/wipp_tfields_2021/

Information Only